Metamorphic evolution in the northern Central Alps: Linking ^{39}Ar-^{40}Ar dating with thermobarometry

Inauguraldissertation
der Philosophisch-narturwissenschaftlichen Fakultät
der Universität Bern

vorgelegt von

Julien Allaz

von Villars-le-Terroir (VD)

Leiter der Arbeit:

Prof. Martin Engi

Institut für Geologie

Prof. Igor M. Villa (Prüfender)	Institut für Geologie, Bern
PD Dr. Alfons Berger (Prüfender)	Institut für Geologie, Bern
Prof. Romain Bousquet (Koreferent)	Institut für Geowissenschaften, Potsdam (D)

Metamorphic evolution in the northern Central Alps: Linking ^{39}Ar-^{40}Ar dating with thermobarometry

Inauguraldissertation
der Philosophisch-narturwissenschaftlichen Fakultät
der Universität Bern

vorgelegt von

Julien Allaz

von Villars-le-Terroir (VD)

Leiter der Arbeit:

Prof. Martin Engi

Institut für Geologie

Prof. Igor M. Villa (Prüfender)	Institut für Geologie, Bern
PD Dr. Alfons Berger (Prüfender)	Institut für Geologie, Bern
Prof. Romain Bousquet (Koreferent)	Institut für Geowissenschaften, Potsdam (D)

Von der Philosophisch-narturwissenschaftlichen Fakultät angenommen.

Bern, 29. Mai 2008

Der Dekan
Prof. Dr. Paul Messerli

Table of Content

Appendix

Further information, pictures... will be soon available on my personnal website!

http://geoloweb.ch/

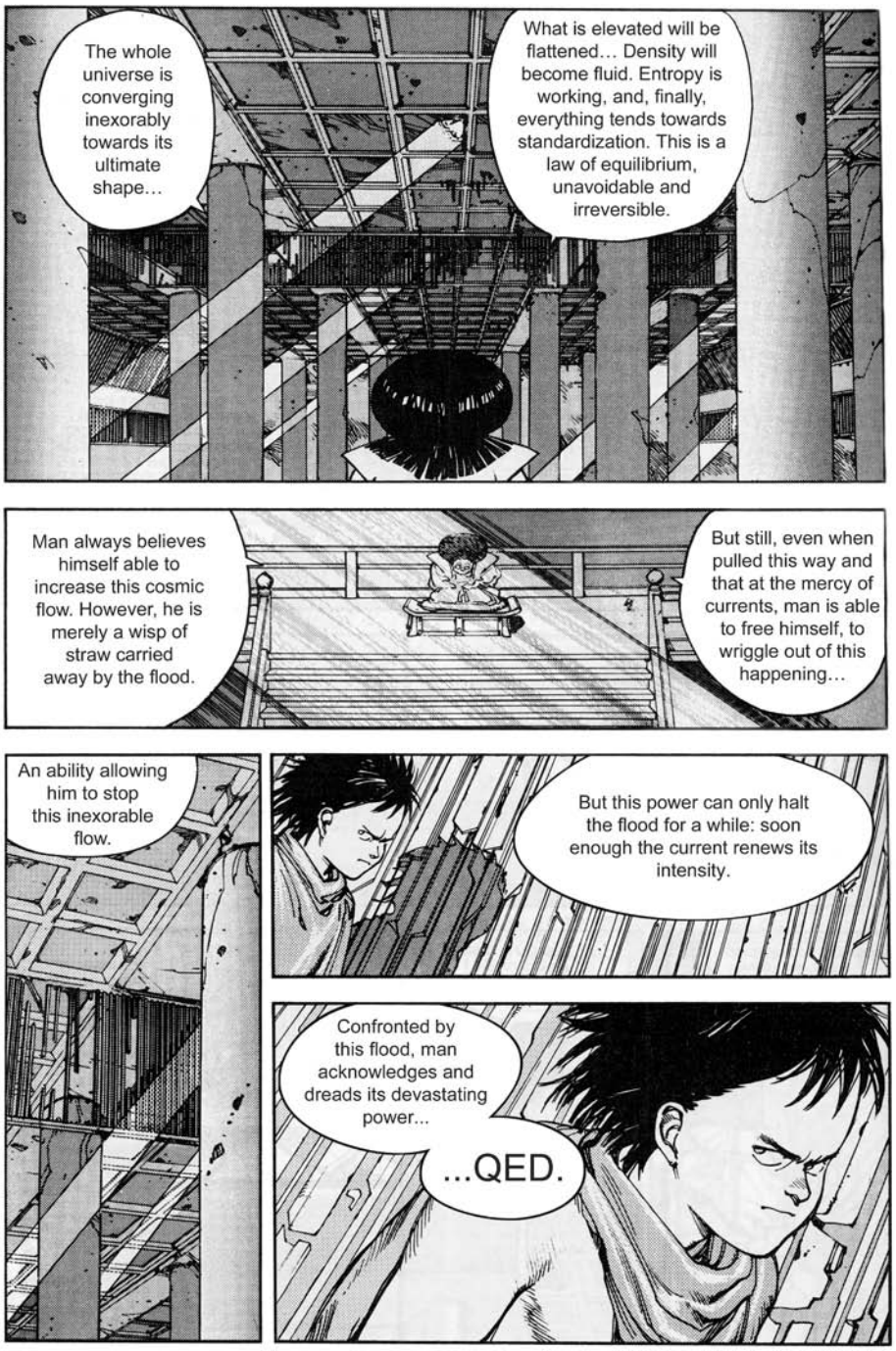

Katsuhiro Otomo,"Akira", volume 4, p. 190

N.d.a: Thank's to uncle Andrew for translation of this strip cartoon!

In memory of...

"Mémé" Denise Allaz-Favre (1914-2005)

"Tonton" André Chambettaz (1934–1999)

"Mon dieu qu'il ferait bon
sur la Terre des Hommes,
si l'on y rencontrait
cette race incongrue...

Cette race importune
et qui partout foisonne,
la race des gens du terroir,
des gens du cru...

Que la vie serait belle
en toute circonstance,
si vous n'aviez tirer
du néant ces jobards...

Preuve peut-être bien
de votre inexistance,
les imbéciles heureux
qui sont nés quelque part..."

Georges Brassens,
repris par Tarmac
"*La ballade des gens qui sont nés quelque part*"

1) Introduction

1.1) Age or not age?

Geochronology is the art of dating a geological process with an absolute age. For instance, the decay of a radioactive isotope and the accumulation of its daughter product(s) inside a mineral are often considered to yield the geological age of this host mineral. However, a meaningful geological interpretation of such an age necessitates a clear relation between the measured isotopic ratio (the age) and the geological processes during formation of the mineral in question and perhaps since that time; hence several processes and conditions need to be identified and characterized. Provided no loss (or gain) of these isotopes has occurred, the dating result obtained should be a "crystallization age", i.e. the time of mineral growth or re-equilibration. Complications commonly arise from the loss or gain of some isotope(s) after crystallization:

A) **Diffusion**. In simple theory, retention of an isotope in a crystalline structure is essentially controlled by temperature. Above a certain "closure temperature", diffusion may induce the complete loss of a daughter isotope and the dating-result is then interpreted as a "cooling age" (Dodson, 1973; Dodson, 1986).

B) **Metamorphic reaction, recrystallization**. Through the increase of metamorphic conditions, a mineral assemblage evolves through different stage of (partial) equilibration. Ideally, a final and complete PT-equilibration is achieved during the thermal climax of metamorphism (at high fluid activity) and corresponds to the closure of all metamorphic reactions and possibly isotopic systems, too. In contrary, re-crystallization induced by a later metamorphic reaction or a penetrative deformation will re-open then system and is likely to be accompanied with an isotopic resetting (e.g. biotite chloritization).

C) **Inheritance**. The presence, even in minor amounts, of relic minerals related to an earlier crystallization stage, is susceptible to yield a geologically meaningless and too old age (of formation). This effect is strong if the inherited material is very old compared to the metamorphic event we aim to date (e.g. inherited Caledonian or Hercynian cores in partially reequilibrated mineral samples, which underwent the Alpine orogeny).

In early geochronological studies, the equilibrium between minerals used for dating was (at best) determined on the basis of textural observations made by optical microscopy, i.e. qualitative documentation at mm-scale. In many cases, Dodson's theory was applied to interpret data as cooling or (re-)crystallization ages (case A). Today, petrology offers the opportunity to study each mineral at µm-scale (e.g. by electron microprobe) or even nm-scale (transmitted electron microscope). This has, in many cases, revealed disequilibrium features or inheritance problems in samples where optical petrography alone would have suggested equilibrium (case B, C).

1.2) Aims of the study

This thesis takes a multidisciplinary approach in an effort to ascertain the correct interpretation of geochronological results. Detailed petrography remains a crucial first step, followed by the analysis of mineral compositions, phase-petrological analysis and multi-equilibrium thermobarometry, completed with Ar-isotopic dating of mica. The methodology is outlined in Figure 1.1 and subsequently detailed in three chapters of this thesis.

Identification, selection, and documentation of suitable samples is critical, of course. To avoid problems of inheritance (case C) only monometamorphic metasediments were collected. The selection of texturally well-equilibrated samples is of utmost importance, in order to minimize effects of retrogression (case B). Pressure and temperature condition were determined using TWQ (Berman, 1991), and the preservation of an equilibrium state was thus quantified. To support the phase-petrological interpretation of textural observations (e.g. compositional zoning of minerals), the stable mineral assemblages were computed in pressure-temperature-fluid composition diagrams (pseudo-sections) using THERIAK-DOMINO (de Capitani, 1994). Only samples, for which the PT-history was thus defined, the age of mica separates was determined by ^{39}Ar-^{40}Ar stepwise heating analysis (5-20 mg of muscovite, biotite, paragonite [Na-mica] and margarite [Ca-mica]). The aim was to answer the following questions:

1. What is the significance of these Ar-ages for micas, notably in relation to the thermobarometric results?

2. Does chemical equilibrium (established for minerals of the major elements) correspond to preserved isotopic equilibrium as well? If not, what processes control the resetting of Ar-ages in micas?

3. Where (minor) disequilibria occur involving the mineral(s) used for dating, is it possible to infer the PT-conditions of reactions responsible for this disequilibration?

4. Given the above approach, i.e. state-of-the-art techniques of quantifying petrological and geochronological results, what new constraints emerge for the pressure-temperature-time (PTt) history, as analyzed in samples from the northern Central Alps?

1.3) Organization of the study

The first question is viewed as the central focus of this thesis and is of course behind the three main chapters comprised. The second question is addressed in the **first chapter**, which discusses the effect of metamorphic reactions (case B) on Ar-ages. For this first study, we investigated (a) the progressive replacement of paragonite by plagioclase in metapelites containing two white micas, (b) the effects of minor chloritization of biotite. Such reactions are susceptible to induce (partial) resetting of the Ar-ages of micas, depending on their chemistry. An effort was made, therefore, to separate muscovite from paragonite, and to determine the age of each mineral. Unfortunately, such separates were usually heterogeneous, containing significant amounts of each type of white mica. However, in addition to ^{36}Ar, ^{39}Ar and ^{40}Ar (which are required to yield an Ar-age), ^{37}Ar and ^{38}Ar were also measured. These isotopes are essentially produced from Ca and Cl during sample irradiation, and the ratios $^{37}Ar/^{39}Ar$ and $^{38}Ar/^{39}Ar$ can be related to Ca/K- and Cl/K-ratios, which yields a good proxy to characterize the gas released in each heating step. Mixtures of muscovite (Ca-free) with Ca-rich mica (margarite) or Ca-poor paragonite typically yields different Ca/K ratio in each analysed step, allowing characterization of the gas released in each step, from which an age for each phase may be determined.

In the **second chapter**, the effect of mineral disequilibria is investigated, using a metapelite from northern the Central Alps. In this sample, there was evidence of growth of K-feldspar, and three different generations of biotite and zoned muscovite (phengite-richer in the core). The aim was to identify the mineral reaction responsible for this (uncommon) K-feldspar growth and the metamorphic conditions of that reaction. If this growth proceeded below the closure temperature of Ar in muscovite or biotite, the Ar-dating of different mica generations would possibly date this process and test for the effect of this disequilibrium reaction on the isotopic reservoir. The detailed petrography and a tightly constrained PT-history are essential to understand such a disequilibrium process.

Paper three is a direct application of the approach outlined above to samples from the northern Central Alps. The PT-conditions (and the PT-path followed) were determined as precisely as possible for well equilibrated metasediment derived from Mesozoic calc-schists and pelites. This part of the Central Alps was selected principally because it has been repeatedly investigated by structural geologists (e.g. Milnes, 1974; Maxelon & Mancktelow, 2005), petrologists (e.g. Frey & Ferreiro Mählmann, 1999), and geochronologists (e.g. Hunziker *et al.*, 1992; Steck & Hunziker, 1994). The latter notably include Jäger, Hunziker and collaborators, who proposed closure-temperatures for K-Ar and Rb-Sr in micas (Armstrong *et al.*, 1966; Purdy & Jäger, 1976) and proposed 38 Ma as the age of Alpine metamorphism in the Central Alps (Hunziker, 1969; Jäger, 1973). Their studies have influenced a generation of geologists, in the Alps and elsewhere, even if some of the results are controversial, e.g. on the closure temperature of Ar in micas (Hammerschmidt & Frank, 1991; Villa & Puxeddu, 1994) and the ages of 22-27 Ma for Alpine monazite (Köppel & Grünenfelder, 1975). The discrepancies and possible significance of these results are reviewed, and an attempt is made to link them to our new ages and the tightly constrained thermobarometry. In a companion study (Janots *et al.*, in preparation), the appearance of Alpine monazite and allanite documented in the northern Central Alps permitted to date these minerals and to link them with PT-conditions established in both studies. These results yield PTt-data, which upon comparison with the present Ar-data and with existing fission track ages on zircon and apatite permit a new assessment of *THE* question: What are we dating with ^{39}Ar-^{40}Ar on micas? Is it possible to distinguish (re)crystallization ages from cooling ages and geologically uninterpretable Ar-isotopic ratios, *i.e.* meaningless ages?

1.4) Published material

1.4.1) Publication

Emilie Janots, Martin Engi, Alfons Berger, Julien Allaz and Oliver Schwarz (accepted in Journal of Metamorphic Geology): *Metamorphic sequence of REE-minerals in pelitic rocks of the Central Alps: Implications on allanite – monazite – xenotime phase relations*.

All three chapters of this thesis are prepared for publication (to be submitted soon).

1.4.2) Talk & Poster

04.2007 Julien Allaz, Martin Engi, Alfons Berger and Igor M. Villa, *Understanding Tertiary metamorphic ages in the northern Central Alps*, **European Geosciences Union, Vienna (Austria)**, Talk.

02.2007 (*) Julien Allaz, Martin Engi, Alfons Berger and Igor M. Villa, *Evolution du métamorphisme Tertiaire dans le Nord des Alpes Centrales*, **Journée de Géologie des Alpes, University of Lausanne (Switzerland)**, Talk.

09.2006 Julien Allaz, Martin Engi, Alfons Berger and Igor M. Villa, *Combining multi-equilibrium thermobarometry and Ar-Ar ages for micas: Results from the northern Lepontine Alps*, **Swiss Geoscience Meeting, Berne (Switzerland)**, Poster.

12.2006 (*) Julien Allaz, Martin Engi, Alfons Berger and Igor M. Villa, *Combining multi-equilibrium thermobarometry and Ar-Ar ages for micas: Results from the northern Lepontine Alps*, Forum Mineralogikum, Bern, Talk.

04.2006 Julien Allaz, Martin Engi, Alfons Berger and Igor M. Villa, *Dating metamorphic processes: combining phase equilibria and multichronometer geochronology*, **European Geosciences Union, Vienna (Austria)**, Talk.

01.2006 (*) Julien Allaz, Martin Engi, Alfons Berger and Igor M. Villa, *Argon dating of micas in Mesozoic metasediments of North Central Alps: crystallization or cooling age*, **Forum Mineralogicum, Bern**, Talk.

11.2004 Julien Allaz, Martin Engi, Alfons Berger and Igor M. Villa, *Age constraints on metamorphism in the Bündnerschiefer of the North Pennine Alps: approach and first results*, **Swiss Geoscience Meeting, Lausanne** (Switzerland), Poster.

(*) No abstract available (internal talk or invited speaker).

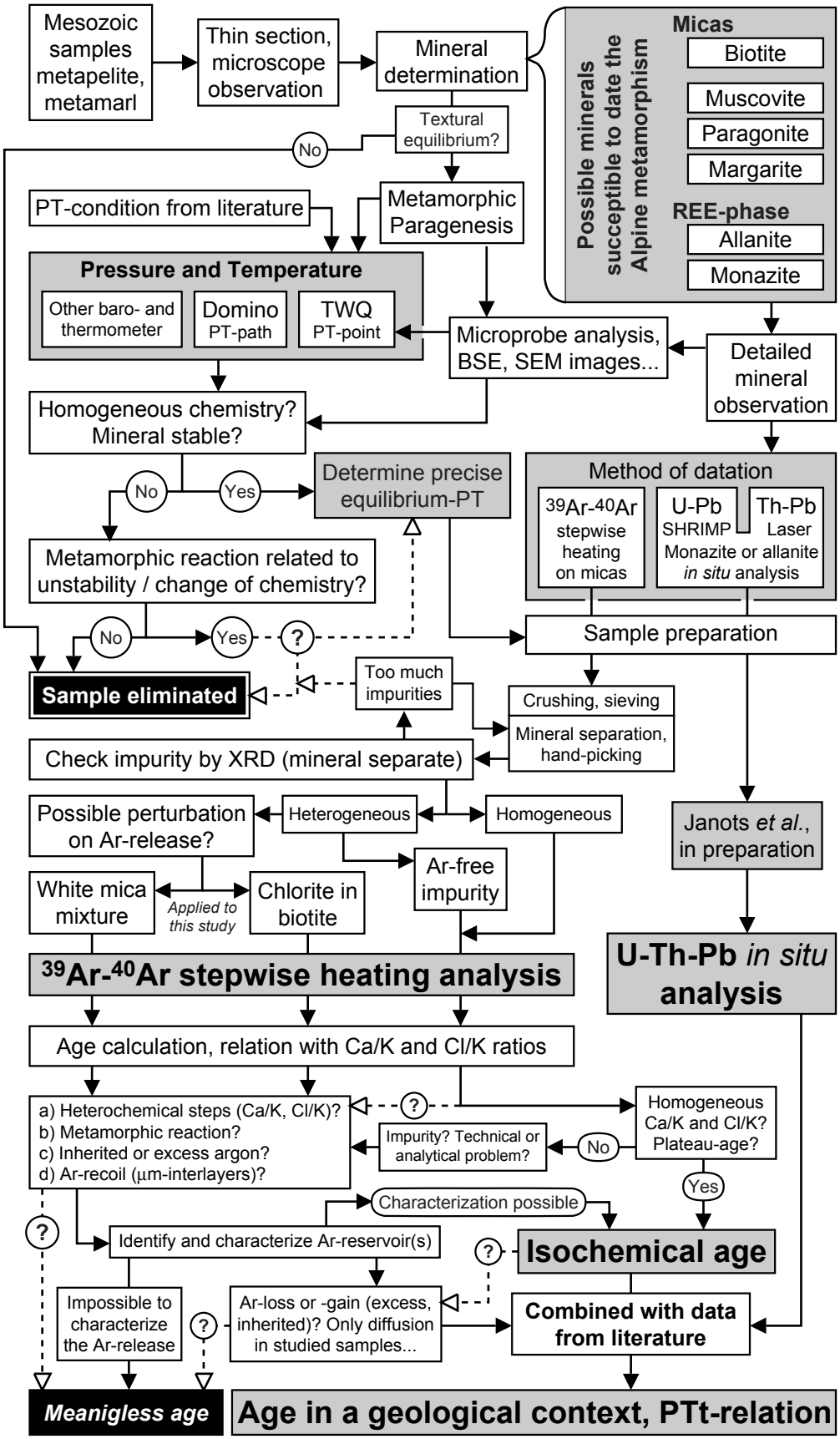

Fig. 1.1: Methods of this study.

2) Diffusion, retrograde reactions, and ^{39}Ar-^{40}Ar ages in homogeneous and heterogeneous micas from the Lepontine Alps

Val Piora from Schenadüi.

J. Allaz, M. Engi, A. Berger & I.M. Villa

2.1) Abstract

Well-equilibrated samples of monometamorphic metasediments from the Lepontine Alps (Switzerland) were studied to obtain precise PT-conditions of mineral equilibration and ^{39}Ar-^{40}Ar ages of micas. Effects of metamorphic reactions occurring during decompression were explored to understand their influence on the ages. Metapelites and metamarls record 500-600 °C, 6-9 kbar. They commonly contain two white mica populations, muscovite with paragonite or margarite. X-ray diffractometry shows that the majority of the separates prepared for Ar-Ar stepwise heating analysis are monomineralic. Accordingly, in these samples $^{37}Ar/^{39}Ar$ and $^{38}Ar/^{39}Ar$ (i.e. Ca/K and Cl/K) ratios are constant, and so are ages. In those samples containing two white mica populations, Ca/K and Cl/K ratios are variable, as they reflect the non-simultaneous degassing of the two heterochemical Ar-reservoirs. These ratios are used to identify each Ar reservoir and to unravel its age.

Muscovite-paragonite separates from Lucomagno (560-580 °C, 7-9 kbar) yield "plateau" ages around 16.5 Ma, with Ca/K ratios in the range expected for muscovite and paragonite. In contrast, step ages are variable for paragonite separates of two samples of Val Piora (560-580 °C, 8-9 kbar) and correlate with the Ca/K ratio. The age extrapolated to the measured Ca/K ratio of paragonite is some 2 Ma younger than muscovite (15-13 Ma versus 17-15). This is interpreted to be due to plagioclase growth during decompression, which involved reequilibration and partial breakdown of paragonite, which in turn led to partial or total resetting of the Ar clock in paragonite. This effect is more pronounced yet at higher grade (Pizzo Molare: 580 °C, 8-9 kbar), where paragonite is 3.5 Ma younger. In a chlorite-margarite-biotite-calcschist equilibrated near 540 °C and 6.5 kbar, biotite and muscovite both yield ages around 18 Ma. All other biotite separates analysed, which were from higher-grade rocks, yield ages younger than muscovite: from 0.5-1.0 Ma (Val Piora and S Lucomagno) to circa 2 Ma (Pizzo Molare). Minor chloritization of biotite on the retrograde path is evident in all studied sample and is apparently a more decisive parameter than temperature in the resetting of the Ar clock; so is the formation of plagioclase from paragonite decomposition. This study thus demonstrates that good constraints on the PT-evolution of samples to be dated are necessary, but not sufficient, to yield geologically meaningful metamorphic ages.

Keywords

^{39}Ar-^{40}Ar dating; equilibrium; metamorphic reactions; muscovite; paragonite; margarite; Central Alps; metapelite.

2.2) Introduction

A classical Barrovian metamorphism resulting from the collision of European and African plates characterizes the Central Alps of Switzerland and its northern area. From North to South, this metamorphism regularly increases from non- and anchi-metamorphism fields in the Jura and the Prealps mountain ranges up to the greenschist-amphibolite facies in the Central Alps. This evolution is well described since a long time (e.g. Frey, 1969; Trommsdorff, 1980; Todd & Engi, 1997; Frey & Ferreiro Mählmann, 1999). Also named the Lepontine Alps (Wenk, 1956; Wenk, 1970), this region is essentially composed of ante-Triassic gneisses (basement) covered by Mesozoic metasediments. Jäger *et al.* (1967) originally proposed the concept of closure temperature, and later its empirical estimation for K-Ar dating of micas, notably 300°C for biotite and 350°C for muscovite (Purdy & Jäger, 1976).

These values are no longer used by any paper of the last 20 years. Because modifying just one of these values entails the collapse of the whole edifice based on them (see the detailed discussion in Villa, 1998b), we decided to re-examine the mica ^{39}Ar-^{40}Ar ages in samples with a very well-constrained petrological characterization. In particular, we strove to consider two classes of problems, which were not known forty-one years ago, namely inheritance and retrogression. To avoid chemical and isotopic inheritance problems from older metamorphic cycles, we sampled only metasediments derived from Mesozoic protoliths. Care was taken to study exclusively texturally and chemically well-equilibrated samples and to ensure the pressure and temperature (PT) conditions of equilibrium are tightly constrained. According to the observed mineral assemblage, chemistry and texture, we identify the possible mineral reactions occurring near the thermal peak and during the retrograde path. This is of major importance for micas we aim to date, as retrograde mineral reaction may induce isotopic resetting (e.g. Chopin & Maluski, 1980; Wijbrans & McDougall, 1986; Villa, 1998b; Di Vincenzo *et al.*, 2004; Villa, 2004; Gouzu *et al.*, 2006; Glodny *et al.*, 2008a; Glodny *et al.*, 2008b). The use of phase diagrams (or pseudo-sections) depicting the evolution of assemblages and the changes in composition of the minerals involved is necessary to ascertain for the state of equilibrium of a specific mineral assemblage. Such diagram also helps to identify the phase possibly involved in retrogression and susceptible to have chemically re-equilibrated (e.g. chloritization, mineral resorption, late blast growth).

We explore the influence of composition, grain size, temperature and mineral reaction on the Ar-Ar ages of micas. The interpretation of Ar-Ar ages for mixtures (muscovite-paragonite and muscovite-margarite) is also investigated and is facilitated by a conspicuous characterization of each mineral separate analysed. Although the K-contents of paragonite (sodic white-mica) and margarite (calcic brittle mica) are low, we test whether it is possible to get meaningful ages for these micas as well. The detailed examination of these Ar-Ar ages in regards of petrography and tightly constrained PT-results appears as a necessary step previous to the geological interpretation. We aim to determine the effect of some specific net-transfer and exchange reactions on micas Ar-ages. These reactions occur along decompression or retrograde PT-path and are believed to play an important role on the Ar-retention properties of studied micas.

2.3) Geological setting

The area of interest is situated in the northern part of the Central Alps (Switzerland). This part of the alpine orogeny results from a collisional stage, during which the combined effects of extension, back-thrusting and rapid erosion lead to rapid exhumation (Schmid *et al.*, 1996; Pfiffner *et al.*, 2000). This frontal part of the Lepontine studied is delimited in the North by polymetamorphic gneiss units of the Aar massif and the Gotthard crystalline nappe, in the South by Pennine basement nappes (Fig. 2.1a; Berger *et al.*, 2005). Samples were collected in three areas from

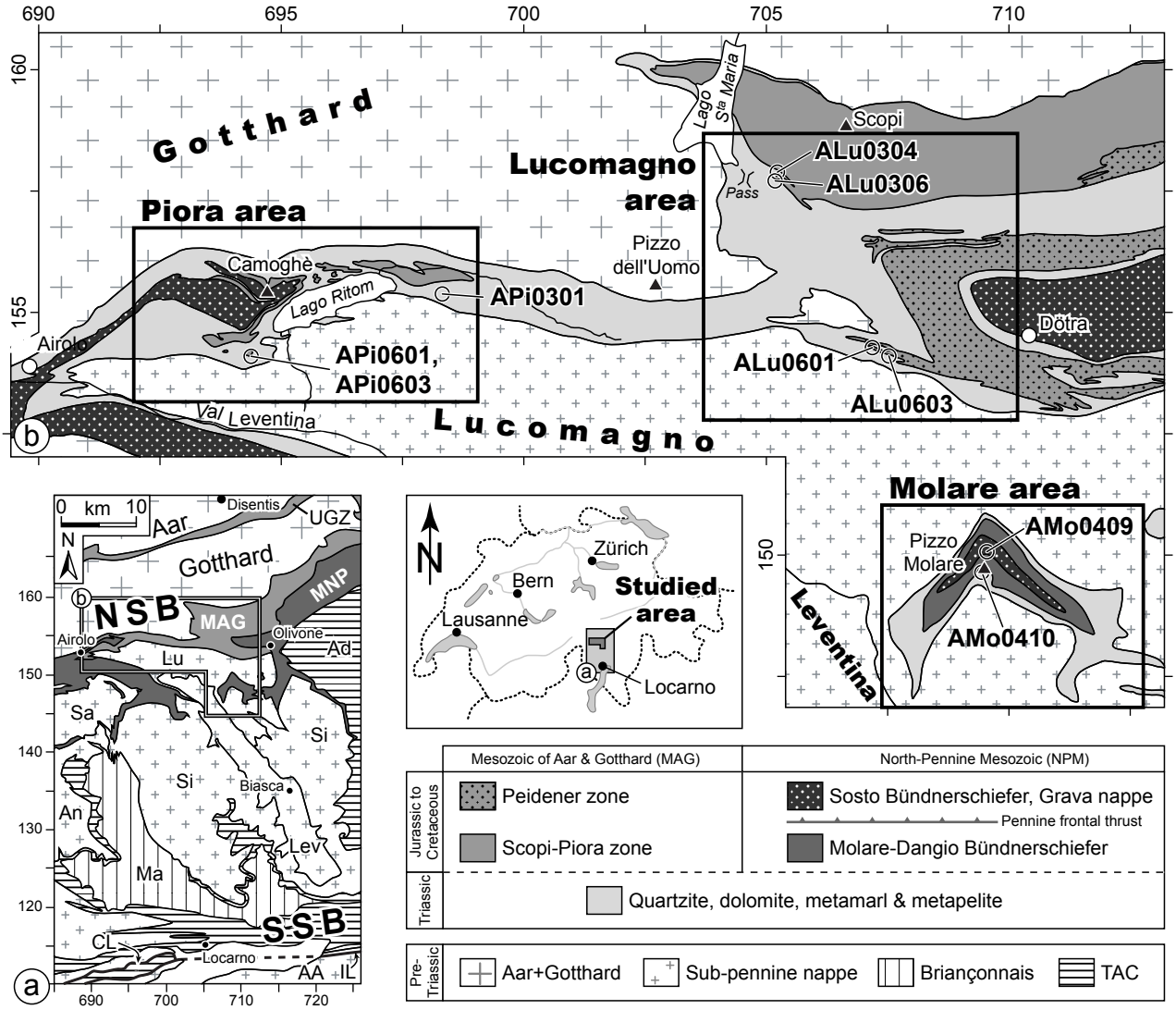

Fig. 2.1: (a) Geological overview of the Central Alps according to Spicher (1972) and Berger *et al.* (2005). In the North are the Aar and Gotthard massifs separated by mesozoic sediments from the Urseren-Garvera Zone (UGZ). Lying on the southern part of this massif is the Northern Steep Belt (NSB) composed of Mesozoic metasediments from Aar and Gotthard (MAG) and from the northern Pennine (NPM). This is our area of interest. NSB is in opposition to the Southern Steep Belt (SSB) situated at the southern limit of the Lepontine Dome. The major Insubric (IL) and Canavese Lines (CL) mark this limit separating European and Briançonnais from Austroalpine nappes (AA). Ad: Adula; An: Antigorio, Bo: Bosco-serie, Le: Lebendun, Lev: Leventina; Lu: Lucomagno, Ma: Maggia; Sa: Sambuco; Si: Simano. **(b)** Geological map of the studied area adapted from Probst (1980), delimited by the Aar and Gotthard massifs to the north and by the European and Briançonnais basement nappes to the south (Lucomagno-Leventina and Sambuco). Open circles stand for sample position. Numbers correspond to Swiss topographic coordinates in kilometre.

metasediments of Mesozoic protoliths: Val Piora, Lucomagno and Pizzo Molare (Fig. 2.1b). Two main tectonic units are distinguished in this area: the Mesozoic of Aar and Gotthard (MAG) and the Northern Pennine Mesozoic (NPM; Probst, 1980). MAG is related to the Aar-Gotthard crystalline massive history remaining at relatively shallow depth during the alpine orogeny. In Lucomagno-Molare area, MAG is subdivided in the Scopi-Piora and Peidener zones, while NPM is subdivided in two units, the Molare-Dangio and Sosto Bündnerschiefer. This later two are separated by a major thrust called the “Frontal Pennine thrust” (e.g. Milnes, 1976; Kamber, 1993), and corresponds notably to the “Grava-Lugnezer-Sosto thrust” (Probst, 1980). Eastwards in Val Piora, this thrust separates the Scopi-Piora Bündnerschiefer from the Sosto schiefer (Probst, 1980).

Both MAG and NPM units are typically composed of a complete series from Triassic up to late Cretaceous, but this order is disjointed, especially in soft metasediments, with common internal repetitions, owning to the strong Alpine folding, shearing and thrusting. Sedimentation started in the lower Triassic with quartzite and dolomite deposits. The Upper Triassic (Quartenschiefer) involves marly to pelitic rocks, on which Jurassic to Cretaceous Bündnerschiefer were deposited (Nabholz, 1945; Nabholz, 1948; Frey, 1969; Hansen, 1972; Bolli *et al.*, 1980; Probst, 1980; Leu, 1986). These are highly variable sediments, comprising mixture of siliciclastic and carbonate members. Bündnerschiefer are generally rich in organic material, which evolved to graphite in the area studied due to the increase in metamorphic grade (Beyssac *et al.*, 2002; Petrova *et al.*, 2002). NPM is richer in calcareous and poorer in carbonaceous material than MAG, in which carbonaceous garnet-schists and impure quartzite are typical. The samples selected for this study in the Lucomagno Pass and Val Santa Maria areas all originate from MAG (Chadwick, 1968; Probst, 1980; Fig. 2.1b). In the Val Piora region, both MAG and NPM appear, but all samples discussed in this paper belong to MAG, with reference to the maps of Krige (1918) and Probst (1980). Finally, samples taken in the Molare area are exclusively from the NPM (Thakur, 1976; Probst, 1980).

The areas sampled are situated in the northern Lepontine metamorphic dome, which is delimited by the Northern and Southern Steep Belts (NSB, SSB; Fig. 2.1a; Milnes, 1974; Maxelon & Mancktelow, 2005). The Gotthard nappe mostly reached but greenschist facies in Alpine times, while MAG and MNP from Piora, Lucomagno and Molare are both in lower amphibolite facies. A rapid increase of the thermal climax of this metamorphism is revealed between Vals-Vrin and Campo Blenio, from 400-450 to 525°C (Wiederkehr *et al.*, submitted). The mineral assemblages in metasediments display this progressive series of transitions clearly and have been widely described in the literature (see review by Frey & Ferreiro Mählmann, 1999). Chloritoid is exclusively found in the northernmost samples or as a relic in porphyroblasts (Niggli, 1970). Staurolite grew at the expense of chloritoid and chlorite, and kyanite appears in Al-rich pelites. Epidote, margarite and paragonite reacted to form prograde plagioclase (Frey & Niggli, 1972; Frey & Orville, 1974; Frey *et al.*, 1982; Bucher-Nurminen *et al.*, 1983; Frank, 1983; Livi *et al.*, 2002). Previous thermobarometric study found PT-conditions around 5.5-6 kbar and 550-600 °C (Todd & Engi, 1997). During Tertiary convergence, the Peidener zone, the Sosto Bündnerschiefer and probably a few Triassic layers were subducted and attained blueschist facies conditions, as attested by relics of carpholite in quartz and calcite veins (Bousquet *et al.*, 2002; Wiederkehr *et al.*, submitted). In the MAG and associated Aar-Gotthard crystalline, as also in the Molare-Dangio Bündnerschiefer, there is no such evidence and these units are thought to have remained at relatively shallow depths (M. Wiederkehr, pers. comm.).

In each of the three elected areas, a range of suitable metasediments was sampled, essentially in the Quartenschiefer unit and in pelitic to marly members of the Bündnerschiefer unit. These samples are advantageous for the purpose of this study for several reasons: firstly, the prograde mineral evolution of metapelite and metamarl at the entry of amphibolite facies crosses several net-transfer reactions and many of them involve devolatilization, which allows for pervasive equilibration and precise thermobarometry. Secondly, large amounts of mica are produced in rocks of such Al-rich bulk composition, making sample preparation for ^{39}Ar-^{40}Ar dating easier. Thirdly, the inheritance of a pre-Alpine component in the mica samples is minimal, as their sedimentary protoliths were post-Variscan. We are thus sure to date thoroughly recrystallized samples that exclusively reflect Alpine metamorphism.

2.4) Sample description

Two to three texturally well-equilibrated samples from four areas were retained for the present study (Fig. 2.1b). From lowest grade to highest grade: Lucomagno Pass (ALu0304, ALu0306), SE Lucomagno (ALu0601, ALu0603),

Val Piora (APi0301, APi0601, APi0603) and Pizzo Molare (AMo0409, AMo0410).

2.4.1) Lucomagno Pass

ALu0306 is a typical metamarl from the Quartenschiefer, while ALu0304 is a Ca-rich metapelite collected in the neighbourhood of ALu0306 at the base of the Scopi Bündnerschiefer (Fig. 2.1b). Both mark the transition from greenschist to amphibolite-epidote facies. Fine flakes of margarite occur in both samples, forming thin layers alternating with quartz. ALu0306 is rich in carbonate (ankerite), contains light green to colourless chlorite, brownish-green biotite and clinozoisite, all aligned in the foliation. ALu0304 is more siliciclastic and contains muscovite, brown biotite, large idioblastic garnet, and rare clinozoisite. This sample is distinctly poorer in carbonate, which are exclusively found as inclusions in garnet. The very first plagioclase appears in these lithologies, either forming small, sparse grains in the matrix (ALu0304) or millimetre-sized neoblasts (ALu0306). Late and local chloritization of biotite is obvious in ALu0304, but chlorite is in textural equilibrium in ALu0306.

2.4.2) SE Lucomagno and Val Piora

The schists from SE Lucomagno stem from the base of Scopi Bündnerschiefer (ALu0601, –03), whereas those from Val Piora are graphite-free Quartenschiefer (APi0301, APi0601, –03; Fig. 2.1b). All samples from both areas are nearby staurolite and kyanite isograds (Niggli & Niggli, 1965). Bulk rock compositions are similar (apart from the carbon contents) and typically rich in Al, but poor in Ca. Quartz and micas are usually the dominant phases. Muscovite typically coexists with paragonite and, due to the variable Na and K contents of the bulk rocks (Appendix 2.1), the modal proportion of the two white micas is highly variable from pure muscovite (ALu0601) to paragonite-rich assemblage (APi0601), and with subequal proportions in ALu0603, APi0301 and APi0603 (Fig. 2.2a). Chlorite is only stable in APi0601 (Mg-richer metapelite), where it forms micrometer-sized interlayers with paragonite and is included in biotite (Fig. 2.2c). Biotite is largely present in APi0601 and –03 and forms large flakes along the schistosity coexisting with oblique books. In samples from SE Lucomagno, biotite is scarce and grows as isolated flakes in the matrix or more currently as small flakes around garnet. This last feature is sign of minor garnet resorption (ALu0601, –03, Fig. 2.2b). Large millimetre- to centimetre-sized garnet is always present together with common sub-idiomorphic and poikiloblastic blast of staurolite and/or kyanite (Fig. 2.2b). Al-rich silicates grow over the schistosity, often along axial plane of late crenulation fold. APi0601, –03 and ALu0601 are distinguishingly richer in kyanite, while ALu0603 and APi0301 are richer in staurolite with or without kyanite. Ovoid blasts of plagioclase are elongated in the schistosity (Fig. 2.2c) and include all matrix minerals, notably biotite, white micas, quartz and epidote. A co-genetic growth of kyanite and plagioclase is deduced from their intimate association. Chloritoid is exclusively included in garnet from staurolite-rich metapelite (ALu0601, –03 and APi0301). Clinozoisite with an allanitic core (REE-epidote) is well preserved as inclusion in garnet or plagioclase and often absent or resorbed in the matrix.

2.4.3) Pizzo Molare

Samples from this area are Al-poor to –rich metapelite from the Quartenschiefer. Both metapelites are composed of white mica, biotite, garnet, plagioclase and kyanite (AMo0410) or staurolite (AMo0409, –10). Garnet-rich layer

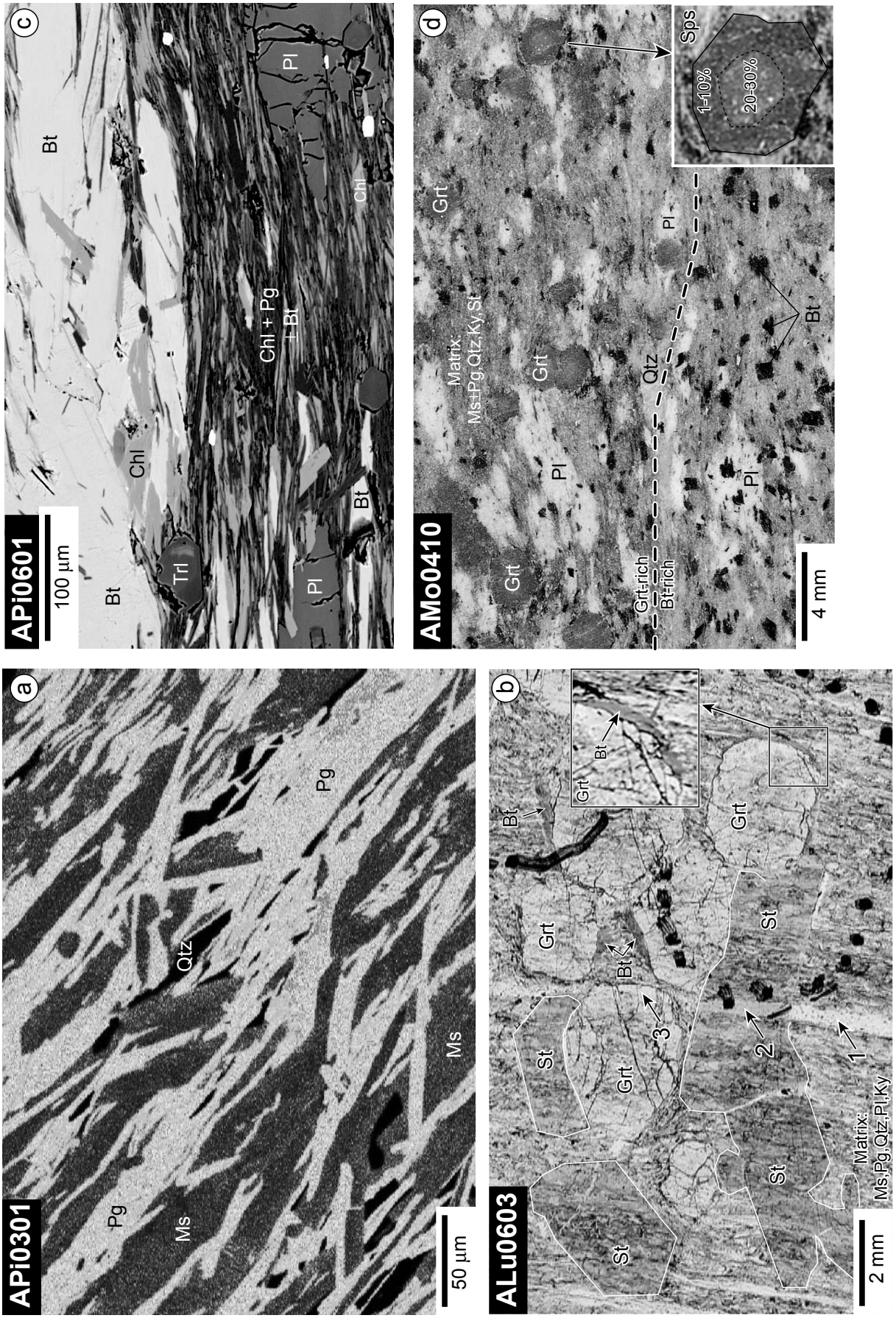
a
APi0301
Pg
Ms
Qtz
Pg
Ms
50 µm
b
ALu0603
Bt
Grt
Bt
Grt
Bt
Grt
St
St
Grt
3
2
1
St
St
Matrix:
Ms,Pg,Qtz,Pl,Ky
2 mm
c
APi0601
100 µm
Bt
Bt
Chl
Trl
Chl + Pg
±Bt
Pl
Pl
Bt
Chl
d
AMo0410
Grt
Matrix:
Ms±Pg,Qtz,Ky,St
Grt
Pl
Grt-rich
Bt-rich
Qtz
Pl
Pl
Bt
4 mm
Sps
1-10%
20-30%

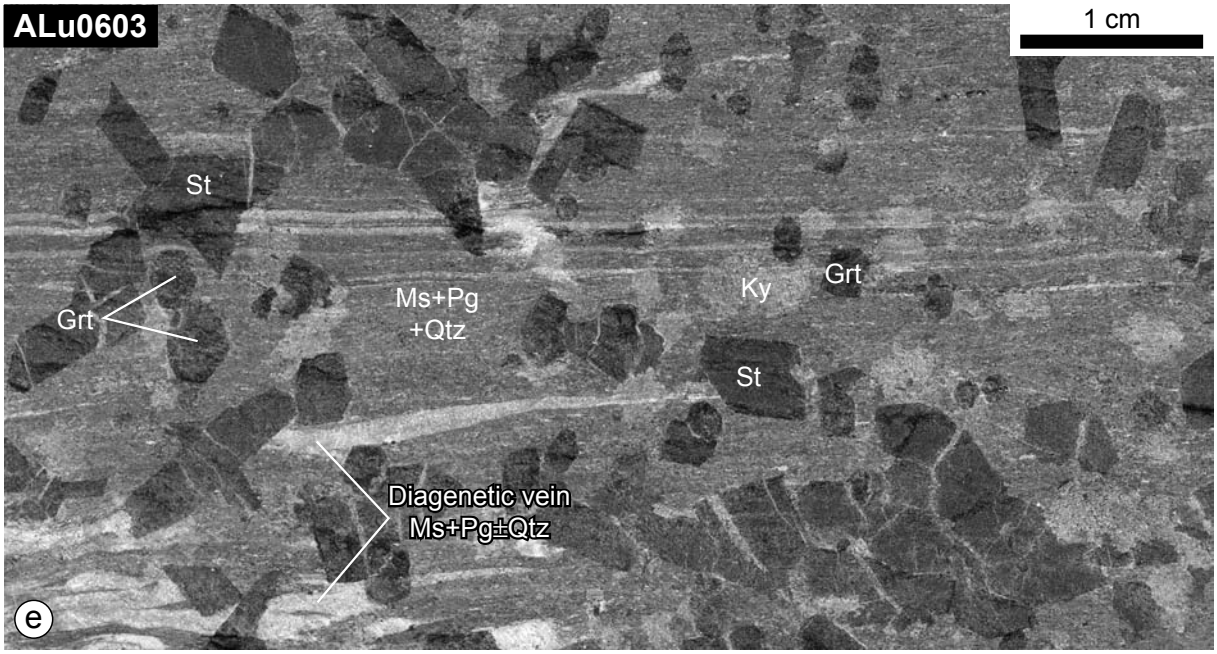

Fig. 2.2: (a) Na element map in the matrix of metapelite APi0301 (WDS mode, 15 kV, 20 nA, beam 2µm, pixel 0.5 µm, dwell-time 50 ms). Such an association of paragonite and muscovite is a typical feature of Al-rich pelite studied here. **(b)** Microphotography of graphite-bearing metapelite ALu0603 showing porphyroblast of garnet and staurolite overgrowing the schistosity. Staurolite is highlighted with a white rim. The graphite-free vein crossing in the middle of the microphotography (arrow 1) is essentially made of white micas and pre-dates porphyroblast growth, as shown by the graphite-free zone in the large staurolite crystal (arrow 2). This effect is similarly observed in garnet (arrow 3). Garnet is slightly resorbed and locally replaced by thin biotite rims, as shown in the inset. Mineral abbreviation according to Kretz (1983). **(c)** Fine association of paragonite and chlorite in the matrix of APi0601 (BSE image). The neoformed plagioclase stems from partial consumption of paragonite. Traces of micrometer-sized muscovite and seldom-larger flakes are also found in the matrix, but are not visible in this image. **(d)** Microphotography of a polished section of sample AMo0410. This Mn- and Al-rich metapelite is made of Grt-rich and Bt-rich layers. This effect is attributed to variation in MnO content of the whole rock, from 6% in Grt-rich layer, falling to <1% in Grt-poor layer. Core of garnet are thus rich in spessartine and are lighter in color, as shown in the inset. **(e)** Polished rock plate in ALu0603 showing the repartition of garnet-staurolite zone and Ky-richer area. Notice also the presence of numerous diagenetic veins overgrown by all porphyroblast. The greyish color of matrix minerals stems from the presence

alternates with biotite-rich layer in AMo0410 (Fig. 2.2d), essentially due to respective richness or poorness of MnO and CaO (from circa 3% each down to < 1% MnO and circa 2% CaO). More interesting in AMo0410 is the occurrence of some scarce paragonite, in apparent textural equilibrium with muscovite and plagioclase. Further south at higher T, paragonite is totally absent from any metapelite assemblage and only muscovite remains stable. Notice that margarite is found in garnet core, suggesting a former coexistence of the three white micas along the prograde path, as it is observed in samples from UGZ (Fig. 2.1a; Frey, 1969; Livi *et al.*, 1997; Livi *et al.*, 2008).

2.4.4) Summary of mineral evolution

This suite of Al-rich to –poor metapelites presents a regular increase of the alpine metamorphism, characterized by the successive disappearance of chloritoid, chlorite, margarite and paragonite in profit of new porphyroblast such as plagioclase, kyanite and staurolite. Chlorite is stable in a few assemblages (ALu0306, APi0601), but is rapidly consumed to form biotite, staurolite and garnet. Notice that it is also found as a retrogression product of biotite. Association of muscovite, paragonite and margarite is restricted to lower grade zone (e.g. UGZ; Fig. 2.1a; Frey, 1969; Livi *et al.*, 1997; Livi *et al.*, 2008). In UGZ, white micas are intimately intergrowth at sub-micrometer scale and evolve to discrete grains (Livi *et al.*, 2008). This is for instance the case in the northern part of the studied

area, where either margarite or paragonite is found in equilibrium with muscovite and the very first plagioclase in Al-rich metapelite. At higher grade, calcic and sodic white micas rapidly disappear around Lucomagno and Val Piora areas (margarite) or southwards of Pizzo Molare (paragonite). Kyanite growth is apparently related to these disappearances. Biotite stability is sometimes strongly affected by the formation of staurolite. In addition and in quite all samples, late retrogression effect induces a local chloritization of some rare biotite in all studied samples. In some case, biotite is quite absent from the assemblage (APi0301, ALu0601, –03). Finally, clinozoisite and allanite are also destabilized in profit of plagioclase, Al-rich silicates and REE-phosphate (Janots *et al.*, in press).

2.5) Analytical methods

2.5.1) Bulk rock and mineral analysis

Bulk rock compositions were obtained by XRF on melted rock powder at the Institut für Geologie, Univeristät Freiburg. Mineral analyses were obtained using either the CAMECA SX-50 or the JEOL-8200 microprobe of the Institut für Geologie, Univeristät Bern (EMP). Results of both instruments overlap within error. In both cases, analytical conditions were 15 kV and 20 nA with a minimum beam size for garnet, staurolite and ilmenite. To minimise volatilization of alkalis, plagioclase and micas were analysed using a defocused beam (5 to 10 µm). Representative average analyses for white micas, biotite, chlorite, staurolite, chloritoid, garnet, plagioclase and clinozoisite are available in Appendix 2.1. A minimum of at least 3 to 5 analyses is performed on each grain to ensure homogeneity. More care is taken for micas we aim to date, with usually more than 20 analyses each mica in one single thin section. Analytical cross-sections are completed in zoned mineral, plagioclase and garnet.

2.5.2) Thermobarometry

Mineral analyses were used for thermobarometry using TWQ (Berman, 1991). The thermodynamic database "JUN92.dat" (Berman, 1988; Berman, 1991) was augmented by the staurolite model defined by Nagel *et al.* (2002a). Phase equilibria were calculated in system SiO_2-Al_2O_3-TiO_2-FeO-MgO-CaO-Na_2O-K_2O-H_2O (TiCNKFMASH). Fe_2O_3 was ignored in TWQ for the following reasons. (1) No Fe^{3+} mineral is stable in any assemblage, except for epidote-clinozoisite; (2) Charge balance calculated for garnet and biotite indicates only a few percent of Fe_{total} is Fe^{3+}, which would change pressure and temperature (PT) estimates by no more than 0.1 kbar and 10°C; (3) graphite is present in the Lucomagno samples, implying a low oxygen fugacity. Mn was not considered in the system, as the only Mn-bearing phase defined in the database used is garnet.

For use in thermobarometry, coexisting minerals were analysed in millimetre-sized domains, often around a garnet porphyroblast. This minimizes apparent disequilibrium effects related to local variations in bulk composition. Care has been taken to characterize and understand mineral zonation; samples in which disequilibrium became evident (e.g. disequilibrium texture, abnormal mineral assemblage compared to estimated metamorphic condition, strong garnet resorption, chloritization of biotite, or late Fe-Mg reequilibration) were not included in this study.

To display stable phase assemblages in pressure (P) - temperature (T) - fluid composition diagrams (sometimes referred to as "pseudo-sections"), we used THERIAK-DOMINO (de Capitani & Brown, 1987; de Capitani, 1994). Compare to TWQ, Mn is added to the chemical system. Iron is input as total FeO and the QFM

buffer was imposed to control Fe_2O_3 contents. References to solid-solution models and thermodynamic data used by TWQ or THERIAK-DOMINO are given in Table 2.1. Databases used are both based on similar thermodynamic data (Berman, 1988) and are thus comparable. Nevertheless, THERIAK-DOMINO is more up-to-date, with notably new models for white micas (Keller *et al.*, 2005), biotite and chlorite (Hunziker, 2003).

Table 2.1: List of different solid-solution models used in the two similar thermodynamic databases considered here, TWQ and THERIAK-DOMINO. in TWQ, margarite activity is calculated either with a ideal model (activity = xCa) or with the model from Worley & Powell (1998): $a(Mrg) = 0.25*xCa*(1+xCa)^2$ and xCa = Ca/(Ca+Na+K).

Based on…	Berman (1988, 1991)	
Mineral	**TWQ**	**DOMINO**
Garnet	Alm-Prp-Grs, Berman (1990) Berman & Koziol (1991)	Alm-Prp-Grs-Sps de Capitani, pers.comm.
Biotite	McMullin et al. (1991)	Hunziker (2003)
White micas	Chatterjee and Froese (1975)	Keller (2005)
Chlorite	-	Hunziker (2003)
Plagioclase	Fuhrman and Lindsley (1988)	
Staurolite	Nagel et al. (2002a)	
Chloritoid	-	Vidal et al. (1999)
Margarite	Ideal (Ca-Na-K) or activity model from Worley & Powell (1998)	Pure phase
Ilmenite	Ideal (Fe-Mg-Mn)	Ideal (Fe-Mg)
H_2O-CO_2	Haar et al. (1984); Mäder and Berman (1991) Kerrick and Jacobs (1981)	

2.5.3) Mineral separation and XRD

In a majority of samples used for ^{39}Ar-^{40}Ar dating, two different grain sizes have been separated. Fraction size is selected according to the average grain size observed in thin section: a fine fraction 50-150 µm (abrogated Ms100 or Bt100) and a coarser one at 150-250 µm (Ms200 or Bt200). It is difficult to deal with a fraction larger than 250 µm due to the pronounced presence of impurities especially in biotite separates or due to the thinness of muscovite-paragonite interlayer. A vibrating table was used to enrich micas, and a Frantz™ magnetic separator to separate biotite from white micas. Using a small grain-size fraction allows a more efficient separation of paragonite from muscovite or of biotite with chlorite interlayer from one without. After sieving, mechanical and magnetic separation, mineral separates are cleaned a few minutes in ultrasonic bath with deionised water and then with acetone. A prolonged ultrasonic bath (15-30 minutes) disaggregated mica sheets and impurities glued on or within them (quartz, chlorite, graphite). In such case, a second sieving is necessary to withdraw smaller flakes. Final handpicking under a binocular microscope ensures better purity, which visually (i.e. with a resolution of 20 µm) appeared as high as 99% in all except one sample. In ALu0306, margarite and muscovite are difficult to separate from quartz and chlorite, even after multiple attempts by gravimetric and magnetic techniques. Biotites from some samples were not prepared for ^{39}Ar-^{40}Ar dating, as this mineral is extremely rare and a good separation was not successful, due to a large amount of impurities, notably chlorite and ilmenite (APi0301, ALu0601, –03). The presence of graphite is a serious problem. Analyses of low-grade graphite-rich rocks from the Apennines (Villa, unpublished data, 1990) had shown that hydrocarbon interference, especially on mass 36, can predominate over Ar from the sample, making corrections the largest source of uncertainty and probably causing incorrect age estimates based on the constancy of the ratio of masses 41 and 36. Therefore it was deemed desirable to remove graphite from our minerals. Oxidation with H_2O_2, while in principle a viable option, is potentially dangerous, as excessively strong oxidants can damage the biotite structure, discolouring grains and extracting cations (Villa, unpublished data, 1990). Therefore, it was decided to concentrate the separation efforts on graphite-poor rocks and push handpicking to new lengths, until no graphite was visible under the binocular microscope.

Separates purity is checked by XRD on a Panalytical X'Pert-Pro X-ray diffractometer at the Institut für Geologie, Univeristät Bern. This instrument is equipped with a Cu-anode tube ($K_{\alpha 1}$, λ = 1.5406 Å) set to operate at 40 kV and 40 mA and cover a 2θ range from 4° to 40°. To enhance [00l] reflections, mica separates

were sedimented with acetone on a glass slide. The intensity-ratios of muscovite and paragonite [006] peaks can be used to semi-quantify paragonite-muscovite mixtures (%Ms = $I_{Ms}/I_{Ms}+I_{Pg}$; Frey, 1977). When large amounts of paragonite and quartz, but only traces of muscovite are present, the [006] peak ratio cannot be used, due to strong peak interference with quartz [101]. Instead, a qualitative intensity-ratio between muscovite and paragonite [004] peaks is given. In studied margarite-bearing sample, peak ratio cannot be accurately calculated due to weak muscovite peaks and the pronounced presence of quartz. Regarding biotite separates, a qualitative intensity-ratio between chlorite [004] and biotite [006] peaks characterized the proportion of chlorite in separate ($I_{Chl}/I_{Chl}+I_{Bt}$).

2.5.4) ^{39}Ar-^{40}Ar stepwise heating

Aliquots of 6 to 21 mg were weighted and packed in aluminium foil before irradiation. All samples were irradiated for circa 8 hours at Pavia University (Italy) or McMaster University (Hamilton, Canada) reactors. Fast neutron flux was monitored by use of MMhb standards (523.1±4.6 Ma; Renne *et al.*, 1998) intercalated between analysed samples. Ar-analyses were performed at the Institut für Geologie, Universität Bern, using an all-metal extraction line attached to a double-vacuum resistance oven and a thermocouple on the external part of the crucible (Belluso *et al.*, 2000). After a pre-cleaning stage at 400°C for at least 15', mineral separate is heated by steps of 10 to 100 °C from circa 500 to more than 1400 °C. When samples are analysed successively and when crucible and resistance condition is similar, the intra-sample temperature bias is believed to be better than ±5 °C. This is the case for the four samples ALu0601, –03 and APi0601, –03 analysed successively. The uncertainty on absolute temperatures between different series of analyses is very conservatively estimated as ±30 °C.

Analyses presented here have been obtained during three independent series: (Ar-A) comprised of samples ALu0306 and APi0301; (Ar-B) of AMo0409 and AMo0410; (Ar-C) of ALu0601, –03, APi0601, –03. The Ar extraction and the cleaning system remain identical, only line blank, spectrometer background and data acquisition may modestly change. A first Zr-Ti-V getter immediately cleans the extracted gas. After a minimum of 15' degassing in furnace, the released gas is transferred to a reduced volume equipped with two other getters. Time in getter is here variable from 10 minutes for lasts steps and up to one hour for firsts. Gas is then sent in mass spectrometer and masses 40 to 36 are measured on a MAP-215B rare gas mass spectrometer. Masses 40, 39 and 36, and backgrounds on masses 40.5, 38.5 and 35.5, are measured successively on a Faraday cup equipped with a 10^{11} Ω resistance amplifier. Values are read with a 7 1/2 digits voltmeter (Solatron 7071). In series Ar-B, also masses 38 and 37, and background mass 39.5, were measured on the Faraday cup. In series Ar-A and Ar-C, masses 39 to 36 and background masses 39.5 and 35.5 were measured on a MasCom electron multiplier, which has 19 Cu-Be dynodes at 2.00 kV total potential. In series Ar-A, the electron multiplier was used in analogue mode by connecting the output to a 10^8 Ω resistor. In series Ar-C, the multiplier was used in pulse-counting mode using a NI-DAQ digital acquisition card. The signal was amplified through a pulse preamplifier WMT PAD06 set at 40 ns dead time, identical to electron multiplier. A threshold value of –4.5 mV is selected to reduce most of electronic noise. Values are corrected for dead time according to the following equation (from ThermoLinear GmbH, Bremen, Germany; J. Kramers, pers. comm.): $a = C \cdot e^{C \cdot D}$; $b = C \cdot e^{a \cdot D}$; $X = C \cdot e^{b \cdot D}$, where C is the measured count rate (in counts per second, cps), D the dead time (in seconds) and X is the corrected count rate. This mathematical correction is insignificant up to 10^5 cps (+0.4% correction) and increases dramatically over 10^6 cps (> +4%). The highest ^{39}Ar signals were below $2*10^6$ cps (0.32 pA on the Faraday cup).

When faraday cup and multiplier measurements were acquired simultaneously (Ar-A and Ar-C), the gain factor is calculated for each step on one of the masses measured with both collectors. Normally, we used mass 39 because of its higher signal intensity. The multiplier/faraday gain was constant over the entire series (5.9±0.1 *

10^{18} cps/A for series Ar-C). When both 39 and 36 masses were too low for a reliable gain factor calculation, the fixed average gain was used.

Spectrometer background was determined according to the stable dynamic and static blanks acquired between each analysis. Following background values are obtained on masses 40 to 36, respectively: 1.2, 3.0, 1.6, 1.1 and 1.9 fL (series Ar-A), 9.4, 1.0, 0.4, 0.5 and 1.0 fL (series Ar-B) and 2.6, 18.9, 1.2, 1.8 and 1.3 fL (series Ar-C). The abnormally high background on mass 39 of Ar-C is likely to be attributed to hydrocarbon H_3C_3. In any case, backgrounds remain insignificant compare to the smallest steps measured (usually the first and last steps, which always had >100000, >10000, and >100 fL ^{40}Ar, ^{39}Ar and ^{36}Ar, respectively). Furnace blanks constantly yield an atmospheric composition in all series. Typically, ^{40}Ar blanks ranged from 3 pL/min at 400°C, 4.5 at 700°C and 14.3 at 1000°C. Interference and production factors for Ca, Cl and K are those used by Belluso *et al.* (2000).

For each run, K, Cl and Ca concentrations are calculated from the total ^{39}Ar, ^{38}Ar and ^{37}Ar, respectively. In the present study, those totals are used to recalculate the percentage of impurity in the mineral separate. Impurities identified by XRD (e.g. quartz, chlorite or kyanite) are assumed to be completely free of K and Ca. This may be an oversimplification in those rare cases where a finely intergrown chlorite gains ^{37}Ar and ^{39}Ar by recoil during irradiation. In all other cases, we can solve the following linear system (similar equation for muscovite-margarite mixture):

$$K_{tot} = X_{Ms} * K_{Ms} + X_{Pg} * K_{Pg}$$

$$Ca_{tot} = X_{Ms} * Ca_{Ms} + X_{Pg} * Ca_{Pg}$$

$$X_{Ms} + X_{Pg} + X_{imp} = 100\%$$

K_{tot} and Ca_{tot} are the total-K and –Ca concentrations; X_{Ms}, X_{Pg} and X_{imp} are the modal abundances of muscovite, paragonite, and impurities; K_{Ms}, Ca_{Ms}, K_{Pg} and Ca_{Pg} are the respective K and Ca concentrations determined by electron microprobe. When XRD does not reveal the existence of a third phase in mineral separate, modal abundance of muscovite and paragonite is calculated based exclusively on total-K from Ar-measurement:

$$X_{Ms} = 100\% * [K_{tot} - K_{Pg}] / [K_{Ms} - K_{Pg}]$$

$$X_{Pg} = 100\% - X_{Ms} = [K_{tot} - K_{Ms}] / [K_{Pg} - K_{Ms}]$$

Finally, when no impurities are identified in the mineral separate, the mass calculation is based exclusively on K-concentration.

In the pioneering days, age spectra were only considered to be valid if they were flat (so-called "plateau": e.g. Dalrymple & Lanphere, 1974). In our mineral separates, the presence of at least two white-mica generations is common. Disentangling a mixture requires using common-denominator three-isotope correlation diagrams, such as e.g. the $^{37}Ar/^{39}Ar$ and $^{38}Ar/^{39}Ar$ ratios, which are equivalent to the Ca/K and Cl/K ratios, respectively. This class of diagrams allows the recognition of binary (or ternary: Villa, 2001) mixtures and a characterization of the phase releasing the argon. Thus, stepwise heating results have been demonstrated to yield a significant age, even in absence of a large plateau, because of the possibility to identify the different Ar reservoirs in a sample (e.g. Villa *et al.*, 1996; Belluso *et al.*, 2000; Villa *et al.*, 2000; Di Vincenzo & Palmeri, 2001; Villa, 2004). According to microprobe measurement in all studied samples: $Ca/K_{margarite} >> Ca/K_{paragonite} > Ca/K_{muscovite} \approx Ca/K_{biotite}$ and $Cl/K_{biotite} > Cl/K_{muscovite}$. Cl/K ratios in paragonite and margarite cannot be precisely determined, as Cl-content is usually below or near the detection limit (50 to 120 ppm) and K-content is circa 10 to 50 times lower than muscovite. A mixture of muscovite with paragonite or margarite should essentially yield variation in $^{37}Ar/^{39}Ar$ and to a lesser

extent in $^{38}Ar/^{39}Ar$. A reliable identification is possible either if one or more steps have similar $^{37}Ar/^{39}Ar$ compared to the measured Ca/K ratio of the phase to date (Villa *et al.*, 1996) or, if a linear correlation is observed, by extrapolating the line to the electron microprobe value of the Ca/K or Cl/K ratio (Villa *et al.*, 2000). However, this technique is limited by the electron microprobe detection limit of Ca in muscovite and paragonite or K in margarite and Cl in any studied white mica. At the end, the age assignment is constrained by the average of "isochemical" steps characteristic of one mineral phase (Krumrei *et al.*, 2006; Hetherington & Villa, 2007). Such steps have a similar Ca/K and Cl/K ratios and more important, these ratios are coherent with the independently known value for each phase to date. Moreover, Ca/K and/or Cl/K variations may exclusively be observed if Ar-release temperatures of each phase constituting the separate are different. Otherwise, each step will result in average age, Ca/K and Cl/K, which are geologically difficult to interpret. The degassing behaviours of muscovite, phengite, Fe- or Mg-rich biotite are sufficiently different to allow a discrimination in most cases (e.g. Zimmermann, 1970; Wijbrans & McDougall, 1986).

2.6) Mineral chemistry

As expected from the comparable rock type, mineral assemblage and metamorphic grade, similar mineral chemistry is observed over the six studied metapelite samples. A set of representative averaged analysis is given in Appendix 2.1. Rock chemistry of all samples is comparable (Appendix 2.2). Only the two metamarls ALu0304 and –06 are largely different, richer in CaO, but significantly poorer in Al_2O_3. Moreover, ALu0306 has the largest MgO content (5.5%) of all studied samples. All other samples being rich in Al_2O_3, the presence of muscovite, paragonite, margarite or two of these three white micas is obvious and will depend mainly on PT-condition and on whole rock Ca, Na and K-content (Appendix 2.2).

No chemical zonation is observed in white micas from any sample and all analyses are relatively homogeneous over each entire thin section (Fig. 2.3a). K-content of muscovite is the highest in absence of paragonite or in presence of margarite (> 0.89 xK = K/Ca+Na+K, K-rich samples, Appendix 2.1 and 2.2), while it decreases down to 0.75 xK in muscovite coexisting with paragonite. No significant phengitic-component is present in any muscovite (Fe 0.05-0.16, Mg 0.08-0.12 and Si 3.06-3.17 [apfu]). In parallel to the increase of metamorphic grade from Lucomagno Pass to Pizzo Molare, an increase of Na-content in muscovite is observed in both Al-poor and –rich samples (Fig. 2.3a).

Margarite is exclusively found in metamarls. It shows a solid solution towards paragonite, with up to 0.30 xNa, but only very minor muscovite component <0.02 xK (Fig. 2.3a). At Pizzo Molare, margarite included in garnet yield slightly higher Na-content and could be attributed either to the difference in bulk rock composition or a (re-)crystallization at higher T at Pizzo Molare compared to Lucomagno Pass (e.g. margarite-paragonite solvus from Franz (1977).

Paragonite composition is homogeneous in each grain and over the thin section with 0.83 to 0.87 xNa (Fig. 2.3a). Comparing two muscovite and paragonite metapelites, Ca- and K-content of paragonite are anti-correlated, ranging from 0.10 xCa and 0.07 xK (APi0301) to 0.03 xCa and 0.11 xK (AMo0410) and correlated with an increase of the metamorphic grade. The larger spreading of paragonite composition from AMo0410 is mostly related to fine intergrowth of this mineral with larger muscovite crystal (K-richer analysis, Fig. 2.3a). Analysis of large and pristine muscovite from this sample shows a noticeable larger variation in Na-content compared to other metapelite (Fig. 2.3a) and could be related to the progressive disappearance of paragonite.

Albeit biotite chemistry is almost homogeneous in each grain from any samples, intra-sample variation

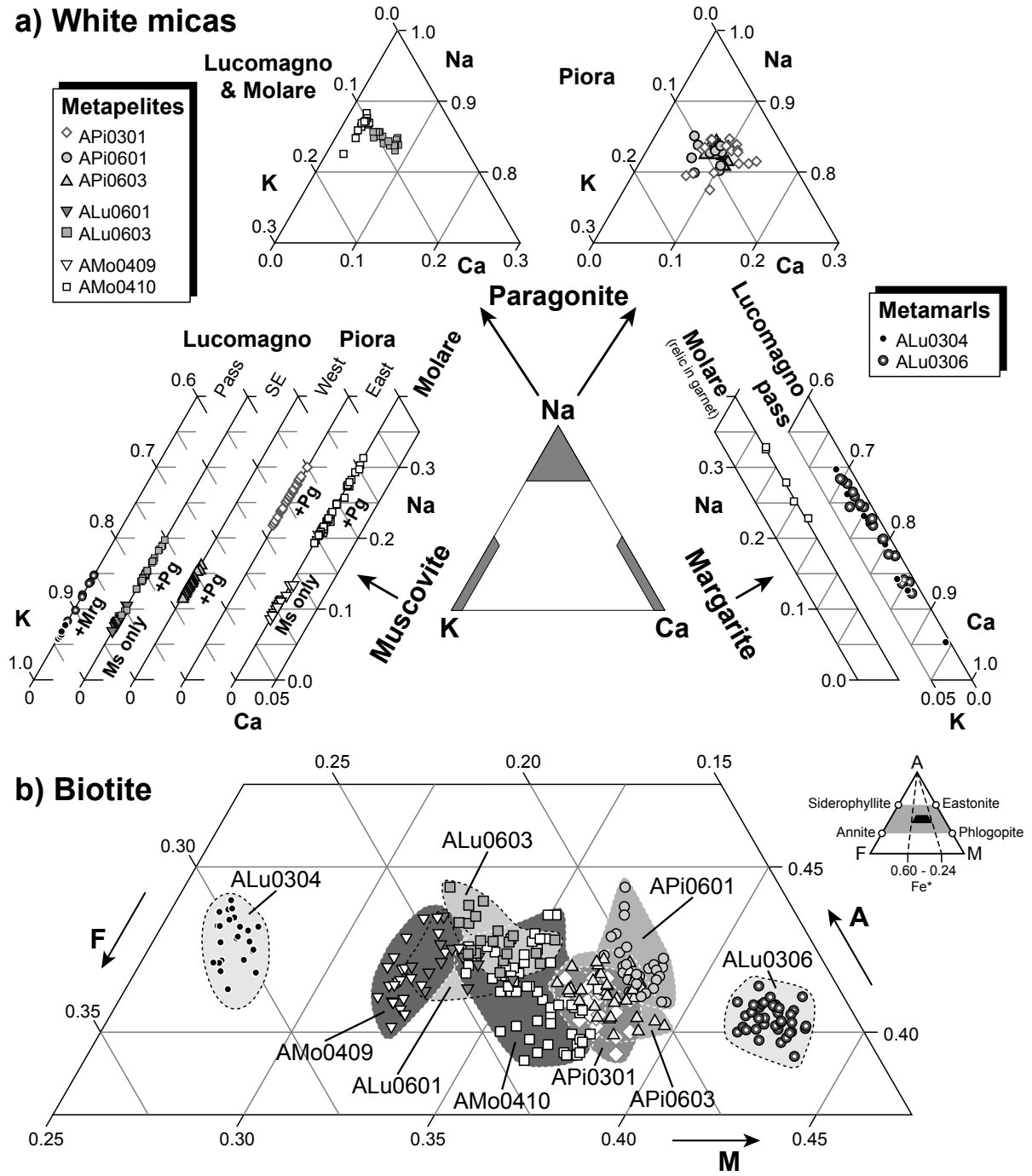

Fig. 2.3: Mica chemistry. **(a)** Ca-Na-K ternary diagram for muscovite (left), paragonite (top) and margarite (right). Insignificant Ca is present in muscovite, while very low K is found in margarite. Paragonite from different samples contains significant but variable amounts of Ca and K. **(b)** Al-Fe-Mg ternary diagram for biotite.

appears from grain to grain at millimetre- to centimetre-scale and reaches ±0.03 Fe*. A larger variation is observed in AMo0410 and is probably related to local variation of rock composition (garnet- or biotite-rich layers). Though that analysed sample stem from Grt-rich zone (Fig. 2.2), we expect some metamorphic segregation around the numerous small but strongly zoned garnet (Fig. 2.4a,b). At almost similar metamorphic grade, Fe* is naturally higher in biotite from Fe-rich metapelite of Lucomagno (0.40-0.45 Fe*) compared to Val Piora (0.33-0.38) or to the Mg-rich metamarl ALu0306 (0.28-0.30; Fig. 2.3b). Chloritization of biotite is present in all studied samples and is usually local and rare. It is clearly identified in BSE images and slightly lower K-content measured at EMP

attests for the omnipresence of chlorite lamellae in biotite of each samples.

When chlorite is resulting from the retrogression of biotite, Fe* ratio of both are very similar. Only chlorite from ALu0306 or APi0601 have a lower Fe* ratio compare to the coexisting biotite. This partitioning attests for a prograde growth of chlorite in these two samples and a chemical equilibrium with biotite during the thermal peak.

Staurolite is present in a majority of elected metapelites and its chemistry is homogeneous. Only in ALu0603 we found two homogeneous staurolite grains with slightly different Fe* (0.77 and 0.81). From sample to sample, Fe* ratio is slightly variable according to the bulk rock chemistry (from 0.74 to 0.83, Appendix 2.1). Small staurolite included near garnet rim in ALu0601 has a typical higher Fe* ratio compared to the larger matrix blast (Fe* 0.88 against 0.79; Appendix 2.1). Chloritoid inclusions in garnet always yield a slightly lower Fe* compared to staurolite (0.74-0.76 Fe*).

Garnet is almandine-rich with a typical prograde zonation showing a regular decrease in Fe*, almandine- and spessartine-component, accompanied by an increase in pyrope-component (Fig. 2.4a,b). Regarding grossular-component, it is generally decreasing from core to rim, except in the kyanite-free sample APi0301.

Plagioclase is usually homogeneous in composition. It rarely presents variation from grain to grain, like the two grains at An_{24} and An_{29} in APi0603. A clear zonation is only visible in APi0601, where An-content decreases from core to rim (An_{28} to An_{18}, Fig. 2.4c).

Clinozoisite present in garnet from metapelite has an allanitic core and a homogeneous clinozoisite-composition rim around 0.65-0.70 xCzo (=[Al-2]/[Ca+Al-2]). Lower value is obtained in the metamarl from lower grade (ALu0306, 0.55-0.60 xCzo), where clinozoisite is a major rock-forming mineral. Some analyses of Appendix 2.1 have a total-oxide sum below 100% related to the presence of REE (allanite-component; Janots *et al.*, in press). Due to low abundance and resorbed aspect of grains, clinozoisite is considered as an unstable and relic phase in Ca-poor metapelites, while it remains stable in metamarls (e.g. ALu0306). Destruction of clinozoisite is a source notably for anorthite in plagioclase.

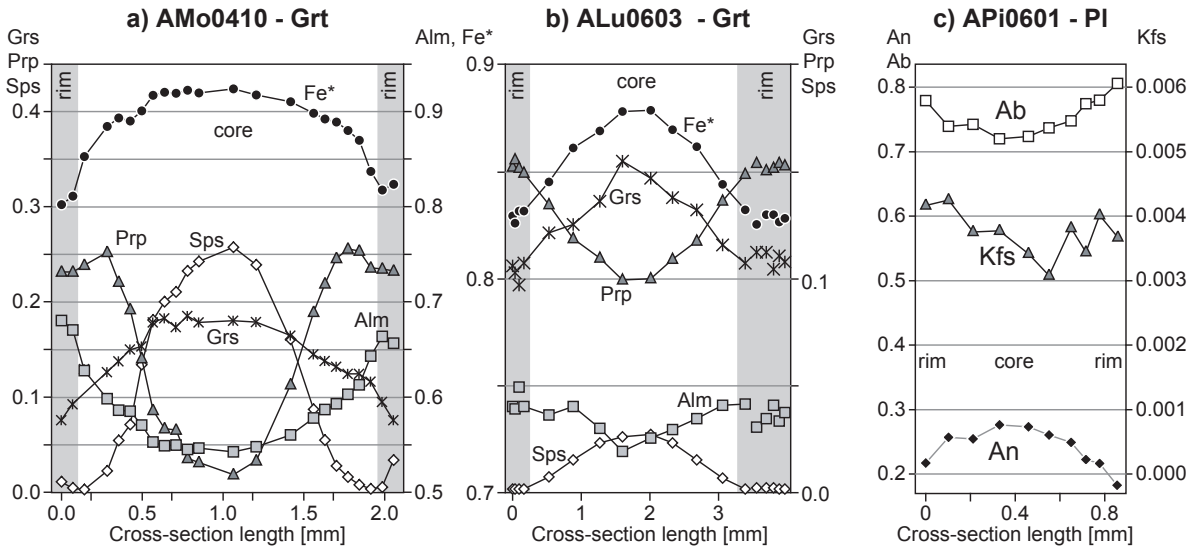

Fig. 2.4: Two typical garnet cross-sections in metapelites from **(a)** Pizzo Molare (AMo0410) and **(b)** Lucomagno (ALu0603). Both show a regular decrease of Fe* related to a growth stage during the prograde path. Fe* = Fe/(Fe+Mg); Alm, Prp, Sps or Grs = Fe, Mg, Mn or Ca/(Fe+Mg+Mn+Ca). At rims of garnet AMo0410, the small increase of Sps and Fe* suggests minor late reequilibration and resorption. **(c)** Peculiar zoned plagioclase in the paragonite-rich metapelite from Val Piora (APi0601) showing a decrease of anorthite-component from core to rim. An, Ab or Or = Ca, Na or K/(Ca+Na+K).

Table 2.2: Thermobarometric results from TWQ in metapelite and marly samples from the three selected areas. A first average is based on the observed mineral assemblage (right-columns). For some samples, biotite was not included in a calculation to check for its equilibrium state (exclusion analysis), but apparently do not lead to large differences in absolute PT-calculation. The second PT-average is based exclusively on a set of well-calibrated equilibria. LIR = number of Linear Independent Reactions.

	LIR	P [kbar]	T [°C]	xH_2O	P	T	Ms	Pg	Mrg	Bt	Grt	St	Pl	Ky	Qtz	Ilm	Rt
Sample	All equilibria				Best eq.		Solid-solutions							Pure		*not in PT*	
ALu0304	5	6.2 ± 0.2	566 ± 8	0.98	6.3	573	X	-	X	X	X	-	X	-	X	X	-
ALu0601	6	7.3 ± 0.6	546 ± 22	0.27	7.5	562	X	-	-	X	X	X	X	X	X	±	X
No biotite	4	7.5 ± 0.3	555 ± 12	0.29	-	-	X	-	-	-	X	X	X				
ALu0603	8	8.8 ± 0.6	577 ± 23	0.36	8.9	580	X	X	-	X	X	X	X	X	X	±	X
No biotite	6	8.7 ± 0.5	569 ± 19	0.34	-	-	X	X	-	-	X	X	X				
APi0301	7	8.3 ± 0.8	570 ± 28	0.46	7.3	511	X	X	-	X	X	X	X	-	X	X	-
No biotite	5	8.5 ± 0.5	585 ± 14	0.55	-	-	X	X	-	-	X	X	X	-	X	X	-
APi0601	4	9.0 ± 0.5	585 ± 16	0.41	8.9	579	-	X	-	X	X	-	X	X	X	X	-
APi0603	8	8.9 ± 0.7	579 ± 24	0.39	8.8	572	X	X	-	X	X	X	X	X	X	-	X
AMo0409	5	6.6 ± 0.2	573 ± 11	0.60	-	-	X	-	-	X	X	X	X	-	X	X	-
AMo0410	7	8.4 ± 0.5	594 ± 14	0.47	8.4	569	X	X	-	X	X	X	X	X	X	X	±

Finally, ilmenite is often present, either in the matrix as stable phase or as relic in blasts. Rutile is also found in the matrix of a few samples, but is apparently never in equilibrium with ilmenite (Table 2.2).

2.7) PT-conditions

According to the detailed petrography, metamorphic equilibration was last achieved under lower amphibolite facies condition, around the kyanite-staurolite mineral isograd in metapelite. The stable mineralogical assemblage is typically made of biotite and one or two white micas (muscovite with paragonite or margarite), together with plagioclase, garnet and often kyanite or staurolite. Table 2.2 give the equilibrium assemblage and PT-results based on mineral equilibrium and calculated with the thermodynamic database of TWQ (Berman, 1991). Considering the close intersections of all computed equilibria (e.g. Fig. 2.5a,c), the chemical equilibrium between rock-forming minerals is well defined and devoid of strong retrogression effect. To get more confidence to these PT-calculations, a second average based on four well-calibrated equilibria is given (Table 2.2, "Best eq.", from file "rxtns_calib. dat" available with TWQ 2.32 package, R. Berman pers. comm.):

pyrope + annite = almandine + phlogopite (Garnet-biotite thermometer) (2.1)

grossular + 2 kyanite + quartz = 3 anorthite (GASP barometer) (2.2)

annite + 3 anorthite = almandine + grossular + muscovite (2.3)

phlogopite + 3 anorthite = pyrope + grossular + muscovite (2.4)

PT errors given in Table 2.2 are exclusively based on intersections of calculated equilibria and do not include analytical errors on mineral analyses. From the first iteration of INTERSX routine, typical error is around ±20°C and ±0.7 kbar, with a lower limit for parallelism of two equilibria set at 15° slope difference. This error is reduced to ±10 °C and ±0.2 kbar, when equilibria more than 1.5 σ outside the average-PT are excluded (not considered here, similar PT-results). In a general manner from our specific mineral assemblage, PT-conditions calculated here are essentially depending on Fe-Mg equilibrium involving garnet, staurolite and biotite, all being

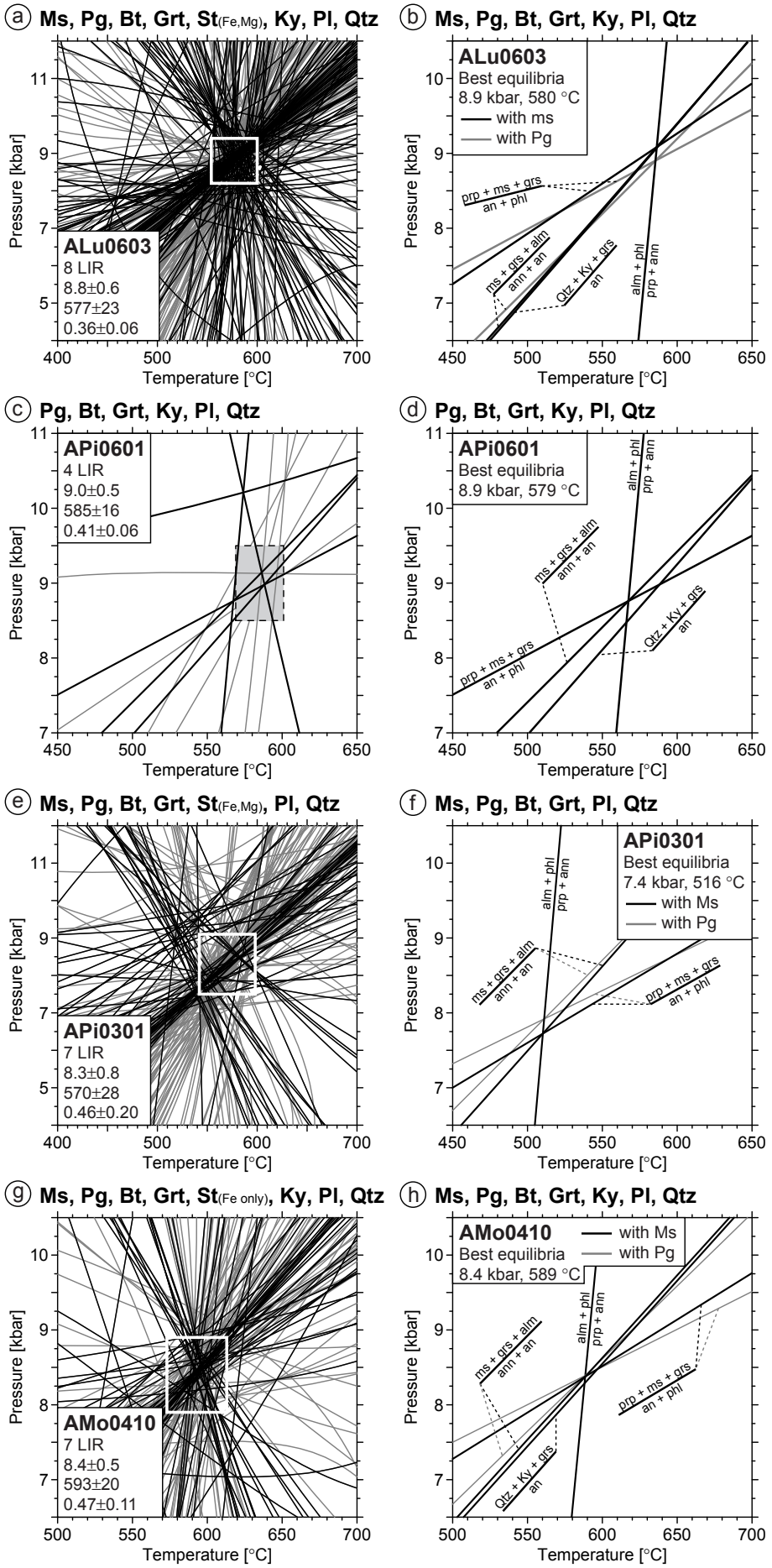

Fig. 2.5: PT-results from TWQ for **(a,b)** typical Al-rich metapelite ALu0603, **(c,d)** paragonite-kyanite-bearing metapelite APi0601, **(e,f)** ill-equilibrated metapelite APi0301 and **(g,h)** Al-poorer garnet-kyanite metapelite AMo0410. Except for APi0301, all computed reactions crosscut in a narrow PT window, significant of a well-preserved state of equilibrium. **(a,c,e,g)** Complete set of equilibria calculated with mineral assemblage given above each PT-diagram. Black curves are fluid-conserved equilibria, while grey curves are dehydration equilibria. White open-square or grey box stands for the average PT-calculation. Identification and listing of all equilibria is available on request. **(b,d,f,h)** A set of four well-calibrated equilibria from TWQ results ensures that garnet, micas, plagioclase and kyanite are fully equilibrated. This is invalid for instance in APi0301, where equilibria intersect in a quite large PT-window, and in those other instances where "best-equilibria" clearly yield PT conditions lower than in the surrounding samples. Reactions involving muscovite are firstly calculated with muscovite-component from muscovite and also from paragonite, when both micas are coexisting (b,f,h: grey equilibria). LIR: number of Linear Independent Reaction.

essentially depending on temperature. White micas and to a less extent, plagioclase compositions usually play a minor role in PT-calculation and a small change in activity do not involve large PT-changes. Temperature is thus extremely well constrained, while pressure determination is constantly subject to large uncertainties.

We are aware that thermobarometric models can only approach the reality without perfectly fitting it (Anderson, 2005). We are also limited to the minerals and solid-solution present in database considered here. All metapelite samples presented here have been investigated with THERIAK-DOMINO and PT-field of stability at unit water activity yields coherent results with respect to the observed stable mineral assemblage and PT-calculations from TWQ. This attests for a good preservation of equilibrium-PT conditions. Moreover, the computation of pseudo-section with THERIAK-DOMINO presents the advantage to give complementary information about change in mineral assemblage and chemistry over variable PT-fluid-conditions.

In the lowest metamorphic grade investigated here, ALu0306 is not suitable for PT-calculation with TWQ, due to absence of garnet in mineral assemblage and the lack of good and consistent thermodynamic data and solution model for quite all major rock-forming minerals: margarite, chlorite, epidote and ankerite. Instead, we consider PT-equilibrium determined in the nearest sample garnet- and margarite-bearing calcschist (ALu0304; Fig. 2.1b). It presents a well-equilibrated texture and achieves equilibrium at 566°C and 6.2 kbar according to TWQ. The thermometry based on Raman spectroscopy of graphite contained in this sample confirms a maximum temperature of 551±13 °C (2σ) according to the calibration given in Beyssac *et al.* (2002); see also Appendix C.4.2). To confirm the validity of such PT-condition in ALu0306, T-fluid pseudosection is computed at various P between 5 and 7 kbar with THERIAK-DOMINO. Thermobarometry in metamarls is not well constrained and suffer lack of good data for silicate-carbonate equilibria, especially Fe-Mg carbonate, epidote and amphibole. Nevertheless, some points about micas and plagioclase are relevant to this study. As expected from similar studies (Worley & Powell, 1998; Livi *et al.*, 2002), the fluid in equilibrium with margarite-bearing assemblage has to be rich in H_2O, but with some necessary CO_2 content (0.74 to 0.94 xH_2O in ALu0306). In this fluid-composition interval, PT-pseudosections are also computed and constrained the stability field for plagioclase, margarite and chlorite around 6-8 kbar and 520-550°C. This is unfortunately inconsistent with the stability of epidote or clinozoisite at higher xH_2O (> 0.95), as also with regards to the theoretic occurrence of biotite and pargasite associated to margarite consumption at slightly higher-T or lower-P (520-575, 5.5-8 kbar). Moreover, muscovite is totally consumed briefly after this reaction. Those considerations suggest margarite is possibly metastable or preserved in some chemically distinct domain, while plagioclase, biotite, chlorite and rare muscovite are stabilized at PT-conditions approaching 6-7 kbar and 540 °C, that is 20 °C above the prograde breakdown of margarite. This is fully in agreement with the TWQ-results from ALu0304 (Table 2.2).

In SE Lucomagno area, two samples (ALu0601, –03; Figs. 2.1b; 2.4a,b) are yielding significantly different PT conditions at 546°C and 7.3 kbar and 577°C and 8.8 kbar, respectively. From the same area, two other samples yield even lower PT-condition at 548-561 °C and 6.0-7.0 kbar (ALu0308 and MF315 from Frey, 1969). Identical results are obtained by considering only best-calibrated equilibria (Table 2.2, “Best eq.”). Textural relation has previously demonstrated that garnet suffer slight resorption and replacement by biotite. However, results with all rock-forming mineral including biotite are often yielding a low-error intersection of calculated equilibria, suggesting that biotite is effectively in equilibrium with the peak assemblage (Fig. 2.5a). This is also confirmed by the similar conditions determined after withdraw of biotite from the stable mineral assemblage (exclusion analysis; Table 2.2, “no biotite”) or by considering exclusively the best calibrated equilibria (Fig. 2.5b). Only a short distance separates both samples and no kilometre-sized post-tectonic feature, like fold or thrust, is identified in this area and cannot explain this PT-variation. We thus argue for a complete reequilibration of matrix minerals, garnet rim and biotite in each sample from this small area, but at slightly different PT-condition. In other words, this suite of PT-condition represents a small part of a decompression path, from 577±23 to 546±22 °C and

8.8±0.6 to 7.3±0.6 kbar.

ALu0603 is a typical Al-rich metapelite, which is representative of some other samples studied here (APi0301 and APi0601) and is thus selected for a detailed examination of the mineral evolution. Hydrous phases dominate the mineralogy and only trace of graphite without any carbonate is present in such samples (0.10% C from bulk rock analysis in ALu0603). We thus compute a PT-grid at water activity approaching unity (xH_2O > 0.99). The observed mineral assemblage is represented by a field starting around 580-590°C and 7.5-8.0 kbar and extending to higher PT up to 650 °C and 10 kbar (darkest field; Fig. 2.6). A partial reconstruction of the prograde path is obtained by computing the garnet zonation (Fig. 2.4b; grey arrow; Fig. 2.6). Rim composition of garnet fit the expected PT-conditions from mineral assemblage and from TWQ. This path is also consistent with the stability of Ti-phases: ilmenite is found in garnet core, while rutile and rare ilmenite are in equilibrium with the matrix minerals. The relic of chloritoid included in garnet yield even more constrain, growing at 550 °C and P > 6.0 kbar. Staurolite also yields precious information. By considering the lowest Fe* measured in a majority of grains (0.75-0.77 Fe*), the PT-stability field is situated at circa 570 °C, 7-9 kbar, consistent with expected PT-conditions of equilibrium. However, the highest Fe* measured in staurolite suggest a later overgrowth during decompression (Fe* > 0.80, T > 550°C, P < 7 kbar). Finally, kyanite and biotite are the only phases present in sample, but apparently unstable at expected equilibrium-PT. From Figure 2.6, biotite is stabilized at lower-P and higher-T after paragonite breakdown. We thus join back the petrological hypothesis, suggesting a later growth of biotite during a nearly adiabatic decompression stage (P < 7.5 kbar). At unit water activity, the biotite-in and chlorite-out reactions occurs at T > 550-595 °C (4-7.5 kbar). A reduction of water activity would shift those reactions at lower T, but similar P (circa –50°C at 0.5 xH_2O). Similar reduction of water activity would also push to lower PT-condition the kyanite stability field (darkest field "+Ky", Fig. 2.6), but not sufficiently to explain the observed kyanite and staurolite stability. The presence of kyanite in ALu0603 is more likely related to a local change in bulk rock composition, as confirmed by its local presence contrasting with staurolite and garnet-rich zone (Fig. 2.2e).

In Val Piora, PT-results are very similar in two samples collected to the western-side of Lake Ritom (APi0601, –03, circa 580°C and 9 kbar; Table 2.2). Both TWQ-results indicate a complete chemical equilibrium, with equilibria cross-cutting in a narrow PT-window (Fig. 2.5c) and similar PT-conditions with the best-calibrated equilibria only (Fig. 2.5d). Eastern-side sample has a similar mineral assemblage and chemistry, but yields slightly lower PT-condition (APi0301, 570°C and 8.3 kbar). The spreading of calculated equilibria over a large PT-window (Fig. 2.5f) combined with the lower PT-condition from best-calibrated equilibria (511°C, 7.3 kbar; Table 2.2, Fig. 2.5f) suggest that APi0301 is suffering slight disequilibrium regarding the stability of biotite (scarcity, partial chloritization) and possibly paragonite too (plagioclase-growth).

Finally, samples from the highest grade studied here are two metapelites from the Quartenschiefer at Pizzo Molare, but stem from two different tectonic units. Sample AMo0410 yields the highest equilibrium-PT at 594 °C, 8.4 kbar (Fig. 2.5g). In this sample, equilibria involving Mg-staurolite have been ignored in TWQ, because they show an abnormally large scatter. AMo0409 lies in a small band of Quartenschiefer, at the contact between Molare-Dangio and Sosto Bündnerschiefer (Fig. 2.1b). TWQ indicates equilibrium at lower PT-condition (6.6 kbar, 573 °C). This difference is viewed either as a tectonic-related problem, a later equilibration along decompression or a disequilibrium effect. This last hypothesis is at first glance excluded, as the mineral assemblage of both samples is in textural equilibrium and all equilibria calculated with TWQ intersects in a narrow PT-window, especially with AMo0409. The contact between both units is a major thrust already playing in the early stage of subduction (Probst, 1980) and is apt to displace the units after the last mineral equilibration. However, the thrust movement is contrary to the calculated P-difference: the Quartenschiefer apparently associated to the Sosto Bündnerschiefer (e.g. AMo0409) should come from a higher-P zone compare to the one associated to Molare-Dangio Bündnerschiefer (e.g. AMo0410). Another tectonic explanation would require a major late folding during

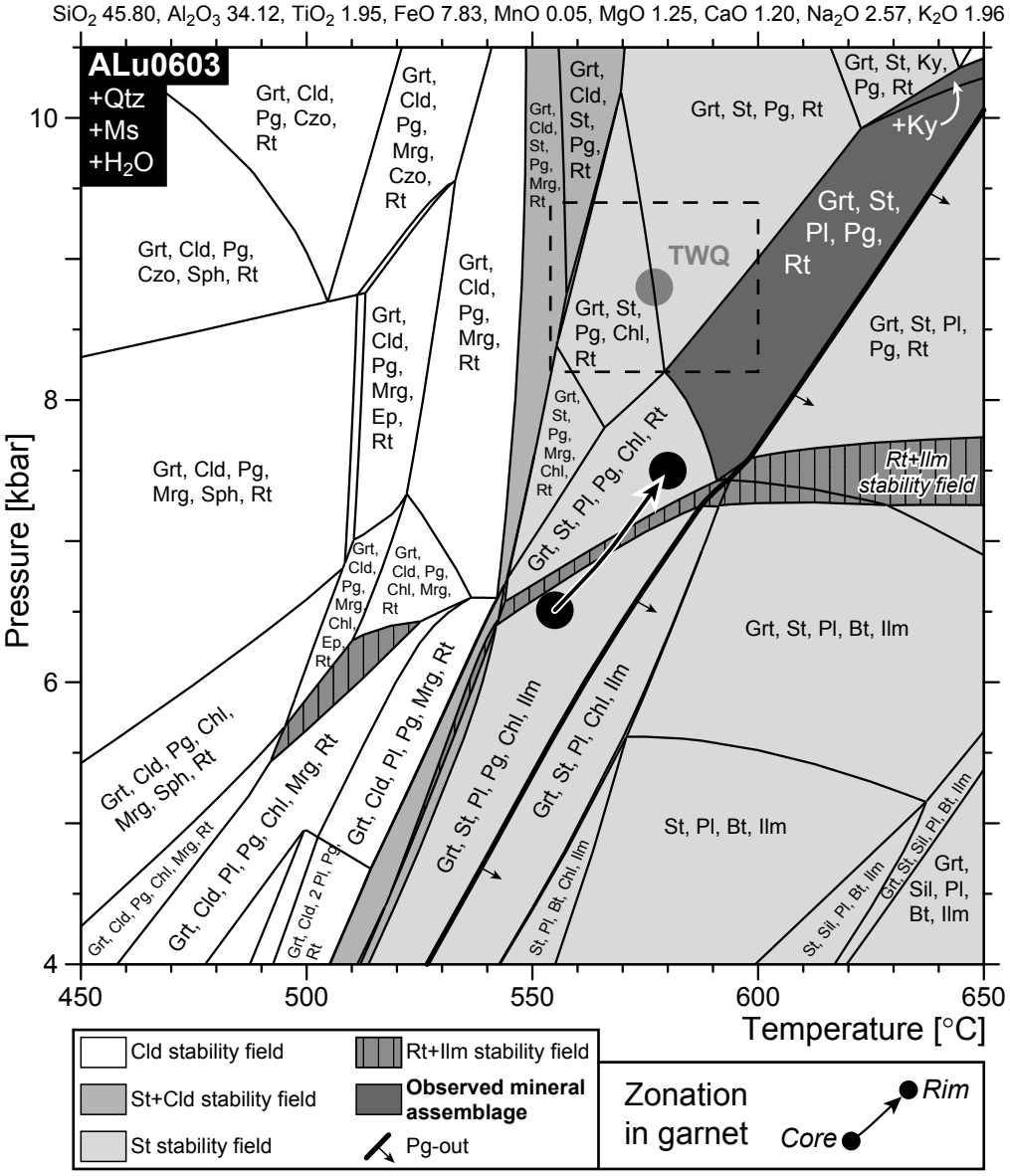

Fig. 2.6: Stable mineral assemblages in metapelite ALu0603 computed with THERIAK-DOMINO at water-saturated condition and for the bulk rock composition given above this PT-pseudosection. Quartz and muscovite stable over the entire PT-window. Some interesting fields discussed in the text are highlighted. The dark dot indicates PT-result from TWQ and grey-dashed box stands for error. Chemical zonation in garnet reveals a prograde growth history from 555, 6.5 to 580 °C, 7.5 kbar.

decompression bringing the Molare-Dangio Bündnerschiefer (high-P) over the Misox unit (low-P). However, even after complete unfolding, the maximum vertical distance is circa 500 m separating both samples and is largely insufficient to explain the 1.8 kbar difference (circa 5 km). A final explanation we support suggests a later equilibration in AMo0409 compare to AMo0410. This is also confirmed by other samples, AMo0406 from Sosto and AMo0504 from Molare-Dangio Bündnerschiefers (573±4 °C, 8.6±0.6 kbar and 586, 7.1, respectively; see Appendix C). The growth of staurolite during decompression supports this idea. Similar to SE Lucomagno area, those PT-conditions are thus viewed as part of the decompression path. Fluid may have percolated after the thermal peak along the major Pennine thrust (Fig. 2.1b) or in its neighbourhood, inducing a late mineral reequilibration. The presence of layers with scapolite or amphibole growing in fan-shape on the schistosity plan attests for this late fluid percolation in the neighbourhood of AMo0409, inducing a later chemical reequilibration.

2.8) ^{39}Ar-^{40}Ar dating

2.8.1) Quality of mineral separate

Prior to Ar-Ar measurement, we characterize the analysed white mica separates by determining the composition of each separate (XRD) and the mineral chemistry of each phase composing each separate (*in situ* microprobe analysis). In margarite, only traces of K are present (< 0.2 weight-% K_2O; Ca/K > 10; Appendix 2.1); paragonite is richer in K (0.5 to 1.0 weight-% K_2O; 0.5 to 2.0 Ca/K).

Grain size and weight of each mineral separate are presented in Table 2.3a, while Table 2.3b summarizes XRD-results and provides indication about mica proportions and presence of impurities. ALu0601 and AMo0409 are the only monomineralic white mica separates according to XRD. All other samples are composed of muscovite (2M1 polymorph) mixed with variable amount of paragonite (1M) or margarite (2M1). Quartz, kyanite or rarely chlorite are other possible impurities in white mica separate. Two difficulties prevent a complete separation: ubiquitous subgrain-scale intergrowths and the identical crystal shape and density of all three white micas. For instance, a 1:1 proportion of muscovite and paragonite constitutes the white mica separate of APi0301. In contrast, APi0601 is rich in paragonite with only trace of muscovite in both white micas separates. However, chlorite is stable in this sample and forms fine interlayers between and within micas (Fig. 2.2c). A significant amount of chlorite is thus inevitable, even after prolonged mineral separation, notably in the coarser fraction (APi0601 Ms200). In APi0603 and ALu0603, muscovite and paragonite were enriched in two fractions by selecting different grain sizes and, in APi0603, different magnetic fractions: muscovite is concentrated in the finest and more magnetic fraction (ALu0603 Ms100 and APi0603 Ms-A), while paragonite remains essentially in the coarser and less magnetic one (ALu0603 Ms200 and APi0603 Ms-D). Two intermediate white mica separates from APi0603 contain approximately 70 and 80% muscovite (Ms-B: fine and less magnetic, Ms-C: coarse and more magnetic). Due to the increase of metamorphic grade in Pizzo Molare area, only a few percent of fine paragonite remains stable in the matrix of AMo0410. The muscovite separate contains < 5% paragonite and traces of quartz and kyanite. No large influence is expected from quartz or kyanite and paragonite will have a minor contribution in the total Ar-release (<1% of total ^{39}Ar-release). XRD results from a first white mica separate of the margarite-bearing metamarl ALu0306 reveal only traces of muscovite with a large amount of margarite and quartz (Mrg-rich). A second separate contains < 10% muscovite (Mrg±Ms). Unfortunately, the combined effect of XRD peak interference between muscovite [006] and quartz [101] and the weak signal of muscovite peaks make it impossible to quantify the muscovite-margarite content before analysis.

All biotite separates contain traces of chlorite. Astonishingly, where chlorite is stable and abundant, biotite separates are among the purest (e.g. APi0601), but Fe* of chlorite and biotite differ (Appendix 2.1). In contrary, two-times more chlorite is present in mineral separates, where chlorite is retrograde (e.g. APi0603). Fe* of biotite

Table 2.3: Major summary of mineral separates and ^{39}Ar-^{40}Ar dating results. **(a)** Mineral prepared for ^{39}Ar-^{40}Ar dating with sample and separate names, weight and grain-size fraction. **(b)** Presence of impurity detected at XRD and peak intensity ratio muscovite [006] to paragonite [006] for white mica separates or Chl [004] to Bt [006] for biotite separates. **(c)** Summary of ^{39}Ar-^{40}Ar ages (errors are given at the 95% confidence level). The first column lists the steps used for averaged age. Next column indicates the status of selected steps: (P) stands for steps yielding a "plateau" age and (I) describe "isochemical" steps (constant Ca/K and Cl/K, coherent with the phase to date), with sometimes some outliers or a larger variation of Ca-, Cl- or K-content (±I). When "heterochemical" steps are selected (i.e. release of Ar from at least two distinct reservoirs), they can always yield a plateau (H–, "heterochemical plateau"). If not, the age variation can be correlated (H+), weakly correlated (±H) or uncorrelated (H_0) with Ca/K and/or Cl/K (see Appendix D and Figure D.5 for details on this classification). Next column is the percentage ^{39}Ar release and the averaged age and error at 95% confidence level. Total K, Cl and Ca concentrations were calculated from the total measured ^{39}Ar, ^{38}Ar and ^{37}Ar. **(d)** Mass balance calculation for the mica generations contained in each separate, based on pure end-member K and Ca concentrations obtained by EMP and on total K and Ca concentrations calculated from artificial Ar isotopes. When only two phases are present in mineral separate, mass balance is exclusively based on K concentration.

	a) Mineral separates				b) XRD results		c) ^{39}Ar-^{40}Ar ages and total K, Ca and Cl							d) Mass balance			
	Sample	Separate	Mesh [µm]	Weight [mg]	Mineral and impurities	Peak ratio *	Steps	State of selected steps	^{39}Ar [%]	**Age [Ma]** error 95% c.l.	Totals K [%]	Totals Ca [%]	Totals Cl [ppm]	% Ms **	% Mrg or Pg **	% Ca-, K-free phase	%^{39}Ar from Ms
WHITE MICA	ALu0306	Mrg-rich	125-250	13.9	Mrg, Qtz, trace of Ms	-	3-10	P, ±H	76.0	**17.6** ± 1.4	0.22	5.89	5.7	1.1	81.1	17.8	43.1
		Mrg±Ms	125-250	29.7	Mrg, Qtz, Ms	-	3-6	P, ±H	97.2	**18.04** ± 0.78	0.85	4.33	9.6	9.0	59.7	31.3	89.1
	ALu0601	Ms100	50-150	14.36	Pure Ms	100	3-8	P, I	90.7	**16.30** ± 0.23	7.20	0.14	54.1	86.3	-	13.7 ?	100.0
		Ms200	150-250	12.10	Pure Ms	100	3-7	P, I	93.9	**16.66** ± 0.20	> 5.44	> 0.17	> 28.6	> 65.1	-	< 34.9 ?	100.0
	ALu0603	Ms100	50-150	11.93	Ms, Trace of Pg	98.8	3-10	P, ±I	95.6	**16.36** ± 0.22	6.27	0.16	47.9	83.7	16.3	-	97.9
		Ms200	150-250	20.51	Pg, Ms, Qtz	13.6	1-6	P, H–	99.9	**16.67** ± 0.39	1.47	0.32	184.6	14.9	46.1	39.0	74.4
	APi0301	Ms+Pg	150-250	14.1	Ms, Pg, trace of Qtz	47.6	4-14	±P, H+	89.6	**16.87** ± 0.35	3.07	0.58	18.0	37.3	50.5	12.3	87.0
	APi0601	Ms100	50-150	11.55	Pg, Qtz, Ms, trace of Chl	ca. 20 #	2	*1 step*	45.8	**15.18** ± 0.70	0.81	0.06	104.4	9.9	8.4	81.7	91.2
		Ms200	150-250	13.75	Pg, Qtz, trace of Ms+Chl	ca. 5 #	2	*1 step*	49.2	**16.42** ± 0.88	0.51	0.33	158.8	1.4	47.4	51.2	20.7
	APi0603	Ms-A	50-150	16.07	Ms, trace of Pg	93.9	4-10	P, I	88.9	**15.88** ± 0.15	6.52	0.21	75.1	85.7	14.3	-	98.3
		Ms-B	50-150	16.97	Ms, Pg	70.9	4-9	P, I	81.0	**15.48** ± 0.19	5.25	0.31	47.7	66.7	33.3	-	95.0
		Ms-C	150-250	15.18	Ms, Pg, trace of Qtz	79.4	3-9	P, I	91.2	**15.73** ± 0.19	5.14	0.26	47.9	65.5	31.5	3.0	95.2
		Ms-D	150-250	20.57	Pg, Qtz, trace of Ms	4.3	3-7	±P, H_0	81.8	**15.0** ± 2.1	0.96	0.66	84.2	4.2	81.2	14.6	33.1
							6-7	I	31.1	**15.7** ± 1.3							
	AMo0409	Ms	200-250	18.3	Pure Ms	100	6-10	P, I	86.3	**17.85** ± 0.61	6.30	0.28	21.7	72.8	-	27.2 ?	100.0
	AMo0410	Ms±Pg	200-250	16.6	Ms±Pg, trace of Ky+Qtz	96.7	4,6,7	I "Ms"	42.6	**18.35** ± 0.59	3.62	1.21	82.6	< 47.3	< 52.7	-	94.9
							5,8-11	I "Ms+Pg"	31.1	**16.87** ± 0.60							

	Sample	Separate	Mesh [µm]	Weight [mg]	Mineral and impurities	Peak ratio *	Steps	Plateau? Isochemical?	^{39}Ar [%]	**Age [Ma]** error 95% c.l.	Totals K [%]	Totals Ca [%]	Totals Cl [ppm]	% Bt	% Chl
BIOTITE	ALu0306	Bt	125-200	6.4	Bt, Chl	2.1	3-8	±P, H+	80.0	**17.65** ± 0.33	6.65	0.86	541.9	80.7	19.3
							3,8	I	41.1	**17.61** ± 0.38					
	APi0601	Bt100	50-150	11.46	Bt, trace of Chl	1.0	3-7	P, I	77.5	**14.85** ± 0.21	6.41	0.13	147.6	83.8	16.2
		Bt200	150-250	11.08	Bt, trace of Chl	0.8	3-9	P, I	92.8	**14.84** ± 0.23	5.94	0.34	569.9	77.7	22.3
	APi0603	Bt100	50-150	9.12	Bt, Chl	2.6	3-8	P, H–	94.6	**14.72** ± 0.26	6.04	0.46	355.1	80.3	19.7
		Bt200	150-250	12.08	Bt, Chl	2.1	4,6-8	P, I	58.0	**15.29** ± 0.25	6.48	0.18	483.9	86.1	13.9
	AMo0409	Bt	50-125	17.3	Bt, trace of Chl	0.2	3-9	P, I	93.8	**16.25** ± 0.81	6.65	0.40	44.6	83.2	16.8
	AMo0410	Bt	50-125	16.6	Bt, Chl	2.6	5,13	I	42.3	**16.37** ± 0.40	6.18	1.09	165.4	83.8	16.2

(*) XRD peak intensity-ratio calculated as following: 100*Ms[006]/(Ms[006]+Pg[006]) and 100*Chl[004]/(Chl[004]+Bt[006]). Peak ratio for white micas is semi-quantitative (Frey, 1977), while chlorite and biotite ratio is only qualitative. No peak ratio for muscovite-margarite mixture from ALu0306 (strong interference of quartz peak [101] and a too small muscovite peak [006]).
(**) If more than three phases are present, as in the two white mica separates of APi0601, this ratio is a maximum value.
(#) The strong interference of quartz [101] on muscovite peak [006] does not allow a precise semi-quantification of paragonite and muscovite content. In this case, these percentages are calculated on [004] peaks and must be considered thus as rough qualitative estimates.

and chlorite is similar in such samples (Appendix 2.1). This precluded a magnetic separation. Prograde chlorite forms larger flakes when it is in equilibrium with biotite (APi0601, Fig. 2.2c), while a retrograde chloritization of biotite is likely to occur at the nanometre-scale (e.g. Di Vincenzo *et al.*, 2003).

In complement to XRD results, the abundance of each micas and possible impurities is recalculated on the basis of K and Ca concentrations from ^{39}Ar and ^{37}Ar (Table 2.3d). In two cases only minimum value are available, either due to a loss of a step (at 1040 °C, ALu0601 Ms200) or due to missing mica analyses (e.g. muscovite in APi0601, too fine interlayer within Pg). Muscovite separates apparently pure according to XRD contain between 95 and 85% of pure muscovite (ALu0601 Ms100, ALu0603 Ms100, AMo0409 Ms). To explain why this number is not perfectly 100%, two possible artefacts (each accounting for a few percent at most) should be considered. One is the external reproducibility of mass spectrometer sensitivity, which is no better than 10%. Another one is the selection of spots on which the K-content of mica analysed at EMP is determined. Indeed, we selected zone devoid of defects and disregarded analyses having low oxide total, low Ca, Na or K content, large apparent mixture with another phase, etc. Thus, an excessively high K-content of mica was probably used to recalculate the muscovite content from the total ^{39}Ar release of a mineral separate. Although EMP analyses are effectively representative of a micrometer-scale area in a mica grain, they may overestimate the real average K-content of a mineral separate made of somehow "imperfect" grains. Therefore, the proportion of "impurity" (quartz, kyanite…) must not be viewed as due to discrete grains (which we would have removed), but as due to intergrowths below optical detection. Nevertheless, ratios calculated from muscovite-paragonite separates are coherent with semi-quantitative XRD ratio and inter-sample comparison in white mica separates is accurate. Moreover, the recalculation of ^{39}Ar release contribution of muscovite compared to paragonite or margarite is expected to be unaffected, as its estimate depends on the ^{37}Ar, ^{38}Ar, ^{39}Ar ratios and not on absolute amounts.

To complete mica abundance estimation and when two K-bearing phase are present in mineral separate, we calculate the percentage of ^{39}Ar-release by each phase to judge of their effect on Ar-spectrum. In mineral separates containing more than 2/3 muscovite (Table 2.3b,d), this mica is clearly dominating Ar-release (> 95% ^{39}Ar-release, ALu0603 Ms100, APi0603 Ms-A to –C, AMo0410). In APi0301, both micas are present in similar quantity, but muscovite is always responsible for 87% of total-^{39}Ar release. Mineral separate ALu0603 Ms200 is composed of more than 80% paragonite, but muscovite always dominates Ar-release with 74% of total-^{39}Ar. The ^{39}Ar-release is essentially related to paragonite only in paragonite-rich separates with 66% of total-^{39}Ar (APi0601 Ms100, APi0603 Ms-D). Finally, in margarite and muscovite mixture (ALu0306; Table 2.3b,d), only a few percent of muscovite are sufficient to dominate the ^{39}Ar-release of separate of both mineral separates, with 89% and 43% of the total-^{39}Ar released by muscovite in Mrg±Ms and Mrg-rich separates, respectively. We thus essentially date the muscovite in Mrg±Ms separate, while an average between muscovite and margarite ages is obtained in the Mrg-rich separate.

2.8.2) Ar-release from micas and mica mixtures

The Ar-release rate from biotite and three white micas (given as percent release per unit time and unit temperature difference) is shown in Figure 2.7. Steps degassing at T below 600 °C usually don't pertain to micas, and moreover mostly contribute an insignificant percentage of the total ^{39}Ar and ^{40}Ar* (Appendix 2.3). Fluid inclusions (notably in quartz) similarly affect only steps below 600 °C (Villa, 2001), and references therein), as they decrepitate at low T during stepwise heating analyses. A higher Cl (and often Ca) characterizes the release of gas from fluid inlcusions. Smaller fluid inclusion may decrepitate at higher T (Villa, 2001). The "fusion" step of each analysis (circa 1400-1500 °C) contains always a minor amount of ^{40}Ar* and ^{39}Ar and ensures that the analysed mica has

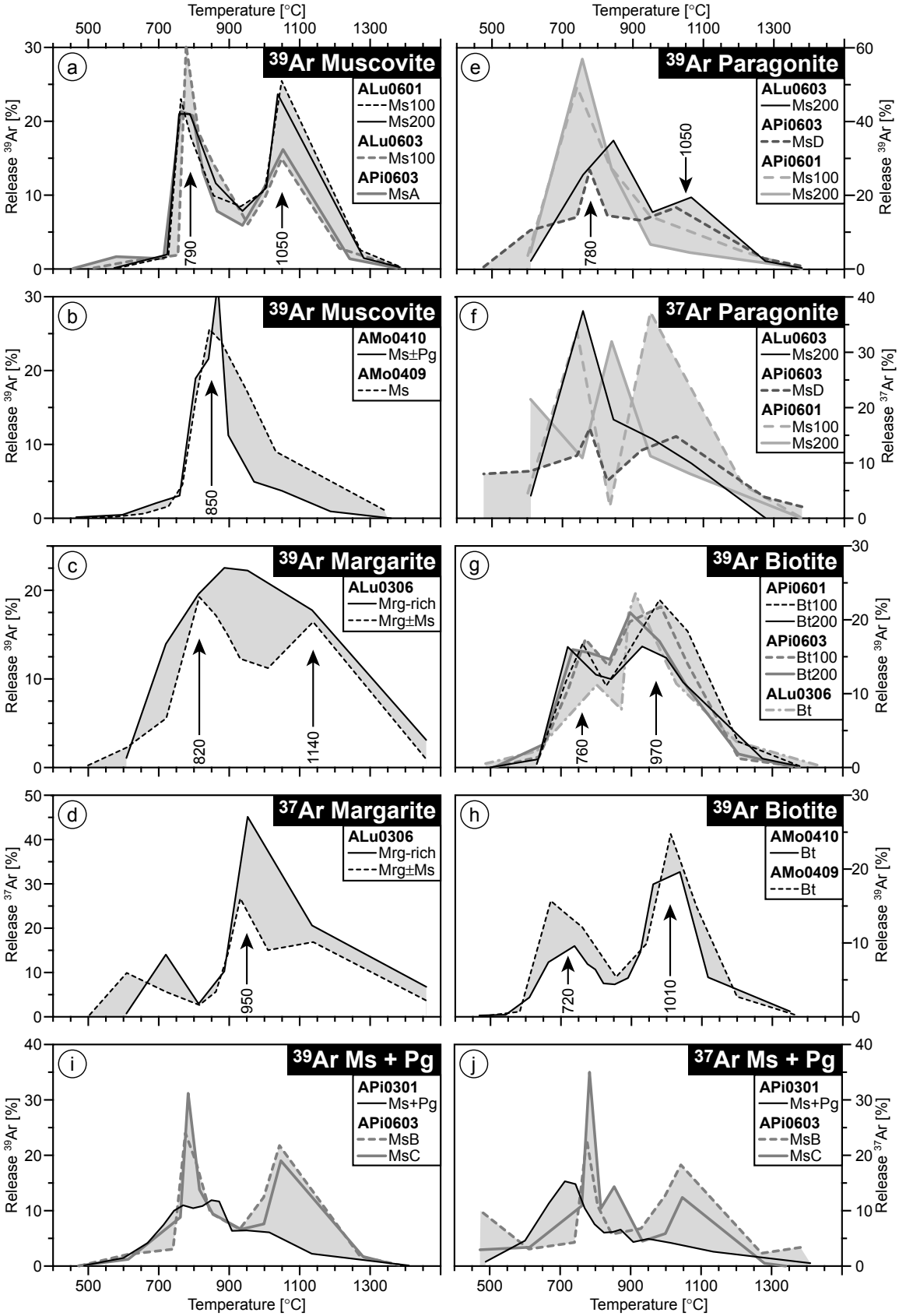

Fig. 2.7: Ar-release rates during *in vacuo* stepwise heating analyses. **(a,b)** ^{39}Ar release rate in pure muscovite separates from **(a)** SE Lucomagno and Piora and **(b)** from Molare. **(c,d)** ^{39}Ar and ^{37}Ar release rates in margarite-rich (Mrg-rich) and margarite-muscovite (Mrg±Ms) separates from Lucomagno Pass. **(e,f)** ^{39}Ar and ^{37}Ar release rates for paragonite. **(g,h)** ^{39}Ar release rate in pure biotite separates from **(i)** SE Lucomagno and Piora and **(j)** from Molare. **(i,j)** ^{39}Ar and ^{37}Ar release rates for muscovite and paragonite mixtures, with circa 50% and 20-30% paragonite in APi0301 and APi0603, respectively.

released its argon entirely.

Pure muscovite separates show two distinct Ar-release patterns. In the Lucomagno and Val Piora areas, two distinct and narrow peaks exist for $^{40}Ar^*$, ^{39}Ar and ^{38}Ar, around 790 and 1050 °C (Fig. 2.7a). At higher grade, in Pizzo Molare region, a single large peak is present around 850 °C and is slightly asymmetric toward higher temperature (Fig. 2.7b). Sletten & Onstott (1998) proposed a two-stage decomposition to explain the double peak. First is a major dehydration and delamination of muscovite. In a second stage, stronger ionic bonds are broken and Ar is released from a dehydroxylate muscovite. These authors suggest a dependence of Ar release upon grain size in muscovite. Our study fails to confirm this conclusion, as different grain size fractions yield a similar Ar release pattern (e.g ALu0601; Fig. 2.7a). Hetherington & Villa (2007) had argued against delamination as the predominant cause of Ar and Xe release from Ba-muscovite. We note that an explanation for the unimodal/bimodal release may require a characterization of polytype modifications as a function of the chemical composition or the metamorphic grade, but a quantitative explanation will not be addressed here.

Both margarite-rich separates from ALu0306 show a $^{40}Ar^*$- and ^{39}Ar-release between 700 and 1150 °C (Fig. 2.7c), while a ^{37}Ar-peak is only present at high temperature between 900 and 1100 °C (Fig. 2.7d). This peak corresponds to the major Ar-release from margarite. In Mrg±Ms separate, the double peaks are in the identical temperature range as the Ar release from pure muscovite separate (Fig. 2.7a,c). Although muscovite represents only a small percentage of this mineral separate (Table 2.3b), the profile of Mrg±Ms separate demonstrates the strong influence of a K-rich phase and confirms that a majority of ^{39}Ar is released from muscovite. Nevertheless, a narrow ^{37}Ar-peak is always present around 950 °C. High-T steps are thus a mixture of ^{39}Ar contributed both by margarite and muscovite, while low-T steps only derive from muscovite.

Paragonite contains only small amounts of K and Ca; because muscovite is constantly present in such mineral separates it dominates the ^{39}Ar release (Fig. 2.7e). The highest ^{37}Ar release rate is observed between 750 and 950 °C, variable from sample to sample (Fig. 2.7f).

Biotite releases Ar in a large range between 600 and 1150 °C. Two peaks are typically visible and may correspond to two decomposition stages: firstly, delamination and dehydration of mica, secondly the dissociation of stronger ionic bonds with the formation of new phases at high-T (spinels, olivine and Si-Al-glass; Zimmermann, 1970; Di Vincenzo *et al.*, 2003; Viti *et al.*, 2004). Those stages happen at different temperature according to the nature of biotite. In Piora and Lucomagno areas, the Ar release profile reveals two peaks around 760 and 970 °C. In Molare area, the two peaks are wider apart (circa 720 and 1010 °C). Biotite chemistry is likely to induce such difference in Ar-release profiles, with a first Ar release peak at higher temperature in Mg-rich biotite (760 °C in APi0601, –03 and ALu0306, 0.35, 0.36 and 0.29 Fe*) compared to Fe-richer ones (720 °C, in AMo0409 and –10, 0.39 and 0.45 Fe*). Zimmermann (1970) had observed a later release of structural water in phlogopite, which is consistent with its higher thermal stability due to shorter and stronger interatomic bonds, proxied by ionic porosity (Dahl, 1996). This is fully corroborated by our observations. A slight increase in metamorphic grade and a change in mineral composition (Fig. 2.3a,b) probably also affect bond strength and therefore control the thermal peak of Ar release rates.

2.8.3) ^{39}Ar-^{40}Ar ages

2.8.3.1) Lucomagno

In metamarl ALu0306, the averaged age over all major steps yield similar results for both Mrg-rich and Mrg±Ms separates, but strong variation in Ca/K and Cl/K (Fig. 2.8a,b). Both minerals apparently record the same event with ages at 17.6±1.4 Ma and 18.04±0.78 for Mrg-rich and Mrg±Ms separates, respectively. Ca/K is usually below the measured value for margarite (46±6 from EMP; Fig. 2.8c). It is the lowest in Mrg±Ms separate (0.8 to 13 Ca/K) and as previously suggested from total ^{39}Ar release, most of the Ar-signal stems from muscovite, notably in steps #4 and 5 (low ^{37}Ar, high ^{39}Ar and $^{40}Ar^*$; Fig. 2.8b). When both results are combined, a weak negative correlation in Ca/K versus the age is visible. Extrapolation toward the microprobe value for margarite (Ca/K = 65±10; Fig. 2.8c) yields a marginally younger age of 17.1±2.5 Ma compared to muscovite at Ca/K = 0 (18.04±0.80 Ma); the two values are statistically indistinguishable. The biotite separate yields a plateau age at 17.65±0.33 and a similar isochemical (steps #3 and #8, lowest Ca/K and Cl/K) age of 17.61±0.38 Ma (Fig. 2.8a,b).

In SE Lucomagno area, ^{39}Ar-^{40}Ar dating in pelitic rocks ALu0601 and 03 yield respectively 16.66±0.20 and 16.67±0.39 Ma for the coarse fraction (150-250 µm) and 16.30±0.23 and 16.36±0.22 Ma for the fine one (50-150 µm; Fig. 2.9a,b). Both muscovite separates in ALu0601 show homogeneous and low Ca/K and Cl/K ratios in the gas-rich steps (Fig. 2.9c). These steps are all isochemical as they reflect the degassing of a single phase; correspondingly, step ages are constant. In contrast, ALu0603 is a mixture of paragonite and muscovite (Table 2.3). Indeed, the Ca/K ratio shows significant variations (Ms100, Ms200; Fig. 2.9c). Step results in Ms100 have Ca/K ratios approaching zero, but vary from 0.15 to 0.50 in Ms200. The coarser fraction is seen to contain much more paragonite (Table 2.3b,d). However, no age difference is observed whether we extrapolate the age at Ca/K value to muscovite (< 0.01) or paragonite (circa 0.84). Both micas record thus the same K-Ar age.

2.8.3.2) Val Piora

All age results of the four white mica separates of APi0603 are similar, three being statistically indistinguishable. Between the two finer fractions Ms-A (15.88±0.15) and Ms-B (15.48±0.19 Ma), the latter has a small but significant difference (Fig. 2.10a; Appendix 2.3). The two coarser fractions (Ms-C and –D) give isochemical ages of 15.73±0.19 and 15.0±2.1 Ma (Fig. 2.10b). The ^{39}Ar release in Ms-A to C is dominated by muscovite notably in Ms-A (Pg-poor), while paragonite dominates in Ms-D (Table 2.3d). Due to low K, Cl and Ca contents, Ms-D has large errors on age and on Ca/K and Cl/K ratios. Two steps from Ms-D at highest Ca/K ratio (#6 and 7) yield an isochemical age at 15.7±1.3 Ma. Combining all four analyses, only a weak dependence of Ca/K on age is observed. Age extrapolation toward the microprobe Ca/K value of paragonite yields an imprecise age of 13.8±1.3 Ma. Most of the age variation between samples Ms-A to –D might also be explained by enhanced Ar diffusion out of paragonite. This was not the case in ALu0603. The same apparent trend is observed in the white mica separate of APi0301. The isochemical age from low-Ca/K steps is 17.04±0.62 Ma; variations in Ca/K anti-correlate with the age and steps at higher Ca/K yield 16.68±0.59 Ma (Fig. 2.11). Extrapolating to the paragonite Ca/K ratio (circa 1.6) of related sample APi0301 suggest that this Na-mica may be younger than muscovite (14.9±5.6 Ma), even if statistically indistinguishable.

Like in previous fraction Ms-D, step ages from the paragonite-rich separates of APi0601 have also large errors due to the low K-content in paragonite and the scarcity of muscovite. Indeed, a fix gain factor between multiplier and faraday was used for these mineral separates. In both separates, one step concentrates more than

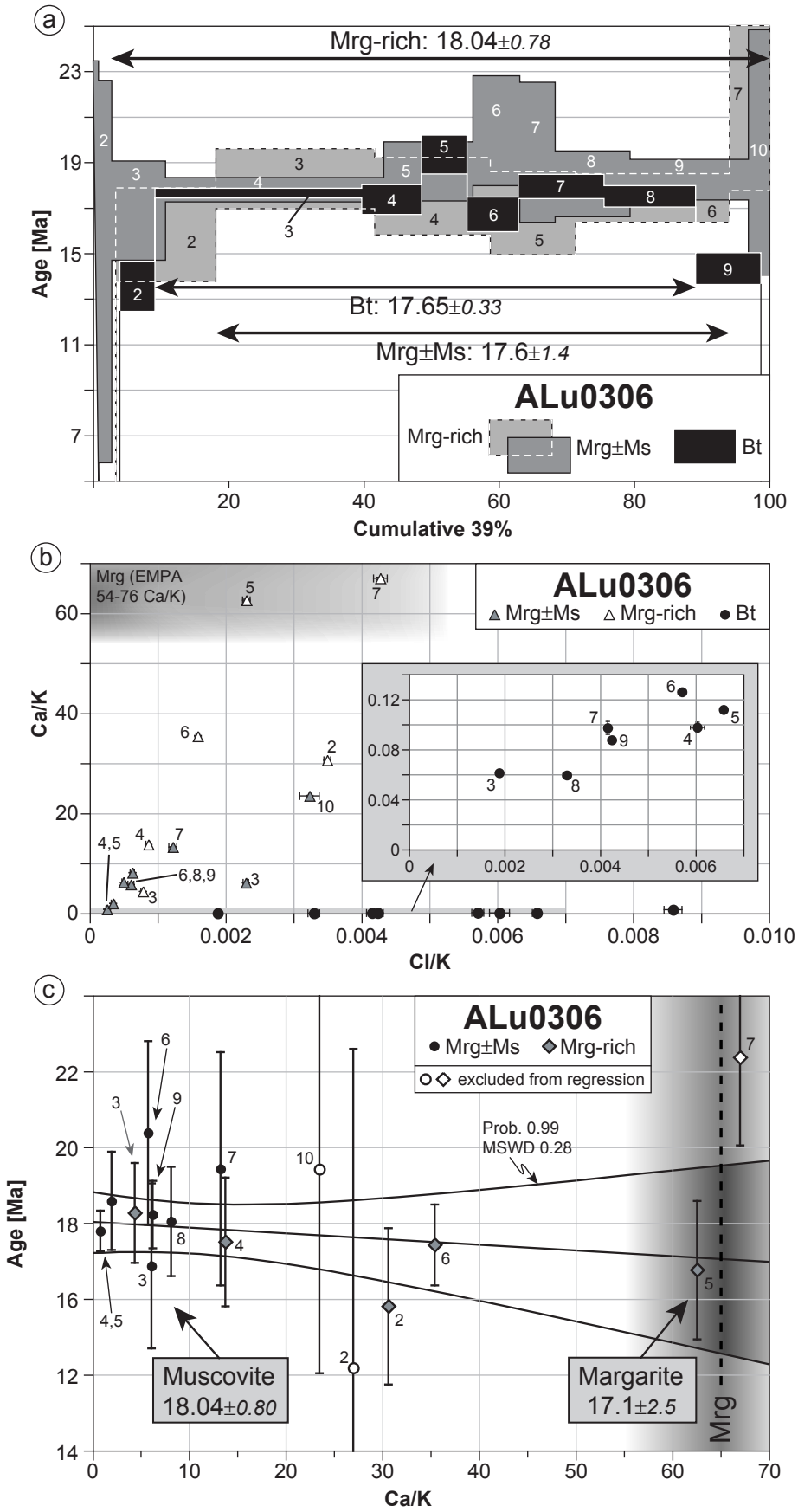

Fig. 2.8: Ar-results from margarite-rich metamarl ALu0306. **(a)** Age spectra for biotite and two white mica separates. Notice the similitude in biotite and white mica age-results. Error on each step in this figure, as in following Ar-spectra, is given at 68.2% confidence level, while average age are calculated at 95% confidence level with Isoplot (Ludwig, 2003). **(b)** Ca/K versus Cl/K correlation in all steps from white mica separates in sample ALu0306, Mrg-rich and Mrg±Ms. The highest Ca/K values obtained for the Mrg-rich separate plot near the electron microprobe determination of Ca/K in margarite and demonstrate the predominance of margarite compared to (minor) muscovite in this separate. High-Ca/K steps yield slightly younger ages than muscovite. In contrast, most steps from the Mrg±Ms separate have a much lower Ca/K, as the 5-10 percent muscovite dominate the ^{39}Ar budget in this separate. Inlet shows the positive correlation of Ca/K versus Cl/K correlation diagram from biotite separate. Isochemical steps #3 and #8 pertain to biotite. **(c)** The Ca/K-age regression is given with a 95% confidence level error envelope and is obtained with Isoplot. Firsts and last steps are excluded from the regression (white diamonds and circles).

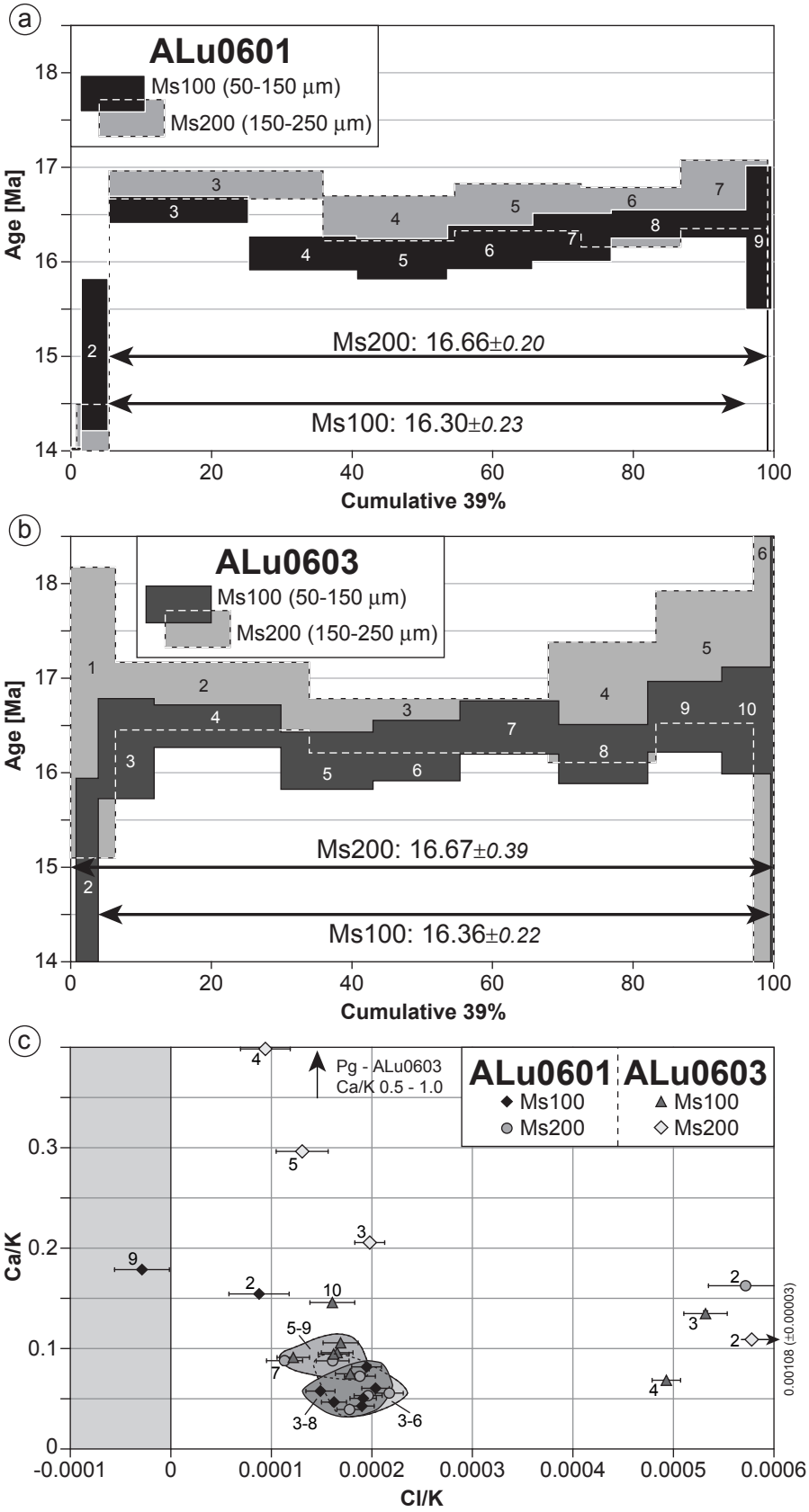

Fig. 2.9: Ar-results from metapelite of SE Lucomagno area. **(a,b)** Age spectra for **(a)** muscovite of ALu0601 and **(b)** muscovite- (Ms100) or paragonite-rich separate (Ms200) of ALu0603. **(c)** Ca/K and Cl/K correlation for mica separates of ALu0601 and –03. Whereas the pure muscovite separates from ALu0601 yield isochemical steps at low Ca/K and Cl/K, the white mica separates of ALu0603 are distinctly enriched in Ca, especially Ms200. This is related to a large amount of paragonite presents in this mineral separate. Nevertheless, even steps #4 and 5 from Ms200 remain below the Ca/K ratio determined for paragonite at electron microprobe (0.5 to 1.0), demonstrating the strongest effect of minor muscovite amount present in this sample (circa 15%). In contrary, a few steps from Ms100 tend towards higher Ca/K ratio compared to muscovite from ALu0603, due to traces of paragonite.

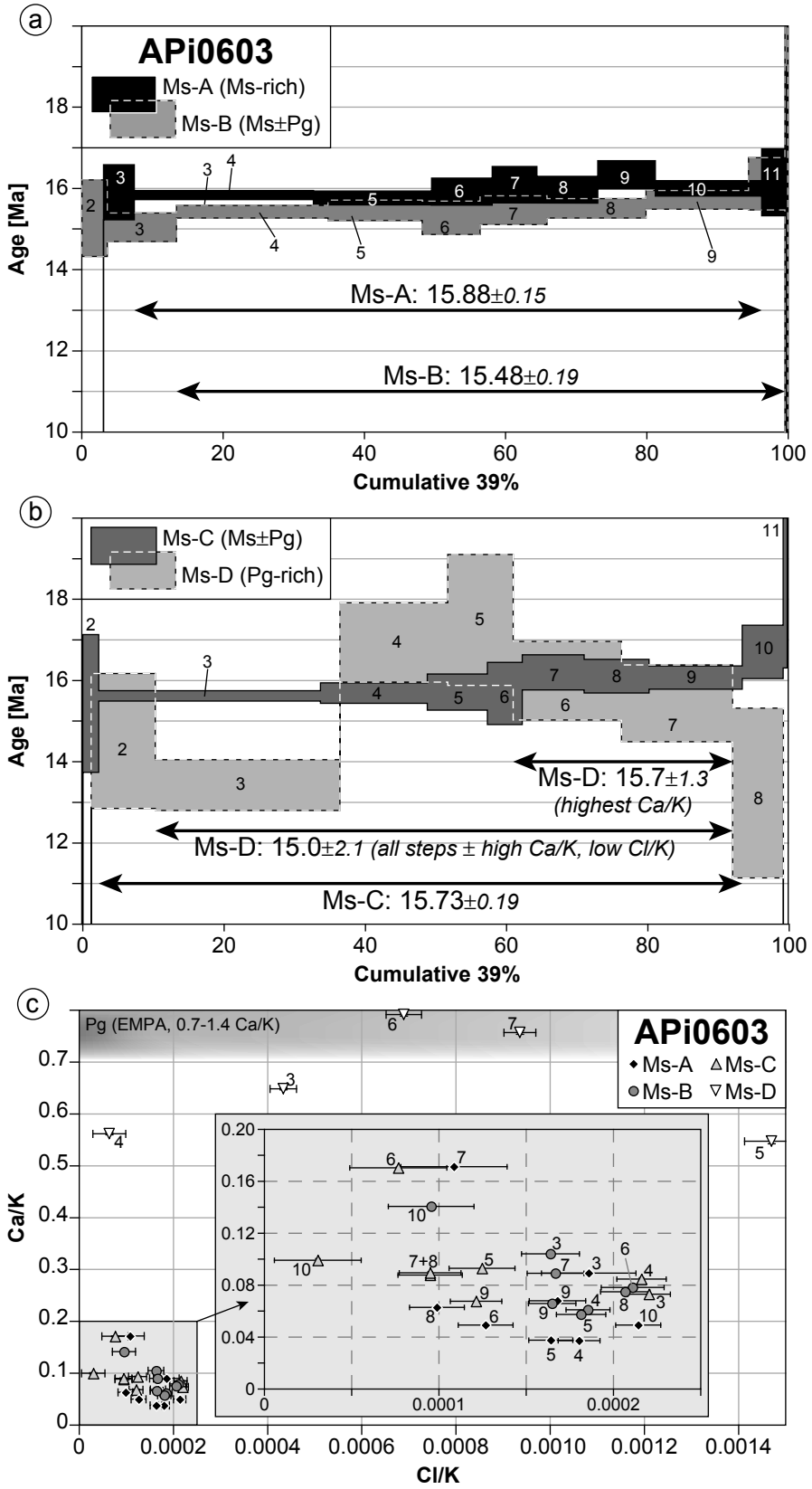

Fig. 2.10: (a,b) Age spectra for the four muscovite-separates from sample APi0603. **(a)** Results for the fine fraction (50-150 µm): Ms-A is muscovite-rich (94%) and Ms-B contains approximately 30% paragonite. **(b)** Age spectra for the coarse fraction (150-250 µm). Ms-D is paragonite-rich (96%), while Ms-C is similar to Ms-B and contains circa 20% paragonite. **(c)** Cl/K versus Ca/K diagram in APi0603. In full agreement with the paragonite content determined in each white mica separate, Ms-D shows the highest Ca/K ratios and reaches value nearby the Ca/K ratio measured at electron microprobe (0.7 to 1.4). On the opposite, Ms-A is poor in paragonite and yields very low Ca/K (< 0.05).

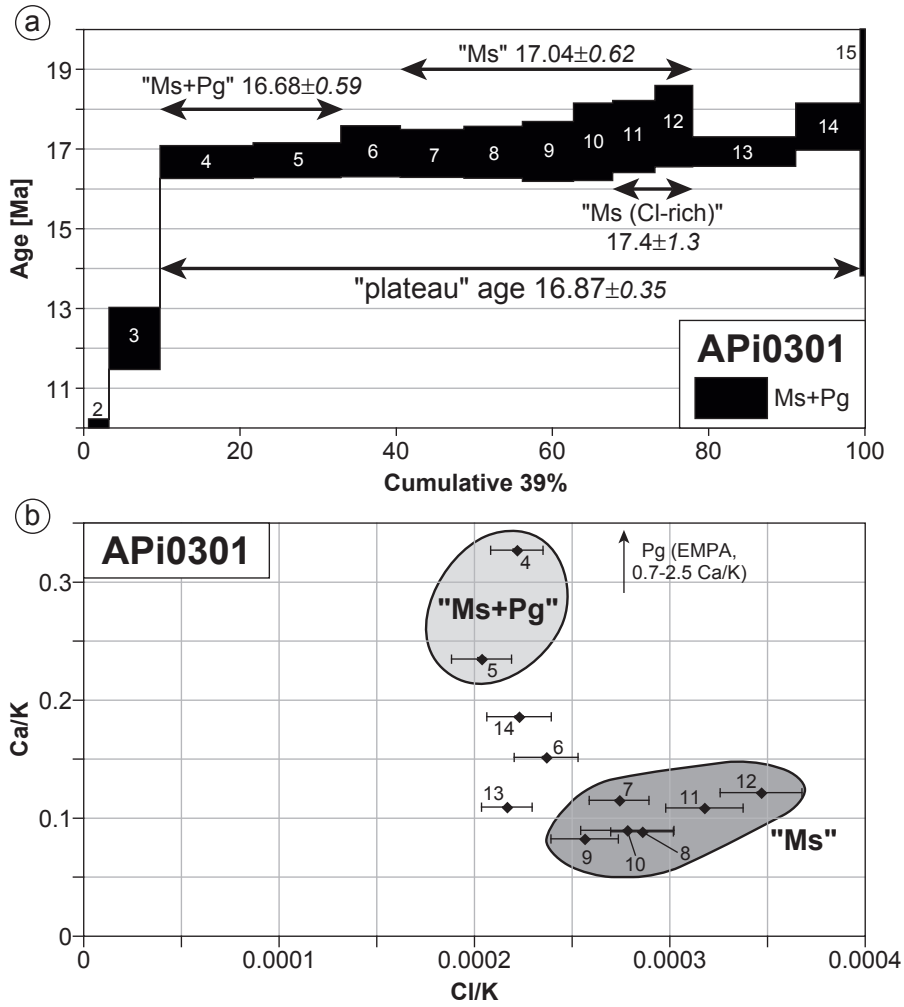

Fig. 2.11: (a) Age spectra for the white mica separate in the muscovite- and paragonite-bearing metapelite APi0301, apparently forming a "plateau" at 16.87±0.35 Ma. **(b)** The Ca/K versus Cl/K correlation diagram shows two distinct fields: one around 0.25 Ca/K (steps 4 and 5), identified as a signature for a mixture muscovite-paragonite, and corresponding to an age of 16.68±0.59 Ma; one with low Ca/K < 0.13 and Cl/K > 0.00025, associated to muscovite degassing (steps 7 to 12). The average age of steps 7-12 suggests that muscovite is slightly older than paragonite. Steps 13 and 14 may reflect an increase of paragonite influence after muscovite is outgassed.

40% of the total-^{39}Ar release and yields an age of 15.18±0.70 Ma (Ms100, #2) and 16.42±0.88 Ma (Ms200, #2; Table 2.3; Fig. 2.12a) at low Ca/K and Cl/K values (Fig. 2.12b). Notice that the step #3 of Ms100 yields the lowest Ca/K and 15.99±1.20 Ma. The age difference may be viewed as a difference between muscovite-richer (Ms100) or –poorer separates (Ms200; Table 2.3b,c), but no clear trend is observed in Ca/K versus age diagram. Therefore the age difference may also derive from a grain-size effect (see discussion below).

Biotite results in Val Piora are constantly younger than white mica separates (Table 2.3d; Fig. 2.13a,b). In APi0601 and 03, coarse fractions yield an isochemical (low Ca/K, low Cl/K; Fig. 2.13c) age of 14.84±0.23 and 15.29±0.25 Ma, respectively, while fine fractions yield 14.85±0.21 and 14.72±0.26 Ma. The ages of fine and coarse fractions are in the error identical in APi0601, whereas their difference in APi0603 is 0.59±0.33 Ma. In separate Bt100 of APi0603, two clusters of points are identified in a Cl/K-Ca/K correlation diagram (Fig. 2.13c), suggesting the existence of two biotite generations having different chemical composition, but texturally distinct biotite generations can only be identified by electron microprobe and not in thin section. The anti-correlation between Fe* and Cl-content in different biotite grains suggests the existence of two chemically distinct generations with higher Cl and lower Fe* concentrations (700-1800 ppm against < 200 ppm and 0.345 % against 0.370 %, respectively). No age difference is recorded by these chemically different biotites: steps 3-5 (having Cl/K = 0.0004 to 0.0005 and Ca/K = 0.09 to 0.11) yield 14.71±0.49 Ma, while steps 6-8 (having Cl/K < 0.00025 and Ca/K = 0.06 to 0.10) give 14.74±0.30 Ma. This implies either a co-genetic growth of Cl-rich and –poor biotite or a concomitant resetting of all grains independently of chemistry.

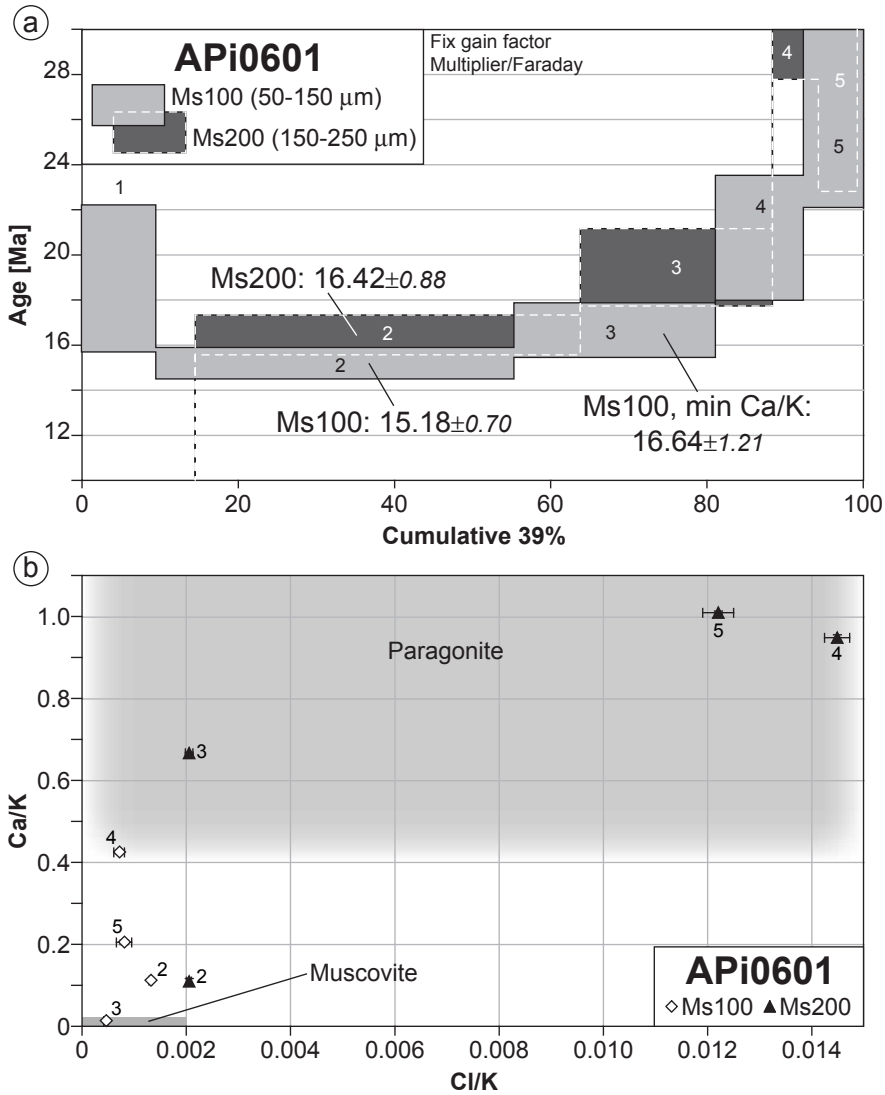

Fig. 2.12: (a) Age spectra for white mica separate in the paragonite-rich metapelite APi0601. **(b)** Ca/K versus Cl/K diagram. As expected from the paragonite-rich character of both white mica separates, Ca/K is extremely variable, reaching values in agreement with paragonite composition (Ms200) or slightly below (Ms100). Due to a more pronounced presence of muscovite in Ms100, Ca/K value tends towards the expected muscovite composition.

2.8.3.3) Molare

In AMo0409, isochemical steps yield 17.85±0.61 Ma and 16.25±0.81 Ma for muscovite and biotite separates, respectively (Table 2.3d; Fig. 2.14a,d,e). AMo0410 records the highest equilibrium-T (Table 2.2). Muscovite separate yields an apparently older age, reaching 18.35±0.59 Ma in steps 4, 6 and 7, while steps 5 and 8 to 10 are younger, 16.89±0.60 Ma (Table 2.3d; Fig. 2.14b,d). As only Faraday measurement was available during analysis series Ar-B, errors are larger compared to other analysed samples. Nevertheless, in a Ca/K versus age diagram, a clear negative trend exists toward a younger phase at Ca/K > 0.1 most likely corresponding to the circa 5% paragonite (Table 2.3b). Actually, the K-content recalculated from the total ^{39}Ar suggests that more paragonite is present in mineral separate (Table 2.3c). The finer grain-size of paragonite in thin section compared to muscovite is most likely the source of underestimation of paragonite content by XRD peak ratio and a few tenth percent or more could effectively be present in the mineral separate. Extrapolation toward the composition of paragonite as determined by EMP, Ca/K = 0.25, yields 13.3±2.3 Ma (Fig. 2.14c). In AMo0410, Ar-release from biotite yield a very discordant spectrum, which we attribute to the high chlorite content in the separate (peak ratio Chl/Bt 2.6%; Table 2.3b). Ca/K and Cl/K are significantly variable (Fig. 2.14e), but no correlation exists with the age variation. The two most gas-rich steps have the lowest Ca/K and low Cl/K ratio; it is also noted that these two steps correspond to the two major ^{39}Ar-release peaks (Fig. 2.7h), and thus probably do reflect the degassing of biotite

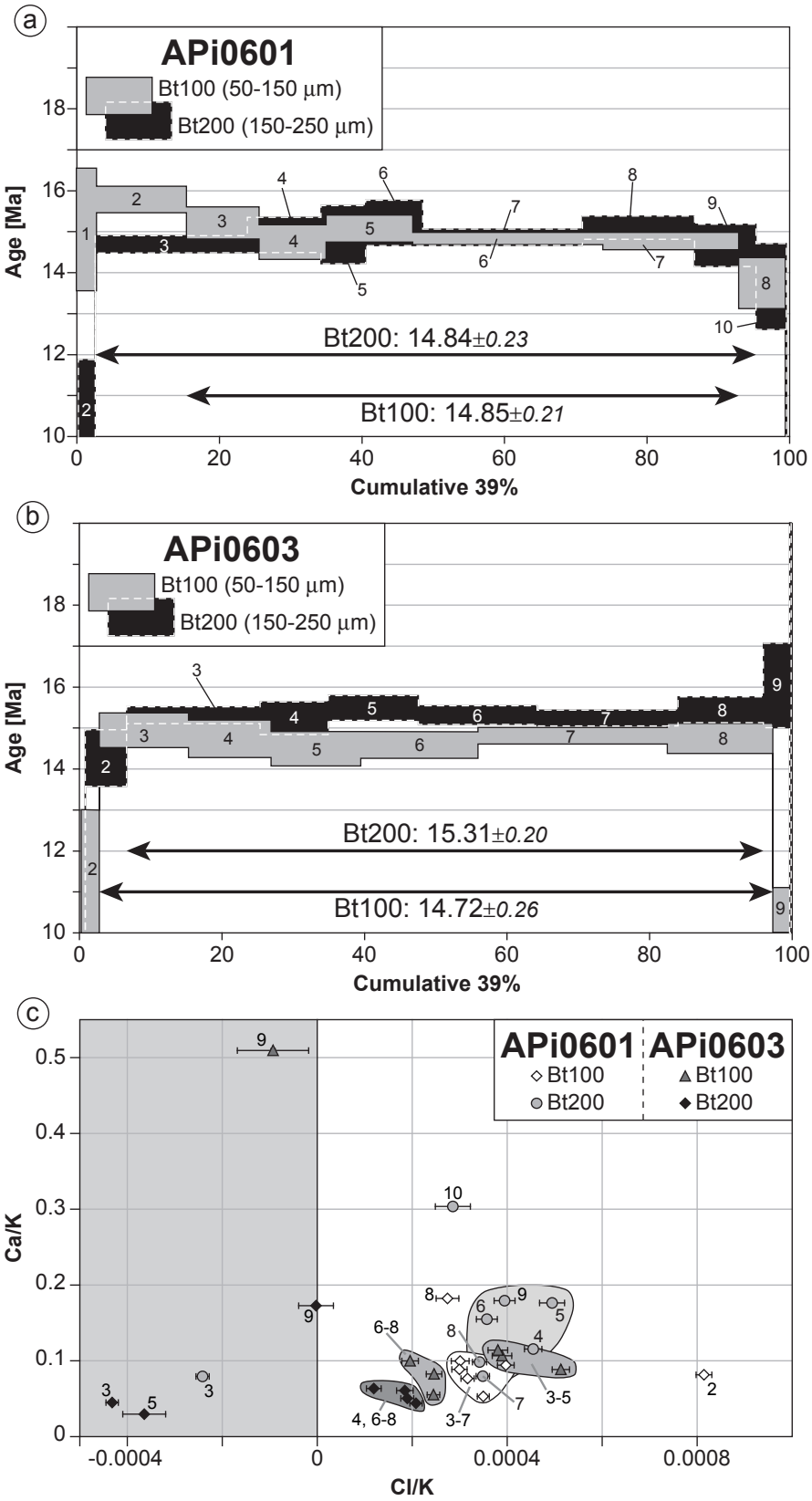

Fig. 2.13: Ar-results for biotite separates from west Val Piora. **(a,b)** Age spectra for biotite separates in metapelites **(a)** APi0601 and **(b)** APi0603. **(c)** Ca/K versus Cl/K correlation diagram. All analysed mineral separates yield low Ca/K, but slightly variable Cl/K, which possibly translates the presence of different biotite generations in both samples. Nevertheless, no age difference is obtained over these two clusters of steps.

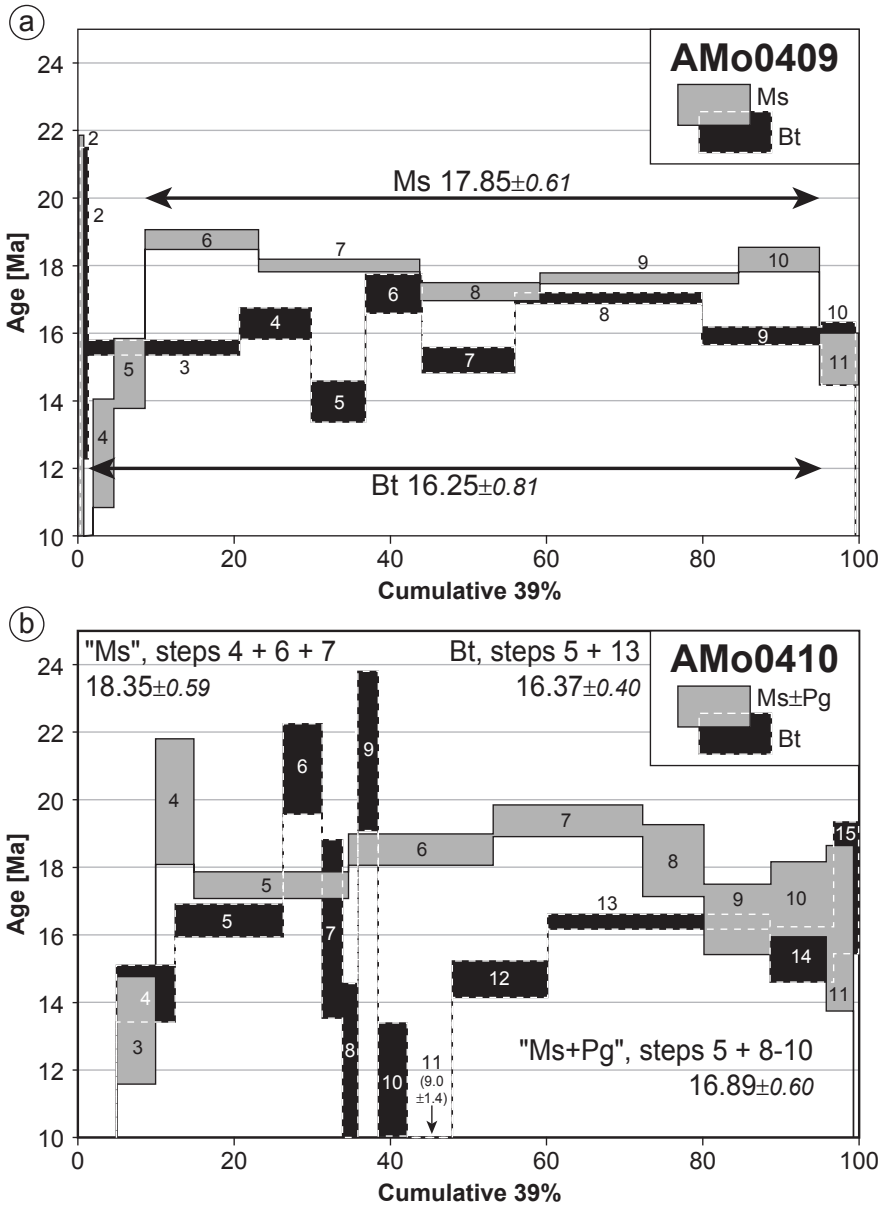

Fig. 2.14: Ar-results from Pizzo Molare. **(a,b)** Ar-Ar spectra for muscovite and biotite separates from **(a)** AMo0409 **(b)** and AMo0410. In this later, the convex shape of muscovite analysis indicates the mixture between two different white mica populations, while the strong chloritization of biotite is responsible for the discordant spectrum of biotite.

sensu stricto. They yield an isochemical age of 16.59±0.43 Ma, coherent with the biotite age from AMo0409, collected in immediate proximity (Fig. 2.1).

2.8.3.4) Summary Ar-results

In three out of five samples where two grain-size fractions were analysed in immediate succession and with both faraday and multiplier collectors (Ar-C series) we observed younger ages in the smaller grain-size fractions: muscovite ALu0601, paragonite APi0601, and biotite APi0603. Age differences are 0.36±0.30, 1.24±1.12, and 0.59±0.33 Ma, respectively. Diffusion would normally be invoked to explain this phenomenon. If diffusion is the only control for the apparent age of mineral grains, then Dodson's approach is applicable (Dodson, 1973; Dodson, 1986). It predicts that all grains are isotopically zoned; large ones are on average older than small ones. While in principle this only holds true if both sizes are no larger than the "effective diffusion grain size", in reality this is

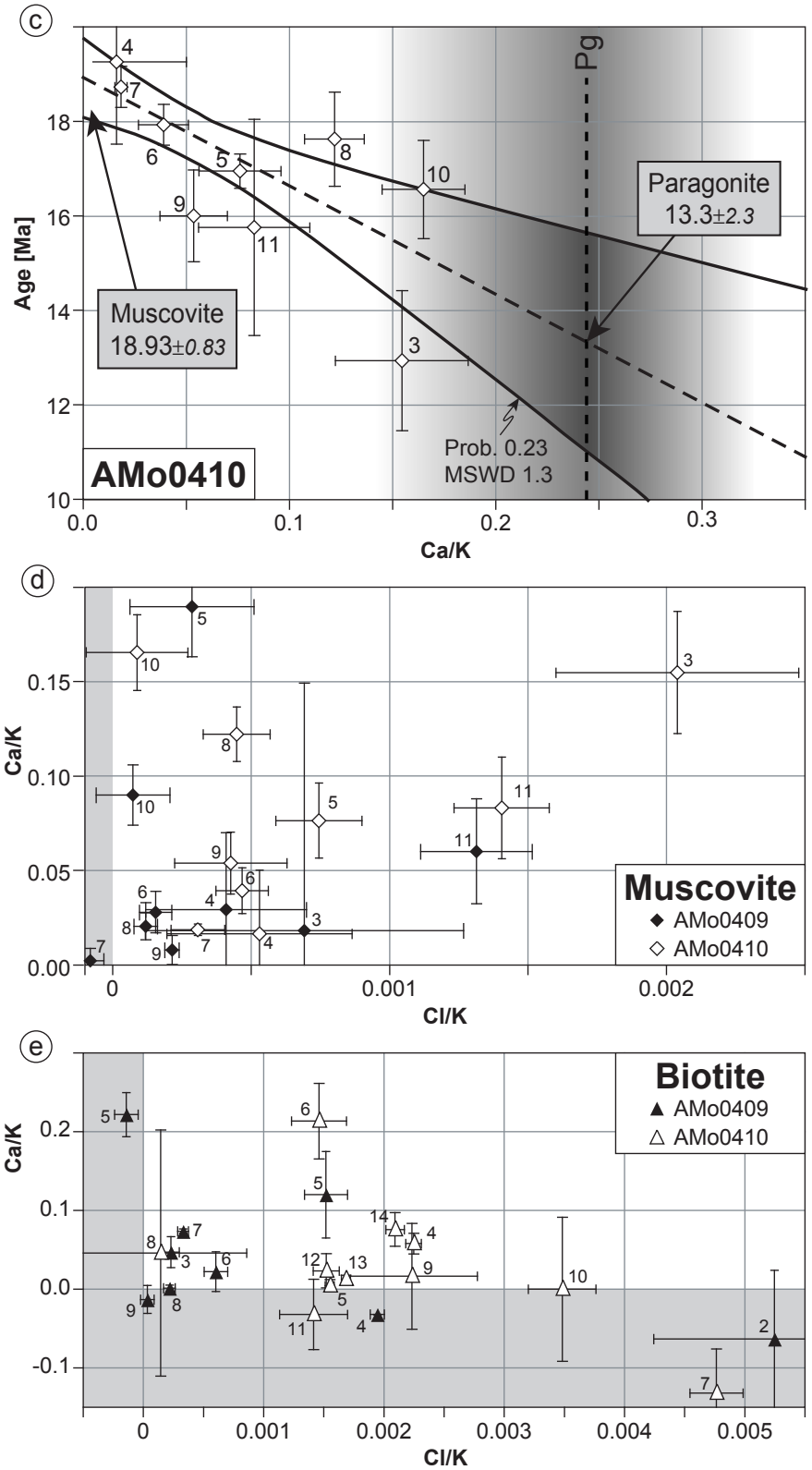

Fig. 2.14: (continued) **(c)** Ca/K versus age correlation diagram. Two major Ar-reservoirs are identified, a young Ca-richer paragonite and an older, Ca-free muscovite. In order to estimate the paragonite age, we extrapolated the correlation line (shown here with its error envelope) toward the Ca/K value in paragonite directly determined by EMP (grey field, depicting EMP uncertainty). White points are steps excluded for age-extrapolation. **(d,e)** Ca/K versus Cl/K correlation diagram **(d)** for muscovite and **(e)** biotite.

always the case, as it was demonstrated that the diffusive grain size of micas coincides with the crystallographically coherent grain-size (Onstott *et al.*, 1991). The apparent relevance of subgrain "domains" in biotite was shown to be due to a misunderstanding of statistical data (see discussion in Villa & Puxeddu, 1994). Sieved grain size fractions are thus expected to show an age difference, albeit to a subdued extent with respect to that of the natural grains. By grinding a large (old) grain, the resulting smaller grains will be both older and younger than the original grain, reflecting Dodson's zoning (Dodson, 1986). Thus, the finer sieve size will contain both whole small, young grains and fragmented large grains, whose sum is exactly as old as the coarser grain size.

If diffusion were the only process affecting mineral ages, one would expect it to be operating in all samples and not just in a few. Rather than explaining why some samples do not follow Dodson's predictions, we should ask what other geological process might have mimicked diffusion and caused small grains to be on average younger that larger ones. One possibility could be the existence of two distinct grain-size generations. This might be the case for biotite, which often shows large and oblique books coexisting with synkinematic and finer flakes. However, for white micas this is an unlikely explanation, as only one synkinematic white mica generation is observed. Another explanation could be admitting a continuous nucleation and growth of micas around the thermal peak and over a certain time-interval (e.g. 0.5 Ma). Each mica flake will thus crystallize at a different time, the distribution of grain size reflecting the length of the growth interval and the distribution of ages reflecting the growth rate.

Ages summarized in Table 2.3c were determined on steps yielding a plateau in the ^{39}Ar spectrum and typically match isochemical steps in monomineralic separates. When two white micas are present in the mineral separate, the Ca/K is typically variable. An extrapolation of the age towards the electron microprobe Ca/K value for muscovite, paragonite or margarite is used to determine the "true" age of each phase composing the mineral separate (Table 2.4). Sometimes, two or more white micas separates are combined to enhance the extrapolation and confirms the general trend observed in a single mineral separate. However, such extrapolation does not take into account of the possible age difference related to the grain-size (up to 0.5 Ma difference).

Typically, ages for muscovite determined in Ar-spectrum are usually identical than ages resulting from extrapolation at Ca/K = 0, though that somehow younger in APi0301 and AMo0410 (–0.31±0.97 and –0.58±1.02 Ma). In sample ALu0306 from Lucomagno Pass, muscovite, margarite and biotite yield statistically indistinguishable ages around 18-17 Ma. Slightly younger, but mutually equal, ages are also recorded within muscovite and paragonite from sample ALu0603 in SE Lucomagno. Paragonite APi0603 from Val Piora gives a much younger age, 13.8±1.3 Ma, against 15.8±0.1 Ma for the coexisting muscovite. Similarly, the two-white-mica-bearing sample from Pizzo Molare, AMo0410, has an isochemical muscovite age of 18.93±0.83 Ma, while the extrapolation toward Ca/K of paragonite yields 13.3±2.3 Ma. There is thus an increasing age difference between paragonite and muscovite from Lucomagno (-0.09±0.30 Ma), Val Piora (2.0±1.3 Ma) up to Pizzo Molare (5.6±2.4 Ma; Table 2.4). The age difference between biotite and muscovite is also increasing from N to S, but less than the muscovite-paragonite difference. The lowest grade sample yields indistinguishable ages for muscovite and biotite (ALu0306) and 0.48±0.23 Ma difference (APi0603). At Pizzo Molare, muscovite and biotite differ by 1.6±0.9 and 2.3±0.9 Ma in AMo0409 and –10, respectively.

Biotite separates usually also yield concordant age spectra. Only AMo0410 shows a strongly disturbed age spectrum. This is one of the most chloritized biotite separates according to XRD (Table 2.3b). We propose that chlorite is responsible for the large age-variation between steps. It is important to point out that chlorite from this sample is a retrograde phase (see above) and forms small interlayer inside biotite. In contrast, in samples ALu0306 and APi0601 chlorite is a stable phase and occurs as relatively large flakes (> 5 µm). Even if these samples have similar bulk chlorite contents as AMo0410, their age spectra are much less discordant. Thus, primary (peak) and secondary (retrogressive) chlorite occurrences have different effects on ^{39}Ar-^{40}Ar systematic. It is only

Table 2.4: Summary of ^{39}Ar-^{40}Ar ages attributed to each mica, including extrapolations from Ca/K-age diagrams for paragonite and margarite. Column "Ca/K" indicates the electron microprobe value assumed for the regression.

Sample		Age from Ar-spectrum	Age from extrapolation…	…at Ca/K	MSWD	Prob.	Age difference
ALu0306	Ms	18.04 ± 0.78	18.04 ± 0.80	0.00	0.28	0.99	1.0 ± 2.0
	Mrg	-	17.1 ± 2.5	65			
ALu0603 *	Ms	"100" 16.67 ± 0.39 "200" 16.36 ± 0.22	16.34 ± 0.23	0.00	0.31	0.98	-0.09 ± 0.30
	Pg	-	16.43 ± 0.20	0.84			
APi0301	Ms	16.87 ± 0.60	17.18 ± 0.76	0.00	0.21	0.993	2.3 ± 5.7
	Pg	-	14.9 ± 5.60	1.58			
APi0603	Ms	15.88 ± 0.15	15.79 ± 0.11	0.00	1.14	0.27	2.0 ± 1.3
	Pg	-	13.81 ± 1.30	1.02			
AMo0410	Ms	18.35 ± 0.59	18.93 ± 0.83	0.00	1.3	0.23	5.6 ± 2.4
	Pg	-	13.3 ± 2.3	0.24			

(*) Excluding step 5 of Ms200.

the secondary retrogression reactions that perturb the isotope record. Moreover, the finer gain size of secondary chlorite produces recoil artefacts during irradiation (Di Vincenzo *et al.*, 2003). The odd isotopes ^{37}Ar and ^{39}Ar have a recoil distance orders of magnitude longer than the even ones, artificial $^{38}Ar_{Cl}$ and radiogenic ^{40}Ar (Onstott *et al.*, 1995; Villa, 1998a). This makes it straightforward to identify a recoil artefact by using three-isotope correlation diagrams having ^{39}Ar as the common denominator and even and/or odd isotopes as numerators. In an even-even diagram (age vs Cl/K), ^{39}Ar recoil into chlorite will manifest itself as a (spurious) correlation line. The diagnostic feature that allows to distinguish a recoil pseudo-correlation from true binary mixing is that the latter can have any slope, while the recoil depletion/enrichment of the common denominator must produce equal relative enrichments/depletions on abscissa and ordinate (see e.g. Villa & Buettner, submitted; their Fig. 2.5). On the contrary, in an even-odd diagram (age versus Ca/K or Cl/K versus Ca/K) the ordinate will be much more weakly anti-correlated to the Ca/K ratio. Such trends are only weakly observed in biotite separate from AMo0410 and the increasing Ca/K ratio in quite all steps except #5 and 13 remains currently unresolved by recoil artefacts. However, this does not exclude the possibility of a strong Ar-loss during chloritization and possible recrystallization of biotite.

The diagnostic pattern of an irradiation artefact is not observed in any of the other mica separates, which consist of large and essentially pristine flakes. At thin section scale and after observation during handpicking, chloritization is very subordinate and only traces are revealed in XRD; therefore, we consider it as minor in our mineral separates. A more precise quantification of this effect would require a TEM study to investigate the crystal structure of all our samples at nm-scale (e.g. Kogure & Banfield, 2000), as also the possible interlayering of muscovite and paragonite. The latter has been documented to occur at lower grade (Livi *et al.*, 1997), but such fine-grained muscovite-paragonite association is apparently no longer present in amphibolite facies, when white micas coarsen to form distinct and large grains (Fig. 2.2a). It is also not identified at the micrometer-scale (BSE imaging, homogeneous muscovite and paragonite electron microprobe analyses).

2.9) PT- time model for mineral evolution

We discuss here the relation between petrography, the state of equilibrium of each sample and the possible progress of some retrogression reaction. This appears to be a necessary step to have a better understanding of age-results.

Diffusion of Ar occurs, but is clearly not able to account alone for the observed mica age variations. We document that metamorphic reactions occurring during decompression or retrogression, wherever they occur, are a more efficient way to achieve loss of Ar and age rejuvenation. Net transfer reactions, like the previously presented prograde and peak reactions, can be quantitatively approached using THERIAK-DOMINO. The stability of micas and chlorite over a certain PT-area is notably of most relevance for this study. A variation of metamorphic conditions (P, T, fluid, bulk rock composition) is always accompanied by a change in mineral stability. This can be translated by a possible change of a) mineral chemistry, e.g. chemical reequilibration, chemical zonation with preservation of growth stage; b) modal abundance of each phase, e.g. progressive disappearance of paragonite or margarite in profit of plagioclase, reaction of biotite or white micas to form staurolite or kyanite; c) fluid composition, e.g. internal change in H_2O-CO_2 fraction according to dehydration or decarbonatation reactions; d) local rock composition, e.g. metamorphic segregation and porphyroblast growth. As shown through petrography between Lucomagno and Molare samples, paragonite is progressively consumed in the small PT-range considered here (6-8 kbar, 500-600 °C) and chlorite is firstly stable (prograde), but may later come back as a retrograde product of biotite (chloritization). Every time such retrogressions take place, they will induce loss of incompatible Ar from micas at a much faster rate than diffusion. As we discussed previously, all samples of this study present a well-equilibrated texture. TWQ calculations do not show large disequilibria. We thus expect only small retrogression occurring near the thermal peak, which are possibly irresolvable with TWQ.

2.9.1) Mica stability

Near PT of equilibrium determined in samples from Lucomagno, paragonite reacts to form plagioclase and can be completely consumed at slightly higher-T or lower-P throughout this dehydration net-transfer reaction:

$$Pg + Qtz \Rightarrow Ab + Ky + H_2O \tag{2.5}$$

As suggested by petrology, paragonite remains stable with plagioclase (Figs. 2.6, 2.11a,b). Within this interval of 50°C, paragonite, plagioclase and muscovite are likely to continuously re-equilibrate with exchange reaction (Ca-Na or Na-K exchange):

$$Pg_{Na} + Pl_{Ca} \Leftrightarrow Pg_{Ca} + Pl_{Na} \tag{2.6}$$

$$Pg_{Na} + Ms_{K} \Leftrightarrow Pg_{K} + Ms_{Na} \tag{2.7}$$

Note that reactions 5 to 7 are easily rewritten for margarite instead of paragonite. Unfortunately, a thermodynamic model for Ca-Na-K micas is missing in both THERIAK-DOMINO and TWQ. Margarite is considered as a pure phase and only the Na-K exchange between muscovite and paragonite is investigated. The determination of a ternary thermodynamic model for white micas would require more work with regard to the composition and the stability of paragonite and margarite. From the numerous microprobe analyses from our white-mica collection, the similitude with the ternary feldspar model is obvious (Fig. 2.3a): minor Ca and K comprises in Na-mica (0.4 to 1.2% each), minor Na and traces of K in margarite. Like muscovite and paragonite, a miscibility gap between margarite and paragonite exists, but remains currently badly constrained (Franz, 1977).

From simple petrological observation, the first plagioclase is not a pure anorthite. Na-component is found in the former coexistence of paragonite and margarite (Frey, 1969; Livi *et al.*, 1997). Both white micas could play together and leave after reaction completion another white mica of different chemistry (x, y from 0 to 1):

$$Mrg + Pg + 2\ Qtz \Rightarrow (Ca_x, Na_{1-x})\text{-}Pl + (Ca_{1-x}, Na_x)\text{-}mica + 2\ Ky + 2\ H_2O \quad (2.8)$$

The destabilization of margarite can thus explain the An-richer plagioclase found in equilibrium with paragonite (e.g. ALu0603, AMo0410). The occurrence of An-richer core in plagioclase from APi0601 is further explained by a first stage of plagioclase growth from margarite, paragonite and carbonate reaction (Ca-rich core; reaction 2.8). After margarite-breakdown, the progressive disappearance of paragonite near the thermal peak involves a large release of Na essentially profitable to plagioclase (Na-richer rim; reaction 2.5). Kyanite from sample collection presented here is essentially resulting from partial destabilization of paragonite (reaction 2.5) and probably margarite, too (reaction 2.8). Kyanite is often intimately related to (Ca,Na)-micas in thin section, while muscovite remains stable and is only slightly affected by kyanite growth. As its stability is usually restricted to high-P field (> 8-10 kbar at unit water activity), kyanite is most likely to grow on the prograde path at thermal peak of equilibrium, near or slightly below the pressure climax. In contrary during decompression, GASP (reaction 2.2) may reasonably cause the total disappearance of kyanite, accompanied by reduction of grossular-component in some Al-rich samples (e.g. APi0301). Adding chlorite or biotite as reactant will produce staurolite and some muscovite instead of kyanite (e.g. ALu0603).

Looking at white mica chemistry, we note that most of the slight variations (±0.03 xK or xNa or xCa; Fig. 2.3a) are related to both subtle reequilibration around equilibrium-PT and to analytical errors. Only an inter-sample comparison reveals significant changes and is correlated with an increase of the metamorphic grade. From lowest (Lucomagno) to highest grade considered here (Pizzo Molare), muscovite present a regular increase of Na-content notably when it coexists with paragonite. This effect is minor in paragonite-free metapelite (ALu0601, AMo0409) or metamarl (ALu0306; Fig. 2.3a), where Na-content of bulk rock composition is among the lowest. In parallel, paragonite is progressively losing Ca in profit of K (Fig. 2.3a). The change in chemistry in paragonite is fully related to the first oligoclase (An_{20-30}) appearing in those lithologies. This is due to reequilibrium between paragonite and plagioclase upon the completion of reaction (2.5):

$$Pg_{Ca,K} + Pl_{Na,K} \Leftrightarrow Pg_{Na,K} + Pl_{Ca} \quad (2.9)$$

The small release of K from the reactant paragonite and albitic plagioclase is probably essentially accommodated in the product paragonite. Note that reaction (2.9) can also explain the formation of an An-richer core in plagioclase of APi0601 during the early stage of paragonite-resorption, though this effect is probably less important than a huge Ca-release from a former margarite.

Margarite present in Ca-rich metapelites (e.g. ALu0304, –06; Appendix 2.1) is also reacting to form plagioclase. According to reaction (2.8), the former occurrence of paragonite together with margarite is the most probable explanation for the higher Na-content in plagioclase compare to margarite. However, it is more difficult to balance the Al-release from plagioclase-formation in metamarl ALu0306. No Al-rich phase is found, but rock is full of chlorite and biotite. As suggested in PT-grid of ALu0306 from THERIAK-DOMINO (Appendix 2.3), the tschermak exchange in chlorite is likely to accommodate this Al-release. We therefore suggest the two following prograde reactions (non-soichiometric) stemming from THERIAK-DOMINO to explain a) the first appearance of plagioclase coexisting with margarite and b) the following disappearance of Ca-mica at slightly higher-T:

$$\text{a) } Ms_{Ms} + Chl_1 + Cc + Qz + Fluid\ (1) \Rightarrow Ms_{Cel} + Chl_2 + \mathbf{Pl} + \mathbf{Mrg} + Fluid\ (2) \quad (2.10)$$

$$\text{b) } Ms_{Ms} + Chl_1 + \mathbf{Mrg} + \mathbf{Pl_{Ab}} \Rightarrow Ms_{Cel} + Chl_2 + \mathbf{Pl_{An}} + H_2O \quad (2.11)$$

Ms_{Ms} design muscovite and paragonite component in muscovite, while Ms_{Cel} stem from celadonite-component. Similarly, Pl_{Ab} describe the albite-component and Pl_{An} is anorthite-component in plagioclase. Chl_1 and Chl_2 are

two chlorite of nearly similar Fe* (depending on the produced celadonite-component in muscovite), but Chl_2 has to be distinguishingly richer in Al (amesite-richer according to chlorite model from Hunziker, 2003). Fluids (1) and (2) stem for a change in H_2O-CO_2 fluid composition in equilibrium. Exact composition depends on the amount of hydrous or carbonaceous phases produced or consumed, but typically evolves toward higher CO_2 composition (reaction 2.10). Note also that carbonate is an ankerite. The effect on PT-condition of reactions involving ankerite instead of calcite or dolomite is unknown. According to THERIAK-DOMINO, those reactions are completed with pargasite as product at high xH_2O (circa 0.93) or dolomite as reactant at higher xCO_2 (circa 0.85). According to the large amount of ankerite present in ALu0306, a higher CO_2 is likely.

Biotite coexists with chlorite exclusively around Lucomagno Pass (e.g. ALu0306) and in a few samples from Val Piora (e.g. APi0601), in typically Mg-richer samples (≥ 0.40 Fe*). In staurolite-rich samples, chlorite and biotite are both completely consumed (ALu0601, –03, APi0301). In such cases, retrogression might induce a reappearance of biotite or chlorite during retrogression as indicated by small garnet resorption rim replaced by biotite and seldom chlorite. Further south, biotite stability within other samples from Val Piora and Lucomagno is clear (e.g. APi0601, –03). However, all such samples denote a partial chloritization: in thin section it is only seldom visible and localized in biotite cleavage; we essentially identified it by EMP (both in BSE images and by quantitative analysis), as also in XRD-spectra from all biotite separates. We now need to consider the mineral evolution of tri- and dioctahedral micas during retrogression and check whether those reactions are effective in our samples and to which extent.

2.9.2) Retrograde paths

PT-conditions determined in various samples from an area show a spreading principally interpreted in term of differential equilibration stage between each sample. Such variation has been previously interpreted in term of a retrogression path from circa 580 °C, 9-8 kbar up to 530, 5 (20 °C/kbar). Similar deduction is also effective in Molare area, at slightly higher-T (590 °C) and following a near-adiabatic decompression path (10 °C/kbar). From PT-grids of ALu0603 (Fig. 2.6), we now consider exclusively the plagioclase-in, paragonite-out and muscovite-out / K-feldspar-in reactions at unit water activity in Al-rich metapelite ALu0603 (Fig. 2.15a), and similarly with the Al-poorer metapelite AMo0410 (Fig. 2.15b). Including CO_2 in PT-calculation assesses the effect of a lower water activity. At 0.4 xH_2O, dehydration reactions involving micas occur at lower-T (-50 °C; Fig. 2.15a), with a weaker effect at low P in AMo0410 (Fig. 2.15b). In contrary and for the same changes of xH_2O, plagioclase-in reaction remains at similar PT-condition (± 20 °C). For similar xH_2O in AMo0410, the presence of carbonate at low-T increases the stability field of plagioclase and paragonite at higher-P, but reduces it at lower-P. Nevertheless, retrograde paths remain fully in the PT-stability field of plagioclase (Fig. 2.15a,b). More questionable is the stability of paragonite: retrograde path and PT-equilibria calculated with TWQ are both in the vicinity of paragonite-out reaction and may override it, notably in Pizzo Molare.

Though we always consider the complete mineral evolution along the retrograde paths, we first restrain the discussion to the modal and chemical evolution of muscovite, paragonite, quartz and plagioclase (Fig. 2.15c,d). Along PT-path in the Al-rich pelite, THERIAK-DOMINO predicts that paragonite is partially consumed and replaced by plagioclase, with a small amount of K liberated from this reaction and balanced by muscovite overgrowth (Fig. 2.15c). The Na-K composition of the remaining paragonite during the progress of reaction is recalculated by THERIAK. Only small changes are calculated along the retrograde path and values are higher than EMP measurement. Lower K and higher xAn are suggested by THERIAK compared to EMP. Paragonite from Pizzo Molare is nearly unstable and totally consumed by plagioclase formation. If decompression lasts,

muscovite also suffers partial resorption and reequilibration after the complete destabilization of paragonite, accompanied by growth of staurolite at pressure below 8-4 kbar (600-530 °C). Like in paragonite, the variation of mica chemistry suggested by THERIAK along decompression and cooling is small (Fig. 2.15d) and is of the order of the normal chemical variation measured by EMP (Fig. 2.3a,b). Small chemical changes in white micas related to such retrogression are thus impossible to identify, either by chemical analysis or by determination of equilibrium PT with TWQ. Very similar PT results in TWQ are calculated, whatever the xNa or xK content of muscovite or paragonite. Equilibria are essentially T-dependent and dominated by reactions involving Fe and Mg, so that disequilibrium involving white micas and plagioclase are hidden behind the large P-error in TWQ. Equilibria (2.3) and (2.4) are first calculated with muscovite (black line) and then with paragonite (grey line), but both equilibria yield nearly identical PT-condition (Fig. 2.5b,f,h).

Concerning the stability of biotite and chlorite, we already discussed the case of ALu0603, where biotite is most likely to occur during the decompression below 7.5 kbar with chlorite at lower T (Fig. 2.6 and 11a). Similarly in AMo0410, biotite is usually stabilized at T > 540 to 600 °C. Equilibrium-PT determined in our rock collection do not fall far away from the chlorite-in reaction at lower-T (Fig. 2.15b). Chloritization is thus likely to occur, providing a fluid-enhanced higher kinetic of reaction along the retrograde path. From petrography, this is obviously the case in all studied biotite, except perhaps the one, where chlorite is stable with biotite (ALu0306, APi0601).

Although not represented in Figure 2.15, some other minerals also show interesting retrogression features commonly observed in thin sections and are identified in PT-grids of ALu0603 (Figure 2.6). Staurolite grows already along the prograde path in ALu0603 and might continue along retrogression, notably during paragonite breakdown. In AMo0410, it grows later from the partial destabilization of garnet and muscovite. Garnet resorption would require a higher energy compared to some dehydration reaction. Even so, such effect is observed in ALu0601 and –03, where biotite and rare chlorite are rimming the resorbed garnet. According to the hydration character of this reaction, some fluid stemming from paragonite-breakdown or from a metamorphic fluid-percolation are necessarily involved. In AMo0410, the analytical cross-section in garnet reveals a small resorption indicated by an increase of spessartine and Fe* at the rim. Stronger chloritization and garnet resorption is observed in carbonaceous Bündnerschiefer from Pizzo Molare and Lucomagno areas, but is never observed in our sample collections. We argue for a resorption starting briefly before the thermal peak of metamorphism or during the early decompression.

In a broader view, we argue for a pronounced late reequilibrium process in paragonite and biotite from Molare area, somehow lower in Piora and quite inexistent in Lucomagno. Such retrogression (disappearance of paragonite, chloritization of biotite) is likely to happen near the thermal peak, probably at P ≈ 7 kbar, where kinetic of reaction is always high. As “dry” environments mostly preserve metastable parageneses in gross disequilibrium with prevailing PT (e.g. Bjørnerud *et al.*, 2002), retrogression necessarily required some fluid flow percolating during exhumation. The PT calculations presented previously have already suggested a differential equilibrium PT in a suite of samples from a narrow area, whereby the spread of calculated pressures between circa 9 and circa 6 kbar is interpreted as due to the degree of retrogression of each sample (e.g. Figure 2.15a,b). Each rock will suffer to different level the possible metamorphic reactions occurring between the maximum of pressure during the thermal peak maximum (not P_{max}!) and the decompression at high-T or during the early cooling history.

2.10) Cooling or (re-)crystallization age?

At the lower boundary of amphibolite facies, indistinguishable ^{39}Ar-^{40}Ar ages are obtained on muscovite,

biotite and margarite from a metamarl of Lucomagno Pass (ALu0306). Metapelites from SE-Lucomagno yield similar muscovite and paragonite ages. The Ca/K versus age diagram from sample APi0301 from Val Piora indicates that the extrapolated paragonite age is younger than muscovite by 2.3±5.7 Ma. An even younger paragonite is presumed in Pizzo Molare, where less than 10% paragonite disturbs the age spectrum of muscovite AMo0410. In this case, the extrapolated Ar-age for paragonite is younger by 5.6±2.4 Ma. Regarding biotite, ^{39}Ar-^{40}Ar ages are always younger than those in muscovite. The age difference between muscovite and biotite increases as the metamorphic grade increases from circa 550 to 600 °C and from 6 to 9 kbar. Moreover, the ^{39}Ar-^{40}Ar age in biotite is younger than in paragonite in APi0601, while in APi0603 and AMo0410 paragonite is younger. This age variation parallels an increase of the metamorphism. Considering the combined evidence from petrography and thermobarometry, and taking into account the ubiquitous retrogression reactions, can we decide whether we date

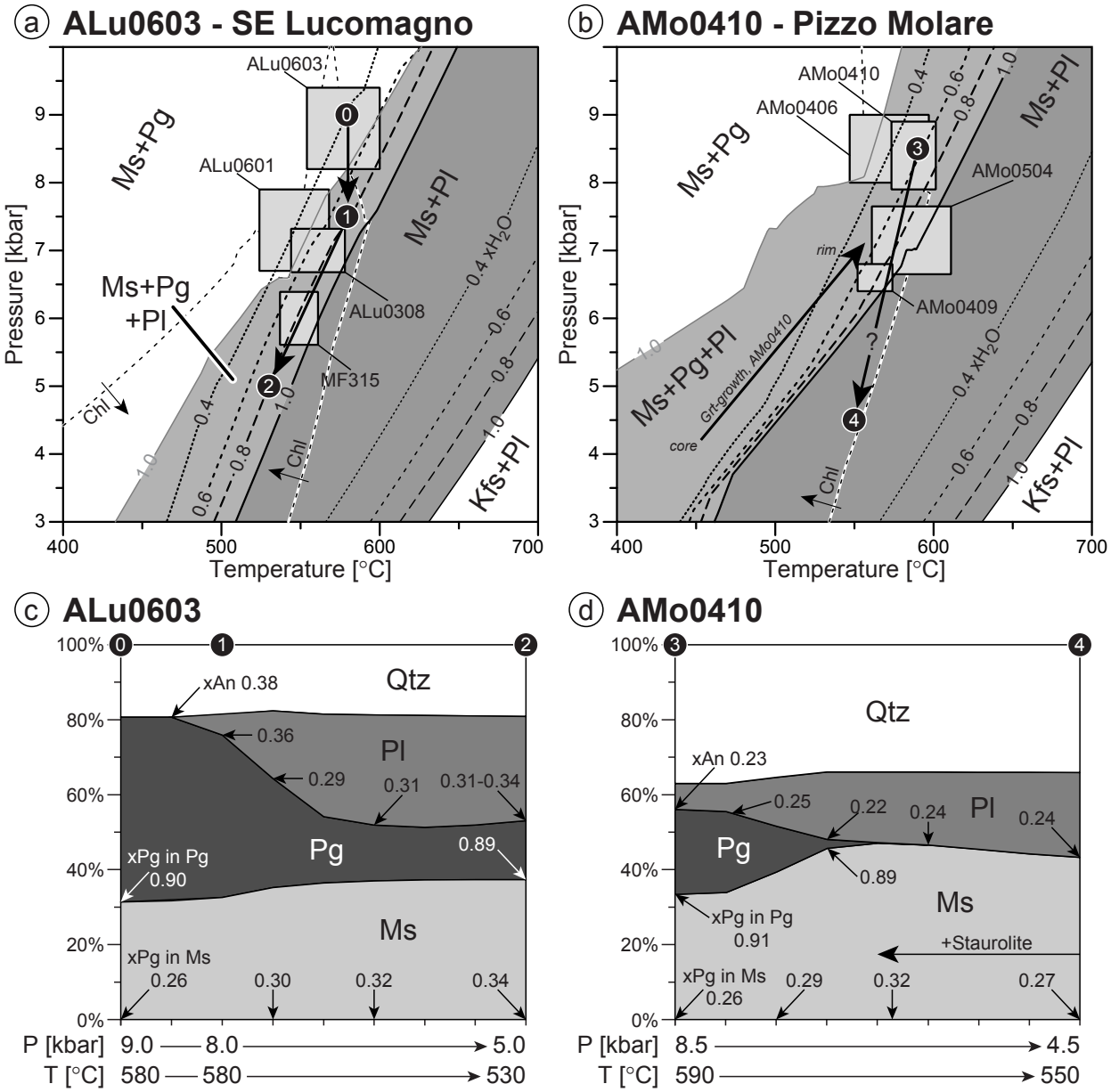

Fig. 2.15: (a,b) Stability of muscovite, paragonite, plagioclase and K-feldspar in Al-rich (ALu0603) and Al-poorer metapelite (AMo0410). Dashed lines stem from the variation of muscovite- or paragonite-out reactions at various H_2O-CO_2 fractions. Grey boxes are PT-results from TWQ relevant to each area (SE Lucomagno and Pizzo Molare). **(c,d)** Modal evolution of muscovite, paragonite, plagioclase and quartz along selected retrograde PT-paths as shown in (a) and (b). Numbers are mineral composition: paragonite-content in paragonite or muscovite and anorthite-content in plagioclase.

crystallization, cooling or recrystallization?

A partial recrystallization and/or exchange reaction (possibly fluid-enhanced) along the retrograde path induces chemical reequilibration and isotopic resetting. Whenever this happens, pure Ar diffusion is overwhelmed by the metamorphic reaction. The role of metamorphic reaction in controlling the isotopic record has been established for a long time (Chopin & Maluski, 1980; Wijbrans & McDougall, 1986; Villa, 1998b; Di Vincenzo *et al.*, 2004; Villa, 2004; Gouzu *et al.*, 2006; Glodny *et al.*, 2008a; Glodny *et al.*, 2008b). In this work, we document in great detail that the blanket term "white mica" hides a complex and variable petrogenesis and hence a multiply controlled isotope record. The growth of plagioclase from partial destabilization of paragonite or margarite is responsible for resetting the Ar record of these white micas in samples AMo0410 and to a less extent ALu0306, APi0301 and APi0603. Paragonite remains stable in SE Lucomagno area and has equilibrated with muscovite and plagioclase during the thermal peak of metamorphism. Retrogression is apparently subordinate or negligible in this sample and ^{39}Ar-^{40}Ar ages for both muscovite and paragonite are similar (Tables 2.3, 2.4). At Pizzo Molare and possibly in Val Piora (Table 2.4) the age attributed to paragonite differs from muscovite. Paragonite from Pizzo Molare is rare, but TWQ shows an apparent well-preserved equilibrium, though not perfect (Fig. 2.4g), between paragonite and other mineral of the assemblage. Along the retrograde path, samples from Pizzo Molare are likely to cross the paragonite-out reaction very briefly after or during the thermal peak of metamorphism. In contrary, the retrograde path suggested for the SE Lucomagno area remains in the stability of paragonite. The case of Val Piora is most likely to represent an intermediate case, where the rock survives a brief passage in the paragonite-out field. Considering biotite, the petrography as well as thermobarometry and mineral analysis demonstrate an omnipresence of stable chlorite in Mg-rich samples or later chloritization in Fe-richer ones. If biotite chemically reacts to form staurolite or chlorite during decompression or cooling, its Ar isotopic record will also be reset. Thermobarometry suggest that late chloritization of biotite along the retrograde path is possible at T < 550 °C. If a complete chemical reequilibration (major element and isotope resetting) between biotite and chlorite is reached, then biotite may date the chloritization event; if the reequilibration is incomplete, the biotite age will lie anywhere between the two events.

Of course, another explanation in addition to (in the absence of) reaction could be diffusion. A higher diffusivity in biotite compared to white mica would yield an age difference between muscovite and the less retentive biotite (corresponding to a lower "closure temperature"). However, we have shown the presence of biotite and white micas having indistinguishable ages at relatively high T (550 °C). This coincidence alone is not sufficient to resolve the long-standing question whether these samples show a practically complete Ar-retention, or whether the age agreement is fortuitous and geologically meaningless, or is evidence of extremely fast cooling. Supplementary information could be gained by using other nuclide pairs to date other minerals, such as U-Pb on monazite. In samples equivalent to APi0601 and ALu0603, alpine monazite growing near the thermal peak of metamorphism were found and dated (18-19 Ma; Janots *et al.*, in preparation; Janots *et al.*, in press). Reader will refer to Chapter 4 for a geological interpretation and discussion of Ar-Ar and U-Pb ages in term of PTt-path in the northern Central Alps. From this parallel paper, the age difference between muscovite Ar-Ar and monazite U-Pb is small and supports a high closure-T for Ar-diffusion in muscovite (> 450 °C). The general regional context encourages us to view the mica ages as very close to the metamorphic peak. On the other hand, the reductionist view consisting in denying validity to all ^{39}Ar-^{40}Ar ages could only be justified if one or two samples showed an exceptional monazite-muscovite-biotite identity or proximity, but certainly not if all samples analysed in sufficient detail conform to it. As for the viability of a "thermochronometric" interpretation of our data, we will show in the following discussion that it conflicts with the overall information available for our samples.

Next to some isochronous biotite-muscovite pairs, some other biotite samples are variably younger than the coexisting muscovite (up to 2.34±0.93 Ma at Pizzo Molare, the sample with the highest PT conditions, viz.

circa 590 °C and 8 kbar). A similar behaviour is observed between muscovite and paragonite Ar-ages, the age difference being again largest at Pizzo Molare, with a younger age for paragonite than biotite. A priori arguments (Dahl, 1996) predict very similar "closure temperatures" for pure Ar diffusion in muscovite and paragonite, both being higher than biotite. Our observations contradict this and imply that pure diffusion was not the sole cause of the measured paragonite ages. The estimates of "closure temperatures" for Ar diffusion in micas originally proposed by Purdy & Jäger (1976) are thus too low by at least 100 °C, because its proponents did not take into account the fact that diffusion will be overwhelmed every time retrograde (aqueous) processes take place, notably metamorphic reactions occurring anywhere along the retrogression path. In absence of inheritance problem, it is the oldest ages in a given field area that most closely approach the purely diffusive behaviour devoid of temperature-independent chemically open-system retrogression. Failing to take into account this fundamental principle may be the cause why indiscriminate averaging of ages obtained on variably preserved parageneses invariably leads to "closure temperature" estimates that are much too low. The literature already demonstrated that Ar retention in micas occurs at high temperature, exceeding 450 °C in biotite and 500 °C in muscovite (Villa, 1998b; Di Vincenzo *et al.*, 2004; Villa, 2006). Even higher "closure temperatures" were proposed for both biotite and white mica, provided the metamorphic environment was dry (Balogh & Dunkl, 2005).

It is worthwhile to note the relation between T and some major metamorphic reaction, such as biotite-in, chlorite-out and paragonite-out. Such similarity does of course not guarantee that complete chemical re-equilibration was achieved, and therefore that isotopic resetting was complete. Thus, the regional age pattern will be further perturbed by isotopic inheritance if the petrographic evidence of unequilibrated relics is neglected. Indeed, a higher Ar-retention in muscovite forces to recognize a more pervasive area possibly affected by inheritance. Some ages from the Aar massive and the Gotthard nappe could thus be affected by this inheritance problem, which may plague the geological interpretation of these ages (see §4.2).

2.11) Conclusions

We report petrological and geochronological observations on mica-bearing Mesozoic metasediments of the northern part of the Central Alps, between Val Piora, Lucomagno Pass and Pizzo Molare. Our detailed observations in thin section combined with precise thermobarometric calculations provide necessary information to identify the presence of equilibrium, disequilibrium or secondary reequilibration. Only a minority of our samples document satisfactory equilibration. Calculated peak pressures and temperatures vary smoothly between 590±20 °C and 7.7±0.7 kbar at Pizzo Molare and 560±20 °C and 6.2±0.2 kbar at Lucomagno Pass. PT-calculations allow the establishment of very sensitive mineral stability fields. Mostly micas from equilibrium parageneses were analysed; in some cases it was unavoidable to resort to samples whose PT trajectories during exhumation led them through mineral stability fields incompatible with the peak assemblage. We observed several examples of destabilization reactions, foremost chloritization of biotite and the resorption of paragonite to give feldspar.

Many analysed white mica fractions were shown by XRD and/or electron microprobe analyses to be mixtures of two white micas, muscovite with paragonite or margarite. Stoichiometry of micas recalculated from the ^{39}Ar-^{40}Ar-gas release was necessary for a quality control on the analysed separates. By using Ca/Cl/K-age correlation diagrams we were able to estimate ages for each white mica composing the mineral separate. Muscovites gave always the oldest ages, very close to the ages of monazite determined on different samples from nearby areas. Biotite and paragonite gave ages that were sometimes indistinguishable, sometimes significantly younger than muscovite. There is no simple, regular pattern of muscovite-biotite-paragonite age relations. We argue that it is the retrogression history of each individual sample, and not the regional temperature field, that has the decisive control

on the isotopic record.

Our age data are best explained in terms of a simple evolution. Amphibolite-facies metamorphism occurred no earlier than 20 Ma ago, probably around 19-18.5 Ma. Muscovite starts retaining Ar at peak conditions (560-590 °C) or immediately thereafter, in any case above 550 °C. Biotite retains Ar simultaneously with muscovite only in the lower-grade samples (560 °C) while it gives younger ages in the highest-grade samples. A simplistic consequence of these findings would be an upward revision of mica "closure temperatures". However, the problem is not whether micas kept at extremely high T will lose Ar. The real problem is if loss of Ar is strictly and only due to diffusion (and thus can be uniquely tied to temperature) or if instead retrograde reactions and recrystallization, two fluid-assisted processes, will overrun diffusion whenever they occur. Such retrograde processes are only vaguely related to P and T, as their limiting factor is rather fluid activity. Fortunately thermobarometry can help in identifying and quantifying such conditions. Upon cooling and decompression, samples along typical PT-paths generally encounter one of the reactions delimiting the stability of biotite, paragonite, and margarite, and this limit is crossed at relatively high temperature, hence reaction progress is likely to lead to local retrogression of these micas. Petrographic evidence for this is common at grain scale (chlorite specks and rims in or around biotite), but even where detectable only in the EMP analyses (e.g. low alkali contents in biotite formula), the data in this study show that the effect on Ar-Ar data is noticeable and usually exceeds the purely diffusional effect on Ar-ages. The same stands for paragonite and margarite, which are likely to form plagioclase. Through the increase of metamorphism, Ar-ages of paragonite are progressively firstly similar to muscovite (Lucomagno, 550-570 °C) but rapidly get younger at Molare (nearly 600°C), when PT-path crosses the paragonite-out reaction near or slightly after the equilibrium-PT conditions. By contrast, retrograde PT-paths, at least for metapelites and metagranitoids, remain within the stability field of muscovite all the way to the surface, except near hydrothermal veins. Diffusion is the fastest process only in the absence of chemical retrogression and fluid-assisted recrystallization. This condition is fairly exceptional and needs detailed petrological equilibrium tests to be demonstrated on a sample-by-sample basis. Only in these cases is the concept of "closure temperature" legitimate; our field-based calibration demonstrates that Ar is retained in equilibrium parageneses at very high temperatures: over 550 °C by muscovites, and circa 550 °C by biotites.

This work demonstrates the necessity of a detailed petrological and thermobarometrical study prior to any geochronological analysis. This is required to assess the equilibrium condition of the studied paragenesis, the presence or absence of retrograde reactions, the stability history of the analysed minerals, and the identification of the possible metamorphic reactions with consequent age resetting. Whenever a reaction occurs, it will overwhelm any pure volume diffusion of Ar or any other radiogenic isotope. Without this ground truth assessment, isotopic ages might be erroneously interpreted in terms of "cooling ages". The determination of the state of equilibrium in a mineral assemblage is thus a critical point for any geochronological investigation, as prograde and retrograde metamorphic reactions alike induce not only a reequilibrium of major elements, but also the resetting of isotopic systems.

Appendix 2.1: Bulk rock composition (XRF analysis) and representative average of several points (electron microprobe analysis, see following pages). Pts avg = number of points used for average. Complete set of analysis for each sample is available on CD.

Bulk rock composition (XRF)

Sample	ALu0306	APi0301	APi0601	APi0603	ALu0601	ALu0603	AMo0409	AMo0410
SiO2	60.58	51.42	62.56	50.69	55.17	45.80	63.14	59.29
Al2O3	13.87	30.65	20.41	33.20	27.68	34.12	17.68	21.92
TiO2	0.78	1.46	1.03	2.05	1.32	1.95	0.78	0.92
FeO	3.84	6.52	4.22	5.06	4.93	7.83	6.37	6.64
MnO	0.06	0.03	0.01	0.06	0.04	0.05	0.01	0.34
MgO	5.52	1.21	3.51	1.57	1.00	1.25	3.10	1.93
CaO	6.20	0.96	0.87	1.60	1.38	1.20	0.51	1.05
Na2O	0.79	2.63	2.42	2.47	1.00	2.57	1.30	2.26
K2O	1.48	2.52	2.07	1.22	4.25	1.96	5.24	3.10
H2O	6.51	2.18	2.20	1.30	2.30	2.10	2.23	1.83
Total	99.62	99.58	99.30	99.22	99.07	98.83	100.37	99.29

Appendix 2.1: (continued) Normalization: white micas 12 O + 2 OH; xCa, xNa or xK = (Ca, Na or K)/(Ca+Na+K).

Muscovite

Sample	ALu0304	ALu0306	ALu0601	ALu0603	APi0301	APi0603	AMo0409	AMo0410
Pts avg	9	9	21	29	12	35	17	46
SiO2	48.21	48.04	47.14	47.41	46.26	47.67	45.97	46.45
Al2O3	34.92	35.04	35.68	35.99	35.24	35.50	33.89	35.10
TiO2	0.32	0.20	0.33	0.32	0.27	0.25	0.41	0.34
FeO	1.49	1.60	1.02	0.88	0.90	0.95	2.84	2.06
MnO	<0.01	0.01	<0.01	<0.01	0.02	<0.01	<0.01	0.01
MgO	1.12	1.19	0.94	0.85	0.86	1.09	1.19	1.03
CaO	0.02	0.01	0.01	0.01	0.01	0.01	0.01	0.01
Na2O	0.48	1.04	0.59	1.05	2.04	0.93	0.83	1.80
K2O	10.23	9.82	10.06	8.83	8.64	9.00	10.43	8.75
H2O	4.59	4.60	4.47	4.50	4.41	4.53	4.46	4.51
F	<0.03	<0.03	0.15	0.12	0.15	0.07	0.01	0.03
Cl	<0.01	<0.01	<0.01	0.01	0.01	0.01	0.03	0.01
Total	101.37	101.55	100.41	99.96	98.82	100.00	100.06	100.10
Si	3.146	3.131	3.103	3.112	3.088	3.130	3.082	3.076
Al IV	0.854	0.854	0.897	0.888	0.912	0.870	0.918	0.924
Al VI	1.832	1.832	1.871	1.896	1.861	1.877	1.760	1.817
Ti	0.016	0.010	0.016	0.016	0.014	0.013	0.021	0.017
Fe2+	0.081	0.087	0.056	0.048	0.050	0.052	0.159	0.114
Mn	-	0.000	-	-	0.001	-	-	0.000
Mg	0.109	0.116	0.092	0.083	0.086	0.106	0.119	0.102
Ca	0.001	0.001	0.001	0.000	0.001	0.000	0.001	0.001
Na	0.060	0.132	0.076	0.134	0.263	0.118	0.108	0.231
K	0.852	0.816	0.845	0.739	0.736	0.754	0.892	0.739
Cations	6.951	6.987	6.957	6.917	7.012	6.920	7.058	7.022
H	2.000	2.000	1.964	1.971	1.962	1.983	1.994	1.992
F	-	-	0.035	0.028	0.036	0.017	0.002	0.007
Cl	-	-	-	0.001	0.002	0.001	0.004	0.001
xCa	0.005	0.001	0.001	0.000	0.001	0.000	0.001	0.001
xNa	0.065	0.082	0.082	0.153	0.263	0.135	0.108	0.238
xK	0.930	0.916	0.917	0.846	0.736	0.864	0.892	0.761

	Paragonite					Margarite		
Sample	ALu0603	APi0301	APi0601	APi0603	AMo4010	ALu0304	ALu0306	AMo0410
Pts avg	10	17	18	25	15	13	15	5
Comment								Incl. Grt
SiO2	45.75	44.29	45.49	45.72	46.13	32.22	33.12	31.82
Al2O3	40.92	40.50	40.63	41.27	40.10	50.74	49.60	50.85
TiO2	n.d.	0.10	n.d.	n.d.	0.11	0.08	0.10	0.11
FeO	0.46	0.29	0.58	0.26	0.86	0.44	0.46	1.04
MnO	<0.01	0.02	0.01	<0.01	0.04	<0.01	<0.01	0.17
MgO	0.08	0.08	0.37	0.09	0.08	0.13	0.40	0.18
CaO	0.97	1.58	0.99	1.13	0.35	11.24	10.01	9.90
Na2O	6.11	7.19	5.88	6.07	6.67	1.38	1.93	2.13
K2O	0.98	0.91	1.02	0.95	1.24	0.16	0.14	0.05
H2O	4.69	4.59	4.67	4.70	4.68	4.59	4.57	4.57
F	n.d.	0.08	n.d.	n.d.	<0.01	<0.01	<0.01	<0.01
Cl	<0.01	0.02	<0.01	<0.01	<0.01	<0.01	<0.01	<0.01
Total	99.97	99.64	99.63	100.19	100.25	100.98	100.34	100.81
Si	2.927	2.866	2.922	2.916	2.953	2.105	2.172	2.087
Al IV	1.073	1.134	1.078	1.084	1.047	0.854	0.854	1.913
Al VI	2.012	1.956	1.998	2.019	1.979	1.832	1.832	2.019
Ti	-	0.005	-	-	0.005	0.004	0.005	0.005
Fe2+	0.025	0.016	0.031	0.014	0.046	0.024	0.025	0.057
Mn	-	0.001	0.000	-	0.002	-	-	0.010
Mg	0.008	0.008	0.036	0.008	0.008	0.013	0.039	0.017
Ca	0.066	0.110	0.068	0.077	0.024	0.787	0.703	0.696
Na	0.758	0.902	0.732	0.751	0.828	0.174	0.245	0.271
K	0.080	0.075	0.083	0.077	0.101	0.014	0.012	0.004
Cations	6.950	7.072	6.948	6.946	6.993	7.030	7.035	7.079
H	2.000	1.981	2.000	2.000	2.000	2.000	2.000	2.000
F	-	0.017	-	-	-	-	-	-
Cl	-	0.002	-	-	-	-	-	-
xCa	0.073	0.101	0.077	0.085	0.025	0.820	0.724	0.717
xNa	0.838	0.830	0.829	0.829	0.868	0.168	0.261	0.279
xK	0.089	0.069	0.094	0.085	0.106	0.012	0.016	0.004

Appendix 2.1: (continued) Normalization: biotite 12 O + 2 OH, chlorite 10 O + 8 OH; Fe* = Fe/(Fe+Mg).

Biotite

Sample	ALu0304	ALu0306	ALu0601	ALu0603	APi0301	APi0601	APi0603	AMo0409	AMo0410
Pts avg	7	26	16	15	27	29	20	15	39
SiO2	36.12	38.91	37.20	37.48	37.73	37.89	37.58	36.15	36.78
Al2O3	19.11	19.12	19.35	20.13	19.21	19.90	19.28	18.91	19.40
TiO2	1.85	1.30	1.62	1.18	1.17	1.19	1.36	1.94	1.35
FeO	19.54	11.59	16.13	15.39	14.37	13.23	13.85	17.00	15.22
MnO	0.03	0.08	0.01	0.01	<0.01	0.01	0.01	0.01	0.03
MgO	9.74	15.78	12.10	12.37	13.95	13.93	14.14	11.54	13.30
CaO	0.02	0.05	0.01	0.01	<0.01	0.02	0.01	<0.01	0.01
Na2O	0.15	0.23	0.12	0.16	0.36	0.17	0.19	0.25	0.35
K2O	9.12	9.92	9.41	8.87	8.97	9.20	8.96	8.97	8.87
H2O	3.78	3.94	3.54	3.63	3.92	3.90	3.77	3.81	3.89
F	0.33	0.45	0.95	0.81	0.31	0.38	0.56	0.31	0.28
Cl	0.01	0.04	0.01	0.01	0.02	0.02	0.03	0.02	0.02
Total	99.80	101.40	100.46	100.05	100.01	99.84	99.75	99.57	99.49
Si	2.727	2.789	2.752	2.758	2.766	2.767	2.758	2.715	2.725
Al IV	1.273	1.211	1.248	1.242	1.234	1.233	1.242	1.285	1.275
Al VI	0.429	0.404	0.438	0.505	0.425	0.479	0.426	0.390	0.419
Ti	0.105	0.070	0.090	0.065	0.065	0.066	0.075	0.109	0.075
Fe2+	1.234	0.695	0.998	0.947	0.880	0.807	0.850	1.068	0.943
Mn	0.002	0.005	0.001	0.001	-	0.000	0.000	-	0.002
Mg	1.096	1.686	1.334	1.356	1.524	1.516	1.547	1.292	1.469
Ca	0.001	0.004	0.001	0.001	-	0.002	0.001	0.000	0.001
Na	0.021	0.031	0.018	0.023	0.052	0.024	0.028	0.036	0.050
K	0.878	0.907	0.887	0.832	0.838	0.857	0.839	0.922	0.838
Cations	7.767	7.802	7.767	7.731	7.785	7.752	7.766	7.817	7.797
H	1.906	1.883	1.744	1.784	1.915	1.897	1.847	1.911	1.922
F	0.093	0.112	0.254	0.215	0.081	0.100	0.149	0.086	0.075
Cl	0.001	0.005	0.002	0.001	0.003	0.002	0.004	0.003	0.003
Fe*	0.530	0.292	0.428	0.411	0.366	0.347	0.355	0.452	0.391

Chlorite

Sample	ALu0306	ALu0601	ALu0603	APi0301	APi0601	APi0603
Pts avg	9	3	8	8	6	3
SiO2	27.12	26.14	25.50	26.02	26.54	26.43
Al2O3	24.10	23.31	23.91	23.70	24.29	23.58
TiO2	0.07	0.09	0.09	0.10	0.09	0.13
FeO	14.17	22.54	22.58	20.03	16.75	17.11
MnO	0.09	0.03	0.02	<0.01	0.01	0.02
MgO	22.89	17.22	16.97	18.41	20.43	21.07
CaO	0.11	0.03	0.01	<0.01	0.02	0.03
Na2O	<0.01	<0.01	0.01	<0.01	0.04	0.02
K2O	<0.01	0.04	<0.01	<0.01	0.04	0.00
H2O	12.21	11.58	11.60	11.49	11.98	11.96
F	<0.03	0.11	0.08	0.14	0.03	0.02
Cl	0.04	0.01	0.00	0.02	0.01	0.03
Total	100.81	101.09	100.76	99.91	100.22	100.40
Si	2.653	2.647	2.594	2.634	2.641	2.633
Al IV	1.347	1.353	1.406	1.366	1.359	1.367
Al VI	1.432	1.431	1.462	1.462	1.490	1.402
Ti	0.005	0.007	0.007	0.007	0.007	0.010
Fe2+	1.159	1.909	1.921	1.696	1.394	1.425
Mn	0.008	0.002	0.002	-	0.001	0.002
Mg	3.337	2.599	2.573	2.778	3.029	3.129
Ca	0.012	0.003	0.001	-	0.002	0.003
Na	-	-	0.001	-	0.007	0.004
K	-	0.005	0.000	-	0.004	0.000
Cations	9.953	9.956	9.966	9.944	9.934	9.975
H	7.965	7.825	7.873	7.758	7.948	7.947
F	-	0.165	0.124	0.224	0.043	0.033
Cl	0.035	0.010	0.003	0.018	0.009	0.021
Fe*	0.258	0.423	0.427	0.379	0.315	0.313

Appendix 2.1: (continued) Normalization: garnet 12 O + 8 cations, staurolite 48 O + 30 cat + 4 OH, chloritoid 14 O + 8 cations + 4 OH; Fe* = Fe/(Fe+Mg), xAlm, xSps, xPrp or xGrs = (Fe, Mn, Mg or Ca)/(Fe+Mn+Mg+Ca).

Garnet

Sample	ALu0304		ALu0601		ALu0603		APi0301	APi0601		APi0603		AMo0409		AMo0410	
Pts avg	11	5	20	3	16	2	2	2	2	9	8	5	5	4	4
Comment	Rim	Core	Rim	Core	Rim	Core	Rim	Rim	Core	Rim	Core	Rim	Core	Rim	Core
SiO2	37.98	37.94	38.10	37.76	37.85	37.73	37.96	37.99	37.78	37.90	37.71	37.37	37.19	37.38	36.89
Al2O3	21.74	21.80	21.33	21.05	21.28	21.11	22.05	21.37	21.11	21.31	21.17	21.84	21.85	21.68	21.17
TiO2	0.08	0.13	0.06	0.09	0.06	0.07	0.08	0.02	0.09	0.03	0.09	0.05	0.10	0.02	0.14
FeO	31.14	31.92	31.14	31.60	33.14	32.45	33.49	31.38	31.98	31.47	31.01	31.04	30.46	32.72	20.95
MnO	1.69	1.32	0.12	1.04	0.09	1.21	0.23	0.32	0.59	0.23	1.06	0.48	1.40	0.22	12.82
MgO	2.09	2.07	3.80	2.36	3.93	2.57	3.02	4.63	3.40	4.10	2.91	3.40	3.14	3.52	1.03
CaO	6.66	6.17	5.77	6.39	3.89	5.40	5.12	3.86	5.11	4.77	5.98	5.38	5.53	4.18	6.43
Na2O	0.01	0.01	0.01	0.01	0.01	<0.01	<0.01	0.03	0.02	0.01	0.01	0.02	<0.01	0.03	0.05
K2O	0.00	0.01	<0.01	<0.01	<0.01	<0.01	<0.01	<0.01	<0.01	<0.01	<0.01	<0.01	<0.01	<0.01	<0.01
Total	101.38	101.38	100.33	100.30	100.26	100.53	101.94	99.59	100.06	99.82	99.94	99.58	99.67	99.76	99.49
Si	2.993	2.992	3.008	3.010	3.003	3.005	2.973	3.012	3.006	3.007	3.005	2.977	2.967	2.982	2.985
Al total	2.020	2.027	1.985	1.977	1.990	1.982	2.036	1.997	1.980	1.993	1.989	2.051	2.055	2.039	2.020
Ti	0.005	0.008	0.004	0.005	0.004	0.004	0.005	0.001	0.005	0.002	0.006	0.003	0.006	0.001	0.009
Fe2+	2.052	2.105	2.056	2.106	2.199	2.162	2.194	2.080	2.128	2.087	2.066	2.068	2.032	2.183	1.418
Mn	0.113	0.088	0.008	0.070	0.006	0.082	0.015	0.021	0.040	0.015	0.072	0.032	0.095	0.015	0.879
Mg	0.246	0.243	0.447	0.281	0.465	0.305	0.352	0.547	0.403	0.485	0.346	0.403	0.374	0.419	0.125
Ca	0.562	0.522	0.488	0.546	0.331	0.460	0.430	0.327	0.436	0.405	0.510	0.459	0.473	0.357	0.558
Na	0.002	0.001	0.001	0.002	0.002	-	-	0.004	0.003	0.002	0.001	0.003	-	0.005	0.008
K	0.000	0.001	-	-	-	-	-	-	-	-	-	-	-	-	-
Cations	7.993	7.987	7.996	7.997	7.999	8.000	8.004	7.991	8.000	7.996	7.995	7.996	8.000	8.000	8.000
Fe*	0.893	0.896	0.821	0.882	0.826	0.876	0.862	0.792	0.841	0.811	0.857	0.837	0.845	0.839	0.919
xAlm	0.690	0.712	0.686	0.701	0.733	0.718	0.733	0.699	0.708	0.697	0.690	0.698	0.683	0.734	0.476
xSps	0.038	0.030	0.003	0.023	0.002	0.027	0.005	0.007	0.013	0.005	0.024	0.011	0.032	0.005	0.295
xPrp	0.083	0.082	0.149	0.094	0.155	0.101	0.118	0.184	0.134	0.162	0.115	0.136	0.126	0.141	0.042
xGrs	0.189	0.176	0.163	0.182	0.110	0.153	0.144	0.110	0.145	0.135	0.170	0.155	0.159	0.120	0.187

Staurolite

Sample	ALu0601		ALu0603	APi0301	APi0601	APi0603	AMo0409	AMo0410
Pts avg	8	5	12	30	10	17	13	16
Comment		Incl. Grt						
SiO2	28.26	27.19	28.17	28.59	28.01	27.93	28.32	28.02
Al2O3	54.94	56.42	54.79	55.30	55.49	54.94	54.25	55.09
TiO2	0.56	0.30	0.58	0.61	0.52	0.56	0.56	0.40
FeO	13.06	13.88	13.26	13.16	12.34	12.33	13.43	12.57
MnO	0.04	0.07	0.01	<0.01	0.02	0.02	0.03	0.15
MgO	1.93	1.03	2.28	1.98	2.16	2.41	2.07	1.97
ZnO	0.17	0.06	0.04	<0.01	0.16	0.08	0.20	0.12
CaO	<0.01	0.01	<0.01	<0.01	<0.01	0.01	<0.01	<0.01
Na2O	0.02	<0.01	<0.01	<0.01	0.01	<0.01	<0.01	<0.01
K2O	<0.01	<0.01	<0.01	<0.01	<0.01	<0.01	<0.01	<0.01
H2O	2.20	2.19	2.20	2.21	2.20	2.19	2.19	2.19
Total	101.17	101.14	101.33	101.85	100.92	100.48	101.04	100.51
Si	7.713	7.451	7.684	7.744	7.639	7.654	7.755	7.684
Al total	17.676	18.226	17.618	17.658	17.840	17.746	17.514	17.805
Ti	0.115	0.061	0.119	0.123	0.107	0.115	0.115	0.083
Fe2+	2.980	3.180	3.025	2.980	2.815	2.826	3.075	2.883
Mn	0.009	0.015	0.003	-	0.005	0.005	0.007	0.035
Mg	0.785	0.419	0.927	0.798	0.876	0.985	0.845	0.805
Zn	0.033	0.012	0.008	-	0.032	0.016	0.041	0.025
Ca	0.001	0.004	0.001	-	0.001	0.002	-	-
Na	0.008	0.002	0.002	-	0.006	0.002	-	-
K	0.001	0.001	0.001	-	0.001	0.001	-	-
Cations	29.322	29.370	29.386	29.304	29.322	29.351	29.352	29.319
H	4.000	4.000	4.000	4.000	4.000	4.000	4.000	4.000
Fe*	0.791	0.884	0.765	0.789	0.763	0.742	0.784	0.782

Chloritoid

Sample	ALu0304	ALu0601		ALu0603	APi0301
Pts avg	7	5	5	8	14
Comment		Grain 1	Grain 2		
SiO2	24.55	24.45	24.60	24.69	24.40
Al2O3	42.04	42.06	42.20	42.27	41.76
TiO2	0.01	0.01	0.01	0.01	0.04
FeO	22.05	22.39	21.43	21.46	21.39
MnO	0.17	0.03	0.02	0.07	0.07
MgO	3.74	3.48	4.39	4.20	4.01
ZnO	n.d.	n.d.	n.d.	n.d.	n.d.
CaO	0.03	0.03	0.02	0.02	0.02
Na2O	<0.01	0.01	0.01	0.01	0.01
K2O	<0.01	<0.01	<0.01	<0.01	0.01
H2O	7.38	7.36	7.41	7.42	7.33
Total	99.97	99.83	100.11	100.15	99.02
Si	1.995	1.993	1.990	1.996	1.996
Al total	4.028	4.040	4.024	4.028	4.029
Ti	0.001	0.000	0.001	0.001	0.002
Fe2+	1.499	1.526	1.450	1.451	1.463
Mn	0.012	0.002	0.002	0.005	0.005
Mg	0.453	0.423	0.529	0.506	0.489
Zn	-	-	-	-	-
Ca	0.002	0.002	0.002	0.002	0.002
Na	0.000	0.001	0.002	0.001	0.001
K	0.000	0.000	0.000	0.000	0.001
Cations	7.990	7.988	7.999	7.990	7.988
H	4.000	4.000	4.000	4.000	4.000
Fe*	0.768	0.783	0.733	0.741	0.749

Appendix 2.1: (continued) Normalization: plagioclase 8 O + 5 cations, ankerite 1 O + 1 cations + 1 CO_2, epidote 12.5 O + 8 cations + 1 OH, xAn, xAb or xKfs = (Ca, Na or K)/(Ca+Na+K), xCal, xSid or xDol = (Ca, Fe or Mg)/(Ca+Fe+Mg), xCzo = (Al-2)/(Fe+Al-2).

Plagioclase

Sample	ALu0304	ALu0306		ALu0601		ALu0603	APi0301		APi0601		APi0603	
Pts avg	3	2	3	5	14	24	6	3	5	6	10	17
Comment		Min An	Max An	Min An	Max An	-	Min An	Max An	Min An	Max An	Grain 1	Grain 2
SiO2	46.52	59.42	57.39	61.60	60.43	64.36	62.06	61.80	63.63	61.90	61.90	63.25
Al2O3	34.99	26.93	27.61	25.35	26.02	23.37	24.52	24.80	23.90	25.16	25.28	24.27
TiO2	<0.03	<0.03	<0.03	0.01	0.01	0.01	<0.01	<0.01	<0.01	0.01	0.01	0.01
FeO	0.11	0.02	<0.01	0.05	0.08	0.03	<0.01	<0.01	0.08	0.04	0.05	0.04
MnO	0.01	0.01	0.03	<0.01	<0.01	<0.01	<0.01	<0.01	<0.01	<0.01	<0.01	<0.01
MgO	0.01	<0.02	<0.01	<0.01	<0.01	<0.01	<0.01	<0.01	<0.01	<0.01	<0.01	<0.01
CaO	17.31	8.02	9.09	6.19	6.84	3.89	5.47	5.82	4.20	5.65	5.87	4.70
Na2O	1.50	7.34	6.78	7.60	7.29	8.98	8.84	8.62	8.68	7.94	7.82	8.43
K2O	0.02	0.04	0.07	0.08	0.07	0.07	0.07	0.07	0.07	0.06	0.06	0.07
Total	100.47	101.78	100.98	100.88	100.76	100.71	100.94	101.11	100.57	100.75	100.99	100.76
Si	2.126	2.609	2.551	2.706	2.665	2.814	2.729	2.715	2.788	2.719	2.714	2.770
Al total	1.885	1.394	1.447	1.313	1.353	1.204	1.271	1.284	1.235	1.303	1.306	1.252
Ti	-	-	-	0.000	0.000	0.000	-	-	-	0.000	0.000	0.000
Fe2+	0.004	0.001	-	0.002	0.003	0.001	-	-	0.003	0.002	0.002	0.001
Mn	0.000	0.000	0.001	-	-	-	-	-	-	-	-	-
Mg	0.000	-	-	-	-	-	-	-	-	-	-	-
Ca	0.848	0.377	0.433	0.291	0.323	0.182	0.257	0.274	0.197	0.266	0.276	0.220
Na	0.133	0.625	0.584	0.647	0.624	0.761	0.754	0.734	0.738	0.676	0.665	0.715
K	0.001	0.002	0.004	0.004	0.004	0.004	0.004	0.004	0.004	0.003	0.003	0.004
Cations	4.998	5.008	5.020	4.963	4.972	4.966	5.014	5.012	4.965	4.969	4.967	4.963
xAn	0.863	0.376	0.424	0.309	0.340	0.192	0.254	0.271	0.210	0.281	0.292	0.235
xAb	0.135	0.622	0.572	0.686	0.656	0.804	0.743	0.725	0.786	0.715	0.705	0.761
xKfs	0.001	0.002	0.004	0.005	0.004	0.004	0.004	0.004	0.004	0.004	0.003	0.004

	Plagioclase					Ankerite			Epidote			
Sample	AMo0409		AMo0410			ALu0304	ALu0306		ALu0304	ALu0306	APi0601	APi0603
Pts avg	4	1	7	4		2	5		16	3	5	12
Comment	Min An	Max An	Min An	Max An							Incl. Grt	Incl. Grt
SiO2	58.26	55.99	64.65	64.09		<0.02	<0.02		38.45	39.49	37.78	38.18
Al2O3	26.39	28.74	22.50	23.29		<0.03	<0.03		29.49	29.17	28.85	29.27
TiO2	<0.01	<0.01	<0.01	<0.01		<0.03	<0.03		0.15	0.49	0.07	0.60
FeO	<0.01	<0.01	<0.01	<0.01		13.20	6.85	Fe2O3 →	5.93	7.01	5.40	5.14
MnO	<0.01	<0.01	<0.01	<0.01		0.66	0.35		0.09	0.02	0.05	0.07
MgO	<0.01	<0.01	<0.01	<0.01		11.84	16.37		0.01	0.01	0.02	<0.01
CaO	7.84	10.33	2.86	3.53		29.64	29.39		23.43	23.49	22.38	23.14
Na2O	7.28	6.00	10.22	9.92		<0.03	<0.03		0.01	<0.01	0.01	0.01
K2O	0.09	0.06	0.07	0.06		<0.03	<0.03		<0.01	<0.01	<0.01	<0.01
H2O						44.69	45.35		1.93	2.03	1.94	1.98
Total	99.85	101.12	100.30	100.89		100.03	98.31		99.49	101.72	96.49	98.40
Si	2.608	2.492	2.840	2.805		-	-		2.863	2.919	2.921	2.897
Al IV	1.392	1.508	1.165	1.202		-	-		2.000	2.000	2.000	2.000
Al VI	-	-	-	-		-	-		0.589	0.541	0.628	0.617
Ti	-	-	-	-		-	-		0.008	0.027	0.004	0.034
Fe2+	-	-	-	-		0.181	0.092	Fe3+ →	0.332	0.433	0.349	0.326
Mn	-	-	-	-		0.009	0.005		0.006	0.002	0.003	0.004
Mg	-	-	-	-		0.289	0.394		0.001	0.002	0.002	-
Ca	0.376	0.493	0.135	0.166		0.521	0.509		1.869	1.860	1.853	1.881
Na	0.632	0.518	0.870	0.841		-	-		0.001	-	0.001	0.001
K	0.005	0.003	0.004	0.003		-	-		-	-		-
Cations	5.014	5.014	5.014	5.017		1.000	1.000		7.669	7.783	7.762	7.761
xAn	0.371	0.486	0.133	0.164	H	-	-		1.000	1.000	1.000	1.000
xAb	0.624	0.511	0.863	0.833	C	1.000	1.000		-	-	-	-
xKfs	0.005	0.003	0.004	0.003								
					xCal	0.525	0.511	xCzo	0.640	0.555	0.643	0.654
					xSid	0.183	0.093					
					xDol	0.292	0.396					

Appendix 2.2: Ar-Ar stepwise heating results for biotite and white mica(s) separates from Piora, Lucomagno and Molare areas.

#	T°C	^{39}Ar [%]	Age [Ma]	^{40}Ar$_{tot}$ [pL]	^{40}Ar* [pL]	^{39}Ar [pL]	^{38}Ar [pL]	^{37}Ar [pL]	^{36}Ar [pL]	Ca/K	Cl/K	39/40	36/40	STP File
ALu0306 Mrg±Ms (13.9 [mg], J = 0.003716, K = 0.85 [%], Cl = 9.6 [ppm], Ca = 43326 [ppm])														
1	500	0.80%	1.44 ± 22.02	361.0 ± 1.8	4.0	18.79 ± 0.24	3.71 ± 0.02	54.7 ± 0.7	1.22 ± 0.21	5.83 E+0 ± 7.7 E-2	3.09 E-2 ± 4.3 E-4	5.20 E-2 ± 7.1 E-4	3.35 E-3 ± 5.8 E-4	R15146
2	610	2.78%	14.18 ± 8.41	771.2 ± 1.3	98.0	46.56 ± 0.07	3.67 ± 0.04	623.0 ± 2.5	2.44 ± 0.21	2.70 E+1 ± 1.1 E-1	1.06 E-2 ± 2.1 E-4	5.98 E-2 ± 1.3 E-4	2.95 E-3 ± 2.6 E-4	R15147
3	722	10.70%	16.87 ± 2.18	2115.3 ± 0.6	470.9	186.64 ± 0.18	5.56 ± 0.01	569.0 ± 1.6	5.71 ± 0.21	6.11 E+0 ± 1.7 E-2	2.30 E-3 ± 4.1 E-5	8.81 E-2 ± 8.8 E-5	2.63 E-3 ± 9.7 E-5	R15148
4	816	42.99%	17.79 ± 0.54	3190.8 ± 2.9	2026.2	760.09 ± 1.00	10.71 ± 0.02	312.1 ± 0.9	4.02 ± 0.21	8.22 E-1 ± 2.4 E-3	2.52 E-4 ± 1.5 E-5	2.38 E-1 ± 3.8 E-4	1.24 E-3 ± 6.5 E-5	R15149
5	863	56.18%	18.58 ± 1.30	1670.3 ± 0.7	864.6	310.49 ± 0.27	4.71 ± 0.01	306.9 ± 0.9	2.81 ± 0.21	1.98 E+0 ± 5.9 E-3	3.41 E-4 ± 2.6 E-5	1.86 E-1 ± 1.8 E-4	1.63 E-3 ± 1.2 E-4	R15150
6	897	63.12%	20.38 ± 2.42	1249.6 ± 0.3	498.6	163.44 ± 0.31	2.89 ± 0.01	470.3 ± 1.6	2.66 ± 0.21	5.77 E+0 ± 2.0 E-2	6.06 E-4 ± 4.5 E-5	1.31 E-1 ± 2.5 E-4	2.03 E-3 ± 1.6 E-4	R15151
7	932	68.35%	19.43 ± 3.07	985.1 ± 0.3	357.6	123.27 ± 0.12	2.58 ± 0.01	813.7 ± 2.3	2.33 ± 0.21	1.33 E+1 ± 3.7 E-2	1.22 E-3 ± 5.8 E-5	1.25 E-1 ± 1.3 E-4	2.16 E-3 ± 2.0 E-4	R15152
8	1011	79.41%	18.04 ± 1.44	1450.5 ± 0.1	702.2	260.36 ± 0.28	4.30 ± 0.01	1057.5 ± 3.0	2.80 ± 0.21	8.15 E+0 ± 2.3 E-2	6.26 E-4 ± 3.0 E-5	1.79 E-1 ± 2.0 E-4	1.75 E-3 ± 1.3 E-4	R15153
9	1139	96.92%	18.22 ± 0.89	1851.7 ± 0.0	1123.5	412.10 ± 0.45	6.27 ± 0.01	1282.2 ± 3.8	2.79 ± 0.21	6.24 E+0 ± 1.8 E-2	4.96 E-4 ± 2.1 E-5	2.22 E-1 ± 2.4 E-4	1.33 E-3 ± 1.0 E-4	R15154
10	1459	100.00%	19.42 ± 5.39	1149.0 ± 1.1	209.8	72.60 ± 0.12	2.65 ± 0.04	846.3 ± 2.8	3.39 ± 0.21	2.35 E+1 ± 7.9 E-2	3.23 E-3 ± 1.4 E-4	6.27 E-2 ± 1.2 E-4	2.77 E-3 ± 1.7 E-4	R15155
ALu0306 Mrg-rich (29.7 [mg], J = 0.003710, K = 0.22 [%], Cl = 5.7 [ppm], Ca = 58876 [ppm])														
1	609	3.33%	-16.01 ± 9.51	535.9 ± 2.7	-100.8	42.62 ± 0.93	6.90 ± 0.06	415.2 ± 9.2	2.26 ± 0.21	1.96 E+1 ± 4.3 E-1	2.53 E-2 ± 3.1 E-4	7.90 E-2 ± 1.8 E-3	4.02 E-3 ± 3.8 E-4	R15156
2	721	18.15%	15.80 ± 2.06	2975.5 ± 0.8	445.1	189.65 ± 0.34	7.15 ± 0.04	2875.0 ± 9.4	9.30 ± 0.21	3.06 E+1 ± 1.0 E-1	3.50 E-3 ± 5.1 E-5	6.31 E-2 ± 1.1 E-4	2.88 E-3 ± 6.5 E-5	R15157
3	814	41.63%	18.26 ± 1.32	1881.6 ± 2.2	822.7	300.41 ± 0.27	5.43 ± 0.01	659.3 ± 1.9	3.75 ± 0.21	4.40 E+0 ± 1.2 E-2	7.80 E-4 ± 2.6 E-5	1.59 E-1 ± 2.4 E-4	1.90 E-3 ± 1.1 E-4	R15158
4	887	58.74%	17.50 ± 1.70	1480.8 ± 1.0	572.5	218.92 ± 0.37	4.00 ± 0.01	1498.8 ± 4.7	3.46 ± 0.21	1.38 E+1 ± 4.3 E-2	8.62 E-4 ± 3.5 E-5	1.47 E-1 ± 2.7 E-4	2.08 E-3 ± 1.3 E-4	R15159
5	953	71.34%	16.76 ± 1.82	1233.7 ± 1.3	397.3	161.26 ± 0.19	3.81 ± 0.03	4941.8 ± 14.4	4.09 ± 0.21	6.26 E+1 ± 1.8 E-1	2.31 E-3 ± 5.6 E-5	1.28 E-1 ± 2.1 E-4	2.29 E-3 ± 1.2 E-4	R15160
6	1136	94.12%	17.42 ± 1.07	1828.0 ± 0.3	753.2	291.38 ± 0.31	5.98 ± 0.01	5098.3 ± 17.0	4.94 ± 0.21	3.54 E+1 ± 1.2 E-1	1.59 E-3 ± 2.7 E-5	1.58 E-1 ± 1.7 E-4	1.99 E-3 ± 8.5 E-5	R15161
7	1460	100.00%	22.38 ± 4.63	1110.7 ± 2.4	247.7	75.26 ± 0.15	2.89 ± 0.01	2464.1 ± 8.2	3.55 ± 0.21	6.69 E+1 ± 2.2 E-1	4.28 E-3 ± 1.0 E-4	6.63 E-2 ± 1.9 E-4	2.63 E-3 ± 1.6 E-4	R15162
ALu0601 Ms100 (14.36 [mg], J = 0.001934, K = 7.20 [%], Cl = 54.1 [ppm], Ca = 5745 [ppm])														
1	574	1.46%	12.08 ± 1.96	1370.2 ± 1.4	201.0	57.90 ± 0.17	14.56 ± 0.06	25.41 ± 0.34	3.96 ± 0.11	8.78 E-1 ± 1.2 E-2	4.04 E-2 ± 2.0 E-4	4.22 E-2 ± 1.3 E-4	2.89 E-3 ± 8.0 E-5	R16653
2	728	5.27%	15.02 ± 0.81	4295.2 ± 0.4	650.3	150.46 ± 0.13	4.15 ± 0.01	11.61 ± 0.07	12.34 ± 0.12	1.54 E-1 ± 9.4 E-4	8.78 E-5 ± 3.0 E-5	3.50 E-2 ± 3.1 E-5	2.87 E-3 ± 2.6 E-5	R16654
3	763	25.24%	16.55 ± 0.14	4961.1 ± 1.2	3761.5	789.50 ± 0.74	10.89 ± 0.02	16.89 ± 0.19	4.06 ± 0.11	4.28 E-2 ± 4.9 E-4	1.90 E-4 ± 1.2 E-5	1.59 E-1 ± 1.5 E-4	8.18 E-4 ± 2.2 E-5	R16655
4	792	40.61%	16.09 ± 0.19	3369.5 ± 0.1	2812.3	607.26 ± 0.53	8.15 ± 0.02	15.31 ± 0.10	1.89 ± 0.11	5.04 E-2 ± 3.1 E-4	1.91 E-4 ± 1.3 E-5	1.80 E-1 ± 1.6 E-4	5.60 E-4 ± 3.3 E-5	R16656
5	856	53.58%	16.03 ± 0.22	2821.4 ± 1.2	2366.4	512.95 ± 0.45	6.75 ± 0.02	14.80 ± 0.13	1.54 ± 0.11	5.77 E-2 ± 5.0 E-4	1.49 E-4 ± 1.4 E-5	1.82 E-1 ± 1.8 E-4	5.46 E-4 ± 3.9 E-5	R16657
6	933	65.69%	16.15 ± 0.24	2804.2 ± 0.4	2224.5	478.45 ± 0.49	6.54 ± 0.01	14.45 ± 0.04	1.97 ± 0.11	6.04 E-2 ± 1.8 E-4	2.04 E-4 ± 1.4 E-5	1.71 E-1 ± 1.8 E-4	7.00 E-4 ± 3.9 E-5	R16658
7	1001	76.86%	16.26 ± 0.25	2581.2 ± 0.1	2067.0	441.62 ± 0.41	6.00 ± 0.02	18.04 ± 0.06	1.74 ± 0.11	8.17 E-2 ± 2.6 E-4	1.95 E-4 ± 1.5 E-5	1.71 E-1 ± 1.6 E-4	6.74 E-4 ± 4.3 E-5	R16661
8	1049	95.99%	16.40 ± 0.15	4045.7 ± 2.1	3570.1	756.15 ± 0.67	9.88 ± 0.02	17.63 ± 0.08	1.61 ± 0.11	4.66 E-2 ± 2.1 E-4	1.62 E-4 ± 1.2 E-5	1.87 E-1 ± 1.9 E-4	3.98 E-4 ± 2.7 E-5	R16662
9	1273	99.72%	16.26 ± 0.76	1021.4 ± 0.1	691.3	147.72 ± 0.13	1.92 ± 0.00	13.19 ± 0.05	1.12 ± 0.11	1.79 E-1 ± 6.3 E-4	-2.87 E-5 ± 2.7 E-5	1.45 E-1 ± 1.3 E-4	1.09 E-3 ± 1.1 E-4	R16663
10	1386	100.00%	-26.31 ± 10.56	423.0 ± 0.1	-81.6	10.91 ± 0.01	0.28 ± 0.00	18.58 ± 0.10	1.71 ± 0.11	3.41 E+0 ± 1.8 E-2	-2.73 E-3 ± 3.4 E-4	2.58 E-2 ± 2.9 E-5	4.04 E-3 ± 2.6 E-4	R16664
ALu0601 Ms200 (12.1 [mg], J = 0.001938, K = 7.05 [%], Cl = 33.9 [ppm], Ca = 6782 [ppm])														
1	579	0.62%	-34.88 ± 5.85	573.7 ± 1.3	-200.7	20.34 ± 0.09	5.30 ± 0.01	51.85 ± 0.51	2.63 ± 0.11	5.11 E+0 ± 5.0 E-2	4.01 E-2 ± 2.3 E-4	3.54 E-2 ± 1.8 E-4	4.57 E-3 ± 2.0 E-4	R16667
2	723	4.20%	13.47 ± 1.03	3813.2 ± 1.9	452.2	116.97 ± 0.12	3.88 ± 0.01	9.51 ± 0.15	11.38 ± 0.12	1.63 E-1 ± 2.5 E-3	5.72 E-4 ± 3.7 E-5	3.07 E-2 ± 3.6 E-5	2.98 E-3 ± 2.9 E-5	R16668
3	758	27.68%	16.81 ± 0.15	4517.4 ± 0.8	3706.6	767.12 ± 0.76	10.30 ± 0.02	15.08 ± 0.23	2.75 ± 0.11	3.93 E-2 ± 5.9 E-4	1.78 E-4 ± 1.2 E-5	1.70 E-1 ± 1.7 E-4	6.07 E-4 ± 2.4 E-5	R16669
4	789	42.16%	16.46 ± 0.24	2525.5 ± 0.5	2237.3	473.05 ± 0.44	6.27 ± 0.01	12.58 ± 0.07	0.98 ± 0.11	5.32 E-2 ± 2.9 E-4	1.96 E-4 ± 1.4 E-5	1.87 E-1 ± 1.8 E-4	3.86 E-4 ± 4.3 E-5	R16670
5	862	56.04%	16.58 ± 0.25	2504.9 ± 0.3	2160.3	453.54 ± 0.41	6.11 ± 0.01	12.62 ± 0.06	1.17 ± 0.11	5.57 E-2 ± 2.7 E-4	2.17 E-4 ± 1.4 E-5	1.81 E-1 ± 1.6 E-4	4.66 E-4 ± 4.4 E-5	R16671
6	938	67.00%	16.47 ± 0.31	2044.6 ± 0.3	1694.8	358.10 ± 0.32	4.81 ± 0.01	12.96 ± 0.06	1.19 ± 0.11	7.24 E-2 ± 3.4 E-4	1.88 E-4 ± 1.5 E-5	1.75 E-1 ± 1.6 E-4	5.79 E-4 ± 5.4 E-5	R16672
7	1006	77.73%	17.32 ± 0.35	2001.6 ± 2.2	1746.5	350.80 ± 2.97	4.51 ± 0.02	15.42 ± 0.83	0.87 ± 0.11	8.79 E-2 ± 4.7 E-3	1.13 E-4 ± 1.8 E-5	1.75 E-1 ± 1.5 E-3	4.31 E-4 ± 5.5 E-5	R16673
8	1038	89.91%	18.61 ± 0.29	2317.5 ± 2.8	2129.4	397.89 ± 1.16	5.94 ± 0.01	5.67 ± 0.18	0.64 ± 0.11	2.85 E-2 ± 8.9 E-4	5.12 E-4 ± 1.5 E-5	1.72 E-1 ± 5.4 E-4	2.75 E-4 ± 4.7 E-5	R16674
9	1282	99.46%	16.71 ± 0.36	2002.0 ± 1.5	1498.7	312.05 ± 0.36	4.27 ± 0.01	13.69 ± 0.10	1.71 ± 0.11	8.77 E-2 ± 6.2 E-4	1.61 E-4 ± 1.6 E-5	1.56 E-1 ± 2.1 E-4	8.51 E-4 ± 5.5 E-5	R16675
10	1385	100.00%	-15.17 ± 6.55	760.9 ± 0.2	-75.9	17.58 ± 0.03	0.74 ± 0.00	15.95 ± 0.05	2.84 ± 0.11	1.82 E+0 ± 5.9 E-3	1.97 E-5 ± 2.1 E-4	2.31 E-2 ± 4.4 E-5	3.72 E-3 ± 1.4 E-4	R16676

Appendix 2.2 (continued)

#	T°C	^{39}Ar [%]	Age [Ma]	^{40}Ar$_{tot}$ [pL]	^{40}Ar* [pL]	^{39}Ar [pL]	^{38}Ar [pL]	^{37}Ar [pL]	^{36}Ar [pL]	Ca/K	Cl/K	39/40	36/40	STP File
ALu0603 Ms100 (Ms-rich, 11.93 [mg], J = 0.001928, K = 6.27 [%], Cl = 47.9 [ppm], Ca = 7435 [ppm])														
1	516	0.76%	-52.00 ±5.41	438.4 ±0.7	-317.3	21.54 ±0.02	8.48 ±0.01	26.50 ±0.24	2.56 ±0.11	2.46 E+0 ±2.2 E-2	6.40 E-2 ±2.1 E-4	4.91 E-2 ±8.5 E-5	5.83 E-3 ±2.5 E-4	R16640
2	621	3.92%	14.66 ±1.28	2282.3 ±0.1	380.8	89.94 ±0.08	2.89 ±0.01	6.64 ±0.05	6.44 ±0.11	1.48 E-1 ±1.0 E-3	1.25 E-3 ±4.7 E-5	3.94 E-2 ±3.5 E-5	2.82 E-3 ±4.8 E-5	R16641
3	755	11.87%	16.26 ±0.53	2722.4 ±0.8	1060.2	225.80 ±1.05	4.38 ±0.01	15.22 ±0.30	5.63 ±0.12	1.35 E-1 ±2.7 E-3	5.32 E-4 ±2.2 E-5	8.29 E-2 ±3.9 E-4	2.07 E-3 ±4.2 E-5	R16642
4	778	29.90%	16.49 ±0.23	3058.3 ±0.8	2439.8	512.11 ±1.62	7.83 ±0.02	17.52 ±0.14	2.10 ±0.11	6.84 E-2 ±5.3 E-4	4.93 E-4 ±1.4 E-5	1.67 E-1 ±5.3 E-4	6.84 E-4 ±3.6 E-5	R16643
5	813	43.00%	16.13 ±0.30	2170.0 ±0.1	1733.1	372.05 ±0.58	4.91 ±0.02	16.96 ±0.05	1.48 ±0.11	9.12 E-2 ±2.8 E-4	1.22 E-4 ±1.6 E-5	1.71 E-1 ±2.7 E-4	6.81 E-4 ±5.1 E-5	R16644
6	854	55.37%	16.23 ±0.32	2095.5 ±0.3	1648.1	351.47 ±0.35	4.74 ±0.01	16.85 ±0.07	1.52 ±0.11	9.59 E-2 ±4.0 E-4	1.65 E-4 ±1.6 E-5	1.68 E-1 ±1.7 E-4	7.23 E-4 ±5.2 E-5	R16645
7	953	69.42%	16.48 ±0.28	2526.6 ±0.6	1899.0	398.97 ±0.35	5.49 ±0.01	14.93 ±0.15	2.13 ±0.11	7.49 E-2 ±7.3 E-4	1.79 E-4 ±1.5 E-5	1.58 E-1 ±1.4 E-4	8.41 E-4 ±4.3 E-5	R16646
8	1003	82.07%	16.20 ±0.31	2234.9 ±0.3	1682.4	359.58 ±0.36	4.90 ±0.01	17.00 ±0.05	1.87 ±0.11	9.46 E-2 ±2.7 E-4	1.62 E-4 ±1.5 E-5	1.61 E-1 ±1.6 E-4	8.37 E-4 ±4.9 E-5	R16647
9	1049	92.61%	16.59 ±0.37	1790.9 ±0.1	1434.8	299.36 ±0.31	4.03 ±0.01	15.82 ±0.09	1.21 ±0.11	1.06 E-1 ±5.9 E-4	1.69 E-4 ±1.7 E-5	1.67 E-1 ±1.7 E-4	6.73 E-4 ±6.1 E-5	R16648
10	1213	99.57%	16.55 ±0.57	1204.8 ±0.3	944.8	197.59 ±0.17	2.67 ±0.01	14.41 ±0.13	0.88 ±0.11	1.46 E-1 ±1.3 E-3	1.61 E-4 ±2.2 E-5	1.64 E-1 ±1.5 E-4	7.30 E-4 ±9.1 E-5	R16649
11	1385	100.00%	10.75 ±9.17	349.6 ±0.0	37.9	12.24 ±0.03	0.27 ±0.01	15.40 ±0.25	1.06 ±0.11	2.52 E+0 ±4.1 E-2	-9.64 E-4 ±3.1 E-4	3.50 E-2 ±8.3 E-5	3.02 E-3 ±3.1 E-4	R16650
ALu0603 Ms200 (Prg-rich, 20.57 [mg], J = 0.001931, K = 1.47 [%], Cl = 184.6 [ppm], Ca = 5288 [ppm])														
1	611	6.37%	16.64 ±1.54	843.1 ±0.8	350.1	73.00 ±0.13	79.54 ±0.17	30.82 ±0.10	1.68 ±0.11	8.45 E-1 ±2.7 E-3	1.91 E-1 ±4.1 E-4	8.66 E-2 ±1.7 E-4	1.98 E-3 ±1.3 E-4	R16631
2	759	33.94%	16.81 ±0.36	2891.3 ±0.7	1531.9	316.10 ±0.30	6.49 ±0.04	77.01 ±0.22	4.62 ±0.11	4.87 E-1 ±1.4 E-3	1.08 E-3 ±2.8 E-5	1.09 E-1 ±1.1 E-4	1.59 E-3 ±3.8 E-5	R16632
3	845	67.95%	16.50 ±0.29	2301.6 ±2.7	1854.6	389.94 ±0.35	5.30 ±0.01	40.07 ±0.11	1.52 ±0.11	2.06 E-1 ±5.9 E-4	1.98 E-4 ±1.5 E-5	1.69 E-1 ±2.5 E-4	6.57 E-4 ±4.8 E-5	R16633
4	956	83.24%	16.74 ±0.64	1184.5 ±0.0	846.3	175.31 ±0.16	2.36 ±0.01	34.91 ±0.13	1.15 ±0.11	3.98 E-1 ±1.5 E-3	9.41 E-5 ±2.5 E-5	1.48 E-1 ±1.3 E-4	9.66 E-4 ±9.2 E-5	R16634
5	1066	97.13%	17.22 ±0.70	1028.4 ±0.8	790.9	159.25 ±0.15	2.14 ±0.00	23.59 ±0.13	0.81 ±0.11	2.96 E-1 ±1.7 E-3	1.31 E-4 ±2.6 E-5	1.55 E-1 ±1.9 E-4	7.81 E-4 ±1.1 E-4	R16635
6	1276	99.85%	16.49 ±3.60	389.1 ±0.0	148.0	31.12 ±0.04	0.51 ±0.00	9.29 ±0.10	0.82 ±0.11	5.97 E-1 ±6.6 E-3	-6.13 E-5 ±1.2 E-4	8.00 E-2 ±1.1 E-4	2.10 E-3 ±2.8 E-4	R16636
7	1380	100.00%	-64.17 ±66.74	214.3 ±0.1	-31.8	1.76 ±0.02	0.17 ±0.00	1.47 ±0.02	0.83 ±0.11	1.67 E+0 ±2.0 E-2	-1.78 E-4 ±2.1 E-3	8.21 E-3 ±7.4 E-5	3.89 E-3 ±5.1 E-4	R16637
AMo0409 Ms (18.3 [mg], J = 0.0009961, K = 6.30 [%], Cl = 18.7 [ppm], Ca = 2700 [ppm])														
1	464	0.23%	-89.10 ±18.30	1068.8 ±1.5	-441.5	9.14 ±0.12	2.88 ±0.11	14.92 ±3.07	5.11 ±0.30	3.27 E+0 ±6.7 E-1	3.55 E-2 ±2.4 E-3	8.54 E-3 ±1.2 E-4	4.78 E-3 ±2.8 E-4	R15727
2	574	0.82%	15.30 ±6.56	636.7 ±1.3	198.6	23.23 ±0.20	1.20 ±0.22	15.17 ±2.65	1.49 ±0.29	1.31 E+0 ±2.3 E-1	4.98 E-3 ±1.7 E-3	3.65 E-2 ±3.2 E-4	2.33 E-3 ±4.5 E-4	R15728
3	658	2.04%	2.73 ±3.43	807.3 ±0.3	73.6	48.37 ±0.10	1.22 ±0.14	0.43 ±3.17	2.48 ±0.31	1.76 E-2 ±1.3 E-1	6.96 E-4 ±5.7 E-4	5.99 E-2 ±1.3 E-4	3.08 E-3 ±3.9 E-4	R15729
4	728	4.70%	12.43 ±1.61	1729.7 ±1.5	730.1	105.20 ±0.45	2.11 ±0.16	1.51 ±2.14	3.38 ±0.32	2.87 E-2 ±4.1 E-2	4.13 E-4 ±2.9 E-4	6.08 E-2 ±2.6 E-4	1.96 E-3 ±1.9 E-4	R15730
5	768	8.69%	14.79 ±1.04	2903.2 ±2.2	1305.9	157.98 ±0.26	3.12 ±0.19	14.94 ±2.09	5.41 ±0.31	1.89 E-1 ±2.7 E-2	2.90 E-4 ±2.2 E-4	5.44 E-2 ±1.0 E-4	1.86 E-3 ±1.1 E-4	R15731
6	807	23.19%	18.77 ±0.29	7395.3 ±0.7	6022.3	573.67 ±0.55	8.13 ±0.18	7.83 ±3.13	4.65 ±0.32	2.73 E-2 ±1.1 E-2	1.58 E-4 ±5.8 E-5	7.76 E-2 ±7.4 E-5	6.28 E-4 ±4.3 E-5	R15732
7	844	43.81%	17.99 ±0.19	8998.1 ±7.4	8209.3	815.74 ±1.01	9.74 ±0.21	0.64 ±2.68	2.67 ±0.29	1.58 E-3 ±6.6 E-3	-7.70 E-5 ±4.9 E-5	9.07 E-2 ±1.3 E-4	2.97 E-4 ±3.2 E-5	R15733
8	877	59.22%	17.22 ±0.27	6709.7 ±12.1	5869.2	609.55 ±0.65	8.12 ±0.13	6.03 ±2.18	2.85 ±0.31	1.98 E-2 ±7.1 E-3	1.22 E-4 ±4.2 E-5	9.08 E-2 ±1.9 E-4	4.24 E-4 ±4.6 E-5	R15734
9	951	84.65%	17.62 ±0.16	11057.4 ±0.8	9912.0	1006.12 ±0.90	13.79 ±0.12	3.62 ±3.89	3.88 ±0.31	7.20 E-3 ±7.7 E-3	2.17 E-4 ±2.6 E-5	9.10 E-2 ±8.2 E-5	3.51 E-4 ±2.8 E-5	R15735
10	1033	95.00%	18.18 ±0.37	4661.4 ±1.8	4162.0	409.46 ±0.51	5.31 ±0.30	18.28 ±3.29	1.69 ±0.28	8.93 E-2 ±1.6 E-2	7.66 E-5 ±1.3 E-4	8.78 E-2 ±1.1 E-4	3.63 E-4 ±6.1 E-5	R15736
11	1340	100.00%	15.22 ±0.77	2449.2 ±1.3	1682.6	197.80 ±0.22	4.27 ±0.22	5.88 ±2.75	2.60 ±0.29	5.95 E-2 ±2.8 E-2	1.32 E-3 ±2.0 E-4	8.08 E-2 ±1.0 E-4	1.06 E-3 ±1.2 E-4	R15737
AMo0410 Ms (16.6 [mg], J = 0.0010015, K = 3.62 [%], Cl = 82.6 [ppm], Ca = 12133 [ppm])														
1	466	3.15%	-56.16 ±2.95	198.4 ±0.8	-1997.4	65.40 ±1.04	16.49 ±0.44	203.04 ±4.56	7.48 ±0.33	6.22 E+0 ±1.4 E-1	3.91 E-2 ±1.2 E-3	3.29 E-1 ±5.4 E-3	3.75 E-2 ±1.7 E-3	R15754
2	597	5.05%	-46.50 ±4.37	573.8 ±0.5	-999.3	39.39 ±0.30	6.02 ±0.19	89.35 ±3.93	5.35 ±0.31	4.54 E+0 ±2.0 E-1	2.07 E-2 ±8.8 E-4	6.85 E-2 ±5.3 E-4	9.28 E-3 ±5.4 E-4	R15755
3	694	10.03%	12.94 ±1.48	1765.6 ±2.5	742.8	103.37 ±0.21	3.05 ±0.25	7.98 ±1.67	3.46 ±0.29	1.54 E-1 ±3.2 E-2	2.04 E-3 ±4.4 E-4	5.85 E-2 ±1.4 E-4	1.96 E-3 ±1.6 E-4	R15756
4	760	14.93%	19.26 ±1.74	1445.0 ±2.2	1090.8	101.79 ±0.10	1.73 ±0.18	0.82 ±1.72	1.20 ±0.34	1.61 E-2 ±3.4 E-2	5.32 E-4 ±3.3 E-4	7.04 E-2 ±1.3 E-4	8.29 E-4 ±2.3 E-4	R15758
5	805	34.71%	16.95 ±0.36	4763.7 ±4.6	3869.2	410.51 ±0.41	7.11 ±0.35	15.61 ±4.08	3.03 ±0.28	7.61 E-2 ±2.0 E-2	7.46 E-4 ±1.6 E-4	8.62 E-2 ±1.2 E-4	6.35 E-4 ±5.9 E-5	R15759
6	842	53.22%	17.93 ±0.43	4291.6 ±1.9	3831.4	384.19 ±0.40	5.82 ±0.19	7.48 ±2.33	1.56 ±0.31	3.90 E-2 ±1.2 E-2	4.69 E-4 ±9.5 E-5	8.95 E-2 ±1.0 E-4	3.63 E-4 ±7.3 E-5	R15760
7	868	72.35%	18.73 ±0.44	4437.1 ±1.8	4138.0	397.10 ±0.42	5.55 ±0.21	3.64 ±0.59	1.01 ±0.33	1.83 E-2 ±3.0 E-3	3.09 E-4 ±9.7 E-5	8.95 E-2 ±1.0 E-4	2.28 E-4 ±7.4 E-5	R15761
8	898	80.22%	17.63 ±1.00	1932.8 ±1.1	1601.1	163.32 ±0.16	2.54 ±0.09	9.94 ±1.18	1.13 ±0.31	1.22 E-1 ±1.4 E-2	4.50 E-4 ±1.2 E-4	8.45 E-2 ±9.4 E-5	5.81 E-4 ±1.6 E-4	R15762
9	971	88.80%	16.00 ±0.97	2176.4 ±1.7	1583.4	177.98 ±0.21	2.90 ±0.19	4.77 ±1.45	2.01 ±0.33	5.36 E-2 ±1.6 E-2	4.29 E-4 ±2.0 E-4	8.18 E-2 ±1.1 E-4	9.22 E-4 ±1.5 E-4	R15763
10	1050	95.87%	16.56 ±1.04	1910.6 ±2.4	1351.5	146.79 ±0.18	2.15 ±0.14	12.11 ±1.47	1.90 ±0.29	1.65 E-1 ±2.0 E-2	8.95 E-5 ±1.8 E-4	7.68 E-2 ±1.3 E-4	9.90 E-4 ±1.5 E-4	R15764
11	1188	99.35%	15.76 ±2.29	1197.9 ±0.5	633.2	72.28 ±0.11	1.78 ±0.04	3.00 ±0.97	1.91 ±0.31	8.29 E-2 ±2.7 E-2	1.41 E-3 ±1.7 E-4	6.03 E-2 ±9.1 E-5	1.60 E-3 ±2.6 E-4	R15765
12	1360	100.00%	-2.50 ±11.97	779.1 ±0.3	-18.6	13.49 ±0.13	1.90 ±0.11	7.96 ±3.26	2.70 ±0.30	1.18 E+0 ±4.8 E-1	1.64 E-2 ±1.7 E-3	1.73 E-2 ±1.7 E-4	3.47 E-3 ±3.9 E-4	R15766

Appendix 2.2 (continued)

#	T°C	^{39}Ar [%]	Age [Ma]	$^{40}Ar_{tot}$ [pL]	$^{40}Ar^*$ [pL]	^{39}Ar [pL]	^{38}Ar [pL]	^{37}Ar [pL]	^{36}Ar [pL]	Ca/K	Cl/K	39/40	36/40	STP File
APi0301 Ms+Prg (14.1 [mg], J = 0.003721, K = 3.07 [%], Cl = 18.0 [ppm], Ca = 5772 [ppm])														
1	489	0.68%	-33.21 ± 7.54	463.7 ± 3.8	-281.7	57.49 ± 0.09	9.90 ± 0.20	34.21 ± 0.99	2.53 ± 0.21	1.19 E+0 ± 3.5 E-2	2.71 E-2 ± 6.2 E-4	1.24 E-1 ± 1.0 E-3	5.44 E-3 ± 4.6 E-4	R15129
2	601	3.30%	8.34 ± 1.88	1174.3 ± 1.8	276.2	221.90 ± 0.30	7.56 ± 0.11	55.17 ± 0.72	3.05 ± 0.21	4.97 E-1 ± 6.4 E-3	3.52 E-3 ± 9.1 E-5	1.89 E-1 ± 3.8 E-4	2.59 E-3 ± 1.8 E-4	R15130
3	669	9.85%	12.23 ± 0.78	2566.3 ± 0.8	1012.5	553.80 ± 0.56	11.14 ± 0.14	119.48 ± 0.50	5.29 ± 0.22	4.32 E-1 ± 1.8 E-3	1.18 E-3 ± 4.8 E-5	2.16 E-1 ± 2.3 E-4	2.05 E-3 ± 8.5 E-5	R15131
4	714	21.75%	16.66 ± 0.41	3587.1 ± 0.8	2510.4	1006.88 ± 1.38	13.76 ± 0.03	164.39 ± 0.50	3.69 ± 0.21	3.27 E-1 ± 1.0 E-3	2.22 E-4 ± 1.3 E-5	2.81 E-1 ± 3.9 E-4	1.02 E-3 ± 5.9 E-5	R15132
5	744	32.96%	16.70 ± 0.44	3417.6 ± 2.5	2372.4	949.11 ± 3.03	12.90 ± 0.04	111.23 ± 0.50	3.57 ± 0.21	2.34 E-1 ± 1.1 E-3	2.04 E-4 ± 1.5 E-5	2.78 E-1 ± 9.1 E-4	1.03 E-3 ± 6.1 E-5	R15133
6	770	40.58%	16.93 ± 0.64	2272.5 ± 0.5	1632.9	644.57 ± 0.58	8.84 ± 0.02	48.72 ± 0.21	2.18 ± 0.21	1.51 E-1 ± 6.7 E-4	2.37 E-4 ± 1.6 E-5	2.84 E-1 ± 2.6 E-4	9.52 E-4 ± 9.2 E-5	R15134
7	798	48.73%	16.88 ± 0.60	2432.9 ± 0.1	1741.2	689.36 ± 1.11	9.60 ± 0.02	39.54 ± 0.13	2.35 ± 0.21	1.15 E-1 ± 3.9 E-4	2.74 E-4 ± 1.5 E-5	2.83 E-1 ± 4.6 E-4	9.62 E-4 ± 8.7 E-5	R15135
8	825	56.21%	16.90 ± 0.65	2224.0 ± 1.2	1600.7	632.72 ± 0.79	8.85 ± 0.02	27.81 ± 0.09	2.12 ± 0.21	8.79 E-2 ± 2.7 E-4	2.86 E-4 ± 1.6 E-5	2.84 E-1 ± 3.9 E-4	9.48 E-4 ± 9.4 E-5	R15136
9	850	62.73%	16.93 ± 0.75	1958.0 ± 0.9	1398.7	552.15 ± 0.66	7.64 ± 0.02	22.67 ± 0.07	1.90 ± 0.21	8.21 E-2 ± 2.4 E-4	2.57 E-4 ± 1.7 E-5	2.82 E-1 ± 3.6 E-4	9.67 E-4 ± 1.1 E-4	R15137
10	872	67.76%	17.17 ± 0.97	1724.4 ± 1.7	1092.6	425.15 ± 0.43	6.06 ± 0.03	18.97 ± 0.06	2.14 ± 0.21	8.92 E-2 ± 3.0 E-4	2.78 E-4 ± 2.4 E-5	2.47 E-1 ± 3.5 E-4	1.24 E-3 ± 1.2 E-4	R15138
11	908	73.18%	17.30 ± 0.90	1870.4 ± 0.3	1188.0	458.80 ± 0.51	6.65 ± 0.02	24.81 ± 0.10	2.32 ± 0.21	1.08 E-1 ± 4.3 E-4	3.18 E-4 ± 2.0 E-5	2.45 E-1 ± 2.8 E-4	1.23 E-3 ± 1.1 E-4	R15139
12	950	77.99%	17.56 ± 1.02	1673.6 ± 2.7	1069.1	406.74 ± 0.81	5.96 ± 0.01	24.65 ± 0.09	2.05 ± 0.21	1.21 E-1 ± 4.4 E-4	3.47 E-4 ± 2.1 E-5	2.43 E-1 ± 6.2 E-4	1.22 E-3 ± 1.3 E-4	R15140
13	1014	91.18%	16.92 ± 0.37	3935.4 ± 0.4	2826.6	1116.18 ± 0.98	15.18 ± 0.03	60.81 ± 0.18	3.77 ± 0.21	1.09 E-1 ± 3.2 E-4	2.17 E-4 ± 1.3 E-5	2.84 E-1 ± 2.5 E-4	9.54 E-4 ± 5.3 E-5	R15141
14	1135	99.42%	17.55 ± 0.59	2753.6 ± 0.8	1831.1	697.13 ± 0.66	9.65 ± 0.03	64.66 ± 0.26	3.14 ± 0.21	1.86 E-1 ± 7.6 E-4	2.23 E-4 ± 1.7 E-5	2.53 E-1 ± 2.5 E-4	1.13 E-3 ± 7.6 E-5	R15142
15	1410	100.00%	22.15 ± 8.34	767.4 ± 0.6	164.0	49.42 ± 0.10	1.52 ± 0.01	20.87 ± 0.11	2.05 ± 0.21	8.45 E-1 ± 4.3 E-3	2.02 E-3 ± 1.5 E-4	6.44 E-2 ± 1.3 E-4	2.66 E-3 ± 2.7 E-4	R15143
APi0601 Ms100 (Prg-rich, 11.55 [mg], J = 0.001919, K = 0.87 [%], Cl = 114.1 [ppm], Ca = 4785 [ppm]; fix gain factor multiplier/faraday)														
1	602	9.52%	18.94 ± 3.26	712.7 ± 0.1	188.2	34.22 ± 0.05	24.99 ± 0.09	3.43 ± 0.01	1.78 ± 0.11	2.00 E-1 ± 6.8 E-4	1.26 E-1 ± 5.0 E-4	4.80 E-2 ± 7.3 E-5	2.49 E-3 ± 1.5 E-4	R16719
2	742	55.30%	15.18 ± 0.70	3134.0 ± 1.2	724.9	164.66 ± 0.15	4.69 ± 0.01	9.12 ± 0.04	8.16 ± 0.11	1.11 E-1 ± 4.6 E-4	1.32 E-3 ± 2.8 E-5	5.25 E-2 ± 5.3 E-5	2.60 E-3 ± 3.5 E-5	R16720
3	835	81.05%	16.64 ± 1.21	1612.2 ± 0.2	447.3	92.63 ± 0.08	2.07 ± 0.01	0.55 ± 0.00	3.94 ± 0.11	1.20 E-2 ± 5.7 E-5	4.66 E-4 ± 4.3 E-5	5.75 E-2 ± 5.2 E-5	2.45 E-3 ± 6.8 E-5	R16721
4	950	92.31%	20.73 ± 2.77	1534.5 ± 0.3	244.0	40.51 ± 0.05	1.46 ± 0.01	8.58 ± 0.07	4.37 ± 0.11	4.24 E-1 ± 3.4 E-3	7.22 E-4 ± 1.0 E-4	2.64 E-2 ± 3.5 E-5	2.85 E-3 ± 7.2 E-5	R16722
5	1212	100.00%	26.27 ± 4.18	2894.9 ± 0.1	211.3	27.64 ± 0.02	2.15 ± 0.01	2.81 ± 0.07	9.08 ± 0.11	2.04 E-1 ± 5.3 E-3	8.16 E-4 ± 1.5 E-4	9.55 E-3 ± 8.4 E-6	3.14 E-3 ± 3.8 E-5	R16723
6	1379	-	-	3604.7 ± 1.2	123.3	-0.26 ± 0.01	2.17 ± 0.01	-10.58 ± 0.25	11.78 ± 0.12	8.24 E+1 ± 1.9 E+0	2.10 E-2 ± 1.6 E-2	-7.12 E-5 ± 1.6 E-6	3.27 E-3 ± 3.1 E-5	R16724
APi0601 Ms200 (Prg-rich, 13.75 [mg], J = 0.001922, K = 0.57 [%], Cl = 189.3 [ppm], Ca = 6211 [ppm]; fix gain factor multiplier/faraday)														
1	610	14.58%	1.92 ± 3.08	971.9 ± 4.8	21.3	38.50 ± 0.16	42.67 ± 0.24	50.46 ± 0.89	3.23 ± 0.12	2.62 E+0 ± 4.7 E-2	1.92 E-1 ± 1.1 E-3	3.96 E-2 ± 2.6 E-4	3.31 E-3 ± 1.2 E-4	R16677
2	757	63.82%	16.42 ± 0.88	2430.0 ± 0.1	618.8	130.05 ± 0.59	4.18 ± 0.03	7.00 ± 0.50	6.13 ± 0.11	1.08 E-1 ± 7.7 E-3	2.06 E-3 ± 4.7 E-5	5.35 E-2 ± 2.4 E-4	2.52 E-3 ± 4.5 E-5	R16678
3	840	88.42%	19.43 ± 1.72	932.9 ± 0.1	365.9	64.96 ± 0.06	1.87 ± 0.02	21.63 ± 0.08	1.92 ± 0.11	6.66 E-1 ± 2.5 E-3	2.06 E-3 ± 7.2 E-5	6.96 E-2 ± 6.9 E-5	2.06 E-3 ± 1.2 E-4	R16679
4	950	94.30%	34.88 ± 7.12	525.9 ± 0.5	157.7	15.52 ± 0.06	1.68 ± 0.00	7.36 ± 0.05	1.25 ± 0.11	9.48 E-1 ± 6.8 E-3	1.45 E-2 ± 2.4 E-4	2.95 E-2 ± 1.1 E-4	2.37 E-3 ± 2.1 E-4	R16680
5	1062	99.26%	31.29 ± 8.50	974.2 ± 0.1	119.2	13.10 ± 0.03	1.59 ± 0.01	6.61 ± 0.02	2.90 ± 0.11	1.01 E+0 ± 3.4 E-3	1.22 E-2 ± 3.0 E-4	1.34 E-2 ± 2.6 E-5	2.97 E-3 ± 1.1 E-4	R16681
6	1377	100.00%	191.02 ± 52.48	1378.9 ± 0.4	113.5	1.95 ± 0.01	1.49 ± 0.00	-1.07 ± 0.06	4.28 ± 0.11	-1.10 E+0 ± 5.7 E-2	6.03 E-2 ± 1.9 E-3	1.42 E-3 ± 5.4 E-6	3.11 E-3 ± 8.0 E-5	R16682

Appendix 2.2 (continued)

#	T°C	^{39}Ar [%]	Age [Ma]	^{40}Ar$_{tot}$ [pL]	^{40}Ar* [pL]	^{39}Ar [pL]	^{38}Ar [pL]	^{37}Ar [pL]	^{36}Ar [pL]	Ca/K	Cl/K	39/40	36/40	STP File
APi0603 Ms-A (Ms-rich, 16.07 [mg], J = 0.001912, K = 6.52 [%], Cl = 75.1 [ppm], Ca = 4760 [ppm])														
1	457	0.17%	40.47 ± 17.67	314.4 ± 0.2	77.5	6.54 ± 0.61	12.22 ± 0.20	20.28 ± 2.81	0.81 ± 0.11	6.21 E+0 ± 8.6 E-1	3.26 E-1 ± 5.4 E-3	2.08 E-2 ± 1.9 E-3	2.55 E-3 ± 3.6 E-4	R16567
2	580	3.14%	-9.50 ± 0.99	1211.8 ± 0.0	-318.9	116.10 ± 0.38	12.96 ± 0.06	20.75 ± 0.35	5.19 ± 0.11	3.57 E-1 ± 6.0 E-3	1.63 E-2 ± 1.0 E-4	9.58 E-2 ± 3.1 E-4	4.27 E-3 ± 9.1 E-5	R16568
3	714	7.50%	15.89 ± 0.68	3171.2 ± 0.7	786.5	169.97 ± 0.15	3.68 ± 0.01	7.57 ± 0.02	8.07 ± 0.11	8.90 E-2 ± 2.7 E-4	1.86 E-4 ± 2.7 E-5	5.36 E-2 ± 4.9 E-5	2.54 E-3 ± 3.5 E-5	R16569
4	763	32.87%	15.83 ± 0.11	5984.6 ± 0.8	4564.1	990.61 ± 0.88	13.55 ± 0.02	18.31 ± 0.08	4.81 ± 0.11	3.70 E-2 ± 1.7 E-4	1.80 E-4 ± 1.2 E-5	1.66 E-1 ± 1.5 E-4	8.03 E-4 ± 1.8 E-5	R16570
5	797	49.62%	15.75 ± 0.17	3587.7 ± 0.2	2998.2	653.67 ± 0.57	8.66 ± 0.02	12.22 ± 0.10	2.00 ± 0.11	3.74 E-2 ± 3.2 E-4	1.64 E-4 ± 1.3 E-5	1.82 E-1 ± 1.6 E-4	5.56 E-4 ± 3.1 E-5	R16571
6	826	58.20%	15.91 ± 0.33	1934.9 ± 0.0	1552.4	335.15 ± 0.30	4.42 ± 0.01	8.22 ± 0.16	1.30 ± 0.11	4.91 E-2 ± 9.3 E-4	1.27 E-4 ± 1.6 E-5	1.73 E-1 ± 1.5 E-4	6.69 E-4 ± 5.7 E-5	R16572
7	866	64.55%	16.08 ± 0.45	1515.4 ± 0.9	1160.5	247.87 ± 0.30	2.58 ± 0.01	5.40 ± 0.04	1.20 ± 0.11	4.36 E-2 ± 3.5 E-4	-4.04 E-4 ± 2.1 E-5	1.64 E-1 ± 2.2 E-4	7.93 E-4 ± 7.3 E-5	R16573
8	938	73.17%	15.96 ± 0.33	2113.1 ± 0.8	1562.6	336.36 ± 0.33	4.49 ± 0.01	10.53 ± 0.17	1.87 ± 0.11	6.26 E-2 ± 1.0 E-3	9.90 E-5 ± 1.6 E-5	1.59 E-1 ± 1.7 E-4	8.82 E-4 ± 5.2 E-5	R16575
9	992	81.33%	16.32 ± 0.35	1919.7 ± 0.3	1514.1	318.60 ± 0.30	4.30 ± 0.01	10.79 ± 0.05	1.38 ± 0.11	6.77 E-2 ± 3.3 E-4	1.68 E-4 ± 1.6 E-5	1.66 E-1 ± 1.6 E-4	7.15 E-4 ± 5.7 E-5	R16576
10	1053	96.37%	15.99 ± 0.19	3164.3 ± 0.1	2732.5	587.03 ± 0.53	7.88 ± 0.01	14.38 ± 0.05	1.46 ± 0.11	4.90 E-2 ± 1.6 E-4	2.14 E-4 ± 1.3 E-5	1.86 E-1 ± 1.7 E-4	4.62 E-4 ± 3.5 E-5	R16577
11	1242	99.81%	16.14 ± 0.82	833.0 ± 0.1	631.6	134.39 ± 0.12	1.79 ± 0.01	11.49 ± 0.09	0.68 ± 0.11	1.71 E-1 ± 1.4 E-3	1.09 E-4 ± 3.0 E-5	1.61 E-1 ± 1.4 E-4	8.18 E-4 ± 1.3 E-4	R16578
12	1376	100.00%	19.48 ± 15.11	159.8 ± 0.2	41.5	7.31 ± 0.01	0.06 ± 0.00	10.02 ± 0.04	0.40 ± 0.11	2.75 E+0 ± 9.7 E-3	-2.31 E-3 ± 5.1 E-4	4.57 E-2 ± 7.8 E-5	2.51 E-3 ± 6.8 E-4	R16579
APi0603 Ms-B (Ms ± Prg, 16.97 [mg], J = 0.001910, K = 5.25 [%], Cl = 47.7 [ppm], Ca = 5412 [ppm])														
1	475	0.12%	22.18 ± 26.90	163.1 ± 0.1	26.1	4.06 ± 0.02	10.17 ± 0.06	37.92 ± 3.08	0.47 ± 0.11	1.88 E+1 ± 1.5 E+0	4.40 E-1 ± 3.0 E-3	2.47 E-2 ± 1.2 E-4	2.84 E-3 ± 6.6 E-4	R16580
2	612	3.69%	15.26 ± 0.94	1154.0 ± 0.1	526.3	118.39 ± 0.12	5.56 ± 0.01	10.82 ± 0.05	2.13 ± 0.11	1.83 E-1 ± 8.4 E-4	5.67 E-3 ± 3.9 E-5	1.03 E-1 ± 1.0 E-4	1.84 E-3 ± 9.5 E-5	R16581
3	741	13.49%	15.03 ± 0.35	3803.0 ± 2.6	1422.3	324.73 ± 0.29	5.62 ± 0.01	16.86 ± 0.05	8.06 ± 0.11	1.04 E-1 ± 2.9 E-4	1.64 E-4 ± 1.7 E-5	8.54 E-2 ± 9.5 E-5	2.12 E-3 ± 2.9 E-5	R16582
4	776	34.95%	15.41 ± 0.16	3891.6 ± 1.2	3194.6	711.18 ± 0.65	9.55 ± 0.02	21.63 ± 0.08	2.36 ± 0.11	6.08 E-2 ± 2.3 E-4	1.86 E-4 ± 1.3 E-5	1.83 E-1 ± 1.8 E-4	6.06 E-4 ± 2.8 E-5	R16583
5	807	48.29%	15.45 ± 0.25	2481.7 ± 0.6	1990.3	442.08 ± 0.43	5.96 ± 0.01	12.64 ± 0.08	1.67 ± 0.11	5.72 E-2 ± 3.8 E-4	1.82 E-4 ± 1.4 E-5	1.78 E-1 ± 1.8 E-4	6.70 E-4 ± 4.4 E-5	R16584
6	847	56.48%	15.27 ± 0.41	1665.7 ± 0.3	1207.7	271.47 ± 0.25	3.80 ± 0.01	10.59 ± 0.15	1.55 ± 0.11	7.80 E-2 ± 1.1 E-3	2.11 E-4 ± 1.8 E-5	1.63 E-1 ± 1.5 E-4	9.31 E-4 ± 6.6 E-5	R16585
7	930	65.97%	15.45 ± 0.35	1841.1 ± 0.3	1416.1	314.50 ± 0.32	4.26 ± 0.01	13.99 ± 0.20	1.44 ± 0.11	8.90 E-2 ± 1.3 E-3	1.67 E-4 ± 1.6 E-5	1.71 E-1 ± 1.8 E-4	7.81 E-4 ± 6.0 E-5	R16586
8	998	79.99%	15.50 ± 0.24	2680.7 ± 0.4	2098.5	464.71 ± 0.43	6.37 ± 0.01	17.35 ± 0.14	1.97 ± 0.11	7.47 E-2 ± 5.9 E-4	2.07 E-4 ± 1.4 E-5	1.73 E-1 ± 1.6 E-4	7.35 E-4 ± 4.1 E-5	R16587
9	1043	94.52%	15.71 ± 0.23	2566.1 ± 0.1	2204.2	481.46 ± 0.45	6.34 ± 0.01	15.80 ± 0.07	1.23 ± 0.11	6.56 E-2 ± 2.8 E-4	1.65 E-4 ± 1.4 E-5	1.88 E-1 ± 1.7 E-4	4.77 E-4 ± 4.3 E-5	R16588
10	1272	99.69%	16.10 ± 0.65	1022.8 ± 0.2	804.8	171.50 ± 0.15	2.25 ± 0.01	12.04 ± 0.08	0.74 ± 0.11	1.40 E-1 ± 9.5 E-4	9.57 E-5 ± 2.5 E-5	1.68 E-1 ± 1.5 E-4	7.21 E-4 ± 1.1 E-4	R16589
11	1382	100.00%	17.09 ± 10.86	174.6 ± 0.1	50.6	10.17 ± 0.02	0.12 ± 0.00	10.22 ± 0.03	0.42 ± 0.11	2.01 E+0 ± 6.8 E-3	-1.36 E-3 ± 3.6 E-4	5.82 E-2 ± 1.2 E-4	2.40 E-3 ± 6.3 E-4	R16590
APi0603 MsC (Ms ± Prg, 15.18 [mg], J = 0.001909, K = 5.14 [%], Cl = 47.9 [ppm], Ca = 5223 [ppm])														
1	473	0.21%	-43.79 ± 18.56	218.5 ± 0.4	-77.6	6.19 ± 0.02	10.19 ± 0.02	18.33 ± 0.09	1.01 ± 0.11	5.94 E+0 ± 3.0 E-2	2.86 E-1 ± 8.0 E-4	2.83 E-2 ± 1.2 E-4	4.59 E-3 ± 5.0 E-4	R16606
2	614	2.46%	15.42 ± 1.70	867.5 ± 0.4	295.6	65.71 ± 0.07	4.16 ± 0.01	11.44 ± 0.15	1.94 ± 0.11	3.48 E-1 ± 4.6 E-3	8.21 E-3 ± 6.1 E-5	7.57 E-2 ± 9.2 E-5	2.23 E-3 ± 1.3 E-4	R16607
3	762	33.87%	15.61 ± 0.13	7275.6 ± 1.0	4174.4	917.05 ± 0.83	13.88 ± 0.02	33.41 ± 0.14	10.50 ± 0.12	7.29 E-2 ± 3.0 E-4	2.21 E-4 ± 1.2 E-5	1.26 E-1 ± 1.2 E-4	1.44 E-3 ± 1.5 E-5	R16609
4	784	49.01%	15.68 ± 0.25	2466.9 ± 3.1	2021.8	442.10 ± 0.58	6.02 ± 0.01	18.67 ± 0.21	1.51 ± 0.11	8.45 E-2 ± 9.5 E-4	2.16 E-4 ± 1.4 E-5	1.79 E-1 ± 3.3 E-4	6.11 E-4 ± 4.4 E-5	R16610
5	816	57.52%	15.70 ± 0.45	1389.8 ± 0.1	1138.5	248.63 ± 0.22	3.26 ± 0.01	11.53 ± 0.05	0.85 ± 0.11	9.28 E-2 ± 3.9 E-4	1.25 E-4 ± 1.9 E-5	1.79 E-1 ± 1.6 E-4	6.12 E-4 ± 7.9 E-5	R16611
6	854	62.46%	15.67 ± 0.77	868.1 ± 0.3	658.9	144.20 ± 0.13	1.89 ± 0.00	12.27 ± 0.04	0.71 ± 0.11	1.70 E-1 ± 6.0 E-4	7.69 E-5 ± 2.8 E-5	1.66 E-1 ± 1.6 E-4	8.16 E-4 ± 1.3 E-4	R16612
7	934	71.23%	16.19 ± 0.43	1582.7 ± 0.1	1209.7	256.19 ± 0.23	3.39 ± 0.01	11.21 ± 0.08	1.27 ± 0.11	8.75 E-2 ± 6.5 E-4	9.51 E-5 ± 1.8 E-5	1.62 E-1 ± 1.4 E-4	7.98 E-4 ± 6.9 E-5	R16615
8	999	80.42%	16.10 ± 0.41	1538.7 ± 0.3	1260.2	268.41 ± 0.24	3.48 ± 0.01	11.98 ± 0.12	0.95 ± 0.11	8.93 E-2 ± 9.2 E-4	9.51 E-5 ± 1.8 E-5	1.74 E-1 ± 1.6 E-4	6.13 E-4 ± 7.1 E-5	R16616
9	1047	93.64%	16.06 ± 0.29	2039.6 ± 0.2	1808.6	386.01 ± 0.36	4.95 ± 0.01	13.01 ± 0.04	0.79 ± 0.11	6.74 E-2 ± 1.9 E-4	1.21 E-4 ± 1.5 E-5	1.89 E-1 ± 1.8 E-4	3.83 E-4 ± 5.4 E-5	R16617
10	1280	99.41%	16.69 ± 0.66	992.7 ± 0.3	820.0	168.39 ± 0.18	2.12 ± 0.01	8.33 ± 0.10	0.59 ± 0.11	9.89 E-2 ± 1.2 E-3	3.07 E-5 ± 2.5 E-5	1.70 E-1 ± 1.8 E-4	5.89 E-4 ± 1.1 E-4	R16618
11	1340	100.00%	22.71 ± 6.41	266.2 ± 0.2	114.3	17.23 ± 0.10	0.12 ± 0.00	5.84 ± 0.23	0.52 ± 0.11	6.78 E-1 ± 2.6 E-2	-1.86 E-3 ± 2.1 E-4	6.47 E-2 ± 3.6 E-4	1.93 E-3 ± 4.1 E-4	R16619
APi0603 MsD (Prg-rich, 20.57 [mg], J = 0.001908, K = 0.96 [%], Cl = 84.2 [ppm], Ca = 8195 [ppm])														
1	477	1.41%	-123.29 ± 11.63	253.7 ± 0.7	-359.4	10.42 ± 0.11	24.00 ± 0.42	60.64 ± 0.89	2.09 ± 0.11	1.17 E+1 ± 1.7 E-1	4.01 E-1 ± 7.2 E-3	4.09 E-2 ± 4.5 E-4	8.18 E-3 ± 4.3 E-4	R16620
2	609	10.49%	14.50 ± 1.66	926.2 ± 0.2	283.3	67.01 ± 0.08	10.12 ± 0.04	26.60 ± 0.14	2.18 ± 0.11	7.94 E-1 ± 4.1 E-3	2.37 E-2 ± 1.2 E-4	7.23 E-2 ± 8.4 E-5	2.35 E-3 ± 1.2 E-4	R16621
3	741	36.63%	13.41 ± 0.62	4455.9 ± 0.9	754.8	193.03 ± 0.18	5.07 ± 0.02	62.48 ± 0.18	12.54 ± 0.12	6.47 E-1 ± 1.8 E-3	4.34 E-4 ± 2.8 E-5	4.33 E-2 ± 4.1 E-5	2.81 E-3 ± 2.5 E-5	R16622
4	778	51.93%	16.92 ± 0.98	961.7 ± 0.1	557.9	112.96 ± 0.14	1.62 ± 0.00	31.66 ± 0.12	1.37 ± 0.11	5.61 E-1 ± 2.1 E-3	6.51 E-5 ± 3.5 E-5	1.17 E-1 ± 1.5 E-4	1.42 E-3 ± 1.1 E-4	R16623
5	828	61.19%	17.48 ± 1.61	523.4 ± 0.3	348.6	68.34 ± 0.09	1.48 ± 0.01	18.67 ± 0.18	0.60 ± 0.11	5.47 E-1 ± 5.2 E-3	1.47 E-3 ± 5.8 E-5	1.31 E-1 ± 1.8 E-4	1.13 E-3 ± 2.1 E-4	R16624
6	924	76.54%	15.98 ± 0.97	774.7 ± 0.2	528.6	113.37 ± 0.10	1.92 ± 0.01	44.79 ± 0.17	0.84 ± 0.11	7.90 E-1 ± 2.9 E-3	6.90 E-4 ± 3.8 E-5	1.46 E-1 ± 1.3 E-4	1.08 E-3 ± 1.4 E-4	R16625
7	1023	92.27%	15.43 ± 0.95	793.2 ± 0.3	522.5	116.11 ± 0.11	2.14 ± 0.00	43.86 ± 0.20	0.93 ± 0.11	7.56 E-1 ± 3.5 E-3	9.37 E-4 ± 3.4 E-5	1.46 E-1 ± 1.6 E-4	1.16 E-3 ± 1.4 E-4	R16626
8	1273	99.45%	13.22 ± 2.09	702.1 ± 0.1	204.2	53.00 ± 0.06	1.76 ± 0.00	32.75 ± 0.09	1.69 ± 0.11	1.24 E+0 ± 3.6 E-3	2.76 E-3 ± 7.1 E-5	7.55 E-2 ± 9.0 E-5	2.40 E-3 ± 1.6 E-4	R16627
9	1380	100.00%	-49.01 ± 28.18	301.3 ± 0.1	-57.3	4.08 ± 0.05	1.36 ± 0.01	11.05 ± 0.24	1.22 ± 0.11	5.42 E+0 ± 1.2 E-1	4.75 E-2 ± 1.0 E-3	1.35 E-2 ± 1.6 E-4	4.03 E-3 ± 3.6 E-4	R16628

Appendix 2.2 (continued)

#	T°C	^{39}Ar [%]	Age [Ma]	$^{40}Ar_{tot}$ [pL]	$^{40}Ar^*$ [pL]	^{39}Ar [pL]	^{38}Ar [pL]	^{37}Ar [pL]	^{36}Ar [pL]	Ca/K	Cl/K	39/40	36/40	STP File
ALu0306 Bt (6.4 [mg], J = 0.001188, K = 6.65 [%], Cl = 541.9 [ppm], Ca = 8572 [ppm])														
1	487	3.96%	-0.40 ± 2.43	554.7 ± 51.6	-18.6	99.96 ± 0.30	58.98 ± 0.26	19.94 ± 0.22	1.95 ± 0.38	3.99 E-1 ± 4.4 E-3	1.02 E-1 ± 4.8 E-4	1.80 E-1 ± 1.7 E-2	3.50 E-3 ± 7.6 E-4	R14438
2	632	9.14%	13.54 ± 1.11	2058.9 ± 1.6	828.7	130.69 ± 0.27	8.61 ± 0.09	48.74 ± 0.52	4.18 ± 0.23	7.46 E-1 ± 8.0 E-3	8.59 E-3 ± 1.3 E-4	6.35 E-2 ± 1.4 E-4	2.02 E-3 ± 1.1 E-4	R14439
3	802	39.73%	17.63 ± 0.22	8569.9 ± 1.5	6385.1	772.24 ± 0.71	18.64 ± 0.04	23.67 ± 0.07	7.40 ± 0.27	6.13 E-2 ± 1.7 E-4	1.89 E-3 ± 1.8 E-5	9.01 E-2 ± 8.4 E-5	8.63 E-4 ± 3.1 E-5	R14440
4	872	48.60%	17.35 ± 0.66	2854.5 ± 1.4	1821.2	223.89 ± 0.25	10.87 ± 0.18	10.94 ± 0.47	3.50 ± 0.23	9.78 E-2 ± 4.2 E-3	6.03 E-3 ± 1.5 E-4	7.84 E-2 ± 9.4 E-5	1.23 E-3 ± 8.2 E-5	R14441
5	892	55.31%	19.33 ± 0.85	2199.9 ± 0.2	1535.4	169.34 ± 0.39	8.67 ± 0.04	9.48 ± 0.17	2.25 ± 0.23	1.12 E-1 ± 2.0 E-3	6.58 E-3 ± 6.3 E-5	7.70 E-2 ± 1.8 E-4	1.02 E-3 ± 1.0 E-4	R14442
6	912	62.90%	16.70 ± 0.77	2316.7 ± 0.6	1499.8	191.56 ± 0.17	8.92 ± 0.08	12.08 ± 0.06	2.77 ± 0.23	1.26 E-1 ± 6.7 E-4	5.71 E-3 ± 8.8 E-5	8.27 E-2 ± 7.6 E-5	1.19 E-3 ± 1.0 E-4	R14443
7	954	75.58%	17.93 ± 0.53	3643.8 ± 1.1	2691.1	320.04 ± 2.25	11.84 ± 0.13	15.57 ± 0.83	3.23 ± 0.26	9.73 E-2 ± 5.2 E-3	4.15 E-3 ± 7.9 E-5	8.78 E-2 ± 6.2 E-4	8.85 E-4 ± 7.2 E-5	R14444
8	1028	89.12%	17.49 ± 0.47	3564.5 ± 0.2	2804.4	341.99 ± 0.33	10.84 ± 0.16	10.18 ± 0.25	2.57 ± 0.26	5.95 E-2 ± 1.4 E-3	3.30 E-3 ± 8.6 E-5	9.59 E-2 ± 9.3 E-5	7.22 E-4 ± 7.2 E-5	R14445
9	1198	98.77%	14.32 ± 0.70	3075.3 ± 0.9	1633.4	243.52 ± 0.65	9.58 ± 0.10	10.68 ± 0.15	4.88 ± 0.27	8.77 E-2 ± 1.3 E-3	4.24 E-3 ± 8.1 E-5	7.92 E-2 ± 2.1 E-4	1.59 E-3 ± 8.8 E-5	R14446
10	1427	100.00%	-10.82 ± 5.04	4413.9 ± 0.5	-156.1	31.03 ± 0.17	7.90 ± 0.04	10.06 ± 0.46	15.47 ± 0.25	6.49 E-1 ± 3.0 E-2	2.67 E-2 ± 3.4 E-4	7.03 E-3 ± 3.8 E-5	3.50 E-3 ± 5.4 E-5	R14447
AMo0409 Bt (17.3 [mg], J = 0.000991, K = 6.65 [%], Cl = 44.6 [ppm], Ca = 4497 [ppm])														
1	477	0.42%	-20.15 ± 12.51	2111.4 ± 2.0	-182.4	16.31 ± 0.06	5.24 ± 0.46	58.02 ± 4.47	7.78 ± 0.38	7.13 E+0 ± 5.5 E-1	3.94 E-2 ± 5.1 E-3	7.71 E-3 ± 3.0 E-5	3.68 E-3 ± 1.8 E-4	R15841
2	584	1.43%	16.88 ± 4.62	7762.2 ± 33.3	379.0	39.95 ± 0.30	6.32 ± 0.22	-1.28 ± 1.74	24.99 ± 0.35	-6.39 E-2 ± 8.7 E-2	5.25 E-3 ± 1.0 E-3	5.15 E-3 ± 4.5 E-5	3.22 E-3 ± 4.6 E-5	R15842
3	672	20.75%	15.56 ± 0.22	12488.6 ± 14.8	6628.4	758.42 ± 1.50	14.05 ± 0.18	27.63 ± 1.09	19.84 ± 0.31	7.29 E-2 ± 2.9 E-3	3.34 E-4 ± 4.5 E-5	6.07 E-2 ± 1.4 E-4	1.59 E-3 ± 2.4 E-5	R15843
4	720	29.97%	16.28 ± 0.47	6610.4 ± 6.9	3306.5	361.62 ± 1.50	10.30 ± 0.10	-5.96 ± 0.03	11.18 ± 0.32	-3.30 E-2 ± 1.6 E-4	1.95 E-3 ± 5.8 E-5	5.47 E-2 ± 2.3 E-4	1.69 E-3 ± 4.8 E-5	R15844
5	761	36.91%	13.97 ± 0.61	6511.8 ± 30.9	2136.7	272.56 ± 0.24	5.76 ± 0.14	30.08 ± 3.80	14.81 ± 0.31	2.21 E-1 ± 2.8 E-2	-1.37 E-4 ± 9.8 E-5	4.19 E-2 ± 2.0 E-4	2.27 E-3 ± 4.9 E-5	R15845
6	857	44.14%	17.16 ± 0.58	6087.4 ± 7.1	2735.7	283.74 ± 0.39	6.43 ± 0.14	3.03 ± 3.55	11.34 ± 0.31	2.14 E-2 ± 2.5 E-2	6.07 E-4 ± 9.8 E-5	4.66 E-2 ± 8.4 E-5	1.86 E-3 ± 5.1 E-5	R15846
7	943	56.01%	15.19 ± 0.37	7343.3 ± 2.4	3974.1	465.88 ± 0.50	8.22 ± 0.17	10.72 ± 4.58	11.40 ± 0.33	4.60 E-2 ± 2.0 E-2	2.32 E-4 ± 7.1 E-5	6.34 E-2 ± 7.1 E-5	1.55 E-3 ± 4.5 E-5	R15847
8	1012	79.91%	17.03 ± 0.16	12287.8 ± 7.0	8976.2	938.33 ± 0.83	14.30 ± 0.24	0.24 ± 1.82	11.21 ± 0.29	5.06 E-4 ± 3.9 E-3	2.21 E-4 ± 4.9 E-5	7.64 E-2 ± 8.0 E-5	9.12 E-4 ± 2.3 E-5	R15848
9	1086	95.27%	15.91 ± 0.26	10171.7 ± 11.6	5390.0	603.10 ± 1.56	10.25 ± 0.18	-4.19 ± 5.31	16.18 ± 0.30	-1.39 E-2 ± 1.8 E-2	3.83 E-5 ± 5.6 E-5	5.93 E-2 ± 1.7 E-4	1.59 E-3 ± 2.9 E-5	R15849
10	1200	99.59%	15.38 ± 0.93	7076.0 ± 0.5	1464.0	169.52 ± 0.42	6.99 ± 0.16	10.10 ± 4.66	18.99 ± 0.30	1.19 E-1 ± 5.5 E-2	1.52 E-3 ± 1.8 E-4	2.40 E-2 ± 5.9 E-5	2.68 E-3 ± 4.2 E-5	R15850
11	1370	100.00%	-4.09 ± 10.68	5919.0 ± 9.3	-36.6	16.04 ± 0.26	4.49 ± 0.18	-4.45 ± 1.76	20.15 ± 0.32	-5.54 E-1 ± 2.2 E-1	5.90 E-3 ± 2.2 E-3	2.71 E-3 ± 4.4 E-5	3.41 E-3 ± 5.4 E-5	R15851
AMo0410 Bt (11.7 [mg], J = 0.000999, K = 6.18 [%], Cl = 165.4 [ppm], Ca = 10916 [ppm])														
1	469	1.44%	-89.05 ± 5.52	235.3 ± 2.4	-1720.4	35.78 ± 0.17	10.25 ± 0.27	139.87 ± 3.19	6.65 ± 0.35	7.84 E+0 ± 1.8 E-1	4.28 E-2 ± 1.4 E-3	1.52 E-1 ± 1.7 E-3	2.81 E-2 ± 1.5 E-3	R15738
2	544	1.76%	-62.68 ± 19.64	415.6 ± 1.8	-274.0	8.02 ± 0.09	1.27 ± 0.28	11.12 ± 2.93	2.34 ± 0.29	2.77 E+0 ± 7.3 E-1	1.64 E-2 ± 6.4 E-3	1.93 E-2 ± 2.2 E-4	5.62 E-3 ± 6.9 E-4	R15739
3	611	5.02%	5.77 ± 1.95	1735.5 ± 1.7	260.0	81.15 ± 0.25	5.10 ± 0.09	15.38 ± 0.71	5.00 ± 0.30	3.79 E-1 ± 1.8 E-2	7.05 E-3 ± 2.4 E-4	4.68 E-2 ± 1.5 E-4	2.88 E-3 ± 1.7 E-4	R15740
4	665	12.51%	14.23 ± 0.84	2621.0 ± 3.0	1478.5	186.54 ± 0.20	5.28 ± 0.04	5.32 ± 1.23	3.87 ± 0.30	5.70 E-2 ± 1.3 E-2	2.25 E-3 ± 6.4 E-5	7.12 E-2 ± 1.1 E-4	1.48 E-3 ± 1.1 E-4	R15741
5	739	26.35%	16.40 ± 0.48	4057.6 ± 5.2	3147.6	344.39 ± 0.94	7.64 ± 0.04	0.63 ± 1.30	3.08 ± 0.31	3.68 E-3 ± 7.6 E-3	1.56 E-3 ± 3.8 E-5	8.49 E-2 ± 2.6 E-4	7.59 E-4 ± 7.8 E-5	R15742
6	776	31.32%	20.88 ± 1.34	1555.6 ± 0.4	1440.7	123.63 ± 0.20	2.54 ± 0.15	13.14 ± 2.97	0.39 ± 0.32	2.13 E-1 ± 4.8 E-2	1.47 E-3 ± 2.3 E-4	7.95 E-2 ± 1.3 E-4	2.50 E-4 ± 2.0 E-4	R15743
7	798	33.95%	16.15 ± 2.64	922.1 ± 0.4	590.1	65.54 ± 0.17	2.74 ± 0.05	-4.35 ± 1.83	1.12 ± 0.33	-1.33 E-1 ± 5.6 E-2	4.77 E-3 ± 2.2 E-4	7.11 E-2 ± 1.9 E-4	1.22 E-3 ± 3.6 E-4	R15744
8	821	35.90%	11.34 ± 3.19	731.7 ± 0.4	306.5	48.56 ± 0.14	0.88 ± 0.19	1.09 ± 3.80	1.44 ± 0.29	4.51 E-2 ± 1.6 E-1	1.49 E-4 ± 7.1 E-4	6.64 E-2 ± 1.9 E-4	1.97 E-3 ± 4.0 E-4	R15745
9	853	38.53%	21.42 ± 2.36	908.5 ± 0.2	781.9	65.39 ± 0.20	1.67 ± 0.19	0.51 ± 2.19	0.43 ± 0.29	1.55 E-2 ± 6.7 E-2	2.24 E-3 ± 5.4 E-4	7.20 E-2 ± 2.2 E-4	4.72 E-4 ± 3.2 E-4	R15746
10	891	42.24%	11.69 ± 1.67	1406.6 ± 0.3	601.2	92.35 ± 0.20	3.41 ± 0.14	-0.04 ± 4.23	2.73 ± 0.29	-8.98 E-4 ± 9.2 E-2	3.49 E-3 ± 2.8 E-4	6.57 E-2 ± 1.4 E-4	1.94 E-3 ± 2.1 E-4	R15747
11	926	48.01%	8.66 ± 1.32	1683.5 ± 0.9	691.8	143.60 ± 0.23	3.46 ± 0.22	-2.36 ± 3.21	3.36 ± 0.36	-3.28 E-2 ± 4.5 E-2	1.42 E-3 ± 2.8 E-4	8.53 E-2 ± 1.4 E-4	1.99 E-3 ± 2.1 E-4	R15748
12	962	60.22%	14.66 ± 0.54	3221.9 ± 0.5	2481.3	303.85 ± 0.30	6.65 ± 0.17	3.42 ± 3.31	2.51 ± 0.31	2.25 E-2 ± 2.2 E-2	1.53 E-3 ± 1.1 E-4	9.43 E-2 ± 9.5 E-5	7.78 E-4 ± 9.7 E-5	R15749
13	1038	88.66%	16.36 ± 0.23	7241.0 ± 2.2	6456.9	707.98 ± 0.65	15.55 ± 0.13	4.24 ± 1.75	2.65 ± 0.30	1.20 E-2 ± 4.9 E-3	1.69 E-3 ± 3.8 E-5	9.78 E-2 ± 9.5 E-5	3.66 E-4 ± 4.2 E-5	R15750
14	1118	96.79%	15.39 ± 0.81	2478.5 ± 0.7	1735.1	202.25 ± 0.34	5.23 ± 0.06	7.59 ± 2.18	2.52 ± 0.31	7.50 E-2 ± 2.2 E-2	2.10 E-3 ± 7.7 E-5	8.16 E-2 ± 1.4 E-4	1.02 E-3 ± 1.3 E-4	R15751
15	1350	100.00%	17.37 ± 1.95	1289.9 ± 0.0	773.6	79.91 ± 0.21	2.45 ± 0.05	35.74 ± 1.97	1.76 ± 0.30	8.95 E-1 ± 4.9 E-2	2.64 E-3 ± 1.7 E-4	6.19 E-2 ± 1.6 E-4	1.35 E-3 ± 2.3 E-4	R15752

Appendix 2.2 (continued)

#	T°C	^{39}Ar [%]	Age [Ma]	^{40}Ar$_{tot}$ [pL]	^{40}Ar* [pL]	^{39}Ar [pL]	^{38}Ar [pL]	^{37}Ar [pL]	^{36}Ar [pL]	Ca/K	Cl/K	39/40	36/40	STP File
APi0601 Bt100 (11.46 [mg], J = 0.001914, K = 6.41 [%], Cl = 147.6 [ppm], Ca = 6427 [ppm])														
1	631	2.83%	15.04 ± 1.50	3453.4 ± 1.4	346.8	79.30 ± 0.08	33.27 ± 0.14	16.83 ± 0.16	10.52 ± 0.12	4.25 E-1 ± 4.0 E-3	6.82 E-2 ± 3.1 E-4	2.30 E-2 ± 2.5 E-5	3.04 E-3 ± 3.2 E-5	R16708
2	715	15.47%	15.78 ± 0.32	3808.1 ± 0.6	1623.4	353.86 ± 0.34	7.16 ± 0.01	14.44 ± 0.14	7.40 ± 0.11	8.16 E-2 ± 7.7 E-4	8.14 E-4 ± 1.6 E-5	9.29 E-2 ± 9.1 E-5	1.94 E-3 ± 2.9 E-5	R16709
3	762	25.65%	15.21 ± 0.39	1961.9 ± 1.8	1260.7	285.14 ± 0.31	4.43 ± 0.01	13.43 ± 0.11	2.38 ± 0.11	9.42 E-2 ± 7.4 E-4	3.97 E-4 ± 1.7 E-5	1.45 E-1 ± 2.1 E-4	1.21 E-3 ± 5.6 E-5	R16710
4	828	35.06%	14.74 ± 0.42	1801.0 ± 0.6	1128.7	263.42 ± 0.27	3.97 ± 0.01	13.14 ± 0.04	2.28 ± 0.11	9.98 E-2 ± 3.4 E-4	3.01 E-4 ± 1.9 E-5	1.46 E-1 ± 1.6 E-4	1.26 E-3 ± 6.1 E-5	R16711
5	889	47.23%	15.06 ± 0.33	2357.4 ± 0.4	1492.6	340.77 ± 0.35	5.13 ± 0.01	15.11 ± 0.05	2.93 ± 0.11	8.87 E-2 ± 2.7 E-4	2.99 E-4 ± 1.6 E-5	1.45 E-1 ± 1.5 E-4	1.24 E-3 ± 4.7 E-5	R16712
6	980	73.92%	14.82 ± 0.15	4650.0 ± 1.2	3221.2	747.40 ± 0.66	11.16 ± 0.02	19.82 ± 0.12	4.84 ± 0.11	5.30 E-2 ± 3.1 E-4	3.49 E-4 ± 1.3 E-5	1.61 E-1 ± 1.5 E-4	1.04 E-3 ± 2.4 E-5	R16713
7	1060	92.97%	14.76 ± 0.21	4029.6 ± 0.6	2289.3	533.45 ± 0.47	8.32 ± 0.02	20.43 ± 0.15	5.89 ± 0.11	7.66 E-2 ± 5.7 E-4	3.17 E-4 ± 1.4 E-5	1.32 E-1 ± 1.2 E-4	1.46 E-3 ± 2.7 E-5	R16714
8	1204	99.55%	13.73 ± 0.62	2852.2 ± 1.6	735.4	184.23 ± 0.18	3.79 ± 0.01	16.79 ± 0.05	7.17 ± 0.11	1.82 E-1 ± 5.1 E-4	2.74 E-4 ± 2.4 E-5	6.46 E-2 ± 7.2 E-5	2.51 E-3 ± 3.9 E-5	R16715
9	1377	100.00%	-60.28 ± 9.49	1935.7 ± 0.2	-215.6	12.57 ± 0.02	1.39 ± 0.00	17.85 ± 0.14	7.28 ± 0.11	2.84 E+0 ± 2.2 E-2	-1.59 E-3 ± 3.1 E-4	6.49 E-3 ± 8.2 E-6	3.76 E-3 ± 5.7 E-5	R16716
APi0601 Bt200 (11.08 [mg], J = 0.001916, K = 5.94 [%], Cl = 569.9 [ppm], Ca = 9733 [ppm])														
1	503	0.28%	-39.41 ± 16.62	340.9 ± 1.0	-79.1	7.04 ± 0.19	122.05 ± 0.24	38.09 ± 1.03	1.43 ± 0.11	1.09 E+1 ± 2.9 E-1	3.08 E+0 ± 6.1 E-3	2.06 E-2 ± 5.6 E-4	4.17 E-3 ± 3.3 E-4	R16685
2	636	2.63%	9.94 ± 1.93	1829.0 ± 0.3	169.7	58.90 ± 0.05	11.69 ± 0.03	13.58 ± 0.05	5.62 ± 0.11	4.61 E-1 ± 1.6 E-3	3.01 E-2 ± 1.0 E-4	3.22 E-2 ± 2.9 E-5	3.07 E-3 ± 6.0 E-5	R16686
3	720	24.00%	14.68 ± 0.21	3124.3 ± 0.6	2283.7	535.70 ± 0.53	6.10 ± 0.02	21.26 ± 0.21	2.85 ± 0.11	7.94 E-2 ± 7.8 E-4	-2.42 E-4 ± 1.4 E-5	1.71 E-1 ± 1.7 E-4	9.11 E-4 ± 3.5 E-5	R16687
4	768	34.36%	14.91 ± 0.43	1442.1 ± 0.2	1125.3	259.84 ± 0.26	3.92 ± 0.01	15.01 ± 0.07	1.08 ± 0.11	1.16 E-1 ± 5.1 E-4	4.55 E-4 ± 1.8 E-5	1.80 E-1 ± 1.8 E-4	7.43 E-4 ± 7.6 E-5	R16688
5	800	40.62%	14.91 ± 0.71	1120.8 ± 0.3	679.5	156.89 ± 0.20	2.56 ± 0.01	13.83 ± 0.09	1.50 ± 0.11	1.76 E-1 ± 1.2 E-3	4.94 E-4 ± 2.6 E-5	1.40 E-1 ± 1.8 E-4	1.33 E-3 ± 9.8 E-5	R16689
6	843	48.62%	15.20 ± 0.55	1282.0 ± 0.0	886.3	200.74 ± 0.18	3.01 ± 0.01	15.56 ± 0.08	1.34 ± 0.11	1.55 E-1 ± 7.8 E-4	3.57 E-4 ± 2.2 E-5	1.57 E-1 ± 1.4 E-4	1.04 E-3 ± 8.6 E-5	R16690
7	931	71.06%	14.85 ± 0.20	3033.8 ± 1.8	2427.1	562.62 ± 0.50	8.10 ± 0.02	22.44 ± 0.13	2.06 ± 0.11	7.98 E-2 ± 4.5 E-4	3.49 E-4 ± 1.4 E-5	1.85 E-1 ± 2.0 E-4	6.77 E-4 ± 3.6 E-5	R16691
8	999	86.79%	15.09 ± 0.28	2361.2 ± 0.6	1728.3	394.37 ± 0.44	5.79 ± 0.01	19.40 ± 0.06	2.15 ± 0.11	9.84 E-2 ± 3.2 E-4	3.42 E-4 ± 1.5 E-5	1.67 E-1 ± 1.9 E-4	9.07 E-4 ± 4.7 E-5	R16692
9	1047	95.41%	14.65 ± 0.52	1635.4 ± 0.6	919.5	216.06 ± 0.23	3.47 ± 0.01	19.37 ± 0.25	2.43 ± 0.11	1.79 E-1 ± 2.3 E-3	3.94 E-4 ± 2.2 E-5	1.32 E-1 ± 1.5 E-4	1.48 E-3 ± 6.7 E-5	R16693
10	1272	99.66%	13.65 ± 1.05	1340.5 ± 0.3	422.7	106.67 ± 0.10	2.00 ± 0.00	16.19 ± 0.05	3.11 ± 0.11	3.04 E-1 ± 8.6 E-4	2.85 E-4 ± 3.7 E-5	7.96 E-2 ± 7.7 E-5	2.32 E-3 ± 8.2 E-5	R16694
11	1371	100.00%	-129.46 ± 14.51	1227.0 ± 0.4	-305.0	8.46 ± 0.04	1.18 ± 0.00	21.36 ± 0.14	5.19 ± 0.11	5.06 E+0 ± 3.3 E-2	2.40 E-3 ± 4.4 E-4	6.88 E-3 ± 3.3 E-5	4.23 E-3 ± 9.0 E-5	R16695
APi0603 Bt100 (9.12 [mg], J = 0.001908, K = 6.04 [%], Cl = 355.1 [ppm], Ca = 11786 [ppm])														
1	509	0.31%	-122.25 ± 18.90	148.1 ± 1.2	-219.6	6.46 ± 0.14	53.85 ± 0.22	89.74 ± 2.01	1.27 ± 0.11	2.81 E+1 ± 6.3 E-1	1.48 E+0 ± 6.1 E-3	4.32 E-2 ± 1.0 E-3	8.40 E-3 ± 7.4 E-4	R16698
2	638	2.85%	10.87 ± 2.12	1567.6 ± 0.3	168.8	53.31 ± 0.05	13.84 ± 0.04	12.66 ± 0.05	4.74 ± 0.11	4.75 E-1 ± 2.0 E-3	4.12 E-2 ± 1.4 E-4	3.40 E-2 ± 3.1 E-5	3.02 E-3 ± 7.0 E-5	R16699
3	722	15.37%	14.94 ± 0.42	1665.2 ± 0.6	1142.5	262.29 ± 0.24	4.17 ± 0.01	11.61 ± 0.04	1.77 ± 0.11	8.85 E-2 ± 2.7 E-4	5.13 E-4 ± 1.8 E-5	1.58 E-1 ± 1.5 E-4	1.06 E-3 ± 6.6 E-5	R16700
4	770	26.96%	14.73 ± 0.46	1519.3 ± 0.5	1043.2	242.86 ± 0.22	3.69 ± 0.01	12.95 ± 0.04	1.61 ± 0.11	1.07 E-1 ± 3.1 E-4	3.89 E-4 ± 2.1 E-5	1.60 E-1 ± 1.5 E-4	1.06 E-3 ± 7.2 E-5	R16701
5	836	39.58%	14.48 ± 0.42	1725.3 ± 0.6	1116.4	264.31 ± 0.32	4.06 ± 0.02	15.07 ± 0.07	2.06 ± 0.11	1.14 E-1 ± 5.6 E-4	3.80 E-4 ± 2.1 E-5	1.53 E-1 ± 2.0 E-4	1.19 E-3 ± 6.4 E-5	R16702
6	896	56.02%	14.57 ± 0.32	2323.3 ± 1.0	1464.1	344.49 ± 0.32	5.07 ± 0.01	14.24 ± 0.06	2.91 ± 0.11	8.27 E-2 ± 3.6 E-4	2.46 E-4 ± 1.6 E-5	1.48 E-1 ± 1.5 E-4	1.25 E-3 ± 4.7 E-5	R16703
7	984	82.63%	14.80 ± 0.20	3633.1 ± 1.6	2406.5	557.49 ± 0.52	8.10 ± 0.01	15.38 ± 0.04	4.15 ± 0.11	5.52 E-2 ± 1.5 E-4	2.45 E-4 ± 1.3 E-5	1.53 E-1 ± 1.6 E-4	1.14 E-3 ± 3.0 E-5	R16704
8	1060	97.41%	14.74 ± 0.37	3155.6 ± 0.3	1331.0	309.71 ± 0.29	5.14 ± 0.01	15.48 ± 0.10	6.18 ± 0.11	1.00 E-1 ± 6.3 E-4	1.95 E-4 ± 1.7 E-5	9.81 E-2 ± 9.3 E-5	1.96 E-3 ± 3.5 E-5	R16705
9	1205	99.84%	8.89 ± 2.21	1457.1 ± 0.4	131.9	50.97 ± 0.05	1.41 ± 0.00	12.98 ± 0.06	4.49 ± 0.11	5.09 E-1 ± 2.4 E-3	-9.32 E-5 ± 7.5 E-5	3.50 E-2 ± 3.4 E-5	3.08 E-3 ± 7.5 E-5	R16706
10	1377	100.00%	-129.48 ± 36.65	1476.4 ± 0.0	-121.5	3.36 ± 0.00	0.93 ± 0.00	15.00 ± 0.05	5.41 ± 0.11	8.96 E+0 ± 3.0 E-2	-6.02 E-3 ± 1.1 E-3	2.27 E-3 ± 2.1 E-6	3.66 E-3 ± 7.5 E-5	R16707
APi0603 Bt200 (12.08 [mg], J = 0.001908, K = 6.48 [%], Cl = 483.9 [ppm], Ca = 4863 [ppm])														
1	516	0.89%	5.51 ± 4.29	520.3 ± 0.3	41.7	26.02 ± 0.15	118.42 ± 0.69	25.53 ± 0.29	1.63 ± 0.11	1.96 E+0 ± 2.2 E-2	8.06 E-1 ± 4.7 E-3	5.00 E-2 ± 2.9 E-4	3.11 E-3 ± 2.1 E-4	R16593
2	650	6.70%	14.26 ± 0.69	3905.2 ± 0.3	705.0	169.57 ± 0.17	9.15 ± 0.02	8.93 ± 0.03	10.83 ± 0.12	1.05 E-1 ± 3.1 E-4	5.38 E-3 ± 3.1 E-5	4.34 E-2 ± 4.3 E-5	2.77 E-3 ± 2.8 E-5	R16594
3	734	25.43%	15.30 ± 0.20	3149.6 ± 0.9	2438.7	546.28 ± 0.61	5.55 ± 0.01	12.30 ± 0.14	2.41 ± 0.11	4.50 E-2 ± 5.1 E-4	-4.32 E-4 ± 1.3 E-5	1.73 E-1 ± 2.0 E-4	7.64 E-4 ± 3.5 E-5	R16595
4	778	34.98%	15.23 ± 0.40	1588.9 ± 0.1	1238.8	278.90 ± 0.27	3.79 ± 0.01	8.48 ± 0.03	1.19 ± 0.11	6.08 E-2 ± 2.3 E-4	1.84 E-4 ± 1.7 E-5	1.76 E-1 ± 1.7 E-4	7.46 E-4 ± 6.9 E-5	R16596
5	840	47.64%	15.48 ± 0.30	1984.4 ± 0.4	1668.3	369.42 ± 0.68	3.79 ± 0.09	5.50 ± 0.12	1.07 ± 0.11	2.98 E-2 ± 6.4 E-4	-3.64 E-4 ± 4.5 E-5	1.86 E-1 ± 3.5 E-4	5.39 E-4 ± 5.6 E-5	R16597
6	897	64.32%	15.31 ± 0.23	2447.2 ± 0.0	2172.2	486.47 ± 0.48	6.41 ± 0.01	12.26 ± 0.10	0.93 ± 0.11	5.04 E-2 ± 4.1 E-4	1.90 E-4 ± 1.4 E-5	1.99 E-1 ± 2.0 E-4	3.80 E-4 ± 4.5 E-5	R16599
7	980	84.11%	15.23 ± 0.19	2837.6 ± 0.6	2566.2	577.39 ± 0.52	7.64 ± 0.01	12.70 ± 0.05	0.92 ± 0.11	4.40 E-2 ± 1.8 E-4	2.08 E-4 ± 1.3 E-5	2.03 E-1 ± 1.9 E-4	3.24 E-4 ± 3.9 E-5	R16600
8	1060	96.11%	15.43 ± 0.32	1788.8 ± 1.1	1577.3	350.27 ± 0.32	4.49 ± 0.01	11.11 ± 0.11	0.72 ± 0.11	6.35 E-2 ± 6.5 E-4	1.19 E-4 ± 1.6 E-5	1.96 E-1 ± 2.2 E-4	4.00 E-4 ± 6.1 E-5	R16601
9	1204	99.79%	16.03 ± 1.03	628.3 ± 0.1	502.0	107.33 ± 0.10	1.34 ± 0.00	9.27 ± 0.09	0.43 ± 0.11	1.73 E-1 ± 1.6 E-3	-2.57 E-6 ± 3.7 E-5	1.71 E-1 ± 1.6 E-4	6.81 E-4 ± 1.7 E-4	R16602
10	1356	100.00%	27.71 ± 17.85	194.9 ± 0.3	49.9	6.16 ± 0.01	-0.01 ± 0.00	9.14 ± 0.05	0.49 ± 0.11	2.97 E+0 ± 1.7 E-2	-5.01 E-3 ± 6.0 E-4	3.16 E-2 ± 8.2 E-5	2.52 E-3 ± 5.6 E-4	R16603

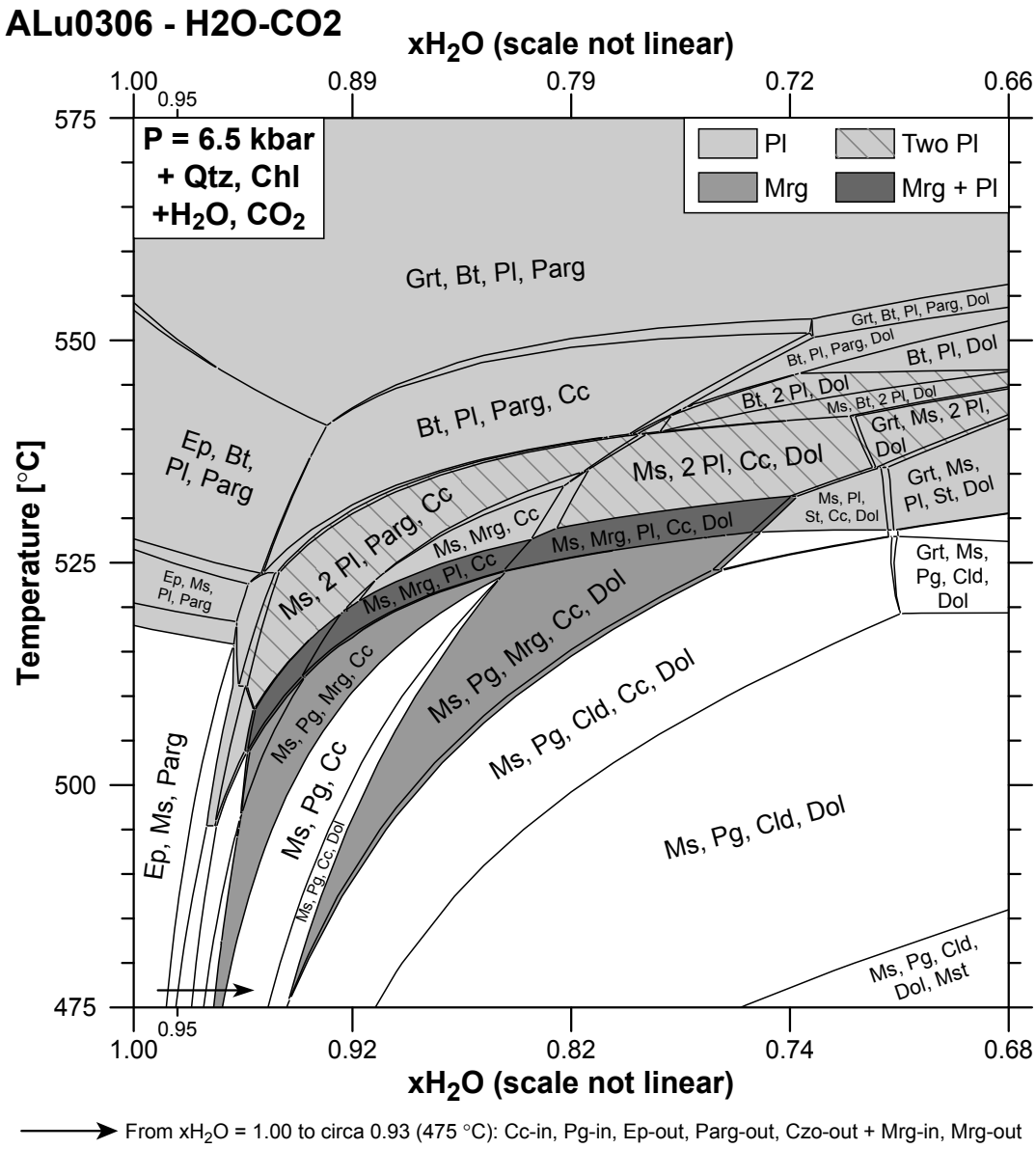

Appendix 2.3: T-xH_2O pseudo-section in margarite-bearing calc-schist ALu0306.

3) Petrogenesis and geochronology of micas: A case study from Val Antabia(Central Alps)

Eastern view from Pianasciom, above Corte Grande (Val Antabia)

J. Allaz, A. Berger, M. Engi & I.M. Villa

3.1) Abstract

Here we address the uncommon growth of K-feldspar in a metapelite of lower amphibolite facies. The thermal peak of metamorphism for this region is tightly constrained at 7.0±0.5 kbar and 570±20 °C. Studied pelitic samples present an apparent well-equilibrated texture corresponding to a complete equilibration in amphibolite facies, with large garnet and plagioclase blasts in a matrix of biotite, muscovite, quartz and rare staurolite. However, a detailed investigation revealed tiny K-feldspar grains (usually <100 µm) growing in the matrix. From petrology and mica chemistry, we identified three distinct biotite generations. These different generations are correlated with thermobarometrical results. Biotite forms a) large millimetre-sized books growing along the prograde path, b) finer flakes in the matrix pertaining to the peak of metamorphism and c) rare flakes associated to chlorite and often surrounding garnet. At least two generations are identified as white micas: synkinematic flakes and larger books overgrowing the schistosity. Both are clearly zoned with a phengite-rich core (3.27 p.f.u. Si against 3.09 at rim). The growth of K-feldspar from K-bearing mica (biotite or muscovite) implies a large release of aluminium, which was essentially balanced by the re-equilbration of phengite-rich to phengite-poor muscovite. This reaction produces the chemical zonation observed in both synkinematic and rare oblique books of muscovite. From thermobarometry, PT-fluid condition necessary to the K-feldspar formation are suggested around 550°C, 4 and 8 kbar and, more importantly, at low water activity (around 0.25-0.45 aH_2O). This corresponds to the early decompression. We suggest that a strong decarbonatation in the surrounding calc-schist and carbonate-rich rocks would externally buffer the fluid composition. The presence of salts and sulphates in this metamorphic fluid may explain the abnormally low water activity calculated.

To complement this metamorphic history, different fractions of muscovite and biotite from metapelite and surrounding calcschist were dated by ^{39}Ar-^{40}Ar stepwise heating analyses. We hypothesised that different mica generation might record different stages of equilibrium, providing that diffusion was (quite) inefficient. Indeed, the largest biotite fraction analysed yield a clearly older age (19-24 Ma) than the finest fraction (13-9 Ma). We suggest that the oldest result obtained in the coarse biotite fraction reflects the age of the mm-sized biotite books, while the youngest ages pertain to the latest biotite generation related to the formation of K-feldspar. In contrary, all white mica separates are essentially composed of the same proportion of phengite-rich and phengite-poor muscovite, thus yielding a constant average age between the two growth stages (ca. 15 Ma).

Keywords

Central Swiss Alps; metapelite; calc-schist; K-feldspar; muscovite; zoned micas; disequilibrium; ^{39}Ar-^{40}Ar geochronology.

3.2) Introduction

Prior to the formation of the Alps, Mesozoic sediments, in Switzerland known as Bündnerschiefer, were deposited in the Valaisan basin and Piedmont Ocean. Following the closure of this ocean, a continental collision occured between the European and Africa plates (see review by Schmid *et al.*, 1996). The Lepontine (or Central) Alps represent the core of the Barrovian metamorphism affecting the Mesozoic sediments and their gneissic basement. This zone of regional metamorphism is characterized by a concentric evolution of the metamorphism from upper greenschist facies in the northernmost area (Aar massif, Gotthard nappe) and a local thermal peak in upper amphibolite-facies near the Insubric Line (Fig. 3.1a). This marks the limit of the African continent and truncates the amphibolite facies metamorphism. The evolution of metamorphism in this area is well-known (e.g. Frey & Ferreiro Mählmann, 1999). In particular, mineral isograds were first recognized to reflect the increasing metamorphic grade from North to South. This depends heavily on the rock type; for instance, chlorite disappears in favour of biotite and garnet in metapelite, followed by staurolite and kyanite (Niggli & Niggli, 1965), whereas Ca-silicates such as margarite, scapolite, tremolite and diopside are typically formed through the progressive decarbonatation of calc-schist and micaceous marble (Trommsdorff, 1966; Trommsdorff, 1980; Steck & Hunziker, 1994; Kuhn *et al.*, 2005). All these mineral isograds depict a half-concentric pattern up to the Insubric Line (Fig. 3.1a), which is also indicated by the increasing PT-conditions (Todd & Engi, 1997). Unfortunately, the mineral growth during decompression or the persistence of relic minerals plagues the definition of some mineral isograds, unless a conspicuous PT and crystallization-deformation history is documented (e.g. Nagel *et al.*, 2002a).

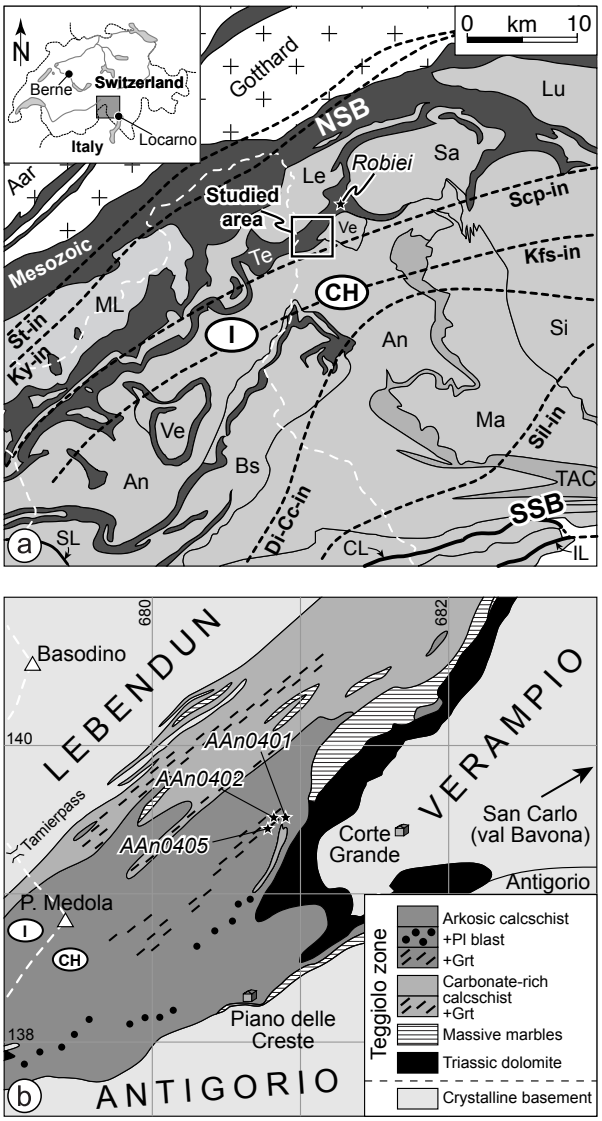

Fig. 3.1: (a) Tectonic overview of the Central Alps, south of the Aar massive and Gotthard nappe, adapted from Steck *et al.* (1999), Berger *et al.* (2005) and Spicher (2005). The area of interest is part of the Teggiolo zone (Te). This limb of Mesozoic metasediments is deposited over the Antigorio and Verampio nappes (An, Ve) and tectonically covered by the Lebendun nappe (Le). Mineral isograds in metapelite (kyanite, sillimanite, staurolite) and calc-schist (K-feldspar, scapolite, diopside + calcite) according to Niggli & Niggli (1965), Trommsdorff (1980) and Kuhn *et al.* (2005). Bs: Bosco series, Lu: Lucomagno/Leventina, Ma: Maggia, ML: Monte Leone, NSB, SSB: Northern and Southern Steep Belts, Sa: Sambuco, Si: Simano, Ve: Verampio, CL, IL, SL: Canavese, Insubric and Simplon Lines. Mineral abbreviation following Kretz (1983). **(b)** Detail geological map according to Burckhardt & Günthert (1957). Stars stand for sample position.

This paper deals with a peculiar outcrop of Mesozoic calc-schist and metapelite situated between the Lebendun and Antigorio nappes (Fig. 3.1). We aim to explain the growth of K-feldspar not only in calc-schist, but

also in metapelite. Mesozoic calc-schist from the Central Alps have been recently reviewed by Kuhn *et al.* (2005) and they notably identified mineral isograds for scapolite and K-feldspar in calc-schist. However, these minerals should be absent from calc-schist in the studied area (Fig. 3.1a). Moreover, the temperature is too low (<600 °C; Todd & Engi, 1997) to induce K-feldspar formation from muscovite in a typical low-Al metapelite at high water activity. Unless fluid percolation has introduced some external elements, micas are the only possible source of potassium in these samples. Indeed, different mica generations are identified in the matrix of metapelite, with fine synkinematic flakes and large oblique books of both muscovite and biotite. These different generations are also identified by significant changes in chemical composition.

The detailed petrography is completed by thermobarometry to determine changes in pressure-temperature or fluid activity responsible of the K-feldspar growth. We use TWQ (Berman, 1991) to yield PT-condition of equilibrium in each samples or to identify assemblages in disequilibrium. Moreover, the stability of a certain mineral assemblage is ascertained by the use of THERIAK-DOMINO (de Capitani, 1994), which models rock-specific equilibrium assemblage diagrams (pseudo-sections) at variable PT and fluid composition. Comparison with petrology and PT-results from other calc-schist and metapelite unaffected by this reaction is used to judge for the precision and accuracy of these thermobarometric calculations.

Secondly, the conservation of chemical zonation pertaining to different growth stage in both micas suggest that at least major elements in micas are partially preserved in the cores of larger books. The isotopic signature might thus be preserved as well, unless a late diffusion-loss occurs after the various growth stages. *In situ* analysis would have been useful, however inapplicable to our case study due to the small size of a majority of mica flakes, a strongly zoned composition of each mica and a presumably too young Ar-age of these minerals (<20 Ma, see below). Instead we carefully selected different grain-fraction of mica for Ar-Ar dating and used ^{39}Ar-^{40}Ar stepwise heating analyses.

The concept of "closure temperature" (Dodson, 1973) has long been the rule for interpretation of geochronological data of metamorphic rocks, notably K-Ar on micas on pelitic and marly rocks from the Central Alps (e.g. Jäger *et al.*, 1967; Dodson, 1973; Purdy & Jäger, 1976; Hurford, 1991; Hunziker *et al.*, 1992). In this way a cooling-path can be investigated, providing the use of multiple geochronometers. The original closure-T for muscovite and biotite Rb-Sr systematic are set at 500 and 300 °C, respectively (Armstrong *et al.*, 1966; Purdy & Jäger, 1976). By comparison, closure-T for muscovite and biotite K-Ar are estimated around 350 °C and 300 °C (Armstrong *et al.*, 1966; Jäger *et al.*, 1967). Recent studies suggest higher closure-T for K-Ar on micas, up to 500 and 450 °C for muscovite and biotite (Hammerschmidt & Frank, 1991; Villa & Puxeddu, 1994). Other studies indicate that diffusion, a process depending mainly on temperature and grain size, is not always the best approach to interpret isotopic ages. Late disequilibrium features and mineral reactions enhanced significantly by late fluid percolation may overwhelm any simple volume diffusion process (Chapter 2; Chopin & Maluski, 1980; Villa, 1998b; Jenkin *et al.*, 2001). In this sense, the use of detailed petrography and thermobarometry aid in identifying the presence of a late retrogression features which may affect the isotopic age of micas. Inheritance problems are also a persist problem in low grade samples (<550 °C) plaguing the geological interpretation of muscovite and biotite Rb-Sr ages (§4.2; Thöni & Jagoutz, 1992). Assuming a recrystallization of mica at a temperature sufficiently low to prevent diffusive Ar-loss, dating-results of muscovite and biotite potentially yields an age for the mineral reaction responsible of K-feldspar growth. In contrary, diffusion might significantly affect the Ar-isotopic signature of micas after mineral reaction completion, rendering the interpretation of such age difficult, if not impossible.

We thus aim to identify first the mineral reaction responsible for this uncommon growth of K-feldspar, as well as the PT-fluid conditions. Comparison with PT-results and other age results (U-Pb on monazite, Ar-Ar or K-Ar from other areas in Central Alps, apatite and zircon fission track) provides a novel way to further interpret Ar-

ages controlled either by diffusion, metamorphic reaction inducing recrystallization (i.e. cooling or recrystallization age) or both. This method is also a powerful tool to identify a meaningless age resulting either from the inheritance of a former metamorphic event or from the Ar-loss through diffusion, retrograde reaction or recoil effect.

3.3) Geological setting

Metapelite samples are from Val Antabia, at the NW end of Val Bavona, south of the Basodino summit (Central Alps, Switzerland, Fig. 3.1a). North and South of this area are three basement nappes: Antigorio, Lebendun and Verampio (Burckhardt, 1942; Günthert, 1954; Steck *et al.*, 1999) separated by a slice of Mesozoic metasediments, representing deposition in a relative shallow marine to submarine environment.

This Mesozoic series starts with a Triassic dolomite, followed by Liassic calc-schists alternating with quartzeous to pelitic layers (Burckhardt, 1942; Leu, 1986). The Liassic and following deposit are known as "Bündnerschiefer" in the Central Alps and are typically composed or dark and graphitic calc-schist. At the base of this Liassic calc-schist are locally present decametre-sized layers of pure marbles, alternating progressively with quartzite in the upper part of the stratigraphy. Calc-schists contain variable carbonaceous, clastic and pelitic components. The base is richer in felsic component with local layers rich in cm-size plagioclase blasts. True calc-schists, with variable but large amount of carbonate, dominate the N-NW part of the field, while mica-rich metasediments are more common SW-W of Corte Grande. Among these is one particular lithology made of pelitic to marly metasediments situated westwards of Corte Grande (Fig. 3.1b). In sedimentary but tectonically folded contact are layers of carbonate-free garnet-bearing pelitic schists interlayered with a felsic calc-schist (Fig. 3.2a). These metasediments are only affected by the Alpine metamorphism and reach early amphibolite facies at PT condition around 575 °C and 6.5 kbar (Todd & Engi, 1997), after staurolite- and kyanite-in in pure metapelite, but before diopside+calcite-in in calc-silicate (Niggli & Niggli, 1965; Trommsdorff, 1980).

These Liassic metasediments are well suited to compare different reaction. Due to the prograde heating, metapelite and calcareous metapelite are affected by dehydration and decarbonatation reactions until a maximum fluid-release relating to last stage equilibration (Proyer, 2003). In contrary to granitic, pure quartzitic or carbonaceous material, a complete equilibration of PT-conditions around the thermal climax is expected. This equilibration is preserved, unless late fluid-percolation induces a late recrystallization. Metapelite and calc-schist are thus sensitive to change in pressure (P), temperature (T), H_2O-CO_2 fluid activity (aH_2O) or bulk rock composition (metamorphic segregation, fluid percolation). They depict a rather complex mineral evolution compared to felsic or carbonate-rich systems and allow tight constraints on metamorphic conditions and on the identification of mineral or chemical disequilibria.

Regarding the age of this Alpine metamorphism, some K-Ar and Rb-Sr ages on mica and U-Pb ages on monazite from the gneissic basements are available (Table 3.1). Unfortunately, analysed samples are only from the old gneissic basement of Antigorio, Lebendun, Sambuco or Verampio nappes. Monazite U-Pb ages are around 22.4 and 22.0±0.5 Ma in the Sambuco nappe, and 19.5±1.1 Ma in the Verampio nappe at (Table 3.1; Köppel & Grünenfelder, 1975; Köppel *et al.*, 1980). Considering the low T-condition calculated for the studied area (550-600 °C; Todd & Engi, 1997), these ages pertain to monazite crystallization (Parrish, 1990), probably near the thermal climax or during the early decompression.

This is in apparent contradiction with Rb-Sr ages on muscovite, which suggest a thermal peak of metamorphism at 38 Ma in the Lepontine Alps (Jäger *et al.*, 1967; Hunziker, 1969). In Chapter 4, we argued for an effective younger metamorphism southwards of the Gotthard nappe around 20 Ma and older southwards,

Table 3.1: K-Ar, Rb-Sr and fission tracks ages from the literature for the NW part of the Central Alps.

		Muscovite		Biotite		Fission tracks		Monazite	
Sample	Lithology	Rb-Sr	K-Ar	Rb-Sr	K-Ar	Zircon	Apatite	U-Pb	Ref.
Sambuco									
#3	Paragneiss (Fusio)	-	-	-	-	-	-	22.4±0.5	1
#13	Paragneiss (Fusio)	-	-	-	-	-	-	22.0±0.5	2
KAW 384	Gneiss (Lago Scuro)	-	-	-	-	-	6.2±0.6	-	3
KAW 386	Gneiss (Lago Scuro)	-	-	-	-	-	6.0±0.6	-	3
KAW 1873	Matorello gneiss (Sambuco)	19.1±1.3	-	15.4±0.2	15.0±0.2	12.7±0.6	6.9±0.7	-	4
KAW 1874	Augengneiss (Scheggia)	25.8±0.3	19.0±0.2	14.3±0.2	14.9±0.1	12.0±0.7	6.7±0.7	-	4
KAW 1875	Matorello gneiss (Naret)	24.9±0.3	17.7±0.2	17.3±0.2	16.0±0.2	12.7±0.6	6.1±0.6	-	4
KAW 1877	Gneiss (Lago Bianco, Robiei)	22.5±1.9	16.8±0.2	15.4±0.2	15.4±0.2	13.5±0.7	7.8±0.8	-	4; 5
KAW 1972	Matorello gneiss (Laghetti)	22.0±0.9	-	15.1±0.2	-	-	-	-	4
KAW 1974	Matorello gneiss (Laghetti)	21.1±0.5	-	15.8±0.2	-	-	-	-	4
Lebendun									
KAW 286	Lebendun gneiss (Cascata Toce)	19.0±3.0	16.6±1.1	13.6±0.8	14.6±1.1	-	4.5±0.5	-	3; 6; 7
B28 a	Lebendun gneiss (Cascata Toce)	-	-	-	14.9±1.0	-	-	-	8
B28 b	Lebendun gneiss (Cascata Toce)	-	-	-	14.4±0.8	-	-	-	8
B28 c	Lebendun gneiss (Cascata Toce)	-	-	-	14.6±1.0	-	-	-	8
Antigorio									
KAW 223	Antigorio gneiss (S Basodino)	-	-	-	-	-	3.2±0.3	-	3
KAW 1876	Antigorio gneiss (Val Bavona)	19.3±0.3	16.6±0.3	13.2±0.2	14.2±0.2	10.9±0.5	5.1±0.5	-	5
Verampio									
KAW 201	Verampio gneiss (Baceno)	15.0±1.9	14.1±0.8	13.4±0.5	12.9±0.8	-	2.2±0.2	-	3; 6; 7
KAW 1706	Quartenschiefer (Baceno)	-	10.6±1.4	-	-	-	-	-	9
KAW 1755	Schist (Baceno)	-	13.0±0.9	-	-	-	-	-	9
Baceno2	Verampio gneiss	-	-	-	-	-	-	19.5±1.1	10

1 = Köppel & Grünenfelder (1975); 2 = Köppel *et al.* (1980); 3 = Wagner *et al.* (1977); 4 = Steiner (1984); 5 = Hurford (1986); 6 = Jäger (1970); 7 = Purdy & Jäger (1976); 8 = Jäger *et al.* (1967); 9 = Frank (1979); 10 = Engi *et al.* (2002).

up to circa 27 Ma near the Insubric Line. More K-Ar (and Rb-Sr) ages are available in the surrounding gneissic basement (Table 3.1; Jäger, 1970; Purdy & Jäger, 1976; Steiner, 1984). Rb-Sr ages from the Sambuco nappe vary from 25.8±0.3 to 19.1±1.3 Ma, likely related to inheritance of a former metamorphic event or disequilibrium problem between white micas and the bulk rock. In contrary, K-Ar ages of this mica are more constant from 17.7±0.2 to 16.6±0.2 Ma and 14.1±0.8 to 10.6±1.4 Ma in Lebendun and Verampio nappes. Biotite K-Ar (and Rb-Sr) ages are constant between 17.3±0.2 and 14.3±0.2 Ma in the Sambuco nappe and gets younger at higher metamorphic degree, yielding 14.9±1.0 to 12.9±0.8 Ma in Lebendun and Verampio nappes.

Rare and precious zircon fission track (FT) data are also available. As their closure-temperature for resetting is well constrained at 280 (+40/-60) °C (Brix *et al.*, 2002; Rahn *et al.*, 2004; Yamada *et al.*, 2007), these data are used to constrained the late cooling history. Most of ages found in the studied area are in the Sambuco nappe and zircon FT ages are broadly constant around 13.5±0.7 and 12.0±0.7 Ma, with a slightly younger age at 10.9±0.5 Ma for the Antigorio nappe. Apatite FT ages are less important here, as they record the very last part of the cooling history yielding ages of 7.8±0.8 to 6.0±0.6 Ma in the Sambuco and 5.1±0.5 to 2.2±0.2 in Lebendun and Antigorio nappes, but at lower elevation (Hurford, 1991).

3.4) Sample description

Here we concentrate on two specific lithologies: a pelitic and a calc-schist facies. The metapelite is garnet bearing, leucocratic and rich in fine muscovite flakes and large biotite books (samples AAn0401-B, AAn0405; Fig. 3.1b). This lithology is restricted to the western part of Corte Grande and forms layers between the second lithology of interest. This second lithology consists of carbonate-rich to plagioclase-rich calc-schist (samples AAn0401-A,

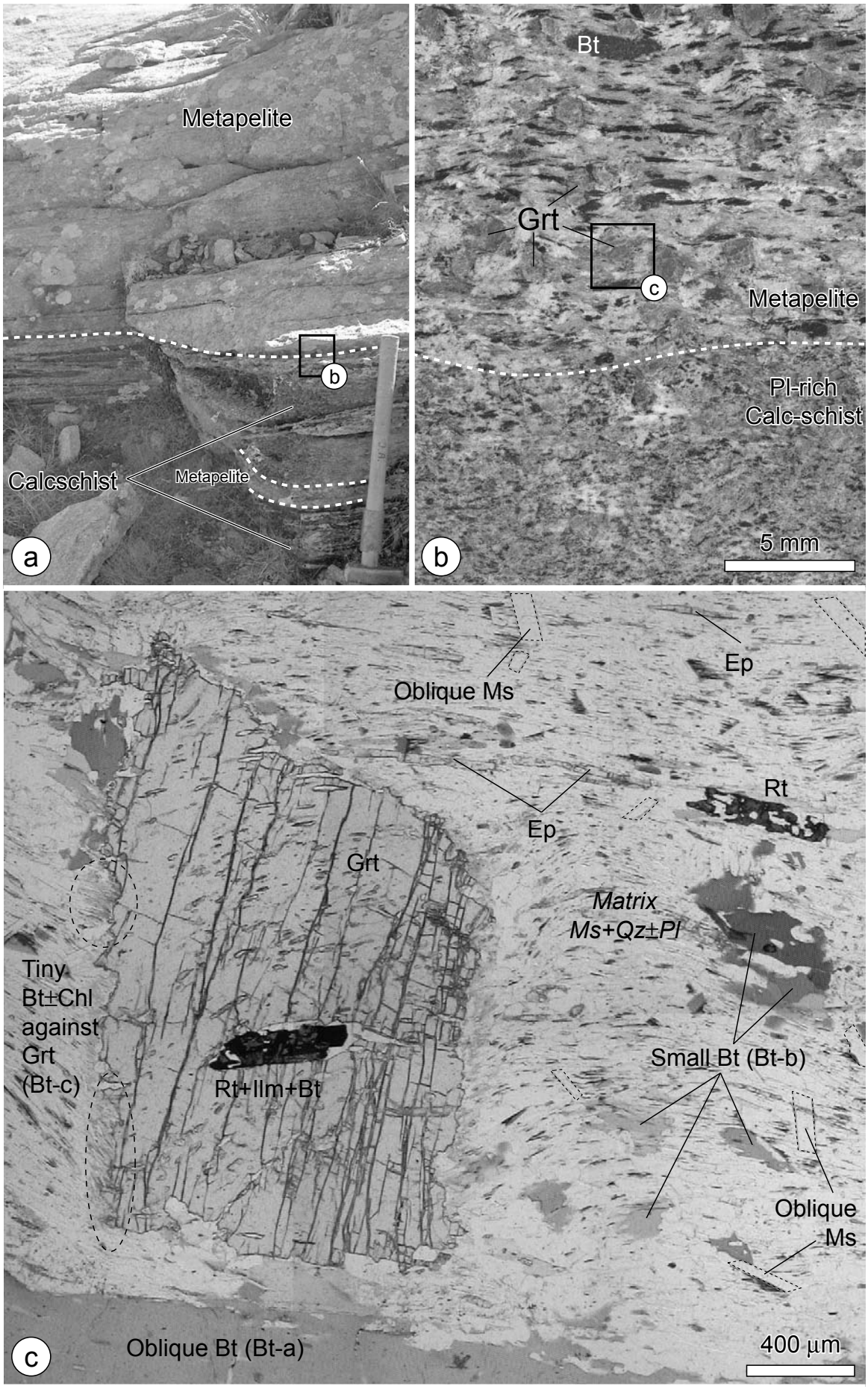
Metapelite
b
Calcschist
Metapelite
a
Bt
Grt
c
Metapelite
Pl-rich
Calc-schist
5 mm
b
Oblique Ms
Ep
Rt
Ep
Grt
Matrix
Ms+Qz±Pl
Tiny
Bt±Chl
against
Grt
(Bt-c)
Rt+Ilm+Bt
Small Bt (Bt-b)
Oblique
Ms
c
Oblique Bt (Bt-a)
400 µm

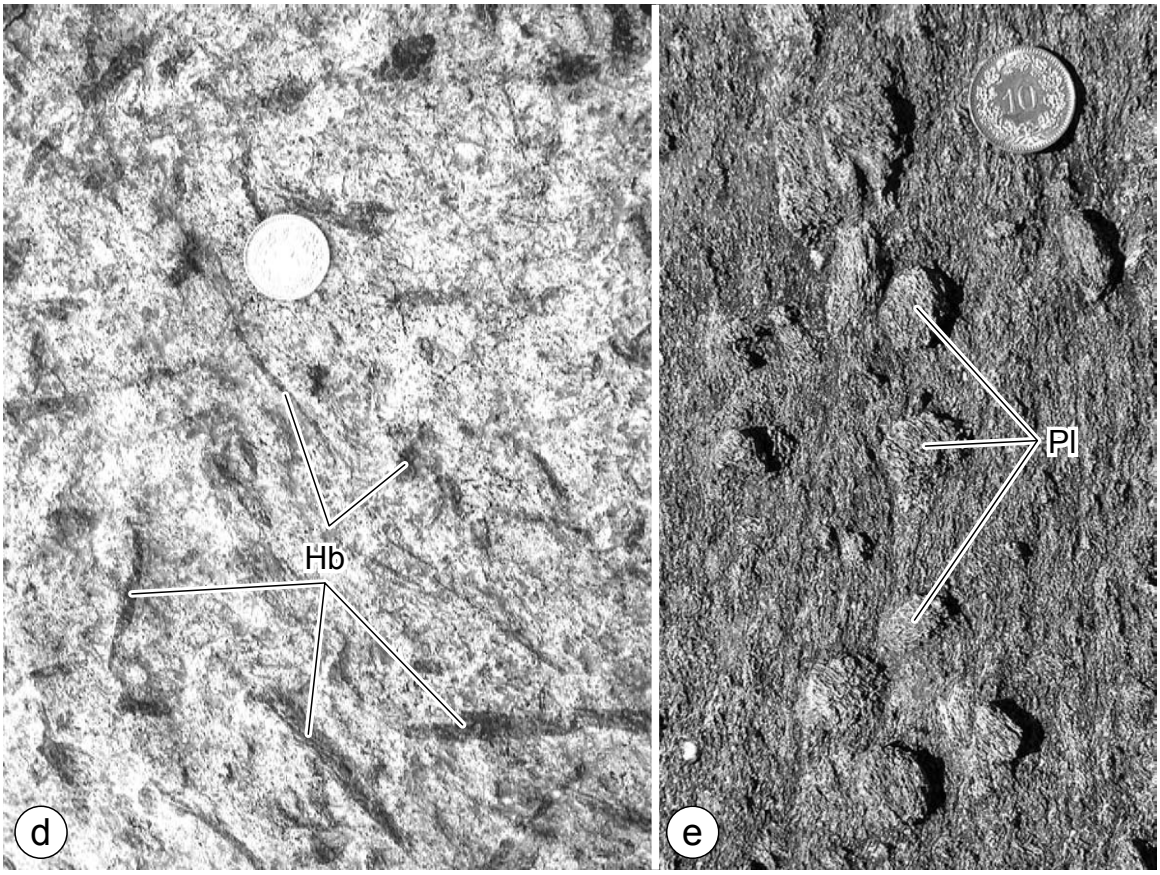

Fig. 3.2: Typical features at the contact of metapelite and calc-schist from Mesozoic metasediment of Val Antabia. **(a)** Contact between metapelite and calc-schist at outcrop of sample AAn0401. Hammer is 60 cm length. **(b)** Polished cut of the contact between metapelite (AAn0401-B) and calc-schist (AAn0401-A). Large garnet and biotite are visible in metapelite and contrast with the finer grain-size of the plagioclase-rich calc-schist. **(c)** Microphotography in metapelite AAn0401-B showing rutile-ilmenite association preserved in core of garnet (with biotite) and exclusively rutile in the matrix. Biotite is found as millimetre-sized crystal oblique to the schistosity (Bt-a), as small grains in the matrix (a few hundreds of micron, Bt-b) or as late growth around garnet often associated to chlorite (<50 µm, Bt-c). Two different white mica generations are distinguished: coarser and oblique books, a few being highlighted by a dashed box, and synkinematic flakes growing along the schistosity, undistinguishable from quartz. **(d)** Local presence of non-orientated hornblende in the metapelite overgrowing all minerals from metapelite, including garnet. Hornblende crystals may be rimmed or totally replaced by biotite and chlorite (late greenschist overprinting). Coin is 2 cm diameter. **(e)** Weathered surface of the plagioclase-rich calc-schist with large plagioclase blast standing out by differential erosion. Scale as in (d).

AAn0402; Fig. 3.1b). For comparison, notably of PT-conditions, a calc-schist from this Bündnerschiefer unit was also selected at Alpe Robiei (sample ARo0601; Fig. 3.1a). The petrography of these lithologies is detailed in the following.

3.4.1) Metapelite

In the felsic facies of the calc-schist local beds are strongly foliated micaschist (Fig. 3.2a). This garnet-bearing micaschist alternates at cm- to dm-scale with the plagioclase-bearing calc-schist. The micaschist is more leucocratic than calc-schist due to richness in white mica, plagioclase and quartz, all three usually reaching an abundance of 75 modal-%. This metapelite is punctuated by reddish garnet and coppery-brown biotite (Fig. 3.2b). Muscovite is by far the most important mineral of this facies, with modal abundance reaching 30 to 50%. Fine muscovites (10-20 µm thickness, <150 µm length) are perfectly aligned in the schistosity and coexist with oblique books reaching

500 µm in length (Fig. 3.2c). Oblique muscovite overgrows the schistosity, can be twin-like associated with biotite flake and is commonly found as inclusion in plagioclase and in large biotite book.

Coarse and oblique biotite books easily reach 3-5 mm length for 1-2 mm thickness and tend to growth along the lineation but perpendicular to the schistosity (Fig. 3.2b). Smaller grains, at least ten-times finer, are also found in the matrix and are usually aligned to the schistosity (synkinematic). A last type of biotite appears around garnet blast and as filling-material of cracks in garnet and plagioclase. This biotite sometimes has a greenish pleochroism and locally coexists with chlorite (Fig. 3.2c) suggesting continuous growth from syn- to post-kinematic biotite, during and after the growth of garnet porphyroblast. Though that rare in this lithology, chloritization of biotite (or seldom garnet) is present locally, occurring either in small biotite flakes around garnet or in marked cleavage of oblique biotite books.

Millimetre-sized blasts of plagioclase form nodules up to 1 centimetre, clearly overgrowing the schistosity and including all matrix minerals, notably quartz, muscovite, biotite, epidote and rutile. Garnet blasts are syn- to postkinematic, typically reaching 1-4 mm in diameter and moulded by quartz, micas and to a less extent plagioclase. They form idiomorphic grains including mainly quartz, rutile, ilmenite, epidote, tourmaline and apatite. Remarkable is the coexistence of rutile and ilmenite in core of garnet, while only rutile is preserved in the matrix (Fig. 3.2c). Partial resorption of the garnet blasts occurs essentially at contact with a calc-schist layer and is accompanied by fracturing of garnet and plagioclase blast. Cracks are filled with chlorite, biotite, feldspar (plagioclase and K-feldspar; see below), minor white mica and calcite.

Locally, some decimetric to metric layers of this micaschist include idiomorphic hornblende crystal up to 10 cm in length (Fig. 3.2d), the richest layer containing up to 5 modal-% (estimated at the outcrop). No preferred orientation is observed and it overgrows all minerals, notably garnet. Alteration leads to the replacement of hornblende by biotite and chlorite. For the purpose of this study, we avoid samples containing amphiboles, as they may be related to a late fluid percolation. They are likely to be parented to the “hornblende garbenschists”, a feature observed in the Alps, at the entry in amphibolite facies (e.g. Wenk *et al.*, 1974; Deutsch & Steiger, 1985; Blackenburg & Villa, 1988; Hoschek, 1998). Accessory phases are apatite, tourmaline, zircon, and rutile is the stable Ti-phase in the matrix. Rare epidote is also present with a typical allanitic core.

At first glance and excluding the local presence of hornblende, mineral assemblage of the metapelite is in textural equilibrium. However, tiny angular grains of K-feldspar generally 20-100 µm in size appears locally at the thin section scale (Fig. 3.3). Such mineral is undistinguishable from quartz microscopically, both appearing as clear and tiny grains devoid of any twin or cleavage; thus modal abundance and repartition over the thin section is difficult. The recognition is easier with electronic imaging, like backscatter electron image (BSE; Fig. 3.3a) or, better, microprobe element mapping (Fig. 3.3b,c). This typically yields 2-5% modal-abundance of K-feldspar and can locally reach 10%. A total abundance of circa 1-3% over the entire thin section is estimated. Grains are usually angular and filling spaces between micas and quartz from the matrix. It occurs all over the thin section, but repartition is irregular, sometimes locally around large and oblique micas (notably mm-sized biotite), along some muscovite-rich layers or in garnet fracture (Appendix 3.1c,d,e), while some millimetre-sized areas remains free of any K-feldspar.

3.4.2) Calc-schist

The Mesozoic metasediments are dominated by calc-schist composed essentially of carbonate (generally calcite), plagioclase, quartz and biotite. Three different types can be differentiated, according to richness in carbonate,

plagioclase or quartz. In detail, all three facies interlayered at metre- to decametre-scale. Muscovite is typically rare and appears both as synkinematic elongated flakes and sericite (plagioclase alteration). Carbonate-rich layers are generally poor in plagioclase, but sometimes rich in biotite and garnet bearing (AAn0402 and ARo0601) or rich in diagenetic calcite-quartz veins (ARo0601). The amount of quartz is variable, generally around 1-10%, but carbonaceous quartzite are also locally present in the calc-schist, especially near the base of this Liassic series. Both plagioclase and garnet have an atoll texture, growing between quartz and calcite grains (Appendix 3.2a). K-feldspar is locally present and intimately associated to plagioclase (Appendix 3.2b,c).

Nodules of plagioclase standing out from the alterated outcrop are a typical feature of plagioclase- and biotite-rich layers (Figs. 3.1b, 3.2e). These micaceous calc-schists are usually garnet bearing and are thus selected, notably for thermobarometry. Calcite is discrete in these rocks, reaching only a few modal percent and is often only found as garnet inclusion. Additionally, carbonates are founds in veins or as a secondary phase together with sericite (AAn0401-A). Fresh samples are grey with centimetric blast of bluish plagioclase moulded by dark brown biotite. Quartz, epidote and white mica are also present in matrix. Garnet blast reaching 1-2 mm is present in the more pelitic layers typically richer in biotite. A few modal percent of epidote with an allanitic core is always present in the matrix and as inclusion in garnet and plagioclase. Accessory phases are rutile and rare ilmenite, sometimes found in association, and also apatite, zircon and tourmaline. Titanite and rutile are stable in carbonate-rich calc-schist (AAn0402). In a general manner, mineral texture in calc-schist shows apparent disequilibrium marked by strongly chloritized biotite (Appendix 3.2d), saussuritization of plagioclase, garnet partially resorbed and surrounded by biotite and chlorite.

3.5) Methods and analytical conditions

Chemical compositions of major minerals from three samples were obtained by *in situ* analysis on a Cameca SX-50 microprobe and then on a JEOL JXA-8200 microprobe of the Institute of Geological Sciences of the University of Berne. Results of both instruments overlap within the analytical error. Analytical conditions were 15kV and 20nA with a minimum beam size for garnet, staurolite, aluminosilicates and ilmenite. To minimise volatilization of alkalis, plagioclase and micas were analysed using a slightly defocused beam (5 to 10 µm). For zoned minerals like garnet and plagioclase, representative analysis of rim and core are given, but only rim analyses were used for thermobarometric calculation. We used TWQ (Berman, 1991) to calculate an equilibrium PT from a selected mineral assemblage and THERIAK-DOMINO (de Capitani, 1994) to compute rock-specific equilibrium assemblage diagrams classically called pseudo-sections at specific PT and fluid composition. For both thermodynamic tools, two slightly different but internally consistent database were used, both based on (Berman, 1988). Further details regarding the various solid-solution models used in this study are given in Table 3.2.

A whole-rock analysis of the pelitic facies was obtained on metapelite sample AAn0405. XRF analysis of major elements was performed on a Philips PW 2400 spectrometer at the University of Fribourg.

The first sample analysed (Ar-A series; AAn0401) is made of two distinct layers and was selected for Ar-Ar dating. We first separate the plagioclase-rich calc-schist (AAn0401-A) from the pelitic part (AAn0401-B). Care has been taken to avoid the contact zone for the mineral separation of each part: a band of approximately 1 cm width has been eliminated each side of this relatively sharp contact (Fig. 3.2b). For comparison, a second purely pelitic sample is selected (AAn0405). We separate micas by conventional techniques as sieving, vibration table and magnetic separator. Quality of the mineral separate with a final purity better than 99.5% was reached by handpicking. XRD analyses on each mineral separates were performed to check for mineral purity and reveal some trace of chlorite within biotite separate and quartz in muscovite separate. Ratio between peak intensity of biotite

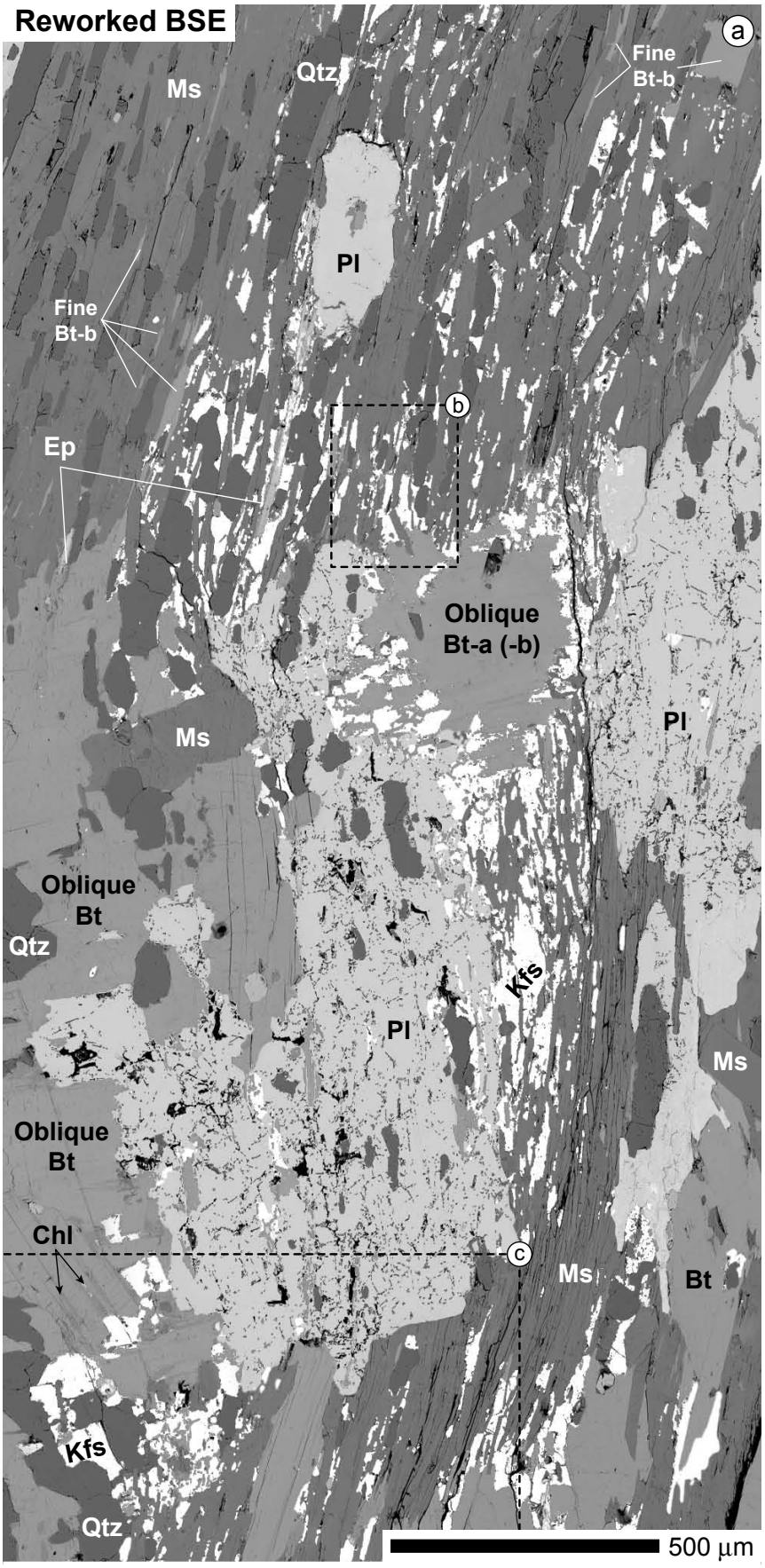

Fig. 3.3: Mineral relations in pelitic facies (AAn0401-B). **a)** Reworked BSE image covering a zone particularly rich in K-feldspar (highlighted in white). The mineral texture indicates K-feldspar formation from both micas. **(b,c)** Inlet of a) shows tiny K-feldspars typically 50 to 100 µm growing along the main schistosity between muscovite flakes (b,c) or in replacement of biotite, together with chlorite (c, top-left corner). **(b)** Distribution map of K; **(c)** difference between K and Fe distribution map (enhanced contrast: dark biotite, medium grey muscovite, light grey K-feldspar). **(d)** Difference between Al and Mg distribution maps, used to enhance the contrast between phengite-rich core (dark grey, Ms1) and phengite-poor rim (light grey, Ms2, same colour for K-feldspar). The two white spots correspond to typical analysis of core and rim, denoted Ms1 and Ms2 in the text. K-feldspar highlighted in white. **(e,f)** Element distribution map of Mg **(e)** and **(f)** Ti showing three biotites generations: Mg-rich books (Bt-a), Ti-richer overgrowth (Bt-b) and fine and Ti-poor flakes against garnet (Bt-c).

Element mappings in WDS mode, 15 kV, 20 nA and:
(b) beam 1 µm, pixel 0.5 µm, dwell-time 20 msec;
(c) 1 µm, 1 µm, 8 msec;
(d) 2 µm, 1 µm, 30 msec;
(e,f) 1 µm, 2 µm, 20 msec.

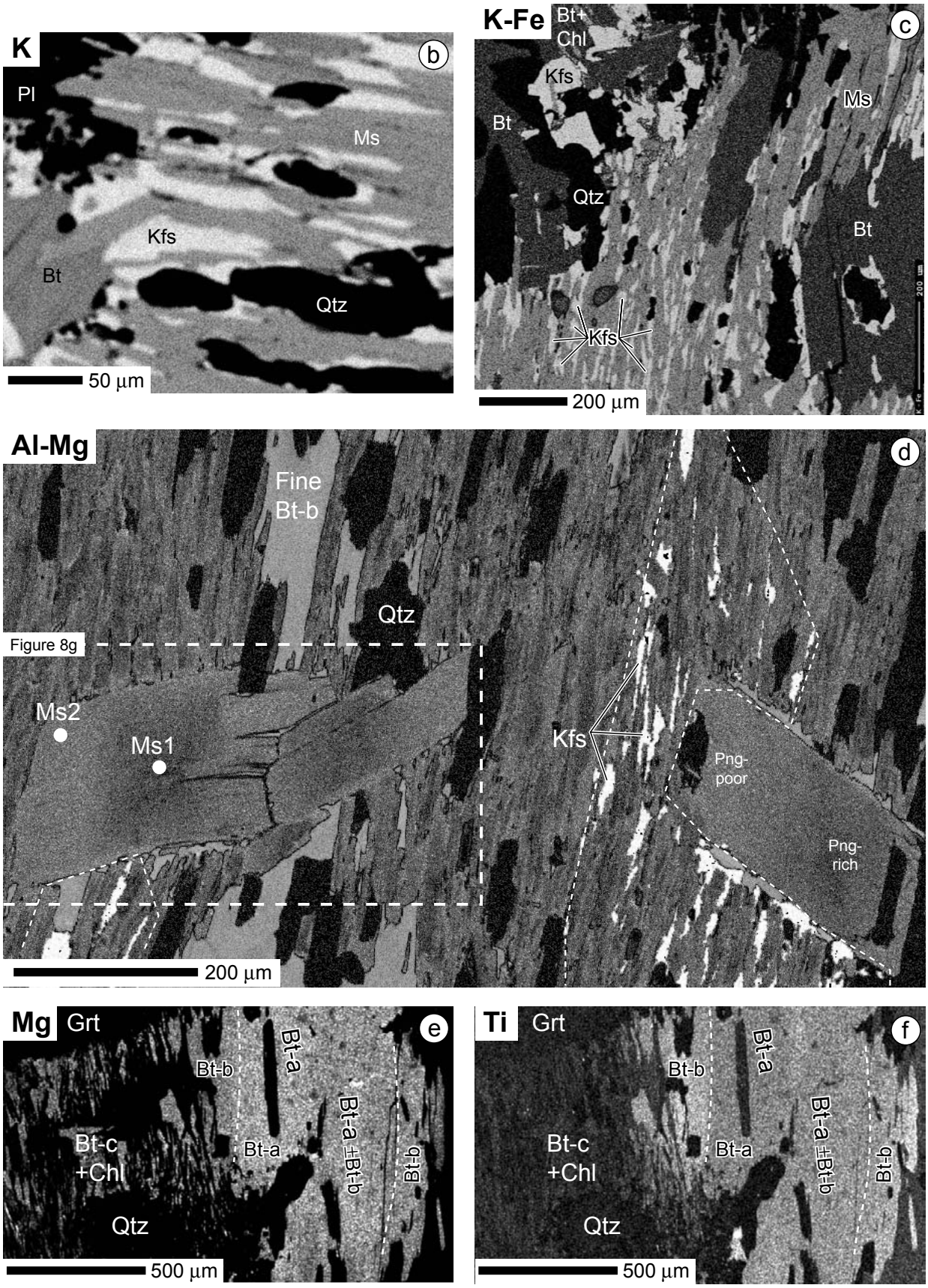
K
b
Pl
Ms
Kfs
Bt
Qtz
50 µm
K-Fe
Bt+
Chl
c
Kfs
Bt
Ms
Qtz
Bt
Kfs
200 µm
Al-Mg
d
Fine
Bt-b
Qtz
Figure 8g
Ms2
Ms1
Kfs
Png-
poor
Png-
rich
200 µm
Mg
Grt
e
Bt-b
Bt-a
Bt-c
+Chl
Bt-a
Bt-a ±Bt-b
Bt-b
Qtz
500 µm
Ti
Grt
f
Bt-b
Bt-a
Bt-c
+Chl
Bt-a
Bt-a ±Bt-b
Bt-b
Qtz
500 µm

Based on…	Berman (1988, 1991)	
Mineral	**TWQ**	**DOMINO**
Garnet	Alm-Prp-Grs, Berman (1990) Berman & Koziol (1991)	Alm-Prp-Grs-Sps de Capitani, pers.comm.
Biotite	McMullin et al. (1991)	Hunziker (2003)
White micas	Chatterjee and Froese (1975)	Keller (2005)
Chlorite	-	Hunziker (2003)
Plagioclase	Fuhrman and Lindsley (1988)	
Staurolite	Nagel et al. (2002a)	
Ilmenite	Ideal (Fe-Mg-Mn)	Ideal (Fe-Mg)
H_2O-CO_2	Haar et al. (1984); Mäder and Berman (1991) Kerrick and Jacobs (1981)	

Table 3.2: Models used in thermodynamic database of TWQ and THERIAK-DOMINO for PT-fluid calculation.

[006] and chlorite [004] or quartz [100] and muscovite [004] are good qualitative indicators of sample purity. We proceed to a second handpicking and XRD analysis, when impurities are too important. This is often necessary for biotite separate, as too much chlorite may strongly disturb the Ar-Ar spectrum (Di Vincenzo *et al.*, 2003).

Ar-Ar stepwise heating analyses were performed at the low argon blank line assembly at the Isotope Geology laboratory of Berne, an all-metal extraction line attached to a double-vacuum resistance oven and an external thermocouple (Villa, 1993). Ar-analyses were performed on a MAP 215-50B rare gas spectrometer, following procedure and corrections factor given in Belluso *et al.* (2000), analysis from AAn0401 and AAn0405 corresponding respectively to analysis series Ar-A and Ar-C from Chapter 2 (§2.5.4). All 5 masses from 40 to 36 were measured on Faraday cup during analysis of AAn0401. In complement to Faraday measurement, multiplier was used for analysis of sample AAn0405, allowing thus a better accuracy and precision on masses 39 to 36. In all Ar-analysis series, blank of spectrometer was controlled by regular dynamic and static background, which all points to a relatively constant background. The same stands for furnace background, which all yields atmospheric ratio. Typically, ^{40}Ar-release from furnace blank ranged from 3 pL/min at 400°C to 14.3 at 1000°C. Unfortunately, this was not the case for analysis of mica separates from AAn0405, where a significant amount of atmospheric argon was remaining from the last sample change. During analysis of Ms200 and Bt200, furnace blank is worst at high release-T (up to 5 times higher than usual), while it rapidly decreases for Ms100 and Bt100 analysis. An irradiation parameter J for each sample analysed has been recalculated on the basis of four MMhb-1 standards placed between samples in the irradiation package. To characterize the source of the extracted gas in each step, the ratio between ^{38}Ar/^{39}Ar and ^{37}Ar/^{39}Ar are used. Such ratios are, after correction, equivalent to ratio of Cl/K and Ca/K respectively (see §2.5.4 for complete methodology and use of these ratio). Such ratio should remain very low, as only traces of Ca and Cl are present in each studied mica (often near detection limit of microprobe).

Table 3.3: Microprobe analysis from metapelite (AAn0401, AAn0405) and calc-schist (ARo0601). One analysis or an average of several points is given for biotite, muscovite, K-feldspar, staurolite, chlorite, clinozoisite, ilmenite and epidote (Nbr pts = number of analysis used for average). Rim and core analysis are given for zoned crystals (garnet and plagioclase, Fig. 3.5). All analyses are accompanied by cation or oxygen normalization and include Fe^{3+} recalculation according to charge balance (cation normalization only).

Fe* = Fe/(Fe+Mg);
xCzo = (Al-2)/(Fe+Al-2);
xK = kfs = K/(Ca+Na+K);
an = Ca/(Ca+Na+K);
ab = Na/(Ca+Na+K);
alm, sps, prp, grs = (M)/(Fe+Mn+Mg+Ca).
(#) as Fe_2O_3.
(*) in addition: Zn0 2.55; Zn 0.537.

Minerals are normalized as following:

- Micas: 12 O, 2 OH.
- Chlorite: 10 O, 10 cations, 8 OH.
- Staurolite: 48 O, 30 cat, 4 OH.
- Clinozoisite: 12.5 O, 8 cat, 1 OH.
- Garnet: 12 O, 8 cat.
- Feldspar: 8 O, 5 cat.
- Ilmenite: 3 O, 2 cat.

	Biotite							Muscovite			Chl	St	Czo
	AAn0405					ARo0601		AAn0405		ARo0601	AAn0401 / –05		AAn405
Comment	Incl. Pl	Core "Bt-a"	Near Grt "Bt-a,b"	Matrix "Bt-b"	at Grt rim "Bt-c"	min Fe*	max Fe*	Ms1 max Png	Ms2 min Png	-	-	-	Low Fe
Nbr pts	7	1	25	8	1	10	14	1	1	25	2	12	4
SiO_2	37.86	38.01	37.33	37.15	36.44	37.69	36.75	48.76	46.32	47.70	26.26	27.75	38.73
TiO_2	1.54	1.43	2.11	2.23	0.75	1.66	2.71	0.33	0.48	0.59	0.21	0.53	0.15
Al_2O_3	18.29	18.55	18.74	18.59	19.68	18.91	18.45	30.79	34.49	33.86	22.59	54.74	29.60
FeO	12.81	14.11	14.69	15.69	18.97	15.14	18.13	1.55	1.37	1.44	22.46	9.34	6.22 #
MnO	0.26	0.24	0.23	0.29	0.29	0.14	0.09	0.01	-	0.01	0.34	0.45	0.03
MgO	13.81	12.90	12.32	11.61	9.97	12.92	10.28	2.15	1.38	1.49	15.75	1.48	n.d.
CaO	0.02	<0.01	0.02	0.04	0.11	0.02	0.03	<0.01	0.02	0.01	0.03	0.01	23.96
Na_2O	0.14	0.08	0.11	0.13	0.17	0.06	0.05	0.13	0.28	0.13	0.01	0.11	0.02
K_2O	9.89	9.93	9.86	9.92	9.72	9.88	9.89	10.78	11.26	10.63	0.02	<0.01	0.01
Cl	0.01	0.02	0.02	0.03	0.05	0.01	0.01	0.01	0.00	0.01	0.02	-	-
F	0.70	0.63	0.52	0.49	0.36	0.36	0.22	0.17	0.09	0.05	0.02	-	-
H2O	3.60	3.71	3.67	3.67	3.72	3.80	3.79	4.37	4.47	4.49	11.46	2.10	1.95
Total	**98.93**	**99.60**	**99.63**	**99.85**	**100.23**	**100.59**	**100.39**	**99.04**	**100.16**	**100.40**	**99.16**	**99.07***	**100.67**
Si	2.807	2.813	2.770	2.767	2.741	2.769	2.747	3.271	3.088	3.151	2.745	7.915	2.975
Al IV	1.193	1.187	1.230	1.233	1.259	1.231	1.253	0.729	0.912	0.849	2.783	18.405	2.001
Al VI	0.406	0.432	0.410	0.399	0.486	0.406	0.373	1.706	1.798	1.788	-	-	0.679
Ti	0.086	0.080	0.118	0.125	0.042	0.092	0.153	0.017	0.024	0.029	0.017	0.115	0.009
Fe^{3+}	-	-	-	-	-	-	-	-	-	-	-	-	0.359
Fe^{2+}	0.794	0.873	0.911	0.977	1.193	0.930	1.133	0.087	0.076	0.080	1.963	2.228	-
Mn	0.016	0.015	0.015	0.018	0.018	0.008	0.006	0.001	-	0.000	0.030	0.110	<0.001
Mg	1.526	1.423	1.362	1.289	1.118	1.414	1.146	0.215	0.138	0.147	2.454	0.628	0.002
Ca	0.002	-	0.001	0.003	0.009	0.002	0.002	-	0.001	0.001	0.003	0.003	1.971
Na	0.020	0.011	0.015	0.018	0.025	0.008	0.007	0.016	0.036	0.016	0.002	0.060	0.002
K	0.936	0.938	0.934	0.943	0.933	0.926	0.943	0.922	0.957	0.896	0.003	0.001	0.001
Cations	**7.785**	**7.772**	**7.767**	**7.772**	**7.823**	**7.788**	**7.762**	**6.964**	**7.030**	**6.957**	**10.000**	**30.000***	**8.000**
Cl	0.001	0.002	0.003	0.004	0.008	0.001	0.002	0.001	0.000	0.001	0.003	-	-
F	0.187	0.167	0.140	0.134	0.099	0.096	0.060	0.041	0.022	0.012	0.005	-	-
H	1.812	1.830	1.857	1.862	1.893	1.903	1.939	1.958	1.977	1.988	7.992	4.000	1.000
OH-grp	2.000	2.000	2.000	2.000	2.000	2.000	2.000	2.000	2.000	2.000	8.000	4.000	1.000
Fe*, xCzo	0.342	0.380	0.401	0.431	0.516	0.397	0.497	0.288	0.421	0.352	0.444	0.780	0.654
xK								0.983	0.963	0.981			

	Garnet						Plagioclase						Kfs	Ilm
	AAn0405				ARo0601		AAn0405		AAn0401-B		ARo0601		AAn0401 / –05	
Comment	Rim 1a	Rim 1b	Core	Rim 2	Rim	Core	Core	Rim	max An	min An	min An	max An	-	-
Nbr pts	6	4	1	5	8	1	3	3	1	1	6	2	5	4
SiO_2	38.42	38.35	38.23	37.72	37.77	37.47	54.91	52.55	54.61	48.73	55.51	49.25	65.27	0.02
TiO_2	0.08	0.07	0.12	<0.08	0.07	0.14	n.d.	n.d.			0.01	<0.01	0.02	50.91
Al_2O_3	21.71	21.78	21.49	21.15	21.03	20.73	29.60	30.99	29.47	33.50	28.99	33.45	18.91	-
Fe_2O_3	-	-	-	0.20	0.60	0.64	-	-	-	-	-	-	-	1.73
FeO	29.53	29.24	25.83	28.58	28.12	27.14	0.02	0.08	0.09	0.06	0.12	0.10	0.06	41.78
MnO	2.07	1.35	6.84	0.63	0.99	3.30	0.01	0.01	n.d.	n.d.	n.d.	n.d.	0.01	3.74
MgO	1.61	1.80	0.86	2.76	2.82	1.29	<0.01	<0.01	<0.01	<0.01	<0.01	<0.01	<0.01	0.08
CaO	8.48	8.74	8.43	8.56	8.48	9.42	10.91	12.75	11.46	16.16	10.87	15.89	<0.01	0.04
Na_2O	0.02	0.02	0.02	<0.01	0.01	0.02	5.22	4.10	4.91	2.22	3.32	1.61	0.48	0.01
K_2O	<0.01	<0.01	<0.01	<0.01	n.d.	n.d.	0.16	0.12	0.17	0.06	0.16	0.05	15.91	<0.01
Total	**101.92**	**101.34**	**101.82**	**99.61**	**99.90**	**100.15**	**100.82**	**100.60**	**100.72**	**100.73**	**98.97**	**100.34**	**100.67**	**98.32**
Si	3.012	3.015	3.016	3.002	2.999	2.997	2.455	2.369	2.450	2.216	2.568	2.260	2.998	<0.001
Al	2.006	2.018	1.998	1.984	1.969	1.954	1.560	1.647	1.559	1.796	1.581	1.809	1.024	-
Ti	0.005	0.004	0.007	-	0.004	0.009	-	-	-	-	<0.001	-	0.001	0.983
Fe^{3+}	-	-	-	0.012	0.036	0.039	-	-	-	-	-	-	-	0.034
Fe^{2+}	1.936	1.922	1.704	1.902	1.867	1.815	0.001	0.003	0.003	0.002	0.005	0.004	0.002	0.897
Mn	0.138	0.090	0.457	0.042	0.067	0.224	0.000	0.001	-	-	-	-	0.001	0.081
Mg	0.188	0.211	0.101	0.328	0.334	0.153	-	-	-	-	-	-	-	0.003
Ca	0.712	0.736	0.713	0.730	0.721	0.807	0.523	0.616	0.551	0.787	0.539	0.781	-	0.001
Na	0.003	0.004	0.003	-	0.002	0.003	0.452	0.358	0.427	0.195	0.298	0.143	0.043	0.000
K	-	-	-	-	n.d.	n.d.	0.009	0.007	0.010	0.003	0.009	0.003	0.932	-
Cations	**8.000**	**8.000**	**8.000**	**8.000**	**8.000**	**8.000**	**5.000**	**5.000**	**5.000**	**5.000**	**4.999**	**5.000**	**5.000**	**2.000**
Fe*, an	0.912	0.901	0.944	0.854	0.851	0.924	0.531	0.628	0.558	0.798	0.637	0.842	-	0.996
alm, ab	0.651	0.650	0.573	0.635	0.629	0.610	0.459	0.365	0.433	0.198	0.352	0.155	0.044	
sps, kfs	0.046	0.030	0.154	0.014	0.022	0.074	0.009	0.007	0.009	0.004	0.011	0.003	0.956	
prp	0.063	0.071	0.034	0.109	0.111	0.051								
grs	0.239	0.249	0.240	0.242	0.238	0.266								

3.6) Mineral chemistry

Representative averages of *in situ* mineral analyses from metapelite (AAn0401-B or –05) and calc-schist (ARo0601) are given in Table 3.3 and all micas analysis are graphically presented for four samples in Figure 3.4a,b (AAn0401-A, –B, AAn0402, AAn0405 and ARo0601). Biotites are affected by the combination of at least two exchange vectors, $FeMg_{-1}$ and $SiR^{2+}Al_{-2}$ (tschermak exchange; R^{2+} = Fe, Mg, Mn), with also smaller and local variation in Ti-, F- and Cl-content. Variation occurs in the same range of AFM compositions (±2% Al and ±5% Fe or Mg, Fig. 3.4a) and occurs generally from grain to grain, each grain being relatively homogeneous with only minor variation in the order of ±0.03 Fe*. Exceptions are the coarser and oblique biotite of metapelites AAn0401-B and AAn0405. They present local variation in Fe* and Ti-richer zone, highlighted by Al, Fe, Mg and Ti element mapping (e.g. Fig. 3.3e,f). Three major biotite generation are distinguished from their textural relationship and also from their chemical composition (Fig. 3.4a,b):

- **Bt-a)** Mg-richer core of oblique book (Fe* 0.41-0.44, intermediate Ti).
- **Bt-b)** Mg-poor rim of oblique book and finer biotite growing in the matrix (Fe* 0.48-0.53, somewhat lower in some flakes situated a few mm away from garnet, usually Ti-rich).
- **Bt-c)** tiny biotite growing at garnet rim, poor in Ti but intermediate Fe* (0.43-0.48).

The maximum Fe* is obtained in a biotite preserved in the core of garnet together with rutile and ilmenite (Fe* 0.57, possible late and local re-equilibration effect) and also in biotite included or stuck against garnet rims. The lowest Fe* is from a biotite included in plagioclase (Fe* 0.34). Lower Fe* between respectively 0.35-0.49 and 0.39-0.45 is also obtained in fine and oblique biotites situated away from garnet. Such a trend is explained either by metamorphic segregation (garnet growth) or by layering during sedimentation. Both effects induce strong variation of biotite chemistry (Fig. 3.4a). Biotite preserved in core of garnet has also a characteristic lower total Al-content than any other biotite (1.55 p.f.u. against >1.60 in all other samples), while Al-content is maximal and variable in biotites from metapelite: 1.60-1.83 p.f.u. in Bt-a, Bt-b from metapelite against 1.55-1.69 in calc-schist. In contrary to Fe-Mg, Al-content in biotite is less susceptible to late exchange with the surrounding minerals present in this inclusion (garnet, ilmenite and rutile), as they exchange essentially divalent cations (Fe, Mg, Mn). Local variation in Ti-content may not only be attributed to change in temperature, but also to the destabilization of a Ti-phase or the late re-equilibration with a Ti-phase situated in the immediate vicinity of biotite. Considering the constantly higher Ti-content in Bt-b, the local Ti-enrichment observed at rim of oblique biotite is most likely related to the destabilization of ilmenite along the prograde or near the thermal peak of metamorphism and is weakly correlated with a decrease of total-Al and an increasing Fe* (Bt-b; Figs. 3.3e,f and 3.4b).

In calc-schist AAn0401-A, Fe* of the unique biotite generation is more homogeneous over the entire thin section (0.43-0.49; Fig. 3.4a,b), but chloritization is more pronounced (Appendix 3.2). AFM variation is local in sample ARo0601 (Fig. 3.4a). Three distinct zones from a single thin section provide three different Fe* ratios. Maximum values are observed in biotite grains near garnet (Fe* 0.50) and minimum value circa 8 mm away from the next garnet (Fe* 0.40). Ti and Al are anti-correlated, with lower Ti in fine biotite around garnet. A weak anti-correlation also exists between divalent cations (R^{2+}), especially Mg (Fig. 3.4b). Concerning Ti, some authors

Fig. 3.4: Chemistry of micas in metapelite and calc-schist samples. **(a)** Ternary Al_2O_3-FeO-MgO (AFM) and **(b)** Fe* versus Ti diagrams of biotite analyses. Typical biotite compositions Bt1 and Bt2 as discussed in the text are shown. **(c)** White mica chemistry in the ternary Al^{IV}-Al^{VI}-(Fe+Mg) diagram from Guidotti (1984). Muscovite from metapelites AAn0401-B and AAn0405 shows a marked trend towards phengite, while those in calc-schist are more homogeneous (ARo0601) or tend towards ferri-muscovite (AAn0401-A, AAn0402). Ms1 and Ms2 are two representative analyses of core and rim of large muscovite books. **(d)** AFM diagram for white micas.

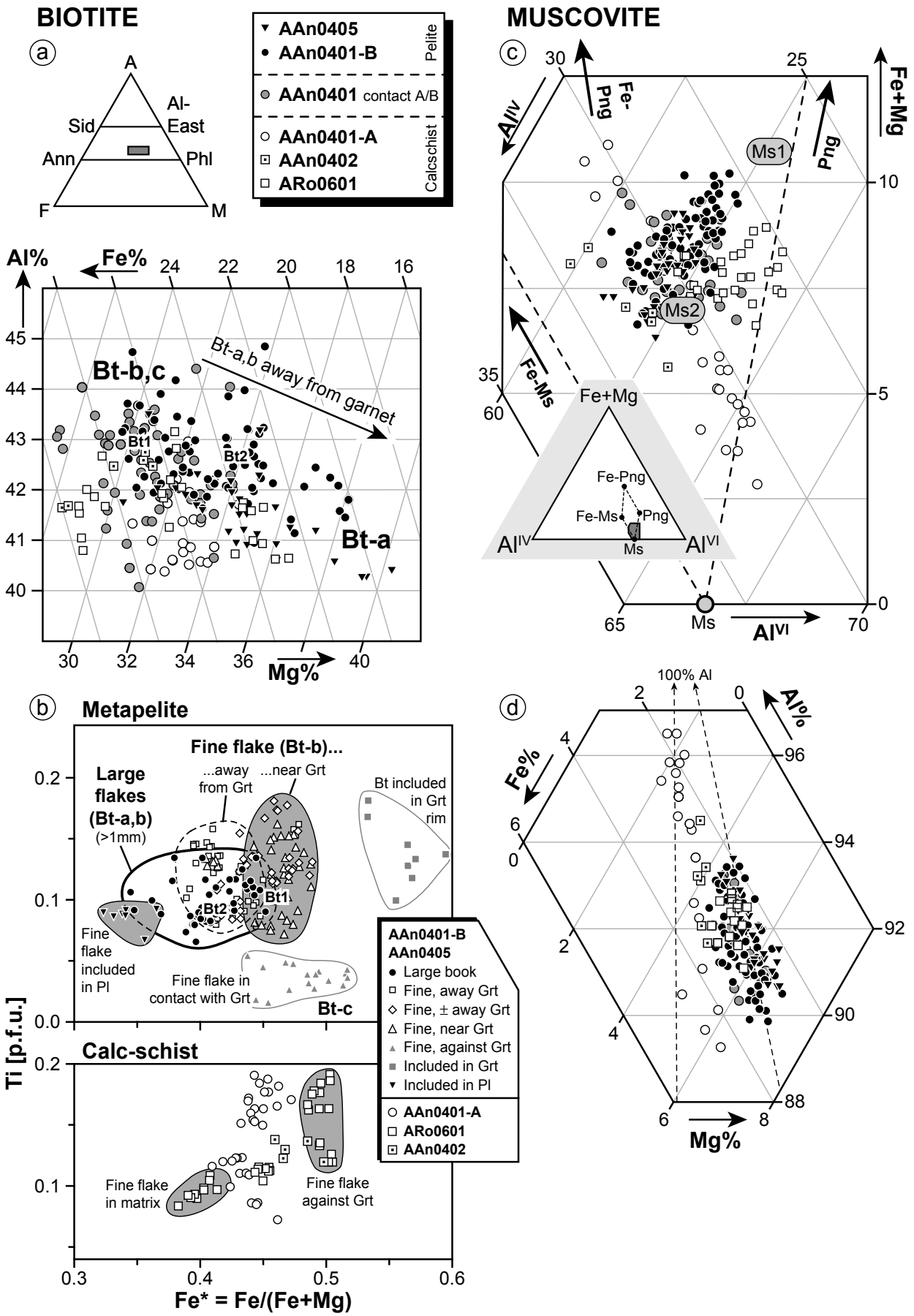
BIOTITE
a
A
Al-East
Sid
Ann
Phl
F
M
AAn0405
AAn0401-B
Pelite
AAn0401 contact A/B
AAn0401-A
AAn0402
ARo0601
Calcschist
Al%
Fe%
Bt-b,c
Bt-a,b away from garnet
Bt1
Bt2
Bt-a
Mg%
MUSCOVITE
c
Fe+Mg
Al^IV
Fe-Png
Ms1
Png
Ms2
Fe-Ms
Fe+Mg
Fe-Png
Fe-Ms
Png
Ms
Al^IV
Al^VI
Ms
Al^VI
b
Metapelite
Fine flake (Bt-b)...
...away from Grt
...near Grt
Large flakes (Bt-a,b) (>1mm)
Bt included in Grt rim
Fine flake included in Pl
Fine flake in contact with Grt
Bt-c
Calc-schist
Fine flake in matrix
Fine flake against Grt
Ti [p.f.u.]
Fe* = Fe/(Fe+Mg)
AAn0401-B
AAn0405
Large book
Fine, away Grt
Fine, ± away Grt
Fine, near Grt
Fine, against Grt
Included in Grt
Included in Pl
AAn0401-A
ARo0601
AAn0402
d
100% Al
Al%
Fe%
Mg%

suggest a dependency of Ti-content and temperature (Dymek, 1983; Kleemann & Reinhardt, 1994; Henry *et al.*, 2005), but it is not clear whether Ti stands in the tetrahedral or the octahedral site. Due to the relation between Ti and Al or R^{2+}, $TiRAl_{-2}$ would be the most conceivable, but we cannot exclude presents of void (revealed by oxide normalization, Table 3.3). The existence of a $Ti\square R_{-2}$ exchange vector, like proposed by Dymek (1983) is thus possible. Local extreme enrichment in Ti-content of biotite like the one depicted in Figure 3.3f reveals former existence in the surrounding of a Ti-phase being now consumed. Like for metapelite, the source of this enrichment is found in the disappearance of ilmenite in profit of rutile.

Similar to its tri-octahedral colleague, white micas from all samples also show variable chemistry (Table 3.2, Fig. 3.4c). Each analysed grain is usually homogeneous and chemical variations are essentially observed at thin-section scale. An impressive intra-grain zonation is exclusively observed in white micas from the metapelite facies in samples AAn0401-B and AAn0405 (dark dot and triangle; Fig. 3.4c). Both samples are made of fine muscovite in matrix and coarser books, and each are zoned with a phengite-rich muscovite core (Ms1) and a phengite-poor rim (Ms2; Fig. 3.3c). Two extreme representative analyses of core and rim variations in oblique muscovite of metapelites AAn0401-B and AAn0405 is given in Table 3.3 and represented in Figures 3.3d and 3.4c. A normalization on 12 oxygens in the reduced NKFMASH system gives:

Phengite-rich core: $(K_{0.92}\ Na_{0.02})\ (Fe_{0.09}\ Mg_{0.22}\ {}^{VI}Al_{1.71})\ (Si_{3.27}\ {}^{IV}Al_{0.73})\ O_{10}\ OH_2$ (Ms1)

Muscovite-rich rim: $(K_{0.96}\ Na_{0.04})\ (Fe_{0.08}\ Mg_{0.14}\ {}^{VI}Al_{1.80})\ (Si_{3.08}\ {}^{IV}Al_{0.91})\ O_{10}\ OH_2$ (Ms2)

The trend towards phengite for the two metapelite AAn0401-B and AAn0405 (Fig. 3.4c) is mainly a $SiMgAl_{-2}$ exchange. The zonation in matrix muscovite is extremely fine and exceed the minimum beam size used for analysis (5 µm). Thus, quite all analyses are intermediate values tending towards Ms2 and only scarce points are approaching the extreme Ms1 analysis.

White micas from plagioclase-rich (AAn0401-A) and carbonate-rich calc-schist (AAn0402) have a different trend, a few analysis yield also higher Fe, Mg and Si but lower Al^{VI} and constant Al^{IV} (Fig. 3.4c). This unusual trend toward Fe-phengite (or Fe-muscovite) is also visible in an AFM diagram (Fig. 3.4d). The increasing Al-content might be related to alteration process and is also suggested by the higher stability of Fe-phengite at lower temperature. Muscovite presents a more pronounced Fe variation compared to the metapelite AAn0401-B (0.04-0.13 p.f.u. in AAn0401-A against 0.06-0.10 in AAn0401-B). At the highest Fe-content, up to 50% Fe^{3+} over the total iron is recalculated after charge balance during cationic normalization (not presented here). However, this ratio is purely indicative, as the exact charge balance in hydrous phase is unknown (possible cation vacancy, double-charged anions, etc.). Microscopic inclusions of biotite, the presence of iron oxides resulting from alteration or a real trend toward ferri-phengite could all explain this variation. According to petrography, yellowish alteration stemming from sulphur and iron oxide leaching is clearly present in white mica and attests for fluid percolation (metamorphic or meteoritic).

Chemistry of muscovite in calcite-rich calc-schist ARo0601 and AAn0402 is more homogeneous than AAn0401-A, though that enrichment in Si (3.13 to 3.21 p.f.u.) and Mg (0.13 to 0.18) is observed and related to a decrease of K (0.94 to 0.86) and Al (2.68 to 2.60). This effect is attributed to the possible presence of voids in mica structure or to mixing effect with a K-poor phase, like chlorite or quartz. However, the chemical composition in each mica flakes remain broadly homogeneous, except K- and Al-variation. A lower sum for total cations is recalculated from oxygen normalization in calc-schists ARo0601 (0.88-0.95) against all other muscovite analysed (0.94-1.00).

The same zoning trend in garnet appears in all samples, calc-schist and metapelite, with approximately

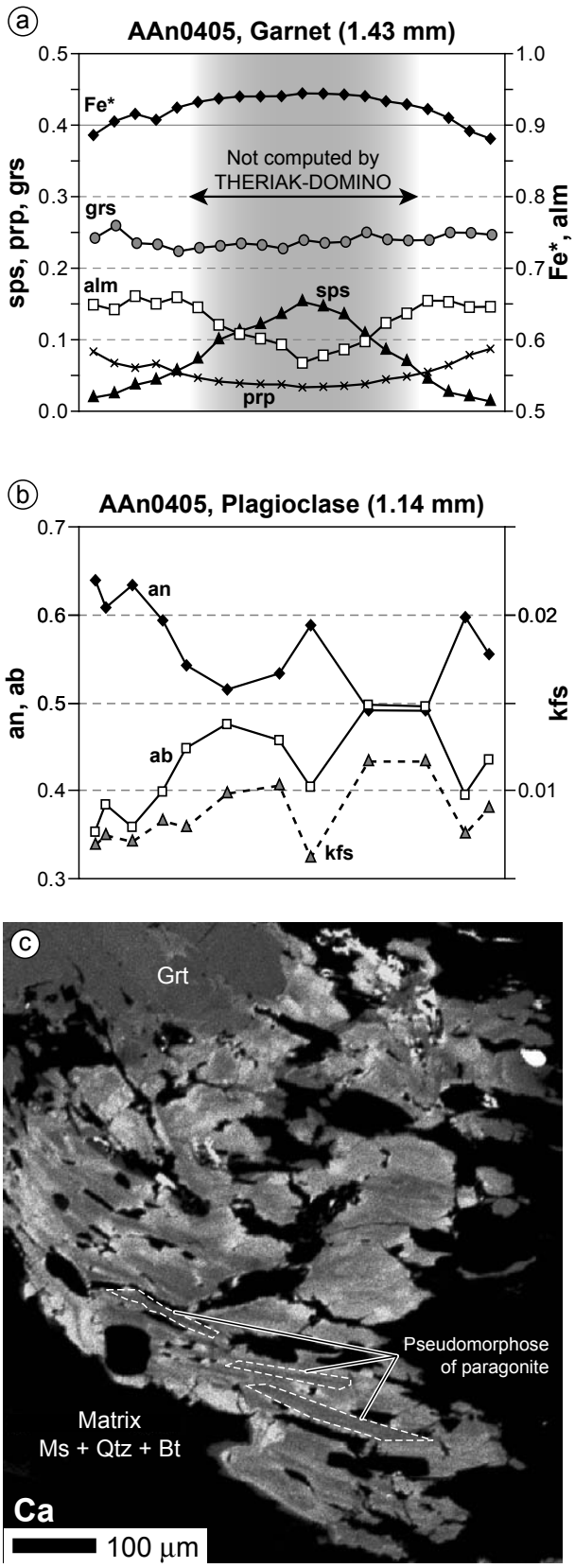

the same range of composition. The regular decreasing of Fe* ratio and spessartine-content in all garnet from any studied sample indicates a regular increase of temperature (prograde path, Fig. 3.5). Grossular-content is relatively homogeneous and quite high for a metapelite, around 25%. This suggests that an important source of calcium like carbonate, Ca-mica (margarite) or epidote was involved in garnet growth reaction. Unfortunately, except the persisting presence of epidote in the matrix, no such inclusions are apparently preserved in porphyroblasts.

Garnet rims may have locally different values, due to the presence of quartz or biotite in direct contact or due to change in local bulk rock chemistry. Garnet rim against quartz yield the lowest Fe* (0.901 at Rim 1b), while the rim against Bt-c yields a slightly higher Fe* (0.912 at Rim 1a; Table 3.3). Though scarce, garnet resorption is present. The latest biotite to appear (Bt-c) results from this resoprtion and yields the maximum Fe* (0.52) compared to biotite from the matrix surrounding garnet (0.40-0.43). Diffusion is unlikely responsible for this higher Fe* in Bt-c (late reequilibration), as garnet should yield lower Fe* in such case (Fe-Mg exchange).

Plagioclase blasts are apparently inhomogeneous zoned in all samples, but present stronger variation in the metapelite. In thin section, the difference in extinction angle highlights the strong zoning pattern occurring especially on rims. Blasts have sometimes a clear intermediate anorthite core (andesine-labradorite, An_{49-60}). Largest blasts without any crack are more homogeneous, but rim is always anorthite-richer and small intra-grain variation are constantly present. Element mapping at the electron microprobe reveals Na-richer slices inside all plagioclase, which most likely pertain to pseudomorphosis of paragonite (Na-mica) during

Fig. 3.5: (a,b) Typical analytical transect in **(a)** garnet and **(b)** plagioclase zonation in metapelite AAn0405. A regular increase of temperature is indicated by the decrease of Fe* and spessartine-component from core to rim of garnet, while plagioclase show a Ca-enrichment at rim and along cracks (middle of the analytical transect). **(c)** Element mapping of Ca in a plagioclase blast near garnet from sample AAn0401-B (WDS mode, 15 kV, 20 nA, beam 1 μm, pixel 1 μm, dwell-time 30 msec). Plagioclase present an irregular zonation, with anorthite-richer zone located preferentially at rim or near contact with included minerals or in cracks. Pseudomorph of paragonite is suggested from Na-richer slices in the plagioclase blast. More element distribution map for plagioclase is available in Appendix 1.

the early plagioclase growth (Fig. 3.5c and Appendix 3.2a,b). However, not only rims, but also cracks and contact with some inclusions are irregularly enriched in anorthite and slightly impoverished in K-content. A typical profile over a grain of circa 1.5 mm from the metapelite is presented together with an element mapping of Ca (Fig. 3.5b,c; see also Appendix 3.2a,b). Both rims reach An_{60-80} (labradorite-bytownite), as does a point in the middle near a crack or around some mineral inclusion. Plagioclase is also identified in garnet fracture and presents chemical zoning from An_{44-48} against garnet to probably $>An_{60}$ in the core of this fracture (Appendix 3.2c,d). The abrupt change in composition and the symmetrical growth of this plagioclase indicate a minimum of two opening stages of this fracture in garnet.

In calc-schist ARo0601 (An_{61-87}), AAn0402 or AAn0401-A (An_{69-83}), zonation is even more inhomogeneous, with unclear textural relation probably related to the small grain size and the locally strong sericitization (alteration). A sudden release of Ca through calcite, dolomite or epidote destabilization is most likely at the origin of a final and irregular anorthite-rich growth of plagioclase.

All other solid solutions are generally homogeneous, except epidote, which has a typical allanitic core and a relative homogeneous clinozoisite rim (65% xCzo; Table 3.3). In pelitic facies, minor albitic component is measured in K-feldspar (Ab_{4-5}). Relics of ilmenite in core of garnet have an important MnO content from 3-4%, up to 8%. Carbonates were not analyzed and EDS scan reveals calcite with only small MgO-content. It is obvious in ARo0601 or AAn0402, but only as minor component in AAn0401-A, where it is essentially grouped in small veins or with sericite in plagioclase. In metapelite AAn0401-B and AAn0405, carbonate is usually absent and rarely located in garnet or plagioclase cracks notably near the contact with the calc-schist AAn0401-A. Local occurrence of tiny staurolite crystal reaching 100-200 µm is possible in metapelite and in country rocks, but remains extremely sparse. They typically appear near garnet blast and are rich in Fe, with a variable but consequent ZnO content from 1.5 to 4.0% (Table 3.3). Very few and tiny Al-Fe-Zn oxides (or spinels?) found in the matrix is possible source for this high ZnO content in staurolite. Its local growth around garnet is also possibly related to metamorphic segregation (induced by garnet growth). From its occurrence and from comparison to other similar outcrops found in the Central Alps (Wenk *et al.*, 1974; Hoschek, 1998), it is probably a Ca-amphibole (tschermakite or pargasite) with an intermediate Fe* growing at amphibolite facies condition or near retrogression (greenschist facies).

3.7) Thermobarometry

The assemblage muscovite, biotite, garnet and rare staurolite indicates equilibration under amphibolite facies condition. To better constrain PT-condition and the state of equilibrium multi-equilibrium thermobarometry was undertaken on garnet-bearing metapelites and calc-schists using TWQ (Berman, 1991). Mineral analyses retained for such calculations are taken from a restricted area of the thin section, about 1 mm diameter, near a garnet rim. Concerning chemically zoned minerals, only rims are considered in equilibrium with the matrix and therefore only one point or an averaged rim analysis of garnet and plagioclase is used for PT calculation. These analyses corresponds to the minimum Fe* ratio in garnet and the maximum anorthite content in plagioclase. Plagioclase is the only mineral for which analysis was sometimes taken 2-4 mm away from garnet.

3.7.1) PT-results

PT-results using muscovite, biotite, plagioclase, garnet and quartz assemblage in metapelite AAn0401-B, AAn0405 or in calc-schist ARo0601 yield similar PT condition around 540-570°C and 6.8-7.4 kbar (Fig. 3.6a). These results

are in good agreement with former PT calculation (Engi *et al.*, 1995). Fluid composition, in term of H_2O-CO_2 content, in equilibrium with the assemblage can also be estimated by TWQ and yield always extremely low value for xH_2O (0.34 in AAn0405 and 0.11-0.15 in all other samples).

The calcite-rich calc-schist AAn0402 yields similar PT conditions at 584°C and 7.65 kbar. This sample is mainly rutile bearing, but scarce titanite is also present in the matrix and associated with rutile in core of garnet. The use of both minerals with a fixed unit activity yields slightly parsed equilibria over a PT range of 540-610°C and 6.5 to 8.5 kbar (dashed lines, Fig. 3.6b). A best fit is obtained with a reduced titanite activity (0.95; full lines in Fig. 3.6b), which suggests disequilibrium. At 0.95 a_{Ttn} and 0.41 xH_2O, PT calculation yields four LIR intersecting in a narrower window (584±14°C and 7.65±0.4 kbar).

TWQ result from the calc-schist AAn0401-A shows a clear disequilibrium (Fig. 3.6c), which is not surprising considering the alteration of biotite, plagioclase and garnet.

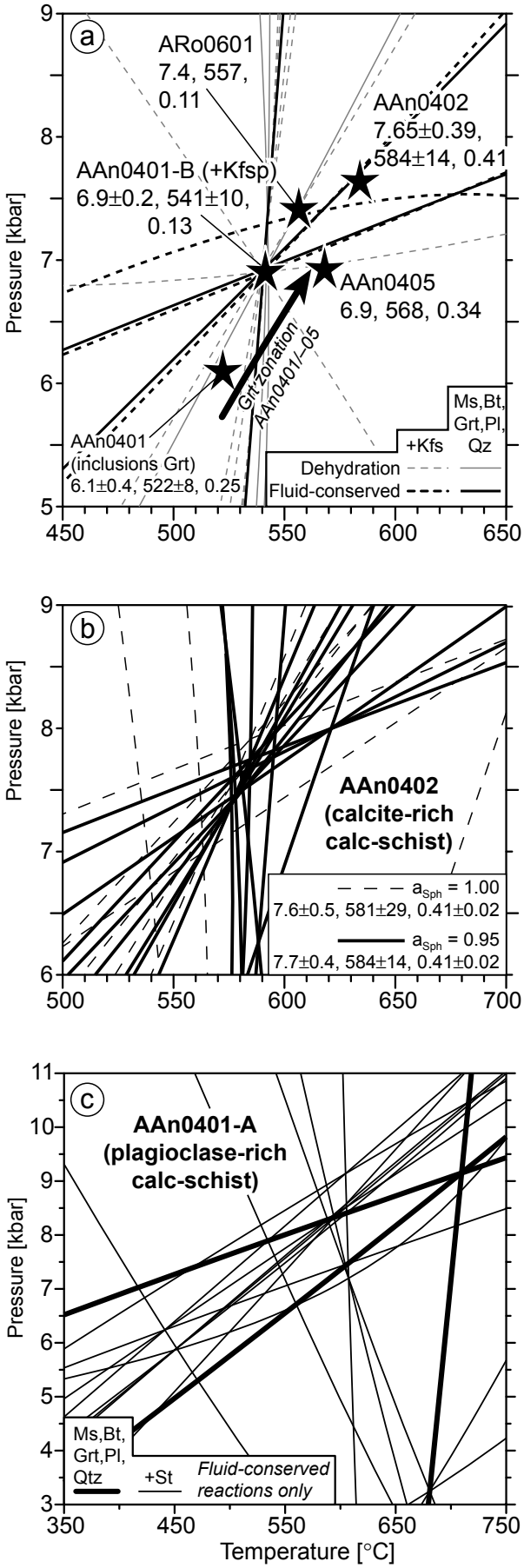

Fig. 3.6: (a) Summary of PT results obtained with TWQ on samples from Antabia (metapelite AAn0401-B and AAn0405, calc-schist AAn0402) and Alpe Robiei (calc-schist ARo0601). All four samples have two linearly independent reactions (LIR). Including H_2O-CO_2 fluids impose a third LIR (dashed lines). The H_2O-CO_2 ratio is obtained from the intersection of calculated equilibria in a P versus $x(H_2O$-$CO_2)$ diagram (not shown here, see CD). Black stars stand for intersection of those reactions and numerical results are given below sample number (P in kbar / T in °C / xH_2O). Both calculations with or without K-feldspar in AAn0401-B (black or grey reactions) yield undistinguishable results. Lower PT-condition for AAn0401-B is obtained by using the assemblage found in core of garnet, notably rutile, ilmenite and biotite (see Figure 2c and text for more details). **(b)** Results for carbonate-rich calc-schist AAn0402. An optimum intersection of reactions is obtained with a slightly reduced activity for titanite (0.95). **(c)** Example of disequilibrium in mineral assemblage from the calc-schist AAn0401-A (notice the larger PT-scale used in this diagram). The same assemblage as in a) is used, but yields impossible PT condition for the studied area, around 715°C and 9.1 kbar (thick lines). Including the rare staurolite growing as tiny crystal near garnet give parsed reactions over this large PT-window (fine lines).

Considering the same minimal assemblage as before, this yields too high PT condition near 680°C and 9 kbar (bold lines in Fig. 3.6c). The addition of staurolite further compounds matters (thin lines in Fig. 3.6c). This Al-rich silicate locally present in the contact zone between metapelite and calc-schist and is either to be considered as a retrograde phase occurring along decompression or in local equilibrium in some chemically distinct domain. The relative high Zn-content (0.54 p.f.u.), and to a less extent also Mn (0.11), compared to FeO and MgO (2.23 and 0.63 respectively) attests for a favoured growth of this crystal related to local ZnO (and MnO) enrichment. The lack of thermodynamic data for Zn- and Mn-staurolite mean only Fe-Mg exchange models can be modelled with TWQ or THERIAK-DOMINO. This accounts for the apparent disequilibria between staurolite and other rock-forming minerals.

All PT calculations performed are essentially dominated by Fe-Mg equilibria. Garnet rim analysis is always used for calculation, while different biotite analyses (and different biotite generation) are available. Considering local equilibrium effect and late exchange reaction between biotite and garnet or ilmenite in contact, only analyses of biotite near garnet, but not in contact with garnet or any other Fe-Mg phase, are retained. A rapid test with TWQ demonstrates that using a biotite analysis with a lower Fe*, which corresponds either to an isolated biotite flake away from garnet or to the core of coarse biotite, TWQ thermobarometry immediately leads to lower PT conditions, around 480-520°C and 6.1-6.6 kbar, which is inconsistent with the observed mineralogy. This demonstrates the effect of local equilibration of rock-forming minerals and metamorphic segregation: growth of large blast, especially garnet, may fractionate elements and affect the apparent local rock analysis. Moreover, we cannot exclude the possible discreet or continuous growth of different biotite generations from near the thermal climax up to the early decompression. Considering the presence of distinct biotite of variable chemistry and textural relationship (included in or at rim of garnet, coexisting fine flakes and large books in matrix), this later hypothesis is preferred.

3.7.2) Mineral stability and PT-path

3.7.2.1) Water-saturated condition

Mineralogical evolution and garnet zoning is modelled with THERIAK-DOMINO (de Capitani, 1994), using the whole rock analysis of the metapelite AAn0405 (Fig. 3.7). We suppose the fluid present in equilibrium with the mineral assemblage is only pure water (Fig. 3.7a), which is apparently coherent considering the large amount of hydrous phases and the absence of carbonate. Garnet isopleths indicate a growth from 520/5.7 to 570/7.0 kbar. The end of this PT-path is consistent with the PT conditions estimated by TWQ (Fig. 3.6a, 3.7a). However, the initial garnet growth might be situated at lower PT-condition, as a part of the garnet zoning is not modelled by THERIAK-DOMINO (Fig. 3.5a). This inadequacy is most likely related to the spessartine end-member defined in the thermodynamic database used (Table 3.2). Nevertheless, mineralogical evolution is consistent with computed PT-grids: rutile and ilmenite are stable at beginning of garnet growth and ends in the rutile stability field.

To constrain possible PT condition at the time garnet starts to grow, we calculate PT condition with TWQ using a core analysis of garnet, an included biotite in garnet near this core analysis and we added rutile and ilmenite (Fig. 3.6a). This assemblage corresponds to mineral found in core of garnet (Fig. 3.2c). Both muscovite and plagioclase are stable before garnet-in reaction (Fig. 3.7a), we assume similar muscovite and plagioclase chemistry as the previous calculation, using either maximum or minimum phengite- or anorthite-component. From THERIAK-DOMINO, no large change in mica or plagioclase composition is expected all along the PT-path calculated from garnet growth. Using various composition of plagioclase or muscovite in TWQ has quite

no influence on PT results, as most reactions are controlled by Fe-Mg exchanges between biotite and garnet. Albeit biotite is more easily subject to late re-equilibration with either ilmenite or garnet, calculated PT-condition for the mineral assemblage found in core of garnet is similar to the value obtained for starting point of garnet zonation modelled by THERIAK-DOMINO (522°C, 6.1 kbar; Fig. 3.6a, 3.7a). According to annite-content in biotite computed by THERIAK-DOMINO at xH_2O = 1.00, lowest to intermediate Fe* value around 0.44 are compatible with *PT* around the point estimated by TWQ (580°C, 7 kbar). Higher values, like those of included biotite (0.55 Fe*) are restricted to lower P or T conditions, below 500°C and 5 kbar. Reducing H_2O activity will reduce the stability field for biotite (at higher T and lower P) and lower Fe* ratio are expected for the considered T (0.40-0.42), but may reach higher Fe* than with pure water at T <500°C.

3.7.2.2) K-feldspar growth

Inconsistency of the computed PT-grids regarding the presence of K-feldspar in thin section is obvious. At fluid composition approaching pure water, the disappearance of muscovite in favour of K-feldspar occurs only at temperature well above 650°C, which is not possible in the studied area. However, reduction of water activity would shift the K-feldspar-in reaction towards lower T. We therefore calculate a pseudo-section at fixed T, but variable pressure and fluid composition (580 °C; Fig. 3.7b). In THERIAK-DOMINO, the fluid composition can be modelled either with H_2O-CO_2 mixture (xCO_2) or with a reduction of water activity (aH_2O). Though both process effectively reduce the water activity, this latter is a simple mathematical treatment, which reduces aH_2O without introducing CO_2 in the system, preventing thus the growth of carbonate.

The stability field for muscovite, biotite, garnet and plagioclase with ilmenite or rutile covers a large field at low xCO_2 (medium grey field, Fig. 3.7b). Around 0.7 to 0.8 xCO_2 muscovite starts reacting to form K-feldspar (dark grey field, Fig. 3.7b). At higher xCO_2, all hydrous phase including muscovite react to produce carbonates (biotite to magnesite and ankerite) or feldspar (muscovite to K-feldspar, light grey field, Fig. 3.7b). The xH_2O-P-T modelling indicates a large influence on fluid composition on phase assemblage. Therefore, we consider a comparable PT diagram at a water fraction of 0.20 to have a better idea of the temperature effect and the possible decompression path. Under such conditions, the assemblage muscovite, K-feldspar, plagioclase, garnet, biotite and quartz (dark grey field of Fig. 3.7c) is stable in a PT window starting around 550°C – 4 kbar and closing at 640°C – 9 kbar. The last stable carbonate, a dolomite at low xH_2O or calcite at lower value, is stable up to circa 500°C at 4 kbar and 620°C at 8 kbar. In studied metapelites, no carbonate is stable in the matrix, except as late alteration phase. We therefore argue for an adiabatic decompression path occurring after the regional peak of metamorphism determined by TWQ (path A; Fig. 3.7c). Comparing the Ti-phase between the model and the natural observation, the phase may be slightly modified as indicated by path B (Fig. 3.7c).

At the time Ms2 is growing (phengite-poor muscovite), it coexists with of K-feldspar, biotite and quartz in the matrix. We can thus consider the phengite barometer of Massonne & Szpurka (1997), which yields a P estimation around 3.5-5.0 kbar for 3.08-3.14 p.f.u. Si and a maximum temperature of 550-580 °C. Higher pressure around 7-9 kbar are obtained for phengite-rich core analyses of muscovite (Ms1, Si 3.27), but this value is minimum as K-feldspar was presumably absent from the assemblage at that time. Moreover, questionable is the role of fluid in equilibrium with the assemblage, notable the one related to K-feldspar growth. At time Ms1 was stable, fluid is presumably water rich ($xH_2O \approx 1.00$). However, lower water activity is required to induce K-feldspar formation from the phengite-rich muscovite and phengite barometry requires a water saturation condition. As shown in Massonne & Schreyer (1987), reducing water activity from 1.0 to 0.6 would induce a pressure increase of about 3 kbar. Nevertheless, we argue for a nearly adiabatic decompression at P <7 kbar and T ≈ 550 °C

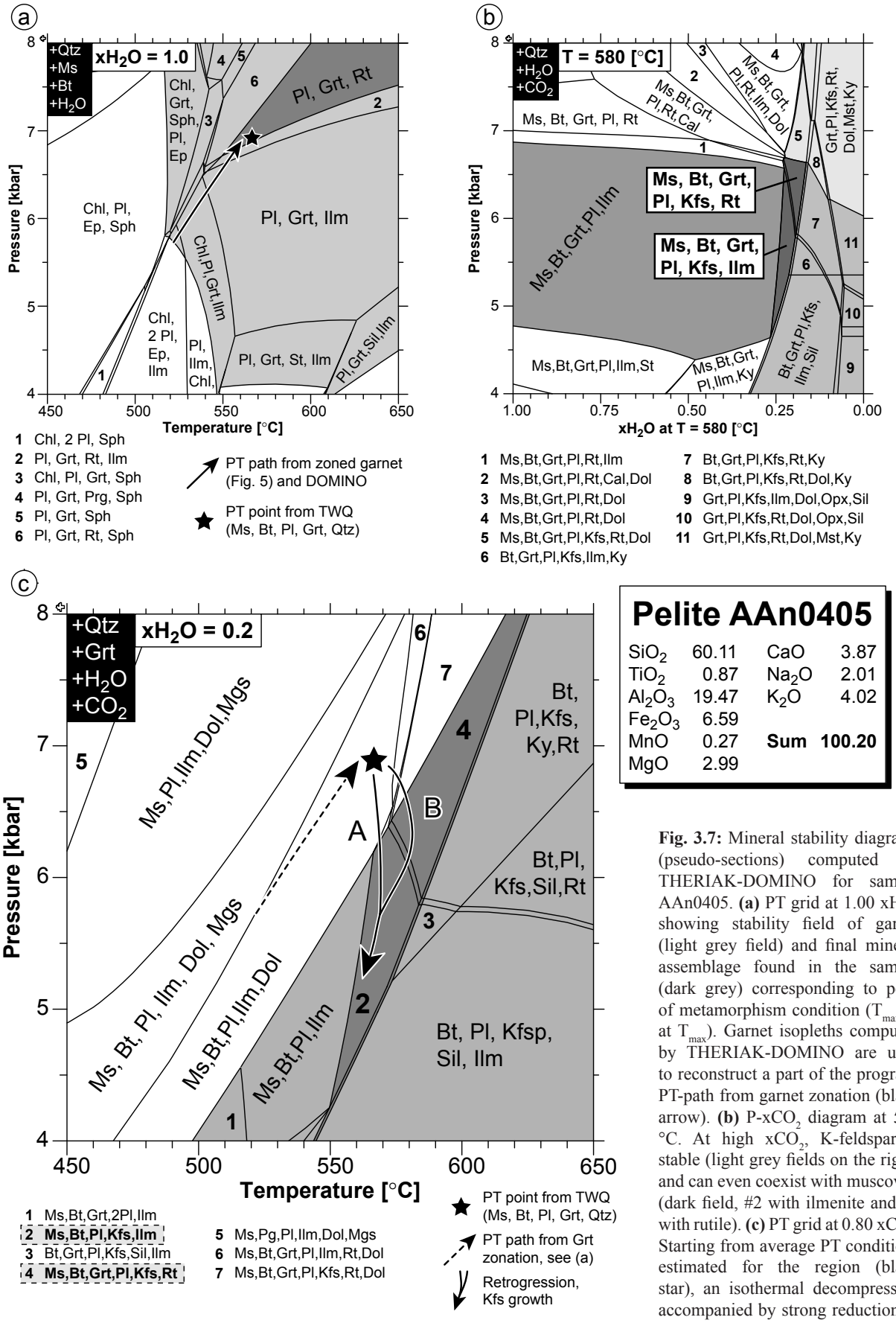

Pelite AAn0405

SiO_2	60.11	CaO	3.87
TiO_2	0.87	Na_2O	2.01
Al_2O_3	19.47	K_2O	4.02
Fe_2O_3	6.59		
MnO	0.27	**Sum**	**100.20**
MgO	2.99		

Fig. 3.7: Mineral stability diagrams (pseudo-sections) computed by THERIAK-DOMINO for sample AAn0405. **(a)** PT grid at 1.00 xH_2O showing stability field of garnet (light grey field) and final mineral assemblage found in the sample (dark grey) corresponding to peak of metamorphism condition (T_{max}, P at T_{max}). Garnet isopleths computed by THERIAK-DOMINO are used to reconstruct a part of the prograde PT-path from garnet zonation (black arrow). **(b)** P-xCO_2 diagram at 580 °C. At high xCO_2, K-feldspar is stable (light grey fields on the right) and can even coexist with muscovite (dark field, #2 with ilmenite and #4 with rutile). **(c)** PT grid at 0.80 xCO_2. Starting from average PT conditions estimated for the region (black star), an isothermal decompression accompanied by strong reduction of water activity permits the association of K-feldspar and muscovite. See text for details.

accompanied by a reduction of water activity well explain the growth of K-feldspar after the thermal climax (Fig. 3.7c). The decompression history inducing K-feldspar growth is estimated around –2.0 kbar after the regional peak of metamorphism (T_{max} and maximum P at T_{max}) determined by TWQ for the region (540-570°C and 6.8-7.4 kbar) and temperature condition remains higher than 550°C but strongly reduced xH_2O.

Water activity suggested from this thermobarometric study might appear unrealistic, due to the rarity of CO_2-rich fluids in metamorphic rocks. Previous studies on calc-schist usually calculate PT-grids in the range 0.0 to 0.5 xCO_2 (e.g. Will *et al.*, 1990; Livi *et al.*, 2002; Kuhn *et al.*, 2005). However, a strong reduction of water activity is always necessary for K-feldspar stability a T <600 °C. In T versus aH_2O diagram at 6.5 kbar for AAn0405 (CO_2-free system, not presented here), muscovite and K-feldspath are stable with biotite, garnet and plagioclase at T >550 or 600 °C and 0.25-0.45 aH_2O. We suggest that other ions stemming from dissolution of sulfate or salt from the Triassic layers (gypsum, pyrite; Fig. 3.1b) could have strongly reduced this water activity, but remains difficult to compute with THERIAK-DOMINO. Moreover, complications arise from the local presence of amphiboles related to fluid-percolation, most likely water-rich. In agreement with the large variety of lithology (from pure pelite to pure carbonate, with variable arkosic material), the fluid composition is believed to have strongly varied, locally in some layers and rapidly. Nevertheless, this effect is local and, up to now, exclusively observed in Val Antabia. No other sample of similar PT-condition collected elsewhere in the Central Alps present such a feature.

3.8) Mineral reactions and PT history

Si/Al ratio is higher in K-feldspar than any mica (2.95 in K-feldspar, 1.5-1.8 in biotite, 1.15-1.25 in muscovite). Thus, growth of K-feldspar from destabilization of muscovite or biotite obligatory induces production of an Al-richer phase. The typical K-feldspar forming reaction includes growth of an aluminosilicate (mineral abbreviation following Kretz, 1983):

$$\text{Ms} + \text{Qtz} \Rightarrow \text{Ky/Sil} + \text{Kfs} + \text{fluid or melt} \qquad (3.1)$$

Addition of biotite to reaction (3.1) permits the formation of staurolite instead of an aluminosilicate. Indeed, traces of staurolite are present. Unfortunately, the very low abundance of staurolite is largely insufficient to explain the large amount of K-feldspar found over the entire thin section (1-3%, locally 5-10%; Fig. 3.3a,c). In contrary, an Al-richer rim is always present in all white micas (large books and fine flakes; Fig. 3.3d). Considering the Na_2O-K_2O-Al_2O_3-SiO_2-H_2O system (NKASH), the destabilization of a phengite-rich muscovite (Ms1) and the production of a phengite-poorer one (Ms2) can explain the K-feldspar formation (Ms1 and Ms2 as defined in the mineral chemistry section):

$$\mathbf{8.99\ Ms1} \Rightarrow \mathbf{1.00\ Kfs} + \mathbf{7.75\ Ms2} + 2.76\ \text{Qtz} + 2.47\ H_2O \qquad (3.2)$$

No supplementary balancing of Na by plagioclase is required in this case, as a similar and always low paragonite-content is present in both Ms1 and Ms2. Using THERIAK-DOMINO to get the right volume of each phase at conditions around 580°C and 4 to 6 kbar allows a rough estimation of possible volume change. For all calculated reactions presented here, no dramatic change is calculated with typically value around –0.5 and +1.5% volume change. In terms of volume-production, the consumption of 12 volume of Ms2 produces 1 volume of K-feldspar, 10 of Ms2 and 0.5 of quartz. Adding FeO and MgO to NKASH system, Ms1 from reaction (3.2) would inevitably release some Mg and to a less extent Fe:

$$9.20\ \text{Ms1} \Rightarrow 1.00\ \text{Kfs} + 7.89\ \text{Ms2} + 2.74\ \text{Qtz} + 2.42\ H_2O + \mathbf{0.20\ Fe} + \mathbf{0.89\ Mg} \qquad (3.3)$$

Thus for a more realistic mass balance of reaction (3.3), Mg- or Fe-bearing phase(s) are required. From textural observation, biotite is also involved in K-feldspar formation (Fig. 3.3a). Different biotite generations are identified. Notably, after the growth of large biotite books (Bt-a) and excluding the Ti-richer rim (related to ilmenite break-down), a later growth of biotite occurs in the matrix (Bt-b) and produces finer flakes essentially aligned in the schistosity (Bt-b; Fig. 3.4a,b). The variable chemical composition of these biotites is suggested to accommodate the Mg- and Fe-excess of reaction (3.3). We therefore consider two biotite of slightly different chemistry (see Fig. 3.4a,b):

Fe-rich: $(K_{0.97}\ Na_{0.01})\ (Fe_{1.07}\ Mg_{1.24}\ {}^{VI}Al_{0.60}\ Ti_{0.10})\ (Si_{2.86}\ {}^{IV}Al_{1.14})\ O_{10}\ OH_2$ (Bt1; 0.46 Fe*)

Fe-poor: $(K_{0.96}\ Na_{0.01})\ (Fe_{0.95}\ Mg_{1.36}\ {}^{VI}Al_{0.62}\ Ti_{0.09})\ (Si_{2.91}\ {}^{IV}Al_{1.09})\ O_{10}\ OH_2$ (Bt2; 0.41 Fe*)

These are two representative analyses of the observed variation of biotite Bt-b composition in the matrix of metapelite samples. A new mass balance calculation gives:

$$14.16\ Ms1 + \mathbf{3.22\ Bt1} \Rightarrow 1.00\ Kfs + 11.89\ Ms2 + 4.18\ Qtz + \mathbf{3.99\ Bt2} + 2.60\ H_2O \quad (3.4)$$

This reaction reflects some similarities with another general K-feldspar formation reaction involving a change in Si-content of phengite as proposed by Massonne & Schreyer (1987):

$$\text{Phengite 1} \Rightarrow \text{Phengite 2} + Kfs + Qtz + Phl \quad (3.5)$$

As show by stoichiometry of reactions (3.2) to (3.4), the formation of K-feldspar is induced by a change of white mica composition towards lower phengite component. Concerning biotite, the only clear correlation between texture and biotite chemistry is the lower Fe* ratio in core of largest grains (Bt-a) and in some finer biotite flakes from the matrix (Bt-b, aways from garnet), which contrasts with the late growth of Fe-rich biotite against garnet (Bt-c). As revealed by the numerous biotite analyses in metapelite and the former discussion, the variation of Fe-Mg in biotite is complex. This is the result of different biotite generations (prograde Bt-a, peak/decompression Bt-b and retrogression Bt-c) combined with some local effects, which are related either to local change in rock composition (metamorphic segregation or sedimentary layering), to the presence of a Ti-phase in the vicinity (Ti-richer biotite) or to a disequilibrium feature (chloritization, diffusional re-equilibration between biotite and garnet, etc.). Late diffusion is also possible and could tend to homogenise the zonation observed in large and oblique biotite (Fig. 3.3e,f).

Nevertheless, we argue for the utmost importance of different biotite generations, which accounts for the largest chemical variation in biotite composition. The youngest biotite generation consist of large books having the lowest Fe*, together with finer biotite flakes preserved in plagioclase (Fig. 3.4b). Various generations related to different PT-conditions will inevitably produce biotite of variable chemical composition. Some variations reflect some specific metamorphic reactions. For instance, ilmenite destabilization involves the overgrowth of a Ti-richer rim on oblique biotite. The partitioning of Ti in biotite will also depend on the bulk rock chemistry, the fluid present and the temperature and will have an effect on Fe* ratio and Al-content (higher Fe* or lower Al for higher Ti-content). Finally, the destabilization of a phase like phengite-rich muscovite may also influence the Fe* ratio of a new biotite generation (reaction 3.4). Although large amounts of Mg are not present in phengite-core of white micas, the large amount of muscovite involved in reaction will produce a significant release of Mg in the system (reaction 3.3). Biotite reacting to form K-feldspar is also inferred from texture (e.g. Fig. 3.3a), but K-feldspar formation through reaction with the large amount of white mica in this pelite is more likely to occur. In any case, no realistic mass balance can be obtained by considering only biotite as a major reacting phase. The only exception is Al-richer biotite preserved in core of garnet, but K-feldspar formation is occurring well after the end of garnet

growth on the retrograde path.

Compiling the petrography, the mineral reaction and chemistry as also the thermobarometric results, we can detect 5 major phases summarized for white micas and K-feldspar relation in Figure 3.8:

1. Prograde path 1: Elongated plagioclase blasts growing over the schistosity are already present together with muscovite (Fig. 3.7a). At this stage it remains unknown, whether oblique mica are already present or not. However, the maximum of pressure is not achieved and it is likely that the main schistosity is always not totally formed. This would suggest an absence of oblique mica (Fig. 3.8a).

2. Prograde path 2: Growth of large garnet blast in a mica-rich matrix, in the stability field of biotite, starting at least at 520°C and 5.8 kbar according to garnet-isopleths. This stage includes the growth of the largest and oblique biotite (Bt-a) and muscovite books.

3. Peak of pressure (near thermal climax): The end of garnet growth and the PT-condition determined from TWQ point to a first complete equilibration near the maximum of pressure (7 kbar). The thermal peak is approached and the kinetic of mineral reaction is at its maximum. The mineral assemblage constituted by garnet rim, biotite (Bt-b), phengite-rich muscovite (Ms1), plagioclase and quartz is equilibrating around 540-570°C and 6.8-7.4 kbar. This PT-condition are similar to calcschist and metapelite from the surrounding area (e.g. Robiei, ARo0601 and results from Todd & Engi, 1997). The release of Ti from ilmenite destabilization accounts for the Ti-richer border (Bt-b) overgrowing the largest biotite books (Bt-a; Fig. 3.3e,f). Due to reduction of stress (pressure will now decrease), growth of oblique muscovite and biotite is enhanced and starts probably just before or near this peak of pressure. Considering the persisting high-T stage, any mica will likely suffer a complete re-equilibration through mineral recrystallization or neocrystallization (Fig. 3.8b). Diffusion in mica may also be responsible for the zonation observed in muscovites (Fig. 3.8c). However, this is unlikely if we consider the slow diffusion of Si and Al in this mica at the considered PT conditions and the relative small time interval available (1-10 Ma). We consider the metamorphic reaction producing K-feldspar as the predominant responsible reaction for the zonation observed in muscovite, without excluding possible later diffusion. This later will tend to homogenize this zonation, smoothing the contrast, especially along a- or b-axis of mica and along marked cleavage and fracture (Fig. 3.8e,g).

4. Decompression: this phase is occurring at isothermal condition, 550-580°C, between 6 and 4.5 kbar and affects mainly hydrous phases, i.e. micas. Decompression induces decarbonatation of the rare carbonate present in the metapelite or, of most probable, in the large amount of carbonaceous material surrounding the relative small metapelite outcrop. The fluid in equilibrium with the metapelite at P_{max}, T_{max} was probably H_2O-rich, but it is suddenly externally buffered by a large amount of CO_2. This influx will induce mineral reaction, especially with the hydrous phases, muscovite and biotite. Through diffusion and recrystallization, phengite-rich muscovite, and to a less extent biotite, reacts to form a phengite-poor muscovite and K-feldspar (Fig. 3.8d,f). Whether the phengite-poor rim is resulting from an dissolution-recrystallization (Fig. 3.8d) or from a volume-diffusion re-equilibration (Fig. 3.8f) remains questionable, but the latter is preferred and would easily explain the texture observed in element mapping (e.g. Fig. 3.8g). We argue for an impossibility for phengite-poor growth or volume-diffusion re-equilibration in absence of a new mineral phase able to balance the large Al and Mg-release from phengite-rich muscovite. K-feldspar formation is exclusively related to a change in muscovite and to a less extent biotite chemistry, accompanied by minor growth of staurolite. Cases presented in Figure 3.8c,d are thus unlikely. A detail observation of the zonation in muscovite (Fig. 3.8g) clearly shows a regular decrease of Al and Mg-content from core to rim along a- or b-axis, parallel to mica sheets. In contrary, along the c-axis of

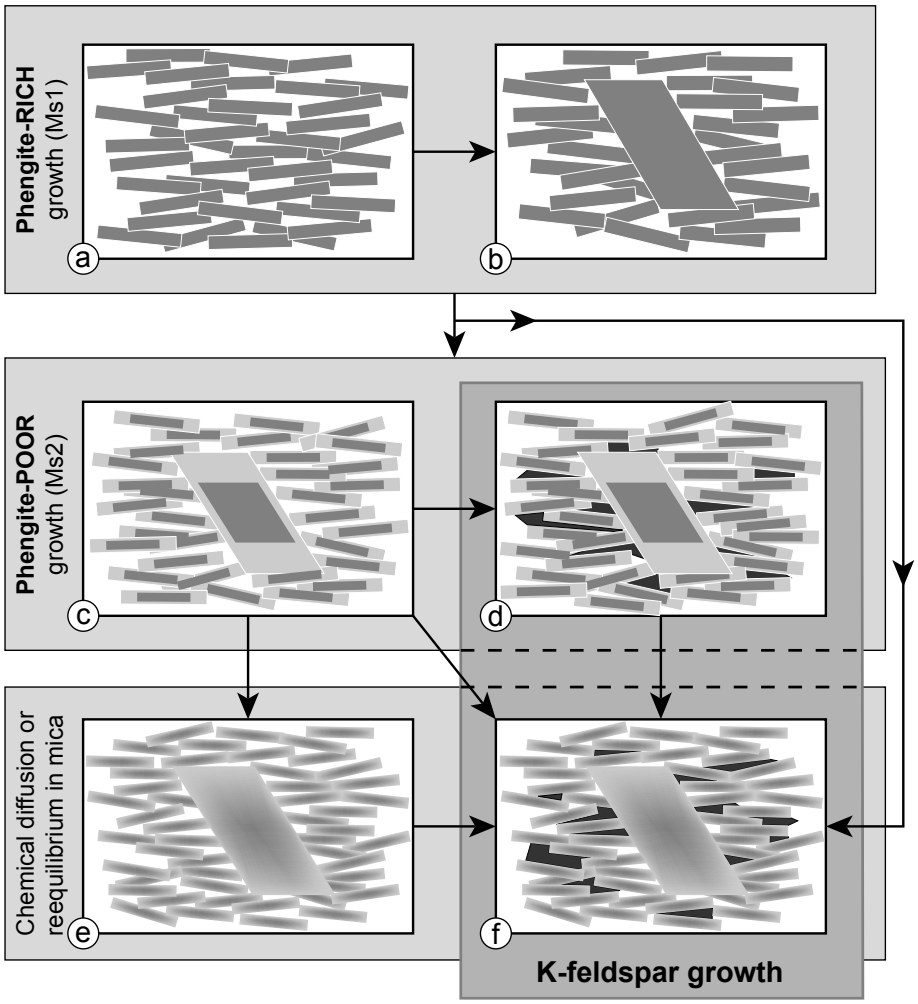

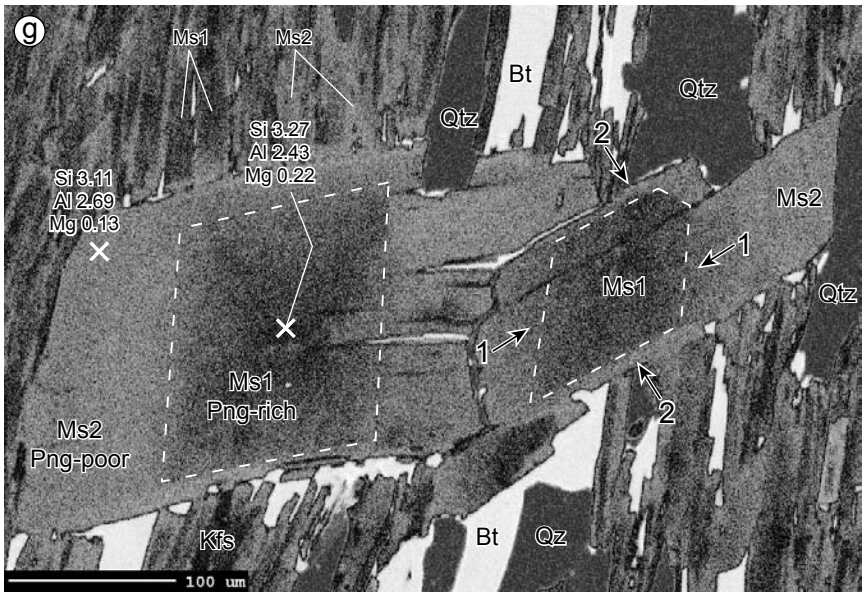

Fig. 3.8: Different models for zonation in muscovite and K-feldspar formation. **(a)** Synkinematic phengite-rich muscovite. **(b)** Growth of larger oblique muscovite (phengite-rich). A complete chemical reequilibration of the synkinematic flakes is possible. **(c)** Overgrowth of muscovite-rich rim on large and synkinematic muscovites independently of K-feldspar growth. This would correspond to the final reequilibration during thermal climax or during early decompression. **(d)** The phengite-poor rim is a recrystallization of phengite-rich to phengite-poor muscovite and induces the growth of K-feldspar. **(e)** Diffusion in micas independent of K-feldspar growth occurring after or during stage (c). **(f)** Apparition of a diffusive contact between phengitic core and muscovitic rim related either to the growth of K-feldspar (a,b => f or a,b => e => f) or occurring afterwards (a,b => d => f). **(g)** Enlarged element mapping from Figure 3d showing in detail the chemical zoning in muscovite (WDS mode, 15 kV, 20 nA, beam 2 μm, pixel 0.5 μm, dwell-time 30 msec). A more diffuse contact is observed along a and b axes of muscovite (e.g. marked cleavage visible in centre) and corresponds to an stronger diffusion in this crystallographic direction (arrow 1, to compare with arrow 2).

muscovite, the boundary is somehow sharper. Such a feature is typically resulting from volume-diffusion, which is clearly higher along a- or b-axis of phyllosilicates due to crystal network. We thus conclude to a volume-diffusion re-equilibration of muscovite during K-feldspar growth, which produces the zoning pattern observed in muscovite (Fig. 3.8f,g). This latter pattern is undistinguishable from the pattern of Figure 3.8e.

5. Retrogression: In a later stage, the entire region is fluxed by water, circulating in some restricted pathway and producing locally those marvellous hornblende garbenschist. Though such samples are excluded from our sample collection, the presence, even locally, of fluids may again induce a recrystallization of some hydrous phase or the hydration of others, such as chloritization of biotite, alteration of muscovite and plagioclase saussuritization. Alteration and recrystallization are often observed in the carbonate-bearing rocks, but seldom in metapelite.

3.9) Argon dating

Calc-schists are often unsuitable for Ar-Ar dating due to scarcity of muscovite and the strong chloritization of biotite (Appendix 3.2), associated to a weak chemical equilibrium in mineral assemblage (Fig. 3.6c). In contrary, metapelites are extremely rich in micas and are thus apparently suitable for Ar-dating. Different crystal sizes obtained after mineral separation were selected and summarized in Table 3.4. In arkosic calc-schist sample AAn0401-A, muscovite is tiny and therefore a grain size between 100 and 200 µm was retained, while a larger grain size was selected for biotite. From petrography and crystallization-deformation relation, different micas generations are identified in metapelite: small flakes (Ms-a) and oblique books (Ms-b) of muscovite on one hand and coarse books (core Bt-a; rim Bt-b), synkinematic flakes (Bt-b) and tiny biotite around garnet (Bt-c) on the other hand. We thus separate two different grain sizes in mica separates of sample AAn0405 (mesh 100-150 and 150-250) to check for age variation according to either different mineral generation or different average grain size. This last point is important, if intra-grain diffusion is regard as the process controlling Ar-retention. Separates of coarser grain size contains oblique mica flakes, while a mix of fine synkinematic micas and coarser books is present in smaller grain size separates. The smallest muscovite related to plagioclase alteration (sericite) or the small biotite growing lately are probably excluded from separate, as in both case the grain size is only a few tenth of micrometer. Due to a too fine grain-size and the relative small abundance of K-feldspar (a few percent), this mineral was not separable and could not be dated.

The presence of chlorite in a biotite separate or presence of a late biotite generation may both disturb the argon-spectrum by argon loss during chloritization and biotite recrystallization or by recoil effect during sample irradiation (Villa, 1998b; Di Vincenzo *et al.*, 2003). See Table 3.4 for mineral separates used for Ar-dating. A few chlorites are found in the biotite separate from calc-schist (XRD ratio Bt/Bt+Chl 1.6%, qualitative ratio), lower in biotite separates from metapelite (0.4 to 1.1%). These qualitative ratios remain low and suggest a low chlorite amount and thus a minimized effect on age.

Ar-dating results are given in Table 3.5 and Figure 3.9. Due to an excellent purity of mineral separate, best results are obtained in the metapelite AAn0401-B. All major steps of both muscovite and biotite Ar-spectrum (Fig. 3.9a) yield a well-defined plateau age at 15.11±0.14 and 14.93±0.43 Ma, respectively. Note, however, that step between 827 and 1007 °C was lost. Thus total-K, –Cl and –Ca recalculated from total ^{39}Ar, ^{38}Ar and ^{37}Ar gives minimum values (Tables 3.4, 3.5). All major steps of muscovite AAn0401-B are restricted to low values of Cl/K and Ca/K ratios with a small spreading (Ca/K <0.063 and Cl/K $<5*10^{-4}$; Fig. 3.10a) and present a small age variation between 14.90±0.17 and 15.33±0.24 Ma (steps 8 and 10; Fig. 3.9a). This plenty justifies the selection of

Table 3.4: Mineral separates and Ar-Ar stepwise heating results. Impurities are typically quartz with muscovite and chlorite with biotite. Trace of epidote is also present in biotite separates from sample AAn0401. See text for further explanations.

a) Mineral separates				b) XRD		c) ^{39}Ar-^{40}Ar stepwise heating results					
Sample, mineral		Mesh [µm]	Weight [mg]	Impurity	Peak ratio *	Steps #	^{39}Ar [%]	Age Error [Ma] [1.95σ]	K [%] from ^{39}Ar	% Ms or Bt **	36/40 ratio at 39/40 = 0
AAn0401 (A, calc-schist)	Ms	100-200	12.6	Qtz	4.86%	5-10	84.0%	**14.95 ± 0.59**	6.09%	66.7%	288.2 ±22.4
						5-8	52.0%	14.52 ± 0.47			
						9-10	32.0%	15.44 ± 0.50			
	Bt	200-250	13.3	Chl, Ep	1.62%	4, 7-11	75.7%	**14.54 ± 0.75**	6.32%	77.9%	256 ±178
AAn0401 (B, pelite)	Ms	200-250	21.1	Qtz	1.09%	4-10	90.9%	**15.11 ± 0.14**	9.15%	100.0%	280.9 ±9.5
	Bt	200-250	14.7	Chl, Ep	0.43%	3-6, 9-10	89.6%	**14.93 ± 0.43**	> 6.36%	85.8%	321.5 ±21.7
AAn0405	Ms	50-150	20.5	Qtz	<0.7%	5-12	85.0%	**15.24 ± 0.45**	8.27%	90.3%	303.0 ±2.3
	Ms	150-250	16.5	Qtz	1.27%	10-15	85.9%	**15.78 ± 0.64**	8.36%	91.2%	294.1 ±2.9
	Bt	50-150	7.1	Chl	1.14%	5-10	77.4%	**11.7 ± 1.9**	6.75%	82.3%	270.3 ±21.2
						7	29.0%	12.98 ± 0.23			
	Bt	150-250	12.8	Chl	0.33%	5-11	73.1%	**19.7 ± 1.3**	7.23%	88.3%	306.8 ±11.3
						11	28.6%	18.94 ± 0.24			

* XRD peak intensity ratio: muscovite Qtz[100] / (Ms[004] + Qtz[100]); biotite Chl[004] / (Bt[006] + Chl[004]). These are *qualitative* ratios.
** Recalculated from K-content determined with total ^{39}Ar measured at mass spectrometer and compared to the theoretical total-K content of separates from microprobe analysis. This percentage reflects the purity of each mineral separate, but due to strong errors on this calculation, a ratio of 90% can be considered as "pure" mineral separate.

steps 4 to 10, as representing the "isochemical age" for muscovite. However, biotite analysis in AAn0401-B are much more inhomogeneous, with values between –3 to +14*10^{-2} Ca/K and 0.8 to 14*10^{-4} Cl/K (Fig. 3.10a). This variation in Ca/K and Cl/K ratios might translates different phase releasing Ar on each steps. From microprobe measurements, biotite is richer in Cl than muscovite, but poorer in K, yielding Cl/K of 5*10^{-4} to 8*10^{-3} in biotite (average 3.4*10^{-3}) against 2*10^{-4} to 4*10^{-3} in muscovite (average 1*10^{-3}, but Cl often nearby detection limit). A sluggish positive correlation is observed between Cl and Fe* in biotite, the highest Cl/K being reached by Fe-rich biotite around garnet rim or in garnet fractures (Cl/K ≈ 2.8 to 8.4*10^{-3}) versus <0.2 to 5.6*10^{-3}). Biotite separates should essentially be composed of Cl-poor biotite related to Bt-a or Bt-b (away from garnet, Mg-richer) and Cl/K should remain <5*10^{-3}. However, some amount of fine biotite Bt-b growing near garnet (Fe- and Cl-richer) is not excluded in the finest fraction (e.g. Bt100, see below). In such case, Cl/K of steps related to this biotite degassing in Ar-Ar analysis is susceptible to yield higher values up to 8*10^{-3}. Actually, Cl/K ratios calculated in biotite from AAn0401 are all yielding low values, suggesting that most of the separate was constituted of Cl-poor biotite, most likely Mg-richer, too (Bt-a, ±Bt-b). Steps 3 to 8 have Ca/K <0.06 and are selected as representing the steps where biotite is degassing ("isochemical age"). Step 6 may be discard due to abnormally high Ca/K ratio (Table 3.5), but this has no significant effect on the calculated age.

In contact with the previous metapelite sample (Fig. 3.2a,b), the calc-schist AAn0401-A shows disturbed Ar-spectra, especially for biotite (Fig. 3.9b), which is the most chloritized sample of this study (Table 3.4). Steps 5 and 6 yield apparent older age (16.5±0.4 and 17.6±0.8 Ma) all while having the lowest Ca/K and Cl/K ratios. Steps 4 and 7 to 11 of biotite are grouped in a cluster at higher, but still low Ca/K (and Cl/K) ratios and yield 14.54±0.75 Ma (Figs. 3.9b, 3.10a), which is again very similar to the previous sample. Regarding the muscovite Ar-spectrum, apparent ages are younger in low temperature steps (14.52±0.47 Ma) and end with significantly older ages (15.44±0.50 Ma), but Ca/K and Cl/K remains clustered at low and are not correlated with the age variation. Steps 3 and 4 yield negative values of ^{38}Ar (and ^{37}Ar) and is most likely related to the very low ^{39}Ar signal suggesting a low amount of released gas, which plagues the determination of very low amount of ^{37}Ar or ^{38}Ar. An average on the overall spectrum, excluding first and last steps at low ^{39}Ar content, gives very similar "plateau age"

at 14.95±0.59 Ma compared to other muscovite separates from pelitic sample.

Taken a few meters away from the calc-schist-metapelite interface, Ar-Ar ages in metapelite AAn0405 are discordant, especially that of biotite. As in metapelite AAn0401-B, steps at abnormally high Ca/K or Cl/K value are withdrawn and correspond to firsts or last analysed steps (outside of Fig. 3.10b; Table 3.5). Biotite separates yield the strongest variation among all analysed samples, from 5 to 13 Ma for fraction 50-150 µm (Bt100) and from 13 to 28 Ma for fraction 150-250 µm (Bt200; Fig. 3.9d). In Bt100, Ca/K and Cl/K are highly variable and only three steps (7 to 9) are yielding low values, while analysed steps from Bt200 are forming a cloud of points at low Ca/K value and slightly variable Cl/K (Fig. 3.10b). An average calculated over the entire spectra yields an older age of 19.7±1.3 Ma in Bt200 compared to 11.7±1.9 Ma in Bt100 (Table 3.4). In each separate, one major step at high temperature release a maximum ^{39}Ar and $^{40}Ar^*$ and yields 12.98 ± 0.23 Ma for the finer fraction (Bt100 step 7) and 18.94 ± 0.24 Ma for the coarser one (Bt200 step 11; Table 3.5). These steps are interpreted as the most significant age for each biotite separates.

Isochemical ages from muscovite analyses are within the error to sample AAn0401-B, with 15.24±0.45 and 14.78±0.64 Ma for Ms100 and Ms200, respectively (Fig. 3.9c). In Ms100, an age average on steps yielding low Ca/K and Cl/K gives even better consistency with the previous Ar-analysis in AAn0401-B (steps 5 and 6; 15.17 ± 0.32 Ma). Ca/K of each major Ar-release steps of the coarser muscovite Ms200 is restricted to circa 2 to $3*10^{-2}$. Larger variations occur in Ms100, but still at low value, from 2 to $3*10^{-2}$ Ca/K (Fig. 3.10b). Differences, notably in Ca, cannot be attributed to two different muscovites, as only trace of Ca is allowed. High value of Ca/K for fraction Ms100 is likely related to traces of Ca-rich impurities undetected at XRD (plagioclase or carbonate). Cl/K ratio is also low at 5 to $7*10^{-4}$ and 0.5 to $3*10^{-4}$ Cl/K in Ms200 and Ms100, respectively. Though that near detection limit, Cl/K calculated from microprobe measurement of phengite-rich or –poor muscovite is constant around $1.2*10^{-4}$ to $2.1*10^{-3}$ Cl/K, coherent with the Cl/K ratio determined from argon measurement.

Albeit mineral separates were quite pure (Table 3.4), the Ar extraction line was unfortunately appreciably polluted by atmospheric argon during the analysis of sample AAn0405, especially during analysis of high temperature steps of Bt200, Ms200 and to a less extent Ms100 (Fig. 3.10d,e,f). In the worst case (Ms200 and Bt200), errors are 2 to 4 times higher and radiogenic $^{40}Ar^*$ of the major steps is only 10 to 30% of the total ^{40}Ar, while it is >60% during all other analyses, including Bt100 (Fig. 3.1d,e,f; Table 3.5). However, considering the identical average ages between the results of AAn0401-B Ms (Ar-A series) and the air-polluted result of AAn0405 Ms200 or Ms100 (Ar-C series), we conclude this high atmospheric argon was accurately corrected away and has no significant effect on average ages. Indeed, at least muscovite results are yielding an atmospheric ratio when projected on ordinates of $^{39}Ar/^{40}Ar$ versus $^{36}Ar/^{40}Ar$ diagram (Fig. 3.10e,f). Biotite separates were analysed between both muscovite separates, in the order Ms200, Bt200, Bt100, Ms100 and a low atmospheric content was present during analysis of Bt100 and Ms100, we argue for a significant age difference between Bt100 and Bt200 (Table 3.4). Whether this age is geologically meaningful will be discussed below. Nevertheless, the presence of excess argon is at first glance excluded by considering the cluster of points for older or younger ages in the isochron diagram (Fig. 3.10e,f); both clusters point towards a value approaching the atmospheric ratio.

3.10) Discussion

Care was taken in this study to collect samples from only Mesozoic metasediment. We are thus to concentrate on Alpine metamorphism, without any inheritance of a former event. However, the detail petrography and relation in PT and P-xH_2O pseudosections reveal a disequilibrium feature related to the late K-feldspar growth occurring after the thermal peak of metamorphism. Such reaction affects micas stability, as revealed by a change in muscovite

Table 3.5: Ar-Ar stepwise heating results for biotite and muscovite separates from samples AAn0401-A, AAn0401-B and AAn0405. All errors are 1σ. In bold are steps retained for average age (generally isochemical and plateau age).

	T°C	Age [Ma]	$^{40}Ar_{tot}$ [pl]	$^{40}Ar^*$ [pl]	...[%]	^{39}Ar [pl]	^{39}Ar%	^{38}Ar [pl]	^{37}Ar [pl]	^{36}Ar [pl]
An0401-A - Ms (12.6 [mg], K = 6.09 [%], Cl = 74 [ppm], Ca = 15880 [ppm], J = 9.847e-4)										
1	473	-56.48 ± 4.71	1812.12 ± 5.10	-1346.21	-	43.16 ± 0.99	1.66	17.42 ± 0.33	227.78 ± 5.32	10.75 ± 0.36
2	617	-13.15 ± 4.65	2481.12 ± 7.54	-259.05	-	35.16 ± 0.26	1.35	6.29 ± 0.14	59.74 ± 2.32	9.29 ± 0.31
3	722	14.61 ± 1.39	3131.99 ± 0.48	907.80	28.98	109.98 ± 0.16	4.22	1.33 ± 0.23	16.84 ± 2.77	7.53 ± 0.29
4	785	16.18 ± 1.20	3076.18 ± 3.16	1293.34	42.04	141.38 ± 0.35	5.43	0.02 ± 0.20	-7.95 ± 1.68	6.03 ± 0.33
5	**820**	**14.09 ± 0.48**	**5694.81 ± 0.67**	**2877.27**	**50.52**	**361.48 ± 0.38**	**13.88**	**6.75 ± 0.16**	**14.17 ± 2.64**	**9.54 ± 0.33**
6	**844**	**14.66 ± 0.45**	**4833.22 ± 0.04**	**3003.94**	**62.15**	**362.50 ± 0.56**	**13.92**	**6.15 ± 0.13**	**8.09 ± 1.34**	**6.19 ± 0.31**
7	**880**	**14.89 ± 0.49**	**4596.79 ± 4.02**	**2786.91**	**60.63**	**331.22 ± 0.39**	**12.72**	**5.89 ± 0.18**	**6.09 ± 1.59**	**6.13 ± 0.31**
8	**915**	**14.43 ± 0.52**	**3921.81 ± 0.59**	**2431.29**	**61.99**	**298.07 ± 0.43**	**11.45**	**3.80 ± 0.11**	**-2.06 ± 1.00**	**5.04 ± 0.30**
9	**1005**	**15.32 ± 0.40**	**4686.14 ± 18.40**	**3246.24**	**69.27**	**374.77 ± 1.01**	**14.39**	**5.57 ± 0.09**	**13.32 ± 2.13**	**4.88 ± 0.29**
10	**1189**	**15.52 ± 0.33**	**5932.99 ± 2.89**	**4023.20**	**67.81**	**458.56 ± 0.42**	**17.61**	**7.62 ± 0.13**	**6.37 ± 3.42**	**6.46 ± 0.29**
11	1362	13.71 ± 1.83	2213.51 ± 0.78	679.27	30.69	87.67 ± 0.31	3.37	1.77 ± 0.16	14.84 ± 4.60	5.20 ± 0.31
An0401-B - Ms (21.1 [mg], K = 9.15 [%], Cl = 41 [ppm], Ca = 7988 [ppm], J = 9.894e-4)										
1	474	-26.96 ± 4.84	1758.73 ± 18.62	-514.54	-	34.38 ± 0.16	0.52	7.48 ± 0.19	98.98 ± 5.45	7.72 ± 0.31
2	617	0.57 ± 3.69	4559.25 ± 27.07	14.61	0.32	45.96 ± 0.06	0.70	5.70 ± 0.17	49.39 ± 3.80	15.39 ± 0.32
3	723	13.61 ± 0.44	8619.61 ± 7.34	2892.24	33.55	378.03 ± 0.82	5.74	9.09 ± 0.23	18.41 ± 3.51	19.39 ± 0.31
4	**793**	**15.06 ± 0.27**	**10498.47 ± 33.56**	**5485.68**	**52.25**	**647.67 ± 0.74**	**9.84**	**11.88 ± 0.13**	**15.41 ± 3.88**	**16.97 ± 0.33**
5	**821**	**15.18 ± 0.20**	**10894.59 ± 31.78**	**7387.46**	**67.81**	**864.93 ± 2.13**	**13.14**	**11.70 ± 0.30**	**27.30 ± 4.11**	**11.88 ± 0.32**
6	**848**	**15.09 ± 0.17**	**11316.73 ± 2.68**	**8156.00**	**72.07**	**960.67 ± 0.89**	**14.59**	**15.84 ± 0.15**	**13.20 ± 2.45**	**10.70 ± 0.31**
7	**885**	**15.07 ± 0.18**	**10684.01 ± 13.66**	**8012.08**	**74.99**	**945.18 ± 1.58**	**14.35**	**13.67 ± 0.16**	**11.94 ± 3.80**	**9.05 ± 0.31**
8	**921**	**14.90 ± 0.17**	**10164.62 ± 4.06**	**7389.85**	**72.70**	**881.58 ± 0.81**	**13.39**	**13.33 ± 0.14**	**10.82 ± 2.86**	**9.39 ± 0.29**
9	**1003**	**15.24 ± 0.16**	**10849.01 ± 0.14**	**8080.62**	**74.48**	**942.24 ± 1.00**	**14.31**	**12.88 ± 0.13**	**26.19 ± 2.44**	**9.38 ± 0.29**
10	**1198**	**15.33 ± 0.24**	**9642.87 ± 2.32**	**6398.63**	**66.36**	**741.96 ± 1.04**	**11.27**	**11.97 ± 0.19**	**-2.95 ± 4.35**	**10.98 ± 0.34**
11	1371	12.11 ± 1.30	4675.64 ± 0.79	965.51	20.65	141.80 ± 0.28	2.15	5.57 ± 0.10	33.67 ± 2.59	12.56 ± 0.35
An0401-A - Bt (13.3 [mg], K = 6.32 [%], Cl = 201 [ppm], Ca = 17962 [ppm], J = 9.823e-4)										
1	471	-75.35 ± 3.77	1113.00 ± 2.59	-1771.64	-	42.72 ± 0.50	1.50	20.59 ± 0.19	262.52 ± 3.19	9.83 ± 0.29
2	583	-34.32 ± 9.19	2283.63 ± 1.91	-330.50	-	17.25 ± 0.42	0.61	6.15 ± 0.13	34.59 ± 1.62	8.86 ± 0.30
3	663	5.20 ± 2.91	1902.39 ± 0.71	152.43	8.01	51.87 ± 0.11	1.82	3.97 ± 0.17	17.65 ± 1.14	5.93 ± 0.29
4	**718**	**14.33 ± 0.32**	**6060.26 ± 2.22**	**3890.79**	**64.20**	**479.41 ± 0.49**	**16.85**	**14.85 ± 0.07**	**20.33 ± 1.62**	**7.35 ± 0.30**
5	760	16.45 ± 0.41	4208.87 ± 1.47	3318.25	78.84	355.83 ± 0.31	12.50	6.02 ± 0.11	3.12 ± 2.71	3.01 ± 0.28
6	824	17.55 ± 0.78	2519.79 ± 3.16	1929.37	76.57	193.85 ± 0.43	6.81	3.71 ± 0.08	-1.27 ± 4.77	2.00 ± 0.29
7	**882**	**15.24 ± 0.97**	**2135.43 ± 1.20**	**1366.37**	**63.99**	**158.17 ± 0.14**	**5.56**	**3.26 ± 0.25**	**5.75 ± 1.19**	**2.60 ± 0.30**
8	**938**	**13.90 ± 0.96**	**2170.59 ± 0.87**	**1308.80**	**60.30**	**166.31 ± 0.52**	**5.84**	**5.22 ± 0.16**	**52.23 ± 3.10**	**2.93 ± 0.31**
9	**1005**	**13.74 ± 0.32**	**4789.38 ± 5.07**	**3606.93**	**75.31**	**463.39 ± 0.46**	**16.28**	**10.76 ± 0.11**	**6.72 ± 1.98**	**4.00 ± 0.29**
10	**1080**	**14.85 ± 0.28**	**5814.05 ± 1.84**	**4717.19**	**81.13**	**560.66 ± 0.79**	**19.70**	**10.40 ± 0.15**	**2.12 ± 1.62**	**3.71 ± 0.31**
11	**1200**	**15.82 ± 0.47**	**3893.50 ± 1.57**	**2914.28**	**74.85**	**324.97 ± 0.91**	**11.42**	**7.86 ± 0.07**	**12.57 ± 3.02**	**3.32 ± 0.29**
12	1368	20.41 ± 4.72	1676.32 ± 3.04	365.39	21.80	31.55 ± 0.08	1.11	2.34 ± 0.13	9.16 ± 3.48	4.44 ± 0.29
An0401-B - Bt (14.7 [mg], K > 6.36 [%], Cl > 123 [ppm], Ca > 11090 [ppm], J = 9.866e-4)										
1	477	-96.84 ± 5.67	1548.95 ± 4.16	-1933.29	-	36.65 ± 1.35	1.16	18.17 ± 0.24	224.05 ± 9.13	11.84 ± 0.28
2	585	11.21 ± 6.39	2704.62 ± 1.06	172.61	6.38	27.33 ± 0.07	0.87	3.31 ± 0.20	-2.48 ± 2.55	8.57 ± 0.33
3	**671**	**15.56 ± 0.34**	**8546.92 ± 16.57**	**4350.08**	**50.90**	**495.53 ± 0.89**	**15.75**	**11.14 ± 0.15**	**-7.84 ± 2.23**	**14.20 ± 0.32**
4	**720**	**14.84 ± 0.28**	**7271.55 ± 9.32**	**4949.57**	**68.07**	**591.35 ± 0.62**	**18.79**	**13.02 ± 0.09**	**17.59 ± 2.04**	**7.86 ± 0.32**
5	**764**	**14.77 ± 0.28**	**5967.05 ± 0.38**	**4356.57**	**73.01**	**522.70 ± 0.50**	**16.61**	**10.14 ± 0.10**	**5.28 ± 1.63**	**5.45 ± 0.28**
6	**827**	**15.94 ± 0.78**	**3121.88 ± 0.62**	**1858.75**	**59.54**	**206.58 ± 0.20**	**6.56**	**3.58 ± 0.08**	**14.67 ± 2.18**	**4.28 ± 0.31**
9	**1004**	**14.24 ± 0.35**	**5821.90 ± 6.14**	**3769.45**	**64.75**	**469.41 ± 0.72**	**14.92**	**7.06 ± 0.08**	**1.77 ± 2.57**	**6.95 ± 0.31**
10	**1087**	**14.93 ± 0.31**	**6843.13 ± 18.44**	**4490.61**	**65.62**	**533.20 ± 1.48**	**16.94**	**10.06 ± 0.23**	**1.20 ± 3.70**	**7.96 ± 0.31**
11	1199	15.57 ± 0.64	4836.01 ± 15.00	2127.41	43.99	242.23 ± 0.46	7.70	7.30 ± 0.18	20.18 ± 3.79	9.17 ± 0.30
12	1370	61.71 ± 6.57	2981.69 ± 6.36	782.56	26.25	22.20 ± 0.34	0.71	3.04 ± 0.14	14.64 ± 2.29	7.45 ± 0.28

Table 3.5 (continued)

	Ca/K	Cl/K	39/40	36/40	STP File
An0401-A - Ms					
1	1.06 E+01 ± 2.47 E-01	6.16 E-02 ± 1.37 E-03	2.37 E-02 ± 5.51 E-04	5.90 E-03 ± 1.98 E-04	R15805
2	3.40 E+00 ± 1.32 E-01	2.10 E-02 ± 7.84 E-04	1.42 E-02 ± 1.12 E-04	3.74 E-03 ± 1.24 E-04	R15806
3	3.06 E-01 ± 5.03 E-02	-2.21 E-03 ± 3.84 E-04	3.51 E-02 ± 5.18 E-05	2.40 E-03 ± 9.33 E-05	R15807
4	-1.12 E-01 ± 2.37 E-02	-3.49 E-03 ± 2.69 E-04	4.60 E-02 ± 1.24 E-04	1.96 E-03 ± 1.06 E-04	R15808
5	**7.84 E-02 ± 1.46 E-02**	**3.53 E-04 ± 8.60 E-05**	**6.35 E-02 ± 6.79 E-05**	**1.67 E-03 ± 5.80 E-05**	**R15809**
6	**4.46 E-02 ± 7.42 E-03**	**3.60 E-04 ± 7.27 E-05**	**7.50 E-02 ± 1.16 E-04**	**1.28 E-03 ± 6.41 E-05**	**R15810**
7	**3.68 E-02 ± 9.60 E-03**	**4.56 E-04 ± 1.00 E-04**	**7.21 E-02 ± 1.06 E-04**	**1.33 E-03 ± 6.77 E-05**	**R15811**
8	**-1.38 E-02 ± 6.68 E-03**	**-3.87 E-04 ± 7.62 E-05**	**7.60 E-02 ± 1.10 E-04**	**1.29 E-03 ± 7.63 E-05**	**R15812**
9	**7.11 E-02 ± 1.14 E-02**	**1.21 E-04 ± 4.96 E-05**	**8.00 E-02 ± 3.81 E-04**	**1.04 E-03 ± 6.11 E-05**	**R15813**
10	**2.78 E-02 ± 1.49 E-02**	**3.97 E-04 ± 5.66 E-05**	**7.73 E-02 ± 7.94 E-05**	**1.09 E-03 ± 4.92 E-05**	**R15814**
11	3.39 E-01 ± 1.05 E-01	-4.61 E-04 ± 3.50 E-04	3.96 E-02 ± 1.42 E-04	2.35 E-03 ± 1.39 E-04	R15815
An0401-B - Ms					
1	5.77 E+00 ± 3.18 E-01	2.93 E-02 ± 1.03 E-03	1.95 E-02 ± 2.26 E-04	4.37 E-03 ± 1.82 E-04	R15829
2	2.15 E+00 ± 1.66 E-01	8.86 E-03 ± 6.90 E-04	1.01 E-02 ± 6.13 E-05	3.37 E-03 ± 7.23 E-05	R15830
3	9.74 E-02 ± 1.86 E-02	4.80 E-04 ± 1.14 E-04	4.39 E-02 ± 1.02 E-04	2.25 E-03 ± 3.57 E-05	R15831
4	**4.76 E-02 ± 1.20 E-02**	**3.01 E-04 ± 4.06 E-05**	**6.17 E-02 ± 2.09 E-04**	**1.62 E-03 ± 3.09 E-05**	**R15832**
5	**6.31 E-02 ± 9.50 E-03**	**-1.42 E-04 ± 6.40 E-05**	**7.94 E-02 ± 3.03 E-04**	**1.09 E-03 ± 2.89 E-05**	**R15833**
6	**2.75 E-02 ± 5.10 E-03**	**4.71 E-04 ± 3.10 E-05**	**8.49 E-02 ± 8.09 E-05**	**9.45 E-04 ± 2.70 E-05**	**R15834**
7	**2.53 E-02 ± 8.04 E-03**	**1.63 E-04 ± 3.35 E-05**	**8.85 E-02 ± 1.86 E-04**	**8.46 E-04 ± 2.90 E-05**	**R15835**
8	**2.46 E-02 ± 6.50 E-03**	**2.42 E-04 ± 3.20 E-05**	**8.67 E-02 ± 8.70 E-05**	**9.24 E-04 ± 2.82 E-05**	**R15836**
9	**5.56 E-02 ± 5.18 E-03**	**9.25 E-06 ± 2.92 E-05**	**8.68 E-02 ± 9.20 E-05**	**8.64 E-04 ± 2.69 E-05**	**R15837**
10	**-7.95 E-03 ± 1.17 E-02**	**2.85 E-04 ± 4.86 E-05**	**7.69 E-02 ± 1.10 E-04**	**1.14 E-03 ± 3.52 E-05**	**R15838**
11	4.75 E-01 ± 3.65 E-02	1.96 E-03 ± 1.55 E-04	3.03 E-02 ± 5.94 E-05	2.69 E-03 ± 7.49 E-05	R15839
An0401-A - Bt					
1	1.23 E+01 ± 1.50 E-01	7.63 E-02 ± 8.37 E-04	3.82 E-02 ± 4.55 E-04	8.77 E-03 ± 2.55 E-04	R15791
2	4.01 E+00 ± 1.88 E-01	4.43 E-02 ± 1.47 E-03	7.55 E-03 ± 1.82 E-04	3.87 E-03 ± 1.29 E-04	R15792
3	6.81 E-01 ± 4.39 E-02	7.74 E-03 ± 5.97 E-04	2.73 E-02 ± 5.63 E-05	3.11 E-03 ± 1.52 E-04	R15794
4	**8.48 E-02 ± 6.77 E-03**	**2.91 E-03 ± 3.59 E-05**	**7.91 E-02 ± 8.63 E-05**	**1.21 E-03 ± 4.88 E-05**	**R15795**
5	1.75 E-02 ± 1.52 E-02	6.36 E-04 ± 6.32 E-05	8.45 E-02 ± 8.04 E-05	7.16 E-04 ± 6.71 E-05	R15796
6	-1.31 E-02 ± 4.92 E-02	9.65 E-04 ± 9.17 E-05	7.69 E-02 ± 1.96 E-04	7.93 E-04 ± 1.16 E-04	R15797
7	**7.27 E-02 ± 1.50 E-02**	**1.03 E-03 ± 2.89 E-04**	**7.41 E-02 ± 7.81 E-05**	**1.22 E-03 ± 1.39 E-04**	**R15798**
8	**6.28 E-01 ± 3.73 E-02**	**2.91 E-03 ± 1.86 E-04**	**7.66 E-02 ± 2.41 E-04**	**1.34 E-03 ± 1.41 E-04**	**R15799**
9	**2.90 E-02 ± 8.56 E-03**	**1.75 E-03 ± 4.71 E-05**	**9.68 E-02 ± 1.40 E-04**	**8.35 E-04 ± 5.94 E-05**	**R15800**
10	**7.56 E-03 ± 5.78 E-03**	**9.87 E-04 ± 5.30 E-05**	**9.64 E-02 ± 1.39 E-04**	**6.38 E-04 ± 5.25 E-05**	**R15801**
11	**7.74 E-02 ± 1.86 E-02**	**1.87 E-03 ± 5.15 E-05**	**8.35 E-02 ± 2.36 E-04**	**8.51 E-04 ± 7.48 E-05**	**R15802**
12	5.81 E-01 ± 2.21 E-01	6.44 E-03 ± 8.04 E-04	1.88 E-02 ± 5.93 E-05	2.65 E-03 ± 1.71 E-04	R15803
An0401-B - Bt					
1	1.23 E+01 ± 5.00 E-01	7.56 E-02 ± 1.22 E-03	2.36 E-02 ± 8.72 E-04	7.61 E-03 ± 1.82 E-04	R15817
2	-1.81 E-01 ± 1.86 E-01	9.01 E-03 ± 1.38 E-03	1.01 E-02 ± 2.63 E-05	3.17 E-03 ± 1.23 E-04	R15818
3	**-3.17 E-02 ± 8.99 E-03**	**9.54 E-04 ± 6.03 E-05**	**5.80 E-02 ± 1.53 E-04**	**1.66 E-03 ± 3.74 E-05**	**R15819**
4	**5.95 E-02 ± 6.89 E-03**	**1.38 E-03 ± 3.47 E-05**	**8.13 E-02 ± 1.35 E-04**	**1.08 E-03 ± 4.39 E-05**	**R15820**
5	**2.02 E-02 ± 6.24 E-03**	**1.01 E-03 ± 3.98 E-05**	**8.76 E-02 ± 8.43 E-05**	**9.13 E-04 ± 4.70 E-05**	**R15821**
6	**1.42 E-01 ± 2.11 E-02**	**3.06 E-04 ± 8.70 E-05**	**6.62 E-02 ± 6.45 E-05**	**1.37 E-03 ± 9.84 E-05**	**R15822**
9	**7.52 E-03 ± 1.09 E-02**	**8.92 E-05 ± 3.84 E-05**	**8.06 E-02 ± 1.50 E-04**	**1.19 E-03 ± 5.35 E-05**	**R15825**
10	**4.51 E-03 ± 1.39 E-02**	**7.68 E-04 ± 7.85 E-05**	**7.79 E-02 ± 3.02 E-04**	**1.16 E-03 ± 4.56 E-05**	**R15826**
11	1.67 E-01 ± 3.13 E-02	2.01 E-03 ± 1.40 E-04	5.01 E-02 ± 1.82 E-04	1.90 E-03 ± 6.11 E-05	R15827
12	1.32 E+00 ± 2.07 E-01	1.12 E-02 ± 1.18 E-03	7.44 E-03 ± 1.14 E-04	2.50 E-03 ± 9.50 E-05	R15828

Table 3.5 (continued) For separates strongly polluted by atmospheric argon (Bt200, Ms200 and Ms100 of AAn0405), one or more steps with maximum ^{39}Ar signal are highlighted with a grey box (maximum Ar-release from biotite or muscovite, minimum air-pollution).

	T°C	Age [Ma]	$^{40}Ar_{tot}$ [pl]	$^{40}Ar^*$ [pl] ...[%]	^{39}Ar [pl]	^{39}Ar%	^{38}Ar [pl]	^{37}Ar [pl]	^{36}Ar [pl]
An0405 - Ms100 (20.5 [mg], K = 8.28 [%], Cl = 260 [ppm], Ca = 8289 [ppm], J = 1.949e-3)									
1	562	14.30 ± 8.12	269.24 ± 0.57	64.54	23.97	15.84 ± 0.12	0.26	67.49 ± 0.58	43.65 ± 0.40	0.70 ± 0.13
2	713	13.32 ± 0.39	1401.09 ± 0.23	787.56	56.21	207.11 ± 0.21	3.41	30.77 ± 0.06	14.97 ± 0.09	2.08 ± 0.08
3	813	10.11 ± 0.53	2941.17 ± 0.25	579.69	19.71	201.06 ± 0.29	3.31	3.94 ± 0.03	11.16 ± 0.06	7.99 ± 0.10
4	888	12.60 ± 0.33	7494.02 ± 65.56	1603.85	21.40	446.04 ± 3.16	7.34	2.51 ± 0.01	10.46 ± 0.23	19.94 ± 0.13
5	**944**	**14.96 ± 0.21**	**30760.15 ± 6.18**	**6687.82**	**21.74**	**1565.38 ± 1.39**	**25.77**	**34.91 ± 0.07**	**12.41 ± 0.43**	**81.47 ± 0.31**
6	**985**	**15.49 ± 0.26**	**25839.34 ± 0.97**	**4662.43**	**18.04**	**1053.99 ± 1.04**	**17.35**	**26.18 ± 0.06**	**11.76 ± 0.05**	**71.67 ± 0.26**
7	**1013**	**16.54 ± 0.65**	**19772.22 ± 0.33**	**2052.99**	**10.38**	**434.38 ± 0.38**	**7.15**	**16.66 ± 0.04**	**14.46 ± 0.16**	**59.97 ± 0.27**
8	**1034**	**15.11 ± 0.71**	**14215.84 ± 7.90**	**1166.15**	**8.20**	**270.29 ± 0.34**	**4.45**	**11.86 ± 0.02**	**16.33 ± 0.09**	**44.17 ± 0.19**
9	**1071**	**16.31 ± 0.79**	**11674.99 ± 0.11**	**1163.40**	**9.96**	**249.63 ± 0.24**	**4.11**	**9.78 ± 0.03**	**12.23 ± 0.04**	**35.58 ± 0.19**
10	**1128**	**16.19 ± 0.48**	**14895.28 ± 4.85**	**2266.48**	**15.22**	**490.04 ± 0.43**	**8.07**	**14.56 ± 0.03**	**25.71 ± 0.17**	**42.74 ± 0.23**
11	**1184**	**14.69 ± 0.28**	**16135.33 ± 6.68**	**2743.58**	**17.00**	**654.22 ± 0.57**	**10.77**	**16.49 ± 0.03**	**18.23 ± 0.09**	**45.32 ± 0.18**
12	**1288**	**15.43 ± 0.44**	**13956.34 ± 0.05**	**1947.36**	**13.95**	**441.99 ± 0.39**	**7.28**	**13.23 ± 0.03**	**15.27 ± 0.06**	**40.64 ± 0.19**
13	1385	-15.37 ± 7.51	17653.69 ± 3.68	-141.29	-	32.47 ± 0.15	0.53	15.53 ± 0.03	34.26 ± 0.19	60.23 ± 0.23
14	1503	-21.13 ± 18.61	9639.01 ± 2.48	-71.05	-	11.94 ± 0.20	0.20	16.71 ± 0.05	79.23 ± 1.42	32.88 ± 0.21
An0405 - Ms200 (16.5 [mg], K = 8.36 [%], Cl = 339 [ppm], Ca = 6221 [ppm], J = 1.953e-3)									
1	528	-158.68 ± 26.60	2574.86 ± 1.33	-319.49	-	7.42 ± 0.34	0.15	38.88 ± 0.47	15.91 ± 0.91	9.80 ± 0.17
2	613	-125.51 ± 19.42	626.63 ± 0.07	-248.82	-	7.24 ± 0.16	0.15	34.94 ± 0.22	12.86 ± 1.13	2.97 ± 0.12
3	718	5.52 ± 2.27	914.14 ± 0.27	113.94	12.46	72.60 ± 0.36	1.46	16.44 ± 0.10	27.26 ± 1.36	2.71 ± 0.16
4	774	12.49 ± 0.86	1354.18 ± 0.64	580.70	42.88	163.15 ± 0.24	3.29	3.61 ± 0.11	7.92 ± 1.43	2.62 ± 0.14
5	804	-5.25 ± 3.82	3961.99 ± 0.33	-60.49	-	40.65 ± 0.16	0.82	3.49 ± 0.13	7.28 ± 1.09	13.61 ± 0.15
6	838	-15.04 ± 6.61	10579.73 ± 0.30	-157.58	-	37.06 ± 0.18	0.75	7.80 ± 0.12	2.68 ± 1.74	36.34 ± 0.23
7	869	12.04 ± 5.07	16978.61 ± 0.07	161.56	0.95	47.12 ± 0.18	0.95	13.85 ± 0.08	2.76 ± 1.66	56.91 ± 0.23
8	890	12.53 ± 3.59	14742.57 ± 1.14	214.87	1.46	60.22 ± 0.14	1.21	11.70 ± 0.15	6.41 ± 1.98	49.16 ± 0.21
9	920	11.51 ± 1.41	14071.11 ± 0.53	513.97	3.65	156.86 ± 0.91	3.16	12.20 ± 0.06	6.21 ± 1.49	45.88 ± 0.21
10	**956**	**14.93 ± 0.45**	**14619.43 ± 1.19**	**2082.24**	**14.24**	**489.12 ± 0.65**	**9.85**	**15.44 ± 0.14**	**5.94 ± 0.50**	**42.43 ± 0.21**
11	**1016**	**14.30 ± 0.27**	**15152.41 ± 0.27**	**4090.55**	**27.00**	**1003.55 ± 0.96**	**20.21**	**22.11 ± 0.09**	**14.03 ± 0.93**	**37.44 ± 0.26**
12	**1078**	**15.09 ± 0.18**	**14818.34 ± 0.65**	**4195.01**	**28.31**	**975.19 ± 0.93**	**19.64**	**20.93 ± 0.10**	**13.31 ± 1.03**	**35.95 ± 0.17**
13	**1170**	**14.25 ± 0.30**	**19490.00 ± 0.96**	**3281.91**	**16.84**	**807.84 ± 0.71**	**16.27**	**22.21 ± 0.15**	**13.70 ± 0.42**	**54.85 ± 0.24**
14	**1260**	**15.97 ± 0.45**	**20709.30 ± 4.67**	**2763.69**	**13.35**	**606.99 ± 0.74**	**12.23**	**20.41 ± 0.15**	**10.75 ± 1.19**	**60.73 ± 0.27**
15	**1335**	**13.52 ± 0.58**	**16753.15 ± 0.05**	**1477.84**	**8.82**	**383.50 ± 1.09**	**7.72**	**17.81 ± 0.23**	**12.93 ± 1.62**	**51.70 ± 0.21**
16	1418	8.41 ± 2.59	14680.57 ± 4.73	209.88	1.43	87.72 ± 0.41	1.77	10.87 ± 0.06	9.74 ± 0.97	48.97 ± 0.22
17	1497	60.84 ± 16.61	20422.83 ± 1.12	331.66	1.62	18.90 ± 0.49	0.38	14.59 ± 0.15	24.78 ± 1.56	68.00 ± 0.31
An0405 - Bt100 (7.1 [mg], K = 6.75 [%], Cl = 138 [ppm], Ca = 14846 [ppm], J = 1.942e-3)									
1	540	-231.47 ± 21.62	158.17 ± 1.05	-311.26	-	5.03 ± 0.09	0.30	0.58 ± 0.08	23.27 ± 0.41	1.59 ± 0.09
2	778	5.44 ± 1.58	3458.81 ± 1.05	160.48	4.64	103.18 ± 0.11	6.18	5.37 ± 0.01	10.28 ± 0.10	11.16 ± 0.16
3	846	11.28 ± 1.49	752.97 ± 0.25	372.17	49.43	115.22 ± 0.15	6.90	3.27 ± 0.01	10.93 ± 0.06	1.29 ± 0.17
4	891	3.89 ± 0.92	528.66 ± 0.44	107.25	20.29	96.45 ± 0.21	5.78	2.72 ± 0.01	12.84 ± 0.13	1.43 ± 0.09
5	**935**	**11.05 ± 0.92**	**579.42 ± 0.14**	**360.19**	**62.16**	**113.84 ± 0.11**	**6.82**	**5.06 ± 0.03**	**24.21 ± 0.14**	**0.75 ± 0.10**
6	**1029**	**10.70 ± 0.80**	**1087.71 ± 0.86**	**618.01**	**56.82**	**201.75 ± 0.18**	**12.09**	**5.56 ± 0.01**	**23.05 ± 0.16**	**1.60 ± 0.16**
7	**1076**	**12.98 ± 0.23**	**2515.85 ± 0.03**	**1802.89**	**71.66**	**484.76 ± 0.43**	**29.04**	**5.43 ± 0.03**	**8.70 ± 0.07**	**2.41 ± 0.11**
8	**1100**	**9.07 ± 0.42**	**1831.53 ± 0.23**	**540.90**	**29.53**	**208.34 ± 0.19**	**12.48**	**3.89 ± 0.06**	**10.61 ± 0.03**	**4.37 ± 0.08**
9	**1150**	**9.98 ± 0.49**	**1568.87 ± 0.49**	**809.11**	**51.57**	**283.16 ± 0.25**	**16.96**	**4.47 ± 0.05**	**13.57 ± 0.09**	**2.57 ± 0.13**
10	**1212**	**9.62 ± 2.29**	**624.81 ± 0.15**	**128.69**	**20.60**	**46.72 ± 0.08**	**2.80**	**2.64 ± 0.01**	**15.57 ± 0.29**	**1.68 ± 0.10**
11	1280	-6.62 ± 10.22	937.34 ± 0.32	-15.65	-1.67	8.30 ± 0.29	0.50	2.92 ± 0.02	17.57 ± 0.62	3.23 ± 0.08
12	1406	365.35 ± 40.52	1524.98 ± 0.22	271.11	17.78	2.36 ± 0.18	0.14	3.71 ± 0.03	22.53 ± 1.73	4.25 ± 0.09
An0405 - Bt200 (12.8 [mg], K = 7.20 [%], Cl = 517 [ppm], Ca = 6482 [ppm], J = 1.946e-3)									
1	527	-592.81 ± 71.97	330.02 ± 0.85	-521.76	-	3.70 ± 0.07	0.11	68.90 ± 0.16	106.99 ± 4.20	2.91 ± 0.18
2	655	-81.55 ± 19.74	845.60 ± 0.21	-202.94	-	8.94 ± 0.36	0.39	42.05 ± 0.34	6.80 ± 1.59	3.55 ± 0.16
3	733	13.17 ± 1.99	1440.59 ± 0.20	336.89	1.66	89.43 ± 0.11	3.15	2.12 ± 0.16	7.88 ± 1.00	3.74 ± 0.17
4	838	14.67 ± 0.33	9841.64 ± 11.74	1665.83	8.22	396.83 ± 0.79	15.42	13.46 ± 0.11	2.08 ± 1.33	27.67 ± 0.13
5	**869**	**20.56 ± 1.05**	**18717.00 ± 0.18**	**1848.06**	**9.12**	**313.64 ± 0.55**	**25.11**	**15.28 ± 0.12**	**1.35 ± 1.24**	**57.09 ± 0.32**
6	**882**	**23.16 ± 1.42**	**12972.67 ± 4.25**	**858.74**	**4.24**	**129.30 ± 0.16**	**29.10**	**10.81 ± 0.02**	**1.87 ± 2.09**	**41.00 ± 0.18**
7	**934**	**23.86 ± 1.37**	**19943.71 ± 0.37**	**1361.01**	**6.71**	**198.90 ± 0.21**	**35.25**	**15.07 ± 0.13**	**-0.41 ± 0.95**	**62.89 ± 0.27**
8	**978**	**21.84 ± 1.14**	**16036.55 ± 2.15**	**1348.24**	**6.65**	**215.37 ± 0.25**	**41.91**	**12.81 ± 0.15**	**1.36 ± 1.27**	**49.71 ± 0.24**
9	**1032**	**19.55 ± 0.84**	**10924.06 ± 1.08**	**1246.00**	**6.15**	**222.53 ± 0.28**	**48.78**	**10.61 ± 0.16**	**7.05 ± 1.57**	**32.75 ± 0.18**
10	**1093**	**21.44 ± 0.50**	**13180.78 ± 0.78**	**2221.54**	**10.96**	**361.55 ± 0.32**	**59.96**	**12.62 ± 0.11**	**3.36 ± 1.18**	**37.09 ± 0.18**
11	**1189**	**18.94 ± 0.24**	**20677.28 ± 3.32**	**5015.22**	**24.74**	**924.59 ± 0.81**	**88.53**	**27.07 ± 0.39**	**6.39 ± 0.84**	**53.00 ± 0.21**
12	1260	28.72 ± 0.73	18189.70 ± 0.27	2355.67	11.62	285.62 ± 0.32	97.35	15.88 ± 0.23	-1.20 ± 0.93	53.58 ± 0.20
13	1346	69.30 ± 3.41	17882.08 ± 2.02	1322.86	6.53	65.72 ± 0.08	99.38	11.45 ± 0.19	2.73 ± 0.97	56.04 ± 0.22
14	1464	113.50 ± 15.90	15747.47 ± 0.94	481.90	2.38	14.44 ± 0.12	99.83	10.43 ± 0.26	2.73 ± 0.06	51.66 ± 0.24
15	1557	129.69 ± 31.49	11965.35 ± 1.08	210.74	1.04	5.50 ± 0.04	100.00	6.57 ± 0.05	3.83 ± 1.53	39.78 ± 0.18

Table 3.5 (continued)

	Ca/K	Cl/K	39/40	36/40	STP File
An0405 - Ms100					
1	5.52 E+00 ± 5.00 E-02	7.55 E-01 ± 6.50 E-03	5.87 E-02 ± 4.59 E-04	2.57 E-03 ± 4.63 E-04	R16528
2	1.45 E-01 ± 8.50 E-04	2.40 E-02 ± 5.73 E-05	1.48 E-01 ± 1.52 E-04	1.48 E-03 ± 5.59 E-05	R16529
3	1.11 E-01 ± 5.89 E-04	7.62 E-05 ± 3.56 E-05	6.84 E-02 ± 9.97 E-05	2.72 E-03 ± 3.41 E-05	R16530
4	4.69 E-02 ± 1.02 E-03	-2.58 E-03 ± 1.49 E-05	5.95 E-02 ± 6.70 E-04	2.66 E-03 ± 2.74 E-05	R16531
5	**1.59 E-02 ± 5.49 E-04**	**1.44 E-04 ± 1.47 E-05**	**5.09 E-02 ± 4.65 E-05**	**2.65 E-03 ± 4.30 E-06**	**R16532**
6	**2.23 E-02 ± 9.48 E-05**	**6.49 E-05 ± 1.73 E-05**	**4.08 E-02 ± 4.01 E-05**	**2.77 E-03 ± 3.18 E-06**	**R16533**
7	**6.66 E-02 ± 7.48 E-04**	**1.41 E-04 ± 2.80 E-05**	**2.20 E-02 ± 1.94 E-05**	**3.03 E-03 ± 8.93 E-06**	**R16534**
8	**1.21 E-01 ± 6.33 E-04**	**2.82 E-04 ± 2.88 E-05**	**1.90 E-02 ± 2.58 E-05**	**3.11 E-03 ± 7.61 E-06**	**R16535**
9	**9.80 E-02 ± 2.91 E-04**	**1.37 E-04 ± 3.34 E-05**	**2.14 E-02 ± 2.04 E-05**	**3.05 E-03 ± 1.24 E-05**	**R16536**
10	**1.05 E-01 ± 6.92 E-04**	**2.93 E-04 ± 2.12 E-05**	**3.29 E-02 ± 3.08 E-05**	**2.87 E-03 ± 1.16 E-05**	**R16537**
11	**5.57 E-02 ± 2.65 E-04**	**8.88 E-05 ± 1.62 E-05**	**4.05 E-02 ± 3.94 E-05**	**2.81 E-03 ± 5.27 E-06**	**R16538**
12	**6.91 E-02 ± 2.66 E-04**	**1.74 E-04 ± 2.17 E-05**	**3.17 E-02 ± 2.81 E-05**	**2.91 E-03 ± 8.88 E-06**	**R16539**
13	2.11 E+00 ± 1.20 E-02	2.14 E-02 ± 2.97 E-04	1.84 E-03 ± 8.72 E-06	3.41 E-03 ± 5.52 E-06	R16540
14	1.33 E+01 ± 2.39 E-01	1.56 E-01 ± 9.99 E-04	1.23 E-03 ± 2.11 E-05	3.41 E-03 ± 1.83 E-05	R16541
An0405 - Ms200					
1	4.30 E+00 ± 2.46 E-01	8.87 E-01 ± 1.12 E-02	2.88 E-03 ± 1.30 E-04	3.80 E-03 ± 6.32 E-05	R16444
2	3.56 E+00 ± 3.12 E-01	8.44 E-01 ± 5.50 E-03	1.15 E-02 ± 2.55 E-04	4.73 E-03 ± 1.98 E-04	R16445
3	7.51 E-01 ± 3.74 E-02	3.70 E-02 ± 2.44 E-04	7.94 E-02 ± 3.95 E-04	2.96 E-03 ± 1.73 E-04	R16446
4	9.71 E-02 ± 1.75 E-02	1.32 E-03 ± 1.22 E-04	1.20 E-01 ± 1.89 E-04	1.93 E-03 ± 9.97 E-05	R16447
5	3.58 E-01 ± 5.38 E-02	2.04 E-03 ± 5.72 E-04	1.03 E-02 ± 3.95 E-05	3.44 E-03 ± 3.56 E-05	R16448
6	1.45 E-01 ± 9.37 E-02	2.75 E-03 ± 6.13 E-04	3.50 E-03 ± 1.66 E-05	3.43 E-03 ± 1.85 E-05	R16449
7	1.17 E-01 ± 7.04 E-02	1.00 E-02 ± 3.55 E-04	2.78 E-03 ± 1.05 E-05	3.35 E-03 ± 6.84 E-06	R16450
8	2.13 E-01 ± 6.59 E-02	5.34 E-03 ± 4.72 E-04	4.08 E-03 ± 9.44 E-06	3.33 E-03 ± 7.99 E-06	R16451
9	7.92 E-02 ± 1.90 E-02	2.02 E-03 ± 8.69 E-05	1.11 E-02 ± 6.48 E-05	3.26 E-03 ± 9.91 E-06	R16452
10	**2.43 E-02 ± 2.05 E-03**	**6.39 E-04 ± 5.43 E-05**	**3.35 E-02 ± 4.43 E-05**	**2.90 E-03 ± 1.04 E-05**	**R16453**
11	**2.80 E-02 ± 1.86 E-03**	**5.86 E-04 ± 2.14 E-05**	**6.62 E-02 ± 6.35 E-05**	**2.47 E-03 ± 1.49 E-05**	**R16454**
12	**2.73 E-02 ± 2.10 E-03**	**5.00 E-04 ± 2.14 E-05**	**6.58 E-02 ± 6.30 E-05**	**2.43 E-03 ± 7.92 E-06**	**R16455**
13	**3.39 E-02 ± 1.04 E-03**	**5.41 E-04 ± 3.65 E-05**	**4.14 E-02 ± 3.64 E-05**	**2.81 E-03 ± 7.08 E-06**	**R16456**
14	**3.54 E-02 ± 3.93 E-03**	**5.64 E-04 ± 4.87 E-05**	**2.93 E-02 ± 3.63 E-05**	**2.93 E-03 ± 7.81 E-06**	**R16457**
15	**6.74 E-02 ± 8.44 E-03**	**1.69 E-03 ± 1.08 E-04**	**2.29 E-02 ± 6.50 E-05**	**3.09 E-03 ± 6.80 E-06**	**R16458**
16	2.22 E-01 ± 2.20 E-02	1.39 E-03 ± 1.48 E-04	5.97 E-03 ± 2.78 E-05	3.34 E-03 ± 9.30 E-06	R16459
17	2.63 E+00 ± 1.66 E-01	1.56 E-02 ± 1.54 E-03	9.25 E-04 ± 2.41 E-05	3.33 E-03 ± 9.71 E-06	R16460
An0405 - Bt100					
1	9.27 E+00 ± 1.62 E-01	7.99 E-03 ± 2.86 E-03	3.17 E-02 ± 5.85 E-04	1.00 E-02 ± 5.73 E-04	R16511
2	1.99 E-01 ± 2.03 E-03	3.58 E-03 ± 5.60 E-05	2.98 E-02 ± 3.18 E-05	3.23 E-03 ± 4.43 E-05	R16512
3	1.90 E-01 ± 1.02 E-03	2.59 E-03 ± 5.16 E-05	1.53 E-01 ± 2.10 E-04	1.71 E-03 ± 2.21 E-04	R16513
4	2.66 E-01 ± 2.73 E-03	2.44 E-03 ± 3.32 E-05	1.82 E-01 ± 4.25 E-04	2.70 E-03 ± 1.63 E-04	R16514
5	**4.25 E-01 ± 2.52 E-03**	**5.60 E-03 ± 5.77 E-05**	**1.96 E-01 ± 1.88 E-04**	**1.28 E-03 ± 1.76 E-04**	**R16515**
6	**2.29 E-01 ± 1.62 E-03**	**2.55 E-03 ± 2.95 E-05**	**1.85 E-01 ± 2.24 E-04**	**1.46 E-03 ± 1.44 E-04**	**R16516**
7	**3.59 E-02 ± 3.09 E-04**	**-2.67 E-04 ± 1.61 E-05**	**1.93 E-01 ± 1.71 E-04**	**9.59 E-04 ± 4.29 E-05**	**R16517**
8	**1.02 E-01 ± 3.29 E-04**	**5.31 E-04 ± 5.67 E-05**	**1.14 E-01 ± 1.06 E-04**	**2.38 E-03 ± 4.55 E-05**	**R16519**
9	**9.59 E-02 ± 6.62 E-04**	**4.16 E-04 ± 3.64 E-05**	**1.80 E-01 ± 1.68 E-04**	**1.64 E-03 ± 8.50 E-05**	**R16520**
10	**6.67 E-01 ± 1.25 E-02**	**6.80 E-03 ± 8.62 E-05**	**7.48 E-02 ± 1.27 E-04**	**2.69 E-03 ± 1.66 E-04**	**R16521**
11	4.24 E+00 ± 1.49 E-01	4.77 E-02 ± 5.18 E-04	8.85 E-03 ± 3.10 E-04	3.44 E-03 ± 8.62 E-05	R16522
12	1.92 E+01 ± 1.48 E+00	2.18 E-01 ± 2.30 E-03	1.54 E-03 ± 1.18 E-04	2.78 E-03 ± 5.65 E-05	R16523
An0405 - Bt200					
1	5.90 E+01 ± 2.32 E+00	3.29 E+00 ± 8.00 E-03	1.10 E-02 ± 1.99 E-04	8.73 E-03 ± 5.40 E-04	R16463
2	1.52 E+00 ± 3.56 E-01	8.22 E-01 ± 6.79 E-03	1.06 E-02 ± 4.30 E-04	4.20 E-03 ± 1.89 E-04	R16464
3	1.76 E-01 ± 2.23 E-02	7.35 E-04 ± 3.20 E-04	6.21 E-02 ± 7.76 E-05	2.59 E-03 ± 1.20 E-04	R16465
4	**1.05 E-02 ± 6.69 E-03**	**1.62 E-03 ± 5.17 E-05**	**4.03 E-02 ± 9.37 E-05**	**2.81 E-03 ± 9.16 E-06**	**R16466**
5	**8.62 E-03 ± 7.93 E-03**	**5.19 E-04 ± 7.81 E-05**	**1.68 E-02 ± 2.92 E-05**	**3.05 E-03 ± 1.33 E-05**	**R16467**
6	**2.89 E-02 ± 3.23 E-02**	**2.24 E-03 ± 5.58 E-05**	**9.97 E-03 ± 1.26 E-05**	**3.16 E-03 ± 8.29 E-06**	**R16468**
7	**-4.13 E-03 ± 9.60 E-03**	**8.71 E-04 ± 1.28 E-04**	**9.97 E-03 ± 1.05 E-05**	**3.15 E-03 ± 7.49 E-06**	**R16469**
8	**1.27 E-02 ± 1.18 E-02**	**8.12 E-04 ± 1.31 E-04**	**1.34 E-02 ± 1.58 E-05**	**3.10 E-03 ± 1.02 E-05**	**R16470**
9	**6.34 E-02 ± 1.41 E-02**	**1.50 E-03 ± 1.34 E-04**	**2.04 E-02 ± 2.58 E-05**	**3.00 E-03 ± 1.28 E-05**	**R16471**
10	**1.86 E-02 ± 6.55 E-03**	**7.04 E-04 ± 5.88 E-05**	**2.74 E-02 ± 2.45 E-05**	**2.81 E-03 ± 9.05 E-06**	**R16472**
11	**1.38 E-02 ± 1.82 E-03**	**1.21 E-03 ± 7.69 E-05**	**4.47 E-02 ± 3.99 E-05**	**2.56 E-03 ± 4.88 E-06**	**R16473**
12	-8.38 E-03 ± 6.50 E-03	1.56 E-03 ± 1.49 E-04	1.57 E-02 ± 1.74 E-05	2.95 E-03 ± 4.45 E-06	R16474
13	8.32 E-02 ± 2.94 E-02	5.53 E-04 ± 5.34 E-04	3.68 E-03 ± 4.64 E-06	3.13 E-03 ± 6.07 E-06	R16475
14	3.78 E-01 ± 7.75 E-03	7.47 E-03 ± 3.21 E-03	9.17 E-04 ± 7.43 E-06	3.28 E-03 ± 9.53 E-06	R16476
15	1.39 E+00 ± 5.55 E-01	-3.01 E-02 ± 1.90 E-03	4.60 E-04 ± 3.05 E-06	3.32 E-03 ± 9.42 E-06	R16477

composition (Ms1 and Ms2) and less visible in biotite composition, too (Bt1 and Bt2). Different micas generation are also identified and not always associated to a drastic change in chemistry: both micas form fine flake or larger book (e.g. for biotite, Bt-a, Bt-b and Bt-c). The evolution of major rock-forming minerals from the metapelite is deduced from detailed petrography and is summarized in Figure 3.11a together with PT-points determined from thermobarometry (prograde, peak and decompression; Fig. 3.11b).

Whether Ar-ages obtained on micas are geologically interpretable needs to be clarified in regard of the previous petrographic and thermobarometric consideration. Firstly, mineral reactions are susceptible to induce a complete resetting of any isotopic system, i.e. the Ar-resetting process is firstly controlled by metamorphic reaction. Such effect is strongly enhanced, when enough fluid is present (Villa, 1998b). Mineral phase surviving such metamorphic reaction may (partially) conserve their primary isotopic signature (Chopin & Maluski, 1980; Di Vincenzo *et al.*, 2004; Mulch & Cosca, 2004; Villa, 2006). Secondly, in absence of any retrogressive mineral reaction, volume-diffusion may induce Ar-loss, providing the temperature is higher than the so-called "closure-temperature" (Dodson, 1973). As suggested in Dodson (1986), a diffusive profile may exist and older ages are present in the core of largest grain. An Ar-analysis on mineral separates constituted of such zoned grains will inevitably yield a geologically meaningless age, unless diffusion is complete. Another problem arises from the estimation of the closure-temperature. We support Ar-Ar closure-T for micas are calculated around 450 and 500 °C for biotite and muscovite, respectively (Hammerschmidt & Frank, 1991; Villa & Puxeddu, 1994; Kirschner

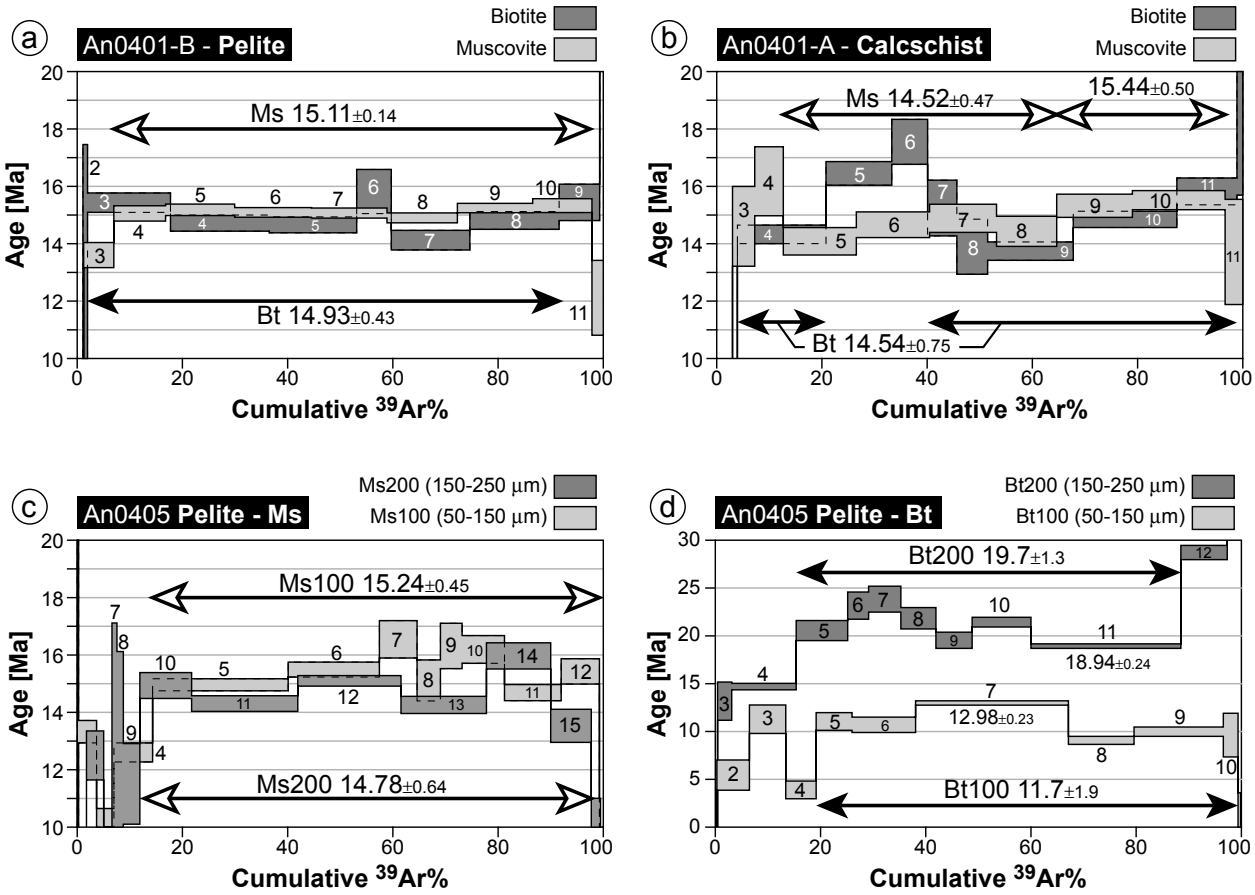

Fig. 3.9: Ar-spectrum for muscovite and biotite separates. Errors on each step age are 1σ and integers are steps number listed in Table 3.5. For all spectra an average on steps as discussed in the text is given (error at 95% confidence). **(a)** Results for muscovite and biotite in metapelite facies (AAn0401-B). (**b,c)** In the equivalent metapelite AAn0405 taken a few meters away from the contact with calc-schist, two different grain-sizes are analysed (50-150 and 150-250 µm). **(d)** Ar-results from the plagioclase-rich calc-schists sample (AAn0401-A). See text for more details.

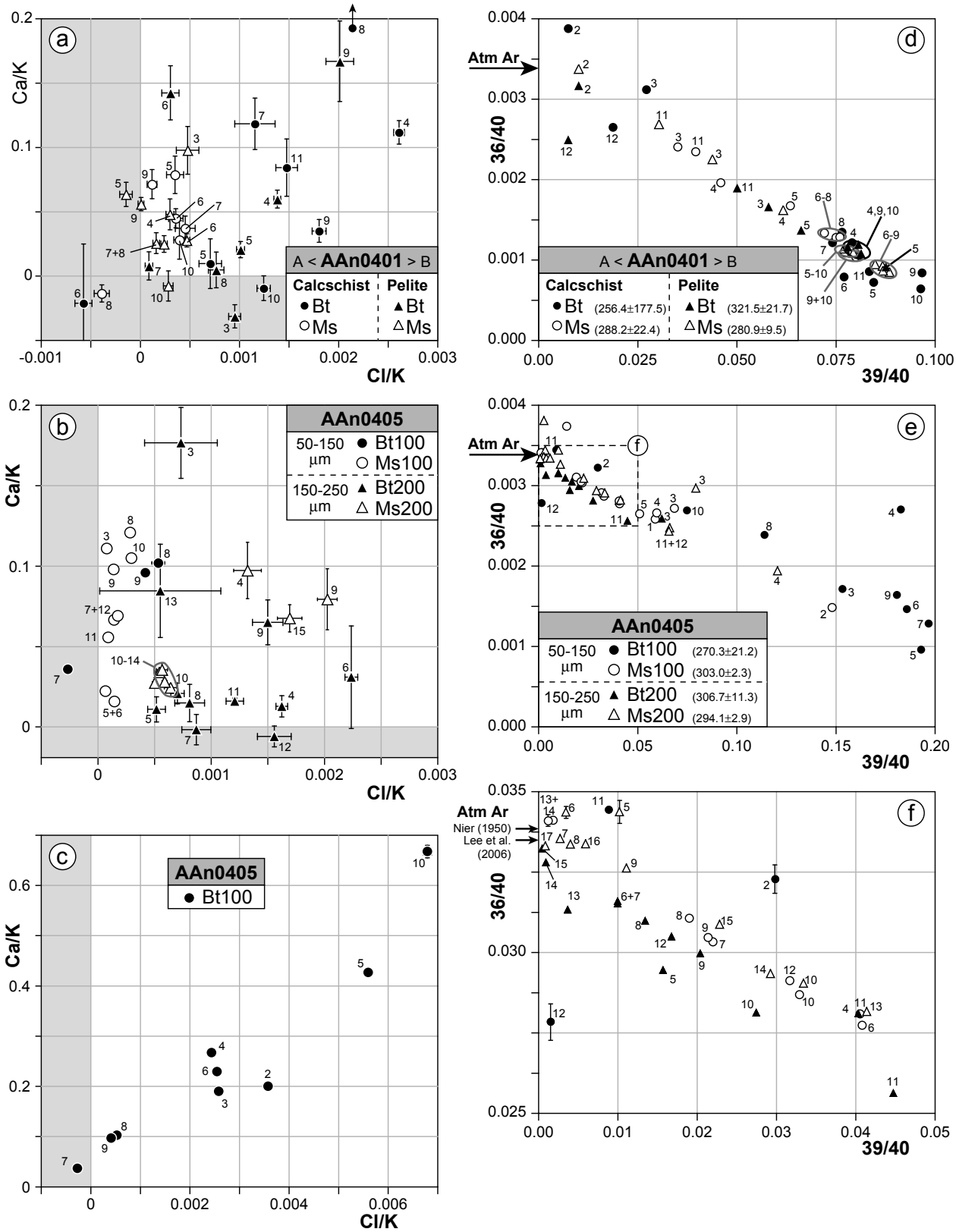

Fig. 3.10: Diagram of Cl/K versus Ca/K calculated from the Ar-stepwise heating results for metapelite samples **(a)** AAn0401 and **(b)** AAn0405. Only points at low Ca/K and Cl/K ratio are presented here and correspond to major steps. Firsts steps and sometimes last one, too, are generally poor in 39Ar and yield abnormally high Ca/K and Cl/K. Both Ca and Cl-content of the two micas are often near detection limit in AAn0401 (Faraday cup measurement only). However, they constantly yield low values, coherent with analysed biotite and muscovite (Table 3.3). **(c)** Larger view on Ca/K versus Cl/K correlation diagram in Bt100 of AAn0405. **(d,e,f)** Isochron diagram for **(d)** AAn0401 and **(e,f)** AAn0405. Most steps yield low $^{36}Ar/^{40}Ar$ in (c), while the air-pollution after sample change accounts for the higher atmospheric content in analysed steps from AAn0405.

et al., 1996). Moreover, phengite better retains argon compared to muscovite (Scaillet *et al.*, 1992; Dahl, 1996). Considering the high-T deduced for the decompression and formation of K-feldspar, volume-diffusion is highly probable after this late retrogressive reaction.

3.10.1) What do we date?

3.10.1.1) Muscovite

In muscovite, Ar-dating always yields circa 15 Ma in any muscovite fraction analysed in metapelite samples (Fig. 3.9a,c). However, both small synkinematic and large oblique muscovites are zoned, which is related to the formation of K-feldspar (Figs. 3.8, 3.11). This latter induces an overgrowth (Fig. 3.8d) or more likely a re-equilibration of muscovite-rims (Fig. 3.8f). This is believed to reset the Ar-signature in muscovite-rim and only the phengite-rich core could have retain its primary isotopic signature (older age, "inherited" argon). Unfortunately, the small size of muscovite flakes and the expected young age disallow the use of *in situ* dating technique, such as laser ablation. This later would require at least 250'000 μm^3 of ablated material to precisely and accurately date a neogene sample (Villa, 2006).

During Ar-Ar stepwise heating analysis, difference in Ar-release from two muscovites of slightly different chemistry is hardly detected (e.g. Ms1 and Ms2). Thus on each analysed step, an average of the gas released by phengite-rich (Ms1) and –poor (Ms2) is analysed, which yields in our case to an apparent plateau age with isochemical steps at constant and low Ca/K and ClK ratios. Different phengite-rich/-poor ratio among the three muscovite-separates could yield small differences, but is unlikely in the present case study; both fine flakes and larger books are composed approximately of the same ratio phengite-rich core versus phengite-poor rim (circa 30 to 50% phengite-rich core, from image analysis of Al and Mg elements mapping; Fig. 3.3c; Appendix 3.3). Except if Ms1 and Ms2 retain an identical Ar-signature, the age calculated from such an analysis is hardly interpretable in terms of geological process. Ar-signature in Ms1 and Ms2 can only be identical, if we consider either a complete Ar-resetting in Ms1 during the metamorphic reaction producing Ms2 or a complete Ar-resetting in Ms1 and Ms2 related to diffusion occurring after this reaction. In other case, the Ar-Ar age is considered as an average age between growth stage of Ms1 and the later equilibration toward Ms2. Of course, volume-diffusion can always affect micas after this reaction, which will result in younger ages, especially at muscovite rim. Due to both higher closure-T and the fact that Ms1 is always enclosed in Ms2, the Ar-retention in phengite-core is presumably higher than the muscovite-rich rim.

We get more information by considering the Ar-dating results from calc-schist. Though alteration is responsible for slightly younger ages in the beginning of Ar-release spectrum (Fig. 3.9b), muscovite Ar-age from the calc-schist sample AAn0401-A yields an identical age compared to metapelite (14.95±0.59 Ma; Table 3.4). Each single muscovite flake from calc-schist is homogeneous in AAn0401-A and the variation of composition, notably in Fe-Mg content, is attributed to local alteration. In contrary to carbonate-rich pelites (e.g. AAn0402), no K-feldspar is identified in this plagioclase-rich facies. The similar age in both samples support the idea of a global event at 15 Ma, which affects both calc-schist and metapelite. Muscovite from calc-schist yields younger ages in the low-T releasing steps, but this is attributed to alteration.

3.10.1.2) Biotite

Consideration of biotite Ar-ages can be used to determined whether this Ar-signature stems from a metamorphic reaction (through fluid percolation, reduction of water activity, brutal change in PT-condition, etc.; model A), a volume-diffusion process (model B) or a combination of both (model AB). If a common metamorphic reaction is affecting both rock types below the closure-T, biotite ages should also be affected in the same way and are thus qualified of recrystallization (or re-equilibration) age. In contrary, when volume-diffusion is responsible for the age resetting, muscovite should be older than biotite, as closure-T for diffusion in biotite is 50° lower (Villa & Puxeddu, 1994, 450 °C for biotite; Hammerschmidt & Frank, 1991, 500 °C for muscovite).

Biotite and muscovite separates from AAn0401-B yield identical Ar-age, which would at first glance invalidate the hypothesis of a resetting through volume-diffusion of argon in micas, preferring thus a recrystallization event at 15 Ma, most likely related to the formation of K-feldspar. In calc-schist, the Ar-spectrum of biotite is discordant due to the strong chloritization of this mineral and selected isochemical steps yield a slightly younger age (14.54±0.75 Ma; Fig. 3.9b). In contrast, two selected biotite fractions in AAn0405 yield different Ar-ages between 18.94±0.24 and 23.86±1.37 for the coarse fraction Bt200 and 9.07±0.42 to 12.98±0.23 Ma for the fine fraction Bt100 (Fig. 3.9d; discordant spectrum). K-feldspar is often intimately associated with biotite (Fig. 3.3a), but was not identified in none of the three biotite-separates. The presence of a large amount of a second K-bearing phase (muscovite or K-feldspar) is excluded from XRD, for which spectrum obtained on all three biotite-separates reveals exclusively biotite with minor chlorite and epidote (Table 3.4). Concerning possible volume-diffusion, a lower closure-T is expected for younger age in the finer fraction compared to the coarser one (Dodson, 1973). However, the age variation is usually small (e.g. <1 Ma in other samples from the northern Central Alps; see §2.8.3.4) and can hardly explain this large age-difference of 6 to 10 Ma between Bt100 and Bt200 (respectively 2 and 4 times less ^{39}Ar and ^{40}Ar* in Bt100).

The occurrence of at least three biotite generations in metapelite is a more important explanation that we support. Those generations are revealed by textural observation (Bt-a, –b and –c; Figs. 3.2c, 3.3e,f, 3.11a), as also by the microprobe analyses of biotite (trend in Fe*, Al and Ti-content). This biotite composition is also variable due to local change of rock chemistry (Fig. 3.4a,b) and thus this criterion is less typical for the crystallization and PT-condition relation than the petrographic evidences (Fig. 3.11). However, the combination of both leads to a conspicuous PT-history with the help of THERIAK-DOMINO. Contrasting with muscovite, which is commonly <200 µm, biotite of first generation forms blast reaching 2 to 5 mm (Bt-a,b), while the later generation is usually <300 µm (Bt-b; Figs. 3.2b,c and 3.3). Whether Ar-Ar signature in those large biotite grains remains discussable. Nevertheless, the older ages obtained for the largest grain size support the idea that the largest biotite books preserved their isotopic signature during decompression and retrogression (Fig. 3.11c, model A). Such preservation of Ar-signature renders obsolete the idea of diffusion-controlled resetting of Ar-ages in the largest biotite grains. The possible presence of excess-Ar (not inherited) tones this conclusion down, but this identification remains difficult (Fig. 3.10d,e). Moreover, it is not excluded that diffusion was effective, but only affects the rim of largest grains (Bt-b) by creating a diffusion profile (Dodson, 1986). Thus, applying Dodson's diffusion theory, the age of Bt-a biotite might even be older (24 Ma?) and the age of 19 Ma represents a cooling age during decompression or early retrogression (Fig. 3.11c, model B).

Secondly during K-feldspar formation, some biotite of first or second generation (Bt-a, Bt-b) are consumed and partially recrystallized in the matrix, forming finer flakes aligned in the schistosity with higher Mg and Al-content (reaction 3.4). Providing volume-diffusion effect occurring after reaction completion is inefficient, age obtained for the finer biotite fraction Bt100 record this event around 12-9 Ma. In other words, either the crystallization of these biotites occurs below the closure-T or, most likely, the fluid-induced metamorphic reaction

is the dominating factors for the Ar-retention in micas. This would again support the preservation of older ages in largest biotite books, which only shows local resorption during K-feldspar formation and the preservation of a chemical zonation in some major elements (Al, Fe, Mg, Ti; Fig. 3.3a,e,f). Finally, the third and last biotite to appear in metapelites (Bt-c) is scarce and associated to chlorite. This stage is related to retrogression in upper greenschist facies (Fig. 3.11a). Such late biotite is excluded from each mineral separate, as those grains are typically <50 µm. Due to their scarcity and to the presence of other major metamorphic reaction disturbing the growth of previous biotite generations, this late growth of biotite and chlorite is believed to leave quite undisturbed Bt-a, remaining thus (quite) unproblematic for Ar-dating.

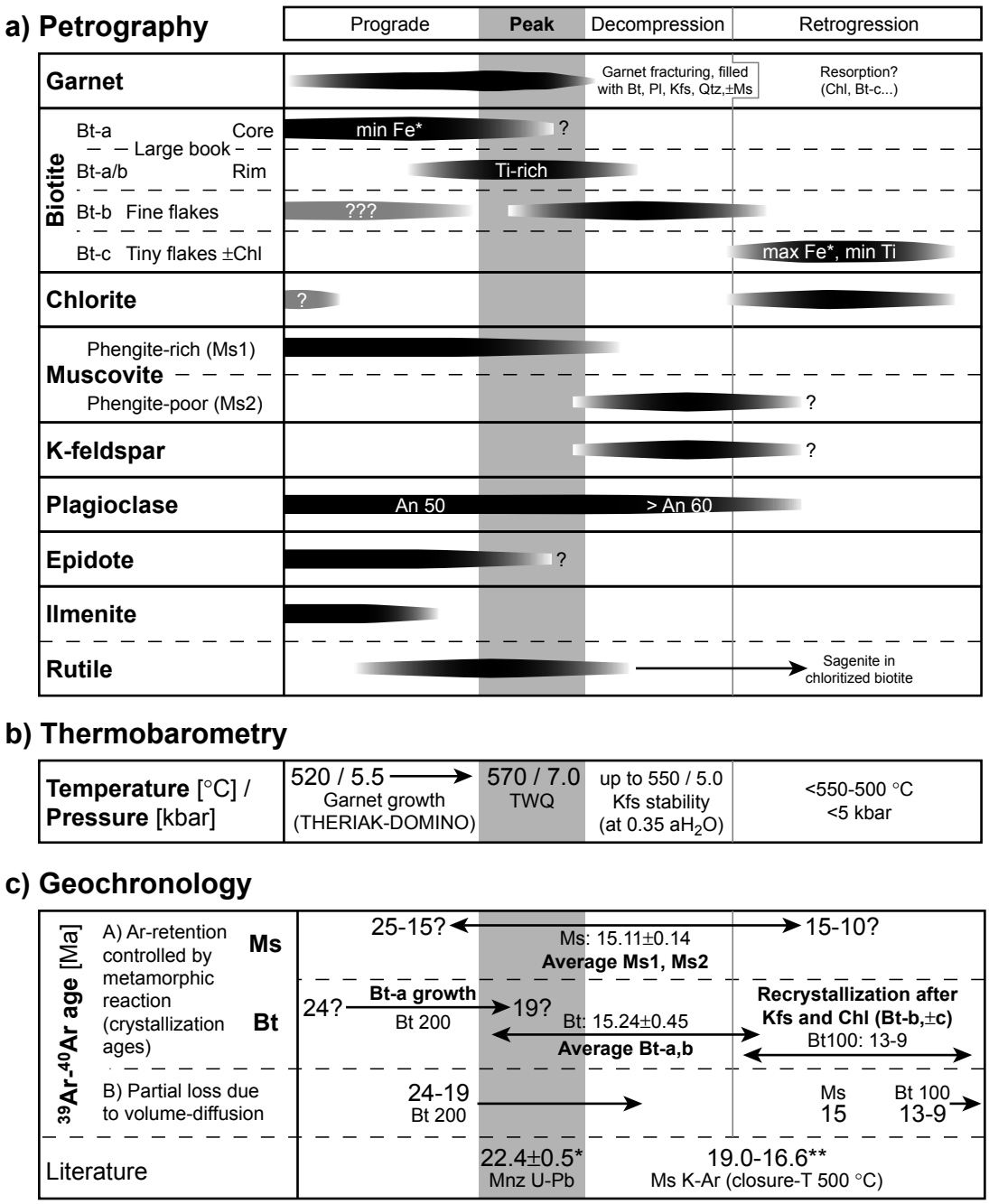

Fig. 3.11: (a) Relations between mineralogy and metamorphism based on detailed petrographic and thermobarometric investigation and including some relevant variation of mineral chemistry for biotite. **(b)** Summary and interpretation of thermobarometric results from this study. **(c)** Two models for the timing of the metamorphism affecting the region and comparison with data from the literature: (*) Köppel & Grünenfelder (1975); (**) Hurford (1986). See text for explanation.

3.11) The relevance of these ages in an Alpine context

Though that hard to replace in a PT evolution due to bad definition of phase relation in REE-bearing phases, growth of monazite and xenotime is suggest to occur around the maximum thermal peak. They are thus best candidate to yield an age for the peak of metamorphism affecting this area of the Central Alps (Janots *et al.*, in preparation; Chapter 4). Unfortunately, no monazite ages are available in the nearest nappes (Antigorio, Lebendun). Nearest ages are found in Fusio (Sambuco nappe, NE of the studied area; 22.0±0.5 Ma) and near Baceno (Verampio window; 19.5±1.1 Ma; Table 3.1). Though uncertain in the studied area, we reasonably admit a peak of metamorphism occurring around 20 Ma, as this is the case southwards of the Gotthard nappe, near Val Piora and Lucomagno (Chapter 4). The age of mineral equilibration estimated by TWQ around 580°C and 7 kbar in Val Antabia is thus expected to occur around 19 to 22 Ma.

Regarding K-Ar ages in Sambuco, Lebendun and Antigorio nappes (Fig. 3.1a; Table 3.1), muscovite and biotite yield respectively 19.0-16.6 Ma and 16.0-14.2 Ma. As suggested by the various authors of these results (Purdy & Jäger, 1976; Frank, 1979; Steiner, 1984; Hurford, 1986), these ages effectively pertain to cooling-ages, but below 500 °C for muscovite and 450 °C for biotite according to more recent studies (e.g. Hammerschmidt & Frank, 1991; Villa & Puxeddu, 1994; §4.6.1). More information regarding the age is taken from the monazite dating suggesting that the peak of metamorphism possibly occurs near 22-20 Ma. From the zircon fission track dating, the cooling below 280 °C occurs around 12-13 Ma in the Sambuco and 10.9±0.5 in Antigorio nappe. Ar-results from our sample collection are younger than those muscovite K-Ar ages, nearly similar than biotite K-Ar ages (except Bt200) and older than zircon fission tracks (except Bt100). We are confronted to two hypothesis summarized in Figure 3.11c.

Model A: The K-feldspar reaction occurs at high T-condition, around 550-580 °C. Nevertheless, a (partial) preservation of Ar-signature is considered in phengite-rich core of muscovite and in the largest biotite books (Bt-a). The older Ar-age from biotite separate Bt200 (19-24 Ma) is interpreted as recording a growth stage along the prograde path or near the thermal maximum (growth of Bt-a, Fig. 3.11a), while Bt100 yield a minimum age for the K-feldspar formation at 13-9 Ma. Due to possible late diffusion effect, this age is a minimum value. Ar-results from all muscovite separates are yielding an average age between phengite-rich core and muscovite-rich rim. The age for the phengite-rich core (Ms1) remain unknown. However, it might be similar to slightly younger than Bt-a (<19 Ma), providing a complete preservation of the isotopic signature during the peak of pressure (Fig. 3.8b). Similarly and compared to Ar-result from Bt100, the muscovite-rich rim is possibly appearing before or at 13 Ma. A mixture of Ms1 and Ms2 will inevitably yield an age around 15 Ma, slightly variable according to the proportion of each mica.

Model B: From K-Ar ages, rocks from this area of Central Alps cool down to 500 °C at circa 17 Ma. Ar-results from this study yield younger ages around 15 Ma (except for Bt200), a resetting has occurred after the cooling to 500 °C. This event at 15 Ma is the K-feldspar reaction occurring in metapelite and is thus dated at 15 Ma by both muscovite and biotite (identical Ar-ages in AAn0401-B). In this hypothesis, the age of Ms1 and Ms2 is identical. However, a contradiction appears from the older (and younger) age obtained in the coarser fraction Bt200 (and the finer Bt100). This could be explained by a partial preservation of the crystallization age of Bt-a, even after diffusion and metamorphic reaction. The younger age of Bt100 is accommodated, providing a temperature for the K-feldspar formation between 500 and 450 °C. This allows diffusion to reset the Ar-signature of the finer biotite, whereas muscovite Ar-age is preserved (crystallization age).

3.12) Conclusion

Detailed petrology and thermobarometry, a model for the K-feldspar growth in a suite of metapelite from Val Antabia is proposed and corroborated with the observed changes in mineral composition:

1) The chemical zonation preserved in garnet constrained a small part of the prograde path from 520, 5.7 to 570 °C, 7.0 kbar.

2) The climax of metamorphism is precisely determined at 7 kbar and 560-580 °C and is situated near the pressure climax or slightly below. From the repartition of monazite ages, this peak of metamorphism is presumably reached around 22-20 Ma. At that time, metapelite was composed of large and oblique biotite books (Bt-a, Mg-rich) coexisting with synkinematic to oblique white micas (phengite-rich, ca. 3.3 p.f.u. Si). Garnet (almandine rich) and plagioclase (An_{40-60}) are the major blast. Before the end of garnet growth, ilmenite disappears and is accompanied by an overgrowth of Ti-richer and Fe-richer rim around largest biotite books.

3) During decompression below 7 kbar, the phengite-rich muscovite and probably some biotites were involved in K-feldspar formation reaction. The recrystallization of a phengite-poor muscovite rim accompanies the growth of K-feldspar. The growth of small biotite flakes in the matrix is also suggested to occur at that time. The growth of K-feldspar in metapelite requires a strong reduction of water activity around 0.25-0.45 aH_2O. We suggest that the decarbonatation of the surrounding calc-schist and carbonate-rich rocks is one possible cause of this strong fluid-percolation, but the extreme high xCO_2 required for this reaction (0.8 xCO_2) seems unrealistic. The help of other diluted ions, such as salts and sulphates from Triassic layers notably, will most likely induce the strong reduction of aH_2O necessary to explain the formation of K-feldspar. For the moment, the source and exact chemical composition for this fluid percolation remain currently unsolved; a detailed study on fluid-inclusion in quartz (produced during K-feldspar formation) would hopefully constrain this part of the metamorphic history from Val Antabia.

Unfortunately, the interpretation of geochronological results on micas from metapelite and calc-schist remains discussable due to the disequilibrium related to the K-feldspar formation. The first series of analysis reveal an identical Ar-age in both muscovite and biotite from metapelite (15.11±0.14 and 14.93±0.43 Ma, respectively), while a small age difference is measured between muscovite and the biotite from the surrounding calc-schist (15.44±0.5 and 14.54±0.75). The careful selection of different grain-sizes for the second series of Ar-analyses confirms the constant age for coarse and fine muscovite fraction, with 15.24±0.24 and 15.78±0.64 Ma, respectively. However, both fractions are broadly composed of the same proportion of phengite-poor and –rich muscovite. This leaves open the question of identical or different age for each muscovite generation.

The results from coarse and fine biotite fraction reveal disturbed plateau, but a significant age difference, with 24 to 19 Ma in the coarse fraction and 9 to 13 Ma in the finer one. In view of the detailed petrographic and thermobarometric analysis, we suggest that the older ages pertain to the signature of the large and oblique biotite books (Bt-a), while the finer fraction is reflecting the age of the finer biotite flakes growing in the matrix and related to the K-feldspar growth. In this idea, diffusion might have occurred, but was inefficient in the large biotite books to totally reset the age signature. From the theory of diffusion in minerals (Dodson, 1986), a diffusive profile can be present with younger ages at rim and older ages possibly pertaining to the growth stage of Bt-a might in the core of the largest biotite book. The average age obtained on biotite separates made on a few hundreds of grain reflect thus a minimum age for the crystallization stage of Bt-a along the prograde path.

Following this interpretation, all three muscovite separates are then viewed as an average age between

the equilibrium stage of phengite-rich muscovite and the phengite-poor re-equilibration during decompression. As approximately 30 to 50% of phengite-rich muscovite is believed to be present in each white mica separate and admitting an age around 9-13 Ma for the later re-equilibration, the phengite-rich muscovite is suggested to yield an Ar-age of 17-19 Ma.

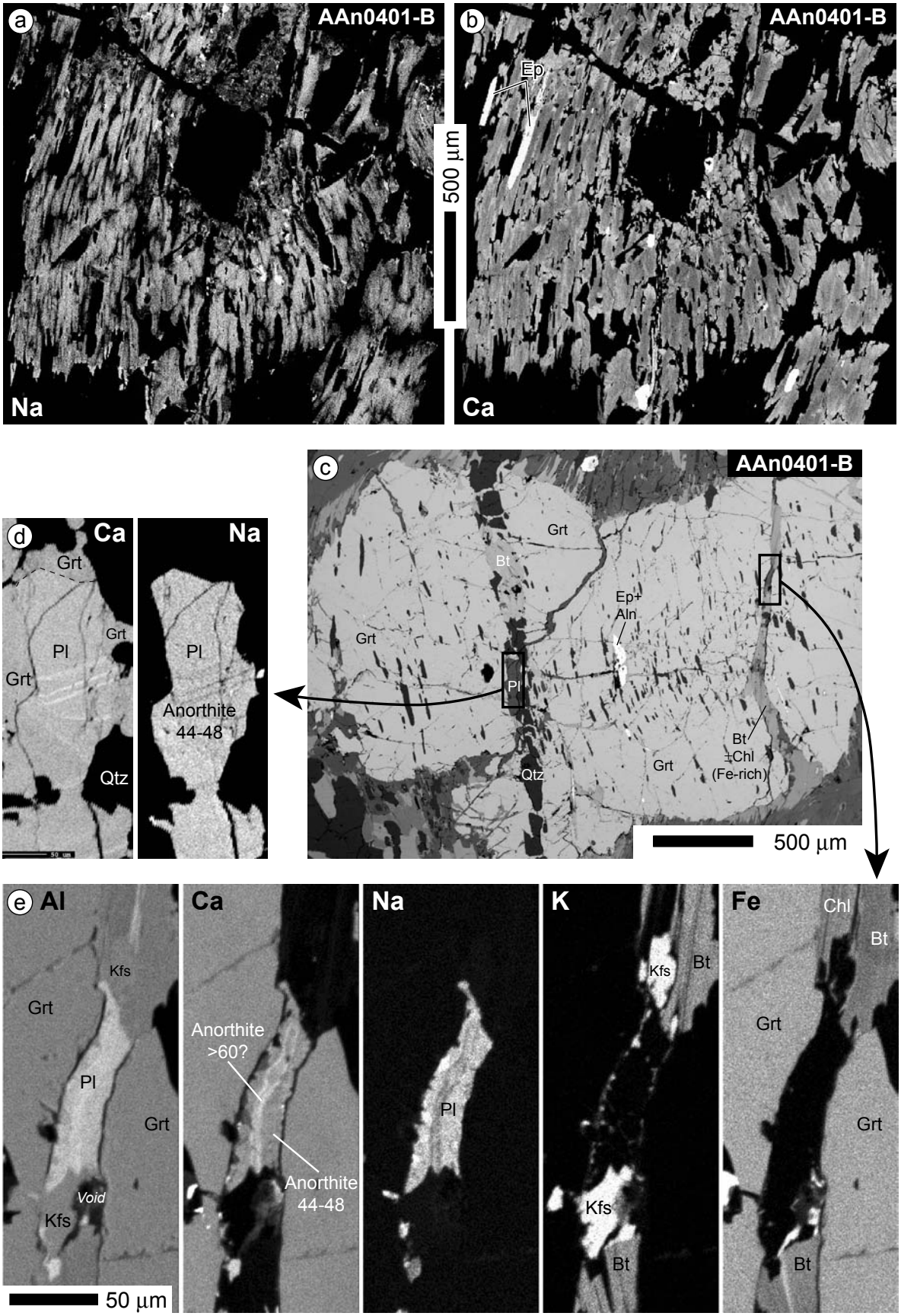

Appendix 3.1: (a,b) Na and Ca composition map in a plagioclase from metapelite AAn0401-B (WDS mode, 15 kV, 20 nA, beam and pixel 2.5 µm, dwell-time 20 msec). **(c,d,e)** In this same sample, plagioclase is found as inclusion in garnet, either as **(d)** grain of homogeneous composition or **(e)** grains in garnet crack with a fracture-filling pattern zoned and associated to K-feldspar (WDS mode, 15 kV, 20 nA, beam 1 µm, pixel 0.5 µm, dwell-time 30 msec).

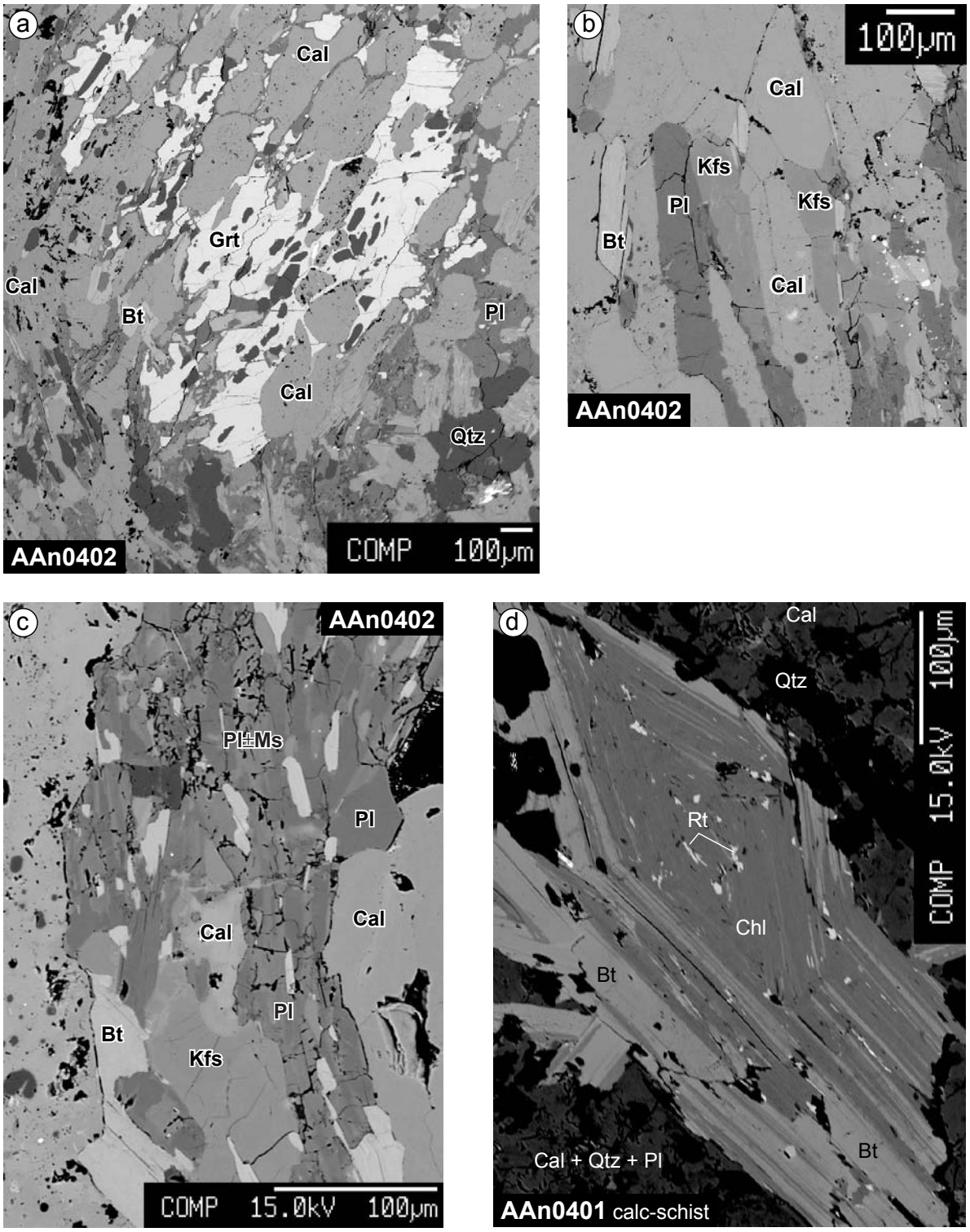

Appendix 3.2: (a,b,c) BSE images in calc-schist AAn0402. **(a)** Local growth of atoll garnet. **(b,c)** Formation of K-feldspar surrounding plagioclase and calcite. **(d)** Strong chloritization in a biotite from calc-schist AAn0401-A (BSE image).

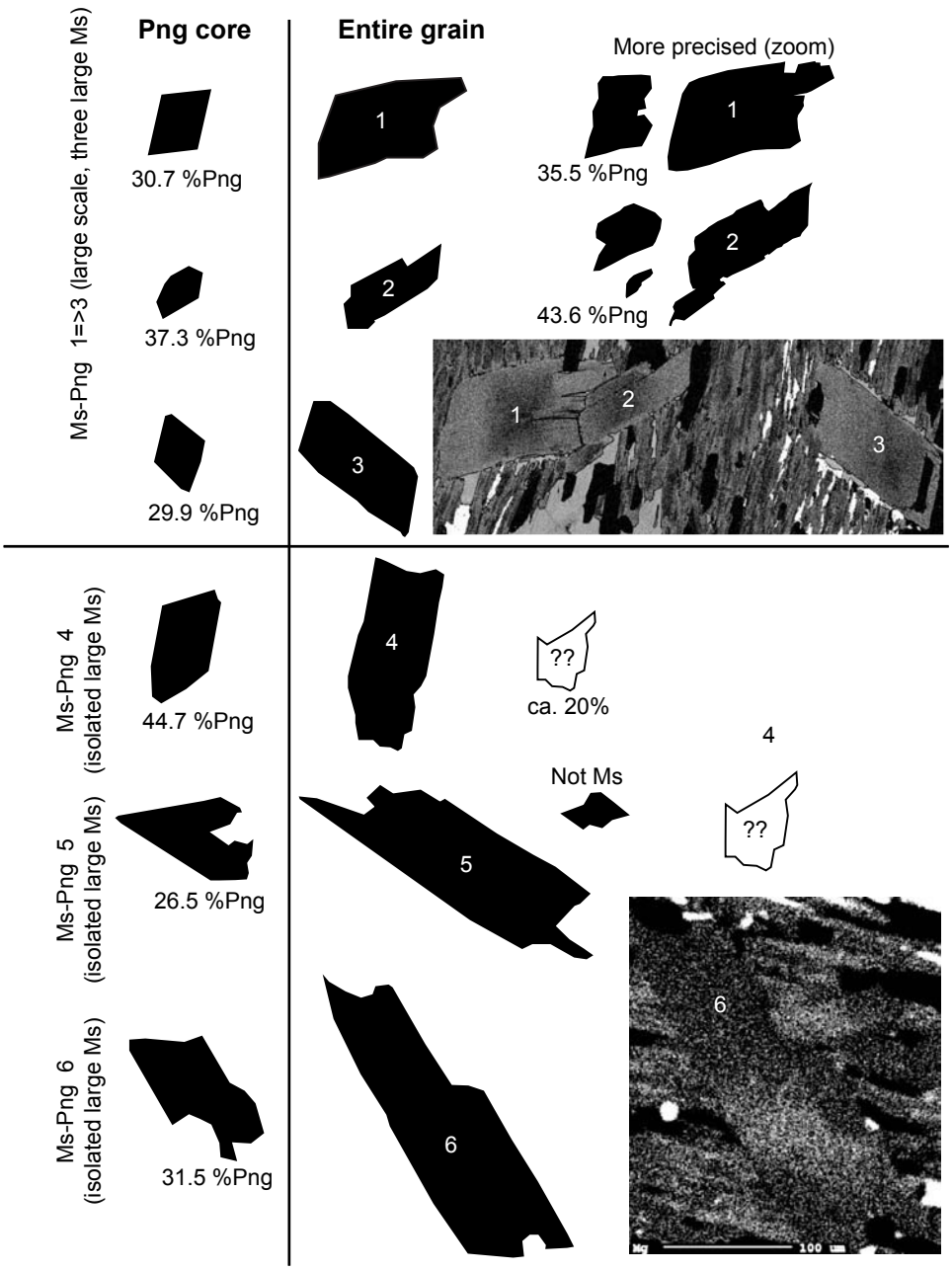

Appendix 3.3: Estimation of the abundance of phengite-core in white mica from AAn0401 and AAn0405, based on element mapping of Al and Mg.

4) PTt-history in the northern Central Alps based on thermobarometry, U-Pb and Ar-Ar ages

From Val Piora (left) to Scopi (right), a view of the studied area from Pizzo Forno (A. Sponda).

J. Allaz, M. Engi, E. Janots, A. Berger & I.M. Villa

4.1) Abstract

Based on multi-chronometry using well-equilibrated metapelites and metamarls from Mesozoic protoliths, the Pressure-Temperature-time (PTt) evolution during the Tertiary Barrovian metamorphism in the northern Central Alps was reconstructed. In samples of lower amphibolite facies grade, the breakdown of allanite to monazite was used to date successive prograde stages by *in situ* analysis of U-Th-Pb isotopy. Coexisting monazite and allanite in close spatial proximity were dated, and their ages were linked to distinct P-T conditions of formation and to the established regional metamorphic field gradient. Relic allanite retained its characteristic growth zoning acquired at greenschist facies conditions even upon after partial replacement of allanite by monazite. Th-Pb and U-Pb dating yield SHRIMP ages between 31.5±1.3 Ma and 29.2±1.0 Ma for allanite, 19.1±0.3 Ma and 18.0±0.3 Ma for monazite.

These results were used to interpret new Ar-Ar data for white mica from the same samples, yielding ages between 18.93±0.83 and 15.79±0.11 Ma for muscovite and 16.37±0.40 and 14.84±0.23 Ma for biotite. The muscovite Ar-ages in this area pertain to conditions near the documented P-T equilibria (7-9 kbar, 550-570 °C), with only minor Ar-loss through diffusion upon cooling from these conditions. Ar-loss is slightly more evident in white mica from a second area, at slightly higher temperatures (580-600 °C). In the same samples, Ar-loss in biotite yields Ar-Ar ages 1-2 Ma lower than muscovite. These results support high Dodson-type closure-temperatures for Ar-Ar in mica (450 °C for biotite, 500°C for muscovite).

Regarding the geodynamic evolution of the Central Alps, the above data have important implications. Prograde conditions near 400 °C were established at 30 Ma (allanite ages) for tectonic units in the northern part of the Lepontine belt, which reached metamorphic peak temperatures at 20-18 Ma (monazite and muscovite ages), following slight decompression. The regional distribution of robust ages across the entire belt shows that the thermal peak was diachronic from the southern to the northern part of the Central Alps, with ages of 30-27 Ma north of the Insubric line and only 20-18 Ma in the northern areas examined in the present study. Considering zircon fission track ages from adjacent areas, an average cooling rate of 31 to 53 °/Ma was determined between 570 and 280 °C.

Keywords

Alpine metamorphism; Central Alps; PTt-path; geochronology; Ar-Ar closure temperature; U-Pb monazite; exhumation rate.

4.2) Introduction

The Alpine orogeny resulted from the closure of Piedmont-Liguria and Valaisan oceans, followed by continental collision of the Eurasian and Adriatic plates. The overall geological architecture of the Central Alps has been reviewed by Schmid *et al.* (1996), Pfiffner *et al.* (2000), Bousquet *et al.* (2002), Schmid *et al.* (2004) and Berger *et al.* (2005). In this area of the regional metamorphic grade increases from north to south, reaching amphibolite facies in the Ticino region. At the southern margin of the belt, the Insubric line truncates this Barrovian metamorphic field. The concentric pattern of metamorphic isograds (Niggli & Niggli, 1965; Trommsdorff, 1966; Wenk & Keller, 1969; Niggli, 1970; Wenk, 1970; Kuhn *et al.*, 2005) and isotherms (Todd & Engi, 1997) cuts across the main tectonic nappe contacts in the Central Alps. This metamorphic field gradient thus peaked after nappe stacking. The Central Alps mostly expose polymetamorphic basement units and only minor metasediments from Mesozoic protoliths. Numerous geochronologists have aimed to relate isotopic ages to tectonic stages or to the Alpine metamorphic imprint, though specific dates pertaining to the Pressure-Temperature-time (PTt-) evolution remain sparse. Various geochronometers have been applied, notably Rb-Sr and K-Ar (or Ar-Ar) on micas, U-Pb on monazite and xenotime, Sm-Nd and Lu-Hf on garnet, as well as fission track data on zircon and apatite. Unfortunately, many of the ages were obtained for samples from the gneissic basement, hence inheritance from pre-Alpine metamorphic stages pose serious problems of interpretation. Moreover, a large number of published papers heavily rely on two-point "isochrons" that never demonstrate the legitimated use of the isochron approach in the first place. The systematic are discussed e.g. by Thöni & Jagoutz (1992) and readers are explicitly referred to it. Especially questionable are muscovite Rb-Sr ages (Hunziker, 1969, assumed a blanket initial $^{87}Sr/^{86}Sr$ ratio of 0.709), as well as garnet ages that do not demonstrate initial polymineralic equilibrium.

The change from Hercynian to Tertiary mica ages is related to the increasing grade of Alpine metamorphism. An overview of literature K-Ar and Rb-Sr mica ages on micas in NSB is given in Figure 4.1a,b. The northern-most samples clearly show variable ages between Hercynian and Alpine orogenies, reflecting an incomplete resetting of both Rb-Sr and K-Ar isotopic systems in micas during the alpine metamorphism. Southwards of the staurolite isograd, muscovite Rb-Sr ages are younger than 38 Ma. Estimated biotite Rb-Sr ages vary from >200 to ca. 30 Ma in correspondence to the stilpnomelane isograd crossing the middle of the Aar-massive (northern part of Fig. 4.1a; Niggli, 1970). Muscovite K-Ar ages yield ca. 25-19 Ma in the Gotthard and 17-16 Ma in the northern Pennine nappes, while biotite ages are more homogeneous around 17 and 16-14 Ma for the respective areas. Data from Mesozoic metasediments are rare and only two sampling localities around the studied area are found in the northern and eastern area at Curaglia and Lumbrein, respectively (Fig. 4.1b). The first of these yielded an illite K-Ar age of 16.4±1.2 Ma for the Urseren-Garvera zone; the second one gave 19.5±3.1 Ma for illite from metasediments situated south of the Gotthard crystalline thrust sheet (Hunziker *et al.*, 1986).

The spatial pattern of muscovite Rb-Sr ages in Central Alps was assumed to be concentric; the younger mica ages W of Monte Rosa were not considered. Jäger *et al.* (1967) and Hunziker (1969) conclude that the Barrovian peak of metamorphism in Central Alps is dated by muscovite Rb-Sr age estimates from the Monte Rosa nappe with a cutoff at 38 Ma (Hunziker, 1969). At higher metamorphic grade in the Central Alps, muscovite Rb-Sr ages are interpreted as a cooling-age below 500 °C. Above this closure-temperature (Dodson, 1973), the isotopic system is opened and the Rb-Sr isotopic system is constantly reset. Comparison of K-Ar and Rb-Sr data in muscovite leads Jäger *et al.* (1967), Jäger (1973) and Purdy & Jäger (1976) to suggest a closure temperature of 350 °C for K-Ar in muscovite. However, Purdy & Jäger (1976; p. 19-20) pointed out that this estimate was subject to larger uncertainties, as the error in the Rb-Sr closure temperature and the errors in K-Ar ages were compounded. Regarding the K-Ar isotopic system, recent studies suggest higher closure temperature in micas: 500 °C for muscovite (Hammerschmidt & Frank, 1991) and 450 °C for biotite (Villa & Puxeddu, 1994). Even higher temperatures have been suggested (up to 550 °C for muscovite) for dry metamorphic environments (Balogh &

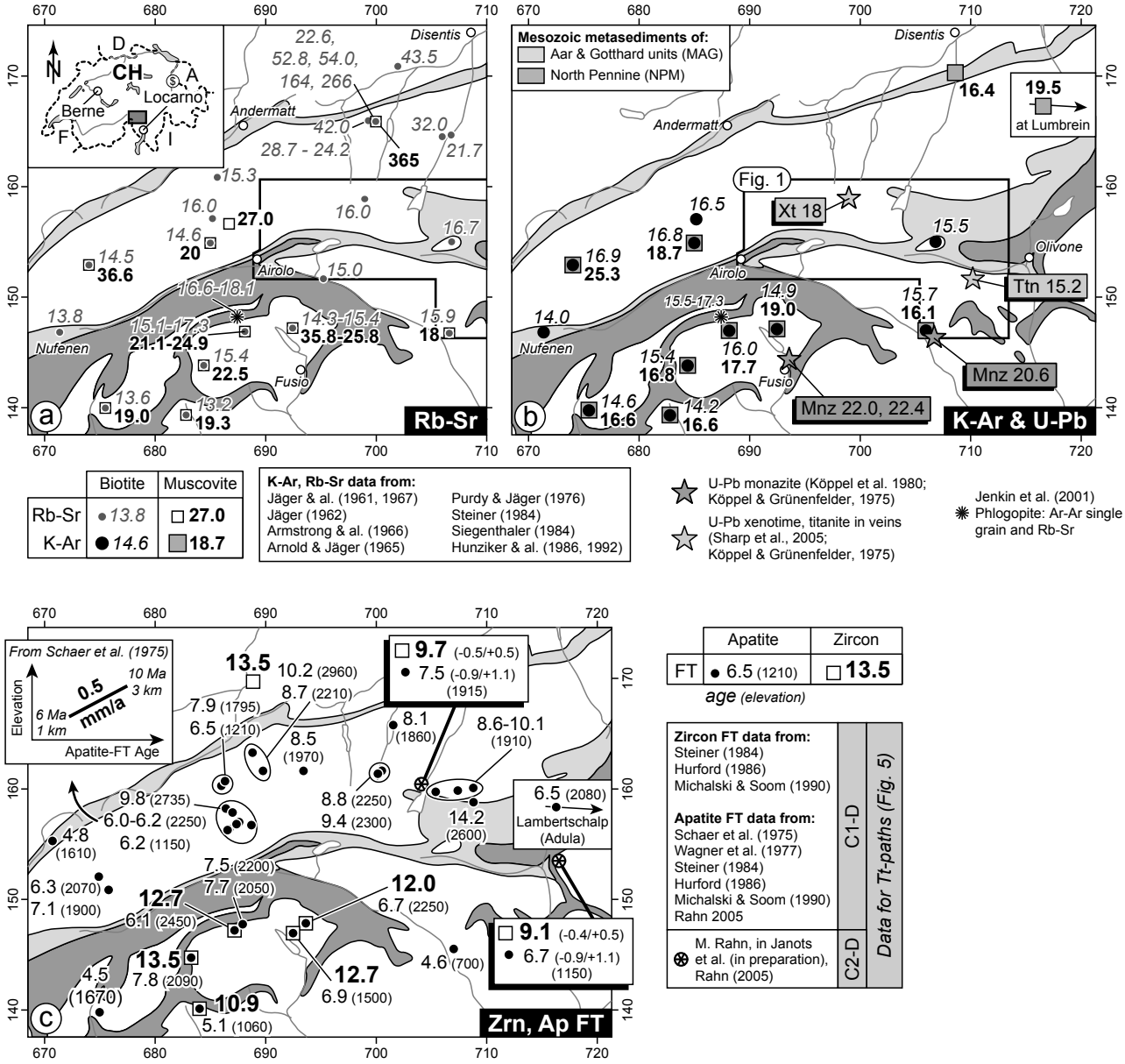

Fig. 4.1: (a) Compilation of muscovite and biotite Rb-Sr ages from the literature in the NSB. MAG and NPM tectonic units according to Probst (1980). Grey curves in background stands for rivers and lakes. **(b)** Same for micas K-Ar data from the NSB. Also shown are the monazite, xenotime and titanite data from basement units and Alpine fissures. Mnz = monazite, Xt = xenotime, Ttn = titanite. **(c)** Same for apatite and zircon fission track (FT) dating. Apatite dating is usually correlated with elevation and therefore can be used to recalculate averaged paleo-exhumation rate. This has been for instance detailed northwards of Airolo in the Gotthard nappe (see inset, from Schaer *et al.*, 1975).

Dunkl, 2005). However, apart from simple volume-diffusion processes, fluids affect the recrystallization behaviour and may induce isotopic resetting (Villa, 1998b; Villa, 2006).

On the other hand, monazite and xenotime U-Pb ages yield 20 to nearly 30 Ma from the northern to the southern part of the Swiss Central Alps (Köppel & Grünenfelder, 1975; Köppel *et al.*, 1980). This observation can be interpreted by two self-consistent but opposing hypotheses for the timing of the Barrovian metamorphism in the Central Alps (see also Villa, 1998b). Steck & Hunziker (1994) consider the model from Jäger *et al.* (1967) as correct, and therefore propose that there was an orogen-wide, simultaneous peak of metamorphism occurring around 38 Ma; in order to achieve consistency, they are forced to propose that monazite ages must be cooling ages, with monazite Pb loss occurring around 450 °C. The alternative hypothesis is based on the observation that the U-

Th-Pb isotopic system in monazite is highly retentive (e.g. Parrish, 1990), and therefore dates the thermal peak of metamorphism in the Central Alps. However, the spatial variation in the monazite and xenotime U-Pb ages from north to south (Engi *et al.*, 1995) relied on diverse samples, many of which were polymetamorphic gneisses, for which an inherited Pb-component could not be excluded. This controversy questioned about the age significance, which may result from an erroneous determination of the closure-T, or the presence of other parameters influencing one of these isotopic systems (e.g. disequilibrium, isotopic loss, inheritance). Recent studies have demonstrated the rather complex behaviour of isotopic systems, which not only suffer of volume diffusion, but also possible late isotopic exchange and fluid-enhanced recrystallization during retrogression (e.g. Villa, 1998b; Jenkin *et al.*, 2001; Di Vincenzo *et al.*, 2004; Balogh & Dunkl, 2005; Villa, 2006; Chapters 2 and 3).

In this paper, we aim to reassess the metamorphic history of Mesozoic metasediments from the Northern Steep Belt (NSB) of the Central Alps by considering new isotopic age data, including ^{39}Ar-^{40}Ar stepwise heating on micas and recent ages based on *in situ* U-Th-Pb isotopic analysis of monazite and allanite (Janots *et al.*, in preparation). Samples were selected for dating based on prior petrological characterisation, including the analysis of the detailed mineral evolution in petrogenetic grids (or pseudo-sections; THERIAK-DOMINO; de Capitani, 1994) and comparing them with the petrographic data. Not only were the PT-conditions and the state of equilibrium ascertained, but care was taken to ensure also that each mineral used for dating did not signs of late re-equilibration or of appreciable metamorphic back-reaction upon decompression and cooling. Given these precautions, the present study yields very tight links between the petrology, PT-conditions and the geochronometric data. This provides a basis to reassess the timing and diachronicity of the Alpine tectono-metamorphic evolution in the Central Alps, as well as the Dodson-type closure temperature for Ar in micas, and the effects of retrograde mineral reactions upon Ar-Ar data.

4.3) Geological setting

The Central Alps in Switzerland are a classic orogen, characterized by a collision-related nappe stack. Its rapid exhumation was triggered by the combined effects of extension, back thrusting and efficient erosion (Schmid *et al.*, 1996; Pfiffner *et al.*, 2000). In the Lepontine area, thrust sheets mainly comprise pre-Alpine basement units and Mesozoic metasediments. Isolated high-pressure relics are confined to slivers of tectonic mélange intercalated within the nappe stack (Engi *et al.*, 2001; Berger *et al.*, 2005; Brouwer *et al.*, 2005), and the entire domain was overprinted at medium pressures. Mineral zones and metamorphic isograds outline a classical Barrovian belt with isotherms organized in a concentric pattern (Todd & Engi, 1997): greenschist to lower amphibolite facies prevail in the northern parts of the Lepontine domain, sillimanite-grade and an Alpine migmatite belt are reached in the south.

This study focuses on a restricted area delimited in the north by the Aar crystalline massif and the Gotthard nappe, in the south by the Leventina and Sambuco nappes (Switzerland; Fig. 4.2). The focus is on essentially pelitic and clastic metasediments, with or without minor carbonate contents. As their protoliths were Mesozoic, i.e. post-Variscan, they experienced but one orogenic cycle and are monometamorphic. Alpine metamorphic conditions in this region straddle to the transition between greenschist and amphibolite facies (Frey & Ferreiro Mählmann, 1999). The dominant tectonic structure is sub-vertical, hence this region was termed the Northern Steep Belt (NSB) by Milnes (1974). Probst (1980) distinguished two major tectonic units in the metasediments from NSB: the Mesozoic unit of the Aar and Gotthard (MAG), and the Northern Pennine Mesozoic (NPM; Fig. 4.2). Both of these units are subdivided in the studied area into two smaller tectonic units. In the MAG, these are the Scopi-Piora and Peidener zones, the latter being present in Lucomagno area only. In the NPM, the “Pennine frontal thrust”

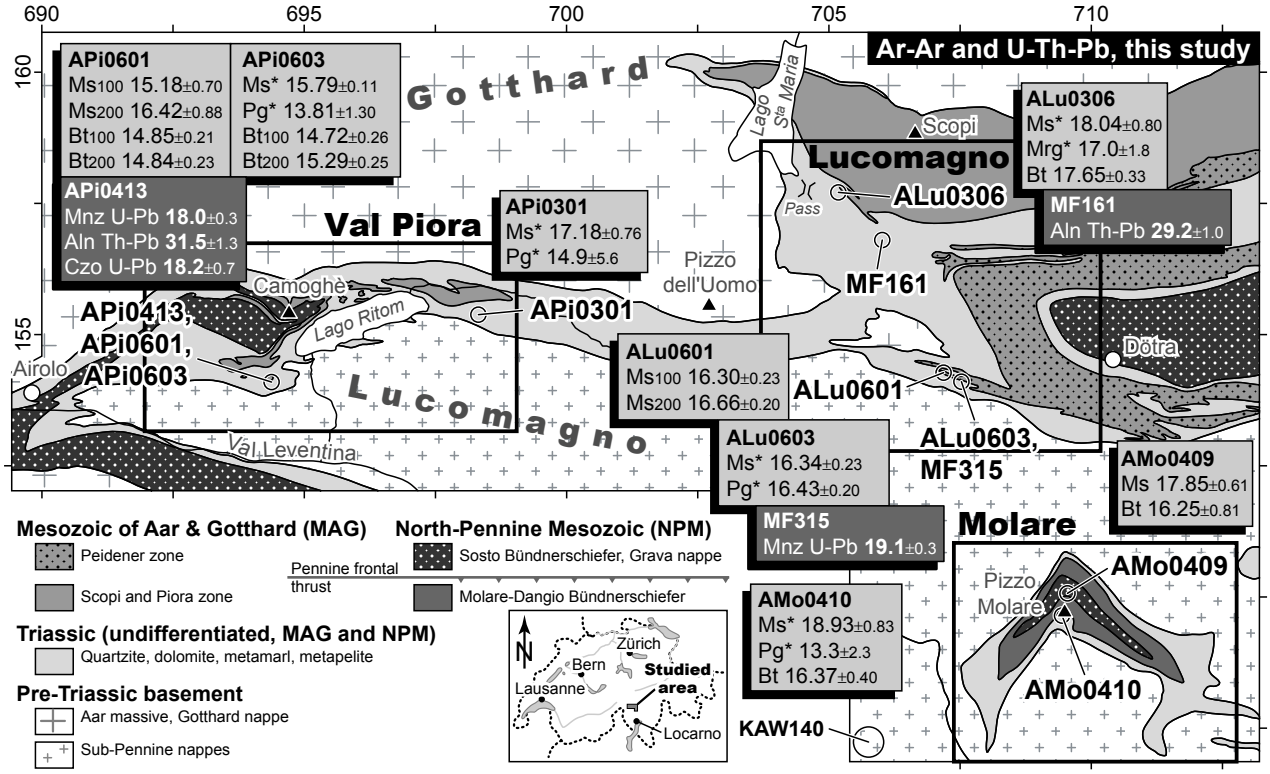

Fig. 4.2: Overview of studied area, situated in the northern part of the Swiss Central Alps (see inset). Sample positions are shown with age data from monazite U-Pb, allanite U-Th (dark grey squares; Janots *et al.* (in preparation) and micas Ar-Ar (light grey squares). Swiss coordinates grid in km; geological map from Probst (1980). Numbers next to mineral abbreviation indicate mineral size fraction analysed ("100" = 50-150 µm, "200" = 150-250 µm). Ages marked with (*) are for mixtures of white micas (muscovite with paragonite or margarite) and imply age extrapolation in a Ca/K versus age diagram (see §2.8.3 for details). Aln = allanite, Bt = biotite, Czo = clinozoisite, Mnz = monazite, Mrg = margarite, Ms = muscovite, Pg = paragonite.

(Milnes, 1976) or the "Grava-Lugnezer-Sosto thrust" (Probst, 1980) separate the Sosto and Molare-Dangio units (Fig. 4.2). The distinction between these different tectonic units may seem small, but it is essential in regard to the PTt-path, as some of the units from NPM probably experienced blueschist-facies metamorphism during the early subduction stage. This inference is based on carpholite relics in fibrous quartz-calcite veins of Valaisan units from the western and eastern parts of the Alps (Petit St. Bernard and Vals-Chur areas, Engadine window; Bousquet *et al.*, 2002). A companion study is currently underway to better document this blueschist stage, and Wiederkehr *et al.* (submitted) already established carpholite relics in the Vals, Vrin, Olivone and Pizzo Molare areas, notably in the Sosto Bündnerschiefer and the Grava nappe. The present study does not address this problem and is based on samples from units, which are not supposed to have implicated in the early-Alpine HP/LT metamorphism.

A few monazite and xenotime ages were already available in Central Alps (Köppel & Grünenfelder, 1975; Köppel *et al.*, 1980; Fig. 4.1b). These ages range from 30-27 Ma in the SSB to 22-20 Ma in the NSB and intermediate ages around 21-24 Ma in the core of the Sub-pennine nappes (Sambuco, Simano, Leventina). Considering monazite as dating the thermal peak of metamorphism implies that the observed variation in PT-conditions from the Central Alps resulted from at least two distinct metamorphic overprints (Engi *et al.*, 1995). The northern part of the Central Alps followed a classical Barrovian type field gradient, while rocks from the SSB were subducted more deeply (reaching eclogite facies) and were reheated during the exhumation and the intrusion of Tertiary granitoids (Engi *et al.*, 1995; Brouwer *et al.*, 2005). A xenotime age from a late-Alpine vein in the Gotthard massif yielded 18 Ma (Fig. 4.1b; Köppel & Grünenfelder, 1975), but remains difficult to relate to a specific temperature. An U-Pb age on sphene from a vein in Lucomagno gneiss yielded 15.2 Ma; its growth was

related to a hydrothermal stage above 270 °C (Fig. 4.1b; Sharp *et al.*, 2005). K-Ar data for hornblende yielded variable ages (26 to 152 Ma; Steiger, 1964; Deutsch & Steiger, 1985) in the Aar massif, the Gotthard nappe, and near the area studied (Val Piora, Lucomagno). South of the staurolite zone boundary (Niggli, 1970), amphibole K-Ar ages are similar to U-Pb monazite ages, and these ages were thus taken to date the Alpine metamorphism around at 23-28 Ma (Deutsch & Steiger, 1985).

Fission track (FT) data are used to constrain the timing of the late exhumation history. As the understanding of resetting processes in zircon FT dating is superior, at least to Ar-Ar, this geochronometer offers an excellent temperature-time reference point (Tt-point) for comparison of micas Ar-Ar and another well-constrained Tt-point given by monazite U-Pb ages. Conclusions of various authors based on both field observations and experiments converge to an annealing interval for zircon in the range between 330 and 200 °C, with an average "closure temperature" of 280 °C (for cooling rates between 10 and 100 °/Ma and a heat duration of 1-10 Ma; Brix *et al.*, 2002; Rahn *et al.*, 2004; Yamada *et al.*, 2007); for apatite FT closure temperatures between 70 and 120 °C are used (Hurford, 1986). Though less readily comparable with Ar-Ar data, apatite FT ages show a dependency to the elevation and allow a recalculation of exhumation rate.

Figure 4.1c summarized currently available FT-dating results on apatite and zircon in the studied area. M. Rahn (pers. comm.) analyzed zircon FT near Lucomagno pass in the Gotthard nappe, which yield 9.1 (-0.4/+0.5) Ma (Janots *et al.*, in preparation). Earlier zircon FT data from the Aar massif yielded 12 to 14 Ma (Michalski & Soom, 1990), in the same range as results from northern Sub-pennine units (Sambuco, Antigorio and Lebendun nappes, 11-14 Ma; Steiner, 1984; Hurford, 1986). FT ages increase southwards, reaching 14-18 Ma in the core of Sub-pennine nappes and 19 Ma in SSB (Hurford, 1986).

Apatite FT ages show a similar trend across the Central Alps, with older ages in the SSB compared to NSB. At Lucomagno pass (1915 m), apatite FT dating yields 7.5 (-0.9/+1.1) Ma (M. Rahn in Janots *et al.*, in

Sample	Swiss-coordinates			Unit	Rock type
	N-S, E-W [km], elev. [m]				
Lucomagno Pass					
ALu0306	157.71	705.18	2'085	MAG, Quartenschiefer	Chl-Bt-Mrg-Pl calcschist (Mg-rich)
ALu0304	157.93	705.27	2'140	MAG, Scopi Bündnerschiefer	Grt-Bt-Mrg-Pl graphitic metapelite (Ca-rich)
MF 161	156.70	706.20	2'175	MAG, Quartenschiefer	Cld-St-Ky metapelite (Al-rich)
Lucomagno South-East					
ALu0601	154.20	707.19	1'760	MAG, Scopi Bündnerschiefer	Grt-St-Ms-Pg-Pl; Graphitic metapelite (Al-rich)
ALu0603	154.05	707.51	1'770		St-rich, Grt-Ky-Ms-Pg-Pl; Graphitic metapelite (Al-rich)
MF 315	153.95	707.65	1'760		St-rich, Grt-Ms-Pg-Pl; Graphitic metapelite (Al-rich)
Val Piora East					
APi0301	155.38	698.32	2'075	MAG, Quartenschiefer	St-rich, Grt-Ms-Pg-Pl metapelite (Al-rich)
Val Piora West					
APi0413	154.10	694.38	2'130	MAG, Quartenschiefer	Heterogeneous metapelite, see APi0601, –03
APi0601					Bt-rich, Grt-Ky-Pg-Pl-Chl metapelite (Al-rich)
APi0603					Ky,Pl-rich, Grt-St-Bt-Ms-Pg metapelite (Al-rich)
Pizzo Molare					
AMo0409	150.13	709.67	2'450	MNP, Quartenschiefer	Grt-Bt-Ms-Pl metapelite (Al-poor)
AMo0410	149.51	709.46	2'555	MNP, Quartenschiefer	Grt-Bt-Ms-Pl, ±Pg,Ky,St metapelite (Al ±rich)

Table 4.1: Position (Swiss coordinate) and rock type for each studied samples. MF161 and MF315 belong to Martin Frey's collection (Frey, 1969).

preparation), which is similar to the results from older studies in the neighbourhood (7-9 Ma at 1500-2500 m; Schaer *et al.*, 1975; Wagner *et al.*, 1977; Michalski & Soom, 1990). The central Sub-pennine nappes (Antigorio, Sambuco, Lebendun) yield 6 to 13 Ma from 300 to 2500 m elevation (Steiner, 1984; Hurford, 1986) and 9-12 Ma in the SSB at 200-500 m elevation (Hurford, 1986; Rahn, 2005). From the apatite FT age versus altitude dependency, means exhumation rate are recalculated and yield 0.45-0.50 mm/a in the Gotthard nappe (e.g. inset of Fig. 4.1c) and slightly lower value near the SSB (Ticino valley and Bergell; 0.34-0.40 and 0.43 mm/a; Wagner *et al.*, 1977). Similar values are suggested from apatite FT in the southern section of Adula nappe, reaching a moderately-correlated exhumation rate of 0.33 mm/a (Rahn, 2005).

4.4) Methods

Prior to geochronological work, detailed petrography and complete mineral analysis was conducted to identify texturally well-equilibrated samples. The major rock-forming minerals of each sample were analysed using a JEOL-8200 electron microprobe, and PT-condition were calculated based on multi-equilibrium thermobarometry using TWQ (Berman, 1988; Berman, 1991). Details about the method are given in §2.5.1 and §2.5.2. Comparison of PT- or P-X(H_2O-CO_2) pseudosections computed with THERIAK-DOMINO (de Capitani, 1994) and the observed mineral assemblage were used to determine the mineral evolution along a PT-path. Bulk rock composition used for this thermobarometric analysis are obtained by XRF, starting with a rock sample of 0.5 to 1.0 kg to minimize inhomogeneities induced by the growth of largest blasts (e.g. garnet, plagioclase, up to 1 cm). Analytical information on mineral zoning was compared to isopleths computed by DOMINO, and calculated mineral abundances (isomode maps) were utilized to infer in which PT-range major net-transfer reactions might have changed the petrography.

The primary criterion used in selecting samples for Ar-dating was an excellent preservation of the equilibrium assemblage, which is thought to reflect the thermal peak of metamorphism. Mineral separation involved crushing and sieving of the samples selected; from mineral mixtures of various size fractions between 50-150 and 200-250 µm muscovite and biotite were extracted by gravity separation and magnetic method. For some samples, two size fractions were selected to check for the effect of grain size on Ar-Ar age (50-150 and 150-250 µm). Final handpicking ensured 99% visual purity. Each separate was then analysed by X-ray diffraction to characterize the impurity contents (see §2.5.3).

Ar-Ar stepwise heating analyses were performed in the isotope laboratory at University of Bern, following procedures detailed in §2.5.4. Usually, only ^{40}Ar, ^{39}Ar and ^{36}Ar are sufficient to calculate an age. However, to enable a better characterization of the degassing phase during each heating step of Ar-analysis, ^{37}Ar and ^{38}Ar were measured together in our study. Constant $^{37}Ar/^{39}Ar$ and $^{38}Ar/^{39}Ar$ ratios (i.e. Ca/K and Cl/K ratios) were obtained over all major analysed steps, which was usually the case for pure mineral separates. In this case, the Ar-data is said to be “isochemical” and typically yielded a well-defined plateau. By contrast, where two Ar-sources of possible different age were present (e.g. muscovite mixed with paragonite or margarite), it was necessary to assess the effect of each phase on the age data, even if an apparent plateau-age is obtained and suggest a homogeneous Ar-reservoir. Whereas ^{39}Ar is essentially released from muscovite (the major K-component, with only traces of Ca), ^{37}Ar stems mostly from paragonite or margarite (the major Ca-component, with minor to traces of K). In the case of mineral mixtures, each step usually yields different Ca/K ratio, which could be attributed to Ca/K values of each phase previously determined by electron microprobe. In successive heating steps, a trend in $^{37}Ar/^{39}Ar$ data versus apparent age is often visible (from “heterochemical” release). Based on the Ca/K ratio on each phase in the mineral separate (from EMP analyses), the “true” age of each K-bearing phase composing the mineral separate is determined.

Table 4.2: Mineral assemblage and modal abundances in our sample collection. Most of these abundances stem from a simple observation of thin sections under microscope and comparison with polished rock plates. They are thus subject to large uncertainties (±5-10%), which are sometimes complicated by layering and small sedimentary heterogeneities, notably quartz-rich layers (see text for further details). ALu0306 is the only calc-schist and contains in addition 10-20% ankerite. Rare ankerite is preserved in ALu0304, as inclusion in garnet.

Sample	Ms	Mrg	Pg	Bt	Chl	Grt	St	Ky	Qz	Pl	Ep	Ilm	Rt	Inclusions in Grt
ALu0304	5-10 *	20-30 *		5-15	<1-1	2-3			30-50	5	<1	<1		Ms-Mrg, Qz, Cld, Ank, ±Rt
ALu0306	1-2 *	10 *		5-15	5-10				40-50	2-3	5		<1	-
MF161 #	*25-30*		*10-15*	*<1*	*3*		*8*	*5*	*23*	*3*	*<1*	*4*		-
ALu0601	50-70			<1-1	<1	10.4 **	2.3 **	8-10	15-20	2-5	<1		<1	Ms, Qz, Cld, Ep, Ilm+Rt
ALu0603	20-30 *		30-45 *	1-2	<1	4.5 **	23.3 **	7.0 **	5-10	5-10	<1		<1	Ms-Pg, Qz, Cld, Rt
MF315 #	*10*		*10-15*	*1*	*1*	*5*	*40*	*<1*	*24*	*5*		*2*		-
APi0301	15-25 *		15-25 *	5-10	<1	1-2	5-15		15-25	5	<1	1-2		Qz, Cld, Ep, Ap, Ilm±Rt
APi0601	1-5 *		10-15 *	25-35	5	2.5 **	0.3 **	10-25	5-20	2-10	<1	<1		Qz, Cld, Ep, Ilm+Rt
APi0603	2-5 *		8-20 *	5-15	<1	4-8	7-10	20-30	5-15	10-20	<1		<1-1	Qz, Cld, Ep, Ilm+Rt
AMo0409	40-50			15-20	<1	2	2		20-30	5	<1	<1		Ms, Qz, St, Ep, Ilm
AMo0410	35 *		<1-5? *	15-20	<1-1	3-5	1-2	1-2	25	10-15		1	<1	Mrg, Ms-Pg, Qz, Ilm

(*) The proportion of muscovite and margarite or paragonite is determined on several Al, Ca, Na and K element mappings at EMP (WDS-mode, up to 2x2 mm, 1 to 2 µm pixel resolution and beam size, 15 kV, 20 nA, 10 to 40 ms dwell-time; see CD).
(**) From image analysis of ca. 10x15 cm polished rock-plate (see CD).
(#) Sample and modal abundances from Frey (1969). MF161 also contains 12% chloritoid.

4.5) Results

4.5.1) Sample description

For geochronometry, care was taken to select the best-equilibrated metasediments, for which equilibrium-PT condition could be clearly defined. As discussed above, all of the samples derive from Mesozoic protoliths, thus minimizing inheritance problems, and almost all of the samples stem from the MAG unit (Table 4.1). Among the metasediments, samples of the Quartenschiefer (Frey, 1969; pelitic to marly upper Triassic; Table 4.1) were best suited for the present study, as they commonly contain large and pristine micas flakes, together with a large variety of minerals yielding well constrained PT-calculations. In comparison, samples from Bündnerschiefer (Jurassic to Tertiary deposits; Table 4.1; Probst, 1980) are very heterogeneous, banded or finely layered at meter- to millimetre-scale, often fine-grained, carbonaceous and poor in micas, except in a few layers. Moreover, they were usually full of sub-micrometric graphite particles included notably in micas, which is a source of complications for mineral separation and Ar-dating.

This paper concentrates on samples from four groups of outcrops (Fig. 4.2) located (a) at Lucomagno Pass (samples ALu0304 and ALu0306; Table 4.1), (b) in the western part (APi0413, APi0601 and APi0603) and the eastern part of Val Piora (APi0301), (c) in the area SE of Lucomagno Pass (MF315 from Frey, 1969), ALu0601 and ALu0603), and (d) near Pizzo Molare (AMo0409 and AMo0410). Mineral assemblage and modal abundances of each studied samples is presented in (Table 4.2). Significant differences are observed between metapelites, mainly due to differences in bulk rock composition, but also due to small changes of PT-conditions.

In the entire studied area typical Al-rich metapelites contain assemblages involving two white micas, biotite, garnet (almandine-rich), plagioclase, and quartz, with chlorite and chloritoid disappearing in favour of biotite, garnet, staurolite and kyanite. Garnet, kyanite and staurolite typically form idiomorphic porphyroblasts

reaching a few millimetres in size and overgrowing the schistosity. Plagioclase blasts can reach similar sizes, but they are more ovoid and elongated in the schistosity. Either ilmenite or rutile is stable, but they are never found together in equilibrium, except sometimes as inclusion in garnet (Table 4.2). Apatite, tourmaline and zircon are ubiquitous accessory phases. In terms of crystallization-deformation relation, the selected samples are quite uniform: Fine mica flakes are typically aligned in the schistosity (typically 100-200 µm length, 10-50 µm thickness) or forming larger oblique books (especially of biotite, mm-size) more or less elongated and sheared along the schistosity; all of the porphyroblasts overgrew the main schistosity, locally also the late crenulation, especially kyanite and staurolite. Chlorite-bearing assemblages may survive up to Val Piora and Lucomagno in Mg-rich bulk compositions of pelite and micaceous calc-schist. The mineral assemblage of all studied samples is detailed below and is necessary to ensure the excellent preservation of mineral stability, which is a prerequisite to PT-condition calculation and to any isotopic dating of a mineral.

4.5.1.1) Area (a): Lucomagno Pass

The northernmost samples bordering the Gotthard nappe marks the transition to amphibolite facies; this represents the lowest metamorphic grade recorded in the sample collection presented in this paper (Table 4.1; Fig. 4.2). ALu0306 is the only calc-schist selected, containing ankerite, chlorite, biotite, quartz, epidote, plagioclase, margarite, and minor muscovite (Table 4.2). This sample is homogeneous, rich in quartz and carbonate. Pleochroic green biotite and pale-green chlorite are in textural equilibrium. Both form large oblique books reaching 0.5-1 mm. Margarite is always synkinematic and aligned in the main schistosity, while tiny muscovite flake crystallized later, as suggested by the absence of a clear preferred orientation in thin section. Latest minerals to grow over the matrix are small plagioclase blasts reaching 0.2-0.5 mm. For petrological comparison and PT-condition, we select in the neighbourhood a typical metapelite (Fig. 4.2); ALu0304 is a homogeneous garnet-biotite metapelite assemblage characterized by the coexistence of muscovite and margarite. Both white micas are intimately associated, aligned in the schistosity and sometimes included in larger and oblique biotite. Garnet forms large porphyroblast, reaches 1 cm and includes notably ankerite.

4.5.1.2) Area (b): Val Piora

Samples of Quartenschiefer were collected near the contact with the Scopi-Piora zone westwards of Lago Ritom (Table 4.1; Fig. 4.2). Irregular layering at meter- to centimetre-scale characterized this outcrop. APi0603 is rich in ferromagnesian minerals (staurolite, garnet, biotite), while APi0601 is leucocratic and contains more kyanite and plagioclase, but only minor muscovite (Table 4.2); APi0413 contains layers of both these types at thin section scale. Large idiomorphic grains of garnet (2-5 mm) and staurolite (2-8 mm) overgrow the foliation in all of these samples and the amount of quartz is quite low, locally below 5 modal-% (Table 4.2). Muscovite from APi0601 forms either very fine interlayer of 10-100 µm length inside paragonite rich matrix or sparse larger flakes reaching 100 µm (see BSE images on CD). Paragonite and biotite clearly dominate the matrix, but biotite clearly forms larger and oblique books reaching 1 mm and coexisting with finer biotite flakes interlayered within paragonite rich layers. In APi0603, both white micas coexist and form larger flakes aligned in the schistosity, with less abundant biotite. Chlorite forms fine lamellae within the paragonite-rich matrix, in textural equilibrium with biotite.

APi0301 is a homogeneous metapelite collected eastwards of Lago Ritom (Fig. 4.2); apart from garnet and plagioclase, this sample is characterized by abundant staurolite (cm-size) overgrowing the matrix. Muscovite

Table 4.3: Summary of mineral compositions in samples used for Ar-dating. For each mineral characteristic values are given: Al = total Al-content in p.f.u., Fe* = Fe/(Fe+Mg), xNa = Na/(Ca+Na+K), xK = K/(Ca+Na+K), Czo = (Al-2)/(Fe+Al-2), Alm, Sps, Prp or Grs = (M)/(Fe+Mn+Mg+Ca), and xAn = Ca/(Ca+Na+K). Complete set of analyses for each sample was presented in §2.6 (see Appendix 2.1).

		MUSCOVITE									
		ALu0304	ALu0306	ALu0601	ALu0603	APi0301	APi0413	APi0601	APi0603	AMo0409	AMo0410
Al	min	2.673	2.673	2.753	2.747	2.733	2.734	-	2.728	2.544	2.617
	Avg	**2.705**	**2.698**	**2.786**	**2.818**	**2.797**	**2.769**	**-**	**2.779**	**2.665**	**2.732**
	max	2.744	2.732	2.842	2.903	2.894	2.830	-	2.852	2.735	2.922
Fe*	min	0.405	0.398	0.332	0.283	0.319	0.393	-	0.278	0.466	0.440
	Avg	**0.427**	**0.429**	**0.379**	**0.369**	**0.371**	**0.406**	**-**	**0.330**	**0.580**	**0.539**
	max	0.455	0.465	0.452	0.495	0.431	0.417	-	0.387	0.664	0.722
xK	min	0.920	0.825	0.895	0.809	0.700	0.745	-	0.828	0.862	0.651
	Avg	**0.933**	**0.860**	**0.917**	**0.846**	**0.745**	**0.791**	**-**	**0.864**	**0.891**	**0.761**
	max	0.941	0.880	0.931	0.872	0.783	0.848	-	0.883	0.914	0.807
xNa	min	0.059	0.119	0.069	0.128	0.217	0.152	-	0.116	0.086	0.193
	Avg	**0.066**	**0.139**	**0.082**	**0.153**	**0.255**	**0.208**	**-**	**0.135**	**0.109**	**0.238**
	max	0.079	0.173	0.105	0.190	0.299	0.254	-	0.168	0.134	0.349

		MARGARITE		PARAGONITE							
		ALu0304	ALu0306	ALu0601	ALu0603	APi0301	APi0413	APi0601	APi0603	AMo0409	AMo0410
Al	min	3.822	3.757	-	2.975	2.944	3.135	3.070	3.095	-	3.004
	Avg	**3.892**	**3.817**	**-**	**3.108**	**3.096**	**3.149**	**3.099**	**3.127**	**-**	**3.029**
	max	3.967	3.892	-	3.160	3.153	3.221	3.136	3.152	-	3.053
Fe*	min	0.588	0.302	-	0.622	0.569	0.451	0.371	0.473	-	0.825
	Avg	**0.648**	**0.450**	**-**	**0.749**	**0.657**	**0.552**	**0.487**	**0.617**	**-**	**0.868**
	max	0.713	0.590	-	0.871	0.776	0.715	0.619	0.731	-	0.887
xK	min	0.005	0.007	-	0.049	0.043	0.067	0.076	0.067	-	0.090
	Avg	**0.014**	**0.013**	**-**	**0.089**	**0.069**	**0.084**	**0.094**	**0.085**	**-**	**0.106**
	max	0.021	0.018	-	0.102	0.129	0.115	0.127	0.103	-	0.153
xNa	min	0.054	0.201	-	0.821	0.774	0.787	0.799	0.808	-	0.763
	Avg	**0.179**	**0.256**	**-**	**0.838**	**0.830**	**0.834**	**0.829**	**0.829**	**-**	**0.848**
	max	0.263	0.313	-	0.848	0.855	0.861	0.868	0.845	-	0.918

		BIOTITE									
		ALu0304	ALu0306	ALu0601	ALu0603	APi0301	APi0413	APi0601	APi0603	AMo0409	AMo0410
Al	min	1.714	1.620	1.704	1.770	1.643	1.724	1.682	1.683	1.666	1.634
	Avg	**1.752**	**1.658**	**1.737**	**1.807**	**1.707**	**1.760**	**1.768**	**1.718**	**1.714**	**1.738**
	max	1.813	1.699	1.793	1.856	1.747	1.812	1.864	1.769	1.773	1.837
Fe*	min	0.514	0.280	0.414	0.398	0.350	0.348	0.330	0.336	0.429	0.362
	Avg	**0.534**	**0.292**	**0.428**	**0.411**	**0.367**	**0.372**	**0.347**	**0.355**	**0.452**	**0.391**
	max	0.534	0.304	0.445	0.425	0.380	0.412	0.374	0.381	0.487	0.440

		CHLORITE (stable in ALu0306 and APi0601, otherwise retrograde)									
		ALu0304	ALu0306	ALu0601	ALu0603	APi0301	APi0413	APi0601	APi0603	AMo0409	AMo0410
Al	min	-	2.763	2.774	2.828	2.775	2.729	2.833	2.776	-	-
	Avg	**-**	**2.795**	**2.795**	**2.877**	**2.844**	**2.801**	**2.868**	**2.815**	**-**	**-**
	max	-	2.840	2.807	2.941	2.906	2.837	2.929	2.887	-	-
Fe*	min	-	0.255	0.403	0.413	0.369	0.348	0.304	0.313	-	-
	Avg	**-**	**0.258**	**0.423**	**0.428**	**0.379**	**0.379**	**0.315**	**0.361**	**-**	**-**
	max	-	0.261	0.446	0.447	0.393	0.415	0.321	0.389	-	-

Table 4.3: (continued).

		GARNET									
		ALu0304	ALu0306	ALu0601	ALu0603	APi0301	APi0413	APi0601	APi0603	AMo0409	AMo0410
Fe*	**Rim**	**0.894**	**-**	**0.822**	**0.827**	**0.852**	**0.815**	**0.794**	**0.813**	**0.841**	**0.843**
	Core	-	-	0.883	0.878	0.871	0.827	0.842	0.857	0.850	0.922
Alm	**Rim**	**0.697**	**-**	**0.687**	**0.735**	**0.732**	**0.701**	**0.701**	**0.699**	**0.705**	**0.739**
	Core	-	-	0.703	0.722	0.753	0.697	0.709	0.691	0.692	0.542
Sps	**Rim**	**0.035**	**-**	**0.003**	**0.002**	**0.005**	**0.010**	**0.007**	**0.005**	**0.011**	**0.005**
	Core	-	-	0.023	0.027	0.016	0.010	0.013	0.024	0.031	0.230
Prp	**Rim**	**0.082**	**-**	**0.148**	**0.154**	**0.128**	**0.160**	**0.182**	**0.161**	**0.133**	**0.138**
	Core	-	-	0.093	0.100	0.111	0.146	0.133	0.115	0.122	0.046
Grs	**Rim**	**0.185**	**-**	**0.162**	**0.109**	**0.135**	**0.129**	**0.109**	**0.135**	**0.152**	**0.118**
	Core	-	-	0.181	0.151	0.119	0.147	0.144	0.170	0.155	0.182

	PLAGIOCLASE									
	ALu0304	ALu0306	ALu0601	ALu0603	APi0301	APi0413	APi0601	APi0603	AMo0409	AMo0410
xAn min	0.836	0.375	0.296	0.186	0.242	0.191	0.182	0.224	0.343	0.130
Avg 1	**0.863**	**0.376**	**0.309**	**0.192**	**0.254**	**0.223**	**0.210**	**0.235**	**0.371**	**0.133**
Avg 2	**-**	**0.424**	**0.340**	**0.198**	**0.271**	**0.244**	**0.281**	**0.292**	**0.463**	**0.164**
max	0.884	0.434	0.353	0.201	0.272	0.273	0.295	0.300	0.486	0.197

	STAUROLITE									
	ALu0304	ALu0306	ALu0601	ALu0603	APi0301	APi0413	APi0601	APi0603	AMo0409	AMo0410
Fe* min	-	-	0.778	0.756	0.770	0.719	0.754	0.739	0.767	0.769
Avg 1	**-**	**-**	**0.792**	**0.765**	**0.790**	**0.765**	**0.764**	**0.748**	**0.785**	**0.782**
Avg 2	**-**	**-**	**(0.884)**	**0.807**	**-**	**-**	**-**	**-**	**-**	**-**
max	-	-	(0.893)	0.823	0.832	0.769	0.784	0.779	0.799	0.814

	WHOLE ROCK analysis									
	ALu0304	ALu0306	ALu0601	ALu0603	APi0301	APi0413	APi0601	APi0603	AMo0409	AMo0410
Si/Al	-	3.71	1.69	1.14	1.42	-	2.60	1.30	3.02	2.30
Fe*	-	0.28	0.74	0.78	0.75	-	0.40	0.64	0.70	0.79
xCa	-	0.66	0.17	0.15	0.11	-	0.11	0.21	0.06	0.12
xNa	-	0.15	0.22	0.57	0.55	-	0.57	0.59	0.26	0.46
xK	-	0.19	0.61	0.29	0.35	-	0.32	0.19	0.68	0.42

ALu0304	+ ankerite included in garnet (xCa = 0.52, xMg = 0.29, xFe = 0.18)
ALu0306	**+ ankerite stable** (xCa = 0.50-0.52, xMg = 0.39-0.41, xFe = 0.09-0.10)

and paragonite in 1:1 proportion composed the matrix with quartz (Table 4.2). Both white micas forms small flakes of identical crystal-size, reaching 200-300 µm for 20-50 µm thickness, and are intimately associated. However, little biotite is present, probably due to consumption by staurolite-formation reactions.

4.5.1.3) Area (c): South-East Lucomagno

Compared to the Piora samples, MF315 and ALu0603 are nearly identical and stem from the same layer (Table 4.1). They are characteristically richer in muscovite and paragonite (ca. 25 vol-% each) and contain 20 vol-% staurolite and even more in MF315 (40%; Table 4.2). Except the presence of graphite in trace and the local appearance of kyanite in ALu0603, all samples from SE Lucomagno are similar to APi0301. Plagioclase is present in apparent equilibrium with paragonite; kyanite occurs locally in staurolite-poor layers. Sample ALu0601 was collected a

few meters away only and is characterized by the absence of paragonite and an abundance of synkinematic flakes and rare oblique books of muscovite reaching 100-150 (up to 200-300 µm for the oblique books). Garnet and kyanite are later porphyroblasts overgrowing the schistosity. Biotite is scarce in all these samples. During the early decompression near thermal climax, minor garnet resorption is possible and induces the growth of tiny biotite and rarely chlorite (see Chapters 2, 3). However, this effect remains minor in the collected samples.

4.5.1.4) Area (d): Pizzo Molare

Pizzo Molare is the only area, where Al-poor (AMo0409) and Al-richer (AMo0410) metapelites stemming from NPM were collected (Table 4.1; Fig. 4.2). AMo0409 is a homogeneous granolepidoblastic metapelite and contains a typical assemblage of garnet, biotite, muscovite, plagioclase, and quartz. Staurolite is sparse and locally present, either partially included in or near garnet rim. Both micas are synkinematic and grow along the schistosity, reaching 0.2-0.6 mm length for 50-100 µm thickness and even thicker for biotite (up to 300 µm). Garnet forms large blast (1 cm) overgrowing the schistosity. AMo0410 is banded at cm- to dm-scale with biotite-rich layers alternating with garnet-rich. Fine muscovite flakes (100-50 µm) are abundant and coexist with a few oblique books reaching 200-400 µm. Two generations are more clearly identified in biotite: huge flakes reaching mm-size coexists with finer synkinematic or oblique biotite in the matrix. Garnet is most abundant in Mn- and Ca- rich layers and has a porphyroblastic core, which notably includes quartz and margarite (Table 4.2). Kyanite and sparse paragonite are only present in AMo0410, together with rare staurolite.

4.5.1.5) REE minerals

In terms of the REE mineralogy in the studied area, allanite (REE-epidote) and/or monazite ($LREEPO_4$) occur in metapelite and metamarl, as detailed in Janots *et al.* (in press). At greenschist facies, detrital Caledonian and Variscian monazite grains vanish and the first allanite appears, notably in the Urseren-Garvera zone, near Curaglia ($T_{formation}$ 400-450 °C). Near the staurolite and kyanite zone boundaries, the first partial replacement of allanite by monazite is observed in metapelites (APi0413, APi0601, MF315, ALu0603). Monazite appearance is restricted to metapelites with low Ca/Na ratios, containing plagioclase with anorthite-contents <0.18; at more calcic compositions allanite remains stable up to higher temperature (Janots *et al.*, in press). At higher metamorphic grade in metapelites and metamarls, tiny monazite <10 µm are commonly present in the matrix or included in the rim of large biotite (e.g. in AMo0410; 580-600 °C).

4.5.1.6) Mineral chemistry

Characteristic range of composition for minerals and bulk rock samples are summarized in Table 4.3 and a complete set of mineral analysis is available in Appendix 2.1. All micas yield relatively homogeneous chemistry in each sample. Small variation of composition is observed in each thin section, but is independent of the possible textural generation identified (e.g. fine flakes and larger books). We suggest a continuous growth and reequilibration of micas up to the final equilibration that we determined by precise thermobarometry (see below). The celadonite-content in muscovite remains low in all studied samples (usually <0.12 p.f.u. Mg) and is insignificant in Ca- or Na-bearing white micas. This content is slightly variable in all studied metapelites (±0.02 p.f.u. Mg) and is maximum

Table 4.4: Summary of PT- and age-results on pelitic and marly samples from the Mesozoic metasediments of NSB. PT-calculation obtained with TWQ (Berman, 1991), monazite U-Th-Pb ages from Janots *et al.* (in preparation) and Ar-Ar ages for the coarser micas fraction as given in §2.8.3.

			PT-results (TWQ)		Ages Ar-Ar, U-Pb, Th-Pb [Ma]				Age differences		
Area		Sample	P [kbar]	T [°C]	Mineral	Age	2σ	Comment	Mnz-Mica	Ms-Bt	Ms-Pg
Lucomagno	Pass	**ALu0306**	500-560 °C, 6.0-7.5 kbar		Ms*	**18.04**	± 0.80	Ca/K vs age	-	0.39	±0.87 -
		ALu0304 >	***6.2***	± *0.2* ***566*** ± *8*	Bt	**17.65**	± 0.33	Plateau	-	-	-
		MF 161	– No calculation –		Aln	**29.2**	± 1.0	In situ Th-Pb analysis	-	-	-
	South-East	**MF 315**	**6.0**	± 0.4 **549** ± 12	Mnz	**19.1**	± 0.3	In situ U-Pb analysis	Reference for ALu0601, –03		
		ALu0601	**7.3**	± 0.6 **546** ± 22	Ms200	**16.66**	± 0.20	Plateau	2.44	±0.36 -	-
		ALu0603	**8.8**	± 0.6 **577** ± 23	Ms*	**16.34**	± 0.23	Ca/K vs age	2.76	±0.38 -	-0.09 ±0.30
					Pg*	**16.43**	± 0.20	Ca/K vs age	2.67	±0.36 -	-
Piora	East	**APi0301**	**8.3**	± 0.8 **570** ± 28	Ms*	**17.18**	± 0.76	Ca/K vs age	-	-	2.3 ±5.7
					Pg*	**14.9**	± 5.6	Ca/K vs age	-	-	-
	West	**APi0413**	**8.4**	± 0.5 **553** ± 21	Mnz	**18.0**	± 0.3	In situ U-Pb analysis	Reference for APi0601, –03		
					Czo	**18.2**	± 0.7	In situ U-Pb analysis	-	-	-
					Aln	**31.5**	± 1.3	In situ Th-Pb analysis	-	-	-
		APi0601	**9.0**	± 0.5 **585** ± 16	Pg (Ms200)	**16.42**	± 0.88	One large step	1.58	±0.93 1.50	±0.91 -
					Bt200	**14.84**	± 0.23	Plateau, isochemical	3.16	±0.38 -	-
		APi0603	**8.9**	± 0.7 **579** ± 24	Ms*	**15.79**	± 0.11	Ca/K vs age	2.21	±0.32 0.50	±0.27 1.98 ±1.30
					Pg*	**13.81**	± 1.30	Ca/K vs age	4.19	±1.33 -1.48	±1.32 -
					Bt200	**15.29**	± 0.25	Plateau, isochemical	2.71	±0.39 -	-
Pizzo Molare		Chiggiogna, Leventina gneiss			Mnz	**20.6**	± 0.5	*Köppel & Grünenfelder (1975)*	Reference for Leventina gneiss **		
					Ms	**16.1**	± 0.8	*Purdy & Jäger (1976)*	4.5	±0.9 0.4	±1.4 -
					Bt	**15.7**	± 1.2		4.9	±1.3 -	-
		AMo0409	**6.6**	± 0.2 **573** ± 11	Ms	**17.85**	± 0.61	Plateau, isochemical	(2.8)	±0.8 1.60	±1.01 -
					Bt	**16.25**	± 0.81	Plateau, isochemical	-	-	-
		AMo0410	**8.4**	± 0.5 **594** ± 14	Ms*	**18.93**	± 0.83	Ca/K vs age	(1.7)	±1.0 1.75	±0.67 3.8 ±2.4
					Pg*	**13.3**	± 2.3	Ca/K vs age	(7.3)	±2.4 -3.1	±2.3 -
					Bt	**16.37**	± 0.40	Isochemical	(4.2)	±0.6 -	-

(*) implies age extrapolation in Ca/K versus age diagram.
(**) Gneiss sample from Val Leventina is *not* directly comparable to samples from the summit of Pizzo Molare (Mesozoic metasediments, 1.5 km elevation difference).

in AMo0410 (3.05 to 3.15 p.f.u. Si and 0.08 to 0.15 p.f.u. Mg). In agreement with the increasing metamorphic grade calculated between Lucomagno Pass and Pizzo Molare (from ca. 550 °C, 6 kbar to 600 °C, 7-9 kbar), muscovite from our sample collection is progressively enriched in Na and paragonite is K-richer and Ca-poorer. A sluggish variation is also observed between the margarite from Lucomagno Pass and the relic margarite preserved in Pizzo Molare (K- and Ca-poorer, Na-richer).

Biotite from each samples are homogeneous in Al-content and Fe* (= Fe/[Fe+Mg]), ranking from 0.24 to 0.60 in our sample collection (Table 4.3). Only sample AMo0410 shows a larger spreading in AFM diagram (±3% Fe or Mg, ±3% Al). Most of this chemical variation is related to local change in bulk rock composition, which was possibly induced by the growth of numerous and strongly zoned garnets. Late chloritization of biotite is also likely to induce some slight variation of composition. However, chlorite is always stable in a few samples. The Mg-rich bulk composition of ALu0306 accounts for the stability of the biotite-chlorite assemblage. Indeed, the most magnesian biotite and chlorite are found in this sample (0.29 Fe* in biotite; 0.26 in chlorite; Table 4.3). APi0601 is also slightly Mg-richer and 5% chlorite is stable together with biotite (0.35 Fe* in biotite; 0.32 in chlorite; Tables

4.2, 4.3). Fe* of chlorite is slightly lower than Fe* of biotite only in samples where both are stable (ALu0306, APi0601). In contrary, when chlorite is a retrogression product of biotite, Fe* of both minerals is nearly identical or slightly higher (e.g. AMo0410; Table 4.3).

The first plagioclase appears in the northern most samples, both in pelite and calc-schist. These are usually anorthite-poor plagioclase, except in the calcium-richer pelite ALu0304. Only samples APi0601 and –03 present either chemical zonation (APi0601, An-richer core) or different grains of variable chemistry (APi0603; Table 4.3). Plagioclases from all other metapelites are all homogeneous in composition (Table 4.3). Its growth is clearly related to the destabilization of margarite and/or paragonite in pelite. In calc-schist and Ca-rich metapelite, the destabilization of carbonate induces the growth of anorthite-richer plagioclase in ALu0304 (An, while the disappearance of paragonite is suggested to produce an albite-richer plagioclase in ALu0306 (Table 4.3). These metamorphic reactions were described and discussed in §2.9.1.

Garnet is almandine-rich (usually >60%) and records a prograde growth marked by a regular decreasing of spessartine-component and Fe* ratio. A higher grossular component is observed in ALu0304 (Grs_{19}), while it usually remains below around Grs_{10-15} in all other studied metapelite (Table 4.3). A large chemical zonation is only recorded in AMo0410 with a core reaching 25-30% spessartine-component. This PT-path is also confirmed by garnet inclusion, with chloritoid in all staurolite-rich samples and margarite in AMo0410. Staurolites are chemically homogeneous and Fe-rich (0.75 to 0.79 Fe*, Table 4.3), with insignificant Mn- and Zn-content. This chemistry is consistent with a staurolite growth near the thermal maximum.

4.5.2) Overview of PT-results in NSB

PT-condition for each studied sample is summarized in Table 4.4. Reader is referred to §2.7 for an extensive discussion of mineral stability and PT-conditions calculated. From multi-equilibrium thermobarometry (TWQ; Berman, 1988; Berman, 1991) and PT- or P-X(H_2O-CO_2) pseudosections computed with THERIAK-DOMINO (de Capitani, 1994), precise PT-conditions are obtained in each area:

(a) At Lucomagno Pass, PT and T-X(H_2O-CO_2) pseudosections in ALu0306 suggests a stability field for the observed mineral assemblage around 500-560 °C and 6.0-7.5 kbar. Sample ALu0304 is essentially retained for thermobarometry as it yields tightly constrained PT-condition at 566±8 °C and 6.2±0.2 kbar.

(b) In Val Piora, TWQ results determined for all three samples are well constrained around 8-9 kbar and 580 °C. From the computation of garnet isopleths in THERIAK-DOMINO, the small garnet zoning yield a prograde garnet growth between 530-550 °C, 5-6 kbar and 570 °C, 7 kbar, consistent with the final equilibrium-PT calculated with TWQ.

(c) PT-conditions in SE Lucomagno area are very similar to those calculated for samples from Val Piora samples, both in terms of PT-point (TWQ) and PT-path (garnet zoning). However, a set of PT-calculations obtained in all samples from SE Lucomagno yield significantly variable pressure (and temperature), from 8-9 kbar, 570-580 °C down to 6 kbar, 560 °C. This is interpreted as a differential PT-equilibration of these samples around the thermal climax but at variable pressure. This suite of PT-results is thus viewed as a record of an early decompression path of the MAG (see details in §2.7).

(d) The strong garnet zonation in a sample from Pizzo Molare (AMo0410) allows the reconstruction of

a longer prograde path from 450 °C, 4.5 kbar to 570 °C, 7.5 kbar. This sample also yield the highest PT-conditions from our sample collection at 580-590 °C and 8-9 kbar. AMo0409 records the lowest PT-conditions at 6.5 kbar and 570 °C, whereas other samples yield intermediates PT-results. Like in SE Lucomagno area, this is interpreted as part of the decompression path followed by the NPM.

A regular increase in PT-conditions from Lucomagno Pass (550 °C, 6.0 kbar) to Pizzo Molare (590 °C, 8-9 kbar) is thus tightly determined, together with essential information about the prograde and decompression path. Except slightly higher temperature in Pizzo Molare, these PT-paths from SE Lucomagno, Val Piora and Pizzo Molare are nearly identical. Nevertheless, the detailed observation of PT-pseudosections shows that a slight higher T at Pizzo Molare is enough to drive the PT-path outside of the stability field of paragonite during the early decompression.

4.5.3) ^{39}Ar-^{40}Ar micas ages

Successful Ar-dating requires at least 5 to 10 mg of inclusion-free, chemically homogenous micas. Most of the carefully selected samples fulfilled these rigorous selection criteria, but in two samples (samples ALu0601 and –03) the micas contain traces of graphite inclusions. Moreover, this was unfortunately not completely successful in the case of white mica separates containing variable amounts of paragonite or margarite with muscovite (ALu0306, APi0301, APi0601, -03, ALu0603, AMo0410; Fig. 4.3). XRD analysis is used to determine as precisely as possible the amount of each phase composing the mineral separate (Table 4.4) and reveal that the fraction of muscovite is variable from less than 5% to more than 90% in two white mica separates (Table 4.4). Quartz is sometimes also present in significant amount in ALu0306 and in traces in a few other samples. However, this mineral is K- and Ca-free and induces insignificant effect on Ar-release. When abundant in thin section, chlorite is usually easily withdrawn from muscovite. However, due to fine association of micas and chlorite in APi0601, a significant amount of chlorite was exceptionally unavoidable in this white-mica separate, possibly with few biotites (Table 4.3).

As the presence of chlorite in biotite separates may strongly disturb the Ar-release, even causing discordant ages (strong and abnormal age variation), particular care was taken to include at most traces of chlorite in the biotite separates. The amount of chlorite in each biotite separate is very low, with XRD peak ratios for chlorite and biotite indicating around 0.2 to 2.6% (qualitative ratio) of chlorite. However, the most important point is not only to minimize the chlorite-content in each mineral separate, but also to select samples, for which chloritization of biotite is also minimal. In this sense, only biotite from AMo0410 shows a stronger chloritization of biotite, though always sparse and local. Chlorite is present in huge amount in sample and in biotite separates from ALu0306 and APi0601. However, the effect of chlorite on Ar-reservoir of biotite is less likely in such samples, as both minerals are in equilibrium and have conserved their chemical composition at equilibrium-PT (i.e. absence of retrogression).

Ar-Ar results are represented on a map, and the complete data set is depicted in a profile-like sequence as well (Figs. 4.2, 4.3). Table 4.4 listed average ages calculated also indicates, whether the Ar-Ar results yield a plateau-age or an isochemical age (see §2.8 and §2.10). This later implies similar Ca/K and Cl/K yielded by a majority of steps during Ar-Ar analysis, in a range consistent with phase to date. Pure muscovite and biotite separates (even with minor chlorite) usually yield isochemical ages and also a plateau. This is usually not the case with paragonite mixtures.

Muscovite constantly yielded the oldest Ar-ages among all of the micas, reaching 18 Ma at Lucomagno pass, decreasing to 16.5 Ma in the area SE Lucomagno and 16 Ma in Val Piora (see Table 4.4 and Fig. 4.2 for sample

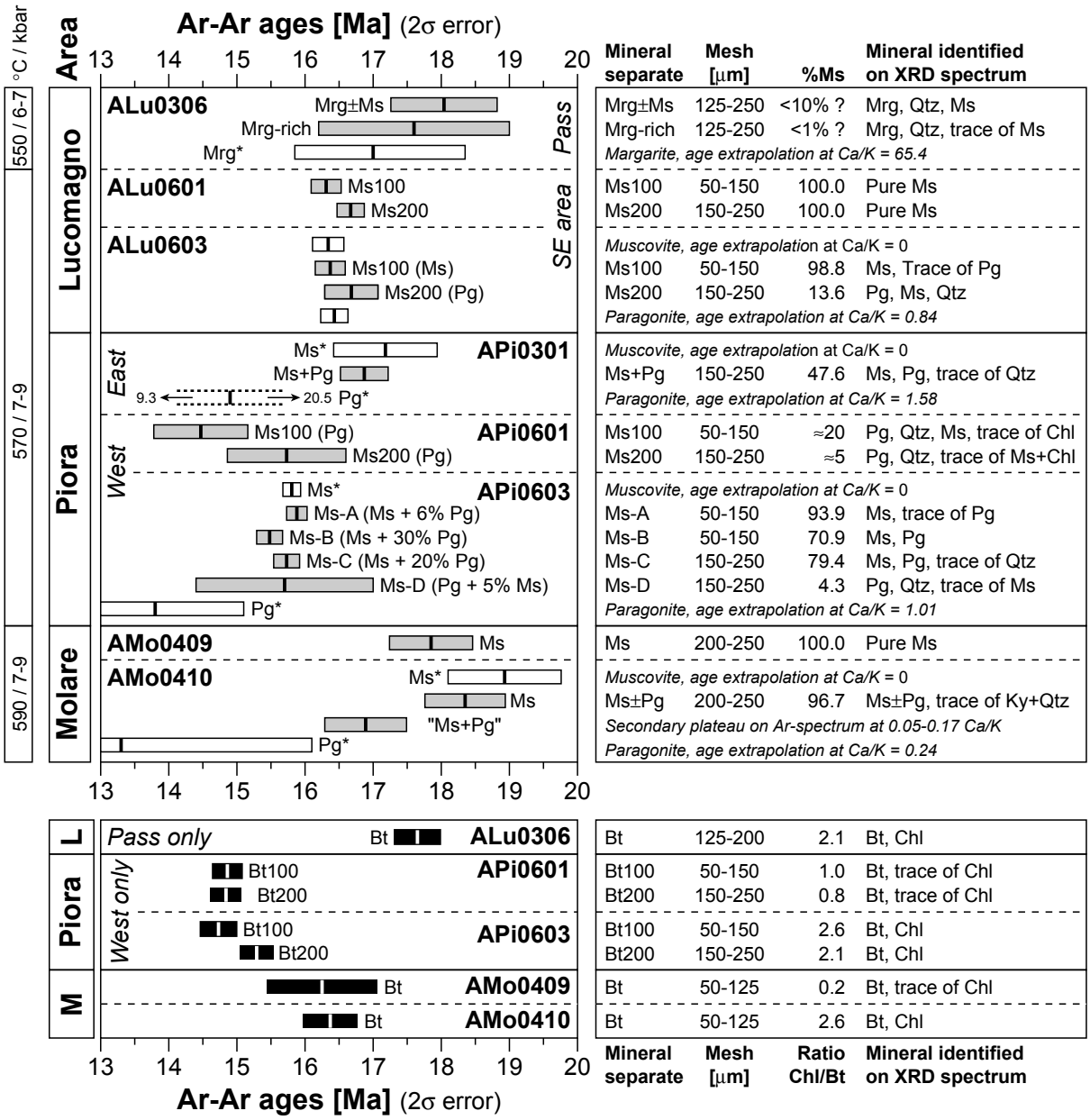

Fig. 4.3: Ar-Ar age results discussed in this paper. Approximate PT-conditions determined for each area in the left border; summary of mineral separates analysed on the right side. The latter contains XRD results, which allow the identification of impurities and estimates of semi-quantitative muscovite/paragonite and qualitative biotite/chlorite abundances (peak ratios of Ms[006] / (Ms[006] + Pg[006]), and of Chl[004] / (Chl[004] + Bt[006]). See §2.8 for details on Ar-Ar analyses.

(*) implies age extrapolation in a Ca/K versus age diagram.

names). At higher grade, around Pizzo Molare, muscovite Ar-ages are older again, around 18 Ma (AMo0409, –10). In samples containing both muscovite and paragonite, Ca/K is variable over the various analysed steps of Ar-analysis, and the age range correlates with the respective amount and composition of each white mica (from ≈0.0 to 0.5-1.5 Ca/K for muscovite with paragonite; >10 with margarite). In samples from SE Lucomagno, the ages remain constant at any Ca/K value, but some paragonite-rich separates from Val Piora (APi0301, APi0603) yield significantly younger ages in steps at higher Ca/K (> 0.2). From electron microprobe analysis, Ca/K in paragonite from Val Piora samples is about 0.8-1.6 and an Ar-Ar age extrapolation toward such value yield ca. 14-15 Ma, which suggests that paragonite is apparently 2 Ma younger than muscovite (Fig. 4.3 and Table 4.4). The effect of paragonite on the Ar-results is even more dramatic for sample of higher metamorphic grade (Pizzo Molare,

AMo0410). Perturbation in the Ar-spectrum marked by younger ages at higher temperature release correlates with higher Ca/K contents (0.10-0.15). We interpreted this as a stronger Ar-release from paragonite at high release temperatures (> 850°C). Extrapolation of the age in a Ca/K diagram indicates only 14.5 Ma for paragonite, which thus appears to be 3.5 Ma younger than muscovite (Fig. 4.3).

In a majority of samples, biotite was present in sufficiently large amounts for analysis. Although XRD spectra reveal the presence of minor amounts chlorite (Fig. 4.3), results of Ar-Ar stepwise heating typically yield isochemical and plateau age. At Lucomagno pass, this biotite Ar-age is 17.5 Ma, only very slightly younger than the muscovite Ar-age. Biotite from two samples of western Val Piora yields plateau ages around 15 Ma. Biotite Ar-ages from Pizzo Molare, like those for muscovite, are significantly older than in Val Piora (Figs. 4.2, 4.3).

4.5.4) U-Th-Pb ages

To assess the potential effectiveness of Ar-diffusion in mica, it is most useful to compare the Ar-ages to more retentive geochronometers, such as U-Th-Pb ages from allanite or monazite, ideally from the same samples. This was possible in a sample from Val Piora and another from SE Lucomagno (Fig. 4.2; Table 4.4; Janots *et al.*, in press). In sample APi0413, Th-Pb measurements on allanite by SHRIMP ion microprobe yielded an age of 31.5±1.3 Ma. U-Pb analyses of monazite from the same sample defined an intercept age on a Tera-Wasserburg diagram of 18.0±0.3 Ma. U-Pb SHRIMP analyses of clinozoisite from the same sample yield an age of 18.2±0.7 Ma, within error of the monazite data. In sample MF315, monazite analyzed by SHRIMP yielded a U-Pb age of 19.1±0.3 Ma with the exclusion of two analyses on a grain preserving an unusual zoning and an apparent older age. Sample MF161 contains allanite, which did not undergo partial prograde replacement by monazite. A Th-Pb age of 29.2±1.0 Ma was obtained from allanite analyzed by SHRIMP. A monazite from the (polymetamorphic) Leventina gneiss yielded a U-Pb age of 20.6±0.5 Ma (Lavorgo-Chiggiogna, ca. 4 km SW of Pizzo Molare; Köppel & Grünenfelder, 1975).

As shown by Janots *et al.* (in press), the preservation of the characteristic textural and chemical zoning of allanite indicates that it did not experience chemical re-equilibration following its prograde formation under greenschist facies conditions between 31.5 and 29.2 Ma. The U-rich clinozoisite rim, which surrounds the allanite core, was dated in sample APi0413 and showed the same age as monazite; this rim is interpreted to have formed or re-equilibrated at the time of allanite breakdown to form monazite (~18 Ma). The textural association of monazite with the highest-grade metamorphic phases, and the absence of monazite in samples below 560 °C indicate that these monazite ages reflect conditions at or close to the thermal peak of metamorphism.

4.6) Discussion

4.6.1) Temperature-time path, petrology and their significance for Ar ages

The U-Th-Pb ages by Janots *et al.* (in preparation) are in conflict with earlier interpretations of Rb-Sr phengite ages, at 35-38 Ma, which were thought to record the metamorphic peak in the northern part of the Lepontine domain (Jäger, 1973; Steck & Hunziker, 1994). Instead, the allanite data suggest that some 30 million years ago the units now comprised within the Northern Steep Belt of the Lepontine Alps were on the prograde path of their metamorphic evolution, near 400-450 °C (allanite formation). The discordance with the Rb-Sr ages may be a result

of disequilibrium in the Rb-Sr isotopic system on the retrograde path, as has been demonstrated in the present area (Fig. 4.1a; Jenkin *et al.*, 2001) and elsewhere in HP to UHP systems (Li *et al.*, 2000; Xie *et al.*, 2004; Jahn *et al.*, 2005). It is also possible that pre-Alpine metamorphic phases remained in the mineral separates used for Rb-Sr dating. In particular, variable amounts of relic muscovite preserved in the core of larger grains would explain the large Rb-Sr age-variation of 5 to 10 Ma observed in muscovite samples (Fig. 4.1a).

As discussed in Proyer (2003), gneissic rocks are more likely to suffer incomplete mineral equilibration compared to metapelite, due to lack of fluids during thermal climax. Moreover, later fluid-percolation may induce a retrogression accompanied notably by chloritization of biotite. Indeed, the presence of sagenite (rutile needles) with some ilmenite in biotite or other secondary phases was already recognized in older Rb-Sr and K-Ar studies (e.g. Jäger, 1962; Arnold & Jäger, 1965; Jäger *et al.*, 1967). Sagenite and ilmenite are clearly related to Ti-exsolution during the chloritization of biotite, plaguing thus the interpretation of these "biotite" separate. By contrast, metapelites may completely preserve the evidence from the climax of metamorphism, as dehydration reactions occur along the prograde path and during early decompression, thus promoting complete equilibration. Following the thermal climax, retrograde reactions are hampered by the dehydrated state, and localized fluid percolation or changes in fluid activity is required to induce partial re-equilibration during decompression or on the retrograde path (e.g. chloritization process, K-feldspar growth in metapelite at T <570 °C, plagioclase or kyanite formation from paragonite and margarite destabilization, etc.).

A detailed examination of the stability and the PT-relation of each phase to date is essential. In this idea, the U-Th-Pb ages by Janots *et al.* (in preparation) for monazite and U-rich clinozoisite represent the best estimate for when the thermal peak of metamorphism was reached in the NSB, i.e. at 18-19 Ma. This recognition has implications for the interpretation of Ar-Ar ages. It is important to recall that muscovite in all of the metapelites selected shows no signs of textural or chemical disequilibrium with other phases from the mineral assemblage. Phase diagrams (e.g. Figs. 2.6, 2.15; many other pseudo-sections on CD) indicate that potassic white mica in these metapelites remained stable along most of the realistically conceivable cooling paths. If minor reactions had occurred upon initial decompression, this should have induced either muscovite resorption (with growth of staurolite or kyanite during decompression; (Nagel *et al.*, 2002b) or overgrowths (K-release from biotite, chloritization, or plagioclase formation from paragonite). The micas analyzed in each sample are chemically uniform, and mica flakes show no chemical zoning. Mica compositions are consistent with the calculated PT-equilibria in these metapelites. Therefore, any difference between the age of the PT-equilibrium determined from monazite dating and the Ar-Ar ages obtained for micas would need to be accounted for as partial Ar-loss from thermally induced volume diffusion (Dodson, 1973).

At the PT-conditions presented here, plagioclase formation by consumption of paragonite was the last dehydration occurring, on decompression or on the earliest retrograde path. According to (Proyer, 2003), this reaction marks the final equilibration of metapelites. Though minor in extent, this reaction may have a strong effect on the Ar-Ar age of paragonite. This age is identical to muscovite Ar-age where both white micas and plagioclase appear to be at equilibrium (e.g. ALu0603). However, at higher grade in Val Piora and more dramatically at Pizzo Molare, paragonite becomes unstable, and its Ar age is lower than the muscovite age. Such mineral reaction processes tend to overwhelm the volume-diffusion effects and render the paragonite age less readily interpretable in the PTt-history we aim to address here (see Chapter 2).

Biotite Ar-Ar ages are consistently younger than the respective muscovite ages (Fig. 4.3; Table 4.4). In the northernmost metamarl from Lucomagno pass, biotite in ALu0306 is clearly richer in Mg than in the other samples. Here Ar-Ar data yield an age-difference <0.5 Ma compared to muscovite. At slightly higher grade in Val Piora (APi0601, –03; 560-580 °C), this difference remains low at around 0.5-1.5 Ma, while it increases to 1.5-2.0 Ma at Pizzo Molare (AMo0409, –10; 580-600 °C; Table 4.4). A similar age differences is observed at Alpe Devero

(600 °C, 8-10 kbar; some 20 km WSW of Val Piora), with pure muscovite separates yielding an Ar-Ar isochemical age of 14.83±0.10 Ma compared with the 13.12±0.22 and 13.09±0.26 Ma obtained on two chlorite-poor biotite separates of different grain-size (Appendix 4.1).

To assess the potential significance of these age differences, several processes are considered: Biotite is commonly affected by local chloritization. Very minor chloritization is difficult to rule out completely, but apart from optics and XRD, EMP-analyses of biotite are a sensitive test, with deficiencies in the total alkalies (K+Na±Ba±Rb) indicating partial chloritization in biotite. In the present samples biotite analyses (Table 4.3; §2.6) show total (K+Na)-values between 0.886 and 0.980 p.f.u. and suggest thus a significant presence of vacancies in this large cationic interlayer sheet (i.e. chloritization). (K+Na)-values higher than 0.95 is restricted to samples ALu0306 and AMo0409, while it is below 0.90 in ALu0603 and APi0603. For comparison, muscovite shows the same trend with ca. 0.88 in ALu0603 and APi0603 against 0.95, 0.99 and 1.00 in ALu0306, APi0301 and AMo0409. This trend is again observed in coexisting paragonite. The presence of 5 to 10% "vacancies" in (K+Na)-interlayer of micas seems to stronger affect a few specific samples (e.g. ALu0601, –03 and APi0603), but they remains usually lower in muscovite than in biotite, sometimes reaching a nearly perfect stoichiometry (e.g. APi0301, AMo0409). Indeed, these samples yield a well-defined plateau age, though that somewhat disturbed by paragonite in APi0301 (heterochemical steps, sluggish Ca/K versus age trend).

The omnipresence of chlorite in our suite of samples is clearly due to the vicinity of the chlorite-stability field at T < 550°C, which is rapidly crossed during the decompression and retrograde path of all studied samples (§2.9.2 and Fig. 2.15). It is also clear that chloritization may enhance Ar loss, either through biotite recrystallization upon chlorite formation or through Ar recoil during sample irradiation (Onstott *et al.*, 1995; Di Vincenzo *et al.*, 2003). This is worst if the incorporation of Ti^{4+} from our biotite (0.06 to 0.10 p.f.u.) is accommodated by a vacancy in octahedral site. Though this cannot explain the low (Na+K)-values, the presence of vacancies in all crystallographic site (except perhaps tetrahedral) will strongly enhance volume-diffusion process. The interpretation of Ar-Ar ages depends on these possibilities. Notably, the age difference may reflect

(a) the time elapsed between closure of Ar-diffusion in muscovite and biotite (diffusional loss only);

(b) the time elapsed between Ar-closure of muscovite (diffusion) and chloritization of biotite (partial recrystallization);

(c) a geologically meaningless interval, owing to a strong recoil effect or a combination of cases (a) and (b).

Case (a) is the commonly accepted explanation and, whatever calibration is used, the difference between closure temperatures for muscovite and biotite is about 50 °C. When the temperature reached by a sample is below the closure temperature for biotite (450 °C; Villa & Puxeddu, 1994), similar ages are expected for both micas. At higher grade, the difference between Ar-Ar ages for the two micas increases up to the closure temperature for muscovite (e.g. Hammerschmidt & Frank, 1991: 500 °C). This age difference remains nearly identical in a sample reaching any thermal climax exceeding the closure temperature for muscovite. The difference between Ar-Ar ages for muscovite and biotite in the NSB increases significantly between 540 and 580 °C (from Lucomagno path to Molare; Fig. 4.3). This is consistent with a closure temperature of muscovite Ar-Ar isotope system around 500-550 °C. This value may be slightly high, as the biotite from the Lucomagno sample is clearly Mg-richer and thus is expected to have a higher closure temperature than biotite from Val Piora or Pizzo Molare (Dahl, 1996).

Concerning cases (b) and (c), partial to total resetting of the Ar-signature in biotite may occur over a large temperature-time window, as chlorite has a stability field in metapelites from near 500-550 °C right up to ambient temperatures. Ages of appreciably chloritized biotite are geologically more or less meaningless. Biotite

separates analyzed in this study essentially depicted large and pristine domains at micro-scale (BSE imaging by EMP), with only minor chlorite revealed by XRD (Table 4.4). Biotite is appreciably chloritized in only one sample (AMo0410); hence, its Ar-spectrum does present large and abnormal variations in age. Both Ca/K and Cl/K in this biotite separate are variable, though uncorrelated. Nevertheless, two steps at low Ca/K and Cl/K are interpreted to represent the Ar-signature of pristine biotite domain, and these two steps are, within error, identical in age to biotite from AMo0409. The precise effects of recoil (case c) are unknown and would require a detailed investigation at the nanometre-scale (TEM, Di Vincenzo *et al.*, 2003; Viti *et al.*, 2004). As only traces of chlorite are present in each separate, case (c) is unlikely to have significantly affected the present age data.

In a regional context, the U-Th-Pb ages and the Ar-Ar data can be assessed also in relation to thermochronological data, notably FT for zircon and apatite. The thermometric and geochronological data available are compared in a temperature-time diagram (Fig. 4.4). The first Tt-point recorded is from allanite growth in metapelites at 31-29 Ma along their prograde path (450 °C; point A on Fig. 4.4). The thermal peak of metamorphism is rather well defined by monazite and clinozoisite growth (point B). The data impliy an average thermal gradient of ca. 8-10 °/Ma for the prograde path between allanite and monazite crystallization (Janots *et al.*, in preparation; path A-B). In order to reconstruct the cooling path, FT data are used. Two paths are shown, based on two zircon FT ages at 14-12 Ma or 9 Ma (Fig. 4.4; point C1; Steiner, 1984; Hurford, 1986) or point C2 (Janots *et al.*, in preparation). Apatite FT ages of 8-6 Ma complete the Tt-cooling history to ca. 120 °C (Fig. 4.4; point D; Schaer *et al.*, 1975; Wagner *et al.*, 1977; Steiner, 1984; Hurford, 1986; Michalski & Soom, 1990; Rahn, 2005).

The impact Ar-data for micas have on the Tt-path is sensitive to the closure temperatures accepted. If relatively low Dodson-type closure temperatures (350 for muscovite and 300 °C for biotite; Armstrong *et al.*, 1966; Purdy & Jäger, 1976), are assumed the Tt-path appear unrealistic (Fig. 4.4, model A): Rapid initial cooling shortly after the thermal climax is followed by a nearly adiabatic decompression or a constant PT-condition around 300 °C from 16 to 10 Ma, and then again by rapid cooling to surface temperatures. The sphene age at 15.2 Ma obtained in a vein from Lucomagno gneiss support this model, as the titanite was believed to have grown at ca. 270 °C (Sharp *et al.*, 2005). A very different evolution emerges if Ar-Ar closure temperatures at 500 °C for muscovite and 450 °C for biotite are assumed (Hammerschmidt & Frank, 1991; Villa & Puxeddu, 1994; Villa, 1998b; Di Vincenzo *et al.*, 2004): A more regular T-t relation is inferred, with increasing cooling rates from <10 °/Ma around 550-500 °C to 65 or even 90 °/Ma approaching the zircon FT data (at C1 or C2, respectively; Fig. 4.4). Models B or C are both consistent with a closure temperature for Ar volume-diffusion in muscovite and biotite around 450-500 °C and 400-450 °C, respectively. In view of the nearly similar age obtained for muscovite and Mg-rich biotite of Lucomagno pass (Figs. 4.2 and 4.3), a Dodson-type closure temperature of 500 °C is suggested for Mg-rich biotite. This is consistent with the expected lower ionic porosity and the related higher Ar retention properties of phlogopite compared to annite (Dahl, 1996).

Although the relation between time and exhumation relations (Pt-path) is poorly constrained for much of the retrograde path, the PT path for the early decompression is known and implies a slow cooling gradient of 10-20 °/kbar, followed by cooling at P<6 kbar (§2.9.2). The timing of this decompression is currently unknown, but exhumation rates can be indirectly evaluated. Equilibrium-PT is dated by monazite at 18 to 19 Ma in Piora and Lucomagno areas, respectively. Considering an equilibrium-P at T_{max} of 7 to 9 kbar (19 to 24 km depth; Table 4.4), an average exhumation rate of 1.00-1.06 to 1.28-1.35 mm/y is obtained. Such value is in agreement with the highest current uplift rate in the Central Alps (0.7 to 1.1 mm/y between Gotthard and SSB; Schlatter *et al.*, 2005), as also with the exhumation rate in the Late Miocene to Pliocene in the Aar massive (0.8-1.0 mm/a; Pfiffner *et al.*, 1997). The dependency of elevation and apatite-FT ages provides further information regarding the average exhumation rate for the last 6-10 Ma. This is estimated at 0.4-0.8 mm/y in the Gotthard nappe (Schaer *et al.*, 1975; Michalski & Soom, 1990). Assuming a similar exhumation rate for the metasediments from the NSB and

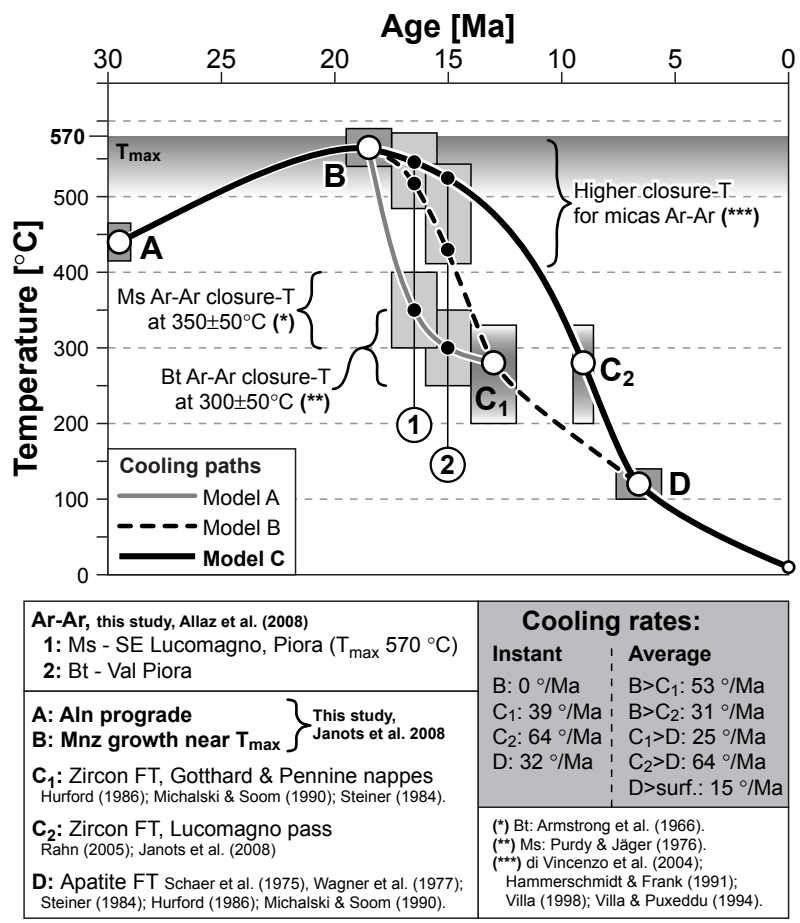

Fig. 4.4: Temperature-time relation in metapelite samples from West Val Piora and SE Lucomagno. Allanite and monazite yield crystallization ages along the prograde path and near the thermal peak, respectively. Three models are distinguished to account for the possible range for closure temperatures of Ar-Ar in micas and the diverse zircon FT ages obtained in the studied area. Models B and C are preferred. See text for discussion.

bearing in mind the average of 1.0-1.4 mm/y calculated from equilibrium-PT, a higher averaged exhumation-rate is inferred for the period between 20 and 10 Ma (>1.4 mm/y), presumably during the nearly adiabatic decompression. An enhanced erosion (and exhumation) rate is also suggested for Miocene time by Schlunegger & Willett (1999), which propose values around 0.4 to 0.5 mm/a in the frontal part of the Alps and below 0.3 for the rear part. However, they consider an older peak of metamorphism at about 35-25 Ma. Therefore, these results yield minimal values for erosion and exhumation rate, if we consider the younger peak of metamorphism determined from monazite dating in the NSB.

A more rapid cooling between 30 and 60 °/Ma and after 15 Ma is suggested from both models B and C. Providing a rapid exhumation accompanying or following the PT-equilibration (i.e. rapid formation of the Lepontine dome), isotherms might have been compressed, increasing thus locally the geothermal gradient. Due to this increasing ΔT and the rapid uplift of "hot" rocks in a colder environment, a rapid cooling is suggested to follow this stage, explaining thus the higher cooling previous to 300 °C. However, in absence of good PT-constraints on pressure along decompression and retrogression, this remains purely hypothetic. New analogue or digital models taking into account of the new timing of alpine metamorphism would possibly give a way to test the precise thermal and exhumation evolution of Mesozoic metasediments in the NSB.

4.6.2) P-T-t evolution and geodynamic consequences

On the basis of the interpretation of geochronological data given, the temperature-time evolution, and the constraints derived from PT paths in the northern Lepontine shed new light on the geodynamic evolution of the Central Alps.

To show small-scale variations, the data are first summarized in a geological section across the area studied; in a second part these considerations are extended to larger scale.

Figure 4.4 compares monazite U-Pb and mica Ar-Ar ages along two parallel N-S geological profiles (Probst, 1980). The first section crosses Lucomagno pass and the area SE and it ends near Pizzo Molare. The second profile is situated 15 km further W, it crosscuts Val Piora near Airolo and ends at Gotthard pass. Sample positions are projected to the respective profiles (max. 5 km), following the fold axes of late NSB-folds crossing the Val Piora and Lucomagno areas (Maxelon & Mancktelow, 2005 and references therein). Data along both profiles show the following trends: Muscovite Ar-Ar ages decrease from Lucomagno pass, Val Piora and the area SE Lucomagno, from 18 Ma down to 17 and 16.5-15.5 Ma, while the PT condition increase from 550-560 °C, 6-7 kbar up to 570-580 °C, 7-9 kbar. Where monazite ages and Ar-Ar ages pertain to the same samples the monazite age is 1.6±0.9 to 2.7±0.4 Ma higher than the muscovite age (West Val Piora and SE Lucomagno; Table 4.4).

Comparisons of the new Ar-ages near Pizzo Molare with the monazite data from Köppel & Grünenfelder (1975) are more difficult to make, as the former samples stem from the NPM, the latter from the (polymetamorphic) Leventina gneiss. K-Ar ages for micas from the latter unit were given by Purdy & Jäger (1976) as 16.1 Ma for muscovite, 15.7 Ma for biotite; monazite age from the similar sample gave 20.6 Ma (Köppel & Grünenfelder, 1975). Our sample from Pizzo Molare was taken at an elevation 1500 m above from the monazite sample and our Ar-ages yield an average of 18.4±1.0 Ma for muscovite, 16.3±0.9 Ma for biotite (Table 4.4). The K-Ar data for micas from Chiggiogna by Purdy & Jäger (1976) are from the same unit (Leventina gneiss) as the monazite data, and in this case the age differences are larger than in Val Piora and SE Lucomagno areas, though more uncertain: 4.5±0.9 Ma (Ms) and 4.9±1.3 Ma (Bt).

Comparing now K-Ar ages from Val Leventina and Ar-Ar age from Pizzo Molare, difference of muscovite ages between is >1.5 Ma; for biotite the difference is within error (0.5±1.3 Ma). In absence of late tectonic feature affecting the distance between both localities, the age difference between muscovite from Val Leventina and Molare can be easily accommodated, assuming an exhumation rate around 1 mm/a (likely in this area, see above) and the distance separating both localities (1.5 km). Moreover, considering a normal geothermal gradient of 30 °/km, Leventina gneiss could be 50 ° hotter, increasing again the age difference (longer time gap between peak of metamorphism and closure of muscovite K-Ar). If diffusion also controls the closure of Ar-Ar in both micas in this area, a similar age difference is expected for biotite. However, biotite age from Leventina gneiss is only 0.7±1.3 Ma younger than biotite from Pizzo Molare, which is statistically undistinguishable. In absence of modern petrological and thermobarometrical study on sample from Leventina gneiss, this discrepancy remains an opened question for biotite.

Between Lucomagno and Val Piora, the younger muscovite ages southwards is explained by an increase of temperature and a higher ΔT between the peak of metamorphism and the closure-temperature of muscovite Ar-Ar. However, micas ages are suddenly older in both samples at Pizzo Molare (Fig. 4.5). The same trend is observed in biotite, though that the older age at Lucomagno Pass is most likely resulting from a higher Ar-retention enhanced by Mg-rich character of this biotite and the absence of late chloritization. Even if all metasediments follow a broadly similar PT-path with slightly higher T at Pizzo Molare (ca. +20°), a small difference in the timing of these PT-paths accounts for the older ages at Pizzo Molare. This suggest that Mesozoic metasediments from Lucomagno-Piora or Molare are two distinct tectonic unit following slightly different PT-*time* path; while samples at Lucomagno-Piora equilibrates around 18-19 Ma and 570 °C, samples from Pizzo Molare are already along the decompression pass (i.e. peak of metamorphism at 590 °C is >20 Ma). Considering a simple diffusion-control of muscovite Ar-ages, this hypothesis suggest an earlier cooling at 500 °C in Pizzo Molare area compared to Lucomagno-Piora. This is supported by the monazite U-Pb ages pattern observed in the Central Alps, which depicted older ages southwards (Köppel & Grünenfelder, 1975; Engi *et al.*, 1995).

At the scale of a N-S cross-section in the Central Alps (Fig. 4.6), the implications of our thermobarometric and geochronological results is best discussed with reference to tectonic reconstruction adapted from the transect in the eastern Central Alps as depicted by Schmid *et al.* (1996). Their tectonic scheme is adapted to the present profile, from Disentis-Curaglia (Urseren-Garvera zone), across the Sub-pennine nappe stack to Bellinzona (SSB) and passing through the Piora-Lucomagno-Molare area (NSB; Fig. 4.6a profile A-B). The reconstructions in Figures 6b-f aim to illustrate the geodynamics in the NSB in particular, where our geochronological and thermobarometric results apply and extend controversially interpreted previous data. This reconstruction is thus accompanied by a reconstruction of P-T-t path (Fig. 4.7). Following Berger *et al.* (2005), three continental and two oceanic domains are distinguished during the Cretaceous. Their tectonic equivalents are identified (Fig. 4.6b), from North to South: European margin, Valaisan, Briançonnais, Piedmont-Liguria, and Adriatic margin (see introduction).

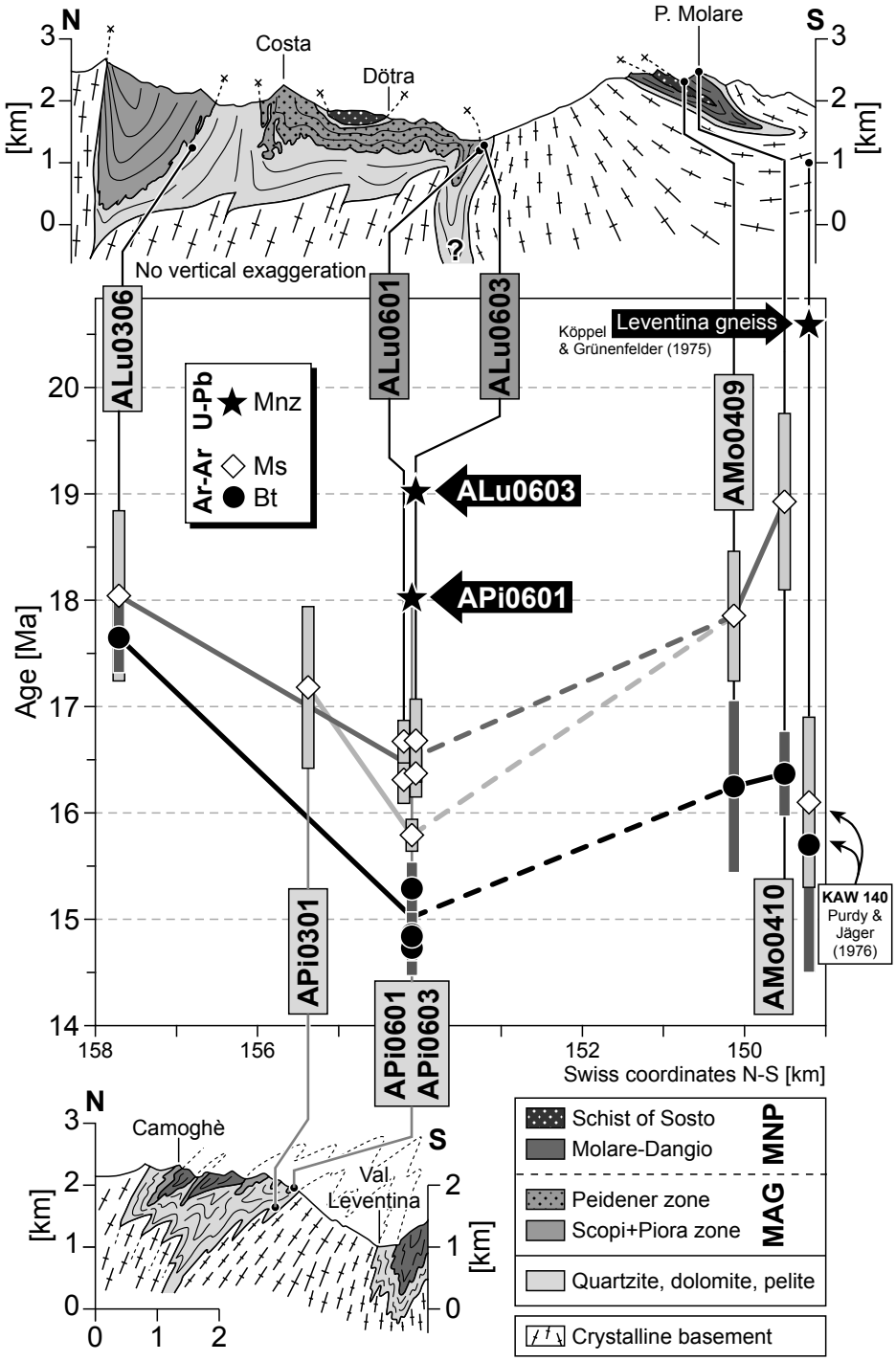

Fig. 4.5: Ar-Ar and U-Th-Pb ages related to tectonic units along two cross-sections (redrawn after Probst, 1980). The two N-S profiles are along the 695 and 710 Swiss coordinates, which broadly correspond to the Val Piora and Lucomagno-Molare areas, respectively (see Fig. 4.2). Ar-Ar results are given with a 2σ error. For comparison, data for the Leventina gneiss sample is also given (Köppel & Grünenfelder, 1975; Purdy & Jäger, 1976). From N to S, the age differences between muscovite and biotite and between muscovite and monazite both increase along this profile. Ar-ages of white micas and biotite initially decrease, but they are distinctly older again at Pizzo Molare. This break between SE Lucomagno and Molare is most likely related to an older and somewhat hotter climax of metamorphism southwards (>20 Ma, 590 °C) compared to Lucomagno-Piora (18-19 Ma, 570 °C). The difference in tectonic origin of each unit (MAG and NPM) is susceptible to accommodate this difference. See text for further explanation.

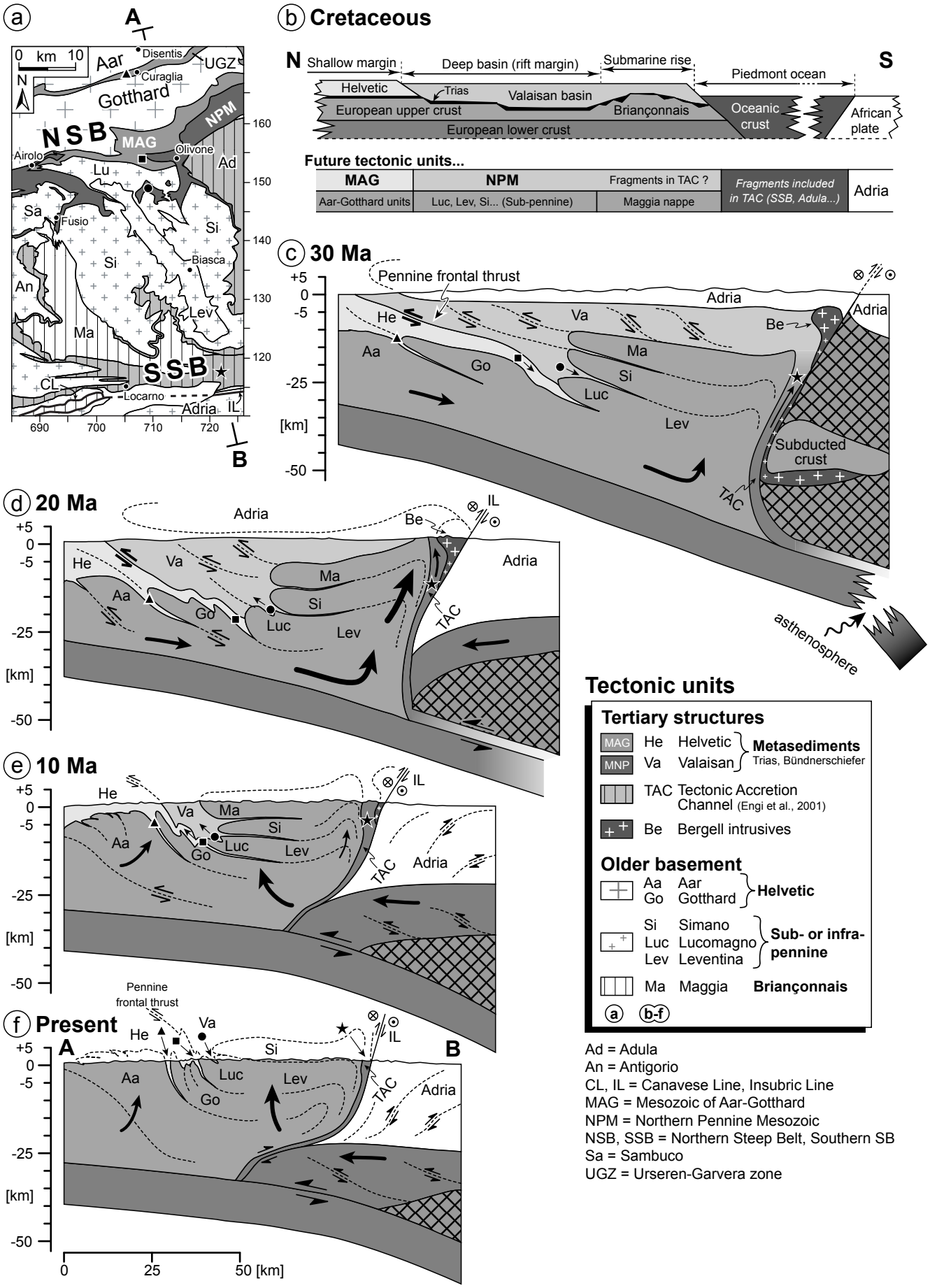

Ad = Adula
An = Antigorio
CL, IL = Canavese Line, Insubric Line
MAG = Mesozoic of Aar-Gotthard
NPM = Northern Pennine Mesozoic
NSB, SSB = Northern Steep Belt, Southern SB
Sa = Sambuco
UGZ = Urseren-Garvera zone

Fig. 4.6: (a) Tectonic overview of the Central Alps showing the major tectonic structures discussed in the following (adapted from Probst, 1980; Berger *et al.*, 2005; Spicher, 2005). **(b-f)** Palinspastic reconstruction along a NNW-SSE profile, from Andermatt-Disentis to Locarno-Bellinzona, which corresponds to the profile A-B located in (a). This schematic reconstruction was adapted from Schmid *et al.* (1996); it schematically summarizes the evolution of Mesozoic metasediments from the NSB (square = Piora-Lucomagno; circle = Molare). A comparison is made with other Mesozoic metasediments from the Central Alps situated northwards and southwards (triangle = Urseren-Garvera zone; star = SSB along the Insubric line). **(b)** Paleogeographic domains prior to the Alpine collision (around Cretaceous). **(c-f)** Reconstruction at 30, 20 and 10 Ma constrained by the new age and PT-results. According to the present position of Bergell and Adamello intrusives, the slab break-off shown in (c) might actually be located further south in a deeper environment. See text for discussion.

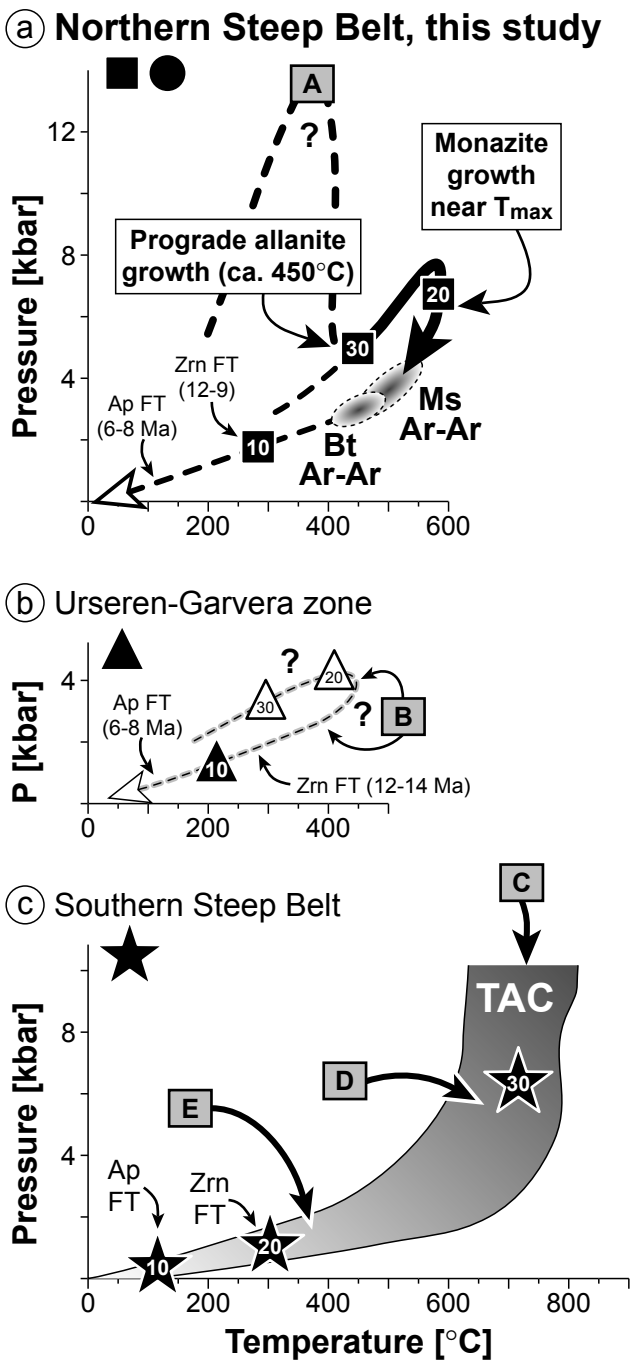

Fig. 4.7: (a) PTt-path for Mesozoic metasediments from NSB based on age and PT-results determined in Piora, Lucomagno and Molare areas. The PTt-path is constrained by thermobarometry on mineral assemblages and garnet zoning, as discussed in the text. These results are strictly valid only for Val Piora and the Lucomagno area; temperature 10-20° higher must be considered for Molare area. The three stages at 30, 20 and 10 Ma depicted in Figure 4.6c-e are represented along the PT-path, using square symbols. This PTt-path is compared to the PTt-path for **(b)** Garvera and **(c)** SSB. Those latter two are constrained by data from the literature (see text).

From the literature:

- **A** — **Unknown age:** Carpholite relic in Qtz-Cc veins (350-400 °C, 11-13 kbar; Bousquet et al. 2002, Wiederkehr et al., in press)
- **B** — **16.4 Ma:** Illite K-Ar (Hunziker et al., 1986)
- **C** — **>70 to 36 Ma:** Eclogite facies, 20-35 kbar, 600-850 °C (Brouwer et al., 2005)
- **D** — **32-28 Ma:** Bergell intrusives (Oberli et al., 2004)
  30-27 Ma: Mnz, Xt (SSB; Köppel & Grünenfelder, 1975)
- **E** — **21-20 Ma:** Ms,Bt K-Ar (Hurford, 1986)

Details on each domains have been recently reviewed by Schmid *et al.* (2004) and Berger *et al.* (2005). For the present purpose, we first consider the evolution of samples from four typical localities of Mesozoic metasediments, which corresponds to four typical domains depicted by symbols in Figures 4.6 and 4.7:

1) A first locality is chosen within the European domain, from a shallow sedimentary domain, which remains at low pressures during convergence and Alpine metamorphism (< 4-6 kbar). This area corresponds to the current Urseren-Garvera zone, which is jammed between Aar massif and the front of the Gotthard nappe (Disentis-Curaglia; triangle in Figs. 4.6c-f, 4.7b).

2) The second locality reflects the southern part of European domain. Mesozoic samples from this area correspond to the present MAG, e.g. in Val Piora and in the Lucomagno area (square; Figs. 4.6c-f, 4.7a).

3) The third locality is situated near the northern flank of Valaisan basin, e.g. in the present NPM of Pizzo Molare (circle; Figs. 4.6c-f). The Pennine frontal thrust crosscuts this area, and some units from this domain may have been subducted more deeply than other localities (Wiederkehr *et al.*, submitted); Fig. 4.7a). Nevertheless, at the scale of the present reconstruction, the PT-history from the later parts of the prograde path onward is probably very similar in the Lucomagno-Piora and Molare areas. The PTt-history for those two localities (Fig. 4.7a) will thus be discussed together.

4) The forth locality we briefly discuss for comparison corresponds to the SSB (Fig. 4.6a). The SSB is part of a tectonic mélange zone, which has been attributed to the tectonic accretion channel (TAC; Engi *et al.*, 2001) formed near the plate margin, during the subduction of oceanic and continental units. Fragments of metasediments from the Valaisan and Briançonnais domain were incorporated with pieces of gneissic basements, mafic bodies and ultramafic lenses from the Piedmont-Ligurian and possibly the Valaisan oceans. Eclogite fragments formed within the TAC and tectonically extruded following slab-breakoff have been investigated by Brouwer *et al.* (2005) and the reader is referred to these studies. Eclogite fragments within the TAC experienced a range of different PT-paths, some cooling-down at 500 °C, some remaining at 600-700 °C, prior to orogenic emplacement in the Alpine nappe stack and the subsequent Barrovian overprint (star; Figs. 6c-f, 7c).

In detail, the link between the PTt-paths constrained in each of these four localities (Figs. 4.1, 4.3) and the large-scale Alpine geodynamics would require consideration of the structural evolution the Central Alps, especially the NSB and surrounding areas (Sibbald, 1971; Milnes, 1974; Leu, 1986; Steck & Hunziker, 1994; Maxelon & Mancktelow, 2005), which is beyond the scope of this discussion. Nappe stacking occurred during the early prograde metamorphism, and no prior information on the PTt-evolution is available for the NSB. Nappe stacking is schematically depicted in the first reconstruction, at 30 Ma, after which time metamorphic and geochronological data can be integrated (Fig. 4.6c).

Up to that stage, European metasediments has apparently followed a regular increase of PT-conditions up to the start of garnet growth (450-550 °C, 4-6 kbar). In Valaisan metasediments, carpholite relics indicate a PT-path through the blueschist facies. Such relics in the Sosto Bündnerschiefer and Grava nappe yield PT-conditions of 350-400 °C and 11-13 kbar (Wiederkehr *et al.*, submitted); Fig. 4.7a). In the area of the present profile, only a few slices in the Pizzo Molare area may have followed such a HP-LT evolution. Already during the late prograde path, the early garnet growth in some metapelites from the summit of Pizzo Molare and the presence of margarite in the core of these require a medium-pressure prograde PT-path, i.e. Barrovian conditions of 4-6 kbar and 450 °C (see also Wiederkehr *et al.*, submitted).

Leaving aside the minor local units that witnessed a HP/LT metamorphic stage, our results constrain a

prograde stage near 30 Ma (Fig. 4.6c), marked in the NSB by the prograde growth of allanite ($T_{formation}$ 400-450 °C; U-Th age 31-29 Ma; Fig. 4.7a). The slope of the subsequent PT-segment is recorded by growth-zoning in garnet, notably in the Pizzo Molare area. Here garnet zoning is impressive and corresponds to the most extensive segment of the PT-path recorded in the sample collection (from 460 °C, 4 kbar to 550-570 °C, 6-7 kbar). At Piora and Lucomagno, garnet yields similar PT-condition, but records a smaller PT-interval of growth at T >500 °C and 6-7 kbar. Allanite being included in garnet, its growth must predate garnet growth, already at P <4-6 kbar (Fig. 4.7a).

In samples from the Urseren-Garvera zone, PT-conditions of the thermal climax were determined around 400-450 °C and 4-5 kbar from graphite crystallinity and fluid inclusion data (Frey & Ferreiro Mählmann, 1999; Janots *et al.*, in press). Direct time information is missing. Only a minimum age for the Alpine metamorphism could be inferred from the youngest Rb-Sr ages on biotite around 22 Ma, which had previously been interpreted as cooling-ages (Jäger, 1962; Arnold & Jäger, 1965; Siegenthaler, 1984). This interpretation stands on uncertain ground, given the large age variation (21.7 to 266 Ma), which most likely pertains to incomplete mineral resetting during Alpine metamorphism (Variscan inheritance).

At the northern margin of the SSB (Castione, NE of Bellinzona) garnet growth in metaclastics was dated by Sm-Nd at 26.7±1.7 Ma (Vance & O'Nions, 1992). Within the SSB, Alpine monazite attributed to this metamorphic stage yielded ages between 27 and 30 Ma (Köppel & Grünenfelder, 1975; Fig. 4.7c). In the SSB, the 30 Ma stage is marked by the Bergell intrusive suite, which intruded the southernmost part of the belt and crystallized between 32-28 Ma (Oberli *et al.*, 2004; Fig. 4.6c). At that stage, elements from the TAC were recording part of their emplacement history, which is summarized in Figure 4.7c (compiled from various PT-paths in the SSB; Brouwer *et al.*, 2005). Comparing the two ends of the profile A-B (Fig.6), exhumation of the TAC units containing eclogite fragments had already started at ca. 40-35 Ma in the southern area, while the northern Mesozoic metasediment still were on the prograde path.

Between 30 and 20 Ma, thrust sheets developed in metasediments of the NSB (Fig. 4.6c,d), duplicating the sedimentary sequence. During that time interval, thrusting is thought to account for the pressure increase of ca. 2-4 kbar in samples from the Piora-Lucomagno and Pizzo Molare areas. The main schistosity was formed then, towards the end of nappe stacking. Amphibolite-facies porphyroblasts (garnet, staurolite, kyanite) essentially overgrew that schistosity, though some growth occurred synchronous with the deformation. Notably, garnet started growing synkinematically in respect to the late deformation (folding) in some samples. Whereas garnet and plagioclase sometimes recorded prograde zoning, micas are homogeneous and may thus have constantly re-equilibrated until the final preserved PT-equilibration stage. PT-results from the isopleths of garnet rims are merged with the final PT-equilibration determined with TWQ. Lower pressure determined in a few samples within each selected areas suggested that rocks reached P_{max} and then rapidly underwent decompression from 9-8 to 6 kbar (§2.9.2).

Considering the repartition of equilibrium-PT over the Central Alps (Todd & Engi, 1997) and the crystallization-deformation relations, the thermal peak of metamorphism dated at 20 Ma post-dates the nappe emplacement and occurs during the early crenulation (late-folding). The exhumation accompanying this thermal climax (decompression path) is associated to back-folding stage in NSB and must thus have occurred near or just before 20 Ma. Equilibrium between the major rock-forming minerals is well constrained around 560-580 °C and 7-9 kbar at Piora-Lucomagno (19-24 km depth) and ca. 10-20 °C more at Pizzo Molare. From monazite U-Pb ages in samples from Piora and Lucomagno, this stage was reached at around 18-19 Ma (Fig. 4.7a). PT-variation between 30 and 20 Ma implies a heating rate of ca. 10 °/Ma (Janots *et al.*, in preparation). In the meantime, samples from SSB were rapidly cooled to ca. 280 °C (Fig. 4.7c), as indicated by zircon FT at 19 Ma (Hurford, 1986). Following intrusion of the Bergell suite, this exhumation was accelerated by back-thrusting and continuing indentation of the Adriatic lower plate into the European basement, as attested by movement along the Insubric line (Fig. 4.6d).

Finally, the onset of backfolding in NSB is active between 20 and 10 Ma. This phase is responsible for the vertical structures found in the northern and southern Central Alps (NSB and SSB; Milnes, 1974). This stage was previously proposed to start around 32 near the Insubric line and regularly propagates towards the Helvetic nappes up to 19 Ma (Schmid *et al.*, 1996). This corresponds to the extremely high exhumation rate determined in the Bergell area (up to 5 mm/a; Giger & Hurford, 1989) and later in the NSB. However, these results were again based on the older and erroneous idea of a thermal peak of metamorphism at 38 Ma in the Central Alps. The concomitant rapid exhumation during the early decompression is probably related to tectonic responds of the Adria indentation, which push-up the European upper crust and involves back folding to accommodate this compression (Fig. 4.6d,e; Schmid *et al.*, 1996). This stage is followed by a regular exhumation and cooling of rocks from 300 °C (10 Ma; Fig. 4.6d) up to the surface (present; Fig. 4.6e), as suggested from zircon and apatite FT dating, closing those the PTt-loop of samples presently found in the Central Alps.

4.7) Conclusions

We argue that inheritance problems affected the polymetamorphic (gneiss) samples from the NSB and the areas of lower metamorphic grade. This has plagued the interpretation of the timing of the Alpine collision in the Central Alps, and the problem has also overshadowed the determination of diffusion-related closure temperatures of the Rb-Sr and K-Ar isotopic systems in micas. Available Rb-Sr ages depict a complex variation inside gneissic basement units, while K-Ar ages on micas were apparently totally reset during the Alpine cycle, and formation or cooling-ages may be inferred.

The use of retentive isotopic systems such as U-Pb on monazite and Th-Pb on allanite provided crystallization ages which, based on thorough petrography and thermobarometry, could be related to well constrained PTt-points. Based on these anchors, Ar-ages for micas were interpreted, and these data support recent studies suggesting closure temperature at 500 and 450 °C for muscovite and biotite Ar-Ar ages. Finally, the integration of zircon and apatite FT ages delineated the cooling-history in various samples from the Central Alps.

The data set as a whole thus yielded critical constraints on orogenic timing, from the late burial to the exhumation history, which are pertinent to tectonic and palinspathic reconstructions for this classic belt. We conclude that the metamorphic history is partly a younger than previously suggested, especially in NSB, with a thermal climax dated by monazite at 18-19 Ma in Piora and Lucomagno areas. Muscovite ages are only 1 to 2 Ma younger than monazite in samples that reached <580 °C, while that age difference increases at higher T due to the increasing effects of diffusion. The same trend is observed in biotite, the age of which is constantly less than that of muscovite, from 0.5-1 Ma difference at Piora-Lucomagno to more than 2 Ma at Pizzo Molare. Even nearly identical muscovite and biotite ages are obtained in one sample at Lucomagno pass, though that the higher Mg-content in this sample implies a higher Ar-retention of biotite from this sample, possibly reaching 450-500 °C.

Whereas slow heating (and perhaps a low compression rate) was inferred for the prograde path, rapid decompression from ca. 8-9 to 6-7 kbar was recorded by differential equilibration of a samples suite from a restricted area. Cooling-rates are low during the early decompression, near the thermal climax at 550-600 °C. Zircon and apatite FT data indicate that cooling was enhanced later, reaching 31 to 64 °/Ma above the closure of zircon FT (ca. 280 °C).

This study demonstrates the need and power of a detailed and combined thermobarometric and geochronological study, if the tectono-metamorphic history is to be understood. It proved essential to avoid problems of inheritance by relying exclusively on Mesozoic metasediments. Careful collection of structurally

Appendix 4.1: Ar-Ar results for Mesozoic gneissic metapelite of Alpe Devero (ADe0302). All separates are composed exclusively of biotite with only traces of chlorite.

#	T°C	^{39}Ar [%]	Age [Ma]	^{40}Ar$_{tot}$ [pL]	^{40}Ar* [pL]	^{39}Ar [pL]	^{38}Ar [pL]	^{37}Ar [pL]	^{36}Ar [pL]	Ca/K	Cl/K	39/40	36/40	STP File
ADe0302 Bt A - steps 5-6, 8-14 = 13.12±0.22 Ma (150-250 µm, 11.1[mg], J = 0.003732, K = 7.05 [%], Cl = 123 [ppm], Ca = 4541 [ppm])														
1	485	0.52%	16.09 ± 5.22	1355.1 ± 3.5	191.4	79.77 ± 0.12	3.22 ± 0.02	8.46 ± 0.04	3.94 ± 0.21	2.12 E-1 ± 9.6 E-4	3.44 E-3 ± 9.6 E-5	5.89 E-2 ± 1.8 E-4	2.91 E-3 ± 1.6 E-4	R15080
2	560	3.32%	7.71 ± 0.98	3245.3 ± 4.3	494.1	430.39 ± 1.31	14.68 ± 0.03	24.09 ± 0.11	9.32 ± 0.21	1.12 E-1 ± 5.1 E-4	3.26 E-3 ± 2.4 E-5	1.33 E-1 ± 4.4 E-4	2.87 E-3 ± 6.5 E-5	R15081
3	634	11.92%	-29.34 ± 4.20	4784.5 ± 2.0	-5705.7	1320.00 ± 8.43	78.16 ± 5.29	284.53 ± 27.3	35.57 ± 2.75	4.31 E-1 ± 4.1 E-2	7.56 E-3 ± 7.2 E-4	2.76 E-1 ± 1.8 E-3	7.42 E-3 ± 5.7 E-4	R15082
4	730	29.25%	11.47 ± 0.19	7349.7 ± 3.6	4547.6	2662.03 ± 3.50	48.77 ± 0.16	30.14 ± 0.66	9.49 ± 0.25	2.26 E-2 ± 4.9 E-4	1.05 E-3 ± 1.5 E-5	3.62 E-1 ± 5.1 E-4	1.29 E-3 ± 3.4 E-5	R15083
5	809	36.43%	13.24 ± 0.38	3773.5 ± 4.9	2178.0	1103.08 ± 1.65	19.21 ± 0.04	9.65 ± 0.03	5.40 ± 0.21	1.75 E-2 ± 5.3 E-5	8.42 E-4 ± 1.4 E-5	2.92 E-1 ± 5.8 E-4	1.43 E-3 ± 5.6 E-5	R15084
6	859	40.39%	13.33 ± 0.69	2375.7 ± 5.3	1206.1	607.10 ± 1.27	10.75 ± 0.03	5.78 ± 0.03	3.96 ± 0.21	1.90 E-2 ± 9.6 E-5	8.40 E-4 ± 1.8 E-5	2.56 E-1 ± 7.9 E-4	1.67 E-3 ± 8.9 E-5	R15085
7	882	43.37%	2.49 ± 1.11	1867.7 ± 4.7	169.2	457.67 ± 0.79	12.17 ± 0.27	26.48 ± 1.49	5.75 ± 0.25	1.16 E-1 ± 6.5 E-3	2.22 E-3 ± 1.1 E-4	2.45 E-1 ± 7.5 E-4	3.08 E-3 ± 1.4 E-4	R15086
8	892	46.08%	13.55 ± 1.00	1718.9 ± 0.3	841.2	416.47 ± 0.37	7.85 ± 0.01	4.40 ± 0.01	2.97 ± 0.21	2.12 E-2 ± 5.9 E-5	1.02 E-3 ± 2.1 E-5	2.42 E-1 ± 2.2 E-4	1.73 E-3 ± 1.2 E-4	R15087
9	905	49.62%	13.45 ± 0.77	2066.0 ± 0.1	1089.9	543.48 ± 0.61	10.00 ± 0.03	4.54 ± 0.03	3.30 ± 0.21	1.67 E-2 ± 1.1 E-4	9.81 E-4 ± 2.0 E-5	2.63 E-1 ± 2.9 E-4	1.60 E-3 ± 1.0 E-4	R15088
10	926	54.27%	13.69 ± 0.58	2350.7 ± 0.0	1458.0	714.16 ± 0.70	13.16 ± 0.04	4.72 ± 0.03	3.02 ± 0.21	1.32 E-2 ± 8.4 E-5	1.05 E-3 ± 1.7 E-5	3.04 E-1 ± 3.0 E-4	1.29 E-3 ± 9.0 E-5	R15089
11	967	65.77%	13.15 ± 0.24	4578.4 ± 2.8	3463.4	1766.85 ± 2.40	30.72 ± 0.06	6.82 ± 0.02	3.78 ± 0.21	7.71 E-3 ± 2.3 E-5	9.30 E-4 ± 1.3 E-5	3.86 E-1 ± 5.7 E-4	8.24 E-4 ± 4.6 E-5	R15090
12	1006	78.83%	13.04 ± 0.21	4910.4 ± 8.0	3898.9	2005.63 ± 2.44	33.60 ± 0.07	6.79 ± 0.02	3.42 ± 0.21	6.77 E-3 ± 2.0 E-5	8.31 E-4 ± 1.3 E-5	4.08 E-1 ± 8.3 E-4	6.97 E-4 ± 4.3 E-5	R15091
13	1045	90.12%	12.98 ± 0.24	4209.3 ± 1.4	3354.5	1734.10 ± 1.55	29.04 ± 0.05	15.68 ± 0.06	2.90 ± 0.21	1.81 E-2 ± 6.4 E-5	8.32 E-4 ± 1.2 E-5	4.12 E-1 ± 4.0 E-4	6.87 E-4 ± 5.0 E-5	R15092
14	1220	98.58%	13.10 ± 0.32	3367.1 ± 0.6	2538.3	1300.02 ± 1.39	21.88 ± 0.08	30.85 ± 0.12	2.81 ± 0.21	4.75 E-2 ± 1.9 E-4	8.30 E-4 ± 1.6 E-5	3.86 E-1 ± 4.2 E-4	8.33 E-4 ± 6.2 E-5	R15093
15	1454	100.00%	-30.48 ± 1.98	1266.8 ± 1.2	-975.5	217.34 ± 0.20	17.47 ± 0.08	57.64 ± 0.21	7.60 ± 0.21	5.31 E-1 ± 1.9 E-3	1.11 E-2 ± 7.3 E-5	1.72 E-1 ± 2.3 E-4	5.99 E-3 ± 1.7 E-4	R15094
ADe0302 Bt B - steps 4-5, 12-15 = 13.09±0.26 Ma (250-500 µm, 11.9[mg], J = 0.003728, K = 7.26 [%], Cl = 68 [ppm], Ca = 1281 [ppm])														
1	483	0.30%	-30.36 ± 8.51	939.2 ± 2.8	-229.0	51.17 ± 0.27	6.32 ± 0.17	19.85 ± 0.68	3.96 ± 0.22	7.76 E-1 ± 2.7 E-2	1.73 E-2 ± 6.1 E-4	5.45 E-2 ± 3.2 E-4	4.21 E-3 ± 2.3 E-4	R15095
2	563	2.50%	7.41 ± 1.10	2620.0 ± 8.1	422.9	382.78 ± 0.90	13.42 ± 0.03	24.90 ± 0.14	7.44 ± 0.21	1.30 E-1 ± 7.2 E-4	3.50 E-3 ± 2.6 E-5	1.46 E-1 ± 5.7 E-4	2.84 E-3 ± 8.1 E-5	R15096
3	633	10.94%	12.13 ± 0.29	5068.6 ± 1.6	2644.8	1461.93 ± 1.39	28.25 ± 0.09	22.48 ± 0.35	8.21 ± 0.21	3.07 E-2 ± 4.8 E-4	1.16 E-3 ± 1.6 E-5	2.88 E-1 ± 2.9 E-4	1.62 E-3 ± 4.2 E-5	R15097
4	700	30.39%	12.83 ± 0.13	9077.4 ± 0.3	6450.5	3369.61 ± 3.05	56.15 ± 0.16	23.34 ± 0.41	8.90 ± 0.21	1.39 E-2 ± 2.4 E-4	7.85 E-4 ± 1.4 E-5	3.71 E-1 ± 3.4 E-4	9.79 E-4 ± 2.3 E-5	R15098
5	757	41.13%	13.10 ± 0.23	5035.4 ± 7.3	3640.9	1862.44 ± 4.43	30.35 ± 0.09	8.93 ± 0.14	4.72 ± 0.21	9.59 E-3 ± 1.5 E-4	7.22 E-4 ± 1.4 E-5	3.70 E-1 ± 1.0 E-3	9.37 E-4 ± 4.2 E-5	R15099
6	809	44.08%	12.72 ± 0.82	2132.7 ± 2.5	968.7	510.43 ± 0.46	9.48 ± 0.02	6.48 ± 0.17	3.94 ± 0.21	2.54 E-2 ± 6.5 E-4	9.56 E-4 ± 1.8 E-5	2.39 E-1 ± 3.6 E-4	1.85 E-3 ± 9.9 E-5	R15100
7	860	46.72%	14.08 ± 0.91	1834.8 ± 3.1	962.6	458.14 ± 0.87	8.29 ± 0.02	4.71 ± 0.09	2.95 ± 0.21	2.05 E-2 ± 4.0 E-4	9.11 E-4 ± 2.0 E-5	2.50 E-1 ± 6.3 E-4	1.61 E-3 ± 1.2 E-4	R15101
8	884	48.67%	13.95 ± 1.24	1383.7 ± 0.7	700.9	336.58 ± 0.44	6.38 ± 0.02	4.10 ± 0.02	2.31 ± 0.21	2.43 E-2 ± 1.1 E-4	1.05 E-3 ± 2.7 E-5	2.43 E-1 ± 3.4 E-4	1.67 E-3 ± 1.5 E-4	R15102
9	895	50.42%	14.43 ± 1.37	1350.9 ± 1.5	653.8	303.59 ± 0.62	5.73 ± 0.01	3.99 ± 0.05	2.36 ± 0.21	2.63 E-2 ± 3.4 E-4	1.01 E-3 ± 2.6 E-5	2.25 E-1 ± 5.2 E-4	1.75 E-3 ± 1.6 E-4	R15103
10	905	52.48%	14.14 ± 1.16	1419.9 ± 2.1	756.1	358.21 ± 0.71	6.76 ± 0.01	4.21 ± 0.03	2.25 ± 0.21	2.35 E-2 ± 1.5 E-4	1.06 E-3 ± 2.3 E-5	2.52 E-1 ± 6.2 E-4	1.58 E-3 ± 1.5 E-4	R15104
11	927	55.47%	13.50 ± 0.81	1774.6 ± 0.2	1040.3	516.54 ± 0.46	9.27 ± 0.03	4.64 ± 0.01	2.49 ± 0.21	1.79 E-2 ± 5.3 E-5	9.40 E-4 ± 2.0 E-5	2.91 E-1 ± 2.6 E-4	1.40 E-3 ± 1.2 E-4	R15105
12	970	62.68%	13.36 ± 0.33	3285.1 ± 0.9	2492.0	1249.53 ± 1.10	21.12 ± 0.11	5.68 ± 0.06	2.69 ± 0.21	9.10 E-3 ± 8.9 E-5	8.44 E-4 ± 2.0 E-5	3.80 E-1 ± 3.5 E-4	8.17 E-4 ± 6.4 E-5	R15106
13	1006	73.99%	13.20 ± 0.21	4648.9 ± 4.9	3863.2	1961.30 ± 2.00	31.79 ± 0.06	6.35 ± 0.09	2.66 ± 0.21	6.48 E-3 ± 9.5 E-5	7.46 E-4 ± 1.2 E-5	4.22 E-1 ± 6.2 E-4	5.72 E-4 ± 4.5 E-5	R15107
14	1046	84.66%	13.20 ± 0.23	4330.4 ± 3.5	3641.0	1848.72 ± 2.63	29.88 ± 0.13	5.76 ± 0.08	2.33 ± 0.21	6.23 E-3 ± 8.5 E-5	7.41 E-4 ± 1.7 E-5	4.27 E-1 ± 7.0 E-4	5.39 E-4 ± 4.9 E-5	R15108
15	1216	98.59%	13.39 ± 0.18	5754.2 ± 3.9	4825.4	2413.92 ± 4.61	38.57 ± 0.08	10.42 ± 0.22	3.15 ± 0.21	8.63 E-3 ± 1.8 E-4	7.06 E-4 ± 1.2 E-5	4.20 E-1 ± 8.5 E-4	5.46 E-4 ± 3.7 E-5	R15109
16	1457	100.00%	13.74 ± 1.71	1353.8 ± 0.3	499.8	243.75 ± 0.29	4.77 ± 0.04	5.10 ± 0.07	2.89 ± 0.21	4.19 E-2 ± 5.4 E-4	9.97 E-4 ± 4.5 E-5	1.80 E-1 ± 2.2 E-4	2.13 E-3 ± 1.6 E-4	R15110

Appendix 4.1: (continued) Ar-results in pure muscovite separate from ADe0302.

#	T°C	^{39}Ar [%]	Age [Ma]	$^{40}Ar_{tot}$ [pL]	$^{40}Ar^*$ [pL]	^{39}Ar [pL]	^{38}Ar [pL]	^{37}Ar [pL]	^{36}Ar [pL]	Ca/K	Cl/K	39/40	36/40	STP File
ADe0302 Ms - steps 5-13 = 14.83±0.10 Ma (250-500 µm, 16.4[mg], J = 0.003724, K = 8.30 [%], Cl = 21 [ppm], Ca = 566 [ppm])														
1	485	0.15%	-64.28 ± 12.16	483.6 ± 1.2	-374.9	39.90 ± 0.60	6.54 ± 0.32	23.86 ± 1.30	2.91 ± 0.24	1.20 E+0 ± 6.5 E-2	2.47 E-2 ± 1.4 E-3	8.25 E-2 ± 1.3 E-3	6.01 E-3 ± 4.9 E-4	R15113
2	600	0.95%	8.32 ± 2.01	1431.5 ± 0.5	272.7	219.68 ± 0.61	6.14 ± 0.07	14.12 ± 0.43	3.93 ± 0.22	1.29 E-1 ± 3.9 E-3	2.29 E-3 ± 7.0 E-5	1.53 E-1 ± 4.3 E-4	2.74 E-3 ± 1.6 E-4	R15114
3	666	2.92%	12.94 ± 0.78	2666.2 ± 1.5	1037.5	536.88 ± 0.50	10.71 ± 0.06	14.14 ± 0.13	5.52 ± 0.21	5.27 E-2 ± 4.8 E-4	1.12 E-3 ± 2.7 E-5	2.01 E-1 ± 2.2 E-4	2.07 E-3 ± 8.0 E-5	R15115
4	713	5.82%	14.33 ± 0.53	3353.4 ± 1.7	1692.8	790.29 ± 0.70	11.59 ± 0.02	5.55 ± 0.06	5.62 ± 0.21	1.40 E-2 ± 1.5 E-4	2.79 E-4 ± 1.5 E-5	2.36 E-1 ± 2.4 E-4	1.68 E-3 ± 6.3 E-5	R15116
5	756	19.96%	14.92 ± 0.11	13133.2 ± 0.0	8593.6	3853.69 ± 5.06	52.83 ± 0.11	5.05 ± 0.02	15.36 ± 0.22	2.62 E-3 ± 8.5 E-6	2.14 E-4 ± 1.2 E-5	2.93 E-1 ± 3.8 E-4	1.17 E-3 ± 1.6 E-5	R15117
6	783	36.75%	14.89 ± 0.09	12136.1 ± 2.6	10188.4	4578.13 ± 4.04	59.71 ± 0.12	4.49 ± 0.01	6.59 ± 0.21	1.96 E-3 ± 6.5 E-6	1.79 E-4 ± 1.1 E-5	3.77 E-1 ± 3.4 E-4	5.43 E-4 ± 1.7 E-5	R15118
7	809	49.24%	14.63 ± 0.12	8769.8 ± 6.2	7437.7	3402.28 ± 4.54	44.16 ± 0.08	3.04 ± 0.02	4.51 ± 0.21	1.79 E-3 ± 9.1 E-6	1.72 E-4 ± 1.1 E-5	3.88 E-1 ± 5.9 E-4	5.14 E-4 ± 2.4 E-5	R15119
8	836	58.92%	14.70 ± 0.16	6820.9 ± 2.2	5802.7	2640.38 ± 3.38	34.32 ± 0.14	2.83 ± 0.04	3.45 ± 0.21	2.14 E-3 ± 3.2 E-5	1.76 E-4 ± 1.4 E-5	3.87 E-1 ± 5.1 E-4	5.05 E-4 ± 3.1 E-5	R15120
9	872	67.50%	14.78 ± 0.18	6193.6 ± 1.6	5167.3	2339.08 ± 2.52	30.71 ± 0.07	2.39 ± 0.02	3.47 ± 0.21	2.04 E-3 ± 1.3 E-5	1.93 E-4 ± 1.2 E-5	3.78 E-1 ± 4.2 E-4	5.61 E-4 ± 3.4 E-5	R15121
10	903	73.32%	14.84 ± 0.26	4430.2 ± 0.8	3512.9	1584.07 ± 2.22	20.93 ± 0.05	2.96 ± 0.02	3.11 ± 0.21	3.74 E-3 ± 2.4 E-5	1.93 E-4 ± 1.3 E-5	3.58 E-1 ± 5.1 E-4	7.01 E-4 ± 4.8 E-5	R15122
11	946	78.57%	14.78 ± 0.29	4060.9 ± 4.0	3163.3	1432.17 ± 1.99	18.88 ± 0.04	2.97 ± 0.01	3.04 ± 0.21	4.15 E-3 ± 1.3 E-5	1.82 E-4 ± 1.3 E-5	3.53 E-1 ± 6.0 E-4	7.48 E-4 ± 5.2 E-5	R15123
12	1007	84.94%	14.88 ± 0.24	4795.4 ± 2.2	3858.7	1735.38 ± 2.52	22.85 ± 0.10	3.27 ± 0.01	3.17 ± 0.21	3.77 E-3 ± 1.7 E-5	1.89 E-4 ± 1.5 E-5	3.62 E-1 ± 5.5 E-4	6.61 E-4 ± 4.4 E-5	R15124
13	1138	96.57%	14.92 ± 0.13	8097.5 ± 5.7	7075.0	3171.63 ± 4.26	40.91 ± 0.07	5.28 ± 0.02	3.46 ± 0.21	3.33 E-3 ± 1.2 E-5	1.66 E-4 ± 1.1 E-5	3.92 E-1 ± 5.9 E-4	4.27 E-4 ± 2.6 E-5	R15125
14	1413	100.00%	15.16 ± 0.44	2939.9 ± 0.5	2117.6	934.65 ± 0.82	12.55 ± 0.04	7.95 ± 0.07	2.78 ± 0.21	1.70 E-2 ± 1.5 E-4	1.98 E-4 ± 1.5 E-5	3.18 E-1 ± 2.8 E-4	9.47 E-4 ± 7.2 E-5	R15126

"The significant problems we have cannot be solved at the same level of thinking with which we created them."

Albert Einstein

5) Concluding remarks

5.1) Geochronology & ^{39}Ar-^{40}Ar dating

1) We have studied (notably) the reaction of paragonite destabilization. The same can be applied at higher grade with for instance the muscovite dehydration reaction to K-feldspar or the K-feldspar alteration towards muscovite. In this case, the Cl-content (i.e. Cl/K ratio) is an excellent proxy to yield a difference between both K-bearing minerals. However, higher temperature means higher diffusion and is something to keep in mind... By extension, any geochronological study *must* include a detailed petrographic to identify the last reaction pertaining to the last equilibration stage. Whenever possible, a thermobarometric study should be considered to ascertain equilibrium condition and to determine as precisely as possible the PT condition. In a similar way, alteration processes, such as sericitization of feldspars can be investigated using the presented methodology.

2) A detail investigation of chloritization process is required to precise its effect over the dating of biotite (meaningless age or valid age?). Is it related to an analytical artefact during irradiation (e.g. recoil)? Who is responsible for the younger ages in biotite: diffusion or metamorphic reaction (chloritization)? The existence of pristine biotite domain and rare chlorite layers suggest a minimized recoil effect. In contrary, regular and thin interlayer at nm-scale will possibly induce a larger Ar-loss through recoil. Transmitted electron microscopy (e.g. Di Vincenzo *et al.*, 2003; Viti *et al.*, 2004), thermobarometry, petrography and Ar-Ar dating (*in situ*, whenever possible, and/or stepwise heating) must be combined to answer this question. Various cases are to be considered, first of all:

    a. Large and pristine biotite and chlorite at equilibrium;

    b. Fine biotite and chlorite interlayer (± at equilibrium, e.g. APi0601);

    c. Chloritization in biotite with conservation of pristine biotite domain;

    d. Chloritization in biotite at nm-scale, absence of pristine µm-scale biotite domain (test for recoil).

3) Geochronology of fine interlayer from Urseren-Garvera zone. Though confronted to problem of disequilibrium, it might be interesting to analyse by stepwise heating these interlayers. As they pertain to Mesozoic metasediment equilibrating (???) around 400-450°C (see Appendix C, §C.4 and Table C.3), dating-results are potentially yielding formation ages. The Ca/K and eventually Cl/K ratios are used as proxy for the determination of age relation between the different interlayer present: illite/muscovite, paragonite and/or margarite. However, the analysis of nm-scale interlayers is complicated by problems of diffusion (stronger effect due to finer diffusion domain) and recoil during irradiation.

4) It must be clearly said: diffusion is *not always* the rule and closure temperatures obtained in the 70's

are highly discussable. New closure temperature at 450 °C for biotite and 500 °C for muscovite seems more realistic (see discussion in Chapter 4). Care should be taken when thermochronology is invoked to interpret some dating results, notably Ar-Ar...

5) Since metamorphic reaction induces re-crystallization and possible Ar-resetting, the effect of deformation is also known as a potential process for Ar-resetting (e.g. Mulch and Cosca, 2004; Di Vincenzo *et al.*, 2007). More than the study of deformation stages, the detail investigation of PT-condition pertaining to the formation of older or newer nuclei may be the key point to the understanding of age-variation.

5.2) Thermobarometry

1) An enhancing of TWQ database is required. Data are missing notably for some interesting phases susceptible to be dated, while some others data are incompletely defined or currently under review:

    a. Muscovite-Margarite–Paragonite solid solution. There may have some similitude with plagioclase ternary model. Indeed, a calibration between micas and feldspars is highly required. The assemblages Ms+Mrg+Pl or Ms+Pg+Pl are common at the upper greenschist to lower amphibolite facies, and a regular change in composition in micas and plagioclase is observed between plagioclase-in and margarite- or paragonite-out isograds (see Chapter 2).

    b. Epidote–Clinozoisite (ideally related to REE-epidote, too);

    c. REE-minerals, notably monazite and allanite (e.g. Janots *et al.*, 2007; Janots *et al.*, in press);

    d. Definition of Mn-garnet end-member in TWQ and reassessement of "spessfalsch" in THERIAK-DOMINO (work in progress, C. De Capitani, M. Engi & R. Berman);

    e. Calculation with staurolite (when present in textural equilibrium) usually yield good results with the model of Nagel *et al.* (2002a), but in some cases, the Mg-staurolite end-member was responsible for a larger spreading of reaction in TWQ. This might reflect an inadequacy of the model to fit equilibria at high xMg (>0.2?) or simply a disequilibrium effect. However, this latter usually implies also some spreading related to Fe-staurolite, too. This was for instance the case in sample AMo0406, where large staurolite porphyroblast are growing locally during retrogression and presents a large disequilibrium with other rock-forming mineral (equilibrium involving staurolite clearly yield lower pressure). This is consistent with the observation of staurolite stability-field at low-P in typical Al-poor pelites, as computed in THERIAK-DOMINO.

2) Small incoherency regarding a too high stability field of chlorite in THERIAK-DOMINO (applied to Al-rich metapelite, notably)? The model from Hunziker (2003) leaves chlorite stable up to too high temperature compared to results from TWQ and field observation (+20 to +50 °C).

3) Variation of pressure conditions determined with TWQ: is it an artefact of the mineral equilibria calculated (essentially T-dependant), or is it real? More works regarding the PT-condition and the structural geology is required here (fieldwork and detailed crystallization-deformation relation). Unfortunately, another major problem remains the lack of good barometers...

5.3) Alpine geology, orogenies & other...

1) Structural geology was leave aside in our study, due to the complexity or the area (quite all phases are parallelized, except in Lucomagno-Molare area). However, mineral equilibration is expected to occur during the back-thrusting in the northern Central Alps. Linking with precision deformation, crystallization, PT-condition of equilibrium and geochronology will obligatory leads to robust results regarding the tectono-metamorphic evolution of the Alps.

2) PT (and time?) relation with the HP-LT stage identified in some specific layers of Bündnerschiefer (carpholite-bearing quartz vein or relic). Such a study is currently in progress, with the work of Prof. Romain Bousquet and his doctorant Michael Wiederkehr, eastwards from our studied area.

3) New computer models for subduction and collision processes in the Alps, based on new PT and age data: re-estimation of erosion and exhumation/uplift rates, global Alpine evolution...

4) A review of other geochronological data based on the concept developed in this thesis is required, if we aim to understand the Alps in its whole. The use of retentive geochronological system (e.g. monazite, zircon) are needed and should be clearly related to a growth stage. This might gives more weight to the interpretation of other geochronological results, such as Ar-dating. Of course, this remark as quite all other presented here applies to any other metamorphic field, not exclusively on the Alps.

5) Alteration is a kind of "metamorphic reaction" occurring at very low grade and might well affect sediments or magmatic rocks (both commonly used for Ar-dating). In such case, what is the meaning of a detrital micas possibly alterated during transport or weathered after deposition? And alterated volcanic material; should we continue whole rock analysis of basaltic chips if not >99.9% "fresh"? What is the effect of hydrothermal fluids? Is it possible to determine the "closure-temperature" of a retrograde process? If yes, is this temperature also applicable to the isotopic system used to date a mineral?

"Bye-bye Central Alps... Hello Southern Alps!"

View from Pizzo Forno, SW direction (A. Sponda)

Many questions which might be solved by one equation...

"1 + 1 = 3"

Bernard Werber, in *L'Encyclopédie du Savoir Relatif et Absolu* and in *Les Fourmis*

(You don't understand? Read these books, or see acknowledgments!)

Appendix

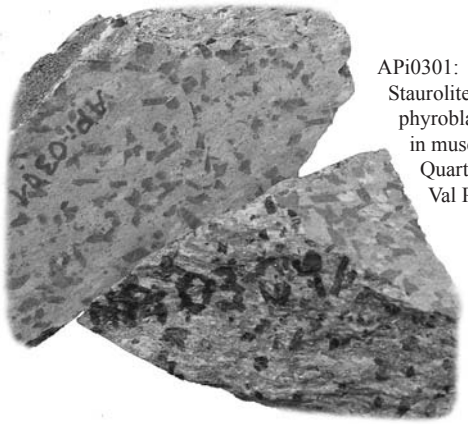

APi0301:
Staurolite and garnet porphyroblast (ca. 1 cm-size) in muscovite–paragonite Quartenschiefer from Val Piora.

A) Sample collection

An overview of the mineral assemblage for each samples with thin section is given in Table A.1. The complete list of studied samples is given in Table A.2 and includes sample position (CH-coordinates) and rock type. Reader is referred to the CD for a raw report on each collected sample: mineralogy in thin section, modal abundance estimated at optical microscope, scan of thin section, comment on each minerals and general observation (Microsoft® Word documents, in French only). Such a report is missing for a majority of the latest collected samples from Lucomagno (ALu06xx), except samples considered for Ar-dating (ALu0601, ALu0603).

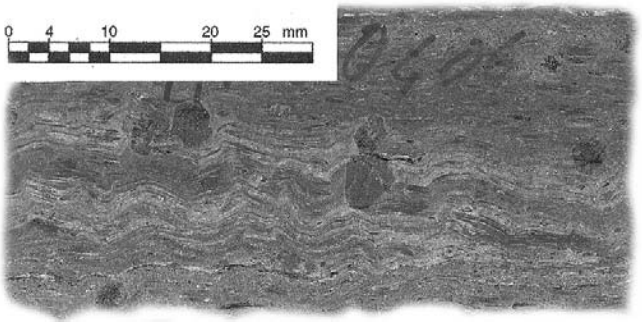

AMo0406:
Garnet-bearing Bündnerschiefer and late staurolite growth. The greyish colour stems from graphite, typical in the studied Bündnerschiefer.

Table A.1: Overview of sample mineralogy. See CD for details on each samples.

Sample	Ms	Pg	Mrg	Bt	Chl	Qz	Pl	Grt	St	Ky	Hb	Ep	Car	Cld	Zoi	Rt	Ilm	Sulf	Grapite	Mineral assemblage (in order of abundance, ± = unstable but present, ? = doubt)
AAn0401	X	.	.	X	r	X	X	X	.	.	.	±	±	.	.	X	X	.	.	Ms – Pl – Qz – Bt – Grt – Rt – Ilm ±Ep ±Carb ±Chl
AAn0402	X			X	r	X	X	X				±	X			X	X		±	Carb – Qz – Bt – Pl – Ms – Grt – Ilm – Rt ±Ep ±C ±Chl
AAn0405	X	.	.	X	r	X	X	X	.	.	.	±	.	.	.	X	±	.	.	Ms – Qz – Bt – Grt – Pl – Rt – Ilm – Carb ±Ep ±Chl
AAq0401	X	.	.	X	r	X	X	X	X	X	.	±	.	.	.	.	X	.	.	Ms – Pl – Qz – Bt – Grt – Ky – St – Ilm – Hem? ±Ep ±Chl
ACb0301	X	.	X	X	r	X	X	X	.	.	.	X	.	.	.	X	X	.	X	Ms – Mrg – Qz – Grt – Bt – Pl – Ilm – Rt – Ep ±Chl - C
ACb0304	X	.	.	X	.	X	.	.	.	.	.	X	.	.	X	.	.	.	X	Zoi – Qz – Ms – Ep – Bt – C
ACb0305	X	.	.	.	X	X	.	.	.	.	.	.	X	.	.	.	.	.	.	Carb – Qz – WM – Chl – …?
ACb0402	X	.	.	±	X	X	X	.	.	.	.	.	X	.	.	.	X	?	.	Qz – Ms – Chl – Carb – Pl – Ilm/Sulf? ±Bt
ACb0404	?	.	?	.	X	X	X	X	.	.	.	X	X	.	.	X	?	?	.	Mrg? – Ms? – Qz – Ep – Pl – Chl – Rt – Ilm?
ACb0406	X	.	X	X	.	X	X	X	.	.	.	±	X	.	.	.	?	X	X	Qz – Ms – Mrg – Grt – Bt – Pl – Ilm/Sulf – Carb – C ±Ep
ADe0301	X	.	.	X	.	X	X	X	.	X	.	±	.	.	.	X	X	.	X	Ms – Qz – Grt – Bt – Pl – Ky – Rt – Ilm – C ±Ep
ADe0302	X	.	.	X	r	X	X	X	.	.	.	.	.	.	.	X	±	.	.	Ms – Qz – Pl – Bt – Grt – Ky – Rt ±Ilm ±Chl
ALu0301	X	.	.	X	.	X	X	X	.	.	.	X	±	±	.	.	X	.	X	Qz – Bt – Ms – Pl – Grt – Ep – Ilm-Hem?– C ±Cld ±Carb
ALu0302	X	.	.	X	.	X	.	.	.	.	.	X	X	.	X	±	?	X	X	Carb – Ms – Zoi – Qz – Ep – Bt – Ilm/Sulf – C ±Rt
ALu0304	X	.	X	X	.	X	X	X	.	.	.	X	±	±	.	±	X	.	.	Qz – Ms – Marg – Bt – Pl – Grt – Ep – Ilm ±Rt ±Cld ±Carb
ALu0305	X	.	.	.	.	X	.	.	.	.	.	.	X	.	X	.	?	X	X	Qz – WM – Carb – Zoi – Sulf/Ilm? – C
ALu0306	X	.	X	X	x	X	X	.	.	.	.	X	X	.	.	X	?	?	.	Qz – Carb – Bt – Mrg – Chl (stable?) – Ms – Ep – Pl – Rt
ALu0308	.	.	X	X	.	X	X	X	X	X	X	X	.	.	.	X	X	.	.	Qz – Bt – Ky – St – Ep – Grt– Pl – Hb – Mrg – Rt
ALu0309	X	.	.	X	X	X	X	.	X	X	.	±	.	.	.	±	X	.	.	Chl – Pl – Qz – Bt – St – Ky – Ilm – Ms ±Ep ±Rt
ALu0310	X	.	.	X	X	X	X	X	.	.	±	X	X	.	.	±	±	.	.	Carb – Qz – Bt – Pl – Ep – Grt – Chl –Ms ±Ilm ±Rt ±Hb
ALu0313	X			.	.	X	?	.	.	.	.	.	X	.	?	.	.	X	X	Qz – WM – Pl – Zoi (Cld ?) – Sulf – Carb – C
ALu0401	±			X		X	?	X	X	X		±				X	±	±		Qz – St – Bt – Grt – Ky – Rt ±Ilm/Sulf ±Ep ±Ms ±Pl?
ALu0402	X	.	.	.	.	X	?	.	.	.	.	.	X	?	X	.	?	X	X	Carb – Qz – Ms – Zoi – Pl? – Oxy/Sulf – C
ALu0404	X				X	X	X					X					?	?		Qz - Pl - Chl - Ep - Ms - Ilm/Sulf
ALu0406	X	.	.	X	r	X	X	.	.	.	.	X	.	.	.	X	.	.	.	Qz – Pl – Bt – Ms – Ep – Rt ±Chl
ALu0601	X	.	.	±	r	X	X	X	X	X	.	r	.	±	.	X	±	.	X	See word file...
ALu0603	X	X	.	±	r	X	X	X	X	X	.	r	.	.	.	X	?	?	X	See word file...

Table A.1 (continued).

Sample	Ms	Pg	Mrg	Bt	Chl	Qz	Pl	Grt	St	Ky	Hb	Ep	Car	Cld	Zoi	Rt	Ilm	Sulf	Grapite	Mineral assemblage (in order of abundance, ± = unstable but present, ? = doubt)
AMo0401	X	.	.	.	.	X	X	.	.	.	.	.	.	.	.	X	.	?	.	Qz – Pl – Magnetite/Sulf? – Ms – Rt
AMo0404	X	.	.	X	r	X	X	X	.	.	.	±	.	.	.	X	X	.	.	Qz – Ms – Bt – Pl – Grt – Ilm – Rt ±Ep ±Chl
AMo0405	X	.	.	X	r	X	X	X	X	X	.	.	.	.	.	.	X	.	.	Ms – Bt – Qz – Pl – Grt – Ky – St – Ilm ±Chl
AMo0406	X	.	.	X	.	X	X	X	X	.	.	±	.	.	.	X	X	.	X	Ms – Pl – Bt – Qz – Grt – Ilm – Rt – St – C ±Ep
AMo0409	X	.	.	X	r	X	X	X	X	.	.	±	.	.	.	.	X	.	.	Ms – Qz – Pl – Bt – Grt – St – Ilm ±Ep ±Chl
AMo0410	X	±	±	X	r	X	X	X	X	X	.	±	.	.	.	±	X	.	.	Ms – Qz – Bt – Pl – Grt – St – Ky – Ilm ±Rt ±Chl ±Ep
AMo0501	X	.	.	X	r	X	X	X	.	.	.	X	X	.	.	X	?	X	.	Lame 1) Grt – Ep – Rt – Rt – Ms? – Qz? – Bt? ±Chl
	X	.	.	X	r	X	X	X	.	.	.	X	X	.	.	X	?	X	.	Lame 2) Qz – Ms – Grt – Bt – Pl – Chl – Ep– Rt – Ilm/Sulf?
AMo0502	X	.	.	X	r	X	X	.	.	.	.	X	X	.	.	X	.	.	.	Carb – Ms – Pl – Bt – Ep – Rt – Qz ±Chl
AMo0503	X	.	.	X	r	X	X	X	±	.	.	X	.	.	.	.	.	.	.	Ms – Qz – Bt – Pl – Grt – Ep ±Chl ±St
AMo0504	X	.	.	X		X	X	X	.	.	.	±	X	.	.	X	±	X	X	Qz – Carb – Pl – Bt – Grt – Ms – Rt – Sulf – C ±Ilm ±Ep
AMo0505	X	.	.	X	r	X	X	X	X	X	.	.	.	.	.	X	X	.	X	Pl – Ms – Qz – St – Ky – Grt – Bt – Ilm – Rt – C ±Chl
AMo0506	X	.	.	X	r	X	X	X	.	.	.	±	±	.	.	X	±	X	X	Pl – Qz – Bt – Ms – Grt– Sulf – Rt – C ±Carb ±Ep ±Ilm ±Chl
AMo0507	X	.	.	X	±	X	X	X	.	.	.	±	.	.	.	X	.	X	.	Ms – Pl – Bt – Grt – Qz – Rt – Sulf ±Ep ±Chl
ANu0301	X	.	?	X	r	X	.	.	.	.	.	.	X	.	X	X	?	X	X	Carb – Qz – Bt – Zoi – Ms (+Mrg?) – Rt – C ±Chl
ANu0302	X	.	X	X	.	X	X	X	.	.	.	±	±	.	.	.	X	X	X	Qz – Ms – Mrg – Bt – Pl – Grt – Ilm/Sulf – C ±Ep ±Carb
ANu0303	X	.	?	X	.	X	X	X	.	.	.	X	X	.	.	.	X	X	X	Carb – Qz – Ms (+Mrg?) – Bt – Grt – Pl – Ep – Oxy/Sulf – C
ANu0304	X	.	X	X	.	X	X	X	.	.	.	±	.	±	.	.	X	X	X	Qz – Ms – Mrg – Bt – Pl – Grt – Ilm/Sulf – C ±Ep ±Cld
ANu0402	±	.	X	X	?	.	X	.	.	.	.	X	.	.	.	.	?	?	.	Chl? – Mrg – Bt – Pl – Ilm/Sulf? – Ep ±Ms
ANu0405	X	.	.	X	r	X	X	.	.	.	.	X	X	.	.	.	?	X	X	Pl – Ms – Bt – Carb – Sulf/Ilm – Ep – Qz – C ±Chl
ANu0408	X	.	.	X	.	X	X	X	.	.	.	±	X	.	.	±	X	?	±	Qz – Carb – Pl – Ms – Bt – Grt – Ilm/Sulf ±Ep ±Rt ±C
ANu0410	X	.	.	X	.	.	±	.	.	.	.	X	.	.	.	X	.	.	.	Ms – Bt – Ep – Rt ±Pl
ANu0411	X	.	±	X	.	X	?	X	.	.	.	X	X	.	?	X	.	±	x	Qz – Carb – Ms – Bt – Grt – Zoi/Pl? – Rt – Ep – C ±Mrg
ANu0413	X	.	.	±	r	X	X	X	.	.	.	±	.	.	.	.	X	X	X	Ms – Qz – Grt – Pl – Ilm/Sulf – C ±Bt ±Chl ±Ep
APi0301	X	X	.	X	r	X	X	X	X	.	.	±	.	±	.	±	X	X	.	Ms – Pg – Qz – St – Bt – Pl – Grt – Ilm ±Ep ±Rt ±Cld ±Chl
APi0302	±	.	X	X	r	X	.	X	X	X	x	X	.	.	.	±	X	.	.	Qz – Bt – Hb – St – Mrg – Ilm – Ky – Grt – Ep ±Ms ±Chl ±Rt
APi0303	X	.	.	X	r	X	X	.	X	X	.	.	.	.	.	.	X	.	.	Ms – Bt – Qz – Ky – Ilm – St – Pl ±Chl
APi0304	X	.	.	X	.	X	X	X	X	X	.	±	.	.	.	±	X	X	X	St – Pl – Ky – Ms – Bt – Qz – Grt – Ilm – Sulf – C ±Rt ±Ep
APi0305	X	.	.	X	.	X	X	X	X	.	.	X	±	.	.	X	X	.	X	Ms – Pl – Qz – Grt – St – Bt – Ep – Ilm – Rt – C ±Carb
APi0306	X	.	.	X	.	X	X	X	X	.	.	X	±	.	.	X	X	X	X	Ms – Pl – Bt – Grt – St – Ep – Qz – Rt – Ilm – Sulf – C ±Carb
APi0401	X	.	.	X	r	X	X	.	.	.	.	±	.	.	.	.	±	.	.	Qz – Ms – Bt – Pl – Ilm/Ulvö/Mt ±Ep ±Chl
APi0402	X	.	.	X	r	X	X	.	.	±	.	X	.	.	.	X	.	.	.	Qz – Ms – Bt – Pl – Ep – Rt ±Chl ±Ky
APi0405	X	X	.	X	r	X	X	X	X	.	.	.	.	±	.	.	X	.	±	Ms – Pg – St – Qz – Pl – Bt – Grt – Ilm ±Cld ±Chl ±C?
APi0407	X	.	.	X	r	X	X	.	X	X	.	±	.	±	.	.	X	±	±	Ms – Pl – St – Ky – Qz – Bt – Ilm ±Ep ±Rt ±Cld ±Chl ±C
APi0408	±	.	X	X	r	X	X	X	.	±	.	±	±	.	.	X	±	.	.	Bt – Qz – Mrg – Grt – Pl – Rt ±Ms ±Ky ±Ilm ±Ep ±Carb ±Chl
APi0409	X	.	.	X	r	X	X	X	±	.	.	X	±	.	.	X	X	.	.	Ms – Qz – Pl – Bt – Grt – Ep – Rt – Ilm ±St ±Chl ±Carb
APi0412	X	.	.	X	r	X	X	X	X	.	.	X	.	±	.	.	X	±	.	Qz – Ms – St – Grt – Bt – Ep – Ilm – Pl ±Rt ±Cld ±Chl
APi0413	?	X	.	X	r	X	X	X	X	X	.	±	.	.	.	X	X	.	.	Pl – Bt – Ky – Prg – Qz – Grt – St – Ilm – Rt ±Ep ±Chl
APi0501	X	.	?	X	r	X	X	X	X	.	.	X	±	±	.	.	.	X	X	Ms – Mrg? – Qz – Pl – Grt – Bt – St – Ep – Rt – Sulf – C
APi0502	X	?	?	±	.	±	X	X	±	X	.	±	.	.	.	X	.	.	.	Lame 1) Pl – Ky – Grt – Ms – Mrg? – Rt ±Bt ±Qz ±St ±Ep
	X	?	?	X	.	X	X	±	X	X	.	±	.	.	.	X	.	.	.	Lame 2) Qz – Ms – Prg? – Bt – Pl – Ky – St – Rt ±Hem ±Ep
APi0503	X	.	.	X	r	X	X	X	X	X	.	±	.	.	.	X	X	.	.	Ms – Qz – Pl – Bt – Grt – St – Ky – Rt – Ilm ±Ep ±Chl
APi0504	X	.	.	X	.	X	X	.	.	.	.	±	X	.	.	.	?	X	X	Carb – Pl – Qz – Ms – Bt – Sulf – C ±Ep ±Ilm? ±Ky ±Ep ±Chl
APi0505	X	.	.	X	r	X	X	X	X	±	.	±	.	X	.	.	X	.	.	Ms – Qz – Cld – Bt – St – Ilm – Grt ±Pl?±Chl ±Ep
APi0506	X	.	.	X	r	X	X	X	X	.	.	±	.	±	.	.	X	.	.	Ms – St – Qz – Pl – Bt – Grt – Ilm ±CldIlm – Ep – C ±Chl
APi0507	X	.	.	X	r	X	?	X	.	.	.	X	X	.	?	.	X	X	X	Carb – Ms – Pl/Zoi? – Qz – Bt – Grt –Sulf – Ilm ±Rt ±Chl
APi0508	X	.	.	X	r	X	X	X	.	.	.	X	X	.	.	±	X	X	.	Carb – Qz – Pl – Ep – Ms – Bt – Grt – C ±St ±Ep ±Chl
APi0509	X			X	r	X	X	X	±			X	X				X	X	X	Qz – Carb – Pl – Bt – Ms – Grt – Ilm – ±Ep ±Chl
APi0510	.	.	X	X	r	X	X	.	X	±	.	±	.	X	.	.	X	.	.	Qz – Mrg – Bt – St – Cld – Pl – Ilm ±KySulf – C ±Ep ±Chl?
APi0511	X	.	.	X	?	X	X	X	.	.	.	±	X	.	.	.	X	X	X	Qz – Pl – Carb – Bt – Grt – Ms – Ilm –
APi0512	X	.	.	X	.	X	X	.	X	X	.	±	.	X	.	.	X	.	±	Ms – Qz – Cld – Bt – St – Ky – Ilm – Pl ±Ep ±C±Cld ±Chl
APi0513	X	.	.	X	r	X	X	X	X	X	.	±	.	±	.	.	X	.	.	Ms – St – Bt – Pl – Grt – Qz – Ky – Ilm
APi0601	X	X	.	X	x	X	X	X	±	X	.	±	.	.	.	.	X	.	.	See word file...
APi0602	x	X	.	X	.	X	X	X	X	X	.	±	.	.	.	X	±	.	.	See word file...
AVr0301 (I)	X	.	.	.	X	X	.	.	.	.	.	.	X	.	.	X	.	.	.	Qz – Cc – WM (various types) – Chl – Rt
AVr0301 (II)	X	.	.	.	.	X	X	.	.	.	.	.	.	.	.	.	.	.	X	Qz – Pl – WM – C – ... ???
AVr0302	X	.	.	.	X	X	.	.	.	.	.	.	X	.	.	?	.	.	.	Carb – Qz – WM – Chl – Rt?

Table A.2: Complete list of studied samples.

Sample	Sampling day	Locality / named-place	CH-coordinates [m] E-W	N-S	Elev.	Tectonic unit
Val Antabia (San Carlo, Val Bavona)						
AAn 0401	26.08.04	Val Antabia - Pianascom	680 900	139 510	2300	Quartenschiefer, Teggiolo
AAn 0402	26.08.04	Val Antabia - Pianascom	680 820	139 510	2310	Quartenschiefer, Teggiolo
AAn 0405	27.08.04	Val Antabia - Pianascom	680 780	139 440	2325	Quartenschiefer, Teggiolo
Aquila (between Olivone & Biasca)						
AAq 0401	06.07.04	E Aquila (in forest)	716 225	151 675	1045	Permian
Campo Blenio						
ACb 0301	30.08.03	Campo Blenio, restaurant "Genziane"	715 000	156 830	1200	Schistes of Sosto
ACb 0304	30.08.03	Road to Lago Luzzone	716 060	157 830	1410	Schistes of Sosto
ACb 0305	30.08.03	Scree along road, N Lago Luzzone	719 150	159 830	1650	Schistes of Sosto
ACb 0402	05.07.04	Val Carassino (SE Campo Blenio)	717 290	156 210	1710	Permian (?)
ACb 0404	25.08.04	Footway Pradasca-Boverina	711 430	157 450	1800	Quartenschiefer
ACb 0406	25.08.04	Footway Pradasca-Boverina	715 050	156 920	1195	Bündnerschiefer (Gotthard)
Alpe Devero						
ADe 0301	27.08.03	Footway near Mte Cazzola	662 310	128 000	2140	Fäldbach series
ADe 0302	28.08.03	Crampiolo, S Lago Devero	664 865	131 010	1790	Fäldbach series
Lucomagno pass and SE area (Frodalera)						
ALu 0301	02.07.03	E Lucomagno pass	705 380	157 940	2150	Bündnerschiefer (Stgir serie)
ALu 0302	02.07.03	E Lucomagno pass	705 370	157 940	2150	Bündnerschiefer (Stgir serie)
ALu 0304	02.07.03	E Lucomagno pass	705 270	157 930	2140	Bündnerschiefer (Stgir serie)
ALu 0305	02.07.03	E Lucomagno pass	705 270	157 770	2105	Bündnerschiefer (Stgir serie)
ALu 0306	02.07.03	E Lucomagno pass	705 180	157 710	2085	Quartenschiefer
ALu 0308	02.07.03	Frodalera	706 910	154 150	1785	Quartenschiefer
ALu 0309	02.07.03	Frodalera	706 910	154 150	1785	Quartenschiefer
ALu 0310	02.07.03	Frodalera	706 910	154 150	1785	Quartenschiefer
ALu 0313	30.08.03	Over road gallery, E Lago Sta Maria	704 580	159 720	1960	Bündnerschiefer (Stgir serie)
ALu 0401	05.07.04	Crossing roads Lucomagno-Frodalera	708 025	154 000	1670	Quartenschiefer
ALu 0402	09.07.04	Gana Negra, below Pizzo Corvo	707 210	157 590	2640	Bündnerschiefer
ALu 0404	09.07.04	E of Gana Negra pass	707 820	156 610	2305	Quartenschiefer
ALu 0406	11.07.04	W of Camperio (in forest)	711 670	153 425	1420	Quartzitic Triassic
ALu0601	01.07.06	Frodalera - Brönich	707 190	154 200	1760	Quartenschiefer
ALu0602	01.07.06	Frodalera - Brönich	707 525	154 030	1770	Quartenschiefer
ALu0603	01.07.06	Frodalera - Brönich	707 505	154 050	1770	Quartenschiefer
ALu0604	01.07.06	Vallone di Casaccia	706 175	157 000	2180	Bündnerschiefer (Stgir serie)
ALu0605	01.07.06	Vallone di Casaccia	706 175	157 000	2180	Bündnerschiefer (Stgir serie)
ALu0606	01.07.06	Vallone di Casaccia	706 175	157 000	2180	Bündnerschiefer (Stgir serie)
ALu0607	01.07.06	Vallone di Casaccia	706 175	157 000	2180	Bündnerschiefer (Stgir serie)
ALu0608	02.07.06	Crest E of Lucomagno (Pizzo Cadrèigh)	709 025	156 210	2395	Bündnerschiefer (Stgir serie)
ALu0609	02.07.06	Crest E of Lucomagno (Pizzo Cadrèigh)	709 220	156 175	2365	Bündnerschiefer (Stgir serie)
ALu0610	02.07.06	Crest E of Lucomagno (Pizzo Cadrèigh)	708 175	156 025	2360	Bündnerschiefer / Quarten?
Pizzo Molare						
AMo 0401	06.07.04	Road E of Molare, near Zóira	713 300	147 680	1105	Permian
AMo 0404	08.07.04	Road E of Molare, near Ticiall	713 280	149 375	1270	Permian / Crystalline basement?
AMo 0405	10.07.04	Alpe San Martino (NE of Molare)	710 780	150 240	2180	Permian
AMo 0406	10.07.04	South of Punta Stou (Molare)	709 590	150 460	2530	Schistes of Sosto
AMo 0409	10.07.04	NW summit "2479m", NE Molare	709 670	150 130	2450	Quartenschiefer
AMo 0410	10.07.04	Crest SSW of Pizzo Molare	709 460	149 510	2555	Quartenschiefer
AMo0501	28.07.05	Summit of Pizzo Molare	709 430	149 510	2540	Quartenschiefer
AMo0502	28.07.05	Summit of Pizzo Molare	709 450	149 505	2560	Quartenschiefer? Molare Bündn.??
AMo0503	28.07.05	SE Punta di Stou	709 630	150 140	2460	Quartenschiefer
AMo0504	28.07.05	SE Punta di Stou	709 780	150 105	2460	Schistes of Sosto
AMo0505	28.07.05	SE Punta di Stou	709 625	150 165	2465	Schistes of Sosto
AMo0506	29.07.05	SE Punta di Stou	709 950	150 000	2410	Schistes of Sosto
AMo0507	29.07.05	SE Punta di Stou	710 100	149 805	2290	Schistes of Sosto

Table A.2 (continued)

Sample	Sampling day	Locality / named-place	CH-coordinates [m] E-W	N-S	Elev.	Tectonic unit
Nufenen pass, Val Bedretto						
ANu 0301	03.07.03	Road for Nufenen, 2-3 km W All'Acqua	677 650	147 560	1820	Bündnerschiefer, Nufenen zone
ANu 0302	03.07.03	Dam of Griessee (NE side of lake)	671 750	146 100	2405	Bündnerschiefer, Nufenen zone
ANu 0303	03.07.03	Dam of Griessee (NE side of lake)	671 770	146 075	2405	Bündnerschiefer, Nufenen zone
ANu 0304	03.07.03	Dam of Griessee (NE side of lake)	671 750	146 100	2405	Bündnerschiefer, Nufenen zone
ANu 0402	12.07.04	Griessee, below "Mändeli"	672 025	146 120	2480	Quartenschiefer
ANu 0405	12.07.04	Footway for val Piana - alpe Valleggia	681 560	149 160	1750	Bündnerschiefer, val Bedretto
ANu 0408	13.07.04	Valleggia, footway dir. Motto di Varoz	681 870	149 125	1800	Bündnerschiefer, val Bedretto
ANu 0410	14.07.04	Misura, South of Fontana	686 075	151 040	1870	Bündnerschiefer, val Bedretto
ANu 0411	14.07.04	Misura, South of Fontana	686 030	151 310	1840	Bündnerschiefer, val Bedretto
ANu 0413	23.08.04	Footway Mändeli-Griespass	672 110	145 890	2460	Bündnerschiefer, Nufenen zone
ANu0601	30.06.06	Footway Ossasco => Alpe Cristallina	684 775	150 580	1740	Bündnerschiefer, val Bedretto
Val Piora, around Lago Ritom						
APi 0301	01.07.03	ESE of SAT Cadagno (Mottone)	698 320	155 380	2075	Quartenschiefer
APi 0302	01.07.03	ESE of SAT Cadagno (Mottone)	698 300	155 480	2030	Quartenschiefer
APi 0303	01.07.03	ESE of SAT Cadagno (Mottone)	698 120	155 420	2055	Quartenschiefer
APi 0304	01.07.03	ESE of SAT Cadagno (Mottone)	698 350	155 310	2045	Quartenschiefer (Bündnerschiefer?)
APi 0305	01.07.03	ESE of SAT Cadagno (Mottone)	696 850	155 820	1920	Bündnerschiefer of Piora (-Scopi)
APi 0306	01.07.03	ESE of SAT Cadagno (Mottone)	696 860	155 820	1920	Bündnerschiefer of Piora (-Scopi)
APi 0401	27.06.04	South of Lago Ritom	695 860	154 725	1780	Quartzitic Triassic
APi 0402	27.06.04	South of ri dei Calcestri (Ganoni)	700 250	154 825	2160	Quartenschiefer
APi 0405	27.06.04	West of Pian di Lecc	695 350	155 610	2090	Quartenschiefer
APi 0407	27.06.04	North of Camoghè	694 725	155 525	2270	Quartenschiefer
APi 0408	27.06.04	East of Foisc	694 510	154 440	2065	Quartenschiefer
APi 0409	27.06.04	South of Pian di Lecc	695 740	155 490	1910	Quartenschiefer? Bündnerschiefer?
APi 0412	25.08.04	South of Foisc	694 260	154 030	2110	Quartenschiefer
APi 0413	25.08.04	South of Foisc	694 375	154 100	2130	Quartenschiefer
APi0501	26.07.05	South of Foisc	694 390	154 010	2095	Bündnerschiefer of Piora (-Scopi)
APi0502	26.07.05	South of Foisc	694 330	154 065	2090	Quartenschiefer? Bündnerschiefer?
APi0503	26.07.05	WSW of Foisc	693 780	154 110	2040	Quartenschiefer
APi0504	26.07.05	Between Foisc & Camoghè	694 110	154 590	2190	Schistes of Sosto
APi0505	26.07.05	NW of Camoghè	694 465	155 625	2195	Quartenschiefer
APi0506	26.07.05	NW of Camoghè	694 425	155 645	2175	Quartenschiefer
APi0507	26.07.05	NW of Camoghè	694 460	155 600	2180	Bündnerschiefer of Piora (-Scopi)
APi0508	27.07.05	North of Camoghè	694 665	155 490	2310	Bündnerschiefer of Piora (-Scopi)
APi0509	27.07.05	Sommet de Camoghè	694 705	155 410	2350	Bündnerschiefer of Piora (-Scopi)
APi0510	27.07.05	North of Camoghè	694 735	155 460	2300	Quartenschiefer
APi0511	27.07.05	North of Camoghè	694 740	155 510	2290	Bündnerschiefer of Piora (-Scopi)
APi0512	27.07.05	North of Camoghè	694 735	155 515	2290	Quartenschiefer? Bündnerschiefer?
APi0513	27.07.05	Entre Camoghè et alpe Tom	695 375	155 595	2070	Quartenschiefer? Bündnerschiefer?
APi0601	03.07.06	South of Foisc, idem APi0413	694 375	154 100	2130	Quartenschiefer
APi0602	03.07.06	South of Foisc, idem APi0413	694 375	154 100	2130	Quartenschiefer
APi0603	03.07.06	South of Foisc, idem APi0413	694 375	154 100	2130	Quartenschiefer
Alpe Robiei						
ARo0601	25.06.06	Alpe Robiei (near Albergo)	683 450	144 150	2010	Bündnerschiefer (from Maggia???)
ARo0602	25.06.06	Alpe Robiei (North, dir. Nufenen)	680 720	146 300	???	Quartenschiefer
ARo0603	25.06.06	Alpe Robiei (North, dir. Nufenen)	680 310	146 155	???	Quartenschiefer
Vrin-Vals (samples not deeply investigated in this work, relic of carpholite-bearing quartz and carbonate veins)						
AVr 0301 (I)	31.08.03	Road dir. Alpe Vaneschia	726 080	165 450	1830	Schistes of Lugnez
AVr 0301 (II)	31.08.03	Road dir. Alpe Vaneschia	726 080	165 450	1830	Schistes of Lugnez
AVr 0302	31.08.03	Road dir. Alpe Vaneschia	726 080	165 450	1830	Schistes of Lugnez

B) Mineral chemistry

Only a few mineral analyses are given in each chapter. Unpublished electron microprobe analyses obtained on a CAMECA SX-50 or a JEOL-8200 are available on CD for the following samples:

- **Antabia, Robiei:** AAn0401, –02, –05, ARo0601.
- **Campo Blenio, Vrin:** ACb0301, –05, ACb0404, –06, AVr0301.
- **Alpe Devero:** ADe0301, –02.
- **Lucomagno:** ALu0304, –06, –08, ALu0601, –03, MF315.
- **Molare, Aquila:** AAq0401, AMo0404, –06, –09, –10, AMo0503, –04, –05, –06.
- **Nufenen pass, Val Bedretto:** ANu0301, –03, –04, ANu0408, –11, –13.
- **Val Piora:** APi0301, –02, –04, –05, APi0401, –05, –07, –08, –09, –13, APi0501, –02, –05, –07, –08, –10, –12, APi0601, –03.

For each sample analysed, an Excel workbook contains one spreadsheet for each analysed mineral and a separate spreadsheet summarizing the most representative average(s). For a complete list of analysed minerals in each sample, please, refer to files "Analysed on JEOL.txt" and "Analysed on CAMECA.txt" (on CD). Most of the data were normalized based on cation normalization, but the macro "JEOL2xls" for Excel can be used to recalculate the original data based on oxide normalization (see help file of this macro at the end of this thesis, p. 193).

The macro "JEOL2xls" for Excel has been developed during this thesis and can be used a) to import element-%, compounds-% and detection limit of JEOL-8200 quantitative results, b) normalize the data (cation- or oxide-based) and c) import and treat Line Scan results. A copy of this macro is also available on CD. Check on my website for (eventual) further updates (URL: http://geoloweb.ch/).

Hundreads Mo of images are also available on CD, essentially backscatter images and element mapping results. These images illustrate some feature discussed in this thesis: association of muscovite and paragonite or margarite, K-feldspar and zoned micas in Val Antabia, garnet and feldspar zonations.... Especially, Some interesting feature regarding margarite (Ca-mica) are visible in element mapping from samples ACb0301 and ANu0304. These are classical Bünderschiefer at Campo Blenio and Nufenen pass. These two garnet-bearing calc-schists present clear relations with a) margarite and the growth of plagioclase (Ca-richer area, "pseudomorphosis" of margarite to plagioclase; ACb0301) and b) the fine occurrence of margarite in matrix and as tiny inclusion in bitotite (ANu0304). This later is visible at the optical microscope, with fine lamellae of low birefringence (1-5 µm thickness for 10-50 µm length; orange 1st order) inside biotite.

C) Thermobarometry

C.1) Programs and databases

All Pressure and Temperature (PT) results from the present thesis were obtained with TWQ (Berman, 1991) and a few samples were also briefly treated with THERMOCALC version 3.25 (Holland & Powell, 1998). Errors calculated by THERMOCALC are also larger and show a larger scatter of PT-results at sensibly higher T compared to TWQ. To complete PT-calcuation, pseudo-sections were sometimes computed with THERIAK-DOMINO (de Capitani & Brown, 1987; de Capitani, 1994) for a few interesting samples, especially metapelite.

Database and solid solutions considered for PT-calculation were presented in Chapters 2 and 3. An electronic version of these databases are found on CD: "JUN92.dat" and "JUN92.sln" for TWQ (with some variant: +staurolite, +two white-micas); "JUN92.basel" for THERIAK-DOMINO. Refer also to CD for the complete set of mineral analysis used for thermobarometric calculation ("oxi" files for TWQ; "th..." files for THERMOCALC), as also for other output files (activity calculation and numerical / graphical results).

C.2) Comments on PT-calculations

C.2.1) Mineral analyses

For each sample elected for PT-calculation, care was taken for the selection of mineral analyses required to compute equilibria in TWQ. This was very important, especially when biotite and garnet are considered. Indeed, both minerals are the majors Fe-Mg phases in equilibrium in quite all studied samples, sometimes associated to chlorite, chloritoid and/or staurolite. PT-calculations are highly sensitive to the Fe* ratio (Fe/Fe+Mg) of these minerals.

For garnet, we admit that its border is in equilibrium with the matrix mineral. In some case, an increase of Fe* at garnet rim is observed and can result from a) a re-equilibration during the thermal climax (slightly after the end of garnet growth) or b) a late retrogression feature (if too strong retrogression, sample is eliminated).

The case of biotite is trickier, as it likes to re-equilibrate with any other Fe-Mg phase at (quite) any moment in a short geological time (e.g. higher diffusion in biotite compared to garnet). Moreover, we suspect some metamorphic segregation or discreet chemical layering (stemming for sedimentation) in some samples to be responsible of local change in Fe* ratio of some biotite flakes (§2.6, §3.6). Though each grain is usually homogeneous, with exception of metapelite from Val Antabia (Chapter 3). Each biotite flake sometimes yields a different chemistry according to its position in thin section: around garnet, in a quartz- and muscovite-rich matrix or in contact with ilmenite. This has been clearly identified in samples from Alpe Devero, where a strong variation is correlated with the presence of garnet blast (ADe0302; Fig. C.1). The same is suspected in sample from Robiei (ARo0601), as also in metapelites from Antabia (see Chapter 3). This effect is probably enhanced if garnet is

strongly zoned and even more complicated in a sample, which presents variation of composition pertaining to different biotite generations (e.g. Antabia).

For PT-calculation, we always consider a biotite analysis in the vicinity of garnet, but we avoid grains in contact with garnet, as they possibly reflect either a later diffusion with garnet or is related to a later growth stage (e.g. garnet resorption, Bt-c in Val Antabia; Chapter 3). It is also essential to avoid biotite flakes in contact with ilmenite (strong diffusion effect, e.g. grain #4 in Figure C.1). An exception is in one PT-calculation of AAn0401-B, where the mineral assemblage found in garnet comprises biotite and rutile-ilmenite in contact (no other choice, used to estimate PT-condition during the early garnet growth). Surprisingly, PT-results yield coherent results with the expected prograde PT-path indicated by garnet zoning from THERIAK-DOMINO (§3.7.2.1).

C.2.2) Summary of PT-results

The entire set of PT-results is given in Table C.1 (from TWQ; Berman 1991). Though some tests were done with THERMOCALC 3.25, these results are not discussed here and are simply given in Table C.2. For a few samples, two or more PT-averages are given with different mineral assemblages, different mineral composition or different area of analysis in a thin section (see especially TWQ results in Table C.1). The molar fraction or activity calculated by TWQ or THERMOCALC is also available in Tables C.1 and C.2. Figure C.2 presents an overview of PT-results over a geological map, with TWQ graphical results (PT-grids including all computed equilibria). In complement, Figure C.3 summarizes in a PT-diagram all PT-results in each samples from this study, with error as calculated in INTERSX (including dehydration reactions).

PT-results at Val Piora present a larger scatter in P and T than any other studied region. This is fairly related to the numerous results obtained in this area (many suitable mineral assemblages for PT-calculation, especially in Quartenschiefer). However, PT-variations along N-S and E-W profiles also suggest some late tectonic feature occurring after the final equilibrium-PT (§C.5 and Fig. C.4).

C.2.3) Bulk rock composition and pseudo-sections

In complement to equilibrium PT-points determined with TWQ, a few pseudo-sections computed with THERIAK-DOMINO were discussed in Chapters 2 and 3 for samples AAn0401, ALu0603 and AMo0410. However, more samples have been treated during this thesis, and results are given on CD (PT-grids, garnet isopleths, etc.).

Bulk rock compositions used for calculation were obtained by XRF analysis at the Departement of Geosciences of Fribourg (Table C.4). To prevent heterogeneities induced by metamorphic segregation (porphyroblast growth), we typically started the crushing with ca. 1 kg material. This has strong effect on a few samples, notably AMo0410 (Pizzo Molare). This latter is clearly layered, with biotite- and garnet-rich layers (garnet-rich layer richer in MnO and CaO; sample SMo0407 from Dr. J.O. Schwarz, pers. comm.). However, bulk composition given in Table C.4 is an average of biotite-rich and garnet-rich layer, more representative of the entire outcrop at cm- to dm-scale. This might induce complications for the computation of PT-grids, i.e. what is the “representative” bulk rock composition for thermobarometric calculation? This question was not addressed in this study, as we prefer “homogeneous” samples, at least at mm-scale (AMo0410 is an exception confirming the rule).

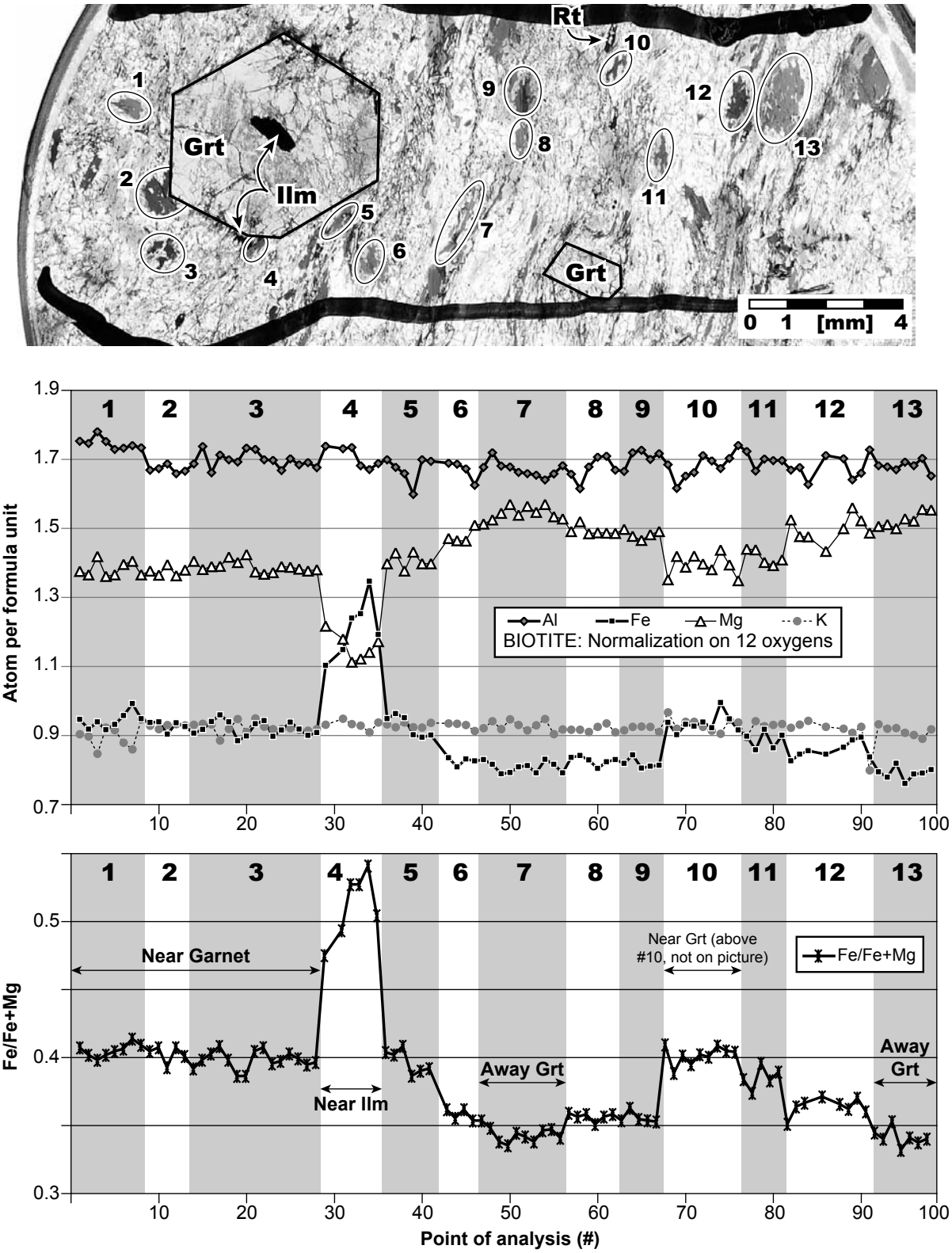

Fig. C.1: Variation of biotite composition in metapelite ADe0302 (Alpe Devero). Numbers in bold in the microphotography and in graphics is used to identify each biotite flake/book.

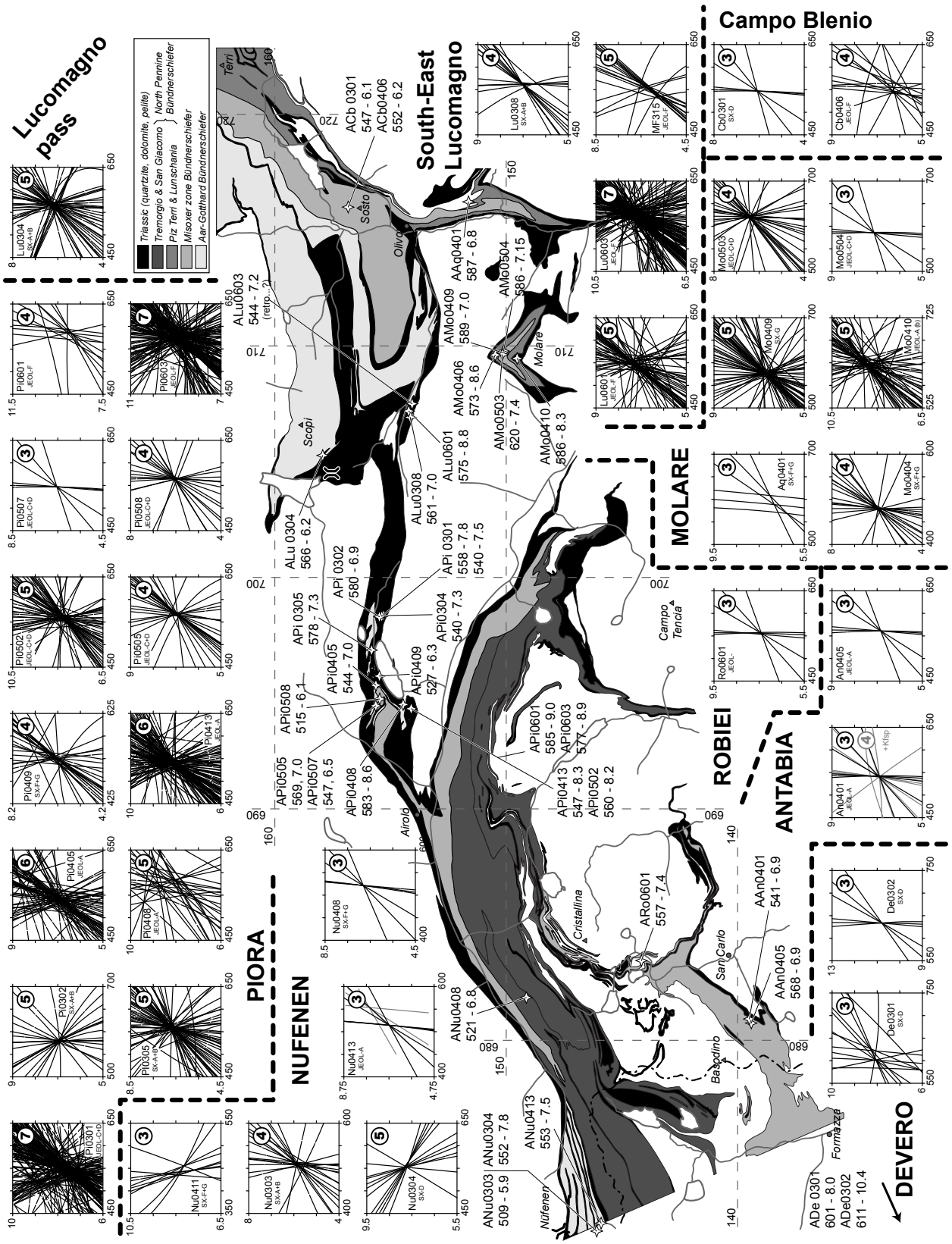

Fig. C.2: PT-results from TWQ over a geological map of Mesozoic metasediments from the northern Central Alps (Probst, 1980). All PT-grids are given with the same P and T range ($\Delta T = 200°C$; $\Delta P = 4$ kbar). Integer in circles corresponds to the number of Linear Independent Reactions (LIR).

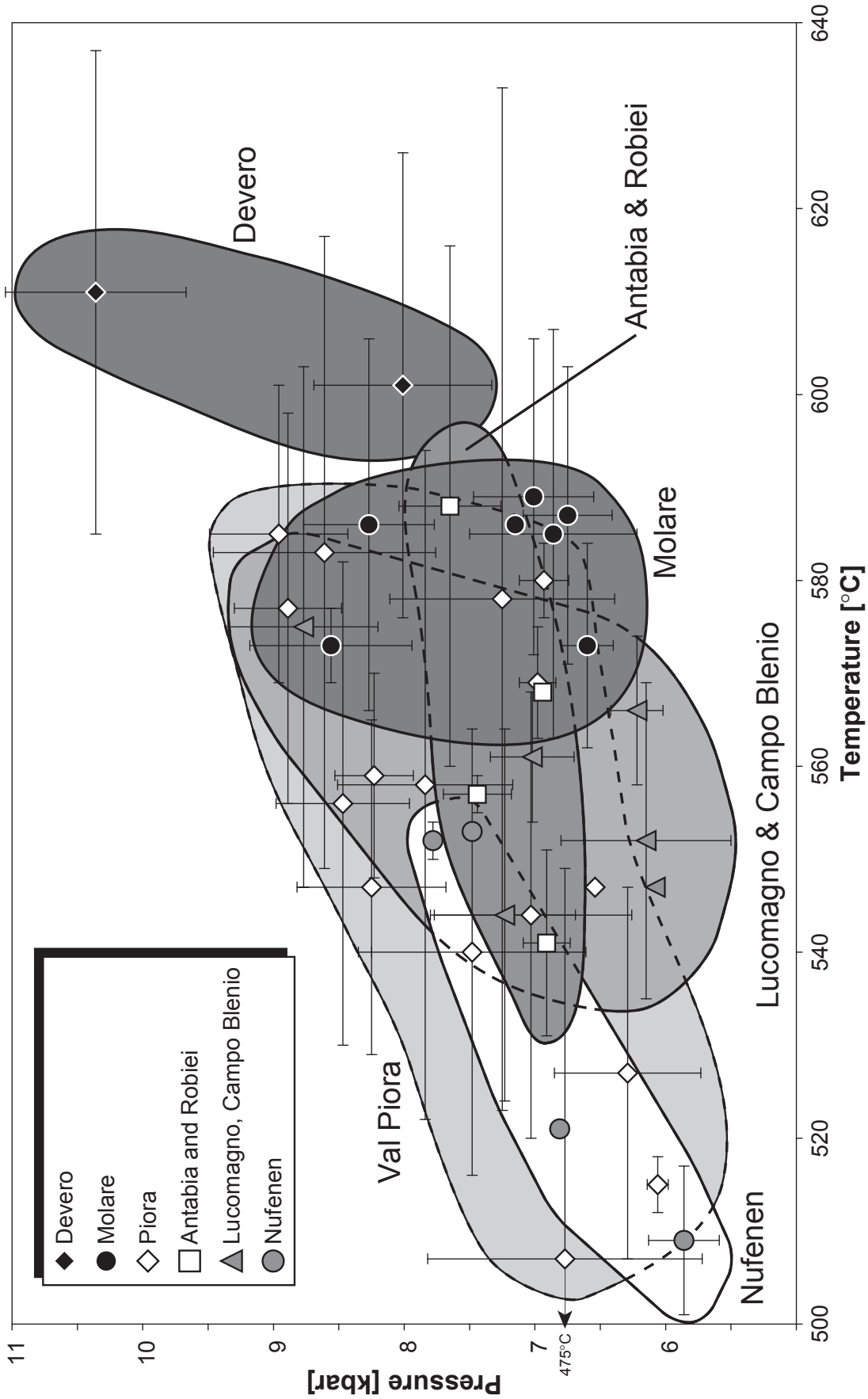

Fig. C.3: PT-condition determined in all studied samples, calculated with INTERSX (considering all equilibria intersecting at an angle > 15°.

C.3) Regional variation

In a broad view, a regular increase of the thermal climax condition towards the south is observed in the northern Central Alps. Temperature increases from Nufenen or Campo Blenio (520-560 °C) up to Alpe Devero or Pizzo Molare (580-620 °C; Fig. C.3). Pressure remains variable between 5-7 kbar at low grade, and slightly increasing around 7-9 kbar in the southern most area. These results are in good agreement with previous PT-results (Todd and Engi, 1997). Higher pressure are suggested in some areas (up to 2 kbar in Piora and Lucomagno) and is likely related to small differences in the thermodynamic database used in our study compared to Todd and Engi (1997).

"Higher" pressure (10-12 kbar) obtained in one sample from Alpe Devero remains discussable and would require a comparison with more PT-results in this area. The problem might be related to the biotite chemistry (Fig. C.1) or to late disequilibrium feature. Concerning all others area, small variation of pressure in a restricted area (±1 kbar) is explained by differential equilibration along the decompression path, with the exception of Val Piora (see below). Each sample will suffer a final equilibration (i.e. a "closure" of mineral composition to cationic exchange), but at variable pressure near the thermal climax. This was addressed notably in §2.7. A problem relative to equilibrium or bad definition of pressure could also account for this difference (most of equilibria are essentially T-dependent). However, all selected samples present a well-equilibrated texture and a good intersection of all equilibria in TWQ when more than 3 LIR are calculated (see Chapters 2, 3 and Fig. C.2).

C.4) Complementary thermometers

C.4.1) Chlorite-chloritoid

Fe-Mg exchange between coexisting chlorite and chloritoid was used to calculate temperature of equilibrium (Vidal *et al.*, 1999). Temperatures determined in samples from Val Piora yields coherent results with the PT-calculation from TWQ at the WNW ends of Val Piora (550-570 °C; Table C.3, Fig. C.3). For comparison, data from the literature for the Urseren-Garvera Zone are also given (Rahn, 2002; Livi *et al.*, 2002) and yield a temperature corresponding to the growth of allanite in Mesozoic metasediments (e.g. Janots *et al.*, in press). Data for chlorite and chloritoid from Vidal et al. (1999) are also suitable for the thermodynamic database of TWQ, but some test yield awful PT diagram with very bad intersection of reactions. Some samples yield abnormally high pressure (>12 kbar), while chloritoid remains poor in Mn (the contrary would have supported HP-condition).

C.4.2) Graphite thermometry

This thermometer is based on the evolution of organic material to graphite. Temperature is determined by the analysis of RAMAN spectrum on graphite in the range 1100-1800 cm^{-1} following the method described in Beyssac *et al.* (2002). Temperatures are comparable than PT-results obtained with TWQ on similar or identical samples (±10 °C). The problem is to find a significant volume of graphite to induce a strong signal on RAMAN spectrometer. This appears to be problematic in a few samples containing very little graphite. The too high or too low temperatures are calculated on spectra presenting a large and variable background (e.g. spectra in Table C.3).

C.5) Val Piora, a special case?

C.5.1) North-South profile

The shift in P (2-3 kbar) and T (30-40°) is essentially observed between samples from Quartenschiefer (Fig. C.4). Southern samples all belong to the MAG, while the origin of northern sample is uncertain (vicinity of the contact MAG/NPM). Three hypotheses are suggested to explain this trend (cases 1 and 2 are preferred):

1. Rapid, but regular increase of the metamorphism. This increase is rapid in Val Piora, but a few kilometres southwards, rocks remain at ca. 600, up to 650 °C in the Southern Steep Belt (Todd & Engi, 1997). Thus, an extrapolation to the South of the abrupt T-increase at Val Piora is not possible.

2. Late major tectonic feature (fault, thurst or fold). E-W oriented thrusts are numerous in this area, notably the Pennine frontal thrust. The soft Mesozoic metasediments are jammed between two large and rigid gneissic bodies (Gotthard and Lucomagno nappes). During exhumation and formation of the Northern Steep Belt (righting of nappes), some thrust movement may persist, enhanced by the compression of tow rigid bodies ("toothpaste tube" model). Some unit from the southern part yielding higher-P (8-9 kbar) are then really originating from deeper level compared to rocks found in the northern part (6-7 kbar).

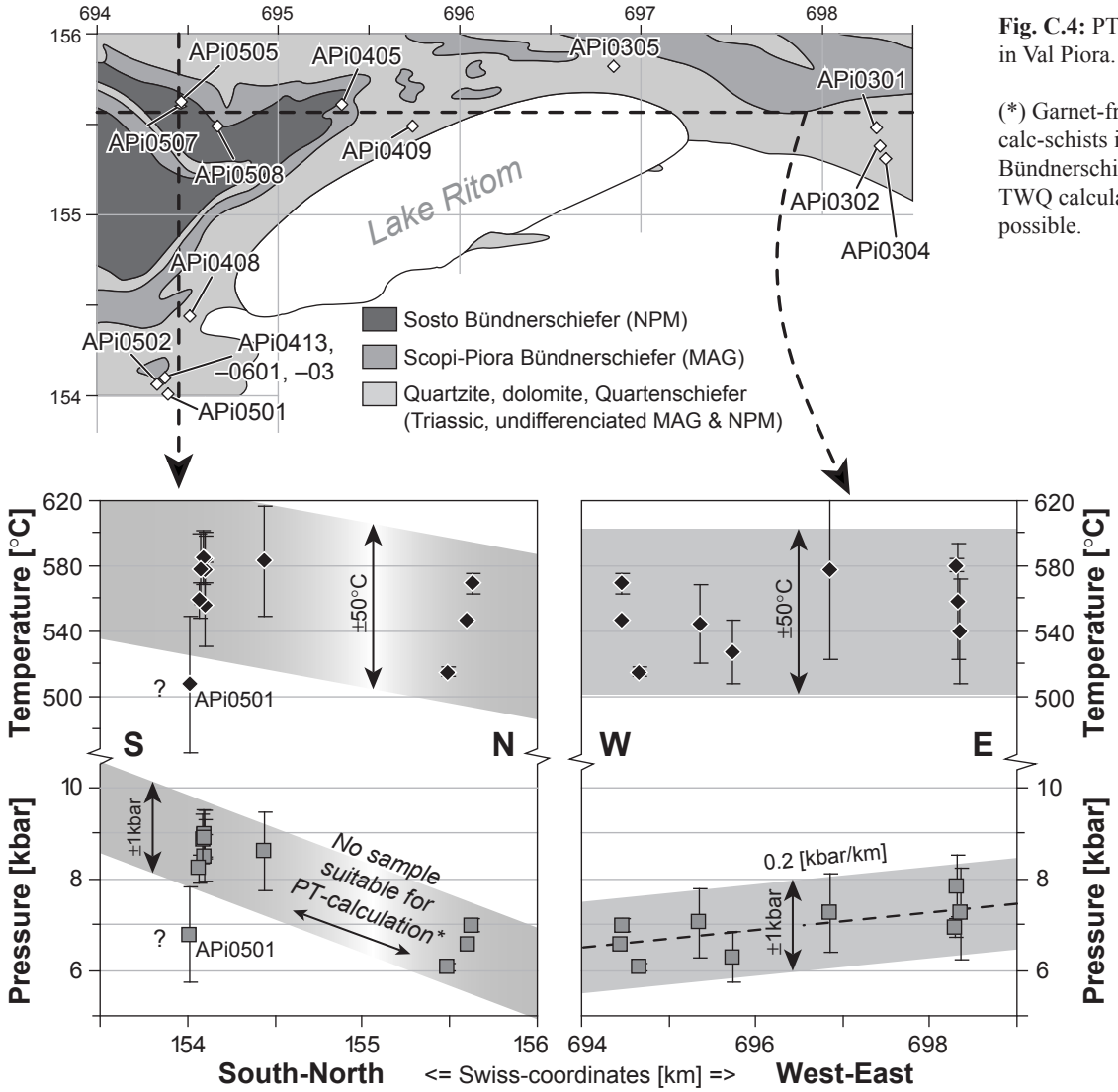

Fig. C.4: PT-results in Val Piora.

(*) Garnet-free calc-schists in Sosto Bündnerschiefer, no TWQ calculation possible.

3. Differential equilibration during the early exhumation and decompression (see §C.3). This is hardly applicable here, as similar results are obtained in a local area (e.g. northern or southern areas). Only the southern most sample yields lower PT-condition and could have recorded a later equilibration during the early decompression (one sample yield 510 °C / 7 kbar versus 560-580 / 8 in other samples).

C.5.2) East-West profile

Along this transect, temperatures calculated remain statistically undistinguishable. However, a sluggish but regular increase of pressure is observed eastwards. This is most likely related to the effect of a late folding, such as the Chièra synform (D4 in Maxelon & Mancktelow, 2005). This is actually the only late major fold occurring in this region susceptible to induce such a trend: pressure increases towards the Sambuco (South-West) and the Lucomagno nappes (East).

Directly related to this observation, we conclude that most of the mineral assemblages found in Val Piora were already equilibrated before the end of the back folding in the northern Central Alps. This is fully consistent with the petrography and the crystallization-deformation. Late porphyroblasts overgrow the schistosity and crystallize sometimes in the hinge of crenulation fold (kyanite, staurolite) or show a slight rotation together with the schistosity (garnet).

Table C.1: results from TWQ for **NUFENEN area**. The black box "OK" signalized results retained for this study (most representative results, usually lowest error). In contrary, the grey box "DISequilibrium" indicates that a larger spreading of equilibria suggests a chemical disequilibrium between minerals from the selected assemblage. Mineral and end-member abbreviations according to Kretz (1983).

In graphics	DISequilib.	OK	OK	OK	OK				
EMP-Analysis		A,B	D	F,G	JEOL-A	JEOL-A	JEOL-A	JEOL-A	JEOL-A
Sample		Nu0303	Nu0304	Nu0408	Nu0413-d	Nu0413-a	Nu0413-b	Nu0413-c	
X		671 770	671 750	681 870	672 110	672 110	672 110	672 110	
Y		146 075	146 100	149 125	145 890	145 890	145 890	145 890	
Altitude		2405	2405	1800	2460	2460	2460	2460	
PT calculation (INTERSX)									
Remarks, Comment					Grt low Fe* Pl high An	Grt high Fe* Pl high An	Grt low Fe* Pl low An	Grt high Fe* Pl low An	
LIR		3	2	2	2	2	2	2	
First iteration	P [kbar]	**5.85**	**7.72**	**6.81**	**7.48**	**6.74**	**7.60**	**6.88**	
	ΔP [kbar]	0.12	-	-	-	-	-	-	
	T [°C]	**509**	**552**	**522**	**553**	**514**	**553**	**515**	
	ΔT [°C]	7	-	-	-	-	-	-	
	xH2O	0.31	1.00	0.50	0.76	0.46	0.72	0.44	
	Δ xH2O	0.25	-	0.00	-	-	-	-	
LIR		4	3	3	3	3	3	3	
First iteration	P [kbar]	**5.86**	**7.78**	**6.81**	**7.48**	**6.74**	**7.63**	**6.88**	
	ΔP [kbar]	0.27	0.05	-	-	-	-	-	
	T [°C]	**509**	**552**	**521**	**553**	**514**	**554**	**515**	
	ΔT [°C]	8	2	-	-	-	-	-	
Solid solutions & activities									
Garnet	grs	0.1890	0.1479	0.2041	0.2043	0.2113	0.2043	0.2113	
	prp	0.0721	0.0739	0.1063	0.0930	0.0806	0.0930	0.0806	
	alm	0.7215	0.7418	0.6733	0.6986	0.7049	0.6986	0.7049	
	sps	0.0174	0.0363	0.0163	0.0040	0.0032	0.0040	0.0032	
Biotite	xMg	0.3915	0.3596	0.4861	0.4141	0.4141	0.4141	0.4141	
	xFe	0.4147	0.4481	0.3260	0.3714	0.3714	0.3714	0.3714	
	xTi	0.0442	0.0331	0.0352	0.0365	0.0365	0.0365	0.0365	
	xAl	0.1492	0.1592	0.1527	0.1775	0.1775	0.1775	0.1775	
	xK	0.9116	0.9069	0.8877	0.8487	0.8487	0.8487	0.8487	
	xOH	1.0000	1.0000	1.0000	1.0000	1.0000	1.0000	1.0000	
Muscovite	xK	0.9284	0.8980	0.9528	0.8396	0.8396	0.8396	0.8396	
	xNa	0.0716	0.1020	0.0472	0.1604	0.1604	0.1604	0.1604	
	xAl	0.9124	0.9133	0.8819	0.9261	0.9261	0.9261	0.9261	
	xOH	1.0000	1.0000	1.0000	1.0000	1.0000	1.0000	1.0000	
Margarite fixed act			0.5400						
Plagioclase	an			0.5783	0.3589	0.3589	0.3402	0.3402	
	ab			0.4154	0.6370	0.6370	0.6563	0.6563	
	or			0.0064	0.0041	0.0041	0.0035	0.0035	
Pure Phase		Ilm, Rt, Qtz	Ilm, Rt, Qtz	Qtz	Qtz	Qtz	Qtz	Qtz	Qtz
Phase not in calcul. (but stable?)		Czo, Carb	Czo	Ilm, ±Rt	Czo, Opaque	Czo, Opaque	Czo, Opaque	Czo, Opaque	Czo, Opaque

Table C.1: (continued) TWQ results for **DEVERO, ANTABIA, ROBIEI areas**.

	In graphics / DISequilib.	OK			OK	OK					DISequilib.	DISequilib.	OK				OK
	EMP-Analysis	D	D	E	D,G,JEOL-D	JEOL-F	JEOL-A,D	JEOL-A,D	JEOL-A,D	JEOL-F	JEOL-F	JEOL-F	JEOL-H	JEOL-H	JEOL-H	JEOL-A,D	JEOL-F
	Sample	De0301	De0301	De0301	De0302	An0401-C	An0401-B	An0401-B	An0401-B	An0401-C	An0401-D	An0401-D	An0402	An0402	An0402	An0405	Ro0601
	X	662 310	662 310	662 310	664 865	680 900	680 900	680 900	680 900	680 900	680 900	680 900	680 820	680 820	680 820	680 780	683 450
	Y	128 000	128 000	128 000	131 010	139 510	139 510	139 510	139 510	139 510	139 510	139 510	139 510	139 510	139 510	139 440	144 150
	Altitude	2140	2140	2140	1790	2300	2300	2300	2300	2300	2300	2300	2310	2310	2310	2325	2010
PT calculation (INTERSX)	Remarks, Comment	NO Ilm	NO Ky, Ilm	With Mrg, analysis from SX-E		Pelite, + Kfs	Contact pelite/calc	Contact pelite/calc	Assemblage in core of garnet	Pelite	PT AWFUL!!	With St, PT AWFUL!! !	Calc-schist (aSph 0.95)	Calc-schist, NO Sph	Calc-schist (aSph 1.00)		
	LIR	3	2	3	2	3	2	2	3	2	2	4	3	2	3	2	2
	First iteration P [kbar]	**8.15**	**8.23**	**8.80**	**10.66**	**6.91**	**8.50**	**6.74**	**6.13**	**6.92**	**9.16**	**6.36**	**7.80**	**7.77**	**7.74**	**6.94**	**7.40**
	First iteration ΔP [kbar]	0.77	-	0.40	-	0.33	-	-	0.28	-	-	1.96	0.62	-	0.58	-	-
	First iteration T [°C]	**612**	**623**	**632**	**637**	**541**	**637**	**529**	**526**	**541**	**673**	**465**	**597**	**595**	**590**	**568**	**554**
	First iteration ΔT [°C]	38	-	18	-	35	-	-	14	-	-	141	16	-	33	-	-
	xH2O	0.88	1.00	1.00	1.00	0.13	0.64	0.14	0.25	0.13			0.41	0.41	0.41	0.34	0.11
	Δ xH2O	0.04	-	-	-	0.01	-	-	0.06	-			-	-	-	-	-
	LIR	4	3	4	3	4	3	3	4	3	NOT calculated	NOT calculated	4	3	4	3	3
	First iteration P [kbar]	**8.01**	**8.08**	**8.68**	**10.36**	**6.91**	**8.54**	**6.77**	**6.06**	**6.94**	...	...	**7.65**	**7.64**	**7.64**	**6.94**	**7.44**
	First iteration ΔP [kbar]	0.68	0.21	0.29	0.69	0.18	-	-	0.37	0.16			0.39	0.18	0.50	-	0.26
	First iteration T [°C]	**601**	**609**	**626**	**611**	**541**	**637**	**531**	**523**	**542**			**584**	**584**	**581**	**568**	**557**
	First iteration ΔT [°C]	25	10	11	26	10	-	-	8	1			14	8	20	-	2
Solid solutions & activities	Garnet grs	0.1910	0.1910	0.1864	0.2143	0.2568	0.2516	0.2618	0.2509	0.2568	0.2283	0.2283	0.2589	0.2589	0.2589	0.2488	0.2385
	Garnet prp	0.1478	0.1478	0.1580	0.1441	0.0817	0.1143	0.0790	0.0545	0.0817	0.1376	0.1376	0.0890	0.0890	0.0890	0.0713	0.1103
	Garnet alm	0.6548	0.6548	0.6501	0.5905	0.6435	0.6222	0.6434	0.6624	0.6435	0.6224	0.6224	0.6035	0.6035	0.6035	0.6496	0.6291
	Garnet sps	0.0065	0.0065	0.0055	0.0511	0.0180	0.0119	0.0157	0.0323	0.0180	0.0116	0.0116	0.0486	0.0486	0.0486	0.0304	0.0220
	Biotite xMg	0.4851	0.4851	0.4850	0.5050	0.4284	0.4404	0.4380	0.3734	0.4284	0.4571	0.4571	0.4199	0.4199	0.4199	0.3732	0.4961
	Biotite xFe	0.3260	0.3260	0.3222	0.3153	0.3694	0.3635	0.3716	0.4585	0.3694	0.3559	0.3559	0.3855	0.3855	0.3855	0.4260	0.3261
	Biotite xTi	0.0247	0.0247	0.0326	0.0305	0.0335	0.0285	0.0379	0.0499	0.0335	0.0337	0.0337	0.0449	0.0449	0.0449	0.0626	0.0322
	Biotite xAl	0.1624	0.1624	0.1588	0.1464	0.1648	0.1637	0.1479	0.1142	0.1648	0.1488	0.1488	0.1493	0.1493	0.1493	0.1309	0.1425
	Biotite xK	0.8508	0.8508	0.8665	0.9212	0.9365	0.9403	0.9502	0.9318	0.9365	0.9357	0.9357	0.9353	0.9353	0.9353	0.9496	0.9258
	Biotite xOH	1.0000	1.0000	1.0000	1.0000	1.0000	1.0000	1.0000	1.0000	1.0000	1.0000	1.0000	1.0000	1.0000	1.0000	1.0000	1.0000
	Muscovite xK	0.8893	0.8893	0.8844	0.9074	0.9797	0.9659	0.9710	0.9659	0.9797	0.9809	0.9809	0.9633	0.9633	0.9633	0.9668	0.9817
	Muscovite xNa	0.1107	0.1107	0.1156	0.0926	0.0203	0.0341	0.0290	0.0341	0.0203	0.0191	0.0191	0.0367	0.0367	0.0367	0.0332	0.0183
	Muscovite xAl	0.9034	0.9034	0.9011	0.8898	0.8661	0.8724	0.8483	0.8724	0.8661	0.8823	0.8823	0.8940	0.8940	0.8940	0.8631	0.8747
	Muscovite xOH	1.0000	1.0000	1.0000	1.0000	1.0000	1.0000	1.0000	1.0000	1.0000	1.0000	1.0000	1.0000	1.0000	1.0000	1.0000	1.0000
	Margarite fixed act			0.6840													
	Plagioclase an	0.6362	0.6362	0.4284	0.2549	0.7029	0.7695	0.7541	0.5832	0.7029	0.6871	0.6871	0.5669	0.5669	0.5669	0.6276	0.7162
	Plagioclase ab	0.3609	0.3609	0.5671	0.7397	0.2883	0.2270	0.2412	0.4087	0.2883	0.3060	0.3060	0.4220	0.4220	0.4220	0.3653	0.2757
	Plagioclase or	0.0028	0.0028	0.0045	0.0054	0.0088	0.0035	0.0047	0.0081	0.0088	0.0068	0.0068	0.0111	0.0111	0.0111	0.0070	0.0081
	K-feldspar an					0.0000							0.0030	0.0030	0.0030		
	K-feldspar ab					0.0439							0.0891	0.0891	0.0891		
	K-feldspar or					0.9561							0.9079	0.9079	0.9079		
	Staurolite xMg											0.2242					
	Staurolite xFe											0.7758					
	Pure Phase	Qtz	Qtz	Qtz	Qtz	Qtz	Qtz	Qtz	Qtz, Ilm, Rt	Qtz	Qtz	Qtz	Qtz, Rt, Sph	Qtz	Qtz, Rt, Sph	Qtz	Qtz
	Phase not in calcul. (but stable?)	Ilm, Rt	Ky	Ilm, Rt	Rt	Czo, Ilm	Czo, Ilm	Czo, Ilm	Czo, ±Carb	Czo, Ilm	Czo, Ilm	Czo, Ilm	Calcite	Rt, Sph, Calcite	Calcite	Czo, Rt, ±Cc?	Rt, Czo

Table C.1: (continued) TWQ results for **AQUILA, CAMPO-BLENIO, LUCOMAGNO areas**.

In graphics	DISequilib.		OK	OK		OK	OK	OK			OK			OK
EMP-Analysis		F,G	D	JEOL-F	JEOL-F	A,B	A,B	JEOL-F	JEOL-F	JEOL-F	JEOL-F	JEOL-F	JEOL-F	JEOL-F
Sample		Aq0401	Cb0301	Cb0406	Cb0406	Lu0304	Lu0308	Lu0601	Lu0601	Lu0601	Lu0603	Lu0603	Lu0603	MF315
X		716 225	715 000	715 050	715 050	705 270	706 910	707 190	707 190	707 190	707 525	707 525	707 525	707 650
Y		151 675	156 830	156 920	156 920	157 930	154 150	154 200	154 200	154 200	154 030	154 030	154 030	153 950
Altitude		1045	1200	1195	1195	2140	1785	1760	1760	1760	1770	1770	1770	1760
PT calculation (INTERSX)	Remarks, Comment	NO Ky, St						NO Ky	With Ky, no Bt	With Ky	With Ky	With Ky, NO Bt	NO Ky	NO Bt
	LIR	3	2	3	2	4	3	4	4	5	7	5	6	Bug Intersx
	First iteration P [kbar]	**6.84**	**6.08**	**6.09**	**6.21**	**6.26**	**7.03**	**7.24**	**7.43**	**7.31**	**8.81**	**8.65**	**8.77**	
	First iteration ΔP [kbar]	0.32	-	0.77	-	0.16	0.53	0.51	0.32	0.63	0.67	0.59	0.57	
	First iteration T [°C]	**590**	**547**	**554**	**541**	**569**	**562**	**545**	**552**	**547**	**576**	**568**	**575**	
	First iteration ΔT [°C]	19	-	26	-	9	2	23	28	26	29	36	28	
	xH2O	0.94	0.74	0.40	0.45	0.97	0.34	0.37	0.29	0.27	0.36	0.34	0.36	0.51
	Δ xH2O	0.00	0.00	-	-	0.05	0.05	0.07	0.06	0.08	Bug Intersx	0.06	Bug Intersx	Bug Intersx
	LIR	4	3	4	3	5	4	5	5	6	8	6	7	5
	First iteration P [kbar]	**6.75**	**6.08**	**6.15**	**6.33**	**6.22**	**7.02**	**7.23**	**7.49**	**7.28**	**8.84**	**8.67**	**8.83**	**6.00**
	First iteration ΔP [kbar]	0.34	-	0.65	0.16	0.20	0.32	0.54	0.31	0.60	0.62	0.48	0.52	0.39
	First iteration T [°C]	**587**	**547**	**552**	**553**	**566**	**561**	**544**	**555**	**546**	**577**	**569**	**577**	**549**
	First iteration ΔT [°C]	16	-	17	8	8	7	20	12	22	23	19	20	12
Solid solutions & activities	Garnet grs	0.1266	0.1947	0.2059	0.2059	0.1851	0.1636	0.1613	0.1613	0.1613	0.1094	0.1094	0.1094	0.0503
	Garnet prp	0.1457	0.0702	0.0736	0.0736	0.0823	0.1390	0.1238	0.1238	0.1238	0.1538	0.1538	0.1538	0.1450
	Garnet alm	0.6258	0.7241	0.7059	0.7059	0.6973	0.6780	0.7109	0.7109	0.7109	0.7349	0.7349	0.7349	0.7959
	Garnet sps	0.1019	0.0110	0.0145	0.0145	0.0353	0.0195	0.0040	0.0040	0.0040	0.0020	0.0020	0.0020	0.0089
	Biotite xMg	0.4891	0.3684	0.3930	0.3930	0.3826	0.4952	0.4662		0.4662	0.4720		0.4720	
	Biotite xFe	0.3379	0.4485	0.4293	0.4293	0.4306	0.3178	0.3487		0.3487	0.3295		0.3295	
	Biotite xTi	0.0236	0.0361	0.0364	0.0364	0.0367	0.0353	0.0315		0.0315	0.0227		0.0227	
	Biotite xAl	0.1472	0.1449	0.1403	0.1403	0.1495	0.1515	0.1534		0.1534	0.1756		0.1756	
	Biotite xK	0.9045	0.9349	0.9174	0.9174	0.8784	0.8927	0.8878		0.8878	0.8327		0.8327	
	Biotite xOH	1.0000	1.0000	1.0000	1.0000	1.0000	1.0000	1.0000		1.0000	1.0000		1.0000	
	Muscovite xK	0.8448	0.9244	0.9513	0.9513	0.9376		0.9181	0.9181	0.9181	0.8469	0.8469	0.8469	0.8224
	Muscovite xNa	0.1552	0.0756	0.0487	0.0487	0.0624		0.0819	0.0819	0.0819	0.1531	0.1531	0.1531	0.1776
	Muscovite xAl	0.8862	0.9072	0.9159	0.9159	0.9011		0.9191	0.9191	0.9191	0.9279	0.9279	0.9279	0.9372
	Muscovite xOH	1.0000	1.0000	1.0000	1.0000	1.0000		1.0000	1.0000	1.0000	1.0000	1.0000	1.0000	1.0000
	Paragonite xK										0.0954	0.0954	0.0954	0.1025
	Paragonite xNa										0.9046	0.9046	0.9046	0.8975
	Paragonite xAl										0.9842	0.9842	0.9842	0.9780
	Paragonite xOH										1.0000	1.0000	1.0000	1.0000
	Margarite fixed act			0.6423		0.7255								
	Plagioclase an	0.3968	0.7965	0.8561	0.8561	0.8771	0.4601	0.3400	0.3400	0.3400	0.1980	0.1980	0.1980	0.1634
	Plagioclase ab	0.5981	0.2017	0.1421	0.1421	0.1217	0.5348	0.6559	0.6559	0.6559	0.7985	0.7985	0.7985	0.8331
	Plagioclase or	0.0052	0.0018	0.0018	0.0018	0.0012	0.0051	0.0041	0.0041	0.0041	0.0035	0.0035	0.0035	0.0035
	Staurolite xMg	0.1629					0.2322	0.2062	0.2062	0.2062	0.2340	0.2340	0.2340	0.2060
	Staurolite xFe	0.8371					0.7678	0.7827	0.7827	0.7827	0.7634	0.7634	0.7634	0.7940
	Pure Phase	Qtz	Qtz	Qtz	Qtz	Ilm, Rt, Qtz	Ky, Qtz	Qtz	Qtz, Ky	Qtz, Ky	Qtz, Ky	Qtz, Ky	Qtz	Qtz
	Phase not in calcul. (but stable?)	Ilm, Ky, St	Ilm, ±Czo	Ilm, ±Czo	Ilm, ±Czo	Czo, Carb	Czo, Ilm, ±Rt	Ky, Rt	Rt, Bt	Rt	Rt, ±Ilm	Rt, ±Ilm, Bt	Ky, Rt, ±Ilm	Bt, Rt

Table C.1: (continued) TWQ results for **MOLARE area**.

In graphics	DISequilib.	OK	OK	DISequilib.	OK				OK		High-T???	OK	DISequilib.	DISequilib.
EMP-Analysis		F,G	JEOL-F	JEOL-F	G	F,G	JEOL-A	JEOL-A	JEOL-A	JEOL-A	JEOL-C,D	JEOL-C,D	JEOL-F	JEOL-F
Sample		Mo0404	Mo0406	Mo0406	Mo0409	Mo0409	Mo0409	Mo0410-a	Mo0410-a	Mo0410-b	Mo0503	Mo0504	Mo0505	Mo0506
X		713 280	709 590	709 590	709 670	709 670	709 670	709 460	709 460	709 460	709 630	709 780	709 625	709 950
Y		149 375	150 460	150 460	150 130	150 130	150 130	149 510	149 510	149 510	150 140	150 105	150 165	150 000
Altitude		1270	2530	2530	2450	2450	2450	2555	2555	2555	2460	2460	2465	2410
PT calculation (INTERSX)	Remarks, Comment		NO St (retrogr.?)	With St, AWFUL PT		NO Mg-St	NO Mg-St	With Ky	With Prg and Ky		Area #2 (thin sct)		NO St,Ky, AWFUL PT	NO St,Ky, AWFUL PT
	LIR	3	2	4	4	3	3	4	6	4	3	3	2	2
	First iteration P [kbar]	**5.96**	**8.48**	**6.84**	**6.66**	**6.72**	**6.90**	**8.23**	**8.45**	**8.83**	**7.44**	**7.14**	**10.98**	**7.79**
	First iteration ΔP [kbar]	0.09	-	2.54	0.27	0.76	0.54	0.60	0.50	0.44	0.08	-	-	-
	First iteration T [°C]	**479**	**568**	**517**	**573**	**580**	**582**	**585**	**595**	**612**	**622**	**585**	**671**	**631**
	First iteration ΔT [°C]	5	-	32	16	35	26	24	14	20	4	-	-	-
	xH2O	0.30	0.49	-	0.60	1.00	0.72	0.40	0.47	0.53	0.99	0.33		
	Δ xH2O	0.04	-	Sans Mg-St	Bug Intersx	-	0.08	0.11	0.11	0.14	0.01	-		
	LIR	4	3	3	5	4	4	5	7	5	4	3	NOT calculated	NOT calculated
	First iteration P [kbar]	**5.97**	**8.56**	**7.76**	**6.63**	**6.86**	**7.01**	**8.27**	**8.43**	**8.84**	**7.42**	**7.15**		
	First iteration ΔP [kbar]	0.10	0.62	2.36	0.24	0.64	0.46	0.50	0.49	0.45	0.11	0.01	...	...
	First iteration T [°C]	**479**	**573**	**507**	**573**	**585**	**589**	**586**	**594**	**616**	**620**	**586**		
	First iteration ΔT [°C]	3	4	42	11	22	17	20	14	17	4	1		
Solid solutions & activities	Garnet grs	0.1987	0.2321	0.2321	0.1505	0.1505	0.1534	0.0837	0.0837	0.0831	0.1676	0.2031	0.1025	0.2174
	Garnet prp	0.0698	0.0927	0.0927	0.1328	0.1328	0.1336	0.1734	0.1734	0.1765	0.1474	0.1026	0.1546	0.1094
	Garnet alm	0.7008	0.6551	0.6551	0.7053	0.7053	0.7035	0.7293	0.7293	0.7365	0.6805	0.6704	0.7400	0.6488
	Garnet sps	0.0307	0.0200	0.0200	0.0114	0.0114	0.0095	0.0136	0.0136	0.0040	0.0045	0.0240	0.0030	0.0244
	Biotite xMg	0.4220	0.4343	0.4343	0.4692	0.4527	0.4530	0.4942	0.4942	0.4761	0.4683	0.4296	0.4322	0.4171
	Biotite xFe	0.3860	0.3694	0.3694	0.3515	0.3750	0.3664	0.3219	0.3219	0.3512	0.3450	0.3802	0.3862	0.3907
	Biotite xTi	0.0439	0.0297	0.0297	0.0357	0.0393	0.0386	0.0224	0.0224	0.0284	0.0352	0.0433	0.0275	0.0635
	Biotite xAl	0.1461	0.1655	0.1655	0.1437	0.1331	0.1414	0.1604	0.1604	0.1435	0.1506	0.1433	0.1538	0.1255
	Biotite xK	0.9280	0.9337	0.9337	0.9380	0.9221	0.9130	0.8600	0.8600	0.8410	0.9151	0.9420	0.8729	0.9470
	Biotite xOH	1.0000	1.0000	1.0000	1.0000	1.0000	1.0000	1.0000	1.0000	1.0000	1.0000	1.0000	1.0000	1.0000
	Muscovite xK	0.9226	0.9254	0.9254	0.8931	0.8931	0.8923	0.7705	0.7705	0.7705	0.9433	0.9686	0.8781	0.9853
	Muscovite xNa	0.0774	0.0746	0.0746	0.1069	0.1069	0.1077	0.2295	0.2295	0.2295	0.0567	0.0314	0.1219	0.0147
	Muscovite xAl	0.9066	0.9166	0.9166	0.8546	0.8546	0.8568	0.8830	0.8830	0.8830	0.8655	0.8433	0.9173	0.8897
	Muscovite xOH	1.0000	1.0000	1.0000	1.0000	1.0000	1.0000	1.0000	1.0000	1.0000	1.0000	1.0000	1.0000	1.0000
	Paragonite xK								0.1090					
	Paragonite xNa								0.8910					
	Paragonite xAl								0.9700					
	Paragonite xOH								1.0000					
	Plagioclase an	0.3498	0.2995	0.2995	0.4858	0.4858	0.4626	0.1970	0.1970	0.1970	0.8693	0.8081	0.1700	0.8825
	Plagioclase ab	0.6435	0.6946	0.6946	0.5108	0.5108	0.5339	0.7979	0.7979	0.7979	0.1307	0.1846	0.8265	0.1137
	Plagioclase or	0.0067	0.0059	0.0059	0.0034	0.0034	0.0035	0.0052	0.0052	0.0052	0.0000	0.0073	0.0036	0.0038
	Staurolite xMg			0.1632	0.2131	0.2196	0.2152	0.2186	0.2186	0.2186	0.1730		0.2088	
	Staurolite xFe			0.7366	0.7757	0.7804	0.7448	0.7814	0.7814	0.7814	0.7110		0.7862	
	Pure Phase	Qtz, Ilm, Rt	Qtz	Qtz	Qtz	Qtz	Qtz	Qtz, Ky	Qtz, Ky		Qtz	Qtz	Qtz	Qtz
	Phase not in calcul. (but stable?)	Czo	Ilm, Rt, ±Czo	Ilm, Rt, ±Czo	Ilm, ±Czo	Ilm, ±Czo, Mg-St	Ilm, ±Czo, Mg-St	Mg-St, Ilm, Rt	Mg-St, Ilm, Rt	Mg-St, Ilm, Rt	Mg-St, Ep	Carb, Czo, Ilm	Ilm, Rt, Ky	Rt, ±Czo, Carb, Ilm

Table C.1: (continued) TWQ results for **PIORA area (1/2)**.

In graphics	DISequilib.	OK					OK	OK			OK	OK	OK	
EMP-Analysis		D,JEOL-D	D,JEOL-D	D,JEOL-D	D,JEOL-D	D,JEOL-D	A,B	A,B	F,G	F,G	JEOL-A	JEOL-A	F,G	F,G
Sample		Pi0301	Pi0301	Pi0301	Pi0301	Pi0301	Pi0302	Pi0305	Pi0304	Pi0304	Pi0405	Pi0408	Pi0409	Pi0409
X		698 320	698 320	698 320	698 320	698 320	698 300	696 850	698 350	698 350	695 350	694 510	695 740	695 740
Y		155 380	155 380	155 380	155 380	155 380	155 480	155 820	155 310	155 310	155 610	154 440	155 490	155 490
Altitude		2075	2075	2075	2075	2075	2030	1920	2045	2045	2090	2065	1910	1910
PT calculation (INTERSX)	Remarks, Comment	+Mg-St	Pg+Ms, max K in Pg, bad equil.	Pg+Ms, min K in Pg	Ms only	Pg (max K) only		Bad equilibrium	With St, bad equilibrium	NO St			With St	NO St
	LIR	6	5	5	3	3	3	3	3	2	5	4	3	2
	First iteration P [kbar]	**7.84**	**7.79**	**7.57**	**7.65**	**7.87**	**6.95**	**7.42**	**6.96**	**6.88**	**7.30**	**8.57**	**6.40**	**6.42**
	First iteration ΔP [kbar]	0.67	0.83	0.73	0.78	0.83	0.33	0.70	0.75	-	0.88	0.89	0.69	-
	First iteration T [°C]	**558**	**548**	**545**	**543**	**552**	**580**	**621**	**530**	**491**	**556**	**591**	**531**	**513**
	First iteration ΔT [°C]	36	27	28	21	36	6	42	29	-	35	33	29	-
	xH2O	0.36	0.36	0.38	0.37	0.37	0.42	0.39	0.40	0.14	0.44	0.49	0.34	0.35
	Δ xH2O	0.10	0.08	0.09	0.11	0.14	0.02	0.11	0.18	0.00	0.12	0.13	0.08	-
	LIR	7	6	6	4	4	4	4	4	3	6	5	4	3
	First iteration P [kbar]	**7.84**	**7.67**	**7.48**	**7.54**	**7.72**	**6.93**	**7.25**	**7.25**	**6.86**	**7.03**	**8.61**	**6.29**	**6.42**
	First iteration ΔP [kbar]	0.82	0.88	0.87	0.55	0.64	0.19	0.86	1.00	-	0.77	0.85	0.56	-
	First iteration T [°C]	**549**	**543**	**540**	**540**	**547**	**580**	**578**	**540**	**490**	**544**	**583**	**527**	**513**
	First iteration ΔT [°C]	24	23	24	18	21	4	55	32	-	24	34	20	-
Solid solutions & activities	Garnet grs	0.1365	0.1365	0.1365	0.1365	0.1365	0.1361	0.1670	0.1309	0.1309	0.1170	0.1613	0.1569	0.1569
	Garnet prp	0.1296	0.1296	0.1296	0.1296	0.1296	0.1354	0.1236	0.1296	0.1296	0.1116	0.1561	0.1108	0.1108
	Garnet alm	0.7293	0.7293	0.7293	0.7293	0.7293	0.6834	0.6925	0.7330	0.7330	0.7472	0.6687	0.7168	0.7168
	Garnet sps	0.0045	0.0045	0.0045	0.0045	0.0045	0.0451	0.0169	0.0065	0.0065	0.0241	0.0139	0.0155	0.0155
	Biotite xMg	0.5179	0.5179	0.5179	0.5179	0.5179	0.4792	0.4749	0.5305	0.5305	0.4613	0.5281	0.4845	0.4845
	Biotite xFe	0.3112	0.3112	0.3112	0.3112	0.3112	0.3466	0.3361	0.3006	0.3006	0.3495	0.2821	0.3378	0.3378
	Biotite xTi	0.0234	0.0234	0.0234	0.0234	0.0234	0.0301	0.0342	0.0254	0.0254	0.0247	0.0256	0.0321	0.0321
	Biotite xAl	0.1475	0.1475	0.1475	0.1475	0.1475	0.1433	0.1539	0.1434	0.1434	0.1636	0.1633	0.1454	0.1454
	Biotite xK	0.8441	0.8441	0.8441	0.8441	0.8441	0.8836	0.9271	0.8464	0.8464	0.8747	0.8785	0.9286	0.9286
	Biotite xOH	1.0000	1.0000	1.0000	1.0000	1.0000	1.0000	1.0000	1.0000	1.0000	1.0000	1.0000	1.0000	1.0000
	Muscovite xK	0.7359	0.7359	0.7359	0.7359			0.9302	0.7593	0.7593	0.7688	0.8399	0.8923	0.8923
	Muscovite xNa	0.2641	0.2641	0.2641	0.2641			0.0698	0.2407	0.2407	0.2312	0.1601	0.1077	0.1077
	Muscovite xAl	0.9252	0.9252	0.9252	0.9252			0.9119	0.9278	0.9278	0.9324	0.9459	0.8951	0.8951
	Muscovite xOH	1.0000	1.0000	1.0000	1.0000			1.0000	1.0000	1.0000	1.0000	1.0000	1.0000	1.0000
	Paragonite xK	0.0862	0.0862	0.0671		0.0862					0.1272			
	Paragonite xNa	0.9138	0.9138	0.9329		0.9138					0.8728			
	Paragonite xAl	0.9841	0.9841	0.9869		0.9841					0.9826			
	Paragonite xOH	1.0000	1.0000	1.0000		1.0000					1.0000			
	Margarite fixed act						0.4971					0.5800		
	Plagioclase an	0.2538	0.2538	0.2538	0.2538	0.2538		0.6796	0.2670	0.2670	0.2518	0.3607	0.3798	0.3798
	Plagioclase ab	0.7424	0.7424	0.7424	0.7424	0.7424		0.3176	0.7297	0.7297	0.7447	0.6352	0.6150	0.6150
	Plagioclase or	0.0039	0.0039	0.0039	0.0039	0.0039		0.0028	0.0034	0.0034	0.0034	0.0041	0.0051	0.0051
	Staurolite xMg	0.2249	0.2249	0.2249	0.2249	0.2249	0.2213	0.2205	0.2240	0.2240	0.2102		0.2170	0.2170
	Staurolite xFe	0.7751	0.7751	0.7751	0.7751	0.7751	0.7787	0.7795	0.7760	0.7760	0.7898		0.7830	0.7830
	Pure Phase	Qtz	Qtz	Qtz	Qtz	Qtz	Ky, Qtz	Qtz	Qtz	Qtz	Qtz	Qtz, Ky	Qtz	Qtz
	Phase not in calcul. (but stable?)	Ilm	Mg-St, Ilm	Mg-St, Ilm	Mg-St, Ilm	Mg-St, Ilm	Ilm, Hb	Czo, Carb, Ilm, ±Rt	Ilm, ±Rt	St, Ilm, ±Rt	Cld, Opaque	Czo, Rt, ±Oxy/Sulf?	Czo, Ilm, ±Rt, St	St, Czo, Ilm, ±Rt

Table C.1: (continued) TWQ results for **PIORA area (2/2)**.

In graphics	DISequilib.	OK			DISequilib?	OK	OK	OK	OK	DISequilib?	OK		OK	
EMP-Analysis		JEOL-A,D	JEOL-A,D	JEOL-A,D	JEOL-C,D	JEOL-C,D	JEOL-C,D	JEOL-C,D	JEOL-C,D	JEOL-C,D	JEOL-F	JEOL-F	JEOL-F	JEOL-F
Sample		Pi0413-a	Pi0413-a	Pi0413-b	Pi0501	Pi0502	Pi0505	Pi0507	Pi0508	Pi0512	Pi0601	Pi0601	Pi0603	Pi0603
X		694 375	694 375	694 375	694 390	694 330	694 465	694 460	694 665	694 735	694 375	694 375	694 375	694 375
Y		154 100	154 100	154 100	154 010	154 065	155 625	155 600	155 490	155 515	154 100	154 100	154 100	154 100
Altitude		2130	2130	2130	2095	2090	2195	2180	2310	2290	2130	2130	2130	2130
PT calculation (INTERSX)	Remarks, Comment	With Mg-St	NO Mg-St, Bt (1)	NO Mg-St, Bt (2)	BAD intersect				Retrograde equilibria?	Bug HP 13kb	Min An in Pl (rim!), NO St	Max An, NO St	Max Fe in Bt, NO Ky	Max Fe in Bt, with Ky
	LIR	6	5	5	3	4	3	2	2	4	3	3	6	7
	First iteration P [kbar]	**8.47**	**8.35**	**8.43**	**6.50**	**8.22**	**6.99**	**6.54**	**6.07**	**12.36**	**8.96**	**7.85**	**9.00**	**8.86**
	First iteration ΔP [kbar]	0.51	0.60	0.52	0.87	0.38	0.16	-	0.08	1.92	0.77	1.12	0.63	0.65
	First iteration T [°C]	**556**	**551**	**560**	**497**	**559**	**569**	**547**	**515**	**567**	**586**	**584**	**576**	**576**
	First iteration ΔT [°C]	26	25	22	43	14	6	-	4	35	27	15	32	29
	xH2O	0.33	0.31		0.18	0.65	0.70	0.44	0.29		0.41	0.55	0.39	0.39
	Δ xH2O	0.08	0.09		0.19	0.06	0.05	-	0.03		0.06	0.16	Bug Intersx	Bug Intersx
	LIR	7	6	NOT calculated	4	5	4	3	4	NOT calculated	4	4	7	8
	First iteration P [kbar]	**8.39**	**8.25**		**6.77**	**8.23**	**6.98**	**6.54**	**6.06**		**8.96**	**8.04**	**8.87**	**8.86**
	First iteration ΔP [kbar]	0.61	0.57	...	1.05	0.30	0.14	-	0.08	...	0.53	0.98	0.56	0.65
	First iteration T [°C]	**553**	**547**		**507**	**559**	**569**	**547**	**515**		**585**	**590**	**579**	**579**
	First iteration ΔT [°C]	21	18		42	11	6	-	3		16	14	21	24
Solid solutions & activities	Garnet grs	0.1458	0.1458	0.1458	0.1788	0.1514	0.1208	0.2103	0.2192		0.1093	0.1093	0.1346	0.1346
	Garnet prp	0.1419	0.1419	0.1419	0.1211	0.1465	0.1262	0.0870	0.0691		0.1823	0.1823	0.1609	0.1609
	Garnet alm	0.7020	0.7020	0.7020	0.6797	0.6780	0.7147	0.6642	0.6844		0.7012	0.7012	0.6994	0.6994
	Garnet sps	0.0102	0.0102	0.0102	0.0203	0.0241	0.0383	0.0384	0.0273		0.0072	0.0072	0.0051	0.0051
	Biotite xMg	0.5238	0.5238	0.5093	0.4929	0.5140	0.4541	0.4149	0.4210	0.4200	0.5248	0.5248	0.5186	0.5186
	Biotite xFe	0.2945	0.2945	0.3047	0.3221	0.2971	0.3478	0.3759	0.4231	0.3917	0.2815	0.2815	0.3022	0.3022
	Biotite xTi	0.0294	0.0294	0.0239	0.0284	0.0278	0.0264	0.0323	0.0381	0.0246	0.0139	0.0139	0.0242	0.0242
	Biotite xAl	0.1519	0.1519	0.1619	0.1549	0.1605	0.1706	0.1758	0.1163	0.1637	0.1798	0.1798	0.1548	0.1548
	Biotite xK	0.8733	0.8733	0.8870	0.9070	0.8862	0.8705	0.9207	0.8672	0.8645	0.8705	0.8705	0.8565	0.8565
	Biotite xOH	1.0000	1.0000	1.0000	1.0000	1.0000	1.0000	1.0000	1.0000	1.0000	1.0000	1.0000	1.0000	1.0000
	Muscovite xK	0.8485	0.8485	0.8485	0.8999	0.8610	0.7742	0.9382	0.9453	0.7195			0.8642	0.8642
	Muscovite xNa	0.1515	0.1515	0.1515	0.1001	0.1390	0.2258	0.0618	0.0547	0.2805			0.1358	0.1358
	Muscovite xAl	0.9252	0.9252	0.9252	0.9002	0.9245	0.9016	0.8959	0.8899	0.9343			0.9164	0.9164
	Muscovite xOH	1.0000	1.0000	1.0000	1.0000	1.0000	1.0000	1.0000	1.0000	1.0000			1.0000	1.0000
	Paragonite xK	0.0884	0.0884	0.0884						0.1168	0.1024	0.1024	0.0933	0.0933
	Paragonite xNa	0.9116	0.9116	0.9116						0.8832	0.8976	0.8976	0.9067	0.9067
	Paragonite xAl	0.9919	0.9919	0.9919						0.9767	0.9675	0.9675	0.9890	0.9890
	Paragonite xOH	1.0000	1.0000	1.0000						1.0000	1.0000	1.0000	1.0000	1.0000
	Margarite fixed act													
	Plagioclase an	0.2430	0.2430	0.2442	0.8177	0.2715	0.3028	0.7457	0.7260	0.2770	0.2100	0.2812	0.2345	0.2345
	Plagioclase ab	0.7512	0.7512	0.7493	0.1787	0.7246	0.6930	0.2489	0.2409	0.7195	0.7858	0.7153	0.7613	0.7613
	Plagioclase or	0.0058	0.0058	0.0064	0.0036	0.0039	0.0042	0.0054	0.0331	0.0035	0.0042	0.0036	0.0042	0.0042
	Staurolite xMg	0.2370	0.2370	0.2657	0.2180	0.2510	0.1948			0.1899	0.2340	0.2340	0.2505	0.2505
	Staurolite xFe	0.7630	0.7630	0.7343	0.7820	0.7490	0.8052			0.8201	0.7560	0.7560	0.7441	0.7441
	Pure Phase	Qtz, Ky	Qtz, Ky	Qtz, Ky	Qtz	Qtz, Ky	Qtz, Ky	Qtz	Qtz, Ilm, Rt	Qtz, Ky	Qtz, Ky	Qtz, Ky	Qtz	Qtz, Ky
	Phase not in calcul. (but stable?)	Mg-St, Rt, Ilm, Czo	Mg-St, Rt, Ilm, Czo	Mg-St, Rt, Ilm, Czo	Ep, Rt, Opaque?	±Czo, Rt	Cld, Ep	Carb, Czo, Ilm/Sulf	Carb, Czo	Cld, Ilm, ±Czo	Chl?, Ilm	Chl?, Ilm	Ky, Rt	Rt

Table C.2: Results from THERMOCALC 3.25 for Campo Blenio, Devero and Molare areas. Mineral abbreviations and end-members as in output of THERMOCALC.

		SX-Analysis Sample	D ACb0301	D ACb0301	E ACb0301	D ADe0301	D ADe0301	E ADe0301	D ADe0302	D+E ADe0302	F+G AMo0404	F+G AMo0409	F+G AMo0410	F+G AMo0410	F+G AMo0410
PT calculation		LIR	8	7	6	8	6	7	6	8	8	9	7	5	7
		P [kb]	**7.7**	**7.7**	**7.0**	**7.4**	**9.2**	**9.5**	**10.8**	**9.9**	**7.6**	**8.7**	**10.6**	**10.8**	**8.8**
		Δ P [kb]	1.1	1.1	1.3	1.0	1.3	1.2	1.4	1.6	1.3	1.1	1.5	1.9	0.9
		T [°C]	**593**	**640**	**570**	**585**	**702**	**636**	**605**	**560**	**564**	**635**	**587**	**632**	**546**
		Δ T [°C]	64	88	92	65	89	70	72	80	97	67	79	115	53
		corr. fact.	0.912	0.729	0.844	0.746	0.797	0.871	0.871	0.882	0.817	0.692	0.617	0.739	0.638
		fit / max	1.05 / 1.45	1.05 / 1.49	1.06 / 1.54	1.25 / 1.45	0.85 / 1.54	0.71 / 1.49	1.09 / 1.54	1.28 / 1.45	1.42 / 1.45	1.12 / 1.42	1.47 / 1.49	1.47 / 1.61	1.06 / 1.49
		xH2O	0.85	1.00	0.45	0.90	1.00	0.60	0.25	0.18	0.40	0.45	0.28	0.60	0.23
		LIR	9	8	7	9	7	8	7	9	9	10	8	6	8
		P [kb]	**7.7**	**7.6**	**6.9**	**7.4**	**8.5**	**9.4**	**10.7**	**9.9**	**7.5**	**8.7**	**10.6**	**10.8**	**8.8**
		Δ P [kb]	0.8	0.8	9.0	0.7	0.9	0.8	0.8	0.9	0.8	0.9	1.2	1.4	0.7
		T [°C]	**595**	**619**	**566**	**585**	**616**	**635**	**604**	**561**	**557**	**632**	**587**	**634**	**545**
		Δ T [°C]	26	29	29	24	30	18	20	22	24	26	23	35	13
		corr. fact.	0.955	0.747	0.791	0.626	0.792	0.734	0.711	0.709	0.651	0.737	0.830	0.810	0.727
		fit / max	0.97 / 1.42	0.97 / 1.45	0.95 / 1.49	1.16 / 1.42	0.93 / 1.49	0.65 / 1.45	0.98 / 1.49	1.19 / 1.42	1.32 / 1.42	1.05 / 1.39	1.34 / 1.45	1.27 / 1.54	0.97 / 1.45
Solid solutions	**Garnet**	py	0.00106	0.00106	0.00106	0.0081	0.0081	0.0097	0.0078	0.0057	0.00124	0.0061	0.0057	0.0057	0.0057
		gr	0.0093	0.0093	0.0093	0.011	0.011	0.0119	0.0146	0.018	0.01	0.0056	0.0028	0.0028	0.0028
		alm	0.34	0.34	0.34	0.24	0.24	0.19	0.17	0.18	0.29	0.27	0.35	0.35	0.35
		spss	1.1E-06	1.1E-06	1.1E-06	-	-	-	(0.0001)	2.6E-06	2.5E-05	1.3E-06	-	-	-
	Biotite	phl	0.041	0.041	0.041	0.092	0.092	0.088	0.086	0.086	0.049	0.078	0.104	0.104	0.104
		ann	0.062	0.062	0.062	0.023	0.023	0.021	0.0107	0.0107	0.049	0.029	0.019	0.019	0.019
		east	0.039	0.039	0.039	0.072	0.072	0.075	0.085	0.085	0.052	0.073	0.078	0.078	0.078
	Muscovite	mu	0.75	0.75	0.77	0.71	0.71	0.73	0.72	0.74	0.76	0.66	0.64	0.64	0.64
		cel	0.022	0.022	0.017	0.029	0.029	0.025	0.029	0.024	0.022	0.028	0.04	0.04	0.04
		fcel	0.017	0.017	0.0125	0.0156	0.0156	0.0124	0.0138	0.0137	0.017	0.0115	0.0131	0.0131	0.0131
		pa	0.341	0.341	0.296	0.435	0.435	0.437	0.347	0.34	0.406	0.343	0.64	0.64	0.64
	Plagioclase	an	0.84	0.84	0.79	0.87	0.87	0.65	0.38	0.4	0.62	0.7	0.27	0.27	0.27
		ab	0.39	0.39	0.47	0.31	0.31	0.58	0.74	0.73	0.65	0.55	0.83	0.83	0.83
	Ilmenite	ilm	0.95	0.95	0.95	0.93	0.93	0.93		0.94	0.93	0.68	0.82	0.82	0.82
		hem	-	-	-	-	-	-		0.0001	-	0.027	0.0064	0.0064	0.0064
		pnt	0.027	0.027	0.027	0.026	0.026	0.026		0.028	0.045	0.0044	0.018	0.018	0.018
		geik	-	-	-	0.0043	0.0043	0.0043		0.0059	0.0045	0.0037	-	-	-
	Staurolite	mst										0.0022	0.0018	0.0018	0.0018
		fst										0.37	0.39	0.39	0.39
	Epidote	cz		0.58	0.58										
		ep		0.32	0.32										
	Pure phase		q, ru	q, ru	q	q, ru, ky	q	q, ky	q, ky	q, ky	q, ru	q	q	q	q, ru
	Phase or end-member excluded			Ep			ru, ky				spss		rt, ky	rt, ky, st	ky, cel

Table C.2 (continued) THERMOCALC results for Lucomagno and Nufenen areas.

		SX-Analysis Sample	A+B ALu0304	A+B ALu0308	A+B ALu0308	A+B ANu0303	A+B ANu0303	D ANu0304	E ANu0304	E ANu0304	F+G ANu0408	F+G ANu0408	F+G ANu0411	F+G ANu0411
PT calculation		LIR	8	10	5	8	7	5	5	5	8	7	6	6
		P [kb]	**6.8**	**8.3**	**9.7**	**7.7**	**7.6**	**7.8**	**8.0**	**8.0**	**8.5**	**8.7**	**9.3**	**8.7**
		Δ P [kb]	1.1	1.0	1.9	1.3	1.2	1.7	1.6	1.6	1.5	1.6	1.6	1.8
		T [°C]	**546**	**627**	**700**	**533**	**594**	**619**	**614**	**614**	**553**	**619**	**694**	**567**
		Δ T [°C]	67	47	94	69	77	105	105	105	85	106	98	94
		corr. fact.	0.930	0.953	0.975	0.934	0.811	0.088	0.116	0.116	0.926	0.837	0.056	0.006
		fit / max	0.78 / 1.45	0.56 / 1.39	0.49 / 1.61	1.15 / 1.45	0.93 / 1.49	0.53 / 1.61	0.56 / 1.61	0.56 / 1.61	1.30 / 1.45	1.21 / 1.49	0.98 / 1.54	1.29 / 1.54
		xH2O	0.50	1.00	1.00	0.27	0.44		1.00		0.18	0.30	1.00	0.85
		LIR	9	11	6	9	8		6		9	8	7	7
		P [kb]	**6.8**	**8.0**	**8.0**	**7.8**	**7.6**	**no** calc.	**7.8**	**no** calc.	**8.6**	**8.6**	**9.0**	**8.7**
		Δ P [kb]	0.8	0.5	0.5	0.8	0.9		1.5		1.0	1.1	1.6	1.6
		T [°C]	**543**	**609**	**609**	**536**	**588**		**566**		**557**	**618**	**587**	**569**
		Δ T [°C]	28	17	18	26	28		60		33	37	50	47
		corr. fact.	0.960	0.825	0.822	0.961	0.788		-0.071		0.962	0.799	-0.129	-0.077
		fit / max	0.72 / 1.42	0.54 / 1.37	0.68 / 1.54	1.07 / 1.42	0.85 / 1.45		0.57 / 1.54		1.21 / 1.42	1.10 / 1.45	1.09 / 1.49	1.16 / 1.49
Solid solutions	**Garnet**	py	0.00156	-	-	0.00118	0.00118	0.00118	0.00118	0.00118	0.0039	0.0039	0.00179	0.00179
		gr	0.0082	0.0098	0.0098	0.0084	0.0084	0.0104	0.0104	0.0104	0.0124	0.0124	0.0132	0.0132
		alm	0.3	0.0075	0.0075	0.33	0.33	0.28	0.28	0.28	0.25	0.25	0.25	0.25
		spss	0.000038	0.25	0.25	4.6E-06	4.6E-06	0.000017	0.000017	0.000017	3.7E-06	3.7E-06	7.1E-05	7.1E-05
	Biotite	phl	0.046	0.091	0.091	0.045	0.045	0.041	0.041	0.041	0.084	0.084	0.051	0.097
		ann	0.053	0.02	0.02	0.046	0.046	0.06	0.06	0.06	0.022	0.022	0.038	0.016
		east	0.043	0.074	0.074	0.046	0.046	0.039	0.039	0.039	0.074	0.074	0.052	0.082
	Muscovite	mu	0.75			0.72	0.72	0.74	0.76	0.76	0.73	0.73	0.77	0.77
		cel	0.018			0.021	0.021	0.019	0.021	0.021	0.03	0.03	0.027	0.027
		fcel	0.0141			0.018	0.018	0.0184	0.0178	0.0178	0.0046	0.0046	0.0134	0.0134
		pa	0.235			0.307	0.307	0.419	0.472	0.472	0.195	0.195	0.251	0.251
	Plagioclase	an	0.89	0.71	0.71	0.72	0.72				0.75	0.75		
		ab	0.28	0.55	0.55	0.57	0.57				0.54	0.54		
	Ilmenite	ilm	0.97			0.96	0.96	0.95	0.95	0.95	0.96	0.96		
		hem						0.00022	0.00022	0.00022	-	-		
		pnt	0.0074			0.01	0.01	0.008	0.008	0.008	0.017	0.017		
		geik	0.01			0.0096	0.0096				0.0064	0.0064		
	Staurolite	mst		0.0027	0.0027								0.0011	0.0011
		fst		0.35	0.35								0.44	0.44
	Epidote	cz	0.61	0.37	0.37	0.6			0.58	0.58	0.56		0.65	0.65
		ep	0.28	0.53	0.53	0.3			0.32	0.32	0.36		0.3	0.3
	Amphibole	tr		0.03952										
		fact		0.000243										
		ts		0.021										
		parg		0.1741										
		gl		0.01303										
	Pure phase		q	q, ky	q, ky	q	q	q	q	q	q	q	q	q
	Phase or end-member excluded		Mrg	WM	Amp, WM	Carb	Carb, Ep	Ep	hem	Ep, hem	Carb, Rt	Carb, Rt	Pl	Pl

Table C.2 (continued) THERMOCALC results for Piora and Aquila areas.

			Zone #2					Zone #3						
	SX-Analysis Sample		D APi0301	D APi0301	D APi0301	A+B APi0302	A+B APi0305	A+B APi0305	F+G APi0304	F+G APi0304	F+G APi0409	F+G APi0409	F+G AAq0401	F+G AAq0401
PT calculation		LIR	8	7	4	8	8	8	6	9	9	9	9	10
		P [kb]	**10.5**	**7.7**	**6.5**	**8.9**	**9.3**	**8.9**	**8.4**	**8.7**	**9.4**	**8.0**	**7.2**	**6.6**
		Δ P [kb]	1.3	1.1	1.0	2.7	1.4	2.0	1.5	1.4	1.2	1.3	0.9	1.2
		T [°C]	**650**	**544**	**459**	**630**	**661**	**648**	**562**	**650**	**655**	**615**	**542**	**598**
		Δ T [°C]	71	77	62	85	82	104	92	78	62	69	51	72
		corr. fact.	0.642	0.676	0.705	0.710	0.699	-0.025	0.735	0.776	0.910	0.949	0.656	0.758
		fit / max	1.26 / 1.45	1.44 / 1.49	1.28 / 1.73	1.18 / 1.45	1.34 / 1.45	1.25 / 1.45	1.34 / 1.54	1.44 / 1.42	1.28 / 1.42	1.38 / 1.42	0.75 / 1.42	1.33 / 1.39
		xH2O		0.60	0.70	1.00	0.60	1.00	0.40	0.36	0.77	1.00	0.25	0.70
		LIR		8	5	9	9	9	7	10	10	10	10	11
		P [kb]	… Bug during avg PT calculation …	**10.3**	**10.6**	**8.1**	**9.3**	**8.7**	**8.1**	**8.7**	**9.4**	**8.0**	**7.3**	**6.7**
		Δ P [kb]		1.1	1.7	1.7	1.1	1.8	0.1	1.0	0.8	0.6	0.8	0.8
		T [°C]		**634**	**652**	**595**	**663**	**596**	**561**	**650**	**654**	**615**	**545**	**602**
		Δ T [°C]		33	35	33	35	52	28	16	25	15	19	16
		corr. fact.		0.827	0.926	0.235	0.735	-0.179	0.813	0.708	0.914	0.779	0.766	0.586
		fit / max		1.24 / 1.45	1.17 / 1.61	1.11 / 1.42	1.24 / 1.42	1.20 / 1.42	1.20 / 1.49	1.34 / 1.39	1.19 / 1.39	1.29 / 1.39	0.70 / 1.39	1.25 / 1.37
Solid solutions	**Garnet**	py	0.0049	0.0049	0.0049	0.0033	0.0046	0.0049	0.0051	0.0051	0.0064	0.0064	0.0049	0.0049
		gr	0.0041	0.0041	0.0041	0.0084	0.0071	0.0059	0.0037	0.0037	0.0058	0.0058	0.0039	0.0039
		alm	0.34	0.34	0.34	0.24	0.29	0.25	0.33	0.33	0.27	0.27	0.29	0.29
		spss	-	-	-	0.00014	4.1E-06	0.00011	-	-	4.4E-06	4.4E-06	0.00009	0.00009
	Biotite	phl	0.112	0.112	0.112	0.095	0.083	0.091	0.112	0.112	0.084	0.084	0.094	0.094
		ann	0.018	0.018	0.018	0.022	0.019	0.023	0.017	0.017	0.025	0.025	0.027	0.027
		east	0.082	0.082	0.082	0.076	0.072	0.071	0.085	0.085	0.071	0.071	0.072	0.072
	Muscovite	mu	0.66	0.66			0.75	0.78	0.69	0.69	0.71	0.71	0.74	0.74
		cel	0.035	0.035			0.028	0.022	0.0264	0.0264	0.027	0.027	0.0095	0.0095
		fcel	0.0207	0.0207			0.0147	0.0146	0.0143	0.0143	0.025	0.025	0.0061	0.0061
		pa	0.8	0.8			0.323	0.387	0.67	0.67	0.53	0.53	0.43	0.43
	Paragonite	mu	-		-									
		cel	-		-									
		fcel	-		-									
		pa	0.75		0.75									
	Plagioclase	an	0.42	0.42	0.42		0.78		0.45	0.45	0.7	0.7	0.61	0.61
		ab	0.74	0.74	0.74		0.47		0.72	0.72	0.58	0.58	0.61	0.61
	Ilmenite	ilm	0.97	0.97	0.97	0.95	0.92	0.94	0.98	0.98	0.96	0.96	0.77	0.77
		hem	-	-	-	-	-	-	-	-	-	-	0.012	0.012
		pnt	0.0021	0.0021	0.0021	0.013	0.047	0.037	-	-	0.021	0.021	0.0062	0.0062
		geik	0.017	0.017	0.017	0.012	0.011	0.01	0.011	0.011	-	-	0.015	0.015
	Staurolite	mst	0.0025	0.0025	0.0025	0.0025	0.0033	0.0021	0.0025	0.0025	0.0011	0.0011	0.0012	0.0012
		fst	0.36	0.36	0.36	0.36	0.33	0.37	0.36	0.36	0.44	0.44	0.43	0.43
	Epidote	cz						0.64			0.35	0.35		
		ep						0.26			0.55	0.55		
	Amphibole	tr				0.021668								
		fact				0.000339								
		ts				0.022								
		parg				0.1062								
		gl				0.00893								
	Pure phase		q	q	q	q	q	q	q	q,ky,ru	q	q, ky	q	q, ky
	Phase or end-member excluded		ru, geik	ru, geik, cel, mst	ru, geik, mst	Mrg, Ky	Carb, Ep	Carb	St, Ky, Rt		ky	fcel	ky	

Table C.3: Complementary thermometers.

Chl-Cld thermometer

From Vidal et al. (1999) $\ln[K] = \ln(xMg_{Chl}^5 * xFe_{Cld}^5) / (xFe_{Chl}^5 * xMg_{Cld}^5) = 5*\ln[Kd]$

$T\,(°C) = 1977.7 / (\ln[K_d] + 0.971) - 273.15$

Reference	Region	Sample	Chlorite Fe	Chlorite Mg	Chloritoid Fe	Chloritoid Mg	Chlorite xFe	Chlorite xMg	Chloritoid xFe	Chloritoid xMg	ln Kd	T [°C]
This thesis	Val Piora	**APi0505**	1.835	2.557	1.443	0.507	0.418	0.582	0.740	0.260	1.378	**569**
	Val Piora	**APi0510**	1.880	2.581	1.460	0.514	0.421	0.579	0.740	0.260	1.361	**575**
	Val Piora	**APi0407**	1.996	2.471	1.484	0.454	0.447	0.553	0.766	0.234	1.398	**562**
Livi et al. (2002)	Garvera	**MF 915**	2.58	1.48	1.800	0.156	0.635	0.365	0.920	0.080	1.890	**418**
		MF 920	1.57	2.40	1.625	0.300	0.395	0.605	0.844	0.156	2.114	**368**
		MF 928	1.80	2.28	1.667	0.250	0.441	0.559	0.870	0.130	2.134	**364**
		MF 931	2.00	2.06	1.652	0.235	0.493	0.507	0.875	0.125	1.980	**397**
	Alp Tgom	**MF 857**	2.140	2.130	1.604	0.307	0.501	0.499	0.839	0.161	1.649	**482**
	Val Gierm	**MF 897**	2.060	2.150	1.620	0.313	0.489	0.511	0.838	0.162	1.687	**471**
	Sedrun	**DrT 1210**	2.550	1.700	1.727	0.233	0.600	0.400	0.881	0.119	1.598	**497**
Rahn et al. (2002)	Curaglia	**MR P 288**	4.384	3.789	1.702	0.208	0.536	0.464	0.891	0.109	1.956	**402**
	Curaglia	**MR P 288**	4.516	3.799	1.664	0.208	0.543	0.457	0.889	0.111	1.907	**414**

Graphit thermometry by RAMAN spectroscopy (from Beyssac et al., 2002)

Analyst: Dr. E. Janots

Sample	T [°C]	2σ
AMo0504-a	598.7	
AMo0504-b	615.2	
AMo0504-c	596.1	
AMo0504-d	612.0	
AMo0504-e	607.8	
AMo0504-f	588.9	
AMo0504-g	605.0	
AMo0504-h	585.7	
AMo0504-i	619.3	
AMo0504-j	614.7	
AMo0504-k	599.1	
	603.9	**±6.5**
SDe0301-a	563.1	
SDe0301-b	586.4	
SDe0301-c	587.1	
SDe0301-d	621.4	
SDe0301-e	589.0	
SDe0301-f	543.8	
SDe0301-g	590.7	
SDe0301-h	574.1	
SDe0301-i	596.8	
SDe0301-j	582.1	
SDe0301-k	637.0	
SDe0301-l	597.4	
SDe0301-m	593.4	
SDe0301-n	589.4	
	589.4	**±11.7**
SPi0306-a	563.1	
SPi0306-b	586.4	
SPi0306-c	587.1	
SPi0306-d	621.4	
SPi0306-e	589.0	
SPi0306-f	571.4	
SPi0306-g	599.7	
SPi0306-h	590.7	
SPi0306-i	574.1	
SPi0306-j	596.8	
SPi0306-k	582.1	
	587.4	**±9.3**

Sample	T [°C]	2σ
ANu0304-b	557.9	
ANu0304-d	558.4	
ANu0304-e	538.4	
ANu0304-f	548.6	
ANu0304-g	557.1	
ANu0304-h	573.8	
ANu0304-i	548.8	
ANu0304-j	566.2	
ANu0304-k	563.4	
ANu0304-l	548.1	
	556.1	**±6.4**
ANu0413-4	518.1	
ANu0413-5	513.3	
ANu0413-6	515.3	
ANu0413-7	534.6	
ANu0413-8	545.2	
ANu0413-9	542.2	
ANu0413-10	546.7	
ANu0413-11	525.8	
ANu0413-12	526.6	
ANu0413-14	550.2	
ANu0413-15	513.3	
ANu0413-16	512.7	
ANu0413-17	530.3	
	528.8	**±7.5**
ACb0301-a	575.4	
ACb0301-b	607.5	
ACb0301-c	572.0	
ACb0301-d	580.6	
ACb0301-e	571.8	
ACb0301-f	575.7	
ACb0301-g	580.1	
ACb0301-h	599.4	
ACb0301-i	606.9	
ACb0301-j	581.9	
ACb0301-k	584.9	
ACb0301-l	569.2	
	583.8	**±7.6**

Analyst: J. Allaz

Sample	T [°C]	Comment / 2σ
APi0501-1	504.7	High bkg, curve down
APi0501-2	571.2	± OK
APi0501-3	525.8	
APi0501-4	603.6	High T???
APi0501-5	538.7	
APi0501-6	522.1	
APi0501-7	469.4	High bkg, low signal
APi0501-8	559.4	High Bkg
APi0501-9	530.9	
APi0501-10	483.1	High bkg, curve down
APi0501-11	540.4	
APi0501-12	504.7	
APi0501-13	499.9	
APi0501-14	503.0	
APi0501-15	498.7	High bkg, low signal
	523.7	**±17.9**
	519.2	**±12.0 (OK only)**
ANu0413-1	459.3	High bkg, low signal
ANu0413-2	451.6	High bkg
ANu0413-3	591.3	High T???
ANu0413-4	496.1	High bkg
ANu0413-5	485.1	High bkg
ANu0413-6	503.4	Very high bkg
ANu0413-7	443.7	High bkg
ANu0413-8	543.9	
ANu0413-9	546.5	High bkg
ANu0413-10	505.7	Very high bkg
ANu0413-11	456.4	High bkg
ANu0413-12	456.7	Very high bkg
ANu0413-14	543.0	
ANu0413-15	508.4	
ANu0413-16	505.6	
ANu0413-17	522.8	
ANu0413-18	517.2	
ANu0413-19	513.0	
ANu0413-20	495.9	High bkg
ANu0413-21	474.6	High bkg
	501.0	**±16.6**
	522.0	**±11.6 (OK only)**

Sample	T [°C]	Comment / 2σ
ALu0304-1	429.4	High bkg, curve down
ALu0304-2	464.9	High bkg, curve down
ALu0304-3	562.7	
ALu0304-4	524.5	High bkg
ALu0304-5	538.2	High bkg
ALu0304-6	532.1	
ALu0304-7	561.3	
ALu0304-8	471.0	High bkg, curve down
ALu0304-9	539.0	
ALu0304-10	551.0	
ALu0304-11	538.7	High bkg
ALu0304-12	546.2	
ALu0304-13	563.3	
ALu0304-14	595.4	
ALu0304-15	496.3	High bkg, low signal
	527.6	**±22.3**
	551.4	**±12.6 (OK only)**
APi0305-1	535.5	
APi0305-2	539.2	
APi0305-3	564.6	
APi0305-4	494.0	
APi0305-5	498.0	
APi0305-6	518.9	
APi0305-7	512.6	
APi0305-8	522.3	
APi0305-9	525.4	
APi0305-10	532.7	
	524.3	**±12.8**

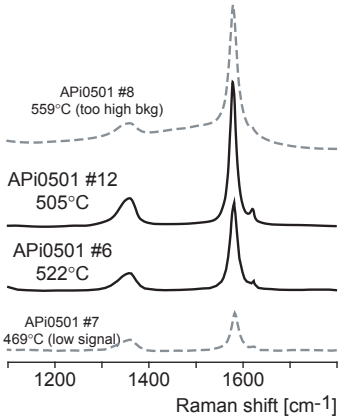

Samples SDe0301 and SPi0306 from Jens-Oliver Schwarz:
Alpe Devero (equivalent of ADe0301) and West Piora (Foïsc).

Table C.4: Bulk rock composition used for computation of pseudo-sections with THERIAK-DOMINO (XRF Analysis).

Sample	SiO_2	TiO_2	Al_2O_3	Fe_2O_3	MnO	MgO	CaO	Na_2O	K_2O	LOI	Total
ACb0301	63.21	0.85	16.93	8.41	0.12	1.33	3.16	0.84	2.64	2.60	100.30
ADe0301	55.05	1.04	22.85	8.78	0.10	3.25	2.40	0.83	3.64	2.03	100.28
ADe0302 (I)	71.82	0.53	14.67	3.85	0.17	1.86	1.12	1.72	3.47	1.59	100.95
ADe0302 (II)	63.86	0.74	18.19	6.22	0.38	1.79	2.30	2.80	3.17	1.22	100.81
ALu0306	60.58	0.78	13.87	4.26	0.06	5.52	6.20	0.79	1.48	6.51	100.21
ALu0309	60.22	0.85	17.94	7.65	0.02	7.03	0.87	1.68	0.98	2.97	100.46
ALu0601	55.17	1.32	27.68	5.48	0.04	1.00	1.38	1.00	4.25	2.30	99.76
ALu0603	45.80	1.95	34.12	8.70	0.05	1.25	1.20	2.57	1.96	2.10	99.73
AMo0404	59.09	0.84	18.27	7.35	0.08	3.49	0.91	1.44	5.63	2.36	99.71
AMo0405	59.11	0.86	19.15	7.20	0.27	2.94	3.81	1.98	3.95	1.69	101.21
AMo0409	63.21	0.77	17.84	7.08	0.01	3.10	0.51	1.29	5.26	2.23	101.51
AMo0410*	59.29	0.92	21.92	7.38	0.34	1.93	1.05	2.26	3.10	1.83	100.21
ANu0301	42.20	0.47	11.02	2.78	0.03	3.71	19.78	0.41	1.53	14.74	97.42
ANu0304	62.11	1.14	19.23	7.33	0.10	1.32	3.22	0.75	2.29	2.60	100.36
ANu0413	59.35	1.08	19.97	7.33	0.09	2.06	1.39	1.97	3.73	4.05	101.20
APi0301	51.42	1.46	30.65	7.24	0.03	1.21	0.96	2.63	2.52	2.18	100.51
APi0305	50.08	1.00	22.83	9.33	0.15	2.71	5.63	1.44	3.32	3.18	100.14
APi0601	62.56	1.03	20.41	4.69	0.01	3.51	0.87	2.42	2.07	2.20	99.84
APi0603	50.69	2.05	33.20	5.62	0.06	1.57	1.60	2.47	1.22	1.30	99.85

* Large variations occurs at mm-scale (garnet-rich layers richer in Ca and Mn), hidden in this bulk analysis.

D) BLABLA comments & bugs

During the five series of analysis, the Ar-extraction line (BLABLA, Bernese Low Argon Blank Line Assembly) remains broadly identical, as detailed in Chapters 2 and 3. A scheme of the extraction line is given in Figure D.1. Each series of analyses are identified according to the name given to the irradiation package (McM = McMaster University, Hamilton, Canada; BEP = Pavia University, Italy). The complete set of results is given on CD, including all analysed standards and background of spectrometer in Excel spreadsheets. Backgrounds and some test on the new multiplier installed in 2007 are also given.

Minor and major bugs apparently unavoidable during (quite) each analysis series are listed below (false bugs and true technical problems, e.g. Fig. D.2). Each bug was objectively solved and negative effects on the age-calculation are minimized. Some general comments, unpublished analysis or secondary conclusion and discovery (not discussed in previous chapters) accompanied this list.

D.1) General comments

- **Mineral separates** were carefully hand-picked. According to petrographic observation, a specific mesh is selected for each sample and each mineral, between 50-125 µm and 250-500 µm (e.g. Fig. D.3). Quality of mineral separate was tested by XRD analysis in the range 4-40° 2Θ (see §2.5.3). These results are available on CD (original "RD" files and vectorized graphics [Illustrator/PDF]). An overview is given in Figure D.3.

- **J-factors** are calculated on the analysis of hornblende standard MMhb, assuming an age of 523.1±4.6 Ma (Renne *et al.*, 1998). The complete list of J-factor calculated from standards is given in Figure D.4. This latter also comprises the J-factor selected for each mineral separate.

- **Sensitivity factor** of mass spectrometer (used for recalculation of K, Ca and Cl) is at maximum when the filament of ion source is new and regularly decreases up to burn out. The factor is adapted according to MMhb standard regularly analysed between samples (based on the known amount of K in standard: 1.555% K).

- **Blanks of furnace** or some parts of the line were regularly measured in all series and constantly yield an atmospheric ratio. Numerous **spectrometer backgrounds** (static and dynamic) accompany all series of analysis. For correction of spectrometer background, an average over all backgrounds is taken (preferentially static background). If a strong change is observed, the background is adapted for each sample analysis. See Chapters 2 and 3 for details about furnace and spectrometer background of each analysis series (in methods for Ar-Ar dating).

- In Chapters 2 and 3, Ar-series are identified as **Ar-A** (McM12, 13), **Ar-B** (McM15) and **Ar-C** (BEP12).

- Series **McM16** yield discussable results and will probably remain **unpublished** (see §D.6).

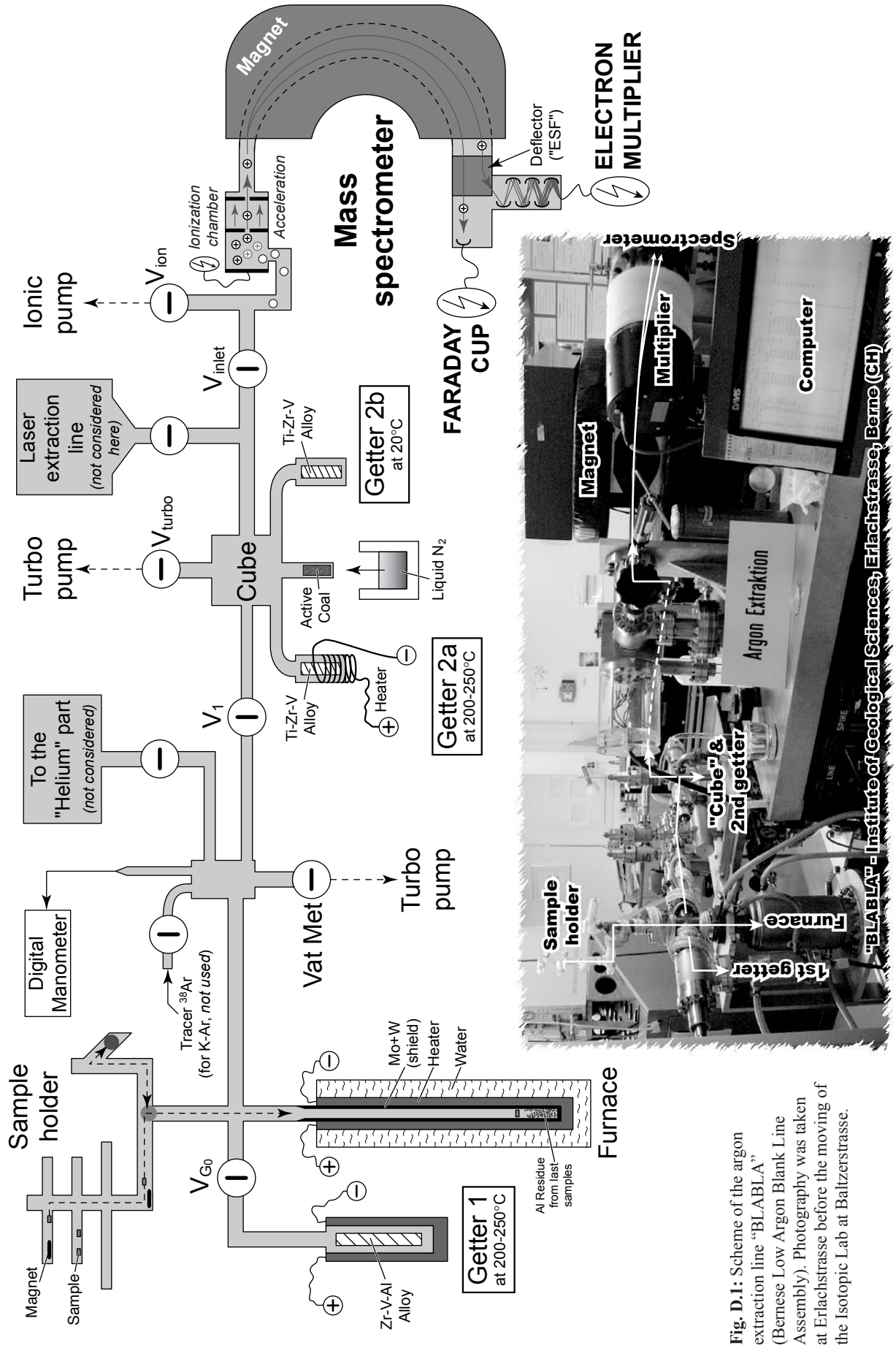

Fig. D.1: Scheme of the argon extraction line "BLABLA" (Bernese Low Argon Blank Line Assembly). Photography was taken at Erlachstrasse before the moving of the Isotopic Lab at Baltzerstrasse.

Fig. D.2: Example of true and false bugs. Below is a view of the furnace resistance in a bad day (these two pictures are from Daniel Rufer and Prof. Jan Kramers), which results from of a short circuit between the shield and the furnace resistance (just after analysis of sample AAn0405, BEP12). Fortunately, the crucible remains unaffected (i.e. no leak in the extraction line). Ar-results remain unaffected by this bug and only the measure of temperature was probably erroneous and variable (±50°?).

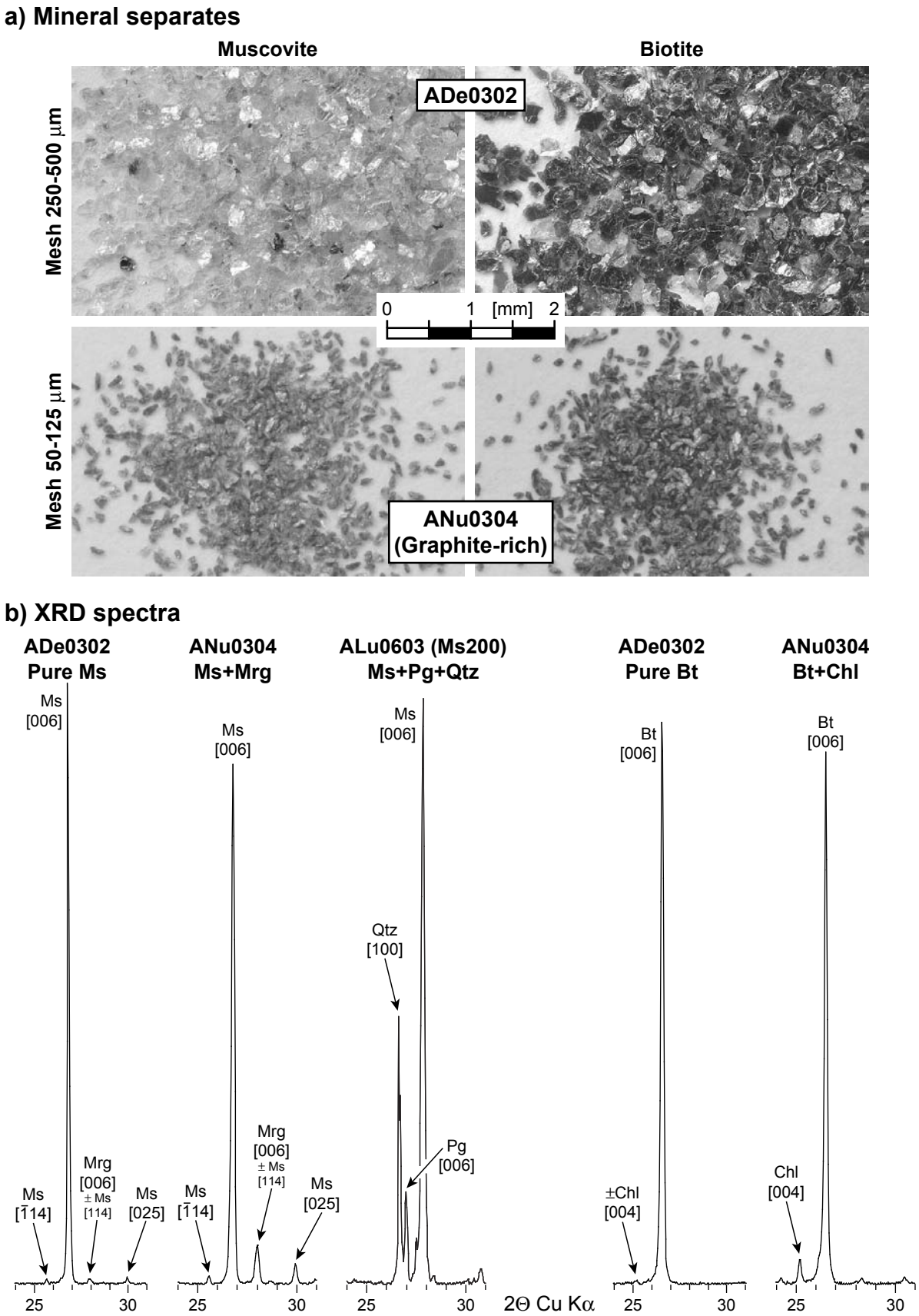

Fig. D.3: (a) Photographies of muscovite and biotite separates previous to hand-picking. Some impurities are always present and are eliminated during hand-picking (aim to reach >99% purity). The presence of graphite in Bündnerschiefer (ANu0304) render hand-picking difficult. **(b)** XRD spectra in the range 4-40° is analysed, but the range 24-31° (2Θ) is given here and allows a good distinction of each mica type and other typical impurities (quartz in white mica, chlorite in biotite).

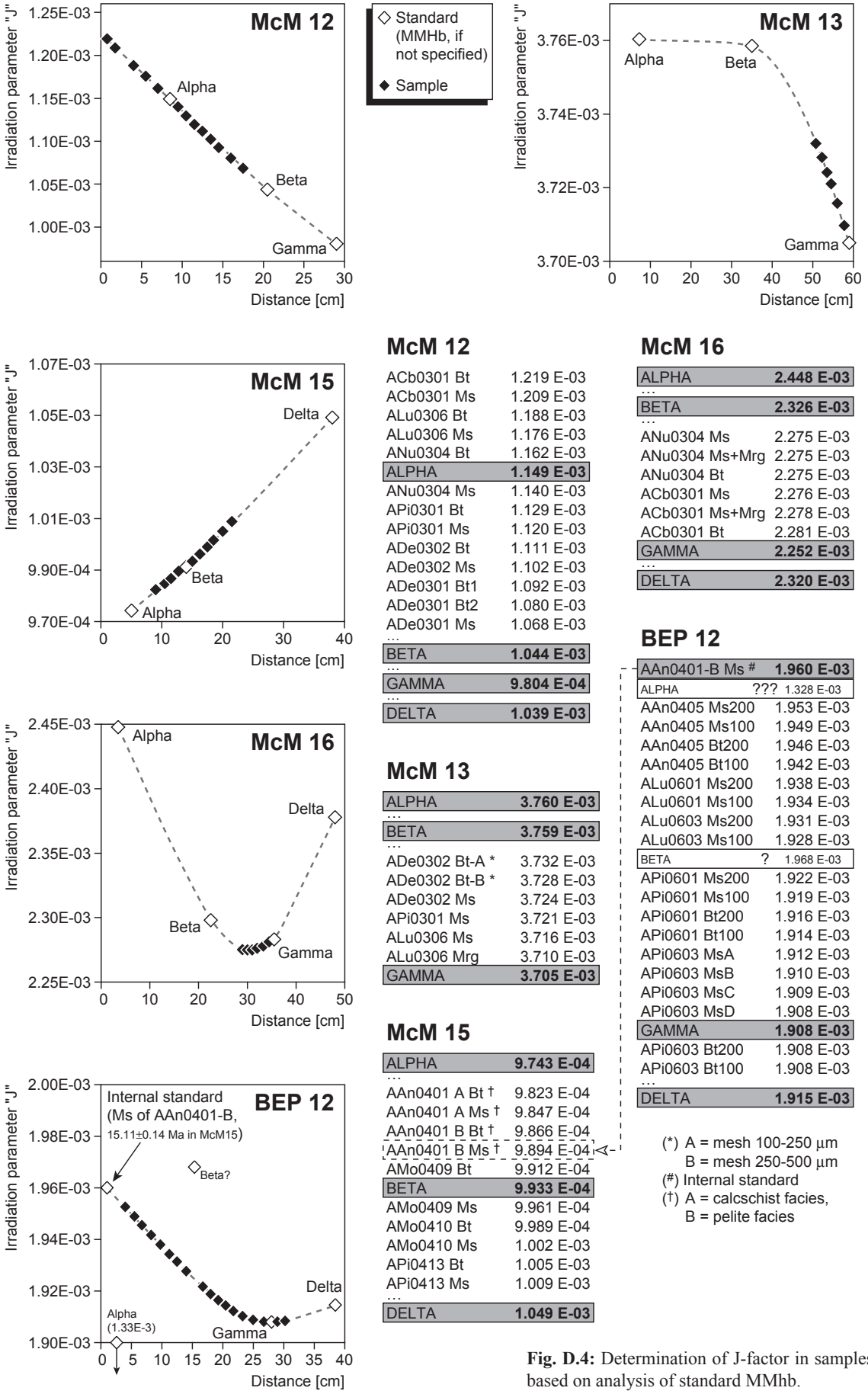

McM 12

ACb0301 Bt	1.219 E-03
ACb0301 Ms	1.209 E-03
ALu0306 Bt	1.188 E-03
ALu0306 Ms	1.176 E-03
ANu0304 Bt	1.162 E-03
ALPHA	**1.149 E-03**
ANu0304 Ms	1.140 E-03
APi0301 Bt	1.129 E-03
APi0301 Ms	1.120 E-03
ADe0302 Bt	1.111 E-03
ADe0302 Ms	1.102 E-03
ADe0301 Bt1	1.092 E-03
ADe0301 Bt2	1.080 E-03
ADe0301 Ms	1.068 E-03
…	
BETA	**1.044 E-03**
…	
GAMMA	**9.804 E-04**
…	
DELTA	**1.039 E-03**

McM 13

ALPHA	**3.760 E-03**
…	
BETA	**3.759 E-03**
…	
ADe0302 Bt-A *	3.732 E-03
ADe0302 Bt-B *	3.728 E-03
ADe0302 Ms	3.724 E-03
APi0301 Ms	3.721 E-03
ALu0306 Ms	3.716 E-03
ALu0306 Mrg	3.710 E-03
GAMMA	**3.705 E-03**

McM 15

ALPHA	**9.743 E-04**
…	
AAn0401 A Bt †	9.823 E-04
AAn0401 A Ms †	9.847 E-04
AAn0401 B Bt †	9.866 E-04
AAn0401 B Ms †	9.894 E-04
AMo0409 Bt	9.912 E-04
BETA	**9.933 E-04**
AMo0409 Ms	9.961 E-04
AMo0410 Bt	9.989 E-04
AMo0410 Ms	1.002 E-03
APi0413 Bt	1.005 E-03
APi0413 Ms	1.009 E-03
…	
DELTA	**1.049 E-03**

McM 16

ALPHA	**2.448 E-03**
…	
BETA	**2.326 E-03**
…	
ANu0304 Ms	2.275 E-03
ANu0304 Ms+Mrg	2.275 E-03
ANu0304 Bt	2.275 E-03
ACb0301 Ms	2.276 E-03
ACb0301 Ms+Mrg	2.278 E-03
ACb0301 Bt	2.281 E-03
GAMMA	**2.252 E-03**
…	
DELTA	**2.320 E-03**

BEP 12

AAn0401-B Ms #	**1.960 E-03**
ALPHA ???	1.328 E-03
AAn0405 Ms200	1.953 E-03
AAn0405 Ms100	1.949 E-03
AAn0405 Bt200	1.946 E-03
AAn0405 Bt100	1.942 E-03
ALu0601 Ms200	1.938 E-03
ALu0601 Ms100	1.934 E-03
ALu0603 Ms200	1.931 E-03
ALu0603 Ms100	1.928 E-03
BETA ?	1.968 E-03
APi0601 Ms200	1.922 E-03
APi0601 Ms100	1.919 E-03
APi0601 Bt200	1.916 E-03
APi0601 Bt100	1.914 E-03
APi0603 MsA	1.912 E-03
APi0603 MsB	1.910 E-03
APi0603 MsC	1.909 E-03
APi0603 MsD	1.908 E-03
GAMMA	**1.908 E-03**
APi0603 Bt200	1.908 E-03
APi0603 Bt100	1.908 E-03
…	
DELTA	**1.915 E-03**

(*) A = mesh 100-250 µm
B = mesh 250-500 µm
(#) Internal standard
(†) A = calcschist facies,
B = pelite facies

Fig. D.4: Determination of J-factor in samples, based on analysis of standard MMhb.

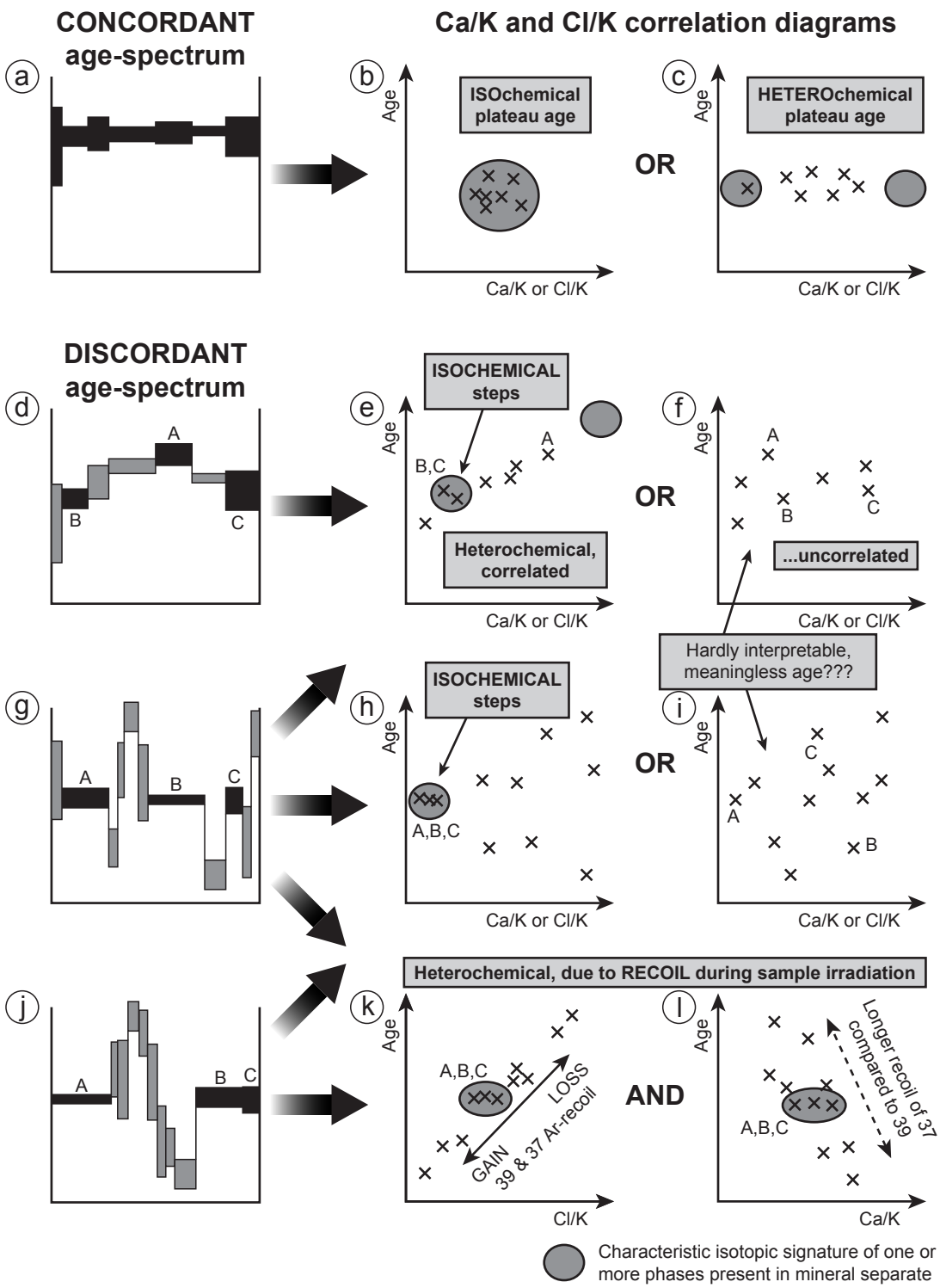

Fig. D.5: Classification of Ar-results according to the concept of isochemical steps: Ca and Cl (i.e. ^{37}Ar and ^{38}Ar) are used to characterize the gas analysed in each steps. This permits the identification of the correct steps pertaining to the degassing of the phase we aim to date. Such characterization is also used to eliminate a doubtful spectrum (analytical or technical problem).

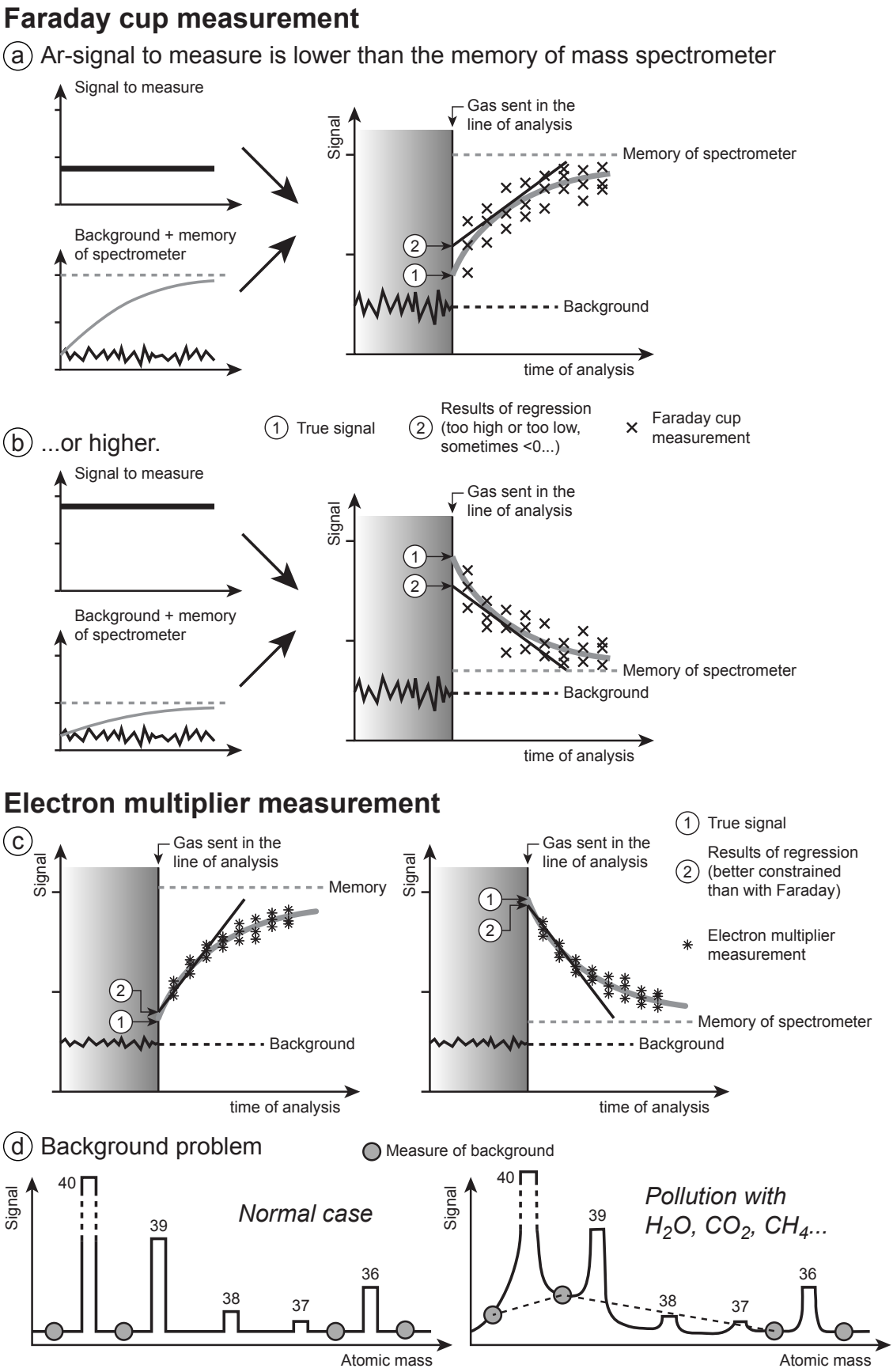

Fig. D.6: The problematic of measuring very low amount of ^{37}Ar and ^{38}Ar. See text for (brief) discussion.

- The **interpretation of argon** stepwise heating analysis in this work is based on the concept of **"isochemical" age**, which corresponds to step yielding similar Ca/K and Cl/K ratios ($^{38}Ar/^{39}Ar$ and $^{37}Ar/^{39}Ar$, respectively). This has been extensively discussed in Chapters 2 and 3. Figure D.5 summarizes this concept by presenting a kind of new classification based on both age-spectra and Ca/Cl/age correlation diagram.

- The **analysis of ^{37}Ar and ^{38}Ar** (Ca and Cl) was correctly measured. However, the analysis of these traces suffer some problems, which sometimes affect the precision of measurement (especially in Ca-poor micas):

  - In all muscovite and biotite, both are present in traces.

  - In contrary to the stable ^{38}Ar, ^{37}Ar is a radioactive isotope with a short half-life of 34.8 days. Unfortunately, samples cannot be analysed immediately due to a) the time required to let the most radioactive elements decay (1-2 months) or b) problems related to the extraction line or the apparatus required for analysis (defect, leak, see following paragraphs). Series McM12, 13 and 16 were analysed 2 months afterwards and 1/4 of the total ^{37}Ar formed during irradiation remained. However, series McM15 and BEP12 were analysed 120 to 150 days after irradiation, leaving thus less than 1/16 of ^{37}Ar created during irradiation.

  - Sometimes, problems stem from the memory of spectrometer, which is the gas "stuck" on walls of the spectrometer and progressively released during the measurement (when the pumping through the ionic pump is stopped; Fig. D.1). This is illustrated in Figure D.6: when only Faraday cup measurement is available and when signal is very low, an error is easily made and imprecision is high (Fig D.6a,b). The problem is sometimes reduced, if a exponential regression is applied. Using multiplier strongly reduces this effect (Fig D.6c), as the shape of the regression is clearly better defined. However, this problem is hardly applicable on ^{37}Ar due to the rapid decay of this isotope (memory of ^{37}Ar should approach the background, Fig. D.6b), unless a huge ^{37}Ar amount was present in a previous sample (e.g. margarite).

  - Background is carefully and regularly analysed between each analyses and usually yield low values. However, the presence of hydrocarbons is likely to produce a higher background on masses 37 and 39 (e.g. C_3H_3). Moreover, a too high pressure in the line during first (and last) analysed steps (stemming from release of H_2O and CO_2), will produce a hump-shape background over masses 40 and 39, especially. The higher background measured on mass 39.5 compared to 36.5 induces an incorrect determination of ^{37}Ar or ^{38}Ar (too low, if not below the average background 39.5-36.5; shown with exaggeration in Figure D.6d).

D.2) McM12 – Preliminary results

D.2.1) 1st series, July 2004 (ACb0301, APi0301-Bt, ADe0301, ADe0302)

- Only faraday cup measurements.

- Large variation of J-factors (±10%).

- Leak in the furnace: possible loss of gas in each analysed steps, which results in "horst and graben" age-spectra. However, comparing results from ADe0302 in McM12 and McM13 (§D.3), average ages remain broadly similar, except larger errors in results from McM12.

- Most of the analysed mineral separates weighted only 3 to 5 mg, especially samples from graphite-rich Bündnerschiefer. This were preliminary results, where we aimed to minimize the possible problem of CH_4,

CO_2... possibly released by this impure mineral separate (e.g. Fig. D.3a) during analysis of such sample. As only 5-8 steps are analysed, the interpretation of these results is difficult. The two or three most significant steps pertaining to mica rarely yield a plateau and are thus quite impossible to interpret.

- **These results were *NOT* considered in this thesis. Reader is referred to the CD to have a look on these *awful* results.**

D.2.2) 2nd series, August 2004 (APi0301-Ms, ALu0306, ANu0304)

- Analyses were acquired with faraday cup and electron multiplier in analogue mode, but "more coherent" results (plateau) were usually obtained by considering exclusively faraday cup measurements (e.g. Fig. D.7). Multiplier unit was apparently ill, with an irregular behaviour of gain factor between faraday and multiplier. This behaviour remains problematic and we thus prefer faraday cup measurements in this series.

- Through pumping, a regular decrease of spectrometer background is observed between each analysed sample. The selection of a representative background for each analysis ensures an optimal correction.

- Only results for biotite ALu0306 are retained and discussed in Chapter 2. White-mica separate from APi0301 yields low signal on many steps (mixture with paragonite: too many steps, too low K-content, too low irradiation) and was re-analysed with a larger amount of mineral separate and a stronger irradiation (McM13). Nevertheless, results remain similar. Results from ANu0304 are not considered as this sample was rich in graphite and weighted only 3 to 5 mg. This sample was lately re-analysed in McM16 (§D.5).

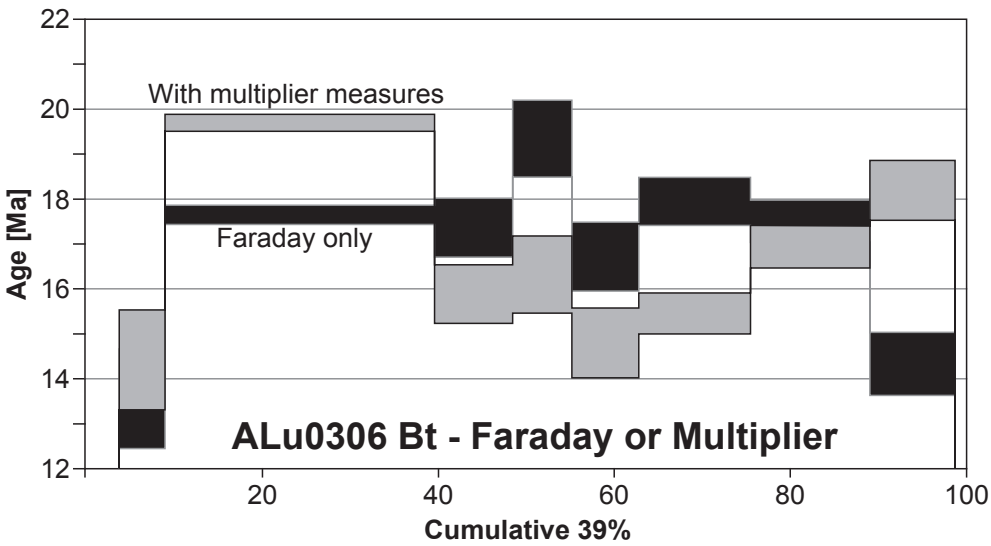

Fig. D.7: Comparison of Ar-result in biotite from ALu0306 obtained with preference given to faraday or multiplier measurements. Mass 40 is analysed on Faraday only, masses 39 and 36 are analysed with both faraday collector and electron muliplier, and masses 37 and 38 are only measured with multiplier. A gain factor is calculated from ratio of faraday and multiplier measurement on mass 39. Masses 37 and 38 are low and do not significantly affects the age-result. Thus, strong variation between measurement of mass 36 on faraday (ok) or multiplier (ill) is essentially the cause of this problem.

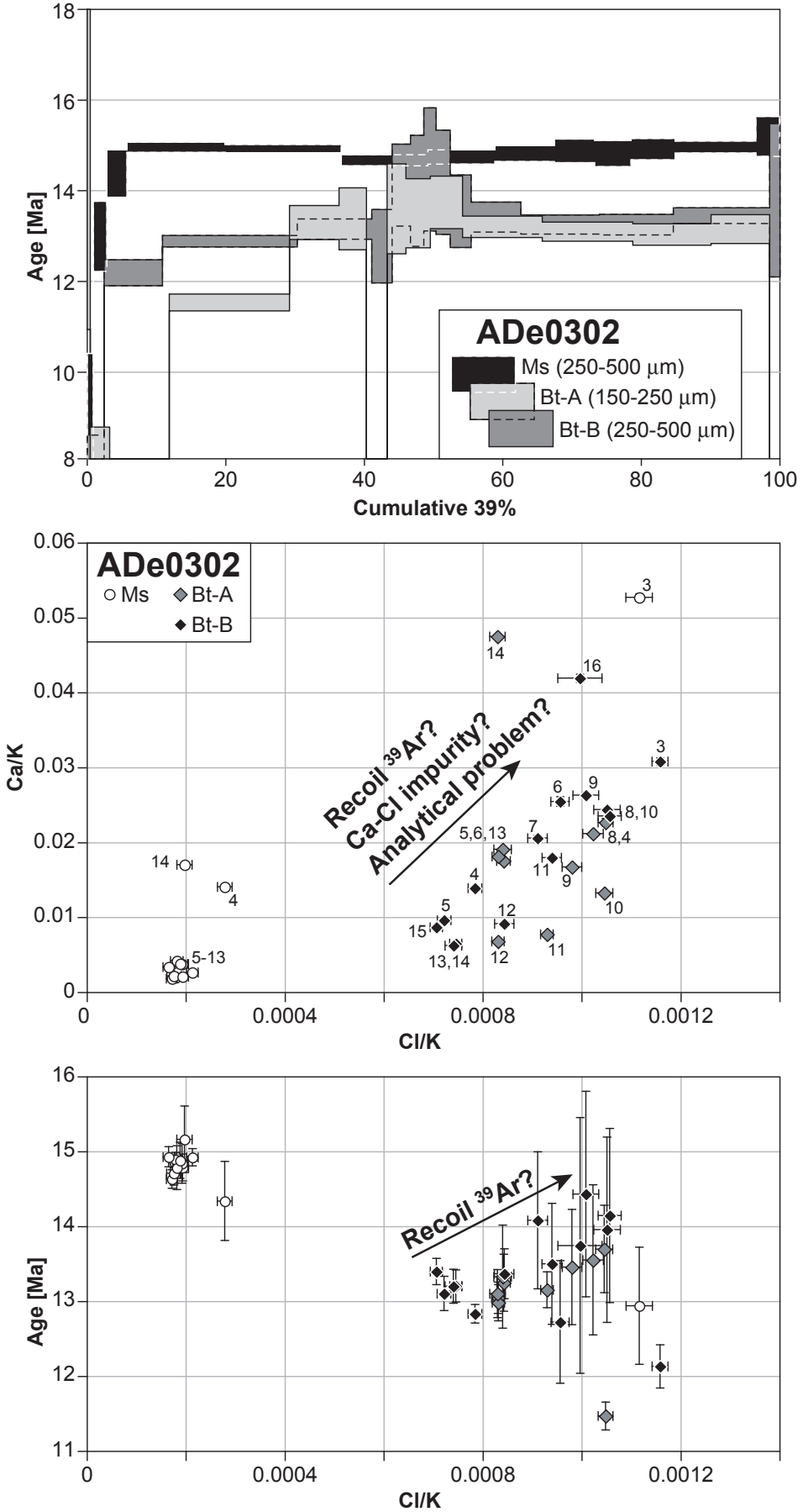

Fig. D.8: Ar-results from ADe0302. Numerical data were given in Appendix 4.1 (Chapter 4).

D.3) McM13 – ALu0306, APi0301, ADe0302

- Analyses were acquired with faraday cup and electron multiplier in analogue mode. No major problem, constant gain factor between faraday cup and multiplier measurements. A similar age is determined when preference is given to faraday or multiplier measurements, but of course a better precision is obtained on masses 36, 37 and 38 measured with multiplier.
- Good background, stable over analyses, slightly high for mass 40, but low for all others.
- Good analysis of J-factor (low variation, ±1%).
- Excellent results for white micas of ALu0306 and APi0301 (Chapter 2), as also one muscovite and two biotite separates from ADe0302. Results from this latter were briefly presented in Chapter 3. In complement to this, age spectra and Ca/K versus Cl/K correlation diagram are given in Figure D.8.

D.4) McM15 – Antabia (I), Val Piora and Molare

- Only faraday cup measurement.
- Good background, stable and low for all masses (slightly higher on mass 39, hydrocarbons?).
- Large, but regular variation of J-factor (±4%).
- During these analyses, the ion source was unstable and caused irregular and sudden drop of the signal intensity during a few seconds. Fortunately, this phenomenon appears "only" one or two times over the 13 cycles of measurement and not all steps where affected. Cycles affected were eliminated for regression to minimize this effect. Only steps yielding very low ^{39}Ar signal might have been disturbed by this effect. Samples from Val Piora and Molare were esstentially affected by this phenomenon. This accounts (partly) for the disturbed spectrum in biotite analysis of AMo0410 (many steps at low ^{39}Ar content) compared to muscovite analysis.

D.5) McM16 – ANu0304 and ACb0301 *(unpublished results)*

- Only faraday cup measurement.
- Good background, stable and low for all except mass 39 (related to some hydrocarbons, e.g. C_3H_3?).
- Large variation of J-factor (±5%, higher value for ALPHA and DELTA), but small variation (±1%) over the analysed samples (Fig. D.4).
- We made a surprising discovery during the hand picking of white micas in these samples. Muscovite and margarite coexists in these two graphite-rich samples (see BSE images and element mapping for this sample, on CD). At the selected grain-size (50-125 µm), graphite is always present as tiny inclusion in some flakes. Where graphite rich flakes were withdrawn, mineral separate were enriched in muscovite (From XRD: 5%

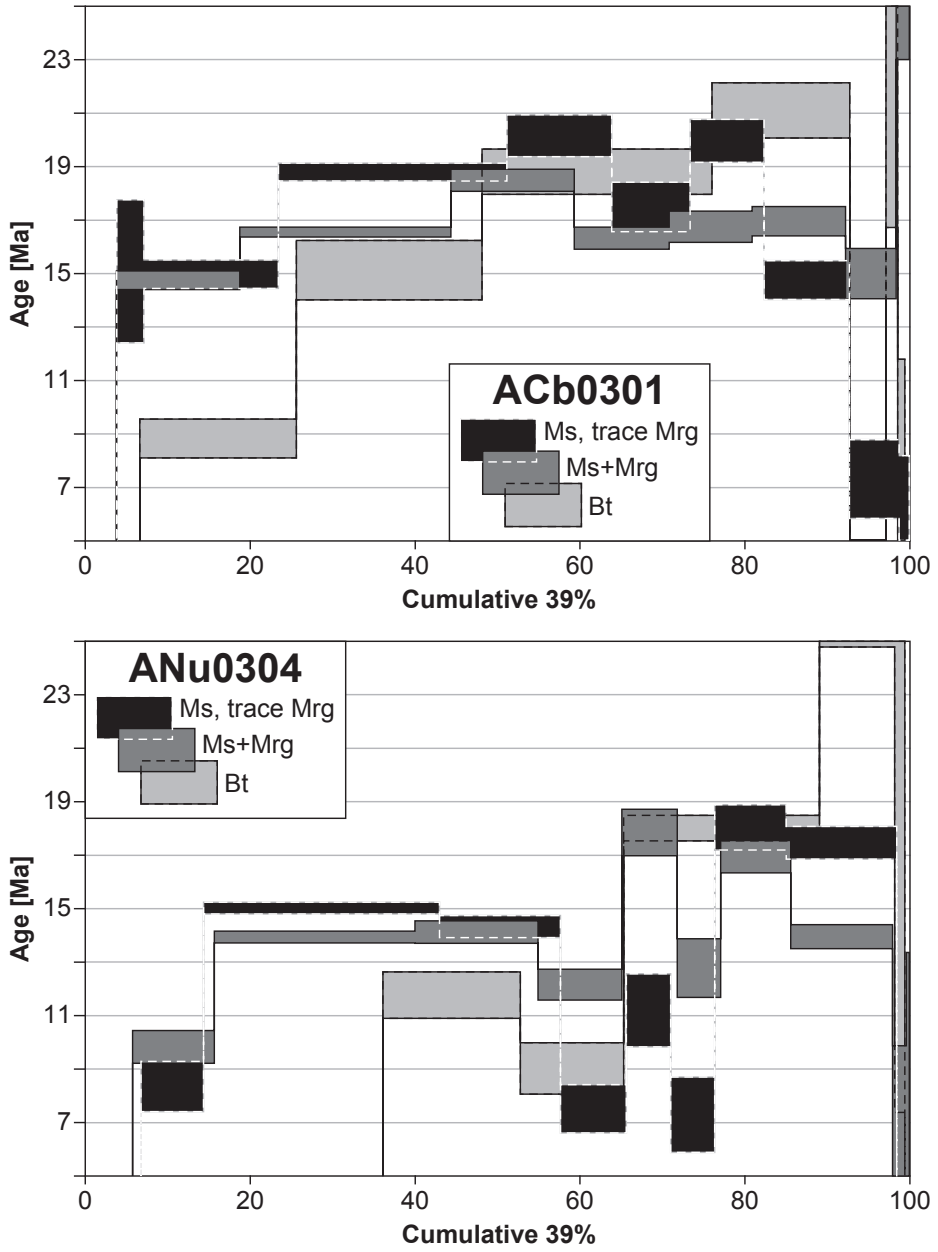

Fig. D.9: Ar-results from calc-schists ANu0304 (Nufenen) and ACb0301 (Campo Blenio). See CD for numerical results and Ca/Cl/K correlation diagrams.

and 15% Mrg in ANu0304 and ACb0301 "Ms"; e.g. Fig. D.3). In contrary, where graphite-rich inclusions remained, the amount of margarite was higher (11% and 30% Mrg in ANu0304 and ACb0301 "Ms+Mrg"). Actually, this is in line with the petrography, which shows graphite-layers inside margarite-rich areas (inclusion of interlayered) and larger muscovite flakes relatively free of graphite (or with graphite surrounding the crystal). The growth of muscovite at higher temperature (larger and pristine flakes) is likely to exclude the graphite from its structure, while margarite has formed aggregates of finer sheets around pseudo-graphite and conserved this aspect at higher grade, up to the formation of plagioclase at higher-T or during decompression. For textural realtions between muscovite and margarite, refer to element mapping of ACb0301 and ACb0406 (on CD).

- All results from white mica separates are yielding large error on ages, with disturbed spectra and no correlation in Ca/Cl/age diagrams (Fig. D.9). Worst are the results from biotite separates (variable, 10 to 20 Ma). This problem remains unresolved, but average ages calculated over all major steps are apparently coherent with the range expected for these regions, especially muscovite of Campo Blenio (compare with ALu0306 from Chapter 2, which yields ca. 18 Ma):

    - **ANu0304, Nufenen: Ms 14.7±2.1 Ms+Mrg 14.1±1.2 Ma**
    - **ACb0301, Campo Blenio: Ms 17.8±2.2 Ms+Mrg 16.8±0.9 Ma**

D.6) BEP12 – Piora, Lucomagno '06, Antabia (II)

- Low spectrometer background, small variation and only slightly adapted for each analysis. As in McM16, some hydrocarbons account for the higher background on mass 39.

- The line was polluted by air during analysis of mineral separates from AAn0405 exclusively, with a reducing pollution from Ms200, Bt200, Ms100 to Bt100 (quite no pollution). This has no dramatic effect on the average age calculated, but induces large error on each step (Chapter 3).

- Again only for analyses of sample AAn0405, a short circuit in furnace induces a bad measurement of temperatures in some steps (possible variation of T-condition during each analysed steps, perhaps ±50 °C; Fig. D.2). Temperatures given for these mineral separates are remains imprecise, especially at higher grade.

- All these problems were solved for sample AAn0401 Ms (used as internal standard, see below), as also for samples APi06xx and ALu06xx (Piora, Lucomagno; "*millésime 2006: la plus raffinée des cuvées"*).

- In this series, only the analysis of standard GAMMA was correctly measured. A small leak at high temperature in the furnace was lately identified *after* the analysis of standards ALPHA, BETA and DELTA. This leak induces a saturation of ^{40}Ar signal; hence, recalculation of J-factor from $^{40}Ar/^{39}Ar$ ratio was not possible, but ^{39}Ar and ^{37}Ar were correctly measured and could only pertain to standard degassing. As the sensitivity factor was "accurately" known (±2-5% ?) from the good analysis of other standards analysed the day before, we recalculated the J-factor required to yield the correct total-K from ^{39}Ar. With this recalculation, results of standards BETA and DELTA are in good agreement with standard GAMMA (Fig. D.4). Excluding standard ALPHA (abnomally low J-factor) and BETA (slightly too high value?), the variation observed remains low (±3%) compared to some other series (up to ±10%, McM12).

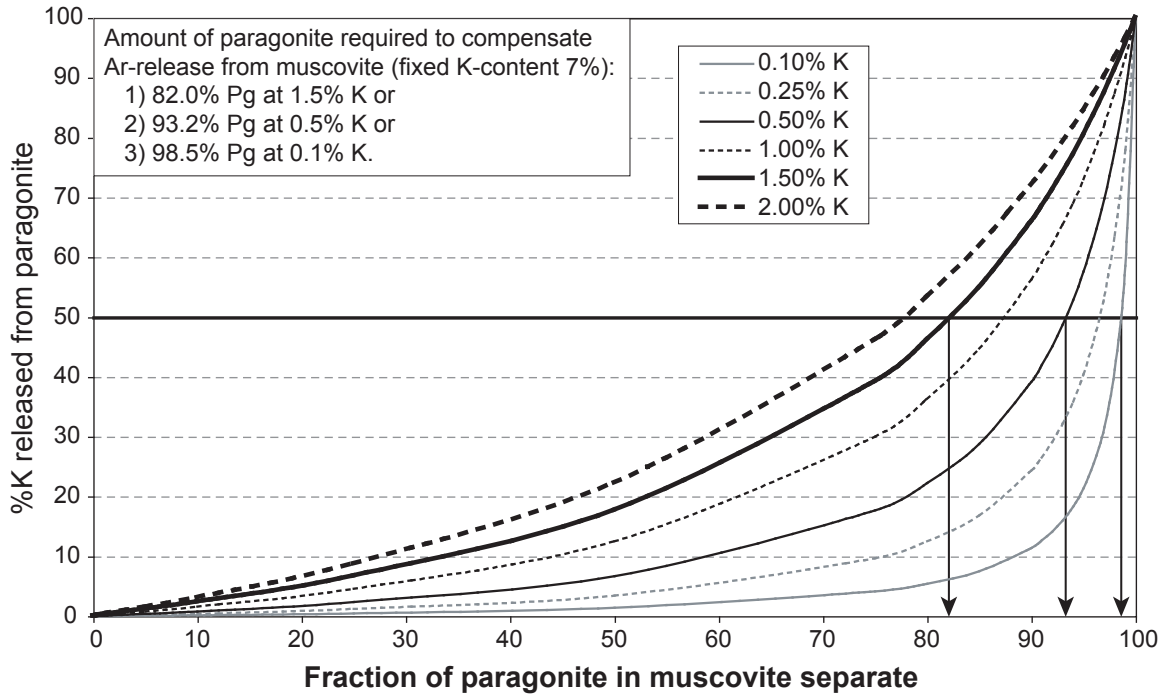

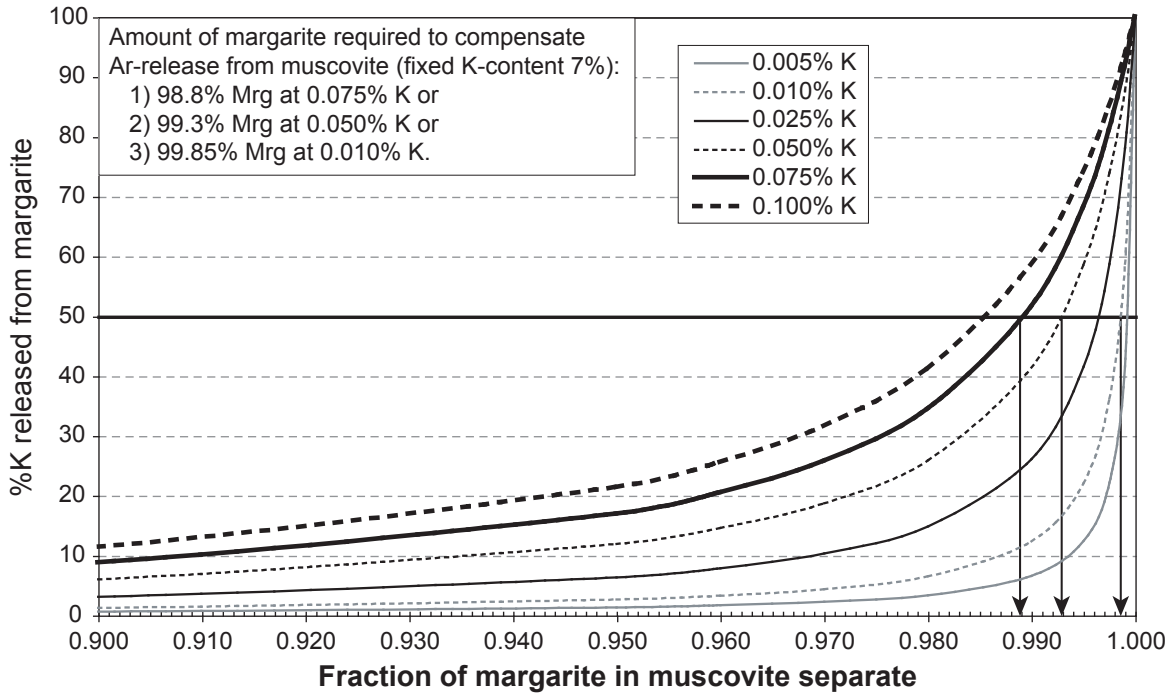

Fig. D.10: Influence of margarite or paragonite (K-poor white micas) on muscovite-rich to -poor mineral separate.

References

Anderson, G. M. (2005). Truth and beauty in thermodynamics. *The Canadian Mineralogist* 43, 11-19.

Armstrong, R. L., Jäger, E. & Eberhardt, P. (1966). A comparison of K-Ar and Rb-Sr ages on Alpine biotites. *Earth and Planetary Science Letters* 1, 13-19.

Arnold, A. & Jäger, E. (1965). Rb-Sr Altersbestimmungen an Glimmern im Grenzbereich zwischen voralpinen Alterswerten und alpiner Verjüngung der Biotite, Messung an Gesteinen des Gotthardmassivs und des Tavetscher Massivs. *Eclogae geologicae Helvetiae* 58, 369-390.

Balogh, K. & Dunkl, I. (2005). Argon and fission track dating of Alpine metamorphism and basement exhumation in the Sopron Mts. (Eastern Alps, Hungary): thermochronology or mineral growth? *Mineralogy and Petrology* 83, 191-218.

Belluso, E., Ruffini, R., Schaller, M. & Villa, I. M. (2000). Electron-microscope and Ar isotope characterization of chemically heterogeneous amphiboles from the Palala Shear Zone, Limpopo Belt, South Africa. *European Journal of Mineralogy* 12, 45-62.

Berger, A., Mercolli, I. & Engi, M. (2005). The central Lepontine Alps: Notes accompanying the tectonic and petrographic map sheet Sopra Ceneri (1:100'000). *Schweizerische Mineralogische und Petrographische Mitteilungen* 85, 109-146.

Berman, R. (1988). Internally-consistent thermodynamic data for minerals in the system Na_2O - K_2O - CaO - MgO - FeO - Fe_2O_3 - Al_2O_3 - SiO_2 - TiO_2 - H_2O - CO_2. *Journal of Petrology* 29, 445-522.

Berman, R. (1990). Mixing properties of Ca-Mg-Fe-Mn garnets. *American Mineralogist* 75, 328-344.

Berman, R. (1991). Thermobarometry using multi-equilibrium calculations: a new technique, with petrological applications. *The Canadian Mineralogist* 29, 833-855.

Berman, R. & Koziol, A. M. (1991). Ternary excess properties of grossular-pyrope-almandine garnet and their influence in geothermobarometry. *American Mineralogist* 76, 1223-1231.

Beyssac, O., Goffé, B., Chopin, C. & Rouzaud, J. N. (2002). Raman spectra of carbonaceous material in metasediments: a new geothermometer. *Journal of Metamorphic Geology* 20, 859-871.

Bjørnerud, M. G., Austrheim, H. & Lund, M. G. (2002). Processes leading to eclogitization (densification) of subducted and tectonically buried crust. *Journal of Geophysical Research* 107, 2252.

Blackenburg, F. v. & Villa, I. M. (1988). Argon retentivity and argon excess in amphiboles from the garbenschists of the western Tauern window, Eastern Alps. *Contributions to Mineralogy and Petrology* 100, 1-11.

Bolli, V. H., Burri, M., Isler, A., Nabholz, W., Pantic, N. & Probst, P. (1980). Der nordpenninische Saum zwischen Westgraubünden und Brig. *Eclogae geologicae Helvetiae* 73, 779-797.

Bousquet, R., Goffé, B., Vidal, O., Oberhänsli, R. & Patriat, M. (2002). The tectono-metamorphic history of the Valaisan domain from the Western to the Central Alps: New constraints on the evolution of the Alps. *Geological Society of America Bulletin* 114, 207-225.

Brix, M. R., Stöckhert, B., Seidel, E., Theye, T., Thomson, S. N. & Küster, M. (2002). Thermobarometric data from a fossil zircon partial annealing zone in high pressure - low temperature rocks of eastern and central Crete, Greece. *Tectonophysics* 349, 309-326.

Brouwer, F. M., Burri, T., Engi, M. & Berger, A. (2005). Eclogite relics in the Central Alps: PT - evolution, Lu-Hf ages and implications for formation of tectonic mélange zones. *Schweizerische Mineralogische und Petrographische Mitteilungen* 85, 147-174.

Bucher-Nurminen, K., Frank, E. & Frey, M. (1983). A model for the progressive regional metamorphism of margarite-bearing rocks in the Central Alps. *American Journal of Science* 283, 370-395.

Burckhardt, C. E. (1942). Geologie und Petrographie des Basodino-Gebietes. *Schweizerische Mineralogische und Petrographische Mitteilungen* 22, 99-186.

Burckhardt, C. E. & Günthert, A. (1957). Geologischer Atlas der Schweiz, Blatt 34: Basodino (1:25'000). *Schweiz. geol. Komm.*

Chadwick, B. (1968). Deformation and Metamorphism in the Lukmanier Region, Central Switzerland. *Geological Society of America Bulletin* 79, 1123-1150.

Chatterjee, N. D. & Froese, E. (1975). A thermodynamic study of the pseudobinary join muscovite-paragonite in the system $NaAlSi_3AlO_{10}(OH)_2$. *American Mineralogist* 60, 985-993.

Chopin, C. & Maluski, H. (1980). ^{40}Ar-^{39}Ar dating of high pressure metamorphic micas from the Gran Paradiso area (Western Alps): evidence against the blocking temperature concept. *Contributions to Mineralogy and Petrology* 74, 109-122.

Dahl, P. S. (1996). The crystal-chemical basis for Ar retention in micas: interences from interlayer partitioning and implications for geochronology. *Contributions to Mineralogy and Petrology* 123, 22-39.

Dalrymple, G. B. & Lanphere, M. A. (1974). $^{40}Ar/^{39}Ar$ age spectra of some undisturbed terrestrial samples. *Geochimica et Cosmochimica Acta* 38, 715-738.

de Capitani, C. (1994). Gleichgewichts-Phasendiagramme: Theorie und Software. *Beihefte zum European Journal of Mineralogy, 72. Jahrestagung der Deutschen Mineralogischen Gesellschaft* 6, 48.

de Capitani, C. & Brown, T. H. (1987). The computation of chemical equilibrium in complex systems containing non-ideal solutions. *Geochimica et Cosmochimica Acta* 51, 2639-2652.

Deutsch, A. & Steiger, R. H. (1985). Hornblende K-Ar ages and the climax of Tertiary metamorphism in the Lepontine Alps (south-central Switzerland): an old problem reassessed. *Earth and Planetary Science Letters* 72, 175-189.

Di Vincenzo, G., Carosi, R. & Palmeri, R. (2004). The relationship between tectono-metamorphic evolution and argon isotope records in white mica: constraints from in situ $^{40}Ar/^{39}Ar$ laser analysis of the variscan basement of Sardinia. *Journal of Petrology* 45, 1013-1043.

Di Vincenzo, G., Carosi, R., Palmeri, R. & Tiepolo, M. (2007). A comparative U-Th-Pb (zircon-monazite) and ^{40}Ar-^{39}Ar (muscovite-biotite) study of shear zones in the northern Victoria Land (Antartica): implications for geochronology and localized reworking of the Ross Orogen. *Journal of Metamorphic Geology* 25, 605-630.

Di Vincenzo, G. & Palmeri, R. (2001). An $^{40}Ar/^{39}Ar$ investigation of high-pressure metamorphism and the retrogressive history of mafic eclogites from the Lanterman Range (Antartica): evidence against a simple temperature control on argon transport in amphibole. *Contributions to Mineralogy and Petrology* 141, 15-35.

Di Vincenzo, G., Viti, C. & Rocchi, S. (2003). The effect of chlorite interlayering on ^{40}Ar-^{39}Ar biotite dating: an ^{40}Ar-^{39}Ar laser-probe and TEM investigations of variable chloritised biotites. *Contributions to Mineralogy and Petrology* 145, 643-658.

Dodson, M. H. (1973). Closure temperature in cooling geochronological and petrological systems. *Contributions to Mineralogy and Petrology* 40, 259-274.

Dodson, M. H. (1986). Closure profiles in cooling systems. *Materials Science Forum* 7, 145-154.

Dymek, R. F. (1983). Titanium, aluminium and interlayer cation substitutions in biotite from high-grade gneisses, West Greenland. *American Mineralogist* 68, 880-899.

Engi, M., Berger, A. & Roselle, G. T. (2001). Role of the tectonic accretion channel in collisional orogeny. *Geology* 29, 1143-1146.

Engi, M., Cheburkin, A. K. & Köppel, V. (2002). Nondestructive chemical dating of young monazite using XRF 1. Design of a mini-probe, age data for samples from the Central Alps, and comparison to U-Pb (TIMS) data. *Chemical Geology* 191, 225-241.

Engi, M., Todd, C. S. & Schmatz, D. R. (1995). Tertiary metamorphic conditions in the eastern Lepontine Alps. *Schweizerische Mineralogische und Petrographische Mitteilungen* 75, 347-369.

Frank, E. (1979). Metamorphose mesozoischer Gesteine im Querprofile Brig-Verampio: mineralogisch-petrographische und isotopengeologische Untersuchungen. University of Berne, 204 pp.

Frank, E. (1983). Alpine metamorphism of calcareous rocks along a cross-section in the Central Alps: occurence and breakdown of muscovite, margarite and paragonite. *Schweizerische Mineralogische und Petrographische Mitteilungen* 63, 37-93.

Franz, G. (1977). Determination of the miscibility gap on the solid solution series paragonite-margarite by means of the infrared spectroscopy. *Contributions to Mineralogy and Petrology* 59, 307-316.

Frey, M. (1969). Die Metamorphose des Keupers vom Tafeljura bis zum Lukmanier-Gebiet. *Beiträge zur Geologischen Karte der Schweiz* 137, 160 pp.

Frey, M. (1977). Progressive low-grade metamorphism of a black shale formation, Central Swiss Alps, with special reference to pyrophyllite and margarite bearing assemblage. *Journal of Petrology* 19, 95-135.

Frey, M., Bucher, K., Frank, E. & Schwander, H. (1982). Margarite in the Central Alps. *Schweizerische Mineralogische und Petrographische Mitteilungen* 62, 21-45.

Frey, M. & Ferreiro Mählmann, R. (1999). Alpine metamorphism of the Central Alps. *Schweizerische Mineralogische und Petrographische Mitteilungen* 79, 135-154.

Frey, M. & Niggli, E. (1972). Margarite, an important rock-forming mineral in regionally metamorphosed low-grade rocks. *Naturwissenschaften* 59, 214-215.

Frey, M. & Orville, P. M. (1974). Plagioclase in margarite-bearing rocks. *American Journal of Science* 274, 31-47.

Fuhrman, M. L. & Lindsley, D. H. (1988). Ternary feldspar modeling and thermometry. *American Mineralogist* 73, 201-215.

Giger, M. & Hurford, A. J. (1989). Tertiary intrusives of the Central Alps: Their uplift, erosion, redeposition and burial in the South-Alpine foreland. *Eclogae geologicae Helvetiae* 82, 857-866.

Glodny, J., Kühn, A. & Austerheim, H. (2008a). Diffusion versus recrystallization processes in Rb-Sr geochronology: Isotopic relics in eclogites facies rocks, Western Gneiss Region, Norway. *Geochimica et Cosmochimica Acta* 72, 506-525.

Glodny, J., Kühn, A. & Austerheim, H. (2008b). Geochronology of fluid-induced eclogite and amphibolite facies metamorphic reactions in a subduction-collision system, Bergen Arcs, Norway. *Contributions to Mineralogy and Petrology* 156.

Gouzu, C., Itaya, T., Hyodo, H. & Matsuda, T. (2006). Excess ^{40}Ar-free phengite in ultrahigh-pressure metamorphic rocks from the Lago di Cignana area, Western Alps. *Lithos* 92, 418-430.

Guidotti, C. V. (1984). Micas in metamorphic rocks. *In Bailey S. W. (editor), "Micas, review in mineralogy", Mineral. Soc. America (Washington D.C.)* 13, 357-468.

Günthert, A. (1954). Beiträge zur Petrographie und Geologie des Maggia-Lappens (NW-Tessin). I) Petrographie des oberen Val Peccia; II) Tektogenese des Maggia-Lappens. *Philosophisch-naturwissenschaftlichen Fakultät*: Universität Basel, 160 pp.

Haar, L., Gallagher, K. & Kell, G. S. (1984). *NBS/NRC steam tables: Thermodynamic and transport properties and computer programs for vapor and liquid states of water in SI units*. Hemisphere, Washington, D.C.

Hammerschmidt, K. & Frank, E. (1991). Relics of high pressure metamorphism in the Lepontine Alps (Switzerland) - ^{40}Ar/^{39}Ar and microprobe analyses on white K-micas. *Schweizerische Mineralogische und Petrographische Mitteilungen* 71, 261-274.

Hansen, J. W. (1972). Zur Geologie, Petrographie und Geochemie der Bündnerschiefer-Serien zwischen Nufenenpass (Schweiz) und Cascata Toce (Italia). *Schweizerische Mineralogische und Petrographische Mitteilungen* 52, 109-153.

Henry, D. J., Guidotti, C. V. & Thomson, J. A. (2005). The Ti-saturation surface for low-to-medium pressure metapelitic biotites: Implications for geothermometry and Ti-substitution mechanims. *American Mineralogist* 90, 316-328.

Hetherington, C. J. & Villa, I. M. (2007). Barium silicates of the Berisal Complex, Switzerland: A study in geochronology and rare-gas release systematics. *Geochimica et Cosmochimica Acta* 71, 3336-3347.

Hoschek, G. (1998). Phase equilibria of hornblende garbenschists from Hohe Tauern, Eastern Alps. *Neues Jahrbuch für Mineralogie, Abhandlungen* 173, 155-187.

Holland, T. J. B. & Powell, R. (1998). An internally consistent thermodynamic dataset for phases of petrological interest. *Journal of Metamorphic Geology* 16, 309-343.

Hunziker, J. C. (1969). Rb-Sr-Alterbestimmungen aus den Walliser Alpen Hellglimmer- und Gesamtgesteinsalterswerte. *Eclogae geologicae Helvetiae* 62, 527-542.

Hunziker, J. C., Desmons, J. & Hurford, A. J. (1992). Thirty-two years of geochronological work in the Central and Western Alps: a review on seven maps. *Mémoires de Géologie (Lausanne)* 13, 59 pp.

Hunziker, J. C., Frey, M., Clauer, N., Dallmeyer, R. D., Friedrichsen, H., Flehmig, H. & Hochstrasser, K. (1986). The evolution of illite to muscovite: mineralogical and isotopic data from the Glarus Alps, Switzerland. *Contributions to Mineralogy and Petrology* 92, 157-180.

Hunziker, P. (2003). The stability of tri-octahedral Fe^{2+}-Mg-Al chlorite. A combined experimental and theoretical study. University of Basel (Switzerland).

Hurford, A. J. (1986). Cooling and uplift patterns in the Lepontine Alps South Central Switzerland and an age of vertical mouvement on the Insubric fault line. *Contributions to Mineralogy and Petrology* 92, 413-427.

Hurford, A. J. (1991). Uplift and cooling pathways derived from fission track analysis and mica dating: a review. *Geologische Rundschau* 80, 349-368.

Jäger, E. (1962). Rb-Sr age determinations on micas and total rocks from the Alps. *Journal of Geophysical Research* 67, 5293-5306.

Jäger, E. (1970). Rb-Sr systems in different degrees of metamorphism. *Eclogae geologicae Helvetiae* 63, 163-172.

Jäger, E. (1973). Die alpine Orogenese im Lichte der radiometrischen Altersbetimmung. *Eclogae geologicae Helvetiae* 66, 11-21.

Jäger, E., Geiss, J., Niggli, E., Streckeisen, A., Wenk, E. & Wüthrich, H. (1961). Rb-Sr-Alter an Gesteinsglimmern der Schweizer Alpen. *Schweizerische Mineralogische und Petrographische Mitteilungen* 41, 255-272.

Jäger, E., Niggli, E. & Wenk, E. (1967). Rb-Sr Altersbestimmungen an Glimmern der Zentralalpen. *Beiträge zur Geologischen Karte der Schweiz* 134, 67 pp.

Jahn, B.-m., Liu, X., Yui, T.-F., Morin, N. & Bouhnik-Le Coz, M. (2005). High-pressure/ultrahigh-pressure eclogites from the Hong'an Block, East-Central China: geochemical characterization, isotope disequilibrium and geochronological controversy. *Contributions to Mineralogy and Petrology* 149, 499-526.

Janots, E., Brunet, F., Goffé, B., Poinssot, C., Burchard, M. & Cemic, L. (2007). Thermochemistry of monazite-(La) and dissakisite-(La): implications for monazite and allanite stability in metapelites. *Contributions to Mineralogy and Petrology* 154, 1-14.

Janots, E., Engi, M., Berger, A., Allaz, J. & Schwarz, O. (in press). Metamorphic sequence of REE-minerals in pelitic rocks of the Central Alps: Implications on allanite-monazite-xenotime phase relations. *Journal of Metamorphic Geology*.

Janots, E., Engi, M., Rubatto, D., Berger, A., Gregory, C. & Rahn, M. K. (in preparation). In-situ determination of heating rates in collisional orogeny. *Geology*.

Jenkin, G. R. T., Ellam, R. M., Rogers, G. & Stuart, F. M. (2001). An investigation of closure temperature of the biotite Rb-Sr system: The importance of cation exchange. *Geochimica et Cosmochimica Acta* 65, 1141-1160.

Kamber, B. (1993). Regional metamorphism and uplift along the southern margin of the Gotthard massive; results from the Nufenenpass area. *Schweizerische Mineralogische und Petrographische Mitteilungen* 73, 241-257.

Keller, L. M., de Capitani, C. & Abart, R. (2005). A quaternary solution model for white micas based on natural coexisting phengite-paragonite pairs. *Journal of Petrology* 46, 2129-2144.

Kerrick, D. M. & Jacobs, G. K. (1981). A modified Redlich-Kwong equation for H_2O, CO_2 and H_2O-CO_2 mixtures at elevated pressure and temperatures. *American Journal of Science* 281, 736-767.

Kirschner, D. L., Cosca, M. A., Masson, H. & Hunziker, J. C. (1996). Staircase $^{40}Ar/^{39}Ar$ spectra of fine-grained white mica: Timing and duration of deformation and empirical constraints on argon diffusion. *Geology* 24, 747-750.

Kleemann, U. & Reinhardt, J. (1994). Garnet-biotite thermometry revisited: the effect of Al^{VI} and Ti in biotite. *European Journal of Mineralogy* 6, 925-941.

Kogure, T. & Banfield, J. F. (2000). New insight into the mechanism for chloritization of biotite using polytype analysis. *American Mineralogist* 85, 1202-1208.

Köppel, V. & Grünenfelder, M. (1975). Concordant U-Pb ages of monazite and xenotime from Central Alps and the timing of the high temperature Alpine metamorphism, a preliminary report. *Schweizerische Mineralogische und Petrographische Mitteilungen* 55, 129-132.

Köppel, V., Günthert, A. & Grünenfelder, M. (1980). Patterns of U-Pb zircon and monazite in polymetamorphic units of the Swiss Central Alps. *Schweizerische Mineralogische und Petrographische Mitteilungen* 61, 97-119.

Kretz, R. (1983). Symbols for rock-forming minerals. *American Mineralogist* 68, 277-279.

Krige, L. J. (1918). Petrographische Untersuchungen im Val Piora und Umgebung. *Eclogae geologicae Helvetiae* 14, 519-654.

Krumrei, T. V., Villa, I. M., Marks, M. A. W. & Markla, G. (2006). A $^{40}Ar/^{39}Ar$ and U/Pb isotopic study of the Ilímaussaq complex, South Greenland: Implications for the ^{40}K decay constant and for the duration of magmatic activity in a peralkaline complex *Chemical Geology* 227, 258-273.

Kuhn, B. K., Reusser, E., Powell, R. & Günther, D. (2005). Metamorphic evolution of calc-schists in the Central Alps, Switzerland. *Schweizerische Mineralogische und Petrographische Mitteilungen* 85, 175-190.

Lee, J. Y., Marti, K., Severinghaus, J. P., Kawamura, K., Yoo, H. S., Lee, J. B. & Kim, J. S. (2006). A redetermination of the isotopic abundances of atmospheric Ar. *Geochimica et Cosmochimica Acta* 70, 4507-4512.

Leu, W. (1986). Lithostratigraphie und Tektonik der nordpenninischen Sedimente in der Region Bedretto-Baceno-Visp. *Eclogae geologicae Helvetiae* 79, 769-824.

Li, S., Jagoutz, E., Chen, Y. & Li, Q. (2000). Sm-Nd and Rb-Sr isotopic chronology and cooling history of ultrahigh pressure metamorphic rocks and their country rocks at Shuanghe in the Dabie Mountains, Central China. *Geochimica et Cosmochimica Acta* 64, 1077-1093.

Livi, K. J. T., Christidis, G. E., Arkai, P. & Veblen, D. R. (2008). White mica domain formation: A model for paragonite, margarite, and muscovite formation during prograde metamorphism *American Mineralogist* 93, 520-527.

Livi, K. J. T., Ferry, J. M., Veblen, D. R., Frey, M. & Connolly, J. A. D. (2002). Reactions and physical conditions during metamorphism of Liassic aluminous black shales and marls in central Switzerland. *European Journal of Mineralogy* 14, 647-672.

Livi, K. J. T., Veblen, D. R., Ferry, J. M. & Frey, M. (1997). Evolution of 2:1 layered silicates in low-grade metamorphosed Liassic shales of Central Switzerland. *Journal of Metamorphic Geology* 15, 323-344.

Ludwig, K. R. (2003). User's manual for Isoplot 3.00, a geochronological toolkit for Microsoft Excel. *Berkley Geochronology Center, Special Publication* 4, 70 pp.

Mäder, U. K. & Berman, R. (1991). An equation of state for carbon dioxide to high pressure and temperature. *American Mineralogist* 76, 1547-1559.

Massonne, H. J. & Schreyer, W. (1987). Phengite geobarometry based on the limiting assemblage with K-feldspar, phlogopite and quartz. *Contributions to Mineralogy and Petrology* 96, 212-224.

Massonne, H. J. & Szpurka, Z. (1997). Thermodynamic proprieties of white micas on the basis of high-pressure experiments in the systems K_2O-MgO-Al_2O_3-SiO_2-H_2O and K_2O-FeO-Al_2O_3-SiO_2-H_2O. *Lithos* 41, 229-250.

Maxelon, M. & Mancktelow, N. S. (2005). Three-dimensional geometry and tectonostratigraphy of the Pennine zone, Central Alps, Switzerland and Northern Italy. *Earth-Science Reviews* 71, 171-227.

McMullin, D. W. A., Berman, R. & Greenwood, H. J. (1991). Calibration of the SGAM thermobarometer for pelitic rocks using data from phase-equilibrium experiments and natural assemblages. *Canadian Mineralogist* 29, 889-908.

Michalski, I. & Soom, M. A. (1990). The Alpine thermo-tectonic evolution of the Aar and Gotthard massifs, Central Switzerland: Fission Track age on zircon and apatite and K-Ar mica age. *Schweizerische Mineralogische und Petrographische Mitteilungen* 70, 373-387.

Milnes, A. G. (1974). Structure of the Pennine Zone (Central Alps): A new working hypothesis. *Geological Society of America Bulletin* 85, 1727-1732.

Milnes, A. G. (1976). Strukturelle Probleme im Bereich der Schweizer Geotraverse - das Lukmanier-Massiv. *Schweizerische Mineralogische und Petrographische Mitteilungen* 56, 615-618.

Mulch, A. & Cosca, M. A. (2004). Recrystallization or cooling ages: *in situ* UV-laser $^{40}Ar/^{39}Ar$ geochronology of muscovite in mylonitic rocks. *Journal of the Geological Society, London* 161, 573-582.

Nabholz, W. K. (1945). Bündnerschiefergebirge zwischen Rheinwald, Valser- und Safiental. *Eclogae geologicae Helvetiae* 38, 1-120.

Nabholz, W. K. (1948). Das Ostende der mesozoischen Schieferhülle des Gotthard-Massivs im Vorrheintal. *Eclogae geologicae Helvetiae* 41, 247-268.

Nagel, T., de Capitani, C. & Frey, M. (2002a). Isograds and P-T evolution in the eastern Lepontine Alps (Graubünden, Switzerland). *Journal of Metamorphic Geology* 20, 309-324.

Nagel, T., de Capitani, C., Frey, M., Froitzheim, N., Stünitz, H. & Schmid, S. M. (2002b). Structural and metamorphic evolution during rapid exhumation in the Lepontine dome (southern Simano and Adula nappes, Central Alps, Switzerland). *Eclogae geologicae Helvetiae* 95, 301-321.

Nier, A. O. (1950). A redetermination of the relative abundances of the isotopes of carbon, nitrogen, argon and potassium. *Phys. Rev.* 77, 789-793.

Niggli, E. (1970). Alpine Metamorphose und alpine Gebirgsbildung. *Fortschritte der Mineralogie* 47, 16-26.

Niggli, E. & Niggli, C. R. (1965). Karten der Verbreitung einiger Mineralien des alpidischen Metamorphose in den Schweizer Alpen (Stilpnomelan, Alkali-Amphibol, Chloritoid, Staurolith, Disthen, Sillimanit). *Eclogae geologicae Helvetiae* 58, 335-368.

Oberli, F., Meier, M., Berger, A., Rosenberg, C. & Gieré, R. (2004). $^{230}Th/^{238}U$ disequilibrium systematics in U-Th-Pb dating: Precise accessory mineral chronology and melt evolution tracing in the Alpine Bergell intrusion. *Geochimica et Cosmochimica Acta* 68, 2534-2560.

Onstott, T. C., Miller, M. L., Ewing, R. C., Arnold, G. W. & Walsh, D. S. (1995). Recoil refinements: Implications for the $^{40}Ar/^{39}Ar$ dating technique. *Geochimica et Cosmochimica Acta* 59, 1821-1834.

Onstott, T. C., Phillips, D. & Pringle-Goodell, L. (1991). Laser microprobe measurement of chlorine and argon zonation in biotite. *Chemical Geology* 90, 145-168.

Parrish, R. R. (1990). U-Pb dating of monazite and its application to geological problems. *Canadian Journal of Earth Sciences* 27, 1431-1450.

Petrova, T. V., Mählmann, R. F., Stern, R. A. & Frey, M. (2002). Application of combustion and DTA-TGA analysis to the study of metamorphic organic matter. *Schweizerische Mineralogische und Petrographische Mitteilungen* 82, 33-53.

Pfiffner, O. A., Ellis, S. & Beaumont, C. (2000). Collision tectonics in the Swiss Alps: insight from geodynamic modeling. *Tectonics* 19, 1065-1094.

Pfiffner, O. A., Sahli, S. & Stäuble, M. (1997). Compression and uplift of the external massifs in the Helvetic zone. In: Pfiffner, O. A., Lehner, P., Heitzmann, P., Müller, S. & Steck, A. (eds.) *NRP-20: Deep structure of the swiss Alps*: Birkhäuser, Switzerland, 139-153.

Probst, P. (1980). Die Bündnerschiefer des nördlichen Penninikums zwischen Valser Tal und Passo di San Giacomo. *Beiträge zur Geologischen Karte der Schweiz* 153, 63 pp.

Proyer, A. (2003). The preservation of high-pressure rocks during exhumation: metagranites and metapelites. *Lithos* 70, 183-194.

Purdy, J. & Jäger, E. (1976). K-Ar ages on rock-forming minerals from the central Alps. *Mem. Instituti Geol. Mineral. Uni. Padova* 30, 31 pp.

Rahn, M. K. (2005). Apatite fission track ages from the Adula nappe: late-stage exhumation and relief evolution. *Schweizerische Mineralogische und Petrographische Mitteilungen* 85, 233-245.

Rahn, M. K., Brandon, M. T., Batt, G. E. & Graver, J. I. (2004). A zero-damage model for fission-track annealing in zircon. *American Mineralogist* 89, 473-484.

Rahn, M. K., Steinmann, M. & Frey, M. (2002). Chloritoid composition and formation in the eastern Central Alps: a comparison between Penninic and Helvetic occurences. *Schweizerische Mineralogische und Petrographische Mitteilungen* 82, 409-426.

Renne, P. R., Swisher, C. C., Deino, A. L., Karner, D. B., Owens, T. L. & DePaolo, D. J. (1998). Intercalibration of standards, absolute ages and uncertainities in $^{40}Ar/^{39}Ar$ dating. *Chemical Geology* 145, 117-152.

Scaillet, S., Feraud, G., Ballèvre, M. & Amouric, M. (1992). Mg/Fe and [(Mg,Fe)Si-Al_2] compositional control on argon behaviour in high-pressure white micas: A $^{40}Ar/^{39}Ar$ continuous laser-probe study from the Dora-Maira nappe of the internal western Alps, Italy. *Geochimica et Cosmochimica Acta* 56, 2851-2872.

Schaer, J. P., Reimer, G. M. & Wagner, G. A. (1975). Actual and ancient uplift rate in the Gotthard region, swiss Alps: a comparison between precise levelling and fission track apatite age. *Tectonophysics* 29, 293-300.

Schlatter, A., Schneider, D., Geiger, A. & Kahle, H. G. (2005). Recent vertical mouvements from precise levelling in the vicinity of the city of Basel, Switzerland. *International Journal of Earth Sciences* 94, 507-514.

Schlunegger, F. & Willett, S. (1999). Spatial and temporal variations in exhumation of the central Swiss Alps and implications for exhumation mechanisms. In: Ring, U., Brandon, M. T., Lister, G. S. & Willett, S. (eds.) *Exhumation processes: normal faulting, ductile flow and erosion*: Geological Society of London Special Publication, 157–179.

Schmid, S. M., Fügenschuh, B., Kissling, E. & Schuster, R. (2004). Tectonic map and overall architecture of the Alpine orogeny. *Eclogae geologicae Helvetiae* 97, 93-117.

Schmid, S. M., Pfiffner, O. A., Froitzheim, N., Schönborn, G. & Kissling, E. (1996). Geophysical-geological transect and tectonic evolution of the Swiss-Italian Alps. *Tectonics* 15, 1036-1064.

Sharp, Z. D. (1992). In situ laser microprobe techniques for stable isotope analysis. *Chemical Geology (Isotope Geoscience Section)* 101, 3-19.

Sharp, Z. D., Masson, H. & Lucchini, R. (2005). Stable isotope geochemistry and formation mechanisms of quartz veins; extreme paleoaltitudes of the central alps in the neogene. *American Journal of Science* 305, 187-219.

Sibbald, T. I. I. (1971). The structural and metamorphic geology of the Val Piora region, Ticino, Switzerland. University of London, 294 pp.

Siegenthaler, R. (1984). Alter und Geochemie von Glimmern und Feldspäten. *Institut für Geologie*: University of Berne.

Sletten, V. W. & Onstott, T. C. (1998). The effect of the instability of muscovite during in vacuo heating on $^{40}Ar/^{39}Ar$ step-heating spectra. *Geochimica et Cosmochimica Acta* 62, 123-141.

Spicher, A. (1972). Tektonische Karte der Schweiz (1:500'000). Basel: Schweizerische geologische Kommission.

Spicher, A. (2005). Tektonische Karte der Schweiz, 1st revision (1:500'000). Bern: Institut für Geologie, Universität Bern, und Bundesamt für Wasser und Geologie.

Steck, A., Epard, J. L., Esher, A., Gouffon, Y. & Masson, H. (2001). Carte tectonique des Alpes de Suisse occidentale et des régions avoisinantes (1:100'000). *Office féd. Eaux Geologie (Berne)* Carte géologique spéciale n° 123, avec notice explicative, 73 pp.

Steck, A. & Hunziker, J. C. (1994). The tertiary structural and thermal evolution of the Central Alps - compressional and extensional structures in an orogenic belt. *Tectonophysics* 238, 229-254.

Steiger, R. H. (1964). Dating of orogenic phases in the Central Alps by K-Ar of Hornblende. *Journal of Geophysical Research* 69, 5407-5421.

Steiner, H. (1984). Radiometrische Altersbestimmungen an Gesteinen der Maggia-Decke (Penninikum der Zentralalpen). *Schweizerische Mineralogische und Petrographische Mitteilungen* 64, 227-259.

Thakur, V. C. (1976). Structural and metamorphic history of the mesozoic metasediments and premesozoic basement rocks of the Molare region, Ticino, Switzerland. *Sciences de la Terre* 20, 265-294.

Thöni, M. & Jagoutz, E. (1992). Some new aspects of dating eclogites in orogenic belts: Sm-Nd, Rb-Sr, and Pb-Pb isotopic results from the Austroalpine Saualpe and Koralpe type-locality (Carinthia/Styria, southeastern Austria). *Geochimica et Cosmochimica Acta* 56, 347-368.

Todd, C. S. & Engi, M. (1997). Metamorphic field gradients in the Central Alps. *Journal of Metamorphic Geology* 15, 513-530.

Trommsdorff, V. (1966). Progressive Metamorphose kieseliger Karbonatgesteine in den Zentralalpen zwischen Bernina und Simplon.

Trommsdorff, V. (1980). Alpine metamorphism and alpine intrusions. In: Trümpy, R. (ed.) *Geology of Switzerland - a guide-book, part A: An outline of the geology of Switzerland*. Basel, New York: Wepf & Co., 82-87.

Vance, D. & O'Nions, R. K. (1992). Prograde and retrograde thermal histories from the Central Swiss Alps. *Earth and Planetary Science Letters* 114, 113-129.

Vidal, O., Goffé, B., Bousquet, R. & Parra, T. (1999). Calibration and testing of an empirical chloritoid-chlorite Mg-Fe exchange thermometer and thermodynamic data for daphnite. *Journal of Metamorphic Geology* 17, 25-39.

Villa, I. M. (1993). On the geological interpretation of radiometric age determinations with the $^{40}Ar/^{39}Ar$ method. Universität Bern, 143 pp.

Villa, I. M. (1998a). Direct determination of ^{39}Ar recoil distance. *Geochimica et Cosmochimica Acta* 61, 689-691.

Villa, I. M. (1998b). Isotopic closure. *Terra Nova* 10, 42-47.

Villa, I. M. (2001). Radiogenic isotopes in fluid inclusions. *Lithos* 55, 115-124.

Villa, I. M. (2004). Geochronology of metamorphic rocks. *Per. Mineral.* 73, 259-271.

Villa, I. M. (2006). From nanometer to megameter: Isotopes, atomic-scale processes, and continent-scale tectonic models. *Lithos* 87, 155-173.

Villa, I. M. & Buettner, A. (submitted). Chronostratigraphy of Monte Vulture Volcano (southern Italy): mineral microtextures, the role of secondary processes, and ^{39}Ar-^{40}Ar systematics. *Bulletin of Volcanology*.

Villa, I. M., Grobéty, B., Kelley, S. P., Trigila, R. W. & Wieler, R. (1996). Assessing Ar transport paths and mechanisms in the McClure Mountains hornblende. *Contributions to Mineralogy and Petrology* 126, 67-80.

Villa, I. M., Hermann, J., Müntener, O. & Trommsdorff, V. (2000). $^{39}Ar/^{40}Ar$ dating of multiply zoned amphibole generations (Malenco, Italian Alps). *Contributions to Mineralogy and Petrology* 140, 363-381.

Villa, I. M. & Puxeddu, M. (1994). Geochronology of the Larderello geothermal field: new data and the "closure temperature" issue. *Contributions to Mineralogy and Petrology* 115, 415-426.

Viti, C., Di Vincenzo, G. & Mellini, M. (2004). Thermal transformations in laser-heated chloritized annite. *Phys. Chem. Minerals* 31, 92-101.

Wagner, G. A., Reimer, G. M. & Jäger, E. (1977). Cooling ages derived by apatite fission track, mica Rb-Sr and K-Ar dating: the uplift and cooling history of the Central Alps. *Mem. Instituti Geol. Mineral. Uni. Padova* 30, 1-27.

Wenk, E. (1956). Die lepontinische Gneissregion und die jungen Granite der Valle della Mera. *Eclogae geologicae Helvetiae* 49, 251-265.

Wenk, E. (1970). Regional metamorphism and ultrametamorphism in the Lepontine Alps. *Fortschritte der Mineralogie* 47, 34-51.

Wenk, E. & Keller, F. (1969). Isograde in Amphibolitserien der Zentralalpen. *Schweizerische Mineralogische und Petrographische Mitteilungen* 49, 157-198.

Wenk, E., Schwander, H. & Stern, W. (1974). On calcic amphiboles and amphibolites from the Lepontine Alps. *Schweizerische Mineralogische und Petrographische Mitteilungen* 54, 97-149.

Wiederkehr, M., Bousquet, R., Schmid, S. M. & Berger, A. (submitted). From subduction- to collision-related metamorphism: Thermal overprint of HP-LT meta-sediments in the northeastern Lepontine Dome (Swiss Alps). *Swiss Journal of Geosciences (Special Volume 8th Alpine Workshop Davos)*.

Wijbrans, J. R. & McDougall, I. (1986). $^{40}Ar/^{39}Ar$ dating of white micas from an Alpine high-pressure metamorphic belt on Naxos (Greece): the resetting of the argon isotopic system. *Contributions to Mineralogy and Petrology* 93, 187-194.

Will, T. M., Powell, R. & Holland, T. J. B. (1990). Calculated greenschist facies mineral equilibria in the system CaO-FeO-MgO-Al_2O_3-SiO_2-CO_2-H_2O. *Contributions to Mineralogy and Petrology* 104, 353-368.

Worley, B. A. & Powell, R. (1998). Singularities in NCKFMASH (Na_2O-CaO-K_2O-FeO-MgO-Al_2O_3-SiO_2-H_2O). *Journal of Metamorphic Geology* 16, 169-188.

Xie, Z., Zheng, Y.-F., Jahn, B.-M., Ballèvre, M., Chen, J., Gautier, P., Gao, T., Gong, B. & Zhou, J. (2004). Sm-Nd and Rb-Sr dating of pyroxene-garnetite from North Dabie in east-central China: problem of isotope disequilibrium due to retrograde metamorphism. *Chemical Geology* 206, 137-158.

Yamada, R., Murakami, M. & Tagami, T. (2007). Statistical modelling of annealing kinetics of fission tracks in zircon; Reassessment of laboratory experiments. *Chemical Geology* 236, 75-91.

Zimmermann, J. L. (1970). Contribution à l'étude de la déshydratation et de la libération de l'argon des micas. *Geochimica et Cosmochimica Acta* 34, 1327-1350.

Help for "JEOL2xls" (ver. 1.04)

A macro for normalizing mineral analysis (PRZ-correction) and treating LineScan from microprobe JEOL-8200
Institut für Geologie, Bern – J. Allaz © 2006-2008 *(and normalization file from ETHZ…)*

General comments:

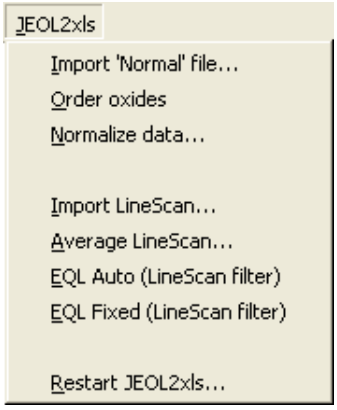

Fig.1, Menu «JEOL2xls» of Excel

Macro files — The entire macro set is comprised in the Excel file "*JEOL2xls.xls*" and is accompanied by a cation normalization file "*CatNorm.xls*" and an oxygen normalization file "*OxyNorm.xls*" (both from ETHZ, should be preserved in "read-only" mode to prevent any changes).

OS — This macro has been developed and tested on both Mac (OS 10.4) and PC (Windows XP), with different version of Excel (98 for Mac and 2000 for PC). No problem should appear on any of these operating systems. As "Visual Basic for Application" is necessary, Excel 5.0 is at least required.

Installation — Copy the three files (macro + normalization files) in the folder of your choice. To start the macro, open "*JEOL2xls.xls*" (file is automatically hidden during opening). If you open it for the first time, you are asked to update the default JEOL2xls directory. Click OK in this first window and then select YOUR copy of file "*JEOL2xls.xls*" and validate. The 'Welcome' form appears and informs you about the updated default path. This start-up form appears each time you open the macro file or you restart the macro JEOL2xls. By clicking "OK", the menu "JEOL2xls" is created at the end of Excel menu bar (Fig. 1).

Treated files
a) For importation processes, use **only EXPORTED TEXT FILE OF JEOL-8200 microprobe** (quantitative analysis or line scan). Importation processes never affected your original data, as a copy of sheet to treat is made before processing. However, a **backup of files to treat is HIGHLY recommended before treating them!** Of course, the author of this macro is NOT responsible of any data loss...
b) Ordering elements or normalization process may be applied **on any type of quantitative analysis file** (be careful, some specific format must be respected, see below "Order oxides" or "Normalize data...").

Normalization — Any kind of silicate, carbonate or oxide (with some restrictions for cation valence) may be normalized, as number of oxygen, cation, OH- and CO2-group can be entered manually. A list of mineral to normalize with default value is also available. Contact me if you want to add one or more mineral in the default list. However, **only following major elements are used** in normalization:

Si^{4+}, Ti^{4+}, Cr^{3+}, Al^{3+}, Fe^{2+}, Fe^{3+}, Mn^{2+}, Ni^{2+}, Mg^{2+}, Ca^{2+}, Na^{+}, K^{+}, Zn^{+}, Cl^{-}, F^{-} (and H^{-}, C^{4+})

If strongly required, some other elements may be added inside process in the future.

Questions? Bugs? Contact me! *jallaz@geo.unibe.ch* [until end 2008] or ***webmaster@geoloweb.ch***

Menu "Import 'Normal' file…" (Importation of QUANTITATIVE ANALYSIS with detection limits)

!!! WARNING !!! This option **only works on data exported from JEOL-8200 microprobe with file type option "Normal" and with option "spreadsheet" activated** (tabulation separates data, instead of spaces). This exportation produces a text file (*.txt) comprising notably the element and oxide components you analysed together with the detection limit (in ppm). Use only quantitative analysis **corrected by the "PRZ" method** (importation of any other method, e.g. "ZAF", will not correctly work).

!!! WARNING !!! **Ensure no other file is opened before applying this process** (except "*JEOL2xls.xls*" of course, should be hidden, see "Window:(un)hide…"). This avoids confusion during file treatments (the "active" file in foreground is normally always treated by the macro, but…).

Open file to treat and click on menu "Import 'normal' file…". You can also directly activate this menu without opening any file: the macro automatically asks you to open a (text) file to treat. Files to treat do not necessary need to be situated in your JEOL2xls default folder.

If an error is produced, it is probably due to a bad file format (the macro tests if cell A2 contains "Intensity and Mass-%", typical of a 'normal' file). If everything is OK, a form opens. **Ensure values for number of element analysed and NOT analysed are correct**. If this is not the case, the file format may be wrong (e.g. ZAF correction has been applied on analysis instead of PRZ) and importation may produce some bugs (see Fig. 2 for correct type of 'normal' file). Elements NOT analysed are all elements determined by differences or by stochiometry (e.g. O, H...). The **total number of analysis is an approximation and just required to be a MINIMAL value** (used for limiting the importation process). Then select your importation options:

	A	B	C	D	E	F	G	H	I
1									
2	Intensity & M	Group : ju	Sample : Fe	Page	1				
3									
4									
5									
6									
7	Unknown Spe	No.	122						
8	Group :	julien_allaz	Sample :	FspJul-MSP					
9	UNK No	122	Comment	MF315a-p1					
10	Stage :	X=	64.921	Y=	60.8765	Z=	11.6478		
11	Acc. Voltage	15	(kV)	Probe Dia. :	5	Scan :	Off		
12	Dated on	############							
13	WDS only	No. of accum	1						
14									
15	Curr.(A) :	2.02E-00							
16	Element	Peak(mm)	Net(cps)	Bg	Bg+	S.D.(%)	D.L.(ppm)		
17	1	Si	77.848	10450.7	52.6	47.8	0.22	134	
18	2	Ti	00.159	9	14.0	12.7	14.90	129	
19	3	K	119.731	18.8	25.8	22.8	9.79	44	
20	4	Na	129.565	2037	53.3	44.3	0.51	98	
21	5	Al	91.035	3772.5	36.1	27.9	0.37	104	
22	6	Fe	134.801	3.1	1.6	1.8	18.39	382	
23	7	Ca	107.431	1154	36.3	32.8	0.68	51	
24	8	Mg	107.513	2.6	103.3	81.3	115.24	99	
25									

Fig. 2, "Normal" file from JEOL-8200 after correct opening. Column H should contain the detection limit (see rows 17 to 24). Those values may be shifted to the right (in column I), but this will be corrected during activation of the "Import 'Normal' file..." process. This correction may take a few seconds, especially if your file contains some hundreds points of analysis...

1. "Check values to import...": detection limit, element-%, compound-% (general information always present).
2. "Parameters for imported values...":
   - Choose if you want to withdraw values below detection limit (and replace them by "< x.xx" where x.xx is detection limit [option 1] or by "-" [option 2] or by " " [nothing, option 3]). Since version 1.04 and for [option 1] you are also asked to give a precision value for detection limit (e.g. if you enter "2", detection limit is "< 0.xx", if 3 => "< 0.xxx", etc.).
   - Check the box "Fe is Fe_2O_3" if you set Fe as Fe^{3+} (Fe_2O_3). If NOT checked, Fe is defined as Fe^{2+} (FeO). Note that during normalization, the Fe^{2+}/Fe^{3+} content can be estimated either by charge difference (cation normalization) or by fixed ratio (oxygen normalization). Estimation with cation normalization is relatively good for solid phases, but should be taken with care for hydrous phases.
   - If you want, select the imported values you want to delete after treatment. Of course, you are not allowed to check all the three options (why then are you using this macro?).
3. "Parameters for normalization":
   - Check option "Order compound-%..." to prepare data for normalization (files "*OxyNorm.xls*" or "*CatNorm.xls*" require a specific ordering of the major elements. Any elements not recognized by the normalization macro are not deleted, but simply put after this list of oxides. The process for ordering oxides can be called after importation (menu "Order oxides", see below).
   - Check option "Normalize data" to continue with normalization process when importation is finished (files "*OxyNorm.xls*" or "*CatNorm.xls*" required, must be present in default folder of JEOL2xls).
   - If you proceed to a second normalization, the existing one is shifted down to prevent overwriting.
4. When everything is okay, start importation and wait until end of the process. If it ends correctly, the importation form is automatically closed. This process should work without limits concerning number of analysis (tested with 450 analysis, but more should work, too) and number or type of elements analysed (tested with 23 elements, REE-mineral analysis)! However, due to Excel limitation of columns (max 256), only 250 analyses can be written in a single sheet. If more analyses are present, the process creates a new sheet (first sheet is named 'Import 1', second one 'Import 2'...). During other automation processes, JEOL2xls searches for any sheet 'Import x' and orders oxides or normalize your data from ALL these sheets!
5. For an easy use, check the very last option ("Normalize data"). **Default importation:** general information, ordered elements (without values below detection limit) and normalization results remains in file. Adapt then this default option to your specific need

!!! WARNING !!! On Mac, importation of 'Normal' file can be very slow compared to PC... To accelerate the process, rapidly move your mouse (don't laugh, this really works! But I cannot explain and correct this bug...).

Note: In older version of JEOL2xls (earlier than version 1.04), importation of date and time was problematic. This is now corrected... If you have trouble with this, close your 'normal' file (without saving it) and re-open it but BY USING THE MENU "Import 'normal' file..." and NOT with the classical "open..." menu of Excel.

Menu "Order oxides"

Use this option to order oxides before using "Normalize data…". Oxides used in normalization MUST BE ordered, otherwise normalization process (see "Normalize data...") never works! The correct order is: SiO_2, TiO_2, Cr_2O_3, Al_2O_3, FeO, Fe_2O_3, MnO, NiO, MgO, CaO, NaO, K_2O, OH/H_2O, CO_2, F, Cl.

To use this process, insert an empty column on the left side of the column containing the oxides to order (must be column "A" and so elements to order is in "B" and first analysis in "C") and **type "Oxide" in the cell situated on the left-hand side of the FIRST compound to order**. Ensure to leave at least two empty rows at the end of the elements to order. Any element not recognized by the ordering process is copied at the end of the ordered oxides.

Menu "Normalize data…"

This option copies your data in the "*OxyNorm.xls*" or "*CatNorm.xls*" file and normalize your data. If you activate this option after the process "Import 'normal' file...", the macro automatically applies the process on each sheets named 'Import x' (x = 1, 2,...). If not, you will be asked to normalize the activate sheet only.

In a same manner than the "Oxide" key word in menu "Order oxides", this process looks first for a **cell named "For Norm" in column A**. This cell MUST BE PRESENT and is automatically added when you treat your data with "Order oxides" or if you have check the option of the same name during in menu "Import 'normal' file...". It is used to indicate the macro, where your ordered oxides start. Remember that oxides present in your file need to be ordered, as described above (see "Order oxides"). Otherwise an error occurs... If everything is okay, a form appears, asking you some parameters required for a the normalization:

- A name for the copy of the normalization file to create (from "*OxyNorm.xls*" or "*CatNorm.xls*"). This file contains the calculation for normalization (choose any name, except "CatNorm", "OxyNorm" or any other name already existing in your JEOL2xls folder). If you don't want a file to be saved, but just to copy-paste the normalized data in your 'normal' file, check the box "Don't save normalization file".

!!! WARNING !!! If the filename you enter already exist in the JEOL2xls default folder, Excel asks you to overwrite the file. If you answer 'No' or 'Cancel', the macro will abnormally stop. When returning to Excel, close the file "*CatNorm.xls*" or "*OxyNorm.xls*" that has been opened, otherwise, a fatal error is produced when restarting the process!

- The row number where are the legend of your data. The content of this row is used a) to recognize your data in the normalization and b) to determine the number of analysis to treat. You can also select a second row of legend. If this latter is not required, just type "0" (zero) and this option is ignored.
- The number of analysis to be treated. If you correctly select the FIRST row legend, this number should be automatically updated (and should be correct...).
- Enter the number of elements not used in normalization (these are the elements, which are not used in the "*OxyNorm.xls*" or "*CatNorm.xls*" files, comprising the 'Total' or 'Sum' of analysed oxides). This value should be determined during opening of the form, but you may correct it. Be careful with this: if the value is incorrect, you may loose some data during processing!
- If you need to normalize your data according to a fixed number of oxygen check the option "use OXYGEN normalization" (file "*OxyNorm.xls*"). In this case, the textbox "# Cation" is change to "Fe3+/Fetot", allowing you to calculate a Fe^{2+} and Fe^{3+} content. If not checked, a normalization based on number of cation is used (file "*CatNorm.xls*").
- Select the type of mineral to normalize with the list. If your mineral is not available, select the first option of the list (named "– (manually) –") and enter the number of oxygen, of cation and of OH or CO_2 group. It is only possible to choose either OH or CO_2 (the macro changes the OH or CO_2 value to zero if you try to enter both...). If you use a cation normalization, enter 0 in # of oxygen to disable Fe^{2+}/Fe^{3+} calculation.
- When everything is okay, click "Normalize the current sheet(s)...". If it ends correctly, the form is closed and normalized data is presented below the ordered oxide.

Note: You can use the options "Order elements" and "Normalize data" at your convenience on any type of file containing oxides-% (and not only files imported from JEOL-8200 ;-). You just have to place "Oxide" in front of the oxides to order or "For Norm" in front of the ordered oxides to normalize...

Menu "Import LineScan…" (For processing LINE ANALYSIS)

!!! WARNING !!! When exporting data **check "Line Intensity/Concentration" option only**. If "Line Measurement conditions" are included in file, you have to **delete the first lines of measurement condition before using this process**. (after this, check that your file is similar to Table 1).

Note: A copy of the original data sheet is made before changing anything!

```
                >>>   Line Intensity/Concentration   <<<
                              Dump (    1) - ( 1000)

Elem-1  Al      Channel 1  WDS         (A=16.3446 : B=1.9850)
-----------------------------------------------------------------------------
>>>>>>>     1 -    50 Points <<
8.84333 10.01399 9.76753 9.89076 10.56851 9.55188 10.59932 9.79834 10.04479
9.18220 10.87658 9.61350 8.96656 …
…
```

Table 1, Example of correct file (only the first few lines)

Open file to treat. ***If Excel automatically opens a "Text Import Wizard", select "Cancel"*** (the macro will automatically do this with the correct options). Load "Import LineScan…" in JEOL2xls menu and ensure if elements found are correct (should be written on the left of each "Channel x"). If this is not the case, your file may be corrupted (see Table 1). Check if it is similar to Table 1! Check the values of the total number of pixels (resolution of your scan). This value should be already correct, as it is taken from your file (second number of the line named "Dump (…) – (…)"). For instance, in Table 1, this is 1000 pixels. Value must be rigorously identical to file content to avoid any bug during treatment. Activate the checkboxes for the channels you want to import (maximum 5 spectrometers and 1 channel for COMP, SEI or TOPO signal). Click "Start importation".

Menu "Average LineScan…" Processing line analysis *AFTER USE OF MACRO "Line_Scan"*

Ensure you have opened and treated your Line Scan results with "Import LineScan…" (do not change file after importation otherwise, it may produce error or bad data treatment). This process will smooth the scan, by calculating a moving average on a certain number of points.

- **Start "Average LineScan…"**
- Check number of pixels and channels (values taken from file: if they are not the one expected, something may be wrong in file).
- Enter number of points to be taken for average. To reduce number of pixels, some averages may be excluded ("jump" of the moving average). For example on a total of 1000 pixels, if you enter "10" in number of points for moving average and 2 as number of points to conserve, this will give you at the end 200 points. The first average is calculated on pixels 1 to 10 and then 6 to 15, 11 to 20, etc… and 191 to 200

!!! WARNING !!! This treatment is not truly statistical. Preferably use a complete mathematical program using recognized smoothing method, especially if you want to publish some results… Here it's fine for "simplification", but some small details (like tiny mineral inclusion producing a sharp peak on the scan) may be highly reduced! A module accompanies the file JEOL2xls (method of EQUIDISTANT LEAST SQUARES © P. Barak 2005). I found it on the web and it is probably a better tool for LineScan treatment. Actually I didn't get into detail with this process, but you may "have a look"… (see **JEOL2xls menu "EQL Auto (LineScan filter)" or "EQL fixed (LineScan filter)"**).

For more detail about the "Equidistant Least Squares" macro, a small part of a huge macro set call "MacroBundle" (**see menu "EQL Auto/Fixed..."**), please, refer to web page... http://www.bowdoin.edu/~rdelevie/excellaneous/

Menu "Restart JEOL2xls…"

Use to reload the macro, unload any extra menu of Excel, test the default directory and reload the JEOL2xls menu.

!!! WARNING !!! If you are using another Excel Add-ins creating a menu (like "Isoplot") it will also be unload!

Julien Allaz, March 2008

For Mac & PC

Design for BLABLA*

Help-file for 'Ar2xls' version 2.4

Data treatment of Argon-Argon extraction line (stepwise heating technique)
Institute of Geological Sciences (Berne) © J. Allaz 2004-2008

READ BEFORE USING THIS MACRO!!!

a) 'Ar2xls' is written for **Mac & PC and Microsoft Excel 98 or later is required** (Visual Basic for Application [VBA] required).

b) When using this macro, **put the 3 files ("*Ar2xls.xls*", "*ArNewBlank.xls*" and "*ArDiffBlank.xls*") in the same folder. DO NOT CHANGE THE NAME OF THESE FILES!!!** Both "*ArNewBlank.xls*" and "*ArDiffBlank.xls*" should be locked to avoid any change, as they are models for new analyses and contain formulae.

c) Only "*ArNewBlank.xls*" may be changed if some constants have to be changed for ALL further analysis treatment (background, J-factor, conversion coefficients...). If you are not sure... DO NOT DO IT and ask an administrator!

d) Preferably **use step files obtained with "MERLIN" program from Berne** (file "*Rxxxxx.STP*", contact Prof. Igor Villa for more information). However, you may adapt your own step files obtained from elsewhere for 'Ar2xls' (refer to § 2.2). STP files are NEVER changed by 'Ar2xls'; when working on it, either close the file without saving or the macro will create a copy of the file.

e) After running any of the routine available in 'Ar2xls' macro, an undo is NOT possible! Therefore, make sure to SAVE YOUR FILE before running an 'Ar2xls' routine. With this security, you can always close your file without saving and re-open it, if something goes wrong...

f) If an **abnormal error occurs during the use of 'Ar2xls' (runtime error or other VBA error), quit Excel – or force to quit – and start 'Ar2xls.xls' again** (even if you click 'Cancel', Microshit Excel remains unstable and fatal error can appear). If error persists, ask an administrator (contact at the end of this manual).

g) Administrators of the 'Ar2xls' macro are NOT responsible of some **data-loss due to a computer crash**. As always when working with a computer, **a copy of the original files** (macro files + STP files + files created by 'Ar2xls') should be kept on an external drive (USB disk, CD, external Hard Drive...)!

Content

* ***B**ernese **L**ow **A**rgon **B**lank **L**ine **A**ssembly*

1. Basic information

This macro aims to replace the older routine "MKLIST", "AGE", and "Stefan's macro for Excel 4.0" used in the BLABLA lab for age calculation. In addition, this new macro allows a rapid treatment of Ar-Ar results, with automation processes for graphic results (age-spectrum, Ca/K and Cl/K, Ar-release…). Iteration process for determination of sensitivity-factor of mass spectrometer and J-factor permits a rapid treatment of standard analyses.

1.1. Files for and from 'Ar2xls"

1.1.1. Macro and blank files (the-files-that-you-should-NEVER-TOUCH!!!!)

"*Ar2xls.xls*" contains all macros (written in VBA for Excel, not accessible in Excel 4.0 or earlier). Access to the macro source is password protected. This file also contains a worksheet with some important information and with a cell containing the path to "*Ar2xls.xls*" (hidden workbook; show it with menu "*Window:Unhide…*"!).

"*ArNewBlank.xls*" is the blank file containing all formulae required to treat results from STP files. In this file, only CST sheet may be changed (*i.e.* when background has changed or if a new J-factor has been calculated). *All other pages contain formulae and should NEVER BE CHANGED*. The file should be kept in read-only mode to avoid any changes.

"*ArNewDiff.xls*" is the blank file containing all formulae and graphics for Arrhenius relation ("Diffusion"). Calculating diffusion coefficient by use of stepwise heating results is totally WRONG, as mineral in the furnace are NOT in equilibrium: Ar release is clearly not dominated by pure volume-diffusion, but by mineral reaction (dehydration, phase change...) through temperature! However, "diffusion" plots may be used to get an idea of difference in release of ^{40}Ar vs ^{39}Ar. This file is also in read-only mode to avoid any changes.

1.1.2. "STP files" and "Run File"

'Ar2xls' is used to treat regression files from the famous BLABLA, the Ar extraction line from the Isotope laboratory of the Geological Institute of Berne (***Rxxxxx.STP***, named "**STP files**" thereafter). Put ALL STP FILES to be treated in the SAME FOLDER as the 'Ar2xls' macro files and ensure the default 'Ar2xls' folder has been correctly defined. If Excel cannot find the "ArNewBlank.xls" file or your own STP files, try first to restart the macro with menu "ArBasic:Restart 'Ar2xls'...". In the following, **Run File** describes any file created by 'Ar2xls' and containing imported values from STP files (this file is a copy of "*ArNewBlank.xls*"). The Run File always contains five sheets:

a) **Info** – sample information and name of STP files needed for importation
b) **STP** – result of the importation (= brut data from all STP files)
c) **Calcul** – some intermediate calculations…
d) **Results** – final results (for publication and graphics)
e) **Cst** – constants (background, J-factor,…) used for the current Run File.

WARNING: To keep Run File compatible with 'Ar2xls', NEVER CHANGE THE NAME OF THESE SHEETS. However, you may add other sheets. Avoid changing values in cells manually in sheets 'STP' (except correction on temperature, cells in orange), 'Calcul' and 'Results'. These sheets are bind with formulae and cell references.

WARNING: If you have to paste data in sheet 'Stp' or 'Cst' (results or change of background…), you should paste value only (by use of menu "Paste special" => check the option "value" => "OK"). Otherwise some formulae may have problems (i.e. instead of containing a value, some cells return an error [#REF!]). Whenever this is possible, change values with one of the 'Ar2xls' menu (i.e. constants, J-factor, background, importation of STP files...)!

1.1.3. Graphics and Print files

When importation and calculation is finished, you will be asked to continue with automatic creation of graphics (spectrum age vs cumulative 39%, Ca/K vs age, Cl/K vs age, Cl/K vs Ca/K and 39/40 vs 36/40). The newly created file is automatically saved as **Graph_***YourRunFileName***.xls** (§ 1.2.7). Exportation of results for printing is named **Print_***YourRunFileName***.xls** (§ 1.2.9), unless you choose a different name. Plot of argon release is named **Release_***YourRunFileName***.xls** (§ 2.1.4), and plot for Arrhenius relation ("Diffusion" graphic) is named **Diff_***YourRunFileName***.xls** (§ 2.1.5).

1.1.4. Faraday and Multiplier measures files

When importing data comprising measures on Faraday cup [F] and Multiplier [M], a special routine creates new files for each original STP files (optional). Each new file is named **MF**_*Rxxxxx*.**STP** (see § 1.2.4). A file comprising calculated gains (*i.e.* the ratio of measure M/F on ^{40}Ar, ^{39}Ar and/or ^{36}Ar) from all "*MF_*.STP*" files may also be saved as **Gain**_*YourRunFileName*.**xls** (optional, see § 1.2.4).

1.2. Starting with 'Ar2xls': the "ArBasic" menu

When starting 'Ar2xls' (by opening the file "*Ar2xls.xls*"), two menus are loaded ("ArBasic" and "ArExtra"). These menus give you access to all routine details of the macro. If an error occurs when selecting one of the options available in these menus, ensure a Run File is open and check if 'Ar2xls' macro filename remain unchanged ("*Ar2xls.xls*") and that path to 'Ar2xls' (in the hidden 'Ar2xls' spreadsheet) is the actual default folder (=> try to restart 'Ar2xls').

The four main commands found in 'Ar2xls' toolbar are explained hereunder. The first menu "*New run…*" automatically drives you through all required information for the importation and calculation of your stepwise heating analysis. However, any option described in following paragraphs can be access at any moment. Remember the macro acts on the activated workbook (in foreground). Therefore, better work with only ONE FILE OPENED!

1.2.1. Starting a new or existing Run File

To start a new run treatment, select "*New run…*" and enter a name for your run file. A copy of the "*ArNewBlank.xls*" file is then created in the 'Ar2xls' folder.

If you have to rework an existing file, simply open it and run one of the 'Ar2xls' option. Note that a test on your file is made before any 'Ar2xls' process: it checks if all required sheets are present and correctly labelled ("Info", "STP", "Calcul", "Results" and "Cst").

1.2.2. "Sample info…" and "New STP-files serie…"

"***Sample info…***" allows you to enter basic information about analysed sample (date of analysis, sample name, mineral analysed, weight of sample <u>*in grams*</u>).

"***New STP-File serie…***" ask you to enter the first step file number (only the *xxxxx* of R*xxxxx*.STP) and allow to enter automatically a continuous numbering of steps. From this point, three possibilities:

a) "**Cancel**": do nothing and to allow you to enter manually the STP file names starting from cell C14 (R14C3) and up to cell C63 (R63C3) of sheet 'Info'. Fill this column without any empty cell between file names otherwise importation process will stop. Return to importation of STP files with menu "Import STP…".

b) "**Back to sheet…**": STP file names are written in 'Info' sheet and form is closed. Then, complete or correct the sequence of STP file names and return to importation of STP files with menu "Import STP…".

c) "**Import Faraday…**": enter sequence of STP file names and continue with importation of STP files containing only 5 measures on Faraday cup or Multiplier.

d) "**Import F+M...**": enter sequence of STP file names and continue with importation of STP files containing up to 10 measures on Faraday cup [F] and Multiplier [M].

WARNING: *Before continuing importation, ensure that all STP files are present in the 'Ar2xls' macro folder!*

1.2.3. "Import STP…"

WARNING: *Do not import STP files with this option, if both Faraday and Multiplier data are in STP files (§ 1.2.4)!*

This menu opens the "normal" routine for importation of STP files. <u>This is for files containing measurements only on a Faraday cup [F] or only on a Multiplier [M]</u>, *i.e.* only 5 lines for measures of ^{40} to ^{36}Ar. Ensure to have all the necessary STP files (whose name is entered in sheet 'Info') and click "OK" to import files. Table 1 present an example of a classical STP file containing only measure on Faraday (but could also have been only multiplier). After importation, enter the correct temperature of each step manually (required for expert option 'diffusion' and 'release', § 2.1.4 and 2.1.5). Note that macro fills automatically this column with the four

first characters present in the comment of each STP file (see Table 1, line 3). This mean that when you type comments on analysed step, first write T° then other comment.

```
Sample Nr: Pi0601 Bt100                                  # General comment on sample #
Run Nr: 16708, Type of run: 11_opt1, Operator: JA        # Nbr of STP file (Run Nr and type) and operator info #
Comment: 631 stp1 linear regression                      # Specific comment on the current step #
 1                                                       # Duration of irradiation (days) #
 100                                                     # Time since irradiation (days) #
 101.6746      4.241969E-02                              # 40Ar on Faraday (measure and error) #
 2.486974      5.002968E-03                              # 39Ar on Faraday (measure and error) #
 .9683607      3.165555E-03                              # 38Ar on Faraday (measure and error) #
 4.530967E-02                2.531936E-04               # 37Ar on Faraday (measure and error) #
 .3101738      4.311676E-04                              # 36Ar on Faraday (measure and error) #
```

Table 1, example of a STP file after regression of the RAW file through the program "MERLIN" (only Faraday measures). Compare this table with your data and make change if necessary (be aware of the empty space at beginning of lines 3 to 9). If you obtain your data in Berne and if you regress it correctly with MERLIN, correction on your STP files are NOT required (#…# are lines of comment, not in file).

1.2.4. "Import F+M…"

When both Faraday cup and Multiplier data are present in STP files, check in one of your STP file to import, which data are present in file: which mass? on Faraday or Multiplier or both?... (see § 2.2 and Table 3 for file example). Close the STP file you may have open, activate again your current Run File and click "Import F+M…". If you treat your RAW data with MERLIN, the masses should be ordered like following: 40[F], 40[M], 39[F], 39[M], 38[F], 38[M], 37[F], 37[M], 36[F], 36[M]. Ensure that all file to import have the same M+F setting (if not, you have to split your filename STP series in as many Run File as there are M+F setting), and proceed as following:

a) Choose which type of measurement should preferably be taken (*Faraday cup* or *Multiplier*). This determines which value is taken preferentially, when both F+M measure are present. Generally, best results are obtained with 'Multiplier' (default option) as the precision is by far better than on Faraday
b) In the next part "*Which masses are in file?*", select ALL masses you analysed. Do not omit one, and cause incorrect importation
c) When data (F or M) have to be transformed in their equivalents (M or F), a gain (ratio M/F) is used to correct the values. *Choose which gain has to be used* either a gain calculated on double mass analysis (M & F) or a fixed value. Usually, "*Gain on 40Ar*" or "*39Ar*" are best option. You can also enter a fixed gain to be used on all STP files. It may be useful to use this option, if calculated gain is badly constrained (e.g. weak signal). Since installation of a new multiplier device on the BLABLA at the Baltzerstrasse, the gain factor M/F appears to be stable around 0.94 (June 2007; MasCom electron multiplier; 19 Cu-Be dynodes at 2.00 kV equipped with preamplifier WMT PAD06; Constant gain M/F calculated over the range 0.1 to 30 mV on Faraday cup). A gain superior than 1.00 should never appear with this setup
d) Check "*Save new STP"* to save each modified STP files in a new Excel spreadsheet ("MF_*Rxxxxx.STP*")
e) Check "*Gains file*" to save a new file comprising all calculated gains from each STP files. The "MF_*Rxxxxx.STP*" file contain both F+M measure and also a line giving the selected value (i.e. M or F measure, or a value corrected with the selected gain)
f) When everything is alright, click "*Import…*".

WARNING: *Ensure that all STP files are present in the 'Ar2xls' macro folder!*

1.2.5. "Import ALL STP…"

The routine "**Import all STP...**" does a similar job as the routine described above (§ 1.2.4), but instead of copying your STP data in a Run File, it creates a new workbook containing ONLY the brut STP data (with or without error). To use it, you just need to define a list of STP file name, in column, without blank line except at the end of your list (STOP signal for the routine). You can choose for this any file of your choice. However, instead of copying your data in a classical Run File, this routine simply copies and paste all your raw data contained in the list of STP file name you give. When activated, proceed as in § 1.2.5 (a, b). Then enter the name of file to create and the starting cell reference of your STP filename list (e.g. enter "A1" or, if you use your Run File, "C14").

1.2.6. "Redo calculation"

Use this routine to **redo calculations in sheets 'Calcul' and 'Results'**. It simply deletes everything except the first line of calculation in both pages and redo a copy-paste of this first line in the lower one, at the condition that a step name (*Rxxxxx.STP*) is present in the first column of sheet 'STP'. However, it is often recommended to redo a complete importation of STP files, especially if an undesirable error is present in the formulae present in sheets 'Calcul' and 'Results'.

1.2.7. "Export Graphic"

A set of five graphics can be drawn automatically after importation: a) age spectrum (age versus cumulative-percent ^{39}Ar), b) age versus Ca/K, c) age versus Cl/K, d) Cl/K versus Ca/K and e) ^{39}Ar/^{40}Ar vs ^{36}Ar/^{40}Ar. A copy of all required data is pasted in a new workbook. This new workbook is automatically saved as "Graph_*YourRunFile*.xls", unless a file of identical name already exist in the 'Ar2xls' default folder.

1.2.8. "Export Print..."

The results of a Run File are pasted in a new workbook and are formatted for printing. In this new workbook, all formulae are suppressed and only values remain. After selection of data you want to export (note the useful buttons to check all values, some default one or none). Sample name, mineral analysed, weight and J-factor are always present in the export file. This new workbook is saved by default as "Print_*YourRunFile*.xls", but you can enter a different name.

1.2.9. "Print sheet (graphic)"

Use this option to generate a "ready-to-print" sheet from a graphic exportation. This option can only be applied on original graphic workbook created by the routine "Export Graphic" from 'Ar2xls'.

1.2.10. Final recommendation

Except sheet 'Cst', all other sheets in your Run Files are originally NOT protected for rewriting. **Pay attention when manipulating the data in these sheets as they are either related to other cells or contained formulae! Avoid also all copy-paste in these cells, notably in sheet 'STP' and do not move them**! It is preferable to copy the data and paste them with the option "Paste special..." => "Value" in a new workbook. You may also use option "Eliminate formulae" (see § 2.1.3) to DEFINITIVELY suppress all formulae and references (this renders the file incompatible with quite all 'Ar2xls' routine...)!

1.2.11. "Restart Ar2xls" and "Close Ar2xls"

When access to blank Run File or any other abnormal error occurs, try first to use option "Restart Ar2xls". With this, default path for Ar2xls are reloaded, while menus "ArBasic" and "ArExtra" are deleted and created again. If you want to restart 'Ar2xls', while menus are inaccessible, you can access to the routine "Restart Ar2xls" through the macro player of Excel ("Tool:Macro:Macro..."). "Close Ar2xls" close the macro file and reset Excel menus. Note that resetting of menus created by Ar2xls has also the effect to deactivate menus from any other Excel Add-ins (e.g. Isoplot).

2. Expert options

2.1. "ArExtra" menu

2.1.1. "Open an STP file"

Select and open STP file(s) of the current Run File. These files must naturally be present in the 'Ar2xls' folder.

2.1.2. "Variate parameters..."

Test the effect on results by varying some run result(s) like Ar masses from STP file, J-factor and irradiation parameters. First, you are asked to enter step number to work on. A form opens, allowing you to

change some value. Click on “RE-CALCULATE NOW!” to validate change. New values you enter are temporarily written in your Run File to get new age. If you want to change step file to test or simply recall in this form the original data, click “Change STP or recall primary data” and enter again a step number.

WARNING: your original data will never be changed at the end of the process. By activating this option, original data are saved and written under each value you can change; by closing the form or by changing step number, original data are recalled. There are NO POSSIBILITIES TO SAVE CHANGES you make in this form! Do you really think you can cheat with data!?!?

2.1.3. “Eliminate formulae”

This option DEFINITIVELY destroys all formulae contained in the actual Run File by doing a copy-paste of values only in all cells. **NO UNDO POSSIBLE and recalculation is impossible after this operation**.

2.1.4. “Export graph Release”

This creates a new workbook (named “Release_*YourRunFileName*.xls”) containing results of argon release (in picoliter per degree) and temperature of each step. Graphic of **Temperature [°C] versus Argon release [pl/°]** is then generated. The graph presents release of ^{40} and ^{39}Ar on the left axis and the right axis stand for release of masses ^{38} to ^{36}Ar. Before using this option, **ensure to have entered the correct temperature value of each step (in sheet STP),** otherwise ‘Ar2xls’ will generate an error!

2.1.5. “Export graph ‘Diffusion’”

It creates an Arrhenius graphic (for “diffusion” with a cylinder model) for ^{40}Ar and ^{39}Ar of the current Run File (new workbook named “Diff_*YourRunFileName*.xls”). **WARNING it is a non-sense to determine a “true” volume-diffusion coefficient of Ar with a stepwise heating technique**, as minerals are not in equilibrium inside furnace (one basic rule of diffusion theory is thus transgressed). However, it may be used qualitatively to check for difference in the release of ^{40}Ar and ^{39}Ar. For instance, the presence of excess ^{40}Ar in fluid inclusion should be well visible with a higher “diffusion” for ^{40}Ar compared to ^{39}Ar.

Before using this option, **ensure to enter the timing of each run (in sheet INFO, columns “time in furnace”) and the correct temperature value of each step (in sheet STP),** otherwise ‘Ar2xls’ will generate an error. If not, enter/correct manually temperature and time of start & end of each degassing step in format hour-minute (hh:mm); the third column “total time in furnace” should be filled automatically, as it contains formula. During exportation of data, time is copy-paste as a value (from original format 02:24 [hh:mm], time is changed in a decimal number 0,1 [day]) and then converted in minutes. If you work over midnight (don’t laugh, this may happen :), the time may be negative. You will have to correct this manually!

2.1.6. "Change Background…"

With this option, you can **change values of spectrometer background (in millivolt).** To **change manually** the background for your Run File, select “Change manually” and enter values. Ensure to use background values corresponding to your measure. You can also **take values from a file** (like “*rrr.bg*”, see Table 2). For this, in “*Change background...*”, select “*Take values from file...*” and enter a file name (this file must be in the ‘Ar2xls’ default folder). In both cases and if needed, do not forget to correct the date of background measure and eventually the relative error on ^{36}Ar background (usually 30% => 0.3). Validate your choice with “Apply changes”.

Your results are automatically recalculated with these new setting, unless you eliminate formulae (§ 2.1.3). If not, refresh calculations by selecting “*Calculation*” in Excel option in menu “*Tool*” and click “*Calc now*” (PC shortcut [F9] or Mac shortcut [Cmd] + [=]). The background of spectrometer may evolve with time. Therefore, regularly check dynamic and static backgrounds you made between analyses.

```
DY.BG                                          # Type of background (dynamic or static) #
                                               # Empty line #
                                               # Empty line #
 .120711          28.389936E-02                # Background of 40Ar on Faraday #
 2.11886E-03      4E-03                        # Background of 39Ar on Faraday #
 .207115E-02      10E-03                       # Background of 38Ar on Faraday #
 2.08385E-03      1.1E-02                      # Background of 37Ar on Faraday #
```

.00210	4.0E-03	# Background of 36Ar on Faraday #

Table 2, example of a background file "rrr.bg". Numerical data are presented as in Table 1: measure and error on each line for each mass.

2.1.7. "Change other constants…"

Allows you to **change all constants from sheet 'Cst'**. You can also unlock sheet 'Cst' and modify value manually (menu "Unprotect CST"). Do not forget to lock 'Cst' sheet again when finish (menu "Protect CST"). **Of course, if you don't know that are these constant, NEVER CHANGE THEM, and ask an administrator (these are not expert options for nothing!!!)**

2.1.8. "J-factor…"

This option is used to **recalculate a J-factor from a standard analysis**. For the moment, only the hornblende standard "MMhb" is present in the macro (age = 523.1 ± 4.6 Ma [*Renne et al. 1998, Chemical Geology, vol. 145, 117-152*], other Ar-standard data available in this paper), but you can select a "Custom..." standard and enter its age manually. More standard references can be added inside the macro, ask an administrator! To proceed with calculation of a new J-factor from a standard analysis:

a) Choose the step n° in the active Run File containing the major step of the standard analysis
b) Select the standard in the list to load data. If not present, choose "Custom..." and enter age manually (in Ma)
c) Click "AUTOCALC" to calculate automatically the J-factor. After iteration, the new J-value is automatically entered in sheet 'Cst' and added in the comment column in sheet 'Info' of the step n° used (added after your existing comments).
d) If you prefer the manual manner, enter a new value for J in "J-factor NEW" field. Then ask to recalculate age (button "Calculate age with J-factor new…"), and validate your J-factor NEW when the calculated age is near the standard age (button "Validate the choice of J-factor NEW and close").
e) By clicking "Cancel", the old J-factor (*i.e.* before accessing to this form) is maintained.

WARNING: It may happen that the result of J-factor calculation return a number but with the wrong delimiter (i.e. if you use the point "." it returns a comma "," or vice-versa). In such case, the formulae will display an error. You will have to change manually.

2.1.9. "Sensitivity-factor #2…"

A "sensitivity-factor" is required to back calculate K-content. Such a factor is in the order of 10^{-11} and is variable (changes with time and ionisation capacity of the filament in mass spectrometer, background of spectrometer…). Similar to J-factor, the use of a standard is required: according to the COMPLETE run analysis of a standard, the total K-content is calculated with the current sensitivity-factor. The first option asks you to enter the K-content of the standard and automatically adjusts the sensitivity factor to yield this theoretic K-amount. Click "Autocalc" to activate this option. The second option allows you to adjust manually this sensitivity-factor and to recalculate the K-content (left-button). Click on the right button to validate your choice or click 'Cancel' at any moment to recall the original value.

2.2. The correct format of STP file

This macro imports only correctly STP files resulting from regression with the program MERLIN (Institut of Geology, Berne). Table 3 is an example of such file (#…# are lines of comment, should not be in file).

The macro takes from this STP file the following values (NO CHANGE IN ORIGINAL FILE, only copy-paste…):

- Lines 1 to 3: are for comments, not obligatory, but quite useful. Reported in sheet STP of the Run File.
- Lines 4 and 5: are for irradiation parameters needed for corrections. Reported in sheet STP.
- Next are all masses measured, accompanied by their error. In Table 3, the maximum of analysis is presented, but some can be missing (however, the order remain the same). If the normal importation process is used, a maximum of 5 lines is needed (exclusively only on Faraday OR on Multiplier).

WARNING: *(if you have to adapt your STP file) there is a space at the beginning of numerical results. Measures are separated by tabulation (a white space should be enough, but I have not tried it yet…).*

If your step files are not from Berne, you may have to adapt it before importation. Why not creating a complementary macro for example… (I can perhaps help you; see final notice ;-)

```
Sample Nr: Pi0601 Bt100                                  # General comment on sample #
Run Nr: 16708, Type of run: 11_opt1,  Operator: JA       # Nbr of STP file (Run Nr and type) and operator info #
Comment: 631 stp1 linear regression                      # Specific comment on the current step #
1                                                        # Duration of irradiation (days) #
100                                                      # Time since irradiation (days) #
 101.6746      4.241969E-02                              # 40Ar on Faraday #
 95.57412      6.365214E-03                              # 40Ar on Multiplier #
 2.486974      5.002968E-03                              # 39Ar on Faraday #
 2.182988      1.050045E-03                              # 39Ar on Multiplier #
 .9205965      1.365145E-02                              # 38Ar on Faraday #
 .8653607      3.165555E-03                              # 38Ar on Multiplier #
 4.405189E-02                9.365245E-03               # 37Ar on Faraday #
 4.140878E-02                2.531936E-04               # 37Ar on Multiplier #
 .3101738      4.311676E-04                              # 36Ar on Faraday #
 .279575       4.258407E-04                              # 36Ar on Multiplier #
```

Table 3, example of a "complete" step file result comprising measure on Faraday cup AND Multiplier for all five masses. This represents the maximum of data 'Ar2xls' can work with. See Table 1 for a description of such file (#…# are lines of comment, should not be in file).

3. Possible errors

Problem: Major crash: Excel is suddenly closed with an "Unexpected Error" or with a message "Unable to save document" or "Device I/O error"...

Solution: With old computers (G3), when starting a new run, your computer may crash generally due to lack of memory: either quit Excel... or update your computer with some RAM. On a newer computer, such error should happen rarely, notably when a process has an abnormal end (with Visual Basic error or so) or when Excel memory is saturated. Sometimes it just crash, without-any-reason...

Problem: The wrong Excel workbook is used by the macro or an error (file not found) occur when an 'Ar2xls' macro is played.

Solution: Ensure the Run File you want to treat is THE CURRENT ACTIVE WORKBOOK (= the one in foreground). If not, simply click on your Run File to activate it! To avoid bad file treatment, it is highly recommended to work with only ONE workbook opened in Excel...

Problem: "Cannot find file [YourFile.xls]…" or "Cannot find [ArNewBlank.xls]" or "…[ArDiffBlank.xls]".

Solution: Ensure to have "*YourFile.xls*" in the same workbook as the 'Ar2xls' files! It may also be due to bad definition of your Ar2xls default folder. To solve problem, restart the macro and check the default folder (menu "ArBasic:Restart Ar2xls...")!

Problem: I cannot access to the source code of the macro…

Solution: This is normal (password protected)! Please, contact Julien Allaz and explain briefly, why you need this access: update, error…

Contact administrator for any encountered errors not listed here or for any question!

Julien Allaz[1]	Igor Villa[2]
	031 / 631.**87.77**
079 / 256.22.45	031 / 972.41.84
	James Bond's Room 007
jallaz@geo.unibe.ch	Baltzerstrasse 1
or **webmaster@geoloweb.ch**	igor@geo.unibe.ch

[1] For problems related to the macro itself
[2] For problems relative to Ar-Ar data and age calculation

Help file of 'Ar2xls' version 2.4 (4th March 2008)

"All parts should go together without forcing. You must remember that the parts you are reassembling were disassembled by you. Therefore, if you can't get them together again, there must be a reason. By all means, do not use a hammer."
1925 IBM Maintenance Manual

"Computers are like bikinis. They save people a lot of guesswork."
Sam Ewing

"To err is human, but to really foul things up you need a computer."
Paul Ehrlich

"Never trust a computer you can't throw out a window."
Steve Wozniak

From http://www.phdcomics.com

Thanks to Allison, Turner and Costa & Igor ;-D

Many thanks to Igor Villa & Daniel Rufer for the argonization of my thesis and Robyn Pickering for zi Änglisch :)

Julien Allaz, 28th April 2008

I WANT YOU FOR PETROLOGY

Acknowledgments

First of all, I am extremely grateful to **Prof. Martin Engi** for providing me this exciting research project in the Central Alps. I will remember and regret these good (and less good or even stressful) moments! This study has demonstrated the fruitful product of a multi-disciplinary approach, which obligatory involved many collaborators and unequivocally leads to greater results ("*1 + 1 = 3 [...] l'union des talents dépasse leur simple addition*" B. Werber). Those collaborators and friends are greatly thanks:

- **Prof. Igor M. Villa** for introducing me to the ^{39}Ar-^{40}Ar dating method, for copious blah blah on BLABLA and also for solving numerous analytical and technical problems (and for *true* italian coffees).
- **Dr. Alfons Berger** for the help at the electron microprobe, as also for fruitful discussions about the geology of the Central Alps and many other petrographic problems.
- **Dr. Edwin Gnos** for assistance at the electron microprobe and pleasant discussions about minerals.
- **Dr. Jens-Oliver Schwarz**, my colleague for these five years. Many thanks for all the good time spent in the field and in the office! Thanks also to **Angie (and little Tobias)** for the funny playing nights (boardgames, poker, billiard...) and other diners and parties!
- **Dr. Emilie Janots**. Many many thanks for her support and her precious help (monazite, allanite dating: that was her job in Berne). Many thanks also for her joy of living, which always brings the sun in our office, even if dark clouds sometimes dominate my petrographic Universe.
- **Danier Rufer** for his highly necessary help before and during my ^{39}Ar-^{40}Ar dating, as also for the rewriting of Ar-Ar analysis program.
- **Prof. Romain Bousquet** for introducing me to the recognition of carpholite veins in Central and Western Alps and to **Michael Wiederkehr** for the fruitful discussion about HP/LT metamorphism and carpholite veins from the Mesozoic of the northern Central Alps.
- **Dr. Meinert Rahn** for providing us his latest fission track results and for introduction to this dating method.
- **Prof. Jan Kramers** for his assistance to install and to program the new electron multiplier for Ar-dating.
- **Dr. Manuel Eggimann** and Dr. **Urs Eggenberger** for assistance at XRD laboratory.
- **Dr. Vincent Serneels** and **Prof. Ivan Mercolli** for providing XRF analysis (I will also remember the snowy field course in Piora with Ivan in 2007...).
- **Dr. Olivier Beyssac** for introducing me to the graphite thermometry.
- **Prof. Christian de Capitani** for the discussion relative to thermobarometry (THERIAK-DOMINO).
- **Robyn Pickering** and **Dr. Carl Spandler** for English corrections.
- **Denise Bussien** and **Dr. Karine Gauchat** for precious information about Antabian and Nufenen areas.
- **Dr. Annett Buettner**, **Dr. Dorothee Hippler**, **Dr. Fraukje Brouwer**, **Dr. Philippe Hunziker** and **Dr. Tom Burri**. These were my first contacts at the institute and I greatly appreciated their help.
- **Ulli Linden** and **Werner Zaugg**, our precious computer engineers. Sorry for all bugs I apparently caused, but this was NOT ALWAYS my fault (check this with Microshit©, please)!
- Our Super-Secretaries were always here when you need help! And they spoke French, which is extremely useful for a *"Welsch"* (or a *"Russe"*) freshly arrived in Berne! Thus, many thanks to **Isabelle Jobin**, **Sarah Antenen** and **Barabara Grose**.
- Our technical staff: **Verena Jakob**, **Jürg Megert** and **Stephan Brechtbühl** (thin sections), as also to **Ruth Maeder** (chemical lab), **Kurt Howald** (isotope lab), **Yves Kruger** (microscope), **Adrian Liechti and**

Hanspeter Bärtschi (technician) and **Daniel Eggimann** (attendant; thanks also to our cleaning ladies :).

- **Marco Antognini** (Museo Cantonale di Storia Naturale, Ticino), for providing necessary permissions for rock sampling in Ticino.

I also thank all members of the Institute of Geological Sciences in Berne, for these marvellous five years spent at the Institute and outside. I will remember these Friday-beer nights with or without BBQ or cheese fondue, as also biking to the Niesen and some nights in the Bierhübeli or elsewhere. The fieldtrips in the Alps, in Czech Republic or in Scotland were also greatly appreciated! Thank you very much to...

Andrea Voegelin (our Dancing Queen), **Sabine Brodhad** and **Nadja Neubert** (the spinning girls), **Greg Van den Bleenken** (Say "cheeeeeese" to the camera), **Dr. Marco Schwab**, **D.J. Glenn Lambrecht** (Jazzy Friday and Sunday rosé), **Kamel Latoui** (French revolution!), **Dr. Bettina Flury** (for sharing stress before our defense), **Dr. Martin Wille**, **Dr. Alexandre Tarantola** (co-locator for a while), **Dr. Monika Painsi** (RAMAN spectrometry), **Dr. Bénédicte Cenki-Tok** (EMP: Zen for me, too), **Notburga Kapferer and Dr. Tonny Thomsen** (the latest arrival in our office), **Dr. Andreas Ebert**, **Dr. Michaela and Dr. Kamil Ustaszewski**, **Dr. Raul Fernandez**, **Lukas Rohrbach** (THE Fridaybeer man), **Matthias Kinkmüller** (the second Fridaybeer man), **Stéphane Kock** (OSL = Old Student Link), **Margarita Koroleva** (Da, da... Vodka! Ach, nein...), **Luca Abbühl** (Another crêpe?), the **Petroseminar group** (Bern-Basel), **Janos Kodolanyi**, **Florian Eichinger**, **Dr. Flurin Vils and Dr. Laure Pelletier** (from Neuchâtel), **Dr. Marek Pekala**, **Prof. Thomas Nägler** (student's Praktikum), **Prof. Larryn W. Diamond** (metamorphic fluids from Antabia remains a mystery to me... For the moment...), **Prof. Othmar Muntener** (Scotland fieldtrip), **Dr. Urs Mäder** (beta-scanner), **Dr. Marco Herwegh** (SEM), **Prof. Jörn Geister** (paleontological excursion to Prag), **Prof. Thomas Pettke**, **Dr. Guido Schreurs**, **Prof. Karl Ramseyer** (moving a lot of heavy things: rocks, tables, notice boards... and interesting discussion, too :), **Dr. Ralph Mettier**, **Jolien Lickens**, **Gabriel Chevalier**, **Katja Lehmann**, **Andreas Dehnert**, **Angela Graf** (Arolla!), **Conradin Zahno**, **Sally Lowick**, **Göktürk Ozan Mert**, **Kay Wache**, **Gonzalez Laura**, **Juan Carlos Silva Tamayo**, **Dr. Peter Alt-Epping**, **Naki Akçar**, **Dr. Ali Al-Kathiri** and all other I could have forgotten...

All my **friends in Vaud: Sybz, Emilie, Héloïse, Sophie, Valérie, Didier, Fred, Romain, Jean, Seb, Jérémy**... *Et la Jeunesse en général, de même que tous les Baulmérans et Bauminé, c-à-d les habituels du café de "La Baumine" qui se reconnaîteront...*, see also http://baumine.ch/). They are intensively thanked for the cool and relaxing moment spent in Baulmes and arounds (even if not so relax these last months...). This allows me to put aside for a while my geological passion. By the way, "beerious" thanks to the **Stella Bernesis! and Stella!** in general. I will never ever forget those Wednesday nights, which render some of my Thursday morning a bit difficult... Special thanks to **Alodie Rey-Mermet** v/o No Smoking!, **Nelson Marreros** v/o Vexe-A-Piles!, **Michaël Berset** v/o Rein-Seth!, **Patrick Studer** v/o Bîte-Ail'R!, **Marie Klauser** v/o Tad-Foîn!, **Thierry Dupont** v/o Lap-Suce! **Séverine Vogt** v/o Bi-Ca'Nal! and **Olivier Petereit** v/o Gouine-Esc(h)e! *Un grand Schluck à toutes et à tous comme quoi... "Labor Omnia Vincit"* (i.e. hardwork conquers all)!

Finally, my parents and family for their enormous support, especially **Patricia Chambettaz** and **Georges Allaz**, their new partner **Marcel Chambettaz** and **Noëlle Saugy-Allaz** and my sister **Danièle Allaz**.

The **Swiss National Funds** is acknowledged for financial support for this thesis and for:

* The project on alpine metamorphic evolution (Grants 200020-101826 and 200020-109637);

* The electron microprobe of Berne (Grant 200021-103479/1).

Julien Allaz, 30th April 2008

Erklärung

gemäss Art. 28 Abs. 2 RSL 05

Name/Vorname: .....

Matrikelnummer: .....

Studiengang: ……

Bachelor ☐ Master ☐ Dissertation ☐

Titel der Arbeit: .....

.....

.....

LeiterIn der Arbeit: .....

.....

Ich erkläre hiermit, dass ich diese Arbeit selbständig verfasst und keine anderen als die angegebenen Quellen benutzt habe. Alle Stellen, die wörtlich oder sinngemäss aus Quellen entnommen wurden, habe ich als solche gekennzeichnet. Mir ist bekannt, dass andernfalls der Senat gemäss Artikel 36 Absatz 1 Buchstabe o des Gesetztes vom 5. September 1996 über die Universität zum Entzug des auf Grund dieser Arbeit verliehenen Titels berechtigt ist.

.....

Ort/Datum

.....

Unterschrift

Curriculum Vitae

Julien ALLAZ (Ph.D. student)

Personal details

Rue du Four jallaz@geo.unibe.ch http://geoloweb.ch/
CH-1446 Baulmes +41 (0)79 256 22 45

Date and place of birth	30.04.1979 in Orbe (Vaud, Switzerland)
Citizenship	Swiss citizen, native of Villars-le-Terroir (Vaud, Switzerland)
Marital status	Single
Language skills	French (mother language), English and German (both fluently spoken and written)

Research interests

- Metamorphic petrology: Mineral analysis (trace and major elements), evolution of mineral assemblage, state of (local) equilibrium, thermobarometry calculation (TWQ, DOMINO [Berman; De Capitani] or THERMOCALC [Holland & Powell]), disequilibrium process.
- Isotope geochemistry: Ar-Ar geochronometry (stepwise heating technique), stable oxygen isotope analysis on silicates, U-Th-Pb dating of monazite and allanite.
- Structural geology: Crystallization-deformation relations, vein formation (e.g. aluminosilicate tension gashes), geological maps.

Education

29th May 2008	Intended completion of Ph.D.
05.2003 - present	Ph.D. student, Institute of Geological Sciences (University of Berne, Switzerland). Subject: Petrography, mineral chemistry, thermobarometry (TWQ, DOMINO) and Ar-Ar geochronology on micas from the Mesozoic metasediments of Central Alps. Aim to understand the dynamics of the Alpine metamorphism, notably to clarify the significance of age data. Collaboration with Dr. Emilie Janots for U-Pb dating of monazite and allanite. Supervisors: Prof. Dr. Martin Engi, PD Dr. Alfons Berger and Prof. Dr. Igor M. Villa. More information: http://thesis.geoloweb.ch/
06.2003	Diploma in Geology (MSc equivalent, viva March 3, 2003), Institute of Mineralogy and Geochemistry (Lausanne, Switzerland). Subject: Structural and metamorphic study with detailed geological mapping (1:5000), mineral chemistry and thermobarometry (THERMOCALC, TWQ). Mineralogical and structural study of the "Knauern" (tension gashes with aluminosilicate) and thermometry by stable oxygen analysis on quartz, garnet and aluminosilicate on vein and host rock. Aim to understand the significance of these veins in term of structural and pressure-temperature condition. Supervisors: PD Dr. Jean-Claude Vannay, Prof. Dr. Albrecht Steck. More information: http://larecc.geoloweb.ch/
1998 – 2003	Undergraduate studies in geology at the University of Lausanne
1994 - 1998	Matura (A-level) in mathematic and sciences at the CESSNOV (Yverdon)

Please, visit my personal website (http://geoloweb.ch) for complete CV and for complementary information about this thesis:

Pictures (fieldwork, rocks and trips), texts & abstracts, links*...

* Currently under review, will be updated in a few months (for summer 2008).